

2014

# Middle Pleistocene to Holocene sea-level changes and coastal evolution on the Mount Gambier coastal plain, southern Australia

Amy Blakemore  
*University of Wollongong*

---

## Recommended Citation

Blakemore, Amy, Middle Pleistocene to Holocene sea-level changes and coastal evolution on the Mount Gambier coastal plain, southern Australia, Doctor of Philosophy thesis, School of Earth and Environmental Sciences, University of Wollongong, 2014.  
<http://ro.uow.edu.au/theses/4243>

## **UNIVERSITY OF WOLLONGONG**

### **COPYRIGHT WARNING**

You may print or download ONE copy of this document for the purpose of your own research or study. The University does not authorise you to copy, communicate or otherwise make available electronically to any other person any copyright material contained on this site. You are reminded of the following:

Copyright owners are entitled to take legal action against persons who infringe their copyright. A reproduction of material that is protected by copyright may be a copyright infringement. A court may impose penalties and award damages in relation to offences and infringements relating to copyright material. Higher penalties may apply, and higher damages may be awarded, for offences and infringements involving the conversion of material into digital or electronic form.

**Middle Pleistocene to Holocene sea-level changes  
and coastal evolution on the Mount Gambier  
coastal plain, southern Australia**

A thesis submitted in fulfilment of the requirements for the award of the  
degree of

Doctor of Philosophy

from

The University of Wollongong

by

**Amy Blakemore**

BSc Hons

School of Earth & Environmental Sciences

2014

I, Amy Blakemore, declare that this thesis, submitted in fulfilment of the requirements for the award of Doctor of Philosophy, in the School of Earth & Environmental Sciences, University of Wollongong, is wholly my own work unless otherwise referenced or acknowledged. The document has not been submitted for qualifications at any other academic institution.

Amy Blakemore

April 2014





Cape Northumberland, South Australia



# Abstract

Reconstruction of palaeo-sea levels provides a framework for determining Quaternary ice volumes and assisting in modelling predictions of future sea-level change. Commonly, records of palaeo-sea level derived from past shorelines only extend back to the last interglacial, marine isotope stage (MIS) 5e, due to erosion of older coastal successions by successive sea-level changes on tectonically stable coastlines. On the Mount Gambier coastal plain, southern Australia, palaeo-shorelines of the Bridgewater Formation, a succession of aeolianite barriers, are preserved by the gentle uplift of the region and the strongly indurated calcrete horizons which blanket the regional landscape, and provide a sea-level archive extending back to at least MIS 17 (680 - 710 ka). The southern continental margin of Australia is within the far-field of former Quaternary ice sheets. Palaeo-sea level records from this region are significant as they are more likely to reflect ice-equivalent sea level with minor but spatially variable hydro-isostatic signals for different coastal sectors.

This thesis provides a geochronological framework for the deposition of interglacial barrier shorelines on the Mount Gambier coastal plain using amino acid racemisation (AAR), radiocarbon, and optically stimulated luminescence (OSL) dating. Depositional environments of barrier successions were reconstructed through stratigraphical analysis and assessments of facies architecture. Fixed and relational palaeo-sea level indicators were identified in the form of back barrier lagoonal and beach facies.

Petrological analysis of bioclastic sediments identified that the carbonate content of the barriers ranges from 66% to 99%. The percentage of quartz increases in inland barriers reflecting greater dissolution of carbonates in older successions. Thin section analysis identified an increase in sparite cements within the calcarenite with age, while XRD analysis highlighted a decrease in proportions of aragonite and an increase of low-Mg calcite. Scanning electron microscope (SEM) analysis of foraminifera indicated that test surface textures reflect transportation and diagenetic environments. Findings reveal a correlation between diagenesis and proposed age of the barriers and aid in constraining the evolution of the coastal plain.

This thesis reveals that the barrier shoreline complexes were formed during successive interglacial sea-level highstands and correlate with the shoreline barriers on the Robe coastal plain, 100 km northwest of the study area. Several barriers are found to be composite features, with facies deposited during separate interglacials. For example, Compton Range,

23 km landward of the present coastline, has a core of MIS 13 subaqueous sediment and overlying MIS 11 aeolian sands. Stacked aeolianites within Robe Range, at the present coastline, were deposited during successive interstadial highstands (MIS 5c, MIS 5a) of the last interglacial. Geochronological analysis also identified several episodes of reworking of older sediments into younger successions during sea-level regression and subsequent transgressional cycles further highlighting the complexity of coastal evolutionary processes within the region. Using a predefined uplift rate for this region, the combination of stratigraphical, petrographical and geochronological analyses allowed for the construction of a palaeo-sea level record of interglacial highstands over the past 680 ka.

This thesis identifies the first recorded example of subaqueously deposited late Pleistocene interstadial coastal strata above present sea level in Australia, represented by a flint conglomerate beach facies with interstratified shells. This deposit is constrained to MIS 5c in age and an uplift-corrected minimum palaeo-sea level of  $-14 \pm 2$  m is derived. OSL analysis confirms that MacDonnell Range, located 7 km from the present coastline, is MIS 5e ( $124 \pm 10$  ka) in age and a correlative of the Woakwine Range which formed during the sea-level highstand of the last interglacial maximum. Palaeo-sea level is also derived for MIS 7 and MIS 9 as 1.5 m and -3.5 m respectively, while minimum sea-level is derived from barrier shorelines deposited during MIS 11, MIS 13 and MIS 17. The sediment volume of individual barriers, predicted using Shuttle Radar Topography Mission (SRTM) data, corresponds with proposed interglacial intensity. The largest barriers on the coastal plain were formed during the more intense interglacials of MIS 5e and MIS 11 whereby warmer temperatures are proposed to have resulted in increased carbonate productivity on the Bonney Shelf, increasing the volume of available sediment for onshore transportation and barrier shoreline construction. AAR analyses revealed that individual foraminiferal tests provide a more accurate indicator of barrier age than AAR whole-rock analyses which are based on the averaging the D/L value of several thousand bioclastic carbonate grains. Analyses of single foraminifer tests allows for the identification and immediate rejection of contaminated, reworked or significantly diagenetically altered grains and provides numeric ages of greater accuracy and precision.

The results of this thesis are generally consistent with palaeo-sea level estimates from other tectonically uplifted coastal successions from the far-field of Quaternary ice sheets and oxygen isotope records. The palaeo-sea level record and coastal evolutionary processes derived from this research will provide an important dataset for modelling Quaternary ice volumes and interglacial climate dynamics.

# Acknowledgements

The last three years have been a steep learning curve for me and there are so many people I would like to thank for their help along the way. Firstly to my supervisor, Professor Colin Murray-Wallace, thank you for allowing me to study such a fascinating part of the world. Your support and encouragement through this process has been greatly appreciated and I have learnt so much under your supervision. To my co-supervisor, Associate Professor Brian Jones, thank you for your prompt reading of many drafts, help with sedimentological analysis and your kindness and encouragement especially through the last few, rather more stressful, months. Dr. Terry Lachlan, your expertise advice and knowledge of AAR has been priceless. Without your support and work in keeping the RP-HPLC up and running this thesis simply would not be here. Thank you for your friendship and your invaluable advice, not only in AAR but through all aspects of thesis life.

This thesis was improved greatly by the knowledge of local residents in the Mount Gambier region. Special thanks go to Bob Delgarno for your enthusiasm and interest in the project. Your knowledge of the local area and network of contacts has been invaluable. Thank you also to Kaye Delgarno for accommodating us on several of our visits down to Mount Gambier. To Don McLennon, thank you for showing me the interesting sites surrounding Dartmoor, western Victoria, and to Robin thanks for the best home-made cake this side of the equator. Thanks also to Ken and David Hurst for allowing me on to their property at Lake Hawdon South and to Laurie Hein for allowing me access to Myora Forest, Mount Gambier. To Jeff Lawson, at South Australia Waters, thank you for drill hole data and fuelling interesting discussions and to Peter Kentish at South Australia Lands, thank you for supplying me with AHD marker data.

To José Abrantes, thank you for producing thin sections, XRD analyses and gold plating of stubs for the SEM and for allowing me to invade your office over multiple lunchtimes to use the dentist drill. To Professor Bert Roberts and Dr. Zenobia Jacobs, thank you for allowing time in your OSL laboratory for my samples to be analysed and to Christina Neudorf and Terry Lachlan, again, for analysing the samples. Thanks also to Dr. Kira Westaway at Macquarie University for analysing the OSL sample from Baxter's Quarry. Dr. Alan Hogg and Dr. Fiona Petchey from the University of Waikato Radiocarbon Dating Laboratory, thank you for conducting the radiocarbon analyses. Thanks also to Dr. Long Nghiem for granting me permission to use the SEM and to Mick Stevens and Heidi Brown for help with GIS.

I would like to thank the University of Wollongong for my International Postgraduate Tuition Fees scholarship that has allowed me to study at the University and for the University Postgraduate Award during the last two years of my candidature. This research has been funded by an Australian Research Grant to Colin Murray-Wallace.

To the Dawson family, for taking me in, for the numerous cooked meals, support and advice; I cannot thank you enough.

Thanks to my fellow PhD students: Nathan Jankowski, Brent Koppel, Stephanie Kermode, Florian Dux, Daniela Mueller, Sarah Eccleshall, Mika Puspaningrum, Claire Perrette and Omar Mohammad. Particular thanks go to Anna Habeck-Fardy and Venera Espanon for riding this rollercoaster with me from the start and to Deirdre Ryan for fantastic help in the field, useful discussions and putting up with me on a daily basis. Thank you to you all for the caffeine, cake and comedy. Without your daily banter and support this whole process would have been much harder and much less enjoyable!

To my family, your love and support has been unwavering, as ever, especially when you are so far away. To my parents, Fi and Mike, thank you for keeping my feet on the ground and believing in me. To Max and Rory, thank you for keeping me smiling along the way and to Ollie, thank you for being my inspiration in everything, as always.

Finally, to Tim, there is so much to thank you for; for reading numerous drafts, assistance in the field, moral support, daily pep-talks, cooked meals and a regular supply of chocolate. Your consistent encouragement has allowed me to reach this end and I am forever grateful.

# Table of contents

Abstract.....	i
Acknowledgements.....	iii
Table of contents.....	v
List of figures.....	xi
List of tables.....	xix

<b>Thesis introduction</b>	<b>1</b>
----------------------------	----------

<b>Chapter 1: Geological and environmental evolution of the Mount Gambier coastal plain, southern Australia.....</b>	<b>3</b>
--	----------

1.1 Introduction.....	3
1.2 Geology of the Mount Gambier coastal plain.....	3
1.2.1 Geological history of the Mount Gambier coastal plain.....	4
1.2.2 Structural features of the Mount Gambier coastal plain.....	9
1.3 Volcanism on the Mount Gambier coastal plain.....	13
1.3.1 Mount Burr volcanic province.....	15
1.3.2 Southern volcanic group.....	16
1.3.3 Neotectonics.....	17
1.4 Climate of the Mount Gambier coastal plain.....	21
1.4.1 Temperature and rainfall.....	21
1.4.2 Wind.....	24
1.4.3 Draining of the land.....	28
1.5 Marine environment.....	28
1.5.1 The Bonney Shelf.....	29
1.5.2 Wave climate.....	30
1.5.3 Ocean currents, sea surface temperatures and salinity.....	30
1.5.4 Modern beaches.....	31
1.6 Preservation of Bridgewater Formation barrier shorelines on the Mount Gambier coastal plain.....	32
1.7 Aims of this study.....	33
1.8 Summary.....	33

<b>Chapter 2: Quaternary interglacial sea levels – a review.....</b>	<b>35</b>
--	-----------

2.1 Introduction.....	35
2.2 Drivers of glacials and interglacials.....	36
2.3 Indicators of interglacial sea level.....	40
2.3.1 Marine-based oxygen isotope records.....	41
2.3.2 Ice core stratigraphy.....	44
2.3.3 Geomorphological record.....	46

2.4 Comparison of global interglacial sea-level records from different indicators.....	50
2.4.1 Marine-cores.....	51
2.4.2 Ice-cores.....	54
2.4.3 Tectonically uplifted coral reefs.....	55
2.4.4 Shoreline barriers and coastal deposits.....	59
2.4.5 Flowstones/speleothems.....	60
2.4.6 Potential reasons for variation in local sea-level reconstructions.....	61
2.5 Duration of interglacials.....	66
2.6 Defining interglacials.....	74
2.7 Last interglacial in Australia.....	76
2.8 Conclusions.....	80

### **Chapter 3: Stratigraphy of the Pleistocene Bridgewater Formation on the Mount Gambier coastal plain, southern Australia.....83**

3.1 Introduction.....	83
3.2 Temperate carbonate sedimentation.....	83
3.2.1 Carbonate platforms.....	84
3.2.2 Cool-water platforms.....	84
3.2.3 Carbonate terminology.....	85
3.2.4 Carbonate classification.....	86
3.2.5 Carbonate sedimentation on the Mount Gambier coastal plain.....	89
3.3 Sedimentary structures of aeolian and beach environments.....	89
3.3.1 Stratigraphical terminology.....	90
3.3.2 Lithostratigraphy and allostratigraphy.....	92
3.3.3 Aeolian environments.....	93
3.3.4 Internal dune morphology.....	94
3.3.5 Beach environment.....	99
3.3.6 Coastal barriers.....	101
3.3.7 Distinguishing between aeolian and sub-aqueous deposition.....	101
3.3.8 Preservation potential of carbonate sand deposits.....	104
3.3.9 Subaerial alteration.....	107
3.4 Calcarene deposition and its role in identifying sea level.....	113
3.4.1 Perth Basin, Western Australia.....	113
3.4.2 Bermuda.....	115
3.4.3 Bahamas.....	116
3.4.4 Mallorca, Western Mediterranean.....	117
3.4.5 South Africa.....	118
3.4.6 Hawaii.....	119
3.4.7 Lord Howe Island.....	120
3.4.8 Discussion of international calcarenite deposits.....	121
3.5 Stratigraphy of the Bridgewater Formation on the Mount Gambier coastal plain.....	123
3.6 Stratigraphical methods.....	123
3.7 Location of study sites.....	123



3.8 Shoreline barriers of the Bridgewater Formation, Mount Gambier coastal plain.....	128
3.8.1 Previous studies.....	129
3.8.2 Modern shoreline of the Mount Gambier coastal plain.....	133
3.8.3 Robe Range.....	141
3.8.4 MacDonnell Range.....	148
3.8.5 Burleigh Range.....	154
3.8.6 Caveton Range.....	164
3.8.7 Gambier Range.....	172
3.8.8 Compton Range.....	176
3.8.9 Mingbool Range.....	186
3.8.10 Dismal Range.....	190
3.8.11 Naracoorte Range.....	204
3.8.12 Summary of stratigraphy at sample sites of the Bridgewater Formation on the Mount Gambier coastal plain.....	207
3.8.13 Siliceous sands.....	211
3.9 Comparison of stratigraphical features observed in the Pleistocene Bridgewater Formation on the Mount Gambier coastal plain with Pleistocene calcarenite elsewhere.....	212
3.10 Chapter summary.....	214

## **Chapter 4: Sedimentary petrography of the Bridgewater Formation, Mount Gambier coastal plain, southern Australia.....215**

4.1 Introduction.....	215
4.2 Carbonate diagenesis.....	215
4.2.1 Meteoric diagenesis.....	217
4.2.2 Karst development.....	217
4.2.3 Shallow marine diagenesis.....	218
4.2.4 Carbonate porosity.....	218
4.2.5 Diagenetic models.....	219
4.3 Petrographic methods adopted within this study.....	221
4.3.1 Thin section analysis.....	221
4.3.2 XRD analysis.....	222
4.3.3 Karst identification.....	222
4.3.4 SEM analysis of foraminifera.....	223
4.4 Sediment texture and fabric of the Pleistocene Bridgewater Formation.....	223
4.4.1 Modern beach, Shelly Beach.....	232
4.4.2 Holocene beach deposit, landward of Port MacDonnell Beach.....	232
4.4.3 Robe Range equivalent, upper aeolianite unit, Port MacDonnell.....	232
4.4.4 Robe Range equivalent, weathered aeolianite, Port MacDonnell.....	233
4.4.5 MacDonnell Range, Swarts Road sand quarry.....	233
4.4.6 Burleigh Range, Rabbitors Road.....	234
4.4.7 Caveton Range, Bucks Hill.....	234
4.4.8 Caveton Range, Rabbitors Road.....	235
4.4.9 Gambier Range, Gooch Road.....	235
4.4.10 Compton Range, Baxter's Quarry.....	236

4.4.11 Dismal Range, Dartmoor Cemetery.....	236
4.4.12 Dismal Range, Fort O'Hare Quarry.....	236
4.4.13 Dismal Range, Mingbool village.....	237
4.4.14 Naracoorte Range, Henschke Quarry.....	237
4.4.15 Summary.....	245
4.5 Mineralogy of sediment on the Mount Gambier coastal plain.....	248
4.6 Karst development.....	252
4.7 Surface textures of foraminifera.....	255
4.7.1 Foraminiferal assemblages on the Bonney Shelf.....	255
4.7.2 Taphonomic processes affecting foraminiferal tests.....	257
4.7.3 Surface textures on foraminifera from depositions within calcarenite on the Mount Gambier coastal plain.....	261
4.8 General petrographic characteristics of the Bridgewater Formation on the Mount Gambier coastal plain – a summary.....	279

## **Chapter 5: Amino acid racemisation, radiocarbon and optically stimulated luminescence dating of the Bridgewater Formation, Mount Gambier coastal plain, southern Australia.....285**

5.1 Introduction.....	285
5.2 Geochronological methods adopted in this study.....	285
5.3 Amino acid racemisation dating – a review.....	287
5.3.1 Principles of amino acid racemisation dating.....	287
5.3.2 Historical review.....	288
5.3.3 Parameters that influence racemisation within natural systems.....	289
5.3.4 Amino acid racemisation as a dating technique.....	295
5.3.5 Kinetics.....	297
5.3.6 Datable material.....	302
5.3.7 Limitations of the AAR technique.....	306
5.3.8 Examples from coastal deposits/marginal marine sequences.....	307
5.3.9 Discussion.....	308
5.3.10 Conclusions.....	310
5.4 Amino acid racemisation methods used in this study.....	310
5.4.1 Definition of terms.....	311
5.4.2 Sample selection.....	311
5.4.3 Laboratory procedure.....	312
5.4.4 Reverse-phase, high-performance liquid chromatography (RP-HPLC).....	313
5.4.5 Data screening.....	313
5.5 Radiocarbon and OSL methods used in this study.....	314
5.5.1 Radiocarbon dating methods.....	314
5.5.2 OSL dating methods.....	315
5.6 Pyrolysis experiments.....	317
5.7 Deriving numeric ages – calibration and kinetic modelling.....	323
5.7.1 Results of radiocarbon and OSL analysis.....	323

5.7.2 AAR calibration curve construction.....	328
5.7.3 Uncertainties.....	331
5.8 Presentation of AAR results.....	333
5.8.1 Modern beach and shell samples.....	334
5.8.2 Port MacDonnell.....	338
5.8.3 Last interglacial (MIS 5e) deposits.....	342
5.8.4 Burleigh Range.....	347
5.8.5 Caveton Range.....	349
5.8.6 Gambier Range and Compton Range.....	353
5.8.7 Mingbool Range and Dismal Range.....	356
5.8.8 Discussion of AAR results.....	359
5.9 Conclusions.....	369

## **Chapter 6: Quaternary coastal evolution of the Mount Gambier coastal plain, southern Australia and the successive development of the**

<b>Bridgewater Formation.....</b>	<b>373</b>
6.1 Introduction.....	373
6.2 Chronostratigraphy of the Bridgewater Formation on the Mount Gambier coastal plain	373
6.2.1 Modern coastline.....	376
6.2.2 Robe Range.....	376
6.2.3 MacDonnell Range.....	377
6.2.4 Burleigh Range.....	377
6.2.5 Caveton Range.....	378
6.2.6 Gambier Range.....	378
6.2.7 Compton Range.....	378
6.2.8 Mingbool Range.....	380
6.2.9 Dismal Range.....	380
6.2.10 Factors that may have altered the morphology of barrier successions.....	381
6.2.11 Discussion of chronostratigraphy.....	386
6.2.12 Comparison of the Bridgewater Formation on the Mount Gambier coastal plain with the stratotype at Bridgewater Lakes, Victoria.....	389
6.3 Sea-level history of the Mount Gambier coastal plain.....	391
6.4 Reliability and significance of results.....	395
6.5 Comparison with barrier successions of the Robe coastal plain.....	398
6.5.1 AAR geochronology.....	399
6.5.2 Palaeo-sea level reconstruction.....	402
6.5.3 Morphology of the barrier shorelines.....	405
6.5.4 New contributions to the southern Australia palaeo-sea level record.....	411
6.6 Comparison with the global interglacial studies.....	412
6.6.1 Global interglacial sea-level.....	412
6.6.2 Insolation forcing.....	418
6.6.3 Interglacial intensity.....	420
6.6.4 Comparison of the thickness of calcarenite deposits on the Mount Gambier coastal plain with other global interglacial calcarenite successions.....	424

6.7 Conclusions.....	426
6.8 Further research.....	429
<b>Bibliography.....</b>	<b>431</b>
<b>Appendices.....</b>	<b>473</b>
<b>Appendix A: Microstructural features of skeletal carbonate grains identified within samples across the Mount Gambier coastal plain, southern Australia.....</b>	<b>473</b>
A.1 Echinoid.....	473
A.2 Foraminifera.....	473
A.3 Mollusc.....	473
A.4 Algal fragment.....	474
A.5 Bryozoan fragment.....	474
A.6 Lithoclast.....	474
A.7 Quartz.....	474
A.8 Opaque grains.....	474
A.9 Cement.....	475
<b>Appendix B: AAR Laboratory procedure.....</b>	<b>476</b>
B.1 Molluscs.....	476
B.2 Whole-rock.....	478
B.3 Foraminifera.....	479
B.4 Pyrolysis experiments.....	480
<b>Appendix C: Statistical analysis of results.....</b>	<b>481</b>

# List of figures

## Chapter 1: Geological and environmental evolution of the Mount Gambier coastal plain

<b>Figure 1.1:</b> The coastline of southern Australia .....	5
<b>Figure 1.2:</b> Otway Basin, southern Australia, modified from Morton (1995).....	5
<b>Figure 1.3:</b> Cross-section between Port MacDonnell and Naracoorte highlighting geological units of the Gambier Embayment.....	9
<b>Figure 1.4:</b> Surface geology of the Mount Gambier coastal plain, southern Australia.....	12
<b>Figure 1.5:</b> Volcanoes of the Mount Gambier coastal plain and sub-crop map of the Mount Gambier volcanic complex.....	14
<b>Figure 1.6:</b> Features of the Mount Gambier coastal plain.....	20
<b>Figure 1.7:</b> Location of weather stations across Mount Gambier coastal plain.....	22
<b>Figure 1.8:</b> Maximum and minimum monthly temperatures across the Mount Gambier coastal plain.....	23
<b>Figure 1.9:</b> Monthly rainfall averages across the Mount Gambier coastal plain.....	24
<b>Figure 1.10:</b> Wind rose diagram indicating wind direction across the Mount Gambier coastal plain.....	27
<b>Figure 1.11:</b> Offshore bathymetry of the Lacepede and Bonney continental shelves of southern Australia.....	29

## Chapter 2: Quaternary sea levels – a review

<b>Figure 2.1:</b> Orbital cycles comprising the 'Astronomical Theory'.....	38
<b>Figure 2.2:</b> Incoming summer insolation at 65°N over the past 800 ka.....	39
<b>Figure 2.3:</b> Changes in zenith angle with latitude.....	40
<b>Figure 2.4:</b> Oxygen isotope record as derived from core V28-238 in the equatorial Pacific (Shackleton and Opdyke, 1973) .....	42
<b>Figure 2.5:</b> $\delta$ deuterium concentration of EPICA Antarctic ice core.....	44
<b>Figure 2.6:</b> Comparison of EPICA Dome C $\delta$ D record from Jouzel <i>et al.</i> (2007) with that of the benthic oxygen isotope record from Lisiecki and Raymo (2005) .....	46
<b>Figure 2.7:</b> Illustration of isostatically depressed land surface.....	48
<b>Figure 2.8:</b> Zonation of global shorelines relative to former areas of continental glaciation.....	48

<b>Figure 2.9:</b> The SPECMAP marine isotopic curve (Imbrie <i>et al.</i> , 1984) .....	51
<b>Figure 2.10:</b> Orbitally-tuned marine oxygen isotope curve of Martinson <i>et al.</i> (1987).....	53
<b>Figure 2.11:</b> Comparison of the $\delta^{18}\text{O}$ record from air trapped within the EPICA ice core (Petit <i>et al.</i> , 1999) with the $\delta^{18}\text{O}$ record from the SPECMAP timescale (Imbrie <i>et al.</i> , 1984).....	55
<b>Figure 2.12:</b> Global interglacial sea level from a variety of sources listed in Table 2.2 plotted in regards to zonation from former Quaternary ice sheets.....	63
<b>Figure 2.13:</b> Reconstruction of a sea-level curve from a range of global sources (Siddall <i>et al.</i> , 2007) .....	64
<b>Figure 2.14:</b> Last interglacial sea level around Australia.....	78
 <b>Chapter 3: Stratigraphy of the Pleistocene Bridgewater Formation on the Mount Gambier coastal plain, southern Australia</b>	
<b>Figure 3.1:</b> Textural classification of carbonate sediments on the basis of lime mud matrix and sparry calcite cement on the abundance and sorting of carbonate grains (after Folk, 1962).....	86
<b>Figure 3.2:</b> Schematic diagram of the internal stratification features in an 'ideal' simple dune	95
<b>Figure 3.3:</b> Bedding within aeolianite deposits from the River Murray mouth region South Australia.....	98
<b>Figure 3.4:</b> Generalised cross-sectional profile of the beach and nearshore identifying principal zones of wave activity.....	99
<b>Figure 3.5:</b> A model of the formation of a succession of littoral deposits, aeolianite and protosols on Bermuda.....	110
<b>Figure 3.6:</b> The potential effects of soil infiltration into karst features (modified from Carew and Mylroie, 1991) .....	112
<b>Figure 3.7:</b> Stratigraphy of calcareous aeolianite deposits at Pollenca Bay, Mallorca (Fornos <i>et al.</i> , 2009) .....	118
<b>Figure 3.8:</b> Exposure of aeolianite units in the Wilderness seaward barrier, South Africa (Bateman <i>et al.</i> , 2011) .....	119
<b>Figure 3.9:</b> Photomosaic of cliffed exposures of dune bedsets in the shorelines at the northern end of Johnsons Beach, Lord Howe Island from Brooke (1999) .....	121
<b>Figure 3.10:</b> Map of shoreline barrier deposits of the Bridgewater Formation and sample sites across the Mount Gambier coastal plain.....	125
<b>Figure 3.11:</b> Map of samples across the Mount Gambier region.....	126
<b>Figure 3.12:</b> SRTM image highlighting the topography of the Mount Gambier coastal plain...	127

<b>Figure 3.13:</b> Barrier shorelines of the Mount Gambier coastal plain, from Sprigg (1952).....	130
<b>Figure 3.14:</b> View looking southward from Centenary Tower, Valley Lake, Mount Gambier indicating the subtlety of the landscape and potential difficulties in identifying barrier sequences.....	132
<b>Figure 3.15:</b> Location of beach transects within Racecourse Bay.....	135
<b>Figure 3.16:</b> Transects across Racecourse Bay.....	135
<b>Figure 3.17:</b> Photographs from transects across Racecourse Bay.....	136
<b>Figure 3.18:</b> Photographs of the modern shoreline along the Mount Gambier coastal plain...	140
<b>Figure 3.19:</b> Aeolianite of Robe Range equivalent in the Port MacDonnell region, South Australia.....	145
<b>Figure 3.20:</b> Multiple unconformities within aeolianite of Robe Range.....	146
<b>Figure 3.21:</b> Composite stratigraphical cross-section illustrating where units of the Robe Range may have lain above the flint conglomerate at Port MacDonnell prior to coastal erosion.....	147
<b>Figure 3.22:</b> Images of MacDonnell Range.....	150
<b>Figure 3.23:</b> Exposure of lagoonal facies within Biscuit Drain, Lake Hawdon South, South Australia.....	152
<b>Figure 3.24:</b> Calcarenite within road cutting, Princes Highway, Narrawong.....	153
<b>Figure 3.25:</b> Scatter plot comparing flint cobbles sizes within Burleigh Range at Rabbitors Road with those on the modern shoreline at Racecourse Bay.....	156
<b>Figure 3.26:</b> Transects along the Burleigh Range derived from SRTM data.....	156
<b>Figure 3.27:</b> Rabbitors Road cutting through Burleigh Range, South Australia.....	160
<b>Figure 3.28:</b> Photographs of stratigraphical features exposed in Burleigh Range at Rabbitors Road.....	161
<b>Figure 3.29:</b> Laslett Road cutting within Burleigh Range, South Australia.....	163
<b>Figure 3.30:</b> Transects across Caveton Range derived from SRTM data.....	166
<b>Figure 3.31:</b> Exposure of lagoonal facies within Caveton Range, South Australia.....	167
<b>Figure 3.32:</b> Interpretative sketches of different units within lagoonal facies of the Caveton Range.....	169
<b>Figure 3.33:</b> Exposure of aeolian facies of Caveton Range at Bucks Hill.....	171
<b>Figure 3.34:</b> Transects across the Gambier Range derived from SRTM data.....	173

<b>Figure 3.35:</b> Photographs of an exposure within Bridgewater Formation, Gambier Range, Myora Forest.....	174
<b>Figure 3.36:</b> Very fine sand exposed in the interdune corridor landward of Gambier Range along Caroline Main Road.....	175
<b>Figure 3.37:</b> Images of Compton Range from SRTM transects and exposures at Grey Street, Mount Gambier.....	177
<b>Figure 3.38:</b> Subaerial exposure structures within Baxter's Quarry, Compton Range.....	180
<b>Figure 3.39:</b> Exposed Bridgewater Formation within the Compton Range, Baxter's Quarry....	181
<b>Figure 3.40:</b> Exposure within the Compton Range at Heritage Industries.....	184
<b>Figure 3.41:</b> Stratigraphical structures within Compton Range at Heritage Industries.....	185
<b>Figure 3.42:</b> Transects across the Mingbool Range derived from SRTM data.....	188
<b>Figure 3.43:</b> Interpretive sketch of exposed facies within the Mingbool Range at Don's Quarry, western Victoria.....	188
<b>Figure 3.44:</b> Stratigraphical features exposed within Don's Quarry, Mingbool Range, western Victoria.....	189
<b>Figure 3.45:</b> Transects across the Dismal Range derived from SRTM data.....	192
<b>Figure 3.46:</b> Exposure of calcarenite within Dismal Range, near Dartmoor Cemetery, western Victoria.....	193
<b>Figure 3.47:</b> Stratigraphical features within exposure at Dartmoor Cemetery, Dismal Range	194
<b>Figure 3.48:</b> Exposure of Dismal Range calcarenite in Fort O'Hare rail cutting, western Victoria.....	198
<b>Figure 3.49:</b> Stratigraphical features exposed within Fort O'Hare rail cutting.....	199
<b>Figure 3.50:</b> Photographs and associated sketches of bedding within small quarry within the Dismal Range near Mingbool village, South Australia.....	201
<b>Figure 3.51:</b> Stratigraphical structures within calcarenite at Mingbool village, Dismal Range	202
<b>Figure 3.52:</b> Transects of Naracoorte Range derived from SRTM data.....	204
<b>Figure 3.53:</b> Calcarenite exposure within Henschke Quarry, Naracoorte, South Australia.....	206
<b>Figure 3.54:</b> Siliceous sands overlying Bridgewater Formation sediment, north of Mount Gambier.....	212



## Chapter 4: Sedimentary petrology of the Bridgewater Formation, Mount Gambier coastal plain, southern Australia

<b>Figure 4.1:</b> Diagenetic environments (modified from Tucker and Wright, 1990).....	216
<b>Figure 4.2:</b> Varying diagenetic grades, modified from Hearty and O'Leary (2008).....	221
<b>Figure 4.3:</b> SEM image of bioconstituents from Port MacDonnell modern beach.....	226
<b>Figure 4.4:</b> Images of the 250-500 µm fraction of samples of bioclastic sediment from the Mount Gambier coastal plain.....	227
<b>Figure 4.5:</b> Images of the 250-500 µm fraction of samples of bioclastic sediment from the Mount Gambier coastal plain.....	228
<b>Figure 4.6:</b> Images of the 250-500 µm fraction of samples of bioclastic sediment from the Dismal Range, Mount Gambier coastal plain.....	229
<b>Figure 4.7:</b> Photomicrographs of thin sections from modern Shelly Beach, Holocene beach at Port MacDonnell, and Robe Range equivalent at Port MacDonnell.....	239
<b>Figure 4.8:</b> Photomicrographs of thin sections from the weathered aeolianite outcrop on Port MacDonnell Beach and the MacDonnell Range exposed at Swarts Road sand quarry.....	240
<b>Figure 4.9:</b> Photomicrographs of thin sections from Burleigh Range at Rabbitors Road and Caveton Range exposed at Bucks Hill and Rabbitors Road.....	241
<b>Figure 4.10:</b> Photomicrographs of thin sections from Gambier Range at Gooch Road Compton Range at Baxter's Quarry and Dismal Range near Dartmoor Cemetery.....	242
<b>Figure 4.11:</b> Photomicrographs of thin sections from Dismal Range exposed at Fort O'Hare Quarry and Mingbool village.....	243
<b>Figure 4.12:</b> Photomicrographs of thin sections from Dismal Range exposed at Mingbool village and Naracoorte Range exposed at Henschke Quarry.....	244
<b>Figure 4.13:</b> Pie charts illustrating the percentage of skeletal carbonate and quartz within sediment samples across the Mount Gambier coastal plain.....	247
<b>Figure 4.14:</b> Area graph highlighting the mineralogical change in sediments from the Bridgewater Formation on the Mount Gambier coastal plain with increasing distance inland and proposed age.....	249
<b>Figure 4.15:</b> Plot identifying trends in mineralogy of sediment samples across the Mount Gambier coastal plain plotted against proposed MIS based on geographical position of barrier successions in relation to the modern shoreline.....	249
<b>Figure 4.16:</b> Ternary plot of XRD results from samples within Bridgewater Formation across the Mount Gambier coastal plain.....	251
<b>Figure 4.17:</b> SEM images of tests of <i>Elphidium crispum</i> from Port MacDonnell Beach.....	270

<b>Figure 4.18:</b> SEM images of foraminifera from upper aeolianite units at Port MacDonnell and Shelly Beach.....	271
<b>Figure 4.19:</b> SEM images of foraminifera from the upper aeolianite units at Port MacDonnell and Shelly Beach.....	272
<b>Figure 4.20:</b> SEM images of foraminifera from the MacDonnell Range at Swarts Road sand quarry and Narrawong.....	273
<b>Figure 4.21:</b> SEM images of foraminifera from the Burleigh Range exposures at Rabbitors Road and Laslett Road.....	274
<b>Figure 4.22:</b> SEM images of foraminifera from Caveton Range lagoonal facies and Gambier Range.....	275
<b>Figure 4.23:</b> SEM images of foraminifera from Compton Range at Baxter's Quarry and Heritage Industries.....	276
<b>Figure 4.24:</b> SEM images of foraminifera from Don's Quarry, Mingbool Range and Dartmoor Cemetery, Dismal Range.....	277
<b>Figure 4.25:</b> SEM images of foraminifera from the Dismal Range at Fort O'Hare Quarry and Mingbool village.....	278

## Chapter 5: Amino acid racemisation, radiocarbon and optically stimulated luminescence dating of the Bridgewater Formation, Mount Gambier coastal plain, southern Australia

<b>Figure 5.1:</b> Diagrammatic representation of amino acid structure.....	287
<b>Figure 5.2:</b> Hydrolysis of peptide bonds in a protein chain, creating terminal and free amino acids.....	293
<b>Figure 5.3:</b> Comparison of the 'extended linear' and 'non-linear' kinetic model options for leucine racemisation in <i>Protothaca</i> , with solid lines representing the extended linear model and dashed lines the non-linear model (Wehmiller, 1984) .....	298
<b>Figure 5.4:</b> A kinetic plot demonstrating the general nature of probable racemisation kinetic pathways in molluscs (Wehmiller, 1982) .....	299
<b>Figure 5.5:</b> Laboratory-induced isoleucine epimerisation at a range of temperatures in modern <i>Mercenaria campechiensis</i> plotted as $\text{alle/Ile}$ against the square root of time (Mitterer and Kriausakul, 1989) .....	301
<b>Figure 5.6:</b> Scatter plots of pyrolysis experiments for <i>Kataysia rhytiphora</i> , <i>Ostrea angasi</i> , whole-rock, <i>Elphidium crispum</i> and <i>Discorbis dimidiatus</i> .....	321
<b>Figure 5.7:</b> Constrained power law functions for D/L data derived from pyrolysis experiments from a range of carbonate material across the Mount Gambier coastal plain to yield forward rate constants for glutamic acid.....	322

<b>Figure 5.8:</b> Single-aliquot OSL equivalent dose ( $D_e$ ) distributions (as radial plots) for Robe II, Port MacDonnell; MacDonnell Range; siliceous sand overlying Bridgewater Formation and Baxter's Quarry.....	327
<b>Figure 5.9:</b> Calibration curve used to derive AAR numeric ages for <i>Turbo undulatus</i> at Port MacDonnell.....	331
<b>Figure 5.10:</b> Scatter plot of aspartic acid (ASP) and glutamic acid (GLU) D/L values derived from AAR analysis of whole-rock, shell and foraminifera at modern beach sample sites.....	336
<b>Figure 5.11:</b> Plots of glutamic acid total hydrolysable (THAA) and free amino acid (FAA) fraction D/L values derived from multiple sub-samples of modern beach sediments at modern beaches across the Mount Gambier coastal plain.....	337
<b>Figure 5.12:</b> Scatter plot of ASP and GLU D/L values from modern beach, Holocene and last interglacial sites across the coastal plain for Whole-rock, <i>Elphidium crispum</i> , and <i>Turbo undulatus</i> .....	344
<b>Figure 5.13:</b> Extent of valine racemization within <i>Anadara trapezia</i> specimens from Australia and New Zealand plotted against current mean annual temperature (CMAT) at each locality, modified from Murray-Wallace <i>et al.</i> (2000).....	345
<b>Figure 5.14:</b> Scatter plots comparing glutamic acid and valine D/L values between samples of whole-rock, foraminifera, and <i>Katelsysia</i> from Burleigh Range and Caveton Range.....	351
<b>Figure 5.15:</b> Scatter plots of D/L values derived from AAR analysis of a variety of molluscan genera from landward of the Woakwine Range (MIS 5e) at Lake Hawdon South, and the Caveton Range (MIS 9) .....	362
<b>Figure 5.16:</b> Plots of GLU D/L values against proposed MIS based on geographical location of barriers from molluscs across the Mount Gambier coastal plain.....	363
<b>Figure 5.17:</b> Plot of GLU D/L values derived from whole-rock samples across the Mount Gambier coastal plain plotted against proposed MIS based on the geographical position of corresponding barrier in relation to the modern shoreline.....	364
<b>Figure 5.18:</b> Plot of GLU D/L values derived from multiple individuals of foraminifers at sample sites across the Mount Gambier coastal plain plotted against proposed MIS based on geographical position of barrier from the present shoreline.....	365
<b>Figure 5.19:</b> Plot compares D/L values of whole-rock samples and <i>Elphidium crispum</i> with the proposed MIS of the barrier sediment was sampled from based on its geographical position.....	366
<b>Figure 5.20:</b> Scatter plot of GLU D/L values between whole-rock and <i>Elphidium crispum</i> samples; illustrates the wider range of D/L values expressed through foraminifera compared with bioclastic sediment samples.....	367

**Figure 5.21:** Scatter plots of D/L values from whole-rock, foraminifera and fossil shells analysed at four of the most inland sites of Early Pleistocene Bridgewater Formation on the Mount Gambier coastal plain..... 368

## **Chapter 6: Quaternary coastal evolution of the Mount Gambier coastal plain, southern Australia and successive development of the Bridgewater Formation**

**Figure 6.1:** Map of the Mount Gambier coastal plain highlighting the successive barrier deposits and sample study sites.....375

**Figure 6.2:** Stratigraphical cross-sections of coastal deposits on Port MacDonnell Beach illustrating chronostratigraphical interpretations..... 377

**Figure 6.3:** Interpretive sketches and the chronostratigraphical interpretation of exposures within Compton Range..... 380

**Figure 6.4:** Correlation of barrier successions on the Robe and Mount Gambier coastal plains with sea-level highstands as identified through the marine oxygen isotope record (Chappell and Shackleton, 1986) ..... 388

**Figure 6.5:** Comparison of cross-sections of the Bridgewater Formation at its type section locality at Cape Bridgewater with the Mount Gambier coastal plain..... 390

**Figure 6.6:** Subcrop map of the elevation of the upper surface of the Oligo-Miocene Gambier Limestone indicating crustal doming associated with centres of Quaternary volcanism..... 397

**Figure 6.7:** Extent of racemisation within skeletal carbonate sands analysed by whole-rock analysis from Bridgewater Formation successions on the Mount Gambier coastal plain, Robe coastal plain (Murray-Wallace *et al.*, 2001) and the River Murray mouth region (Murray-Wallace *et al.*, 2010) plotted against the proposed MIS that the barrier was deposited during based on geographical location.....400

**Figure 6.8:** Scatter plot of ASP and GLU D/L values derived from *Katelsia rhytiphora* from last interglacial deposits between Robe and the River Murray mouth.....401

**Figure 6.9:** Map locating the transects across the coastal plain from which SRTM data in Figures 6.10 to 6.14 are derived.....406

**Figure 6.10:** Transect across the Mount Gambier coastal plain from Port MacDonnell to Dismal Range derived by SRTM data, highlighting the difference in barrier morphology and the elevation of palaeo-sea level markers and the derived numerical age of these deposits from AAR analysis..... 407

**Figure 6.11:** Transect across the Robe coastal plain derived by SRTM data, highlighting the morphology of the barrier shorelines and the elevation and numeric ages (derived by AAR, or TL if in italics) of palaeo-shoreline deposits as described by Murray-Wallace *et al.* (2001)..... 408

<b>Figure 6.12:</b> Comparison of transects (from SRTM data) from the Mount Gambier and Robe coastal plains highlighting the different in the rate of uplift between the two regions.....	409
<b>Figure 6.13:</b> Transect across the Mount Gambier coastal plain between Nelson and Dartmoor using SRTM data and highlighting subaqueous facies identified at Don's Quarry, Fort O'Hare Quarry and Dartmoor Cemetery.....	409
<b>Figure 6.14:</b> Transect of barrier shorelines of the Mount Gambier coastal plain with interglacial sea-level elevations as proposed by Murray-Wallace <i>et al.</i> (2001) adjusted for tectonic uplift in the Mount Gambier region.....	410
<b>Figure 6.15:</b> Various interglacial sea-level deposits plotted in regards to zonation from former Quaternary ice sheets after Clarke <i>et al.</i> (1978) .....	413
<b>Figure 6.16:</b> Comparison of palaeo-sea levels derived from the Mount Gambier coastal plain with marine oxygen isotope records (from the Red Sea: Siddall <i>et al.</i> , 2003 and LR04 stack of Lisiecki and Raymo, 2005) and other morphological indicators from palaeo-shorelines.....	414
<b>Figure 6.17:</b> Comparison of depositional timing of barrier successions on the Mount Gambier coastal plain with northern hemisphere insolation maximum as derived by Berger and Loutre (1991) .....	420
<b>Figure 6.18:</b> Scatter plot of barrier height on the Mount Gambier coastal plain against $\delta D$ from the EPICA Dome C ice-core (Jouzel <i>et al.</i> , 2007) for the corresponding marine isotope stage the barriers were deposited within.....	422

## List of tables

### Chapter 1: Geological and environmental evolution of the Mount Gambier coastal plain

#### Chapter 2: Quaternary interglacial sea levels – a review

<b>Table 2.1:</b> Timing of 65°N insolation maxima over the past four interglacial cycles (from Berger and Loutre, 1991) .....	39
<b>Table 2.2:</b> Comparison of palaeo-sea level reconstructions around the globe for the past four interglacials.....	62
<b>Table 2.3:</b> Oxygen isotopic stage boundaries depicted from a range of marine and ice core records.....	76
<b>Table 2.4:</b> Comparison of palaeo-sea level reconstruction data from around Australia during the last interglacial.....	78
<b>Table 2.5:</b> Ages of barrier shorelines on the Coorong coastal plain, as derived from AAR and TL analysis, and their associated palaeo-sea level elevations (Murray-Wallace, 2002).....	79

### **Chapter 3: Stratigraphy of the Pleistocene Bridgewater Formation on the Mount Gambier coastal plain, southern Australia**

<b>Table 3.1:</b> Folk's (1959; 1962) Classification of carbonates.....	88
<b>Table 3.2:</b> Dunham's (1962) classification of carbonates based on depositional texture.....	88
<b>Table 3.3:</b> Structural terms used throughout this study.....	91
<b>Table 3.4:</b> Characteristics of basic types of aeolian stratification (Hunter, 1977).....	97
<b>Table 3.5:</b> Sedimentary structures of the beach environment.....	100
<b>Table 3.6:</b> Comparison of aeolian and subtidal stratification patterns (from Loope and Abegg, 2001) .....	103
<b>Table 3.7:</b> Comparison of features of the exposed flint lenses either side of Rabbitors Road cutting, Burleigh Range.....	157
<b>Table 3.8:</b> Sedimentological features, fauna and microfauna present within different units of lagoonal facies within Caveton Range, South Australia.....	170
<b>Table 3.9:</b> Summary table of sedimentary structures and depositional facies identified at sample sites within exposures of the Bridgewater Formation on the Mount Gambier coastal plain.....	210

### **Chapter 4: Sedimentary petrology of the Bridgewater Formation, Mount Gambier coastal plain, southern Australia**

<b>Table 4.1:</b> Compositional data of thin sections derived from point counting 400 grains from representative samples across the Mount Gambier coastal plain.....	231
<b>Table 4.2:</b> Mineralogical composition of representative samples across the Mount Gambier coastal plain derived by powdered XRD analysis.....	250
<b>Table 4.3:</b> Summary of karst features found at sample sites across the Mount Gambier coastal plain.....	253
<b>Table 4.4:</b> Surface texture characteristics of foraminifera from sediment samples across the Mount Gambier coastal plain.....	269
<b>Table 4.5:</b> Summary of the diagenetic features observed through petrographic analysis of sediments on the Mount Gambier coastal plain, southern Australia.....	283

### **Chapter 5: Amino acid racemisation, radiocarbon and optically stimulated luminescence dating of the Bridgewater Formation, Mount Gambier coastal plain, southern Australia**

<b>Table 5.1:</b> AAR D/L values derived from pyrolysis experiments on modern molluscs <i>Katelysia</i> , <i>Ostrea</i> , whole-rock sediments and the foraminifers <i>Discorbis</i> and <i>Elphidium</i> .....	320
---	-----

<b>Table 5.2:</b> Forward rate constants derived from pyrolysis experiments for aspartic acid (ASP) and glutamic acid (GLU) .....	320
<b>Table 5.3:</b> Numerical ages derived from radiocarbon analysis of <i>Turbo undulatus</i> opercula from Port MacDonnell, South Australia.....	327
<b>Table 5.4:</b> Results of OSL analysis from aeolian sand samples across the Mount Gambier coastal plain, southern Australia.....	327
<b>Table 5.5:</b> Results of AAR analysis from samples at modern beaches across the Mount Gambier coastal plain.....	335
<b>Table 5.6:</b> Results from AAR analysis of samples from a range of coastal facies at Port MacDonnell, Mount Gambier coastal plain, southern Australia.....	339
<b>Table 5.7:</b> Results from AAR analysis of samples from proposed last interglacial sites within MacDonnell Range, Woakwine Range, Lake Hawdon South, and Narrawong, Victoria.....	343
<b>Table 5.8:</b> Results from AAR analysis within Burleigh Range and Reedy Creek Range, Mount Gambier and Robe coastal plains, southern Australia.....	348
<b>Table 5.9:</b> Results of AAR analysis from the Caveton Range, Mount Gambier coastal plain, southern Australia.....	350
<b>Table 5.10:</b> Results of AAR analysis from Gambier Range and Compton Range, Mount Gambier coastal plain, southern Australia.....	354
<b>Table 5.11:</b> Results of AAR analysis from samples within Mingbool Range and Dismal Range, Mount Gambier coastal plain, southern Australia.....	357
 <b>Chapter 6: Quaternary coastal evolution of the Mount Gambier coastal plain, southern Australia and the successive development of the Bridgewater Formation</b>	
<b>Table 6.1:</b> Summary table of stratigraphic descriptions, diagenetic maturity derived from petrologic analysis and derived numeric ages for representative sample sites across the Mount Gambier coastal plain, southern Australia.....	385
<b>Table 6.2:</b> Interglacial palaeo-sea levels derived from sample sites within Bridgewater Formation successions across the Mount Gambier coastal plain, southern Australia.....	394
<b>Table 6.3:</b> Comparison of derived numeric ages and palaeo-shorelines between the Robe and Mount Gambier coastal plains, southern Australia.....	404
<b>Table 6.4:</b> Comparison of interglacial intensity as defined by Masson-Delmotte <i>et al.</i> (2010) with the height and width of barrier shorelines on the Mount Gambier coastal plain, southern Australia.....	423
<b>Table 6.5:</b> Comparison of global coastal calcarenite deposits during differing interstadial and interglacial sea-level highstands.....	425

## Appendices

### Appendix C

**Table C.1:** Results of Post-Hoc Tukey statistical tests on GLU D/L values from the foraminifer *Elphidium crispum* in sample sites across the Mount Gambier coastal plain..... 482

**Table C.2:** Results of Post-Hoc Tukey statistical tests on GLU D/L values from whole-rock analysis of bioclastic sediment at sample sites across the Mount Gambier coastal plain..... 483

**Table C.3:** Results of post-hoc Tukey statistical tests for GLU D/L values from *Katelsia rhytiphora* samples across the Mount Gambier coastal plain..... 484

**Table C.4:** Results of post-hoc Tukey statistical tests for GLU D/L values from *Ostrea angasi* samples across the Mount Gambier coastal plain..... 484

**Table C.5:** Results of post-hoc Tukey statistical tests for GLU D/L values from *Turbo undulatus* samples across the Mount Gambier coastal plain..... 484

**Table C.6:** Results of post-hoc Tukey statistical test for GLU D/L values for a range of genera collected from an *in situ* assemblage at Lake Hawdon, lagoonal facies, proposed to be MIS 5e in age..... 485

**Table C.7:** Results of post-hoc Tukey statistical tests for GLU D/L values for a range of genera collected from a lagoonal facies within Caveton Range, proposed to be MIS 9 in age.....485



# Thesis introduction

The Mount Gambier coastal plain, southern Australia is dominated by successive barrier shoreline complexes which trend sub-parallel to the modern coastline. The primary aim of this research is to define the nature of relative interglacial sea-level changes for the middle Pleistocene to Holocene from the Mount Gambier coastal plain and to evaluate the results in a global context. Subsidiary aims include to evaluate the morphostratigraphy of barrier successions within a temporal framework for marine and ice-core oxygen isotope records, and to identify trends of diagenesis within the coastal deposits.

The combination of stratigraphical, petrological and geochronological analyses within this thesis examines the Quaternary coastal evolution of the Mount Gambier coastal plain in response to fluctuating interglacial sea-levels. Assessment of facies architecture within exposures of barrier successions of the Bridgewater Formation allow for a palaeo-environmental reconstruction of coastal processes. Markers of palaeo-sea level are identified, and through the use of amino acid racemisation (AAR), optically stimulated luminescence (OSL) and radiocarbon analyses a geochronology of barrier formation is derived and a middle Pleistocene to Holocene record of sea-level highstands is reconstructed.

Previous studies of the Mount Gambier coastal plain have suggested the coastal barriers were formed during interglacials and are correlatives of those 100 km northwest on the Robe coastal plain (Sprigg, 1952). Through extensive stratigraphical, petrological and geochronological analyses throughout this thesis, especially within previously unsampled deposits farther inland, these hypotheses are shown to be correct.

The thesis is organised as follows:

Chapter 1 provides an introduction to the Mount Gambier coastal plain, identifying the geological and environmental evolution of the area, from the formation of the Otway Basin in the Cretaceous to the draining of the land by European settlers in the years following World War II. This discussion identifies that the successive barrier shorelines have been well-preserved due to the combined effects of tectonic uplift, a lack of perennial rivers, and a climate which promotes development of pervasive calcrete horizons.

Chapter 2 provides a contextual framework for the thesis by reviewing the global literature on Quaternary interglacial sea-level records. The advantages and limitations of specific sea-level indicators are identified and the potential reasons for differences between

global records are discussed. The findings from this research are compared with this body of literature later in the thesis to determine the significance of the derived palaeo-sea level record for the Mount Gambier coastal plain.

Chapter 3 examines the stratigraphy of calcarenite deposits across the coastal plain. A review of the literature on temperate carbonate production and the stratigraphy of associated global coastal calcarenite provide criteria with which to compare and determine depositional environments. Facies architecture of exposures of Bridgewater Formation calcarenite allows for the identification of markers of palaeo-sea level and for palaeo-environmental reconstructions from which the coastal evolution of the region can be determined.

Results of petrographical analyses of deposits across the coastal plain are presented in Chapter 4 to assess the extent of diagenesis and to determine whether this increases with the proposed age of the successions. An assessment of karstic features at sample sites, thin-section analysis and scanning electron microscope analysis of foraminiferal tests allows diagenetic environments to be established which supported stratigraphical interpretations of deposition. Assessment of the extent of diagenesis within certain samples may account for discrepancies within geochronological results.

Amino acid racemisation (AAR) was the primary geochronological method used throughout this thesis due to its suitability to bioclastic carbonate deposits and its potential age range of 1.2 Ma within this region (Murray-Wallace *et al.*, 2001). Chapter 5 presents a review of AAR and its application to other coastal successions. Radiocarbon and OSL were also used to constrain the depositional timing of barrier shorelines within this study. Results of all geochronological analyses are presented in this chapter and indicate that the interglacial sea-level record in the Mount Gambier region extends to at least MIS 17. The merits of single-test analyses of foraminifera over the whole-rock technique are also discussed.

Chapter 6 provides a synthesis of coastal evolution on the Mount Gambier coastal plain throughout the middle Pleistocene to Holocene. Stratigraphical and geochronological analyses are combined to derive a chronostratigraphy for barrier deposition which is found to correlate well with the barrier shorelines on Robe coastal plain. Following the establishment of the uplift history of the coastal plain, a palaeo-sea level history for the region is derived and compared with other interglacial sea-level records as discussed in Chapter 2. The reliability, limitations and significance of these results are determined before the major conclusions of this research are presented and ideas for further research are proposed.

# Chapter 1

## Geological and environmental evolution of the Mount Gambier coastal plain, southern Australia

### 1.1 Introduction

The Mount Gambier coastal plain is located in southern Australia between latitude 36°57'S and 38°04'S extending from Naracoorte to the present coastline at Port MacDonnell, and between longitude 37°50 at Lake Bonney to 38°21 at Cape Bridgewater. The Mount Gambier coastal plain is dominated by the coastal dune barrier sequences (locally referred to as 'ranges') of the Bridgewater Formation, a Pleistocene succession of aeolianites which extend sub-parallel with the modern coastline (Sprigg, 1952; Sprigg and Boutakoff, 1953; Boutakoff, 1963). The barriers are correlatives of the dune ranges of the coastal plain between Robe and Naracoorte, where at least thirteen well-preserved high-wave energy barrier shoreline successions and their back-barrier lagoonal facies provide a long record of Pleistocene interglacial sea levels (Hossfeld, 1950; Sprigg, 1952; Murray-Wallace *et al.*, 2001; Murray-Wallace and Woodroffe, 2014). This thesis builds upon previous studies conducted on the Robe coastal plain (Figure 1.1). The barrier sequences on the Mount Gambier coastal plain are located on the eastern side of the Mount Burr volcanic province, South Australia, and extend into western-most Victoria.

This chapter describes the geological history and structures within the region which provide a context for the stratigraphical description of study sites across the Mount Gambier coastal plain (Chapter 3), and for comparison with other global palaeo-sea level study sites (Chapter 6). The volcanic history, climate and modern marine setting are all discussed in turn, and this chapter concludes with their contribution to preservation of the Bridgewater Formation barrier shorelines. The slow epeirogenic uplift of the Mount Gambier coastal plain, particularly, has resulted in the preservation of successive barrier shorelines and provides a lengthy interglacial sea-level record rarely preserved elsewhere in the world.

### 1.2 Geology of the Mount Gambier coastal plain

The following section describes both the underlying and surface geology of the region, from the formation of the Otway Basin during the mid-Jurassic to present day weathering and erosion of calcareous surface deposits which contributed to the karst topography seen on the Mount Gambier coastal plain. Epeirogenic uplift associated with the Mount Burr volcanic

province (Figure 1.5) has resulted in the separation of successive interglacial barrier shorelines. An understanding of the underlying geology of the area will aid in interpretations of the present morphology of the coastal plain, and knowledge of uplift rates will allow calculations of palaeo-sea level.

### **1.2.1 Geological history of the Mount Gambier coastal plain**

This section details the formation of the Otway Basin as Australia rifted away from Antarctica beginning during the Late Jurassic, followed by the deposition of Cretaceous, Palaeogene and Neogene sediments which are found to underlie much of the coastal plain. Paleogene/Neogene sediments include the Gambier Limestone, which is found to crop out across the coastal plain in multiple regions, unlike farther north near Robe where it is not found at the surface. Deposition of the Bridgewater Formation during the Pleistocene and Holocene is then discussed.

#### **Otway Basin**

The Mount Gambier coastal plain lies within the Gambier Embayment of the Otway Basin and is found south of Kingston and Naracoorte (Figure 1.2). Together with the Bass and Gippsland Basins in Victoria, the Otway Basin forms part of the south-eastern coastal margin rift zone of Australia (Morton, 1995). These basins were divided from one another by Cainozoic tectonic movements (Alley and Lindsay, 1995). The geological evolution of the Otway Basin is closely related to the separation of Australia from Antarctica during the mid-Cretaceous, approximately 95 Ma (Veevers, 1986). Continental breakup occurred earliest in the Bight Basin to the west, with a slow rate of spread occurring in the Otway Basin until the Eocene (Morton, 1995). The Otway Basin is a linear, fault-controlled graben that trends east-west, and extends for 500 km west of Melbourne into South Australia (Duddy, 2003).

Major faults trending in a north-westerly direction are suggested to be synthetic growth faults associated with high rates of sedimentation, while isolated faults, commonly found concave to the basin, do not persist laterally and are proposed to have evolved independently (Morton, 1995).



Figure 1.1: The coastline of southern Australia.

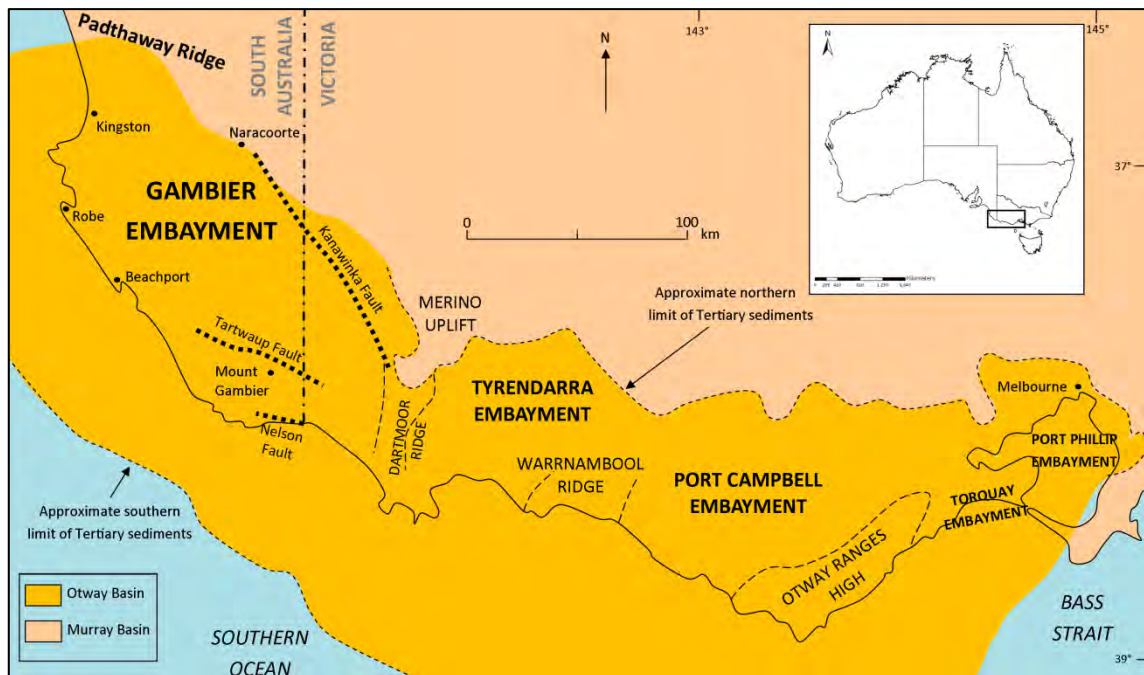


Figure 1.2: Otway Basin, southern Australia, modified from Morton (1995). The Mount Gambier coastal plain is located within the Gambier Embayment.

## Cretaceous

The rifting of Australia from Antarctica resulted in the deposition of sand and silt within the depression of the Otway Basin, which therefore contains thick accumulations of alluvial, deltaic, lacustrine and marine sediments. The Gambier Embayment may be divided into two parts by the north-west trending Tartwaup Fault (Figure 1.2), exhibiting contrasting depositional settings between the Early and Late Cretaceous. The northern segment is

dominated by the Otway Supergroup and the southern by the Sherbrook Group (Morton, 1995). The poorly known Casterton Formation is the earliest deposited unit in the Otway Basin and consists of a succession of interbedded carbonaceous shale and minor feldspathic sandstone and siltstones. The Otway Supergroup consists of the Crayfish Group, Pretty Hill Formation, Laira Formation, Katnook Sandstone and Eumeralla Formation, of which all primarily consist of interbedded carbonaceous siltstone, mudstone, shale and siltstone. These sediments are suggested to have been deposited in a low relief environment of a down-faulted valley during the Late Jurassic and Early Cretaceous (Morton, 1995). These early sedimentary sequences were disturbed by faulting resulting from crustal stresses as Australia separated from Antarctica (Wopfner and Douglas, 1971). The Sherbrook Group consists of the Copa Formation, Waare Sandstone, Flaxman Formation, Belfast Mudstone, Paarette Formation and Timboon Sandstone. These are predominantly carbonaceous shales, muds, and quartz sandstone suggested to have been deposited in a large, deep, saline lake, which may have connected to a restricted sea to the west and east (Morton, 1995) and formed as sea level fluctuated.

### **Paleogene and Neogene**

Increases in subsidence and eastward advancement of the coastline during the Paleogene resulted in the flooding of the Gambier Embayment and much of coastal South Australia. The final separation of Australia from Antarctica (~45 Ma) resulted in the formation of the Southern Ocean, enhancing circum-Antarctic Ocean currents around the Australian margins which in turn promoted carbonate productivity on the southern Australian continental shelf. Bryozoal limestones were therefore deposited largely within the aerated ocean water that contained abundant marine life (Wopfner and Douglas, 1971; James and Bone, 2010).

Paleogene sediments within the Gambier Embayment overlie the Late Cretaceous Sherbrook Group, and can be found to decrease in thickness landwards of Port MacDonnell, where they are at their maximum thickness of 1000 m (Alley and Lindsay, 1995). Sedimentation in the Gambier Embayment began in the Late Palaeocene to Middle Eocene with the Eangerrip Group consisting of the Pebble Point Formation, Pember Mudstone and Dilwyn Formation. These sediments comprise oolitic grits, silty mudstone and sandy sediments (Alley and Lindsay, 1995). During the Late Eocene sediments became increasingly dominated by cool-water carbonates (Holdgate and Gallagher, 2003) leading to the deposition of the marginal-marine Nirranda Group and the open-water marine Gambier Limestone. The Nirranda Group, deposited during the Late Palaeogene to Early-Middle Neogene consists of the carbonate and clastic Mepunga Formation overlain by the carbonate-dominated

Narrawutuk Formation. The Haytesbury Group can be found overlying the Nirranda Group and in the Gambier Embayment it consists of the Gambier Limestone and Gellibrand Marl (Morton and Drexel, 1995).

Sprigg (1952) suggested that the Gambier Limestone is the most extensive Paleogene/Neogene deposit in South Australia, and is composed largely of bryozoal and argillaceous limestones and marls, with numerous flint bands. White (1995) subdivided the Gambier Limestone into three members: the Greenways Member which comprises grey, marly limestone; the Camelback Member (10-250 m thick) which consists of bryozoal calcarenite and ranges from Early Oligocene to Early Miocene age; and the Green Point Member, which is at least 190 m thick and is characterised by a grey colour and abundant chert. Gambier Limestone deposition ceased in the early Middle Miocene as global sea level transgressed (Haq *et al.*, 1987) and uplift occurred along the southern Australian continental margin. Dolomitized zones within the Gambier Limestone are associated with the Tartwaup and Nelson Faults (Alley and Lindsay, 1995). In the Naracoorte region, the Naracoorte Limestone overlies the Gambier Limestone and is up to 6 m thick. It is recognised through its coarse-grained, rubbly appearance and is highly fossiliferous (Alley and Lindsay, 1995). The Naracoorte Limestone is suggested to have been deposited in a warm but not tropical ocean (James and Bone, 1989) and is differentiated from the Gambier Limestone due to the presence of abundant molluscs and gastropods (Ludbrook, 1961). During the Late Miocene both the Gambier and Naracoorte Limestone were exposed to extensive karstification.

### **Quaternary**

The Australian continent became increasingly arid during the Pleistocene with a change from summer to winter-dominated rainfall (Bowler, 1982). The progressive aridity is reflected in the composition of preserved coastal and shallow marine deposits which change from mixed quartz-carbonate sands deposited in the Early Pleistocene to sediments that are increasingly carbonate-dominated and indicative of cooler waters throughout the middle to late Pleistocene (Belperio, 1995). Early Pleistocene deposits include those of the Commandook Formation, which reaches up to 75 m thick in places and consists of sandy limestone, calcareous sandstone, shelly sandstone and clays. The oldest sands of the overlying Bridgewater Formation may be identified by the marine gastropod *Hartungia dennanti chavani* which was identified by Ludbrook (1978) in deposits east of Naracoorte and Keith.

The Quaternary has been dominated by fluctuating volumes of continental ice (discussed further in Chapter 2), and associated sea-level rise and fall. The Bridgewater

Formation refers to bioclastic barrier shoreline deposits that trend sub-parallel to the modern shoreline and are suggested to represent multiple sea-level successions (Sprigg, 1952). The position of these barriers on the Mount Gambier coastal plain is the central focus of this thesis.

The Bridgewater Formation was first formally described by Boutakoff (1963) at Cape Bridgewater, western Victoria, but had previously been described in South Australia by Sprigg (1952). At least 13 well-preserved barrier shorelines and their back-barrier lagoonal facies have been identified across the Coorong coastal plain between Robe and Naracoorte (Hossfeld, 1950; Sprigg, 1952; Murray-Wallace *et al.*, 2001). The Coorong Lagoon and Younghusband Peninsula, which trend along the modern coastline for over 300 km, are modern equivalents of the preserved barrier shorelines.

In the Mount Gambier region the barriers are commonly found to rest unconformably upon Gambier Limestone, which rises up to 60 m above present sea level (APSL) at the Kanawinka escarpment and around the Mount Burr volcanic complex. The barrier shorelines typically range from 30-40 m in height, from 1-2 km in width, and can stand up to 10 km apart from each other on the Mount Gambier coastal plain. Towards the north-west the spacing of the barriers reduces as distance from volcanic complexes increases and associated uplift of these areas diminishes. Towards Lake Alexandrina (~300 km north-west of Mount Gambier) the barriers coalesce into a single calcarenite complex (Belperio and Cann, 1990; Murray-Wallace *et al.*, 2010). Southeast of Mount Gambier the barriers lose expression in the landscape and not all palaeo-shorelines are identifiable (Belperio, 1995).

Belperio (1995) identified five associated sediment facies within the Bridgewater Formation shoreline deposits including (1) skeletal calcarenite and marls deposited in (2) littoral, (3) subtidal, (4) lagoonal and (5) lacustrine environments. These are discussed in more detail in Chapter 3, where they are correlated with exposed facies on the Mount Gambier coastal plain. Previous work has focused on the geochronological history of these barriers on the coastal plain between Robe and Naracoorte, and is also discussed in more detail in Chapters 3 and 6.

After the last glacial maximum (~21-22 ka) sea level rose rapidly, and is suggested to have reached the present coastline in Australia ~7 ka (e.g. Lewis *et al.*, 2013). The continental shelf reduces in width between the Great Australia Bight, where it is 200 km wide, to the Bonney Shelf, where it is only 50 km wide. Loading of the continental shelf with rising sea level has therefore resulted in different degrees of coastal warping and geographically variable sea-



level transgression along the southern Australian coastline (Belperio, 1995). In South Australia all Holocene coastal and shelf sediments deposited in a range of marine settings may be ascribed to the St Kilda Formation, and were described in gulf waters north of Adelaide by Cann and Gostin (1985) and Belperio (1988).

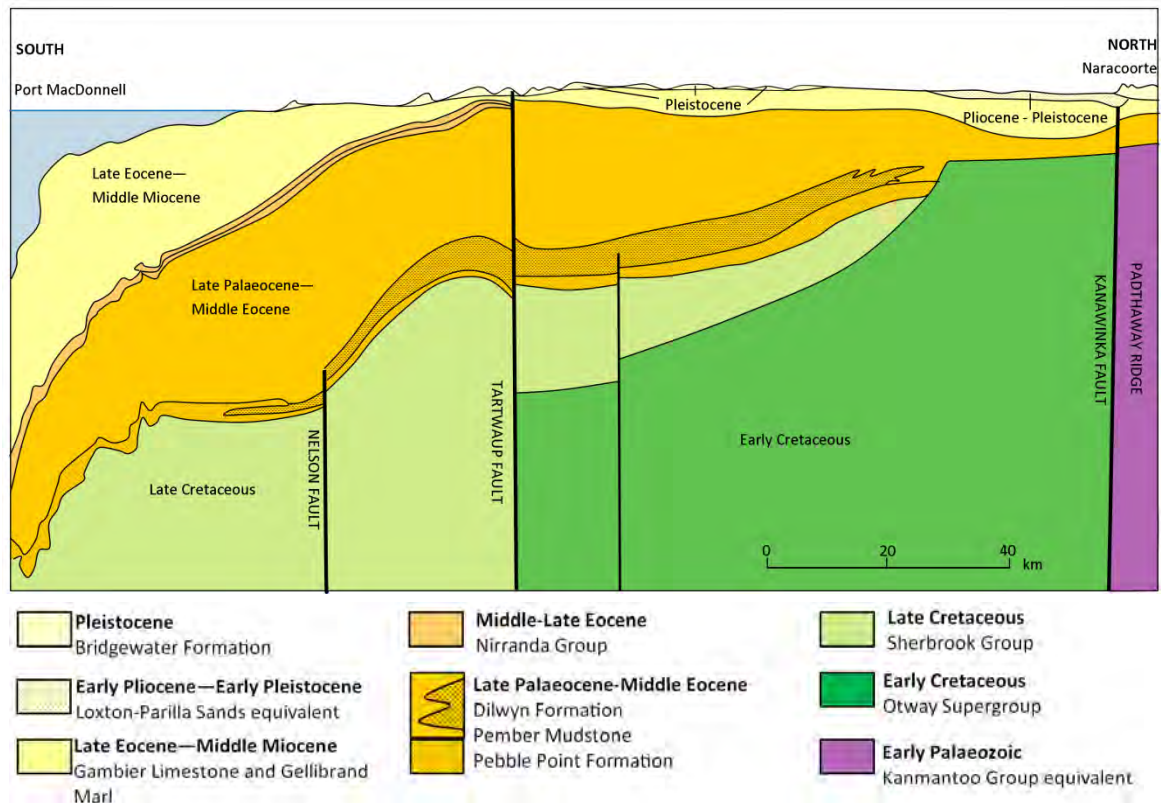


**Figure 1.3:** Cross-section between Port MacDonnell and Naracoorte highlighting geological units of the Gambier Embayment modified from Morton (1995).

### 1.2.2 Structural features of the Mount Gambier coastal plain

A range of structural features found within the study region have a degree of control over local sedimentation patterns. These include boundaries to the Otway Basin such as the Padthaway Ridge, and faults within the Gambier Embayment such as the Kanawinka and Tartwaup Faults.

#### Padthaway Ridge

To the north and west, the Otway Basin is constrained by the fault-bounded Padthaway Ridge, a partly exhumed early Palaeozoic complex consisting of igneous rocks and metasediments. The Padthaway Ridge is a horst-like structure that separates the Otway Basin from the similarly aged Murray and Great Artesian Basins to the north (Sprigg, 1952). Drill holes through the

Padthaway Ridge have indicated that glacial sediments lie upon an irregular bedrock floor (Alley, 1995). The Padthaway Ridge is suggested to be a remnant of initial rifting between Australia and Antarctica, and the intrusive granites within the structure are associated with faulting during the Delmerian Orogeny,  $514 \pm 3$  Ma (Riordan *et al.*, 2011). The granitic rocks of the Padthaway horst are proposed to underlie much of the south-eastern South Australia region, and they crop out sporadically as monadnocks and whaleback on the coastal plains, such as those seen along the modern coastline near Kingston (Murray-Wallace and Cann, 2007).

### **Kanawinka Escarpment**

The shoreline barriers of the Mount Gambier coastal plain are bounded by the extended linear cliff of the Kanawinka Escarpment. The Kanawinka Escarpment ranges from 15 to 100 m in height and trends in a northwest direction for over 100 km from Naracoorte (Kenley, 1971). The formation of the Kanawinka Escarpment has been debated, with numerous suggestions proposed: a low-lying fault scarp (Fenner, 1930); a series of connected faults (Boutakoff, 1952; Kenley, 1971); a palaeo-shoreline cliff (Hossfeld, 1950; Wallace *et al.*, 2005; McLaren *et al.*, 2011) or a combination of a fault and a coincidental palaeo-shoreline (Sprigg, 1952). Kenley (1971) noted the abrupt offset of Paleogene/Neogene strata around the escarpment and suggested this could be explained only by faulting or monoclinal flexing parallel to the escarpment, and interpreted the Kanawinka Fault to lie 2 km southwest of the escarpment. Kenley (1971) also proposed that the displacement along the Kanawinka Fault may have controlled the coastline structurally in the Early Pleistocene, and the escarpment retreated to its present position under the influence of coastal marine erosion.

The Kanawinka Fault system is found at the northern and eastern boundaries of the Gambier Embayment and is a complex of high angle faults and monoclines (Kenley, 1971) that has experienced normal and reverse movement through the late Mesozoic and Paleogene (James and Bone, 1989). The preservation of up to 100 m of Gambier Limestone on the upthrown block is indicative of recurring movement of the escarpment and movement at varying times throughout the Neogene (Kenley, 1971). McLaren *et al.* (2011) suggested that the Kanawinka Escarpment separates the Late Miocene – Early Pliocene Loxton-Parilla Sands from the Quaternary Bridgewater Formation.

The Tartwaup Fault is another north-westerly trending fault that is found to the north of Mount Gambier and extends to 5 km south of Dartmoor in Victoria (Kenley, 1971). Similarly to the Kanawinka Fault, the Tartwaup Faults have throws towards the south-west, and also act

as a structural hinge line separating Cretaceous and Paleogene sediments that increase in thickness towards the south (Love *et al.*, 1993).

### **Loxton-Parilla Sands**

The Loxton-Parilla Sands are located north of the Gambier Embayment within the Murray Basin and consist of more than 600 strandplains (Miranda *et al.*, 2009). In Victoria the Loxton-Parilla Sands are referred to as the Dorodong Sands. The strandlines trend sub-parallel to the modern coastline and the Bridgewater Formation is regarded as a modern analogue for these deposits, as the Loxton-Parilla Sands are also interpreted as transgressive dune complexes (Belperio and Bluck, 1990). These sands are composed of fine shelly material overlain by planar-bedded calcareous to coarse-grained sandstone (Belperio, 1995). The Loxton-Parilla Sands are suggested to represent early Pliocene marine regression (Ludbrook, 1961; Blackburn, 1962). The presence of the foraminifer *Elphidium pseudonodosom* within the sand is also indicative of a Pliocene age (Belperio, 1995). Sea level did not fluctuate significantly during this time, and therefore Miranda *et al.* (2008) suggested that tectonism may have been a primary mechanism in the formation of this strandplain sequence. McLaren *et al.* (2011) proposed that the cessation of Loxton-Parilla Sand deposition was related to the damming and formation of palaeo-lake Lake Bungunnia, which would have deprived the basin of a sediment source and resulted in a change from a progradational to an erosional coastline.

While the Loxton-Parilla Sands are not located within the Gambier Embayment and do not directly relate to the Bridgewater Formation, it is important to be aware of their existence as a potential sediment source of the shoreline deposits on the Mount Gambier coastal plain.

### **Karst features**

Karst topography is well-developed on the Mount Gambier coastal plain and is present in both the Gambier Limestone and the Bridgewater Formation. Sea-level regression during the Late Miocene left the Gambier Limestone exposed for a significant time, allowing for karstification of the ground surface. The Gambier Limestone crops out in the Port MacDonnell, Mount Gambier and Naracoorte regions (Figure 1.4). The physical and chemical properties of the limestone have a strong influence on the geomorphology over the entire coastal plain (Twidale *et al.*, 1983).

The Gambier Limestone is crystalline in structure and well-jointed but poorly bedded (Grimes, 1994). The microcrystalline structure of the limestone prevents the passage of water through the rock body, yet water can readily infiltrate along joints and bedding planes. The geomorphology of the region is therefore influenced by the karstic nature of the Gambier

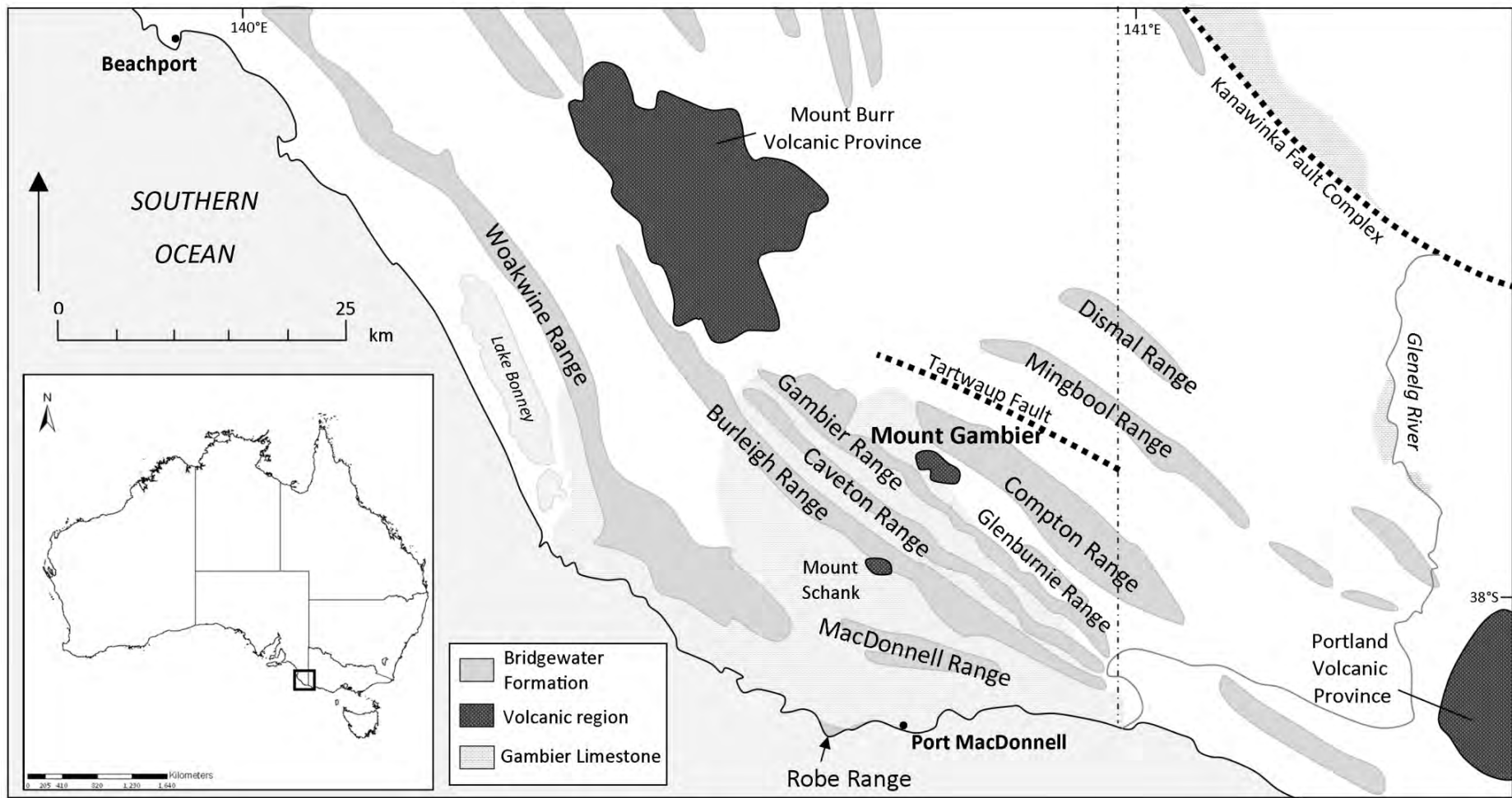


**Figure 1.4:** Surface geology of the Mount Gambier coastal plain, southern Australia. (Geology of the region after Love *et al.*, 1993 and Sheard, 1990).

Limestone in a number of ways: streams commonly descend below the surface resulting in limited overland drainage; joints and bedding planes are enlarged through dissolution to form sinkholes and caves; and occasionally carbonates transported in solution may re-precipitate to form speleothems (Twidale *et al.*, 1983).

Karst features within the Gambier Limestone include collapsed dolines and cenotes. In the Mount Gambier and Naracoorte regions collapsed dolines may reach up to 500 m in width and 8 m in depth (Grimes, 1994). Dolines are suggested to have formed through solution and subsidence of surface soil into larger cavities (Grimes, 1994). The depths to which karst features have developed is found to increase towards the coast as the Gambier Limestone increases in thickness in this region and the karst would have developed during lower sea levels and water tables in Pleistocene glacial episodes (Sheard and Smith, 1995). Cenotes, where dolines extend beneath the water table, are restricted to the southern areas of the Mount Gambier, Schank and coastal regions. Little Blue Lake, for example, is a typical cenote found within the Schank region.

Karst features found within the calcarenite of the Bridgewater Formation may be referred to as syngenetic karst as the structures are forming within soft, porous sediment at the same time as it is being cemented into rock (Grimes, 1994). Syngenetic karst within the palaeo-shoreline deposits include vertical solution pipes and low cave systems (Grimes, 1994), while common pedogenic features include calcrete horizons and calcareous rhizoliths or plant replacement features. Solution pipes are common across the Mount Gambier coastal plain and are seen as vertical cylindrical tubes, up to 1 m in diameter and up to 20 m deep. Commonly, solution pipes have a cemented rim which is harder than the surrounding calcarenite and they may be infilled with *terra rossa* soils.

The presence of karst features on the Mount Gambier coastal plain can influence sub-surface drainage, and identification of these structures may also indicate periods of subaerial exposure of different surfaces. Pedogenic features, such as hard calcrete horizons, can also promote preservation of barrier shoreline deposits.

### **1.3 Volcanism on the Mount Gambier coastal plain**

Quaternary volcanic centres on the Mount Gambier coastal plain have been identified as a source of epeirogenic uplift (Murray-Wallace *et al.*, 1998) and have essentially preserved successive sea-level highstand deposits. Understanding the formation of these volcanic

structures, associated rates of uplift and how these may vary is thus crucial for accurate determination of palaeo-sea level in this region.

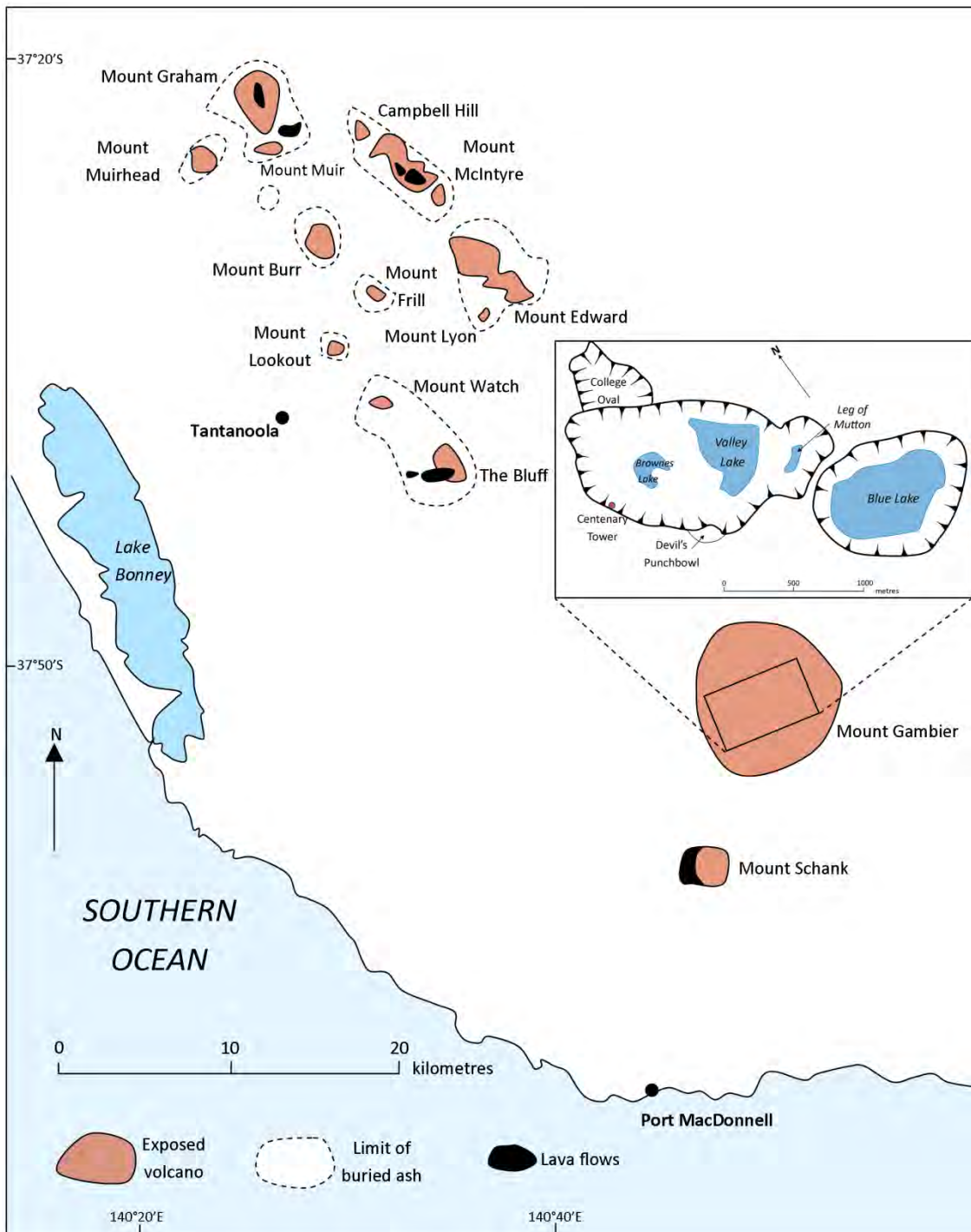


**Figure 1.5:** Volcanoes of the Mount Gambier coastal plain and sub-crop map of the Mount Gambier volcanic complex, modified from Sheard (1990).

Approximately 17 volcanic eruptive centres can be identified on the Mount Gambier coastal plain (Figure 1.5). Volcanoes identified in the southeast of South Australia are the youngest, and form the western most extension of the Neogene and Quaternary Newer

volcanics province of Victoria. In central Victoria over 250 eruption points have been identified and are suggested to be of Plio-Pleistocene age (Copper *et al.*, 2003). Cainozoic volcanism in Victoria has been related to the tectonic effects and rifting associated with the breakup of the Australian and Antarctic continents, but Quaternary volcanism on the Mount Gambier coastal plain is related to the northward drift of the Australian plate over a mantle hot region (Joyce, 1975). The Western District Province, which the volcanoes on the Mount Gambier coastal plain are a part of, generally includes volcanic rocks younger than 4.5 Ma (McDougall *et al.*, 1966), and over 400 separate eruption centres have been identified (Joyce, 1975). The Western District Province can further be divided into two sub-provinces; the Central Highland and the Western Plains. The youngest activity on the Western Plains is generally represented by small cinder cones, maars and lava shields (Price *et al.*, 2003).

Volcanism on the Mount Gambier coastal plain can be separated into two groups; the Mount Burr volcanic province to the north, and the Southern volcanic group which includes Mount Gambier and Mount Schank (Figure 1.5). Sprigg (1952) suggested that these two regions were indicative of two distinct phases of volcanism and that the more northern volcanoes had possibly followed the strike of the Tartwaup Fault.

### **1.3.1 Mount Burr volcanic province**

East of the town of Millicent, the Mount Burr volcanic province includes 15 volcanic centres which are associated with basement faults formed as part of the Otway Basin Graben (Sheard, 1990). Seismic profiling reveals three main fault lines in the Mount Burr region and is reflected in the three trend lines of volcanic centres (Sheard, 1983; 1990). Volcanic structures within this group include lava flows, scoria domes, composite domes and maars. Drilling at The Bluff by Sheard (1983) showed alternating sequences of scoria, lava flows and ash, with the presence of a palaeosol, indicating a significant hiatus between episodes of eruption. The Mount Burr volcanoes are primarily alkaline basalt, with lherzolite identified as xenoliths in lava flows or as volcanic bombs (Sheard, 1995). Geochemical analysis of lava by Irving and Green (1976) indicates olivine analcinite-rich lava erupted from Mount Watch and Mount McIntyre, while lava from Mount Burr was potassium-rich nepheline hawaiite.

Ejecta from this northern group lies directly on top of the Gambier Limestone and is overlain by the Pleistocene sands of the Bridgewater Formation, indicating at least an Early Pleistocene age for the eruptions. In addition to deposition of sands during Quaternary sea-level highstands, marine activity during this time also physically altered the volcanic landforms and distribution of tephra surrounding the eruption centres (Sheard, 1990). For example, the

effect of onshore winds and coastal erosion associated with sea-level highstands has resulted in an asymmetrical cross-section through Mount Muirhead and The Bluff (Sheard, 1990). At Mount Muirhead, high angle cross-bedding and ripple marks are visible within the volcanic layering, suggestive of eruption within a coastal setting (Sheard, 1983).

Dating of the Mount Burr volcanic province has been mostly unsuccessful due to the alteration of rock by weathering, marine action and the presence of secondary calcium carbonate (Sheard, 1995). Palynological work conducted by Dodson (1974) on cores collected near Lake Leake (Figure 1.7) suggested volcanism in this area had ceased by 20 ka. Stratigraphic evidence, in the form of the overlying Pleistocene Bridgewater Formation sediments, indicates eruptions during the Early Pleistocene.

### **1.3.2 Southern volcanic group**

Mount Gambier and Mount Schank comprise the younger (Holocene), southern volcanic group on the Mount Gambier coastal plain. Both Mount Gambier and Mount Schank have erupted through sediments of the barrier shorelines of the Bridgewater Formation, and ejecta from their eruptions are found overlying these marine sands, indicative of significantly younger eruptions than those associated with the Mount Burr volcanic province. These volcanic centres are both complex maar and cone structures produced by phreatomagmatic explosions rather than by structural collapse analogous to calderas (Sheard, 1995). Irving and Green (1976) identified the geochemistry of Mount Gambier as nepheline hawaiite, and Mount Schank as potassium-rich nepheline haeiite or nepheline trachyandesite.

#### **Mount Gambier**

Two episodes of closely-spaced eruptions occurred at Mount Gambier; one at the western end of the volcanic complex and the other near Leg of Mutton Lake Crater (Sheard, 1978, 1983; 1995). Initial eruptions resulted in the formation of small, low maars and the surrounding land was covered in 2 m of ash and lapilli (Sheard, 1978; 1995). Lava then flowed from a fissure near Brownes Lake and a vent near Leg of Mutton Lake, but the two small flows did not coalesce (Sheard, 1983; 1995). A scoria cone developed near this western lava flow towards the end of the first eruption episode. Palaeomagnetic evidence from Barbetti and Sheard (1981) suggested that activity ceased for approximately 300 years, allowing lava to cool and crystallise (Sheard, 1978). The second phase of volcanic activity was of greater intensity and involved a larger area. The percolation of groundwater into the existing volcanic centres and its interaction with ascending magma columns resulted in a range of phreatomagmatic explosions. Many closely-spaced small vents combined and formed the large craters that now



contain Blue, Valley and Brownes Lake (Sheard, 1978). Ejecta, including ash, lapilli and volcanic bombs, are identified up to 8 km away from the eruption centre, with a total volume of 1.3 km<sup>3</sup> of tephra ejected (Sheard, 1995). The final magmatic event was lava fountaining at Brownes Lake.

Radiocarbon dating of charcoal fragments within tuff ejected from Mount Gambier by Blackburn *et al.* (1982) and palaeomagnetic analysis of lava conducted by Barbetti and Sheard (1981) indicate eruptions occurred 4 ka to 4.3 ka. Robertson *et al.* (1996) used thermoluminescence (TL) analysis to date baked tuff underlying the lava flow at Valley Lake, Mount Gambier, and obtained an age of  $4.2 \pm 0.5$  ka, but also suggest an additional eruption event may have occurred approximately 7 ka.

### **Mount Schank**

Mount Schank is located approximately 10 km south of Mount Gambier, and is significantly smaller in size, forming a maar-cone structure. Eruptions from Mount Schank began from a fissure in the underlying Gambier Limestone. From the fissure basaltic ash vented for a short time, followed by the extrusion of lava which flowed westwards and southwards and had an average thickness of 3.5 m (Sheard, 1990; 1995). Eruptive activity was concentrated at the centre of the fissure, where a scoria cone and small maar were constructed. As activity at these two sites ceased a final vent opened forming the main cone present today (Sheard, 1995).

Thermoluminescence analysis of quartz grains from the Bridgewater Formation overlain by lava from Mount Schank was conducted by Smith and Prescott (1987) and yielded an average age of  $4.93 \pm 0.54$  ka.

### **1.3.3 Neotectonics**

The Mount Gambier coastal plain has undergone regional epeirogenic uplift as a result of intraplate Quaternary volcanism associated with emplacement of a magma chamber and dislocation along the Kanawinka Fault (Murray-Wallace *et al.*, 1998). Thus, estimates of last interglacial palaeo-sea level must be sought elsewhere. Murray-Wallace and Belperio (1991) proposed that the most reliable datum for the last interglacial (~125 ka) sea level in Australia can be derived from Eyre Peninsula, whereby a consistent level of 2 m APSL has been recorded for 500 km along the coastline. Eyre Peninsula comprises part of the tectonically stable Precambrian Gawler Craton, rendering it a more reliable sea-level datum than other last interglacial shorelines in Australia from less stable areas (Murray-Wallace and Belperio, 1991). Using this datum for the last interglacial *sensu stricto*, Murray-Wallace *et al.* (1998) were able

to map the spatial variation and neotectonic uplift of last interglacial deposits on the Coorong and Mount Gambier coastal plain.

The Woakwine Range has been identified as a last interglacial deposit (e.g. Murray-Wallace *et al.*, 1999). The height of the back barrier lagoonal facies of the Woakwine Range rises in a south-easterly direction from 1 m APSL at Lake Alexandrina, to 3 m APSL at Salt Creek near Kingston, to 8 m APSL at Robe and 18 m APSL near Mount Gambier (Murray-Wallace *et al.*, 1998). Lagoonal facies yield a more precise palaeo-sea level indicator in the region than beach facies and may be within  $\pm 1$  m of mean sea level (Murray-Wallace *et al.*, 2001). Using the last interglacial sea-level height of 2 m APSL defined by Murray-Wallace and Belperio (1991), Murray-Wallace *et al.* (1998) were able to account for neotectonic uplift across the Coorong to Mount Gambier coastal plain. Back-barrier facies of the last interglacial Woakwine Range at Robe were identified at 8 m APSL which indicates an uplift rate of 50 mm per 1000 years. Lagoonal facies of Reedy Creek Range (MIS 7), at  $18 \pm 1$  m APSL, and West Avenue Range (MIS 9) at  $24 \pm 1$  m APSL, inland of Robe, are suggestive of slightly higher longer-term rates of uplift at 80 mm per 1000 year. Murray-Wallace *et al.* (1998) argued that the uncertainties associated with measuring palaeo-shoreline altitude and inferring sea-level height could mean that longer-term uplift in the Robe region is not significantly different from that calculated from the Woakwine Range. Murray-Wallace *et al.* (1998) therefore proposed an uplift rate of 70 mm per 1000 years.

Beach facies at the southern extremity of the Woakwine Range, near Mount Gambier, have been dated to  $132 \pm 9$  ka through the use of TL analysis (Huntley *et al.*, 1993a). Shell beds in this region are identified up to 18 m APSL, indicative of 16 m of uplift at an uplift rate of 130 mm per 1000 years. These shell beds are the highest occurrence of last interglacial coastal strata found on the Australian mainland (Murray-Wallace *et al.*, 1998). Murray-Wallace *et al.* (1996) identified palaeo-shoreline facies of the Burleigh Range (MIS 7) and Caveton Range (MIS 9) in the Mount Gambier region indicative of uplift rates of 140 and 120 mm per 1000 years respectively, suggesting uplift rates in the Mount Gambier region have continually been greater than at Robe since the late middle Pleistocene (Murray-Wallace *et al.*, 1998).

It is therefore apparent that with greater distance from Quaternary volcanic centres, the source of epeirogenic uplift on the coastal plain, rates of uplift decrease. Towards the River Murray mouth, barrier shorelines of the Bridgewater Formation coalesce. The same pattern appears to occur farther west into Victoria. Uplift rates have not yet been determined for the Mount Gambier coastal plain in western Victoria, and it is not known what, if any,

influence the Portland volcanic province may have on uplift rates in this region. Sherwood *et al.* (1994) identified a shell bed 4 m APSL at Narrawong, western Victoria. Uranium-thorium dating of fossil shell yielded an age of  $100 \pm 20$  ka and amino acid racemisation (AAR) of the gastropod *Turbo undulatus* gave similar D/L values to other last interglacial shells of the same species in South Australia (Murray-Wallace and Belperio, 1991). However, U-series dating of shell has been heavily criticised (e.g. Kaufman *et al.*, 1971; Edwards *et al.*, 2003) and thus this age cannot be relied upon. If these geochronological values are taken as accurate they suggest only 2 m of uplift of the coastal plain in western Victoria over the last 125 ka. However, uplift rates within the Narrawong region are affected by the presence of the Kanawinka Fault, and further work accounting for any tectonic movement associated with the fault needs to be conducted prior to the calculation of uplift rates for this region.

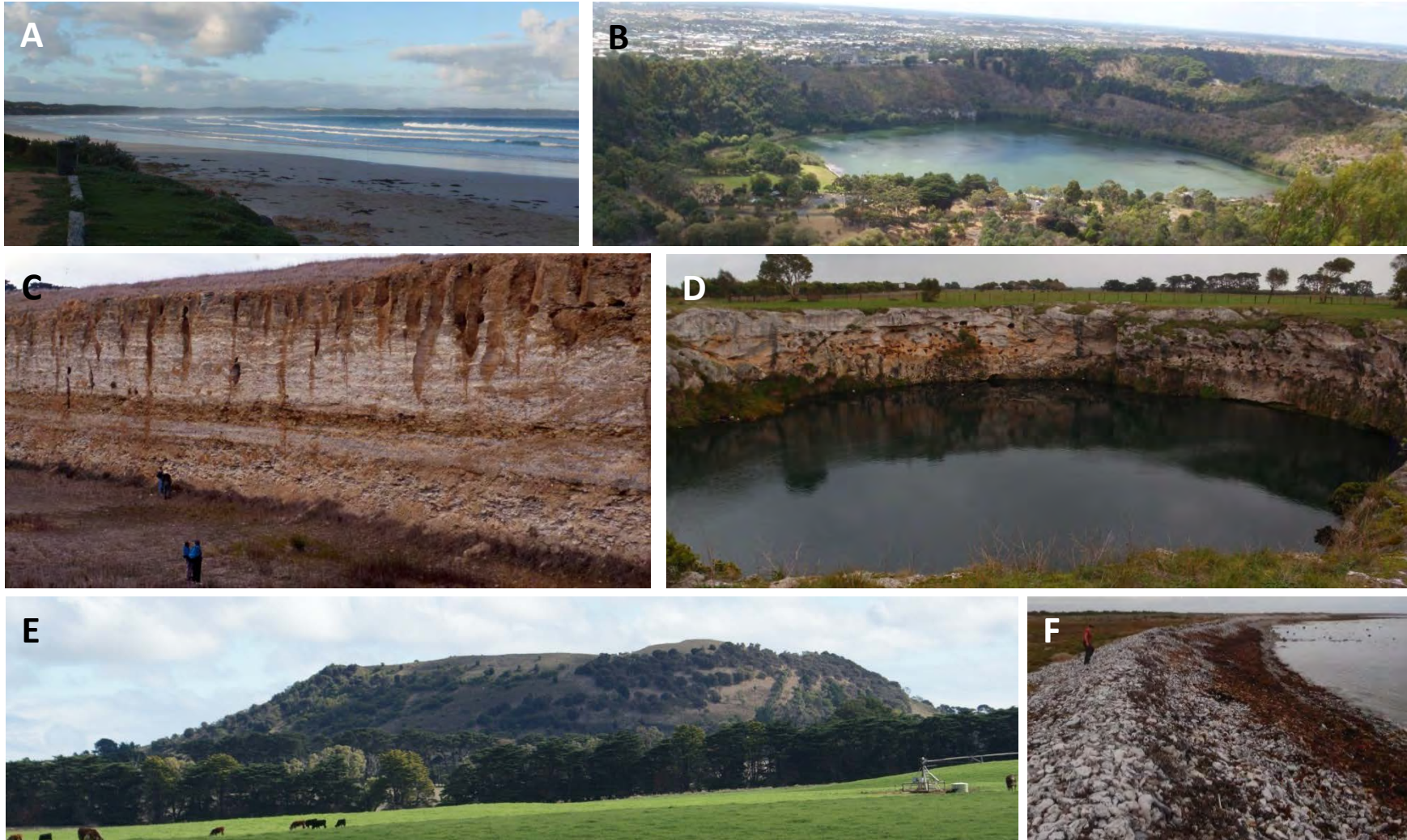


**Figure 1.6:** Features of the Mount Gambier coastal plain. **A:** Dissipative beach at Cape Bridgewater; **B:** Valley Lake, Mount Gambier looking east towards Blue Lake; **C:** Solution pipes in Gambier Limestone within a quarry near Mount Gambier; **D:** Little Blue Lake cenote; **E:** Mount Schank; **F:** Flint cobble beach at Racecourse Bay.

## **1.4 Climate of the Mount Gambier coastal plain**

The Mount Gambier coastal plain experiences a Mediterranean climate, with warm, dry summers, and cooler, wetter winters. Sea surface and air temperatures experience little variation annually in coastal regions but experience larger differences farther inland. Rain is concentrated on coastal regions and is locally affected by topography. Both winds and rainfall are seasonally driven by the sub-tropical high pressure system in summer and the mid-latitude cyclones in winter.

Wind and wave climates can influence the deposition of calcareous sands along the coastline. Identification of primary and secondary wind directions is therefore important when assessing facies architecture within calcarenite deposits. Rainfall and temperature can determine rates of weathering and diagenesis and, in turn, the destruction or potential preservation of barrier shorelines and the development of karst features across the coastal plain. Figure 1.7 illustrates the location of each of the weather stations referred to within the following section.

### **1.4.1 Temperature and rainfall**

Temperatures are mild along the coast and vary little between summer and winter, due to the buffering effect of the ocean. At Robe the mean monthly maximum temperature is 22.6°C (February) and mean monthly minimum temperatures fall to 8.1°C (July), recording a current mean annual temperature (CMAT) of 14.7°C (Bureau of Meteorology, 2013). Similar temperatures are recorded farther southwards along the coast at Portland, where the CMAT is 13.7°C and a maximum temperature range of 15.4°C. Farther inland, annual temperature differences are greater. The CMAT at Mount Gambier, approximately 25 km from the coastline, is 13.3°C and ranges by 16°C annually, and at Naracoorte, 90 km inland, the CMAT is warmer still at 14.7°C, with an annual range of 24.8°C. Figure 1.8 highlights the monthly maximum and minimum temperatures measured across the coastal plain.

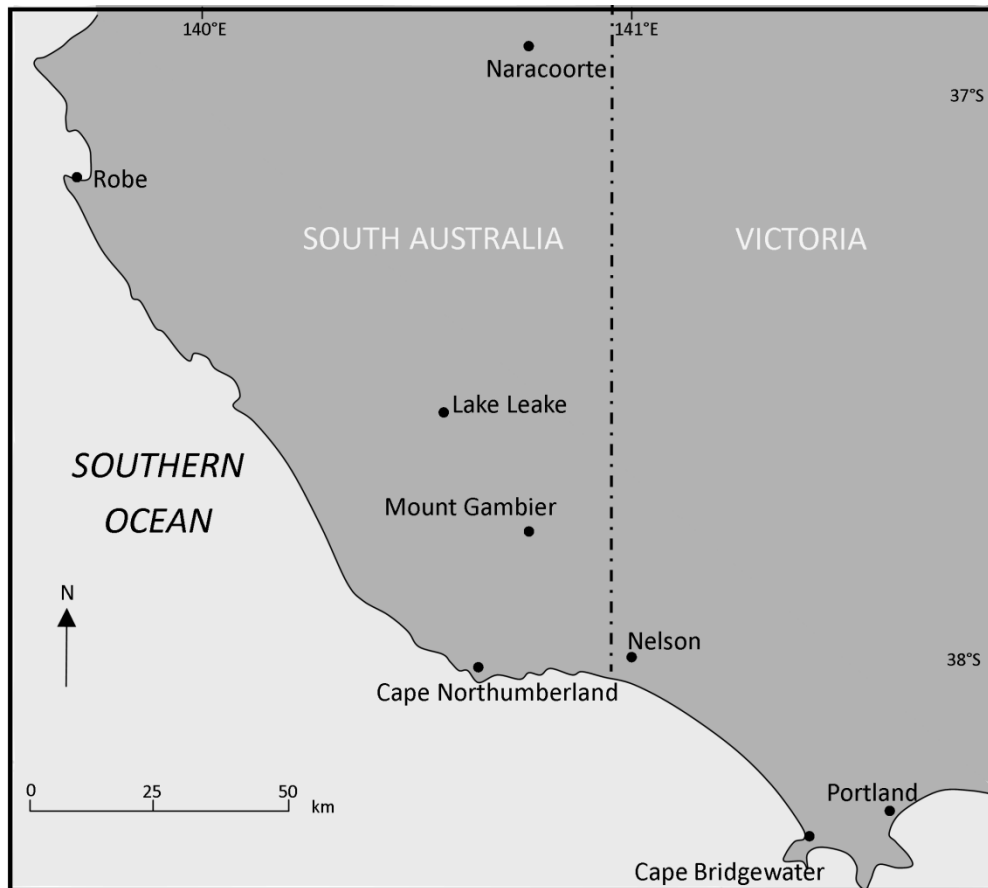


**Figure 1.7** Location of weather stations across Mount Gambier coastal plain.

The climate of southern Australia is dominated by the subtropical high pressure system. During Australian summer this high is located along the latitude of Adelaide and brings dry, stable air conditions, with light winds and clear sky to the southern portion of the continent (Short, 2006). During Australian winter, the subtropical high moves northwards to a latitude of approximately 30°S, permitting mid-latitude cyclones and their associated cold fronts, to bring cooler, wetter weather to southern Australia. Short (2006) recognised three factors influencing rainfall across southern Australian coastline: firstly, rainfall is seasonal, with wet winters and dry summers; secondly, there is distinct decrease in rainfall from south to north, with increased distance from the precipitation source of the mid-latitude cyclones; finally, rainfall is influenced by local topography resulting in orographic effects.

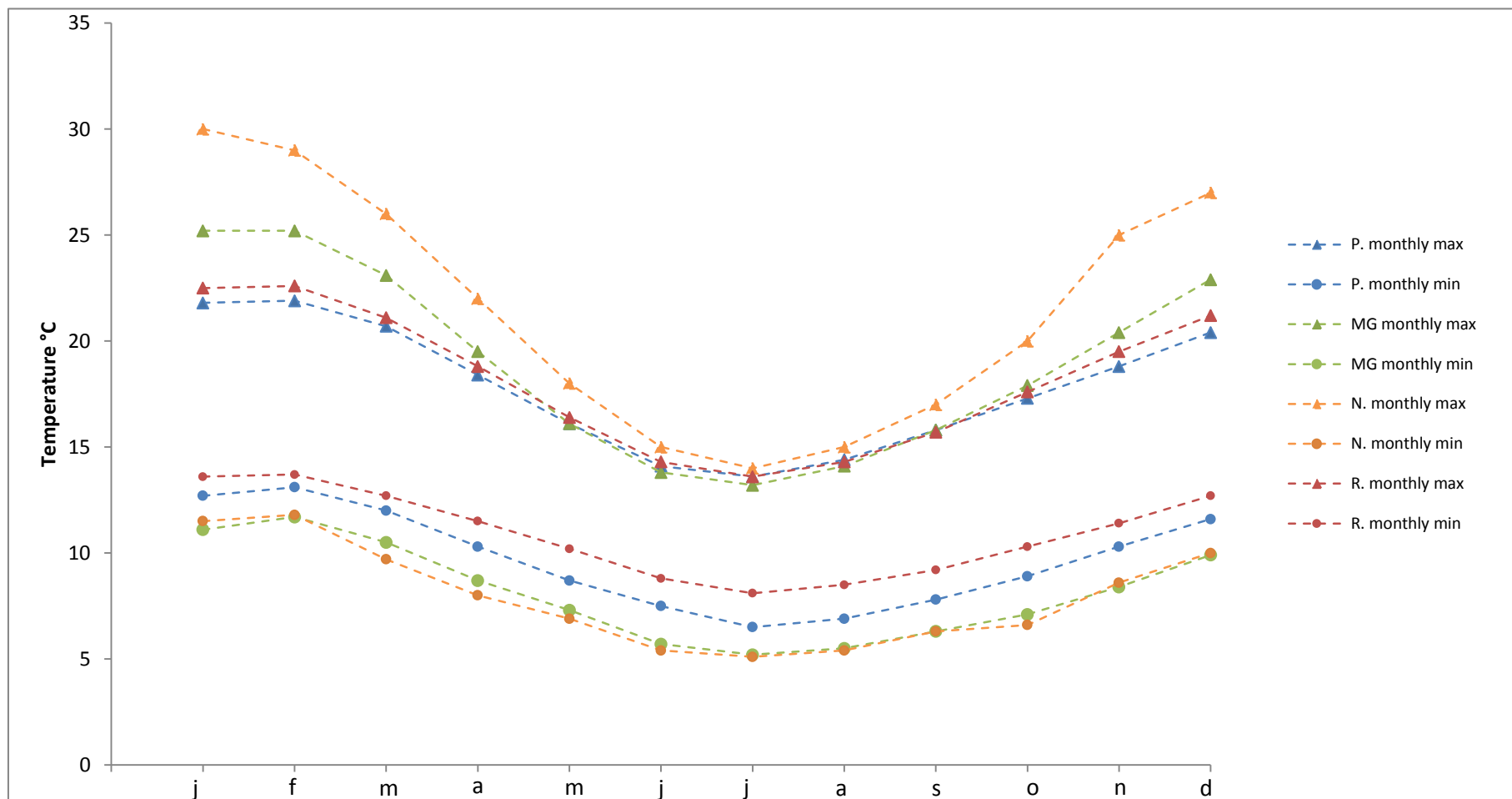


**Figure 1.8:** Maximum and minimum monthly temperatures across the Mount Gambier coastal plain (Bureau of Meteorology, 2013). P=Portland, MG = Mount Gambier Aero, N = Naracoorte, R=Robe.

These three characteristics are illustrated by viewing rainfall data across the Mount Gambier coastal plain. Figure 1.9 shows rainfall data collected by Bureau of Meteorology (2013) across the coastal plain, and at all sites rainfall is shown to increase in winter and decrease in summer, indicating the seasonal influence of the subtropical high pressure system. At Cape Bridgewater a maximum winter (July) rainfall of 115 mm is recorded. Approximately 60 km north-west at Nelson, July rainfall is slightly less at 107 mm, and a farther 150 km north-west at Robe, even lower winter rainfall is recorded at 104 mm, due to increased distance from the mid-latitude cyclone belt. Rainfall differences are also noted with increased distance inland. At Naracoorte, mean annual rainfall is only 491 mm, while at Nelson and Robe, both on the coast, mean annual rainfall is 766 mm and 633 mm, respectively. On the Mount Gambier coastal plain orographic rainfall is influenced by the topographic high of Mount Burr. At Lake Leake, located approximately 35 km inland from Lake Bonney, and within the Mount Burr volcanic province, a mean annual rainfall of 835.6 mm is recorded, while at Mount Gambier, a similar distance inland of the coast, a significantly lower mean annual rainfall of 710.1 mm is recorded.

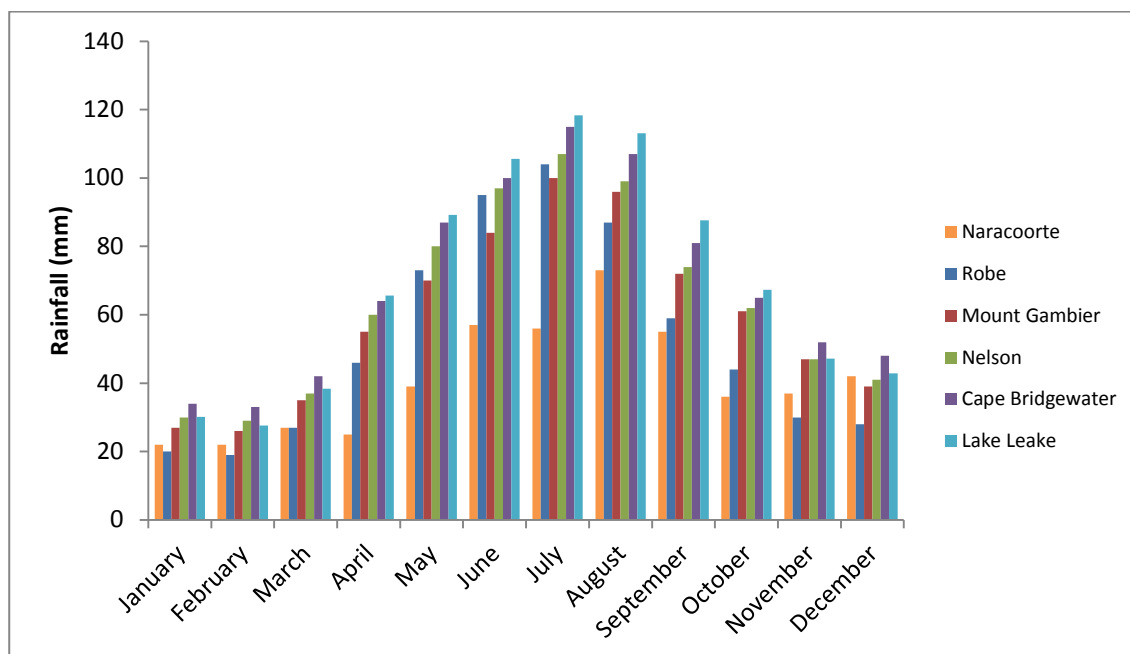


Figure 1.9: Monthly rainfall averages across the Mount Gambier coastal plain (Bureau of Meteorology, 2013).

### 1.4.2 Wind

The subtropical high pressure system that dominates the southern Australian climate during summer brings with it light winds. Warm, dry winds flow in an anti-clockwise direction around the high, with a westerly stream flowing across the southern half of the high and the southern



Australian coastline. These westerlies dominate year-round but are strengthened in winter with the addition of westerly cold fronts associated with the influence of the mid-latitude cyclonic belt, which sits on a latitude of 40-60°S and is referred to as the 'roaring forties' storm belt (Short, 2006).

Winds along the southern Australian coastline are also affected by local sea breezes. Sea breezes result from the differential heating of the land surface compared with the sea, especially during Australian summer when this difference can be greatest. As the hot air rises over the land, it is replaced with cooler air blowing landwards from the sea. These breezes generally develop in the early afternoon, and their direction is dependent on the orientation of the coastline. On south-facing coasts, the southerly sea breeze comes from the southeast, and on west facing coasts from the southwest, and therefore the direction varies along the coastline (Short, 2006).

The Bureau of Meteorology only records wind direction and speed twice daily; at 9am and 3pm. The records reflect the average wind speed and direction in the 30 minutes prior to sample collection. Figure 1.10 is a wind rose diagram illustrating the varying wind directions recorded at 9am and 3pm from various sites across the Mount Gambier coastal plain in both summer (January) and winter (July), derived from data collected by the Bureau of Meteorology (2013). The size of the central circle indicates the number of calms recorded, with larger circle size indicative of a greater number of calms. During winter (July), winds are predominantly northerly in direction, but westerly winds increase in strength (Penny, 1983) due to the influence of the 'roaring forties'. In January, winds are predominantly from the south, southeast and southwest. During summer afternoons, sea breezes add to synoptic wind patterns, and in coastal regions on the Mount Gambier coastal plain they are generally from westerly to southwesterly directions (Penny, 1983). Winds may also be affected by topography, with the most inland shoreline barrier of the Bridgewater Formation, the Naracoorte Range, sheltering the town of Naracoorte from certain winds. This results in a greater recorded number of calms in this area (Penny, 1983), than recorded in coastal regions such as Robe and Cape Northumberland (Figure 1.10).

Studies investigating palaeowind patterns in South Australia coastal deposits are few. Within the last interglacial Woakwine Range, Murray-Wallace *et al.* (1999) describe predominantly landward dipping aeolianite units, indicative of south-westerly winds during this time. From similar studies on Hindmarsh Island, near the River Murray mouth, Murray-Wallace *et al.* (2010) describe MIS 5e aeolianite with beds dipping towards the northeast,

indicative of south-westerly winds. On Kangaroo Island, Lachlan (2011) suggests that palaeowinds were predominantly onshore during deposition of interglacial aeolianite. From the limited information available it could be suggested that winds during interglacials on the South Australian coastline were similar to those of the present Holocene interglacial.

During glacials wind patterns in South Australia may have varied. From studies of desert dunes in more central areas of South Australia wind strength has been suggested to have increased during glacials and a shift in the seasonal pattern of westerlies up to 5° farther north has been proposed (e.g. Bowler, 1975). From a review of palaeowind proxies in the Southern Hemisphere Shulmeister *et al.* (2004) suggested that westerly flow over Australasia was enhanced during the Last Glacial Maximum and was significantly reduced at the start of the Holocene.

Winds are highly important for coastal processes as they generate local sea waves and determine the direction and distance of onshore aeolian transport (Short, 2006). It is therefore imperative to be familiar with the predominant wind directions along the coastline when assessing the facies architecture and bedding structures of calcarenite deposits across the Mount Gambier coastal plain.

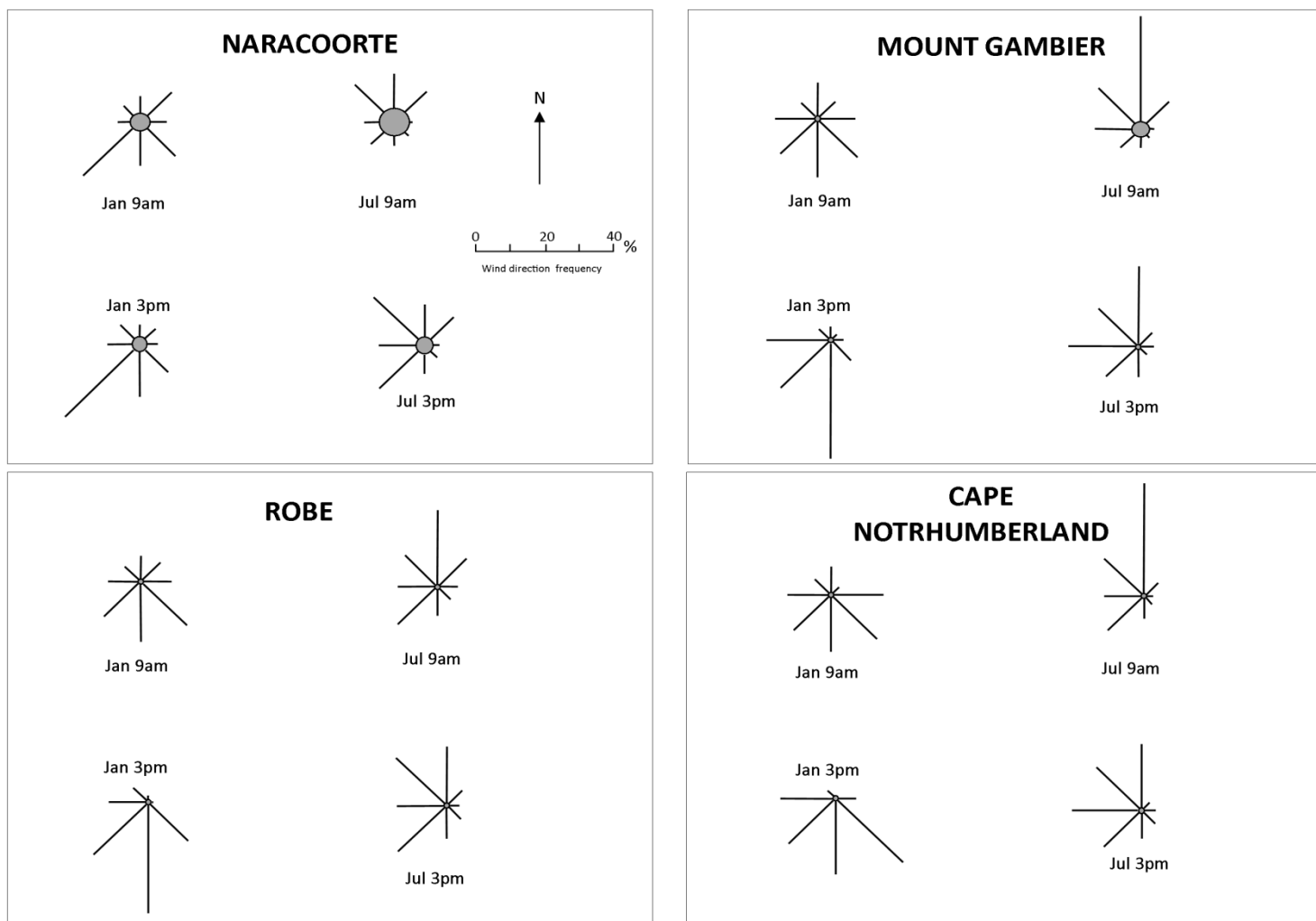


Figure 1.10: Wind rose diagram indicating wind direction across the Mount Gambier coastal plain.

### **1.4.3 Draining of the land**

The combination of geology and climate on the Mount Gambier coastal plain proved difficult for land occupiers when the area was settled by Europeans during the 1880s. The high winter rainfall commonly collected on the flats between the barrier shorelines of the Bridgewater Formation, resulting in a swampy environment due to poor natural drainage. The water-logged land resulted in transportation difficulties and continual puddling made parts of the land impossible to farm or build on.

Due to gradual neotectonic uplift each inter-barrier flat is found at a progressively higher elevation than the one seaward of it, with the most easterly flat at Penola being 60 m above present sea level, while the most westerly is drowned and forms a chain of lakes (Williams, 1977). Flats are also tilted in a north-westerly direction, resulting in natural drainage of the flats towards the west until a barrier shoreline of higher elevation is encountered, deflecting the water in a north-westerly direction. The resulting watercourse is slow moving and ill-defined (Williams, 1977). Water will either find an outlet to the Coorong lagoon or terminate as a swamp.

The first attempt to drain the Mount Gambier region occurred in 1863. Surveyor General Goyder suggested coastal swamps could be drained by cutting channels at right angles through the coastal ranges, allowing the water to drain to the sea (Williams, 1977). Development of drainage systems was slow and limited by a lack of government funding. It was not until 1944, when the state and federal governments decided to re-settle ex-servicemen from the Second World War in the region, that significant drainage development occurred as part of the Anderson Scheme. Between 1944 and 1970 the drainage system was extended and reorientated the natural northwest trending systems towards the west (Williams, 1977). As a result of the extensive anthropogenic drainage system, it is difficult to find any standing water on the flats today, with the exception of a handful of wildlife refuge lagoons.

## **1.5 Marine environment**

The following section examines the modern marine environment of the Mount Gambier coastal plain, discussing the offshore continental shelf, water temperatures, salinity, currents and wave climate. These factors directly influence carbonate production (which is discussed further in Chapter 3) and in turn, deposition of sediments of the Bridgewater Formation.

### 1.5.1 The Bonney Shelf

The Mount Gambier coastal plain is fronted offshore by the Bonney Shelf, a western extension of the Lacepede Shelf (Figure 1.11), and comprises part of the Australian continental passive margin. The Bonney Shelf is an open shelf and generally deeper than 40 m (James *et al.*, 1992). The shelf is narrowest at Portland, where it is less than 35 km wide, and broadens to the east and west. At Robe, the shelf is 60 km wide and is 80 km in width at Warrnambool in Victoria, 150 km east of Port MacDonnell (Boreen *et al.*, 1993).

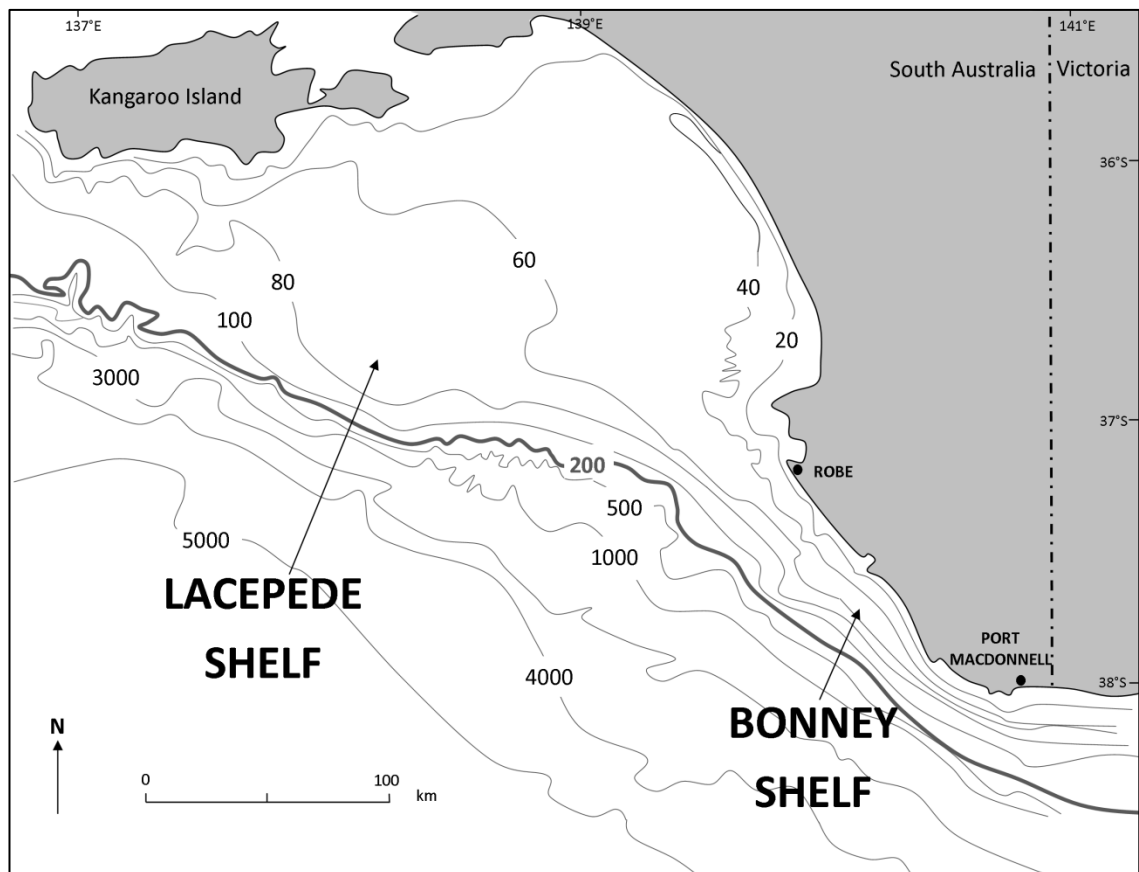


**Figure 1.11:** Offshore bathymetry of the Lacepede and Bonney continental shelves of southern Australia, after James *et al.* (2005). Bathymetry data are in metres.

The main break in shelf slope is identified at a depth of 180 m, and the shelf can be divided into three sections characterised by carbonate production. The shallow shelf, found between 40-70 m water depth, displays subtle local relief and comprises grainy, quartzose, palimpsest facies reflecting the interaction of modern bioclastic sediment production and numerous sea-level highstands during the Late Pleistocene which have mixed sediment and introduced quartz-rich sediments during sea level lowstands (James *et al.*, 1992). Along the middle shelf, between 70-140 m water depth, coarse carbonate sands are mostly modern and

are dominated by bryozoan particles (James *et al.*, 1992). The deep shelf, found between 140-250 m depth, is composed of muddier sediments.

### **1.5.2 Wave climate**

The Mount Gambier coastal plain contains some of the most exposed, high energy coastline in Australia, with large sections directly facing prevailing large south-westerly waves and westerly winds (Short, 2006). The Bonney Shelf is predominantly swell-dominated, and it is this swell that determines the depth of the sediment regions outlined above. Swell is produced year-round from the mid-latitude cyclones, with slightly higher swell experienced in late winter and a minimum during summer (Short, 2006). Swell is predominantly from a westerly and south-westerly direction as dictated by the prevailing winds, and increases in height south-eastwards along the coastline, with Cape Northumberland recording swell between 0-2 m 31% of the year, and swell between 2-4 m for 62% of the year (Short, 2006).

High (>2.5 m) modal deep water waves are common in the region as are long period (>12 s) swell waves, with wave lengths up to 200 m (Short and Hesp, 1982). Reading and Collinson (1996) noted that in order for surface gravity waves to entrain sediment, the depth of water must be less than or equal to approximately half of its wavelength. This depth is commonly referred to as the fair-weather wave base. Therefore, on the Bonney Shelf, sands are potentially subject to oscillatory motion at water depths of 100 m (James *et al.*, 1992).

### **1.5.3 Ocean currents, sea surface temperature and salinity**

The dominant current off South Australia is the Antarctic Circumpolar Current, which moves in an easterly direction, between 50-60°S, driven by the dominant westerly winds of the region. The Leeuwin Current transports warmer water southwards from the tropics along the Western Australia coastline. At Cape Leeuwin, the current turns eastward and brings these warmer waters into the Great Australia Bight. The waters of the Leeuwin Current are significantly warmer than those of the Southern Ocean and strengthening of this warm current in the past (e.g. MIS 5e) is suggested to have brought warmer-water species to the region, such as the foraminifer *Marginopora vertebralis* (Cann and Clarke, 1993; McGowran *et al.*, 1997; Murray-Wallace *et al.*, 2000) which have been identified as far east as Robe. Closer to the coastline, currents are determined by the local winds, which are predominantly westerly. A seasonal reversal in the coastal current can occur across the Bonney Shelf where an easterly flow of water spreads across the shelf from Bass Strait (Short, 2006).

Schahinger (1987) noted that during the summer months, between December and March, waters on the Bonney Shelf are subjected to wind-driven upwelling events, resulting in

offshore flow of surface waters, with onshore flow of cooler water occurring below. Waters are stratified over summer due to strong south-westerly winds bringing deep, cold ocean waters to the shelf (James *et al.*, 1992). Waters are more vertically homogenous in winter.

Sea surface temperatures along the Bonney Shelf range from 17-18°C in summer months to as low as 13-15°C in winter (Short, 2006). These temperatures are cooler than those on the Lacepede Shelf farther west, which are more strongly influenced by the Leeuwin Current that weakens as it travels eastwards. This cool water prevents the development of coral reefs across the carbonate shelves, and is discussed further in Chapter 3. Waters are of open ocean salinity and range from 35.1-35.6‰ on the Bonney Shelf, to more saline conditions of 35.9‰ on the Lacepede Shelf (James *et al.*, 1992).

#### **1.5.4 Modern beaches**

Much of the Mount Gambier coastal plain is dominated by dissipative beaches; high energy beaches with a wide surf zone. As suggested by Short and Hesp (1982), dissipative beaches are formed as a response to modally high wave conditions in regions of abundant medium- to fine-grained sand supply. Dissipative beaches commonly possess wide, low-gradient forms and a moderately stable shoreline (Short and Hesp, 1982). The surf zone along the Mount Gambier coastal plain is high and commonly extends for 500 m seawards.

Three beaches in the Port MacDonnell region have been described by Short (2006). Racecourse Bay, 5 km east of Port MacDonnell, is fronted by shallow limestone shoals and substrates which act to lower wave energy, and supply limestone and flint to the cobble beaches in this vicinity. Western Port MacDonnell Beach is a lower energy, 300-m-long, southwest-facing beach that is also fronted by extensive rock flats. The western-most end of Port MacDonnell Beach is primarily composed of medium-grained sand and is backed by aeolianite cliffs. At Cape Northumberland, directly west of Port MacDonnell, the cape is composed of calcarenite which has been cliffed by wave action. Small pocket beaches are found on the eastern base of these cliffs and are composed of medium-coarse sands. Aeolianite sea stacks are found directly seaward of these beaches. More detailed descriptions of these beaches are given in Chapter 3 (section 3.8.2), but this comparison serves to show the range in beach face structures over a small (10 km) section of coastline. Short and Hesp (1982) noted that landward aeolian transport is greatest where beach topography is low and aerodynamic flow regime is least disrupted, and it is thus potentially highest on dissipative beaches.

Beach types along the coast may change due to varying aspects of the coast in regard with incoming wind and swell energy regimes or the availability of sediment, which may vary with the width of the carbonate shelf and the outcropping of Gambier Limestone at the coast. The type of beach is therefore likely to determine the presence or size of foredunes backing the beach in a specific location. It is important to be aware of these factors and the change in the coastline over a small time scale when analysing the facies architecture of palaeo-shoreline barriers.

### **1.6 Preservation of Bridgewater Formation barrier shorelines on Mount Gambier coastal plain**

The combination of climate, local geology and neotectonic uplift across the Mount Gambier coastal plain has resulted in preservation of the barrier shoreline complexes of the Bridgewater Formation. The Mediterranean climate, with drier summers and cool wet winters, combined with the high calcareous content of underlying sediment, promotes pedogenesis and the formation of surficial calcrete horizons which blanket the landscape. These resistant calcrete horizons have effectively preserved the original morphology of the barriers with minimal landscape lowering. Calcrete formation is discussed in more detail in Chapter 3 (section 3.3.8) in relation to the stratigraphy of the Bridgewater Formation deposits.

The presence of the underlying, highly porous, Gambier Limestone has resulted in little overland drainage across the coastal plain. The lack of rivers has reduced the potential for erosion of the barrier shorelines, and also results in very little terrigenous material reaching the ocean, thus not diluting the dominantly carbonate sediment. The closest river is the Glenelg River in western-most Victoria. This river cuts through the more inland barriers of the Mingbool and Dismal Ranges, and may contribute to the reduced expression of more inland barriers on the Victorian border.

The archive of interglacial palaeo-shorelines preserved across the Coorong and Mount Gambier coastal plain is of global significance. Very few palaeo-shoreline records extend over such a lengthy time frame (Murray-Wallace and Woodroffe, 2014). The primary factor resulting in the preservation of these barriers is the slow and gentle uplift of the coastal plain due to the neotectonics of the Mount Burr and Mount Gambier volcanic provinces. In the Mount Gambier region, the coastal plain has been uplifting at  $0.13 \text{ mm yr}^{-1}$  (Murray-Wallace *et al.*, 1996). This uplift has effectively removed the older barriers from the erosive potential of subsequent sea level highstands, and resulted in Bridgewater Formation deposits increasing in age landward.



### **1.7 Aims of this study**

This study aims to provide a geochronological framework for deposition of interglacial barrier shorelines on the Mount Gambier coastal plain through the use of amino acid racemisation (AAR), optically stimulated luminescence (OSL) and radiocarbon dating techniques. The interpretation of facies architecture and fossil fauna will enable reconstruction of palaeo-depositional environments and combined with petrographical analysis will enhance interpretations of coastal evolution and the elevation of past sea level on the coastal plain.

Previous work (see section 3.8.1 for a review of previous studies) has concentrated on the coastal barriers in the Robe region, while limited studies have been conducted on the barriers within the Mount Gambier area. This study aims to assess whether the barriers on the Mount Gambier coastal plain are correlatives of those farther northwest, as suggested by Sprigg (1952) and to describe and interpret deposits of the more inland barriers which have not previously been reported in detail.

Future sea level is predicted to rise within the next 100 years (IPCC, 2007). Studies of past interglacial height, such as this research, will provide a geological analogue with which to compare future predictions. This study will provide a dataset for modelling Quaternary ice sheet volumes and interglacial climate dynamics.

### **1.8 Summary**

The Mount Gambier coastal plain sits within the Otway Basin, and comprises part of the southern continental margin of Australia that formed during continental rifting from Antarctica during the Jurassic. Cretaceous, carbonaceous siltstones, muds and shales lie beneath the Oligocene-Miocene Gambier Limestone which crops out in the Port MacDonnell, Mount Gambier and Naracoorte regions. Progressive sea-level fall during the Neogene resulted in extensive karstification of the Gambier Limestone. The Pleistocene bioclastic sands of the Bridgewater Formation lie directly above the Gambier Limestone and can be identified in the form of five facies as outlined by Belperio (1995). Shoreline barriers of the Bridgewater Formation extend sub-parallel to the modern shoreline and represent an archive of interglacial sea-level highstands. Quaternary neotectonism has resulted in gradual uplift of the coastal plain and has separated barrier shorelines from one another. Distance between barriers is found to decrease with increasing distance from Mount Burr volcanic province due to differential uplift of the coastal plain.

The climate of the Mount Gambier coastal plain is Mediterranean with warm, dry summers and cool, wet winters. Rainfall increases towards the south and coastal regions and is topographically induced by the Mount Burr volcanic province. Winds are predominantly from the south and west and increase in strength in winter with increased influence from the mid-latitude cyclonic belt. The combination of climate, geology and neotectonics has resulted in the preservation of the barriers of the Bridgewater Formation in this region.

The narrow Bonney Shelf lies offshore of the Mount Gambier coastal plain. Carbonate production on the shelf is high due to little terrigenous material reaching the ocean at this location. Wave lengths are long and result in a deep fair-weather wave base. The coastline is swell-dominated year-round and wave energy is high. Beach type varies across the Mount Gambier coastal plain depending on source material and aspect of the coast in relation to primary wave direction.

Assessment of facies architecture is reliant on an accurate understanding of climatic conditions. For example, knowledge of primarily westerly winds may aid in identifying stoss and lee slopes in aeolian deposits. Knowledge of wave climate may also aid in determining palaeo-shorelines. However, the identification of three different beach types of varying material (coarse sand to limestone and flint cobbles) within a 10 km stretch of coastline highlights how the coast can differ on a small spatial scale and leads us to question how the coastline may have varied in previous interglacial episodes and whether the modern coastline is a suitable analogue for past sea-level highstands. Varying climatic conditions can influence coastal environments. For example, the potential strengthening of the Leeuwin Current during the last interglacial *sensu stricto* resulted in a greater abundance of warmer-water fauna along the South Australian coastline than found in the present interglacial (Cann and Clarke, 1993; McGowran *et al.*, 1997; Murray-Wallace *et al.*, 2000). Accurate assessments of sedimentary structures and faunal assemblages in barrier shorelines of previous interglacials require knowledge of past climates as well as the sea-level of past interglacials. The following chapter addresses the current literature on Quaternary interglacials and will provide a context for which findings derived from the Mount Gambier coastal plain can be compared.

# Chapter 2

## Quaternary interglacial sea levels – a review

### 2.1 Introduction

The Quaternary is characterised by the waxing and waning of continental ice sheets. A range of internal and external mechanisms are proposed as drivers initiating the changes from glacial to interglacial conditions and are assessed in this chapter. Sea-level reconstruction can aid in estimating the global ice volume during these cycles, and can be derived from marine- and ice-cores as well as geomorphological indicators such as palaeo-shorelines.

This chapter reviews sea-level literature derived from studies of these indicators for the past four interglacials, from which the most evidence has been preserved. Variation is evident both in the duration of interglacial episodes and the sea-level elevation during these intervals, and differs with both the type of indicator the data are derived from, and the geographical location of the study site in relation to former continental ice sheets. Duration of interglacials between datasets varies as a result of the accuracy and precision of dating methods, and the lack of a common definition for interglacials; where does a glacial end and an interglacial begin? Potential reasons for variance in sea-level elevation with geographical location may result from glacio-hydro-isostatic effects where the Earth's crust-mantle system readjusts to changes in the load. Differences in sea-level elevation and duration between interglacials derived from a range of sources are analysed within this chapter. As well as comparing a range of interglacial sea-level highstand data sets from sites around the globe, studies of last interglacial sea-level in Australia are also discussed, highlighting the differences between sites close to former ice sheets and those from more remote locations.

A framework of global sea-level literature is established within this chapter with which to compare the data derived from the Mount Gambier coastal plain. By outlining the advantages and limitations of certain sea-level indicators and accounting for differences between global study sites, the Mount Gambier data can be set within a global context. Assessment of the literature establishes that the lengthy record of the Mount Gambier coastal plain, recording at least six sea-level highstands, is a rarity and indicates the unusually good record of this study site.

## 2.2 Drivers of glacials and interglacials

While growth and contraction of continental ice sheets has dominated the Quaternary period, the pattern of ice expansion and reduction has changed throughout the Quaternary and is evident within a range of archives including ice-cores (EPICA community members, 2004; Masson-Delmotte *et al.*, 2010; Schilt *et al.*, 2010) and marine-cores (Shackleton and Opdyke, 1973; Hays *et al.*, 1976; Imbrie *et al.*, 1984; Martinson *et al.*, 1987). In the Early Pleistocene a 41 ka cycle dominated, while from ~1 Ma onwards ice sheet growth has been characterised by a 100 ka cycle (Ruddiman *et al.*, 1986) where climate has oscillated between short-lived interglacial and extended glacial episodes. The six interglacials prior to the Holocene appear to have been asymmetric (or 'saw-toothed') in pattern, with the gradual accumulation of ice over ~90 ka and rapid deglaciations over approximately a tenth of that time (Broecker and van Donk, 1970).

The cause of these fluctuations in ice sheet growth and decay and the reasons for the observed change in their cycle is contentious. Some theorists suggest that external factors such as variations in solar output are the cause, while others propose internal elements, such as changes in deep ocean circulation, have resulted in the detected fluctuations (Hays *et al.*, 1976). More recently, it has been suggested that the driving force controlling a change in climate from glacials to interglacials is the result of orbital forcing changes in atmospheric composition and internal feedback effects (e.g. Paillard, 1998).

One hypothesis explaining the climatic fluctuations resulting in expanding and retreating ice sheets is the 'Astronomical Theory' which was first advocated by Croll (1887) and expanded upon by Milankovitch (1941). The 'Astronomical Theory' suggests that the temperatures at the surface of the Earth vary due to regular changes in the Earth's axis and orbit. Milankovitch's (1941) orbital hypothesis is comprised of three major cyclic processes (eccentricity, obliquity and precession) which determine the axial tilt and shape of the Earth's orbit around the sun, and thus govern the amount of insolation a certain hemisphere will receive at a certain time (Figure 2.1). Eccentricity determines how the shape of the Earth's orbit varies from near circular to elliptical, and thus alters the distance between the Earth and the Sun at aphelion (where the Earth is farthest from the Sun in its orbit) and perihelion (where the Earth is nearest the Sun) and has a period of *ca.* 100 ka. Obliquity controls the angle of tilt of the Earth's rotational axis and has a 41 ka period. The process of precession regulates the 'wobble' of the Earth's axis and alters the seasons at which aphelion and perihelion occur, with a period of ~21 ka.

While changes in these three orbital parameters do not cause significant variations in the total amount of energy that is received in the upper atmosphere of the whole planet over a year, they do result in variations to the geographic distribution of insolation and seasonality (Williams *et al.*, 1998). The geographic distribution of incoming energy can be altered when an increase in obliquity widens the zone of the tropics allowing more energy to reach the polar latitudes when they are tilted towards the sun during summer (Williams *et al.*, 1998). Variations in orbital parameters can also influence seasonality; if summer is reached in one hemisphere during perihelion, insolation will be greater than when summer occurs at aphelion. Changes in the eccentricity of the Earth's orbit may also influence seasonal length. Therefore, while no significant variation in energy occurs at the top of the atmosphere over the entire globe, changes to seasonality and the geographic distribution of energy can result in differences to the amount of solar radiation observed by the Earth-atmosphere system (Williams *et al.*, 1998).

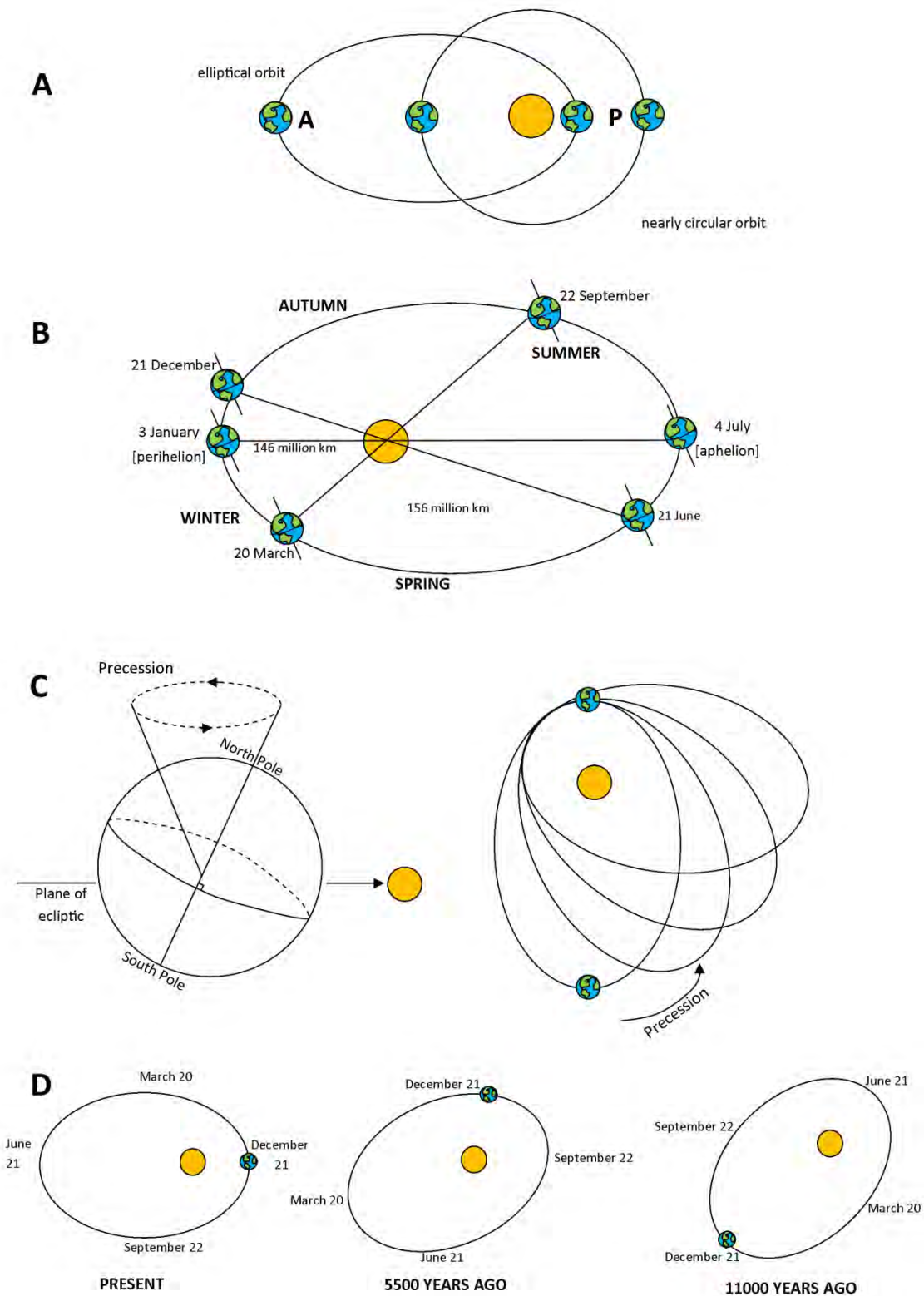


**Figure 2.1:** Orbital cycles comprising the 'Astronomical Theory', illustrating; **A:** Eccentricity (A = aphelion; P = perihelion), **B:** Obliquity, **C:** Precession of the Earth's orbit and **D:** Precession of the equinoxes (modified from Maslin and Ridgwell, 2005).

Milankovitch (1941) suggested that the distribution of summer insolation at 65°N, where landmass is greatest in spatial extent, is critical to the growth and decay of ice sheets. Berger and Loutre (1991) later refined the summer insolation curve at 65°N as seen in Figure 2.2. At high latitudes the effect of obliquity is greatest as the sun is lower in the sky and zenith angles (the angle of incidence measured from the vertical, Figure 2.3) are therefore greater. If a change in obliquity resulted in a decrease of the zenith angle from 65° to 63° at high latitude, the subsequent change in the cosine of the zenith angle would produce an insolation increase of 7%. A similar 2° change in the zenith angle at 10°N however, would only yield a 1% variation in insolation (Williams *et al.*, 1998). Milankovitch (1941) calculated that at 66°N, an increase in obliquity by 1° would result in a 5.9% reduction in radiation. Milankovitch (1941) thus proposed that ice-age climate cycles were directly influenced by summer insolation at mid-latitudes in the Northern Hemisphere, implying that ice sheet collapse should correspond with peaks in Northern Hemisphere June insolation. Conversely, maintenance of winter snow through summer (leading to ice sheet growth) would be maximised when summer insolation at high latitudes is minimal.

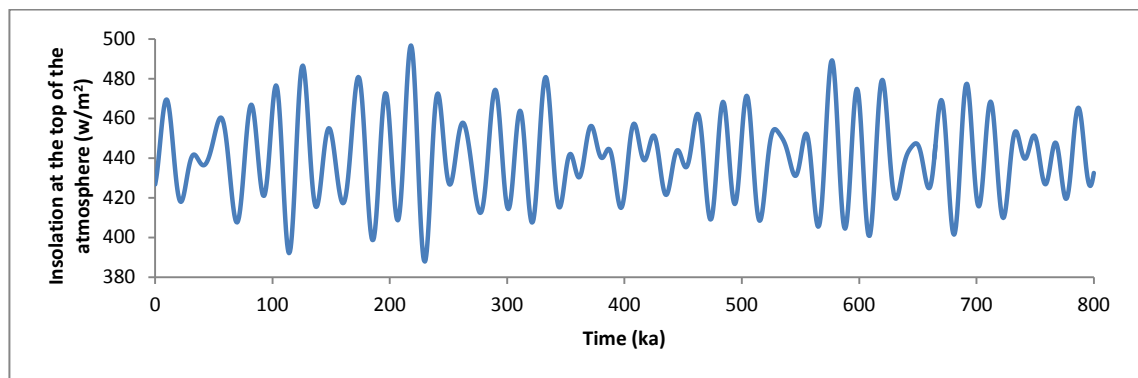


**Figure 2.2:** Incoming summer insolation at 65°N over the past 800 ka (data from Berger and Loutre, 1991).

**Table 2.1:** Timing of 65°N insolation maxima over the past four interglacial cycles (from Berger and Loutre, 1991)

MIS	1	5a	5c	5e	7a	7c	7e	9a	9c	11
Time of NH insolation maximum (ka)	10	82	103	126	201	218	241	311	333	425

An attractive element of Milankovitch's (1941) orbital theory is that it produces a timeframe in which the episodes of glaciation can be predicted. The 'Astronomical Theory' also potentially resolves the change in ice sheet growth from a 41 ka cycle in the Early Pleistocene when obliquity may have been the principal orbital cycle, to the 100 ka cycle of the later Pleistocene as eccentricity dominated. Nevertheless, some aspects of this are still unexplained, as obliquity is one of the weaker forcings, yet the 100 ka cycle is very dominant in the youngest parts of the Quaternary.

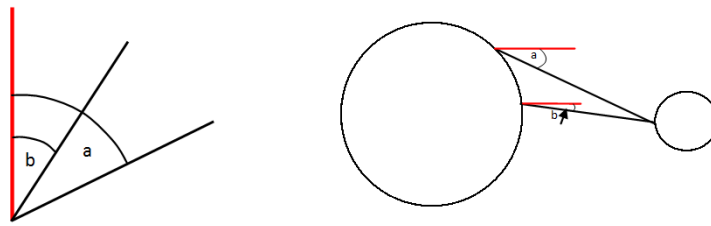


**Figure 2.3:** Changes in zenith angle with latitude; zenith angles are greater at high latitudes (a) than low latitudes (b).

In 1976, the rhythm that Milankovitch (1941) predicted for glacial expansion and contraction was identified within natural archives. Hays *et al.* (1976) reported results of oxygen isotope analyses from the planktonic foraminifer *Globigerina bulloides* in marine-cores RC11-120 and E49-18 from the Southern Indian Ocean. Using spectral analysis methods Hays *et al.* (1976) identified peaks within the record corresponding to periods of 106, 43, 24 and 19 ka. Subsequent studies have replicated and illustrated further evidence for the orbital rhythm within the climatic cycle in: pollen records (Hooghiemstra *et al.*, 1993); loess (Kukla, 1987); tropical lakes (Kutzbach and Street-Perrott, 1985); coral reefs (Aharon, 1984); ice cores (e.g. EPICA community members, 2004); marine-cores (e.g. Shackleton and Opdyke, 1973) and sea-level records (e.g. Mesolella *et al.*, 1969; Veeh and Chappell, 1970). However, records have also been presented and analysed through uranium-series dating that suggest that the timing of the orbital cycles do not accurately correspond with the timing of interglacial and glacial episodes (e.g. Winograd *et al.*, 1992).

## 2.3 Indicators of interglacial sea level

A range of methods have been developed to determine when and for how long interglacials occurred during the Quaternary and the extent of their associated sea-level highstands. These exist in sea-level proxies such as oxygen isotope analysis of marine- and ice-cores which decipher continental ice-volumes; and direct sea-level indicators such as geomorphological evidence of former shorelines preserved in the continental landscape. The sea-level highstand record preserved on the Mount Gambier coastal plain comprises part of the geomorphological record. In order to assess the integrity of this archive it is imperative to determine the strengths and weaknesses of geomorphological and proxy sea-level records against which the Mount Gambier dataset will be compared, to highlight potential weakness in the record, and identify why differences between records may occur.



### 2.3.1 Marine-based oxygen isotope records

A range of organisms inhabiting the ocean commonly secrete calcium-carbonate structures and through the synthesis of these structures oxygen is subtracted from the surrounding ocean water. The oxygen isotope composition ( $\delta^{18}\text{O}$ ) of fossil carbonate organisms buried on the deep-sea-floor should therefore reflect the ratio of oceanic oxygen isotopes in the ocean water and the water temperature at the time of carbonate secretion. Foraminifera are one type of secreting organism that is widely used in oxygen isotope analysis of marine-cores. Commonly used planktonic species include *Neogloboquadrina pachyderma* (Wu and Hillaire-Marcel, 1994) and *Globigerinoides sacculifera* (Shackleton and Opdyke, 1973) and benthic species such as *Uvigerina senticosa* (Shackleton *et al.*, 1983). Benthic species are commonly preferred for oxygen isotope analysis as they are less affected by changes in temperature, local salinity and upwelling than planktonic species (Patience and Kroon, 1991). Benthic species are also suggested to preserve a more positive  $\delta^{18}\text{O}$  than surface species (Pisias *et al.*, 1984; Jansen, 1989).

Emiliani (1955) reported oxygen isotope records from planktonic foraminifera in the Caribbean and tropical Atlantic. The resultant isotopic record was suggested to be reflective of changes in ocean surface temperatures. From this Emiliani (1955) was able to derive what he believed to be a palaeo-temperature sequence for the Pleistocene from which he suggested that surface water temperatures dropped by 6°C during glacial episodes.

Shackleton (1967) conducted further oxygen isotope analysis of marine-cores and concluded that the oxygen isotope composition of foraminiferal tests corresponded with the extraction of large volumes of ocean water (up to 70%) during glacials and the recirculation of water during interglacials. He thought that the differences in isotopic composition through a marine-core primarily reflect the volume of terrestrial ice, and thus in turn proxies of sea level could be derived from marine-cores (Shackleton and Opdyke, 1973). Isotopic fractionation occurs as the lighter isotope  $^{16}\text{O}$  is preferentially evaporated from the water leaving an  $^{18}\text{O}$ -enriched ocean. In polar regions this effect is amplified as colder temperatures result in further reduced absorption of the heavier  $^{18}\text{O}$  isotope. Moisture bearing winds transport the  $^{16}\text{O}$  enriched vapour to polar glaciers where it precipitates as snow and adds mass to growing ice sheets. During glacials there is a relative increase in the abundance of the heavier isotope  $\text{H}_2^{18}\text{O}$  in ocean waters, while during interglacials a relative decrease occurs. The water temperature at the time of carbonate secretion has since been suggested to have a more

minor role, yet the work of Emiliani (1955) still proves important in determining a timescale for terrestrial glacial events.

Within marine-core V28-238 from the equatorial Pacific, where sediment is assumed to have been continuously deposited over the past 870 ka, Shackleton and Opdyke (1973) were able to outline the boundaries of 22 separate isotope stages and proposed they be adopted as the standard for the Pleistocene (Figure 2.4).

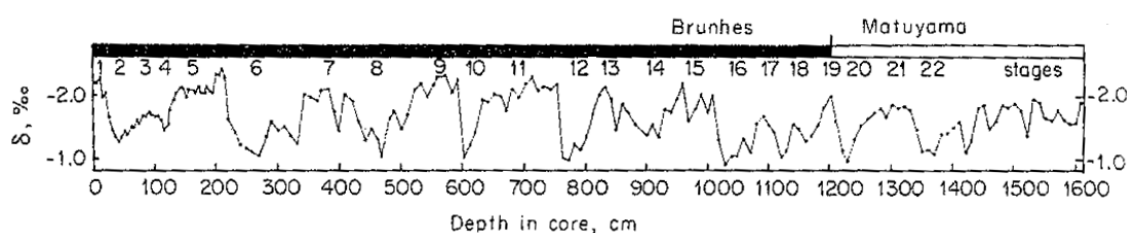


Figure 2.4: Oxygen isotope record as derived from core V28-238 in the equatorial Pacific (Shackleton and Opdyke, 1973).

Close resemblances between marine oxygen isotope records have been identified from different locations within the world's oceans (e.g. Imbrie *et al.*, 1984; Williams *et al.*, 1988). Variations in the quantity of  $^{16}\text{O}$  stored on the continental ice sheets results in changes in the mean  $\delta^{18}\text{O}$  value of the entire ocean. The oxygen isotope record thus is now thought to reflect a global history of continental ice volume (Shackleton, 1987), and suggests that the ocean as a whole has been responding to some common mechanism, lending support to Milankovitch's (1941) orbital hypothesis.

Through detailed analysis of core V28-238, Shackleton and Opdyke (1973) noted that a change in the isotopic record of 1.2‰ correlated with a 120 m drop in sea-level approximately 17,000  $^{14}\text{C}$  yr BP, during the Last Glacial Maximum (LGM). Shackleton and Opdyke (1973) were therefore able to suggest that a 0.01‰ change in the oxygen isotopic record of marine-cores would reflect a 10 m change in sea-level.

The marine-based oxygen isotope profile, while providing a valuable technique for Quaternary palaeoclimate reconstruction, does not yield a direct sea-level curve and only acts as a proxy for estimating sea-level elevation, especially in context of localised glacio-hydro-isostatic adjustment. One limitation of oxygen isotope analysis of marine-cores is that temperature does play a role in  $\delta^{18}\text{O}$  composition, though not to the extent that Emiliani (1955) thought. Another limitation is the varying rates of sedimentation at different locations and over varying timescales within the world's oceans, thus affecting core resolution. In regions where sedimentation rates are slow, cores may span a greater length of time but their

resolution will be small. However, where sedimentation rates are rapid, resolution is high but the time-length captured by the record is short. Problems may also be encountered in the form of diastems, or gaps in the sedimentary record. Different rates of sedimentation within different oceans also create difficulties in record comparison. The use of the isotopic record is also limited by the bioturbation of marine sediments on the ocean floor by bottom dwelling organisms and distortions arising from turbidity currents or compaction through core sampling. Therefore, no marine core will provide a perfect record of the isotopic history of the ocean (Shackleton, 1987) and small scale-events may be obscured.

Species-specific rates of carbonate secretion also need to be considered. Certain species of foraminifera and other organisms will secrete carbonate at different rates, and thus it is essential to know of species-dependent effects and be able to apply necessary corrections to avoid a biased sample (Bradley, 1985).

A further limitation in using the marine oxygen isotope record to establish palaeo-sea level is that the isotopic composition of former ice sheets would have varied with their latitude, size, and the residence time of the ice (Mix and Ruddiman, 1984). Therefore, the isotopic composition of the oceans is not linearly related to the volume of ice (Mix and Ruddiman, 1984; Bintanja *et al.*, 2005), and thus multiple cores from all ocean basins are required.

The interpretation of the marine oxygen isotope record is also complicated by the storage of oxygen isotopes in continental ice, deep water temperatures and the salinity of the surrounding water (both of which may alter the uptake of  $\delta^{18}\text{O}$  in calcite by benthic foraminifera) affecting the isotopic composition record. It can therefore be difficult to decipher a direct relationship to sea-level highstand history. As the marine oxygen isotope record represents the global volume of continental ice, it cannot account for global variations in sea level. Finally, a major problem with the oxygen isotope record in marine cores is that few of them are dated directly. Most, such as SPECMAP (Imbrie *et al.*, 1984; Martinson *et al.*, 1987) are 'tuned' to the astronomical parameters of the Milankovitch cycles. This introduces an element of circularity in the record as there is evidence that orbital forcing does not explain all of the Quaternary glacial-interglacial record (e.g. Winograd *et al.*, 1992).

### **Summary**

Marine-based oxygen isotope curves are a powerful tool for dating and correlating ocean sediments through time. Marine oxygen isotope stratigraphy presumably provides a continuous record of ocean floor sedimentation, and preserves an archive of global ice volume. This record spans the entire length of the Quaternary and as well as allowing for ice volume

estimation throughout that time it also aids in determining the timing and duration of continental glaciations and interglacials. Marine-based oxygen isotope records provide a proxy for global sea-level reconstruction but cannot generate sea-level elevation at various sites around the world as they do not account for local variations in glacio-hydro-isostasy. They must, therefore, be used in conjunction with other corroborative evidence to enable the production of a reliable age model. The global oxygen isotope record of marine-cores can aid in providing a framework for the timing of interglacials and potentially the deposition of shoreline barriers on the Mount Gambier coastal plain, but not in determining interglacial sea-level elevation within this region.

### 2.3.2 Ice core stratigraphy

Continental ice-cores can be of high resolution and are extremely valuable in palaeoclimatic reconstruction as they can resolve short-term climatic events not registered in marine-cores. Ice cores have been analysed in both northern and southern polar regions, and span a record of up to 800 ka, in EPICA Dome C, Antarctica (Masson-Delmotte *et al.*, 2010). The counting of annual layers, measuring of dust and chemical content, and stable isotopic analysis allow for the reconstruction of: local palaeo-temperature; precipitation rates; past wind strength and direction; moisture source conditions; and aerosol fluxes from volcanic, marine and terrestrial sources (Petit *et al.*, 1999). The stable isotope record of deuterium is commonly used in palaeoclimate reconstruction within ice-cores. Isotopic fractionation of deuterium is temperature dependent, and therefore  $\delta D$  can be used as a proxy of Antarctic temperature, as seen in Figure 2.5, taken from the EPICA Antarctic ice core Dome D (Jouzel *et al.*, 2007).

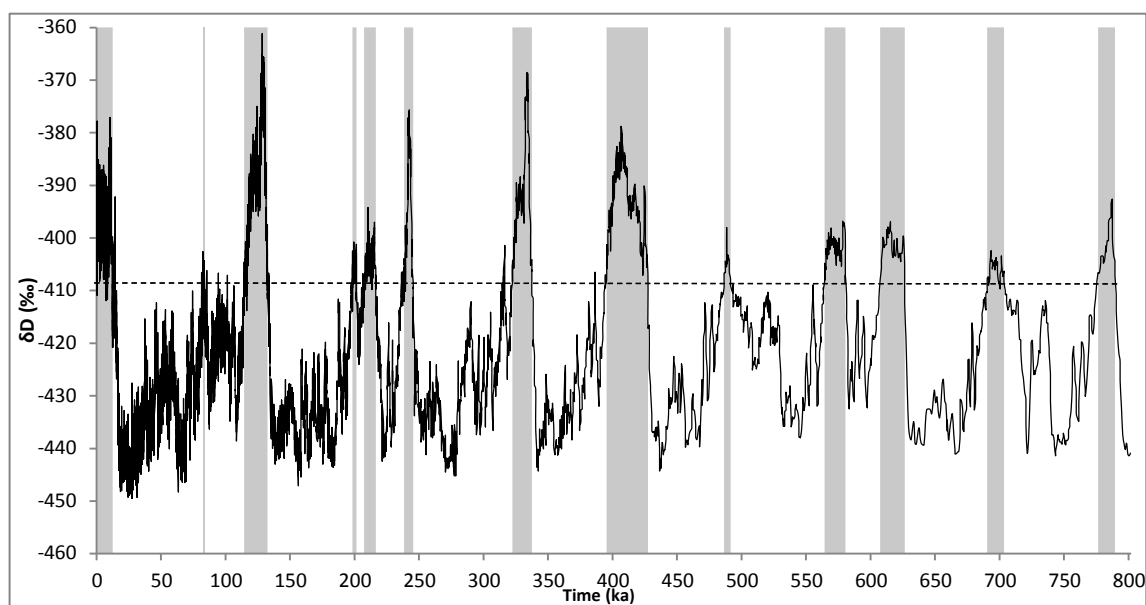


**Figure 2.5:**  $\delta$  deuterium concentration of EPICA Antarctic ice core (Jouzel *et al.*, 2007). Shaded regions highlight interglacial episodes, identified by Schilt *et al.* (2010) as where  $\delta D$  is greater than  $-408\text{‰}$ .

Isotopic curves derived from ice- and marine-cores show high similarity and allow direct comparison between the two archives, enhancing confidence in establishing the time and duration of past glacial and interglacial episodes. This relationship is highlighted in Figure 2.6 where the  $\delta D$  concentration from EPICA Dome C (Jouzel *et al.*, 2007) is compared with a global marine oxygen isotope record from Lisiecki and Raymo (2005).

Ice-cores may be the most direct and resolved records for use in reconstructing palaeoclimate conditions (EPICA community members, 2004). Ice preserves the record of past climates with fine temporal resolution and can provide a greater opportunity to resolve short-term climate changes than is possible with marine sediment records (Murray-Wallace, 2007). Dansgaard-Oeschger (D-O) events, which have an average period of approximately 1460 years and typical amplitude of  $\sim 50 - 70\%$  of a full glacial-interglacial range, have been associated with changes in  $\delta^{18}O$  in the Greenland ice core (Dansgaard *et al.*, 1993). D-O events may result in sea-level changes of several metres, and while present within the ice-core record, they are undetectable within marine-cores, possibly due to the effects of bioturbation and the resolution of sampling.

### **Summary**

Ice-cores can aid in reconstructing the duration of interglacials; as indicated by the  $\delta D$  record in Figure 2.5, Marine Isotope Stage (MIS) 11 appears longer in its duration than any of the past 9 interglacials. Ice-core records also aid in palaeoclimatic reconstructions. For example, MIS 5e (Figure 2.5), is shown to have reached higher temperatures (Jouzel *et al.*, 2007) than the other interglacials and was therefore perhaps more intense than other episodes (Masson-Delmotte *et al.*, 2010). However, while ice-cores provide a diverse record of palaeoclimate, potentially spanning much of the Quaternary period, they do not provide a direct marker of interglacial or glacial sea-level variation.

While, the records derived from ice-cores will not be able to aid in determining sea-level elevation during interglacial highstands on the Mount Gambier coastal plain, they can aid in constraining the timing, duration and intensity of interglacials. The ice-core record provides continuous information on palaeoclimate from around the globe during the Quaternary and these data may be used to compare differences observed in interglacial sea-levels.

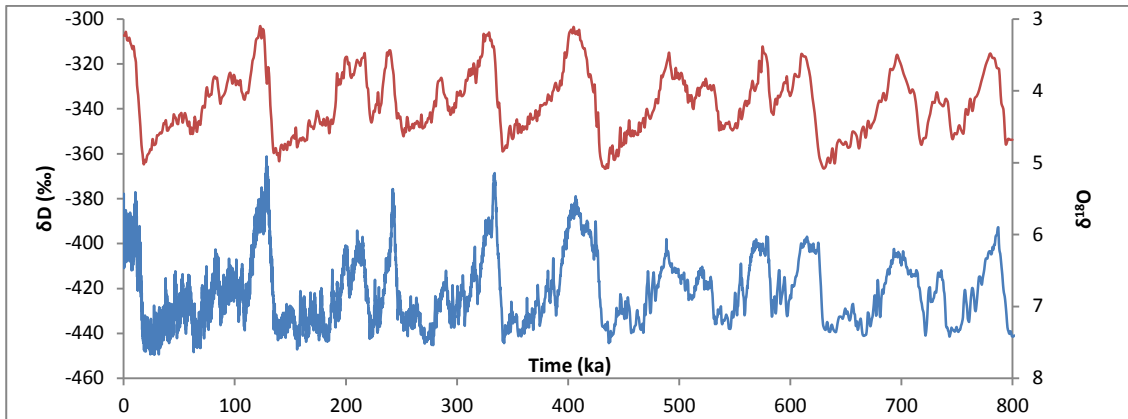


**Figure 2.6:** Comparison of EPICA Dome C  $\delta D$  record (blue line) from Jouzel *et al.* (2007) with that of the benthic oxygen isotope record (red line) from Lisiecki and Raymo (2005).

### 2.3.3 Geomorphological record

Sea level has fluctuated globally as a result of the waxing and waning of continental ice sheets throughout the Quaternary. Evidence of these fluctuations can be found within the geomorphological record where sea level has actively marked its extent along the coastline in physical features such as coral reef tracts, barrier shorelines, uplifted erosional marine terraces, and depositional and erosional features in sand-dominated systems.

Evidence of previous interglacial sea-level highstands is commonly best preserved on tectonically uplifting coastlines, where markers of highstand events are clearly separated from one another, with older deposits found at higher elevations. In rapidly uplifting areas, such as New Guinea, interstadial sea-level highstands (where sea level was lower than in interglacials but significantly higher than during glacials) may also be preserved. Certain corals grow at a known depth below sea level and therefore act as sensitive sea-level indicators. Fairbanks (1989) used fossil corals on the island of Barbados to study meltwater pulses associated with the Younger Dryas; a significant meltwater phase at approximately 11 ka. By examining the coral *Acropora palmata*, which is restricted to the upper 5 m of ocean water depth, Fairbanks (1989) suggested that sea-level rise after the last glacial occurred in two distinct steps. In this regard, uplifted coral reefs may be described as a continuous tape measure, with each coral reef crest representing a peak of sea-level transgression (Pirazzoli, 1993). Uplifted coral reef terraces associated with palaeo-sea level have been studied at several localities around the world including most notably on the Huon Peninsula, Papua New Guinea (e.g. Chappell, 1974a), and the island of Barbados (e.g. Broecker *et al.*, 1968).

Global sea-level variation may also be deduced from the study of uplifted or submerged ancient shorelines (Pirazzoli, 1996). Stratigraphical analysis of facies architecture of uplifted coastal deposits can aid in the detection of palaeo-sea level elevation. Palaeo-sea

level may be marked by geomorphological indicators of coastal processes that have left certain features associated with contemporary sea-level position (Pirazzoli, 2007). These marks include erosional indicators such as; wave cut notches, erosion platforms with palaeo-sea cliffs at their landward margins, beaches, tafoni, caves, arches and grooves, while depositional indicators include marine terraces, coral conglomerates and speleothems (Pirazzoli, 2007). Sedimentary markers of palaeo-sea-level include gravel and boulder beaches and beachrock (Cooper, 2007). Identification of macro- and microfossils within coastal deposits (such as marine molluscs and/or foraminifera) can aid in reconstructing depositional environments and determining palaeo-sea level when the vertical ranges of such organisms in the modern-tidal environment can be compared with their fossil counterparts (Gehrels, 2007). Chappell (1987) suggested that sea-level indicators within the geomorphological record fall within two categories; those which always form at a fixed elevation to tidal datum and those which fall above or below tidal datum. These are labelled fixed and relative indicators respectively.

Rapidly growing corals, such as *Acropora palmata* in the Caribbean, 'keep up' with sea level as it rises and therefore can record the early portion of an interglacial. Erosional marine terraces are modified throughout the early part of an interglacial with bench-cutting and sea cliff retreat. Therefore, fossils left behind on such terraces may record the later part of an interglacial, yet both of these can be classed as 'fixed' indicators.

Many regional factors are superimposed upon the ice volume signal of sea level, such as uplift and subsidence of coastal areas associated with glacial- and hydro-isostasy, while tectonic processes also complicate palaeo-sea level interpretations. Therefore, no single value of sea level at one specific locality can be representative of sea level at all sites around the globe. As ice sheets melt, a spatial surface variation within the ocean is formed as different parts of the oceanic floor and continental land surface deform under time-dependent water and ice loads, referred to as glacio-hydro-isostatic contributions to sea level (Lambeck and Chappell, 2001). Lambeck and Nakada (1992) addressed the concept of the isostatic response of the lithosphere and the mantle to changes in ice volume and water loading and unloading. The influence of glacio-hydro-isostatic effects varies in relation to proximity to former continental ice sheets. Near to glaciated areas, glacio-isostatic processes are a dominant factor controlling local sea level during and after glaciation. As the ice melts the coastline is elevated due to the reduced weight on the continent resulting in a relative drop in sea level (Lambeck and Chappell, 2001). During glaciation the mantle beneath a mass of ice will flow outwards towards the perimeter of the ice, creating a bulge (Figure 2.7). When the ice begins

to melt, the mantle returns to its original position and the bulge subsides, thus resulting in relative sea-level rise once melting has ceased. As the ice retreats, the originally lowered land surface beneath the ice rebounds and thus, in coastal areas in close proximity to ice sheets, relative sea-level lowering is experienced during deglaciation.

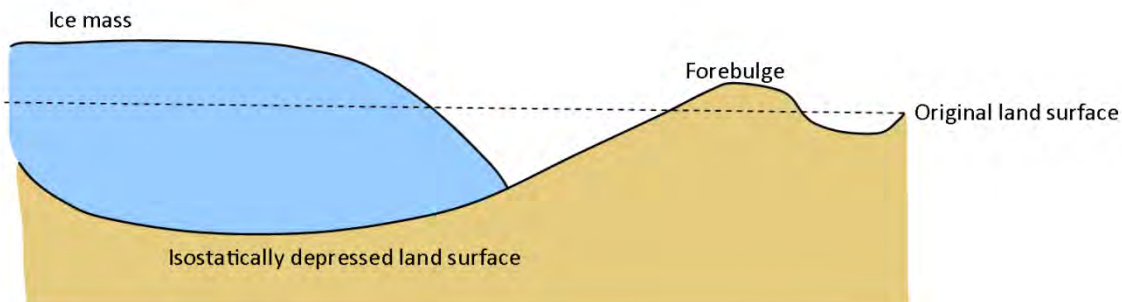


**Figure 2.7:** Illustration of isostatically depressed land surface.

Regions around the world can be classified into near-field, intermediate-field, and far-field zones based on their distance from former glaciated areas. This thesis adopts the zonation proposed by Clark *et al.* (1978), and is highlighted in Figure 2.8, with zone 1 being closest to glaciated regions and zone 5 being the farthest away. While Clark *et al.* (1978) used these zones as post glacial markers they also directly relate to previous glacial cycles.

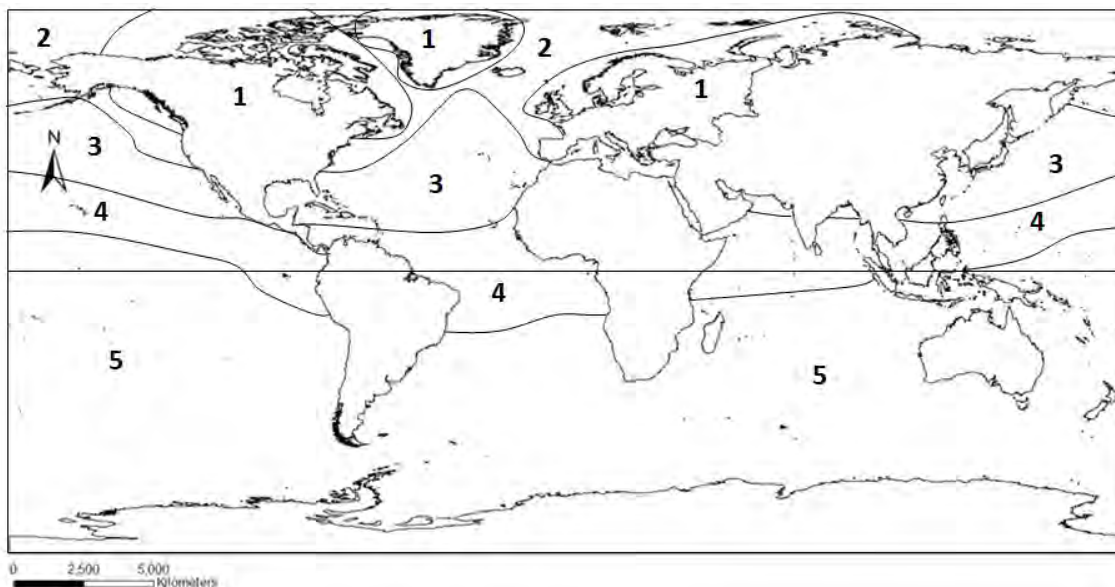


**Figure 2.8:** Zonation of global shorelines relative to former areas of continental glaciation (Zonation follows that of Clark *et al.*, 1978). World continents Copyright ESRI (2002).



In far-field sites (zones 4 and 5), considerable distances from former glaciated regions, sea level is thought to be primarily eustatic and controlled mostly by the volume of water in the ocean; directly influenced by the volume of ice sheet melt. However, loading (during deglaciation) and unloading (during glaciation) of water into the ocean can also create subsidence and rebounding of the ocean floor respectively. These hydro-isostatic effects may vary spatially with contrasting continental shelf width at different locations resulting in local sea-level variations as the mantle beneath readjusts to fluctuating water volumes.

The surface of the ocean is not a regular surface but is of a complex configuration known as the geoid. The height of the sea surface corresponds to the equipotential surface, the effects of tides and currents and other sea level anomalies (Murray-Wallace and Woodroffe, 2014). Several significant anomalies in the geoid are associated with volcanic plateaus, deep seafloors and hotspot swells (Caznave *et al.*, 1988) as well as oceanic islands (Woodroffe *et al.*, 2012). Therefore, the differences in geoid should be accounted for when assessing palaeo-sea level in near and far field sites.

Unlike the marine- and ice-core record, evidence of palaeoclimate and associated sea-level within morphological archives is not commonly preserved over the majority of the Quaternary. The advance and retreat of subsequent ice sheets and shorelines has effectively eroded previous indications and records of palaeo-sea level. Early Pleistocene sea-level fluctuations were of a significantly smaller frequency and amplitude, as suggested by Shackleton and Opdyke (1973), and records of these are likely now submerged, if not eroded, by the ocean.

### **Summary**

In conclusion, several limitations are inherent in geomorphological evidence to analyse past sea level. When uplifted coral reefs and shorelines are used, it is commonly difficult to ascertain whether rates of uplift have been constant throughout time (Chappell and Veeh, 1978) and they are therefore sometimes assumed and extrapolated. The effects of isostasy and resulting variation in relative sea level need to also be accounted for in order to estimate accurately the change in sea level resulting from ice volume change alone. The effects of glacio-hydro-isostasy vary globally depending on the position of a shoreline in relation to former continental ice sheets, and thus it may be difficult to accurately compare sea level derived from one site with another. The exact relationship of a sea level indicator to a palaeo-sea level is commonly challenging to accurately ascertain. For example, a beach deposit may be within  $\pm 6$  m on a macro-tidal coast and will depend on the palaeo-tidal range. Different

species of coral reef will also grow at varying depths below the sea surface. The precision of geomorphological indicators of is therefore reliant on the accuracy of palaeo-environmental reconstruction. A further limitation of geomorphic sea-level indicators is that they are dependent on dating techniques and their associated drawbacks. The sea-level record derived from geomorphic evidence is not continuous throughout the Quaternary, as sea-level lowstands are commonly not preserved as they have been eroded by sequential highstands. Finally, due to the erosional effects of advancing ice and shorelines throughout the Quaternary it is commonly difficult to locate lengthy archives of Pleistocene palaeo-sea level.

As the Mount Gambier coastal plain preserves a geomorphological record of sea-level highstands in the form of successive barrier shorelines, knowledge of the advantages and limitations of such records can aid in determining the integrity of the derived results when comparing global archives. Familiarity with the impacts of the glacio-hydro-isostatic effects upon the southern Australian margin is required before determining the palaeo-sea level record from the Mount Gambier coastal plain.

## **2.4 Comparison of global interglacial sea-level records from different indicators**

To assess how the sea-level record preserved on the Mount Gambier coastal plain contributes to constraining the timing, duration and intensity of interglacial episodes, it is useful to view global interglacial sea-level literature derived from the range of interglacial indicators. The following section discusses middle to late Pleistocene interglacial sea-level records from: marine-cores such as SPECMAP; geomorphological records such as the coral reefs in Papua New Guinea, Barbados, the Bahamas and Japan; ice cores; and speleothem data. Interglacial palaeo-sea level has been reconstructed at numerous sites globally and from a range of records, yet there still remains a degree of variation in the estimated height and duration of former sea-level highstands. This section describes the salient details of several classic studies of palaeo-shoreline reconstruction and explores potential reasons for variation.

### 2.4.1 Marine-cores

#### The SPECMAP timescale

The SPECTral MAPPING Project (SPECMAP), conducted by Imbrie *et al.* (1984) attempted to create an orbitally tuned, standard chronology for marine oxygen isotope records. The oxygen isotope record from planktonic foraminifera within 5 rapidly accumulating deep sea cores (RC-11-120, V28-238, DSDP 502, V30-40, and V22-174) was amalgamated. A composite curve was constructed, smoothed, filtered and tuned to the calculated astronomical cycles (Figure 2.9).

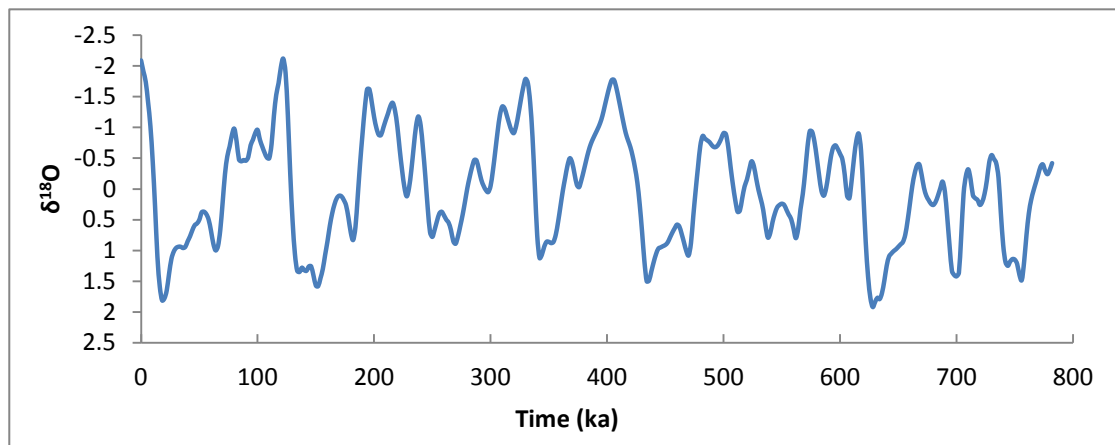


Figure 2.9: The SPECMAP marine isotopic curve (Imbrie *et al.*, 1984).

An advantage of the SPECMAP timescale is that it presents a global standard chronology and can be used as a parameter in defining isotopic stage boundaries. However, several researchers have found discrepancies with the timescale. Gallup *et al.* (1994) identified corals on Barbados that formed during the penultimate deglaciation (MIS 6). Through combined  $^{230}\text{Th}$  and  $^{231}\text{Pa}$  dating Gallup *et al.* (1994) suggested that sea level on Barbados had reached  $-18 \pm 3$  m below present, 80% of its rise from full glacial to full interglacial conditions, by 135 ka, while June insolation only peaked at 127 ka. Gallup *et al.* (2002) proposed that the Milankovitch orbital hypothesis cannot explain the termination of the penultimate glaciation, thus bringing into contention the timing of the penultimate glacial period as derived by the SPECMAP record.

A range of other studies have also suggested that the timing of the penultimate glaciation does not directly correspond with the June insolation record and, through the use of uranium-thorium dating, suggest this climatic change may have occurred up to 15 ka earlier. From aragonitic-rich sediments on the Bahamian slopes, Henderson and Slowey (2000) used uranium-thorium dating to determine the midpoint of the penultimate deglaciation to be  $135 \pm 2.5$  ka. Zhu *et al.* (1993) used thermal ionisation mass spectrometry (TIMS) U-series dating of

coral on the Houtman Abrolhos Islands, Western Australia, to suggest that sea level was 2 m above present sea level (APSL) at 133 ka, while from marine deposits on the island of Oahu, Hawaii, Szabo *et al.* (1994) used Th<sup>230</sup> dating to indicate sea level extended to 1-2 m APSL at 131 ka.

While these data sets question the orbitally tuned timing of glacial and interglacial episodes, there is a need to assess critically the validity of the ages derived from U-series dating. A significant assumption of uranium-series dating is that the dated material is a closed-system (Broecker, 1963). A common problem in the dating of coral reefs by uranium-series methods is that the back-calculated uranium isotope activity ratios ( $\delta^{234}\text{U}$ ) are frequently higher than sea water values (e.g. Bard *et al.*, 1991; Henderson *et al.*, 1993). The higher activity ratios are attributed to post-depositional diagenesis, whereby the fossil corals have not behaved as closed systems to uranium and thorium (e.g. Gallup *et al.*, 1994; Scholz *et al.*, 2004) and analyses may yield results with an older age. The accuracy of U-series derived ages is therefore limited more by isotopic anomalies than by analytical precision (Scholz *et al.*, 2004; Bard *et al.*, 2002).

Thompson and Goldstein (2006) attempted to resolve this problem and presented a sea-level reconstruction for the past 240 ka, derived from a selection of U-Th data across the Barbados coral dating literature, by correcting ages for bias imposed by open-system behaviour. Thompson and Goldstein (2006) suggested that their data are of sufficient resolution to be correlated to the marine oxygen isotope record. In regards to the significant differences illustrated between the radiometric and orbitally tuned timescales near the MIS 6/7 boundary, as highlighted by Gallup *et al.* (2002) and Henderson and Slowey (2000), Thompson and Goldstein (2006) suggested that their comparison of radiometric and SPECMAP ages of identical isotopic events illustrate that the SPECMAP timescale is quite accurate and that its errors have been overestimated.

The above discussion highlights significant issues in comparing records derived from a range of sources. While further screening of potential diagenetic influences on coral reefs are necessary, these older dates for the last interglacial sea-level highstand serve as a reminder of the need to further qualify the marine-derived oxygen isotope records. It is potentially necessary to verify both U-series and marine-based oxygen isotope records with additional data before they are used as robust estimates for the timing of glacial and interglacial episodes.

### Other oxygen isotope derived sea-level reconstructions

Martinson *et al.* (1987) constructed an orbitally tuned marine isotope timescale using the high resolution staked marine oxygen isotope stratigraphy of Pisias *et al.* (1984). Martinson *et al.* (1987) used four separate orbital tuning parameters to develop a high resolution, deep-sea chronology, spanning the last 300,000 years. They were able to develop a chronology from core RC11-120 from the southwest Indian Ocean that provided five climatically sensitive data sets: planktonic oxygen-isotope measurements; relative abundance of the radiolarian *Cycladophora davisiana*; summer sea surface temperature estimates; carbon isotope measurements; and calcium carbonate percentages. Similarities in peaks and troughs were found throughout each of these parameters, allowing Martinson *et al.* (1987) to test and improve orbital tuning approaches free from the bias of using only a solitary climate signal.

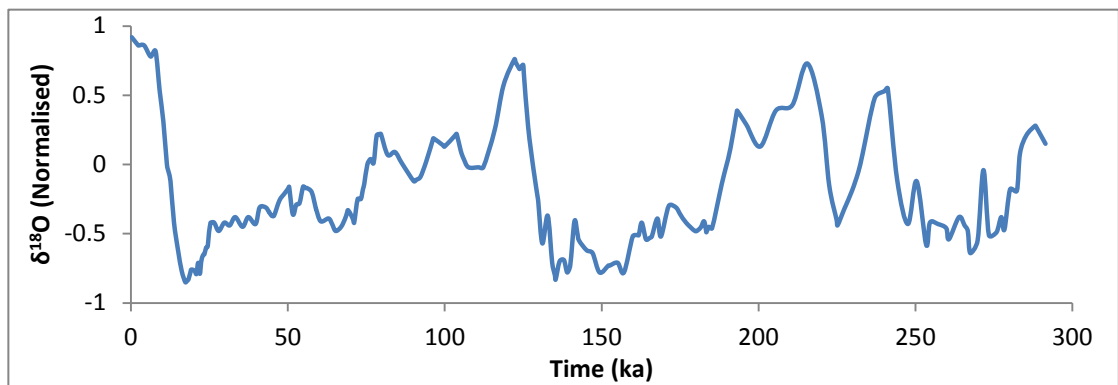


Figure 2.10: Orbitally-tuned marine oxygen isotope curve of Martinson *et al.* (1987).

Each of the four orbital tuning approaches was combined and an average was calculated (Figure 2.10). The final chronology has an average error of  $\pm 5$  ka. Age estimates from the final chronology were compared with a variety of estimates derived from radiometric techniques and found to agree well, and were comparable to the lower portion of the SPECMAP timescale (Martinson *et al.*, 1987). While the SPECMAP timescale (Imbrie *et al.*, 1984) spans over 800 ka, the timescale derived by Martinson *et al.* (1987) is of higher resolution and more applicable for younger datasets. Martinson *et al.* (1987) suggested that this chronology provides a globally representative climatic record, and is transferable to any other oxygen isotope record to aid in establishing a standard and consistent chronostratigraphy for comparing and evaluating individual time slices or entire archives.

Siddall *et al.* (2003) used oxygen isotope records from marine-cores within the Red Sea to reconstruct water residence times over the past 470 ka. The Red Sea is highly evaporative and changes in residency time of the water are reflected by oxygen isotope records. As sea level falls, salinity values in the Red Sea increase and the basin becomes relatively enriched

with  $\delta^{18}\text{O}$  (Rohling *et al.*, 1998; Siddall *et al.*, 2003). By using a hydraulic model of water exchange between the Red Sea and the world ocean Siddall *et al.* (2003) were able to derive the sill depth, and thus reconstruct a local sea level over the last glacial cycle. They found that sea level could change at rates of  $2 \text{ cm yr}^{-1}$ . Siddall *et al.* (2003) suggested that their reconstruction was accurate to  $\pm 12 \text{ m}$  and agrees well with fossil reef data from the Huon Peninsula, Papua New Guinea. Rohling *et al.* (2009) further constrained the Red Sea sea-level chronology record through graphic correlation to the EPICA Dome C ice core Antarctic temperature record of Jouzel *et al.* (2007).

#### **2.4.2 Ice-cores**

Shackleton (2000) derived global sea-level variations from the record of  $\delta^{18}\text{O}$  trapped within atmospheric air bubbles ( $\delta^{18}\text{O}_{\text{atm}}$ ) in the Vostok ice core presented by Petit *et al.* (1999). The  $\delta^{18}\text{O}$  content of the atmosphere differs from that of marine water, due to a relative enrichment of  $^{18}\text{O}$  in the atmosphere primarily as a result of the preferential absorption of  $^{16}\text{O}$  by most species. The difference between  $\delta^{18}\text{O}_{\text{atm}}$  and  $\delta^{18}\text{O}$  of seawater ( $\delta^{18}\text{O}_{\text{sw}}$ ) is known as the Dole effect, and has a present day value of  $\sim 23.5\text{‰}$  (Kroopnick and Craig, 1972).  $\delta^{18}\text{O}_{\text{atm}}$  is thus determined by complex fractionation processes occurring during photosynthesis and respiration.

Shackleton (2000) argued that the record of  $\delta^{18}\text{O}_{\text{atm}}$  within ice-cores must therefore reflect changes in  $\delta^{18}\text{O}_{\text{sw}}$ , with a small delay controlled by the balance between the rate of global photosynthesis and the atmospheric oxygen reservoir estimated to have a turnover time of approximately 1 ka (Bender *et al.*, 1994). Shackleton (2000) then orbitally tuned the  $\delta^{18}\text{O}_{\text{atm}}$  record by assuming that its phase, relative to the precession cycle and insolation changes, was constant and that change in the Dole effect could be linearly related to orbital parameters. Jouzel *et al.* (2002) suggested that this was a significant simplification of highly complex processes.

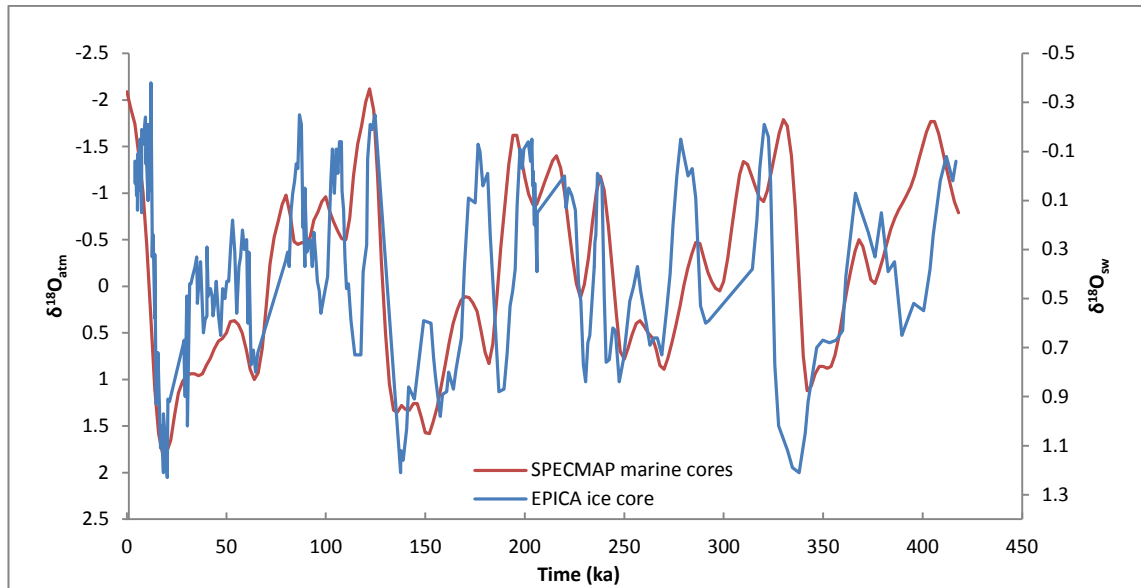


**Figure 2.11:** Comparison of the  $\delta^{18}\text{O}$  record from air trapped within the EPICA ice core (Petit *et al.*, 1999) with the  $\delta^{18}\text{O}$  record from the SPECMAP timescale (Imbrie *et al.*, 1984).

Problems with ice-core palaeo-reconstruction are also experienced in dating the ice core itself. The location of the Vostok drilling station in East Antarctica, for example, is not situated on a dome. Therefore, ice found at depth within the core has not been deposited *in situ*, but would have been deposited farther upslope and flowed to this location, thus seriously complicating the estimation of accumulation rates (Jouzel *et al.*, 2002). Problems are also associated with the weight of the overlying ice distorting the record at depth. Determining sea level from ice cores may prove challenging, yet the palaeoclimatic records derived from such archives are important for determining ice sheet stability and can potentially account for differences in sea-level elevation and highstand duration between interglacials.

### 2.4.3 Tectonically uplifted coral reefs

Coral reefs are excellent indicators of sea level as they commonly grow at confined water depths. When this depth is known the sea level at their time of growth can be calculated. On tectonically uplifted coastlines, coral reef terraces that formed during subsequent highstands may be vertically separated from one another, allowing for the dating of these highstand events. Many significant sea-level archives are preserved in uplifted fossil coral reefs and the findings of some of these studies are discussed here and will be later compared with results derived from this thesis (Chapter 6).

### **Huon Peninsula, Papua New Guinea**

The Huon Peninsula represents one of the most detailed archives of eustatic sea-level change throughout the Quaternary, as the emergent fringing reef terraces preserve evidence of multiple interglacial and later interstadial sea-level highstands. The Huon Peninsula lies within the collision zone between the advancing Pacific and Indo-Australian plates and is thus subject to continuous tectonic influences resulting in steady uplift of the area. The uplifted coral terraces have developed for more than 80 km along the coastline and rise to more than 1000 m in height (Chappell, 1974a). Each reef terrace developed when sea level was rising at a greater rate than the land was uplifting, and thus each reef crest represents the approximate peaks of each sea-level transgression (Chappell and Shackleton, 1986). High rates of uplift in the area result in reef crests lying above present sea level, with each reef crest topographically higher than those formed in the subsequent highstand. Due to the equatorial location of Papua New Guinea, a considerable distance from former ice sheets (Figure 2.8), the documented sea level may be regarded as eustatic once tectonic uplift has been accounted for.

Through facies analysis of coral reefs and assessment of U-series chronologies (Veeh and Chappell, 1970; Bloom *et al.*, 1974), Chappell (1974a) was able to identify past sea-level maxima at 30, 40-50, 60, 80, 105, 120, 140, 185 and 220 ka, which he noted compared well with Emiliani's (1955) sea-level curve. The reef sequences on the Huon Peninsula have been illustrated to support Milankovitch's (1941) astronomical cycles (Veeh and Chappell, 1970; Aharon, 1983; 1984), and the sea-level record is suggested to be synchronous with precessional changes in solar radiation at times when orbital eccentricity was largest (Chappell, 1974b). Chappell and Shackleton (1986) correlated the Huon Peninsula reef record with marine-core V19-30 in the Pacific and indicated that both revealed a common ice-volume signal.

The archive of sea-level change on the Huon Peninsula has been shown to be highly sensitive to fluctuations in ocean surface elevation. Short-term sea-level changes such as Dansgaard-Osleger (D-O) events (Chappell, 2002); Heinrich events from the North Atlantic (Yokoyama *et al.*, 2001); and meltwater pulses associated with the Younger Dryas (Chappell and Polach, 1991) have been correlated with certain coral reef crests on the Huon Peninsula. Six episodes of sea-level rise and fall between 9 and 20 m, up to 1-2 ka in duration, have been identified between 65 and 3 ka and are proposed to correlate to the Heinrich events in the North Atlantic (Chappell, 2002).



Chappell (2002) noted that the sea-level highstands at 38, 44.5 and 52 ka coincided with D-O interstadials 8, 12 and 14, while Heinrich events 4, 5 and 5.2 were identified during sea-level transgressions. The representation of these minor fluctuations within the Huon Peninsula coral reef archive highlights the acute sensitivity of this record that is commonly unseen within composite marine-cores.

Discrepancies with the sea-level record derived from the Huon Peninsula may be related to errors in U-series dating as previously outlined or due to assumptions in the tectonic uplift of the region.

### **Barbados**

The island of Barbados, located in the Caribbean Sea, is another classic example of palaeo-shoreline reconstruction in response to Quaternary sea-level changes. Barbados, a fore-arc ridge, formed as the North American plate subducted underneath the Caribbean plate resulting in large volumes of sedimentation and the formation of an accretionary prism (Schellmann and Radtke, 2004). As the island emerged during the Pleistocene the coralline limestone formed a series of fringing reefs. The uplift rate of the island has been rapid enough to separate the coral terraces formed at successive sea-level highstands (Broecker *et al.*, 1968). While Barbados lies within the intermediate zone from former continental ice sheets (zone 3/4), Peltier (2002) suggested that the island is not influenced by glacio- or hydro-isostatic effects and therefore records of palaeo-sea level should correlate to ice-equivalent eustatic values (Schellmann and Radtke, 2004).

Mesolella *et al.* (1969) identified 19 exposures of reef tracts on the island, with higher reefs proving to be older in age. Broecker *et al.* (1968) documented three distinct highstands during the last interglacial *sensu lato*; the first at 122 ka with an assumed sea-level elevation of 6 m APSL, one at 103 ka and a final one at 82 ka with sea level approximately 13 m below present sea level (BPSL). Combined with the Holocene sea-level highstand, Broecker *et al.* (1968) suggested that these four highstands correlated with the last four prominent warm peaks (at 126, 103, 82, and 10 ka) in the summer insolation curve and thus supported the Milankovitch hypothesis. Gallup *et al.* (1994) also noted that during the last three interglacial and two intervening interstadial episodes on Barbados, sea level peaked at or after summer insolation maxima in the Northern Hemisphere, which further supports the orbital-driven timing of interglacials.

More recently the uplifted reefs on Barbados have been studied using electron spin resonance (ESR) and U-series dating to provide an improved reconstruction of glacio-eustatic

sea-level (Schellmann and Radtke, 2004). Schellmann and Radtke (2004) calculated Quaternary sea-level on Barbados by using the globally recognised sea level datum of 6 m APSL for the last interglacial highstand. Using this figure to calculate an uplift rate, and assuming it has been constant through time, they suggested that sea-level would have extended to 8 m and 18 m APSL for MIS 9 and 11 respectively, much higher than had previously been predicted for these episodes by marine core oxygen isotope analysis (e.g. Imbrie *et al.*, 1984). However, by substituting the 6 m value with a sea-level more similar to that of present, their sea-level reconstructions produced elevations similar or slightly below present for the previous four interglacials in Barbados (Schellmann and Radtke, 2004). Through their extensive dating of the raised fossil corals on Barbados, Schellmann and Radtke (2004) suggested the sea level had oscillated in a more complex fashion than previously thought in the past 400 ka, with several sub-stage elevations identified during MIS 5a, 5c, 7a and 7c.

Sea-level highstands at ~200 ka, ~120 ka, ~100 ka and ~80 ka have been observed on both the Barbados and the Huon Peninsula coral records (Mesolella *et al.*, 1969; Bloom *et al.*, 1974; Chappell, 1974a) and this demonstrates that sea-level change over the Quaternary at these two sites is an expression of global-eustatic processes.

#### **Ryukyu Islands, Japan**

The Ryukyu Islands lie to the southwest of Japan in a curved formation known as the Ryukyu Arc and well-developed fringing coral reefs surround most of the islands (Sugihara *et al.*, 2004). Nakamori *et al.* (1995) identified a range of facies within the coral thought to be controlled by sea-level rise throughout the Pleistocene. Corals on Kikai Island in the central Ryukyus have been correlated with reef terraces on the Huon Peninsula which relate to sea-level highstands at ~55, 62 and 66 ka (Sasaki *et al.*, 2004) and ~80 and ~100 ka (Ota and Omura, 1992).

#### **Timor and Atauro Island**

Chappell and Veeh (1978) identified sets of raised coral terraces on the northern coast of East Timor and Atauro Island, which they attributed to past sea-level highstands. Through the use of  $^{230}\text{Th}/^{234}\text{U}$  dating, Chappell and Veeh (1978) were able to date three reef terraces to 84, 105 and 120 ka which correlate well with MIS 5a, 5c and 5e respectively. By calculating uplift rates on the island, and assuming these rates had been constant Chappell and Veeh (1978) determined that sea level reached -20 m at 84 ka, -14 m at 105 ka and +6.5 m during the last interglacial *sensu stricto* at 120 ka. These findings closely correspond with data from both Barbados and the Huon Peninsula.

#### **2.4.4 Shoreline barriers and coastal deposits**

Geomorphological indicators that document the presence of palaeo-shorelines can be identified through the analysis of facies architecture of coastal deposits, usually best preserved in tectonically uplifted areas where deposits are protected from the erosive forces of subsequent sea-level highstands. Detailed analysis and identification of facies can determine the depositional environment of the sediment and lead to the detection of palaeo-sea level elevation (the identification of these facies will be detailed further in Chapter 3). A range of classic palaeo-shoreline studies are presented here and can be used to directly compare with the sea-level data derived from geomorphological evidence reported within this thesis.

##### **Bahamas**

Certain geomorphological features found on the Bahamian Islands are thought to be the product of sea-level changes throughout the Late Quaternary (e.g. Garrett and Gould, 1984). Accelerated rates of carbonate sedimentation have been correlated to sea-level rise above the shelf margin.

The tectonic stability of the Bahamas islands has been debated (Kindler *et al.*, 2007 and references therein). Certain researchers have suggested that the entire Bahamian archipelago behaved as a single, stable tectonic entity throughout the Late Quaternary (Carew and Mylroie, 1995), while others have suggested that its proximity to a plate boundary results in the islands being tectonically active (e.g. Mullins *et al.*, 1991). Hearty (1998) discounted tectonic uplift as a factor attributing to relative sea-level change on the Bahamas for two reasons: the good concordance of interglacial sea-level highstands between the Bahamas and Bermuda; and the absence of historical earthquake activity within the region. Accurate assessment of this tectonic setting is required to determine whether measured elevation of such indicators is the direct response of elevated sea-level.

Hearty (1998) analysed eight palaeosol-limestone parasequences on the island of Eleuthera. Hearty suggested that enhanced carbonate deposits were deposited during interglacials while the bands of *terra rossa* soils are indicative of reduced sedimentation rates in glacial times. Through the use of amino acid racemisation (AAR) Hearty (1998) correlated these carbonate deposits with previous interglacials from MIS 1 to 13 and recognised sea-level highstands at +2, 7 and 20 m APSL which he suggested were formed during MIS 9/11. Hearty *et al.* (1999) suggested that for a +20 m increase in sea level on Eleuthera, the entire Greenland and West Antarctic ice sheets would have had to melt, as well as a portion of the East Antarctic ice sheet. The abnormally high sea level proposed for the Bahamas during MIS

11 has sparked controversy. Mylroie (2008) suggested that the high carbonate deposits on Eleuthera are the result of storm events and not sustained sea-level highstands. Identification of the MIS 11 highstand on the Mount Gambier coastal plain, a relatively stable site (due to slow epeirogenic uplift over the last 1 Ma at a rate of  $0.13 \text{ mm yr}^{-1}$ ), located far from Quaternary ice sheets, could aid in constraining sea level during this time.

### **Italy**

Ferranti *et al.* (2006) assessed tectonic displacement along the Italian coastline by identifying elevation of the last interglacial *sensu stricto* shoreline. Morphological indicators were used to recognise palaeo-shoreline deposits and included the identification of: lagoonal, beach and foreshore deposits; erosional markings such as marine terraces and tidal notches; and biological indicators including certain faunal and floral assemblages (Ferranti *et al.* 2006). Ferranti *et al.* (2006) illustrated the significant difference in elevation between last interglacial shorelines along the Italian coastline and suggested that the best reference of eustatic sea-level height for the Mediterranean was found on the Sardinian coast where MIS 5 sea level was recorded at  $6 \pm 3 \text{ m APSL}$ .

### **2.4.5 Flowstones / Speleothems**

In regions geologically dominated by limestone, caves are common features. Within these caves precipitation of carbonate can occur from dripping water, forming speleothems such as flowstones, stalagmites and stalactites. These deposits can be used in sea-level reconstruction studies as their growth only occurs during vadose conditions, and thus significant hiatuses in calcite deposition represent episodes of sea-level highstands when caves are located below sea level. While these deposits cannot determine the maximum height of interglacial sea-level they provide valuable records to constrain the timing of these episodes. Two studies using speleothem records are presented here and their records of sea-level highstands will later be correlated with results from the Mount Gambier coastal plain (section 6.6).

### **Lucayan Cave, Bahamas**

A speleothem within the Lucayan Caverns on Grand Bahama Island has been studied to identify sea-level fluctuation between -10 and -15 m (which is significantly higher than glacial sea level) over the past 300 ka (Lundberg and Ford, 1994). During times of lower sea level, caves on the island would have experienced vadose conditions and promoted the deposition of calcite stalactites, stalagmites and flowstones. Rising sea level would have interrupted the growth of the speleothems and these hiatuses in calcite deposition are marked by some erosion of the preceding calcite layer and deposition of a fine layer of mud (Lundberg and Ford,

1994). Through U-series dating Lundberg and Ford (1994) recognised sea-level highstands at 233, 215, 125 and 100 ka which correlate well with the orbitally tuned marine isotope record.

#### **Argentarola Cave, Italy**

Uranium-thorium dating of a stalagmite within the Argentarola Cave, central Italy, has aided in constraining the age, duration and elevation of sea-level highstands (Bard *et al.*, 2002). At times of higher sea-level the coastal cave would have flooded and thick marine crusts of calcitic tubes formed by marine worms were deposited on speleothems within the cave that had formed previously. In glacial episodes speleothem calcite would be deposited. From U-Th analysis of speleothems, along a tectonically stable portion of the Italian coast, Bard *et al.* (2002) identified a sea-level highstand associated with MIS 7a at 202-190 ka, and when compared with the flowstone from Grand Bahama Island (Lundberg and Ford, 1994) suggested that global sea level at this time was likely between -18 and -19 m BPSL.

#### **2.4.6 Potential reasons for variation in local sea-level reconstructions**

As previously mentioned different techniques of interglacial sea-level assessment have significant strengths and weaknesses, which must be considered when comparing records derived from a range of sources. Interglacial climates have been shown to vary over the past 800 ka, with some interglacial episodes experiencing a single sea-level highstand associated with one peak of interglacial intensity (e.g. MIS 11), while others may experience two or three peaks (MIS 9, MIS 7, MIS 5) associated with interstadial intervals (Table 2.2). For example, the last interglacial *sensu lato* (MIS 5) comprises three peaks in ice volume/sea level; the last interglacial maximum ~125 ka, whereby sea level was as high or above present, followed by two interstadials MIS 5c (~105 ka), and MIS 5a (~82 ka), where sea level was considerably lower than today, but significantly higher than in glacials. Some archives of palaeo-sea level contain evidence of multiple peaks during the last interglacial, while others do not. This may be because of the precision obtained from specific types of deposit of sea-level records.

The variation in sea-level elevation at certain sites around the world is highlighted in Table 2.2 and Figures 2.12 and 2.13. Some variation may be derived from comparing sea level obtained from different sources. This section discusses other potential reasons for variation in sea-level reconstructions including: differences in palaeo-temperature between interglacials; different glacio- and hydro-isostatic effects between regions; and tectonic stability. It is important to be aware of reasons for sea-level elevation variation when comparing sea level data derived from the Mount Gambier coastal plain with other records from around the world.

**Table 2.2:** Comparison of palaeo-sea level reconstructions around the globe for the past four interglacials

MIS	Sea level height	Date of sample	Dating method	Location	Corresponding zone in relation to former ice sheets	Found by whom?
11	+20 ± 3 m		AAR dating	Government Quarry, Bermuda. Beach sediments found in a sea cave	3	Hearty <i>et al.</i> (1999)
	+21.3 m	399±11 ka	AAR dating	Calonectris Quarry, Bermuda	3	Olson and Hearty (2009)
	+2m, +7.5m and +21 m	At or before 420±30 ka	AAR dating	Eleuthera, Bahamas. Beach deposits along middle Pleistocene cliffs	3	Hearty (1998)
	-9.0 to -5.5 m	>400 ka	U-series dating of unconformity surface	Ironshore Formation, Grand Cayman, West Indies	3	Vezina <i>et al.</i> (1999)
	As high or above modern sea level	418-400 ka	Oxygen isotope analysis	Cariaco Basin		Poore and Dowsett (2001)
9	-8 to +18 m	398-410 ka	ESR of coral reefs	Barbados	3/4	Schellmann and Radtke (2004)
	-3 m	420ka	Thermoluminescence dating	East Avenue Range, Coorong Coastal Plain, S. Australia	5	Murray-Wallace (2002)
	+4 m	339-303 ka	U-series, AAR, ESR and palaeomagnetism	Palaeosol and limestone sequences in Bermuda and Bahamas	3	Hearty and Kindler (1995)
	-3 to +0.5 m	~346 ka	Th/U series dating	Ironshore Formation, Grand Cayman, West Indies	3	Vezina <i>et al.</i> (1999)
	-1 m	350ka	TL and AAR dating	West Avenue Range, Coorong Coastal Plain, S. Australia	5	Murray-Wallace (2002)
7	-3 to +8 m	300-384 ka	ESR of coral reefs	Barbados	3/4	Schellmann and Radtke (2004)
	-6 to +9 m	193 to 201 ka	<sup>234</sup> U/ <sup>238</sup> U	Barbados	3/4	Gallup <i>et al.</i> (1994)
	-2.5 to +1.1 m	~229ka	Th/U series dating	Ironshore Formation, Grand Cayman, West Indies	3	Vezina <i>et al.</i> (1999)
	-18 to -9 m	3 substages; 195, 216 and 238 ka	U-Th dating – TIMS of submerged speleothem	Argentrola Cave, Italy	2	Bard <i>et al.</i> (2002)
	<-5 to +1 m	>204 ka	ESR of coral reefs	Barbados	3/4	Schellmann and Radtke (2004)
5	Near or slightly above present	~200 ka	U-series	Florida Keys	3	Muhs <i>et al.</i> (2011)
	-11 to -18 m	212 ± 5 and 227 ± 6.5 ka	U-Th	Mururoa atoll, French Polynesia	5	Camoin <i>et al.</i> (2001)
	-3.3 to +2.3 m	~200 ka	U-series	Cortalein unit, Lower Terrace, Curaçao, Leeward Antilles islands	4	Muhs <i>et al.</i> (2012a)
	-6 m	250 ka (MIS 7e)	TL and AAR dating	Reedy Creek Formation, Coorong Coastal Plain, South Australia	5	Murray-Wallace (2002)
	0 m	200 ka (MIS 7a)		Dairy Creek Formation, Coorong Coastal Plain, South Australia		
5	+3 m	128±1 to 116±1ka	U – series dating	Western Australia	5	Stirling <i>et al.</i> (1998)
	0 to +6 m*	74-132 ka	ESR of coral reefs	Barbados	3/4	Schellmann and Radtke (2004)
	+5 to +8 m	5e	Oxygen isotope analysis of Giant Clam <i>Tridacna gigas</i> within reef	Huon Peninsula	5	Aharon (1983)
	-13 to -14 m	5c and 5a	<sup>230</sup> T/ <sup>234</sup> U dating	Barbados	3/4	Broecker <i>et al.</i> (1968)
	+6 m*	122 ka				
	Below -13 m	103 and 82 ka				
	+2.5 m	132 – 125 ka	AAR dating	Bahamas	3/4	Hearty and Neumann (2001) and Neumann and Hearty (1996)
	+6 to +8.5 m	118 ka				
	+2.5 to +6 m	~131 ka	Th/U series dating	Ironshore Formation, Grand Cayman, West Indies	3	Vezina <i>et al.</i> (1999)
	+6 m*	124 ka	Th/U series dating	Uplifted coral reefs, Papua New Guinea	5	Chappell and Shackleton (1986)
	-9 ± 3 m	100 ka				
	-19 ± 5 m	81 ka				
	+5 m	130.5 ± 5	U-series dating	Uplifted coral reefs, North-western Peninsula of Haiti	3	Dumas <i>et al.</i> (2006)
	-8 m	107.3 ± 5				
	-11 m	82.6 ± 2 ka				
	+2 to 8 m*	120 -130 ka	U-series dating	Coral terraces, Barbados	3/4	Gallup <i>et al.</i> (1994)
	-12 to -17 m	104 ka				
	-13 to -18 m	83.3 ± 0.3 ka				
	+2m	125ka (MIS 5e)	TL and AAR dating	Woakwine I Range, Coorong Coastal Plain, S. Australia	5	Murray-Wallace (2002)
	-9m	105ka (MIS 5c)		Robe III Range, Coorong Coastal Plain, S. Australia		

\*Assumed values derived from other regions that researchers have used to calculate uplift rates for other highstands

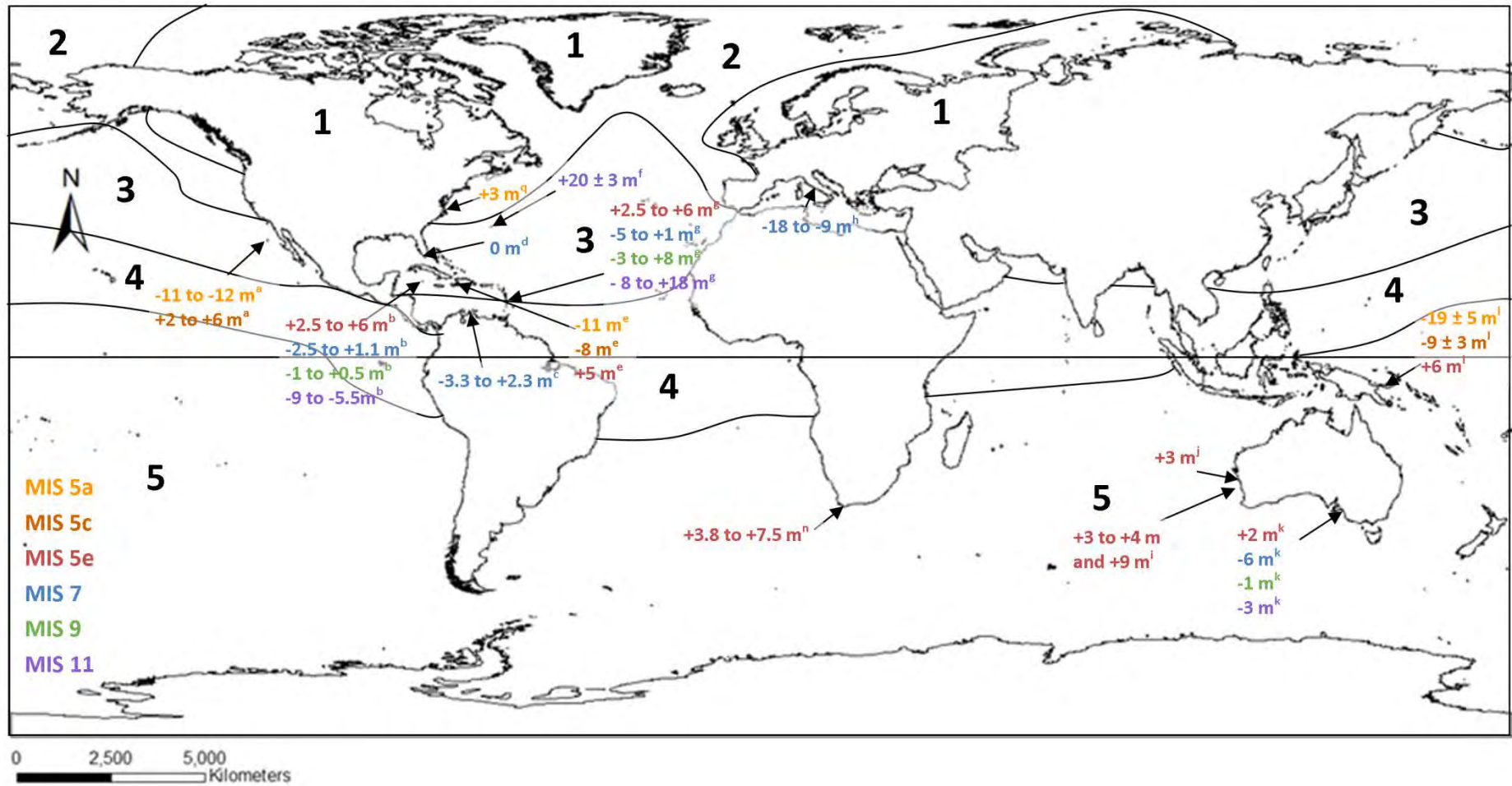


**Figure 2.12:** Global interglacial sea level from a variety of sources listed in Table 2.2 plotted in regards to zonation from former Quaternary ice sheets after Clark *et al.* (1978). <sup>a</sup>San Nicolas Island, California, Muhs *et al.* (2012a); <sup>b</sup>Ironshore Formation, Grand Cayman Island, Vezina *et al.*, (1999); <sup>c</sup>Curaçao, Leeward Antilles Islands, Muhs *et al.* (2012a); <sup>d</sup>Florida Keys, Muhs *et al.* (2011); <sup>e</sup>North-western Peninsula, Haiti, Dumas *et al.* (2006); <sup>f</sup>Government Quarry, Bermuda, Hearty *et al.* (1999); <sup>g</sup>Barbados, Schellmann and Radtke (2004); <sup>h</sup>Argentrola Cave, Italy, Bard *et al.* (2002); <sup>i</sup>Quobba Ridge, Western Australia, O'Leary *et al.* (2013); <sup>j</sup>Cape Range, Western Australia, Stirling *et al.* (1998); <sup>k</sup>Coorong coastal plain, South Australia, Murray-Wallace (2002); <sup>l</sup>Huon Peninsula, Papua New Guinea, Chappell and Shackleton (1986), <sup>n</sup>Cape Agulhas, South Africa, Carr *et al.* (2010).

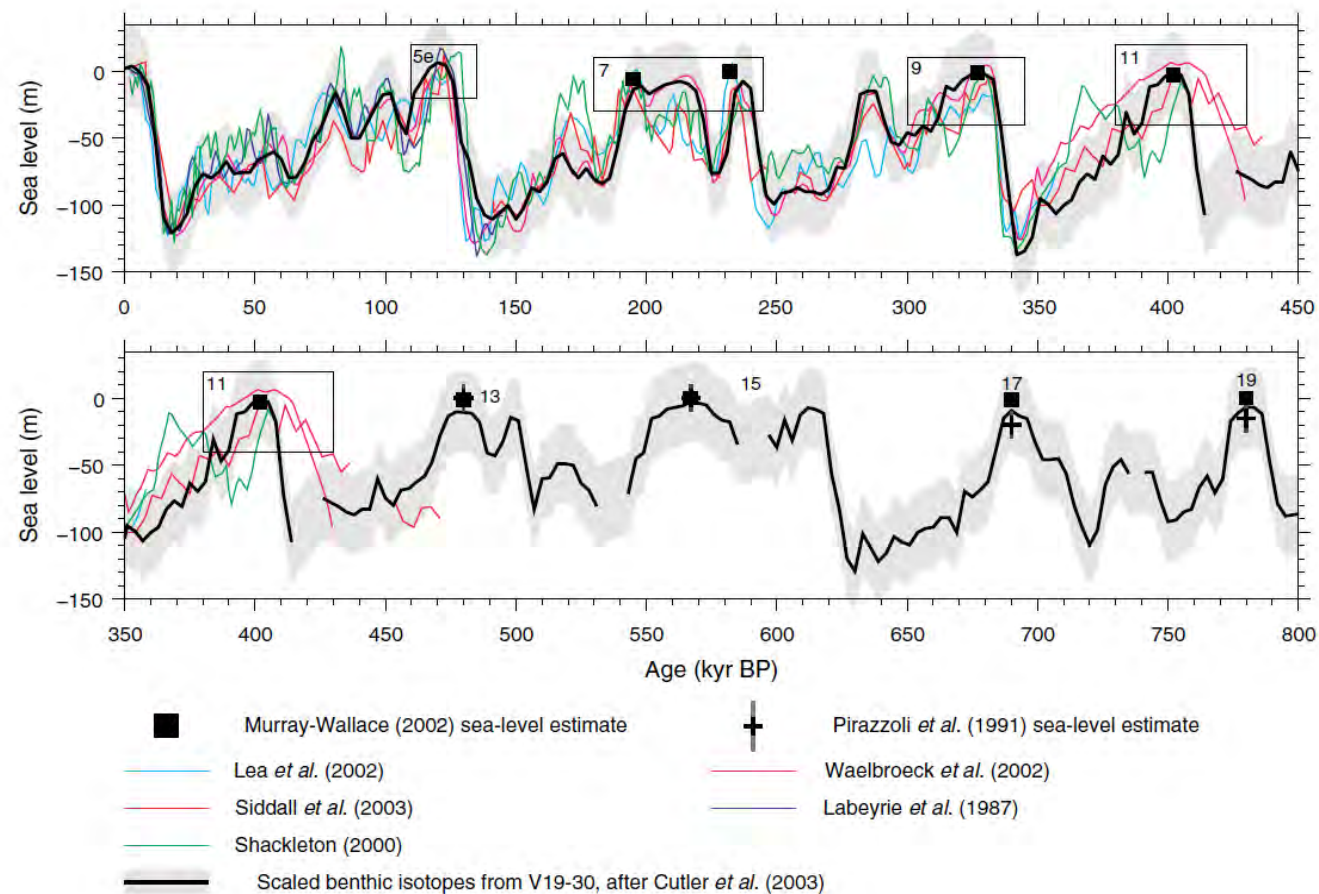


**Figure 2.13:** Reconstruction of a sea-level curve from a range of global sources (Siddall *et al.*, 2007). Lea *et al.* (2002) planktonic temperatures from foraminifera; Waelbroeck *et al.* (2002) North Atlantic and equatorial Pacific benthonic oxygen isotope records; Shackleton (2000) benthonic oxygen isotope records from the equatorial Pacific (V19-30) and the Vostok air oxygen isotope ratio record; Siddall *et al.* (2003) Red Sea oxygen isotope record; Labeyrie *et al.* (1987) benthonic oxygen isotope records from the Norwegian Sea and equatorial Pacific (V19-30). Dating of sea level estimates of Murray-Wallace (2002) sea level estimates in southern Australia and sea level estimates of Pirazzoli *et al.* (1991) sea level estimates from Indonesia is by correction with the benthonic isotope record of V19-30.



### **Palaeo-temperature**

A possible reason for the variation in sea-level amplitude identified between the past four interglacials may relate to the palaeo-temperature experienced at each of these times. Isotopic analysis of deuterium within ice cores allows palaeo-temperature reconstruction at the time of deposition. Masson-Delmotte *et al.* (2010) identified the 'intensity' of interglacials over the past 800 ka through the study of stable isotopes such as deuterium and other interglacial proxies such as dust, sodium, calcium, methane and carbon dioxide within the EPICA Dome C ice core, Antarctica. The strength of interglacials is suggested to have varied throughout the record (Jouzel *et al.*, 2007) with MIS 5e and MIS 11 found to be the warmest and most intense episodes, while MIS 13 and 17 were proposed to be the weakest (Masson-Delmotte *et al.*, 2010). These findings correspond with the high sea-level elevations recorded for MIS 5e and MIS 11 where sea level has been proposed to have reached up to 6 m and 13 m APSL, respectively (e.g. Mesolella *et al.*, 1969; Dumas *et al.*, 2005; Raymo and Mitrovica, 2012).

An interaction between obliquity and precession orbital cycles has been proposed as a possible reason for the varied strength of interglacials throughout the record (Jouzel *et al.*, 2007). When the summer insolation at 65°N and obliquity peaks are in phase (within 5 ka) of each other their collective effects may stimulate strong interglacial episodes, whereas in antiphase, the effects induce weaker interglacials (Jouzel *et al.*, 2007).

### **Glacio-hydro-isostasy**

Global sea-level may vary not solely due to differences in ice volume, but also as a result of differences in the proximity to former areas of glaciation (Figure 2.12). Lambeck and Nakada (1992) addressed the concept of the isostatic response of the lithosphere and the mantle to change in ice volume and water loading and unloading and argued that shoreline elevations around the globe cannot be directly compared without accounting for these differences. Lambeck and Nakada (1992) compared palaeo-shoreline elevations in Western Australia (zone 5) with those in Bermuda located within the sphere of rebound influence of former North American ice sheets (zone 3). It was found that at intermediate-field sites the highest sea levels occurred towards the end of interglacial interval, when the contribution from glacial unloading had partly relaxed and prior to sea-level lowering in response to the following glacial period (Lambeck and Nakada, 1992).

In the western North Atlantic a disparity in shoreline elevations has been noted during substage MIS 5a. Sea level during this interstadial have been found to range from between -15 and -18 m as recorded in speleothems in underground caves of the Bahamas (Richards *et al.*,

1994), to 1-2 m APSL from emergent coast deposits in Bermuda (Ludwig *et al.*, 1996) to 4-10 m APSL in coral deposits in Virginia, USA (Szabo, 1985; Wehmiller *et al.*, 2004). Potter and Lambeck (2003) addressed the issue of a north-south gradient in intertidal sea-level variation in the western North Atlantic and suggested this disparity was related to glacio-isostatic effects associated with the North American ice sheets of the penultimate glacial. Lambeck *et al.* (2012) stated that interglacial sea levels cannot be interpreted directly in terms of ice volume as they are a function of the entire glacial history prior to the interglacial, and that spatial variability in sea level is likely to be significant across multiple regions. Present sea level is also not level and is affected by the Coriolis Effect and currents such as El Niño (Davis and Fitzgerald, 2004).

### **Tectonic stability**

Sea level may also appear to vary globally due to differences in tectonic setting. The accuracy of reconstructed sea-level curves is dependent upon the information regarding the tectonic history of the region (Dawson, 1992). At sites of palaeo-sea level reconstruction where tectonic processes are evident, it is commonly assumed that uplift (or subsidence) has been constant over a certain period of time. For example, Ota and Chappell (1996) suggested that up to six regressive coral terraces on the Holocene raised reef tract of the Huon Peninsula, Papua New Guinea, represent repeated episodic uplift caused by earthquakes. Local variations in palaeo-sea level reconstruction may therefore be due to errors in uplift or subsidence calculation.

### **Summary**

Variations in sea-level reconstruction may be due to errors in accounting for glacio-hydro-isostatic effects, as suggested by Potter and Lambeck (2003) for sea-level variation during MIS 5a in the North Atlantic, or errors in calculating rates of tectonic uplift. These factors may account for variations observed between different records during the same interglacial. Differences in sea-level elevation recorded in separate interglacials may be a result of differences in interglacial intensity due to phasing between summer insolation at 65°N and the obliquity cycle (Jouzel *et al.*, 2007).

## **2.5 Duration of interglacials**

Interglacials are significantly shorter in length than glacials though their duration has varied from interglacial to interglacial with earlier interglacials (such as MIS 11) suggested to have lasted for more than 30 ka (Raynaud *et al.*, 2005; Loutre and Berger, 2003). This section reviews the literature on the duration of the past four interglacials, for which more data are available than earlier ones. Examining data from palaeo-sea level studies can aid in

constraining the timing of interglacial sea-level highstands and whether there is any correlation between the distance of a site from former glaciated areas and the timing of the sea-level highstand. This section will address reasons for variation in interglacial length.

Defining the duration of interglacial episodes will potentially aid in constraining the timing of sea-level highstand deposits and may account for variation in calcium carbonate productivity on the Bonney Shelf and differences in barrier size and morphology on the Mount Gambier coastal plain. Determining timing of when a sea-level highstand occurred within an interglacial in other far-field regions will allow comparisons with the Mount Gambier coastal plain record and aid in clarifying the glacio-hydro-isostatic response to the region.

Forsström (2001) noted that the length of interglacials have varied substantially and suggested the variation is bound to the summer solar radiation maximum in the Northern Hemisphere. Evidence from the  $\delta^{18}\text{O}$  record of a calcite vein from Devils Hole, Nevada, where Winograd *et al.* (1992, 1997) suggest that interglacials may have been up to twice as long as that indicated by the marine oxygen isotope record (e.g. SPECMAP record, Imbrie *et al.*, 1984). Winograd *et al.* (1992, 1997) reconstructed a palaeo-temperature record for the past 500 ka and proposed that MIS 11c, MIS 9c, MIS 7e and MIS 5e were ~20 ka, ~20 ka, ~26 ka and ~22 ka in length respectively, indicating distinct deviations from Milankovitch cycles. However, Imbrie *et al.* (1993) argued that it is inappropriate to transfer the chronology derived from Devils Hole to that of the marine record due to the physical differences associated with each archive. The Devils Hole calcite vein reflects the isotopic distillation of moisture from the atmosphere and is linked with the local temperature at which  $\text{CaCO}_3$  precipitation occurred, resulting in lighter isotopic values during glacials. The SPECMAP time series is an average of stacked marine-cores and heavier isotope values are experienced during glacials, all of which are tuned to the astronomical timescale. Imbrie *et al.* (1993) therefore concluded that the application of Devils Hole chronology to oceanic cores requires 'physically implausible changes in sedimentation rates'. Both the SPECMAP record and the Devils Hole chronology have certain limitations. The SPECMAP records averages a range of marine-cores and thus lacks the resolution of other records (e.g. ice cores) while the Devils Hole chronology uses palaeo-temperature rather than the volume of ice cover to define interglacials. The comparison of these records highlights the potential pitfalls of paralleling interglacial records derived from different deposits, and indicates that set criteria are used for defining interglacial episodes.

A further limitation of the Devils Hole chronology is that it suggests that the last four interglacials were similar in length, while most other proxies suggest interglacial lengths varied

quite significantly. For example, from the Vostok ice core record, Antarctica, Petit *et al.* (1999) suggested that MIS 5e and MIS 9c were similar in duration and amplitude and that both interglacials display a warm period of ~4 ka followed by relatively rapid cooling. From the Vostok record, Petit *et al.* (1999) proposed that MIS 7e differed in that it had a much shorter duration of only ~7 ka, compared with 17 ka and 20 ka for stages MIS 5e and MIS 9c, respectively. They deduced this may be a result of a different configuration of the Earth's orbit during this time.

### **MIS 11**

The duration of MIS 11 (~420 ka) is highly contested. Loutre and Berger (2003) suggested that it was the longest interglacial of the past 0.5 Ma, and that interglacial conditions continued for over 60 ka. Desperat *et al.* (2007) proposed that the warmest stage of MIS 11 was longer than during subsequent interglacials and that MIS 11 was three times longer than the current (incomplete) Holocene interglacial. Raynaud *et al.* (2005) suggested that MIS 11 lasted approximately 30,000 years and proposed that solar energy and CO<sub>2</sub> may have contributed to the exceptionally long interglacial. Certain works (e.g. Howard, 1997; Droxler and Farrell, 2000; Berstad *et al.*, 2002) contended that the warmest phase of MIS 11 recorded the highest temperatures of the last 0.5 Ma, with further studies suggesting that the Antarctic temperatures were also warmer during MIS 11 than currently experienced in the Holocene (EPICA community members, 2004), indicating a more intense interglacial (Masson-Delmotte *et al.*, 2010).

Hoddell *et al.* (2000) reconstructed oxygen and carbon isotopic gradients within the Southern Ocean and proposed that the sea surface temperatures (SST) of the ocean were no greater during this time than in other interglacials but the duration of this warm period was much greater than for other Late Pleistocene interglacials. The orbitally tuned SPECMAP timescale also suggests a lengthy MIS 11 duration of ~33 ka (Imbrie *et al.*, 1984). Why this interval was perhaps longer than other Pleistocene interglacials is a matter of debate. One suggestion is that episodes of sustained warmth are controlled by the eccentricity modulation of the precession cycle, and that during MIS 11 eccentricity was low and the amplitude of the precessional cycle was reduced, resulting in fewer cold substages within the interglacial (Hoddell *et al.*, 2000). This idea is supported by oxygen isotopic evidence which highlights a sustained warm period throughout the interglacial with no apparent sub-stage events (e.g. Shackleton and Opdyke, 1979; Imbrie *et al.*, 1984).

It has been suggested that sea-level highstands were also higher during this interglacial. On the islands of Bermuda and the Bahamas a range of studies (Hearty *et al.*, 1999; Hearty, 1998; Olson and Hearty, 2009; van Hengstum *et al.*, 2009) have suggested that sea level during MIS 11 reached 21 m APSL. McMurtry *et al.* (2007) and Mylroie (2008) suggested that these highly elevated features may have in fact been deposited by tsunami or storm events rather than a sustained sea-level highstand. MIS 11 sea level on the Canary Islands has been suggested to have been at least +9 m relative to present and may have been up to +24 m (Muhs *et al.*, 2014). Bowen (2010) surveyed a range of MIS 11 sea-level records worldwide and suggested that peak sea level may have reached 6-9 m APSL. However, Bowen (2010) excluded a range of outliers in his calculations including those of the Bermuda and Bahamas sites. Raymo and Mitrovica (2012) proposed that these studies have ignored the potential signal from glacial isostatic adjustment (GIA) as both the Bahamas and Bermuda are located within the peripheral bulge of the Laurentian ice complex. By accounting for glacial isostatic adjustment Raymo and Mitrovica (2012) concluded that eustatic sea level in the Bahamas and Bermuda would have reached 6-13 m APSL in the late stages of MIS 11.

Due to the lack of well-preserved sites and the difficulties in dating precision of these older deposits it is challenging to constrain the exact timing of MIS 11 sea-level highstands independently from the orbitally tuned marine-oxygen isotope records. However, multiple studies have suggested that this was an exceptionally long interglacial, highlighting that not all interglacials follow the same pattern of duration. Further work is required to constrain sea level elevation during this time and to account for glacial-isostatic effects. Sea-level data derived from the Mount Gambier coastal plain during MIS 11 may aid with this.

### **MIS 9**

Oxygen isotope records (e.g. Imbrie *et al.*, 1984) suggest that MIS 9 comprised a dominant sea level peak at 331 ka (MIS 9c) followed by a smaller secondary peak at 310 ka (MIS 9c), which correlate with the insolation maximum at 65°N recorded at 333 and 311 ka. As with MIS 11, geomorphological evidence associated with the MIS 9 highstand is challenging to date accurately due to the increased likelihood of samples being affected by diagenesis.

A study of coral reefs on Henderson Island in the South Pacific suggested that MIS 9 lasted from  $324 \pm 4$  to  $306 \pm 4$  ka, with the MIS 9 sea-level highstand occurring between  $324 \pm 3$  to  $318 \pm 3$  ka (Stirling *et al.*, 2001). Further research on the Henderson Island corals conducted by Anderson *et al.* (2010) also identified separate reef building episodes during MIS 9 and indicated a peak MIS 9c sea level at  $322 \pm 3$  ka, and a peak MIS 9a highstand at

307 ± 1 ka. On the Mururoa atoll, French Polynesia, Camoin *et al.* (2001) indicated that the MIS 9c sea-level highstand occurred at 332 ± 12 ka. These studies suggest that MIS 9 sea-level highstands occurred after the insolation maximum at ~333 ka. However, Henderson *et al.* (2006) constructed a  $\delta^{18}\text{O}$  chronology from the Bahamas Banks ODP site 1008A and proposed that full interglacial conditions were established by 343 ka, ~8 ka prior to the Northern Hemisphere summer insolation maximum. The reliability of the dataset derived by Henderson *et al.* (2006) is questionable, however, as only three dates are presented, with one rejected on the grounds of diagenetic alteration.

### **MIS 7**

The penultimate interglacial, MIS 7, is suggested to have consisted of three sea-level highstands from marine oxygen isotope records. The SPECMAP timescale indicates that MIS 7e, where interglacial sea levels were highest of the three highstands, lasted for ~12 ka. A study of submerged speleothem from Argentarola Cave, Italy, suggested that the MIS 7e sea-level highstand occurred between 202 and 190 ka, yielding a MIS 7e duration of 11 ± 2 ka, in agreement with the SPECMAP chronology (Bard *et al.*, 2002). Further work was conducted on these speleothems by Dutton *et al.* (2009) who constrained the timing of sea-level highstands during MIS 7 as occurring from 248.9 ± 1.9 to 231.0 ± 3 ka (duration 18 ka) for MIS 7e, from 217.2 ± 1.9 to 206 ± 1.9 ka (duration 11 ka) for MIS 7c; and from 201.5 ± 1.7 to 189.7 ± 1.5 ka (duration 12 ka) for MIS 7a. These findings suggest that sea-level highstands associated with MIS 7 occurred before the Northern Hemisphere summer insolation maximum at ~241 ka. Dutton *et al.* (2009) further suggested that although the MIS 7c highstand coincided with the insolation maximum (at ~218 ka) it did not reach much higher than -18 m BPSL.

While the work of Dutton *et al.* (2009) may provide a more precise chronology it is limited in that it only identifies when sea level is higher than -18 m, which was used as the boundary for interglacial timing in this study. Problems associated with dating speleothem hiatuses should also be accounted for; such as diagenesis of outer growth layers. A study of fossil reef complexes on Henderson Island (Anderson *et al.*, 2010) suggested that MIS 7e peak sea level was attained by 240.3 ± 0.8 ka and compared well with U-series dating of corals from Barbados which indicated that peak sea level was reached between 243 ± 4 ka and 239 ± 6 ka (Thompson and Goldstein, 2005). U-series dating of the flowstone of a Bahamian speleothem also correlates with these records and suggests that MIS 7e occurred between 235 and 230 ka, while the MIS 7c sea-level highstand was reached between 220 and 212 ka (Lundberg and Ford, 1994). These studies coincide well with the predicted timing of peak summer insolation at 65°N at ~241 ka and ~218 ka lending support to the Milankovitch hypothesis.

Evidence of only two prominent highstands at ~233 and ~215 ka is suggested from U-series dating of a submerged speleothem in the Bahamas (Lundberg and Ford, 1994). However, a sea-level highstand may have occurred where sea level did not reach above -15 m and thus did not fill the cave. In fact, the Barbados reef record shows three terraces dating to MIS 7 (Bender *et al.*, 1979). Robinson *et al.* (2002) used U-Th dating of  $\delta^{18}\text{O}$  records from aragonitic rich Bahamian slope sediments (core ODP Leg 166) to constrain the duration of MIS 7e to 9 ka from ~237 to 228 ka. They also indicated that MIS 7c began at 215 ka and while unable to determine the timing of MIS 7a suggested that the end of MIS 7 was highly complex and ended up to 10 ka after that predicted by orbitally tuned records. Further evidence for a complicated end to the penultimate interglacial is derived from U-Th dating of bulk sediment and an improved  $\delta^{18}\text{O}$  chronology from benthic foraminifera within ODP Site 1008A on the slopes of the Bahamas Banks (Henderson *et al.*, 2006). From this study it was suggested that while the start of MIS 7 may be in accord with the timing predicted by Northern Hemisphere summer insolation, the presence of an additional highstand post-dates the expected end of MIS 7 by up to 10 ka (Henderson *et al.*, 2006).

While evidence from an Italian speleothem (Dutton *et al.*, 2009) suggests that MIS 7 consisted of three sea-level highstands with sea level elevation being highest in MIS 7e, (similar to that of MIS 5), Desperat *et al.* (2007) indicated that MIS 7 does not follow the same pattern as other interglacials. Desperat *et al.* (2007) suggested that MIS 7 consisted of a very short first warm stage in comparison to other interglacials (such as MIS 5) which appear to have a lengthy first warm stage, and proposed that this may be due to the large insolation oscillation recorded during this episode.

It is apparent that there are discrepancies in the MIS 7 records; some studies indicate MIS 7 consisted of three sea-level highstands while others only record two. This may be due to a lower sea level in this last highstand, as suggested by the marine oxygen isotope record (e.g. Imbrie *et al.*, 1984) compared with others and thus is simply not recorded in certain archives. However, Rowe *et al.* (2014) suggested that relative mean sea level on Bermuda may have been at least 4.5 m APSL. Timing of MIS 7 also appears to vary significantly with certain records indicating sea-level highstands prior to that of Northern Hemisphere summer insolation maxima and others indicating sea levels that coincide or slightly post-date it. Further dating of MIS 7 sea level highstands deposits and a greater understanding of glacio-isostatic responses during this interval are required.

## MIS 5

Sea level during MIS 5e has been suggested to be up to +6 m higher than that of today (e.g. Dutton and Lambeck, 2012) resulting in the preservation of more last interglacial *sensu stricto* deposits than those of previous interglacials. This has, in turn, led to a great volume of research which has attempted to constrain the timing and elevation of the last interglacial sea-level highstand. However, rather than yielding a more precise timing for the duration of the interglacial, the vast quantity of studies pose more questions as to the timing and duration of this event, with certain works (e.g. Chen *et al.*, 1991; Szabo *et al.*, 1994; Esat *et al.*, 1999) proposing that MIS 5e began well before the Northern Hemisphere insolation maximum and demanding the need for other hypotheses to explain the timing of interglacial episodes.

Shackleton (1969) identified that the last interglacial (or Eemian as it is referred to in Europe) *sensu stricto* only corresponded to a portion of MIS 5. This is confirmed in other oxygen isotope records (e.g. Martinson *et al.*, 1987) where it is apparent that MIS 5 consisted of three episodes of high sea level, similar to the pattern observed in MIS 7. MIS 5e, the first of the three sea-level highstands, displayed the highest sea-level elevation of the interglacial, while sea levels in MIS 5c and MIS 5a are found to be several metres below that of present (e.g. Rohling *et al.*, 2008). Preservation of markers of these interstadial episodes are therefore reduced as is the volume of morphological data surrounding them.

SPECMAP chronology suggests that MIS 5e lasted for 13,000 years, from 128-115 ka (Imbrie *et al.*, 1984); while Shackleton proposed that if the start of MIS 5e is taken as the mid-point of the MIS 5e/6 transition the interglacial *sensu stricto* would have been ~11 ka in length. However, several studies of palaeo-shorelines have suggested that the onset of MIS 5e occurred well before the Northern Hemisphere insolation maximum at ~126 ka.

The development of thermal ionisation mass spectrometry (TIMS) has allowed for greater precision in dating deposits, particularly from the last interglacial, and has been used to further test the Milankovitch hypothesis (e.g. Edwards, 1987). Zhu *et al.* (1993) used TIMS U-series dating on corals from the Abrolhos Islands, Western Australia, and proposed significant sea-level rise associated with MIS 5e occurred prior to 134 ka. Further TIMS U-series dating of coral reefs on Bermuda, the Bahamas, Hawaii and Australia also lead Muhs (2002) to suggest that the last interglacial *sensu stricto* derived from the coral record is of greater duration than that indicated by the oxygen isotope record.

From the analysis of  $^{230}\text{Th}/^{234}\text{U}$  dating of fossil coral reefs in the Bahamas, Chen *et al.* (1991) suggested that MIS 5e sea-level highstand had likely started by 132 ka and certainly by



129 ka. On the island of Oahu, Hawaii, Szabo *et al.* (1997) used  $\text{Th}^{230}$  dating to establish that marine sediments were deposited between ~131 and ~114 ka, indicating duration of ~17 ka for the interglacial. Esat *et al.* (1999) analysed last interglacial coral reefs from within Aladdin's Cave, Huon Peninsula, and identified a sea-level highstand at 135 ka. Esat *et al.* (1999) proposed that the elevated sea-level was not sustained and that there was a return to glacial conditions before a further warming and sea-level rise between 128-126 ka. In an assessment of interglacial sea-level highstand studies in the Caribbean (Chen *et al.*, 1991; Woodroffe *et al.*, 1983; Szabo *et al.*, 1978; Harmon *et al.*, 1983; Neumann and Moore, 1975; Hamelin *et al.*, 1991) and Australia (Veeh and France, 1988; Szabo, 1979; Veeh *et al.*, 1979) from glacio-hydro-isostatic rebound models, Lambeck and Nakada (1992) concluded MIS 5e occurred between 135 and 120 ka.

The early onset for the last interglacial is also indicated from certain non-marine records. Waelbroeck *et al.* (2008) suggested that the penultimate glacial to last interglacial boundary was  $131.2 \pm 2$  ka, as indicated by an abrupt increase in atmospheric  $\text{CH}_4$  and North Atlantic surface temperature. From the analysis of the Vostok ice core, eastern Antarctica, Jouzel *et al.* (1993) proposed that the last interglacial was 5 ka longer than that suggested from deep sea records. Kukla *et al.* (1997) orbitally tuned La Grande Pile pollen record in eastern France (Woillard, 1975) with the stratigraphy of marine core V29-191 from the North Atlantic (McManus *et al.*, 1994). From this they proposed the last interglacial *sensu stricto* lasted from 130 to 107 ka, a duration of 23 ka which is nearly twice as long as that implied from the marine oxygen isotope record. However, Tzedakis (2003) highlights the potential lag effects in interglacial terrestrial evidence and the pitfalls of correlating records of different proxies from various geographical regions.

In contrast, a range of studies also suggest that the MIS 5e sea-level highstand corresponded well with the timing of the Northern Hemisphere insolation peak. For example; studies of U-series dating on fossil reefs from South Florida by Muhs *et al.* (2011) indicated that MIS 5e was well underway by 123 ka and lasted at least 9 ka until 114 ka. Muhs *et al.* (2011) suggested that the younger ages derived from the Florida corals compared with those from the nearby Bahamas (e.g. Chen *et al.*, 1991) may result from the absence of rapidly growing corals, such as *Acropora palmata*, in Florida.

It is apparent that discrepancies occur in relation to the timing and duration of the last interglacial. The observed differences may reflect a complex interglacial or perhaps reflect differing interpretations from various deposits.

## **Summary**

Differences in interglacial duration are observed from a brief review of the literature. The timing and length of interglacials are found to vary when different interglacials are compared and also when the same interglacial is compared from various deposits. Some evidence suggests that the beginning of interglacials is governed by the timing of the Northern Hemisphere insolation maximum while others indicate that additional forces may be involved. The difference in sea-level highstand maxima may also be related to the distance of the site from Quaternary ice sheets, and highlights the potential pitfalls of not only comparing sea level data from varying sources but from differing geographic localities.

Beyond MIS 5e, interglacial deposits are commonly less well-preserved and dating techniques cannot yield ages to the same degree of precision. This therefore brings into question whether the contention surrounding timing of the start of the last interglacial, in relation to Northern Hemisphere insolation, is a matter of the complexity of this interval compared to others, or simply that we have a greater knowledge of this interglacial than of others. It is apparent that the past four interglacials have varied in their duration as well as the number and elevation of associated sea-level highstands. This variability therefore questions which (if any) past interglacial is most analogous with the present Holocene interglacial.

The duration of an interglacial essentially relates to how we define an interglacial episode and through which criteria we use to define where isotopic stage boundaries are drawn. These ideas are discussed in the following section.

## **2.6 Defining interglacials**

As shown through a brief examination of interglacial studies, there is disparity in the recorded duration of these intervals. This section assesses how interglacials are defined and the boundaries that are used to identify them. As previously discussed, sea-level highstands can occur at different times during the interglacial depending on their position relative to former ice sheets. Thus, it is necessary to determine the overall timing of interglacial intervals so it is possible to constrain the timing of interglacial deposits on the Mount Gambier coastal plain.

The duration of interglacials varies between records and this opens the question of how isotopic stage boundaries have been defined and whether all isotope records are using the same criteria to define stage boundaries. Where exactly does a glacial end and an interglacial begin?

In determining where isotopic stage boundaries should lie, Emiliani (1955) used the mid-point between successive isotopic minima and maxima. This approach was also adopted by Shackleton and Opdyke (1973) in their analysis of marine core V28-238 from the equatorial Pacific. Shackleton and Opdyke (1973) identified 22 stage boundaries over 870,000 years and established stage boundaries on the basis of a uniform sedimentation rate within the core, calibrated by the presence of the Brunhes-Matuyama magnetic reversal (700 ka) at 1200 cm deep, within isotope stage 19. The mid-point approach to defining isotopic stage boundaries was also used by Pisias *et al.* (1984) as they evaluated the resolution of marine oxygen isotope stratigraphy.

Prell *et al.* (1986) defined stage boundaries as centring on isotopic peaks, rather than mid-points as suggested by Shackleton and Opdyke. In establishing the SPECMAP record Imbrie *et al.* (1984) used the numerical system and identified stage boundaries as corresponding to rapid and monotonic shifts in the isotopic curve. However, Patience and Kroon (1991) suggested that the absolute ages and positions of the isotopic stage boundaries within the SPECMAP curve may be erroneous due to the linear interpolation used to correlate between radiocarbon dated control points (0-35 ka) and the K-Ar dated Brunhes-Matuyama boundary. Prell *et al.* (1986) also defined stage boundaries as centring on isotopic peaks rather than mid-points, and Patience and Kroon (1991) proposed that this is a less subjective approach. Shackleton (2006) has also criticised the decimal labelling approach of Prell *et al.* (1986), and suggests that the decimal isotope events actually only signify points within the record rather than intervals which the alphabetically labelled method defines. Shackleton (2006) noted using the decimal system on a range of cores, especially those that are poorly sampled, will result in gaps between the positions of successive events, whereas the alphabetically labelled method spans the full stratigraphic record.

Table 2.3 presents the stage boundaries as defined from a range of marine oxygen isotope chronologies, and attempts to derive a simple average of these boundaries in which to compare results derived from the Mount Gambier coastal plain. These averages do not consider the ages derived from the morphological record because, as noted by Patience and Kroon (1991), determining stage boundaries from such a record is more challenging as the archive is not continuous. Geochronological results from the Mount Gambier coastal plain will also be compared with these morphological records.

**Table 2.3:** Oxygen isotopic stage boundaries depicted from a range of marine and ice core records

Stage Boundary	Shackleton and Opdyke (1973)	Hays <i>et al.</i> (1976)	Imbrie <i>et al.</i> (1984) SPECMAP	Williams <i>et al.</i> (1988)	Masson-Delmotte <i>et al.</i> (2010)	Martinson <i>et al.</i> (1987)	Jouzel <i>et al.</i> (2007)	Timing of stage boundary Derived from simple averages of listed works
Age (ka)								
1-2	13	10	12		11.6	12.05	12.3	12 ± 1
2-3	32	29	24		35.6	24.11		29 ± 5
3-4	64	61	59			58.96		61 ± 2
4-5	75	73	71			73.91	82.5	75 ± 4
5-6	128	127	128	128	132.0	129.84	132.8	129 ± 2
6-7	195	190	(186)	194	153	189.61	197.9	187 ± 14
7-8	251	247	(245)	258	245.6	244.18	245.1	245 ± 5
8-9	297	276	(303)	313	278		322.1	298 ± 17
9-10	347	336	(339)	359	335.6		337.7	342 ± 8
10-11	367	356	362	386	360		394.8	371 ± 14
11-12	440	~425	(423)	430	424.6		427.0	429 ± 6
12-13	472	~457	(478)	486	451		486.3	475 ± 13
13-14	502		524	521	529.6		491.1	514 ± 15
14-15	542		(565)	544	548			550 ± 9
15-16	592		(620)	589	628		580.9	602 ± 19
16-17	627		(659)	622	651		690.6	650 ± 25
17-18	647		689	658	720		704.0	684 ± 27
18-19	688		(726)	695	755.6		775.4	728 ± 34
19-20	706		(736)	729	791.6		789.6	750 ± 35
20-21	729		(763)	743	801.6			759 ± 27
21-22	782		(790)	786				786 ± 3

\*Ages in parenthesis have been determined by interpolation between adjacent ages with reference to stratigraphic level of corresponding event in core V28-238 (Imbrie *et al.*, 1984). Note that the derived means are dependent on the number of works used, which is not an extensive list. Also note that several records (e.g. Imbrie *et al.*, 1984) are orbitally tuned and are thus already averaged from several records.

Shackleton (2006) has also criticised attempts to determine the exact transitions between stage boundaries, stating that due to bioturbation and differences between foraminiferal species used to derive marine oxygen isotope records, these transitions will differ for each core. However, oxygen isotope stratigraphy is also used on land as a reference, as well as in the oceans. For example, the application of AAR may be more precise and a more powerful tool when correlated with oxygen isotope stratigraphy of nearby marine-cores (Bowen, 1978; Shackleton, 2006).

## 2.7 Last interglacial in Australia

As mentioned in Chapter 1, the Coorong coastal plain in southern Australia preserves one of the longest sea-level highstand records found on emergent coastlines in the world, due to the steady tectonic uplift of the region and the semi-arid climate which promotes the production of a protective calcrete capping. In order to find a context for the timing of interglacial deposits derived from the Mount Gambier coastal plain it is necessary to assess other interglacial sea-level highstand studies from around Australia, and to determine how Australian data correlate with highstand data derived from the elsewhere in the world.

Australia experienced limited glaciation during glacial times (Colhoun *et al.*, 2010) and lies far from previous continental ice sheets (zone 5, Figures 2.8, 2.12). As with many other coastal regions, last interglacial shoreline deposits are more widely preserved than other previous sea-level highstands in Australia, and are therefore the focus of more research. The

+4 to 6 m benchmark for the last interglacial (MIS 5e) sea level is commonly held as a *de facto* eustatic sea level and used in establishing uplift rates at sites globally. Dutton and Lambeck (2012) suggested that this is not a valid approach, as the position of last interglacial sea level can be expected to vary depending on the location of the site in relation to the position of former and subsequent ice sheets, and the associated resultant isostatic adjustments of ice and water loading.

From the study of several last interglacial shorelines in Australia it has been suggested that sea level did not extend as high as the +6 m *de facto* datum (Table 2.4, Figure 2.14). Through U-series dating from the fossil coral reefs of the Houtman Islands, Western Australia, Zhu *et al.* (1993) and further work by Eisenhauer *et al.* (1996) suggested that at approximately 124 ka sea level was 3.3 m APSL. Hearty *et al.* (2007) studied marine deposits in the Perth and Rottnest Island region of Western Australia. Here they suggested that sea level on Fairbridge Bluff, Rottnest Island, did not exceed +2 m during the last interglacial. Hearty *et al.* (2007) suggested that a sea level of +6 m may have only been reached for a few hundred years in Western Australia while a +2.5 m sea level was sustained for several thousand years during the early half of MIS 5e. U-series dating on the Ningaloo Reef, northern Western Australia (WA) suggested that between  $129 \pm 1$  and  $119 \pm 1$  ka, sea level was between 2-4 m APSL (McCulloch and Esat, 2000). As shown in Table 2.4 some of the last interglacial deposits in Australia correspond well with the Northern Hemisphere summer insolation maximum (e.g. Cape Range, WA, Stirling *et al.*, 1998; Ningaloo Reef, WA; McCulloch and Esat, 2000) while others, such as corals from the Houtman Islands, WA indicated the possibility of an earlier start to MIS 5e (Zhu *et al.*, 1993). The lower Last Interglacial sea level recorded in Australia compared with other global MIS 5e sea level datum may relate to the absence of widespread glaciation in Australia. Glacio-isostatic effects therefore, do not contribute to sea level in Australia and shorelines reflect hydro-isostatically modified global sea levels (Murray-Wallace and Belperio, 1991).

More recently, further work has been conducted on the coral reefs of Western Australia, and while suggesting that sea-level remained between 3-4 m APSL for the majority of the last interglacial *sensu stricto* (127 to 119 ka), this work has suggested a jump in sea level to 9 m APSL at the end of MIS 5e (O'Leary *et al.*, 2013). This sharp sea level increase at the end MIS 5e has also been recorded in the Bahamas by Neumann and Hearty (1996) who suggested sea level increased to between 6 and 8.5 m APSL at 118 ka. However, a lack of numerical ages within this study cast doubt on their interpretation.

**Table 2.4:** Comparison of palaeo-sea level reconstruction data from around Australia during the last interglacial

Location	Sea level height	Date of sample	Dating method	Tectonic Setting	Reference
Houtman Abrolhos	4 m BPSL	134 ka	U-series	Stable	Zhu <i>et al.</i> (1993)
Islands, Western Australia - coral reef	2-4 m APSL	133 – 116 ka			
Cape Range National Park, Western Australia - coral reef	3.3 m APSL	124 ka	TIMS U-series	Stable / negligible	Eisenhauer <i>et al.</i> (1996)
Ningaloo Reef, Western Australia	>3m APSL	128 ± 1 to 121 ± 1 ka	U-series	Stable	Stirling <i>et al.</i> (1998)
Quobba Ridge, Western Australia	>4 m APSL	128 ± 1 ka	U-series	Stable	McCulloch and Esat (2000)
Spencer Gulf Region, South Australia	3-4 m APSL	127 to 119 ka	U-series	Stable	O'Leary <i>et al.</i> (2013)
Eyre Peninsula, South Australia - intertidal facies	9 m APSL	118 ka			
	1 m APSL	ca. 125 ka	TL and AAR		Hails <i>et al.</i> (1984)
Tasmania and Bass Strait Islands – coastal sediments	2m APSL	Last interglacial?	AAR	Stable	Murray-Wallace (1987); Murray-Wallace and Belperio (1991)
	24.6 m AHD – Mary Ann Bay, TAS		AAR and ESR	Unstable - uplifted	Murray-Wallace and Geode (1991, 1995)
	12.3 m AHD – Montagu, TAS				
	14.3 m AHD (m) – Broadmeadows, TAS				
	3.7 m AHD – Yellow Rock River, King Island				
Lord Howe Island, coral and marine sediments	2-4 m APSL	136 ka (average)	U-series	Stable	Woodroffe <i>et al.</i> (1995)
Largs, New South Wales - <i>Anadara trapezia</i>	4 ± 1 m APSL	138 ± 21 ka	TL	Stable	
Evans Head, Northern New South Wales – coral	5 ± 1 m APSL	Last interglacial	AAR	Stable	Thom and Murray-Wallace (1988)
Fairbridge Bluff, Rottnest Island, Western Australia – coral	>3 m APSL	119 ± 4 ka	U-series	Stable	Pickett <i>et al.</i> , (1989); Marshall and Thom (1976)
North Stradbroke Island, Queensland	>3 m APSL	127 to 122 ka	TIMS U-series	Stable	Stirling <i>et al.</i> (1995)
	-6 to +2 m APSL	119 ± 3 ka	U-series	Stable	Pickett <i>et al.</i> (1985); Pickett <i>et al.</i> (1989)

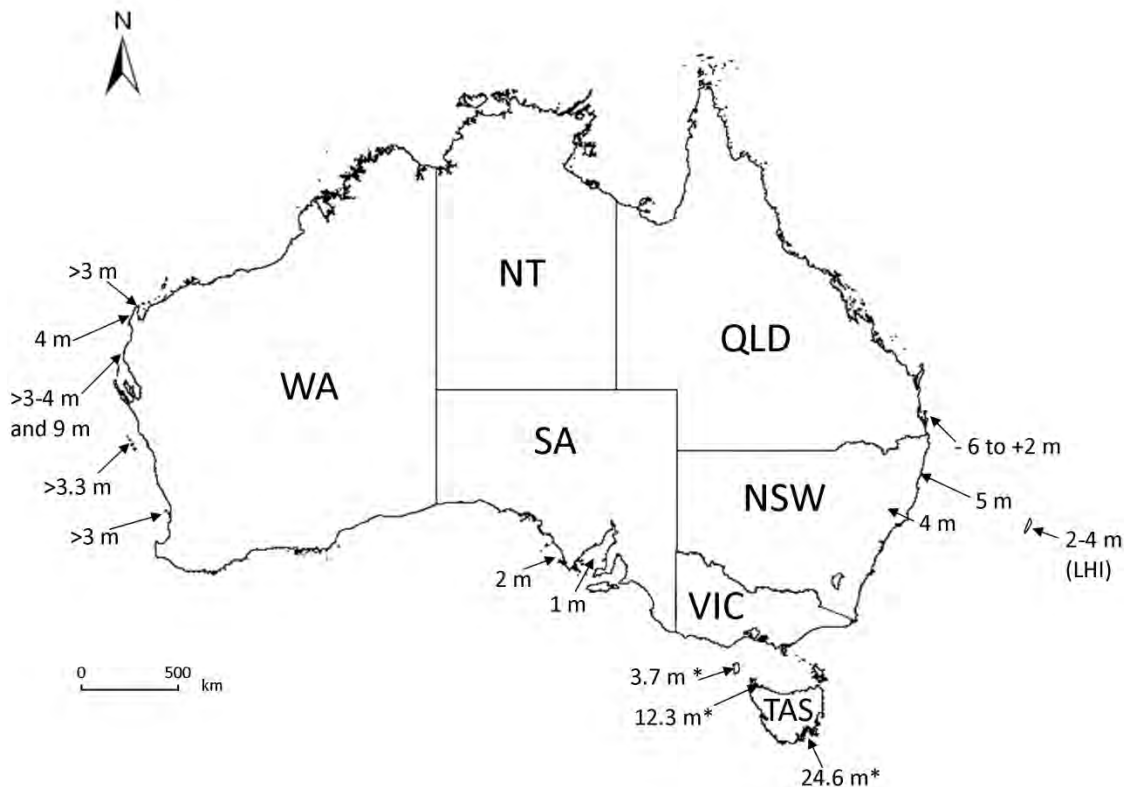


**Figure 2.14:** Last interglacial sea level around Australia. \*Marks sites that are not tectonically stable. LHI = Lord Howe Island.

Interpretation of palaeo-shorelines from coral reefs are limited to the warmer waters found along the northern and western coasts of Australia. On the coast of southern Australia palaeo-shoreline interpretations are restricted to non-reefal marine sediments. Murray-Wallace and Belperio (1991) proposed that the most reliable height datum of the last interglacial sea level in Australia can be derived from Eyre Peninsula, South Australia, whereby a consistent sea-level elevation of +2 m APSL has been recorded for 500 km along the coastline. Eyre Peninsula comprises part of the Precambrian Gawler Craton and thus has a long record of geological stability in comparison to other interglacial shorelines in Australia that display variations in elevation in relation to regional neotectonic deformation (Murray-Wallace and Belperio, 1991).

Sea-level elevation on the Coorong coastal plain, 500 km south-east of Eyre Peninsula, has been shown not to deviate more than 6 m from present sea level over the last 1 Ma (Belperio and Cann, 1990; Murray-Wallace *et al.*, 2001) with no apparent higher sea level experienced during MIS 11, as proposed in the Bahamas by Hearty *et al.* (1999). Table 2.5 highlights the uplift-corrected shoreline elevations between Robe and Naracoorte, South Australia as derived by Murray-Wallace (2002), and calculated by using the 2 m APSL reference sea level from the Eyre Peninsula for the last interglacial maximum (Murray-Wallace and Belperio, 1991). Dating of the barrier shorelines through thermoluminescence (TL) analysis was conducted by Huntley *et al.* (1993a; 1994) and through amino acid racemisation (AAR) by Murray-Wallace *et al.* (2001). These results were then correlated to marine oxygen isotope stages based on the chronology of Williams *et al.* (1988).

**Table 2.5:** Ages of barrier shorelines on the Coorong coastal plain, as derived from AAR and TL analysis, and their associated palaeo-sea level elevations (Murray-Wallace, 2002)

Dune Range	Marine $\delta^{18}\text{O}$ stage <sup>a</sup>	TL age (ka) <sup>b</sup>	AAR age (ka) <sup>c</sup>	Uplift corrected sea-level (m) <sup>d</sup>
Younghusband Peninsula	1	-	-	0
Robe III	5c	116 ± 6	127 ± 24	-9
Woakwine I	5e	132 ± 9	-	+2
Reedy Creek	7e	258 ± 25	251 ± 48	0
West Avenue	9	342 ± 32	382 ± 73	-1
East Avenue	11	414 ± 29	-	-3
Baker	13	456 ± 37	438 ± 83	-1
Peacock/Woolumbool	15	-	-	0
Harper/Stewart	17	585 ± 44	693 ± 132	-1
West Naracoorte I	19	800 ± 100	543 ± 102	0
East Naracoorte	25-29	720 ± 70	935 ± 178	-

<sup>a</sup>Marine oxygen isotope stages and ages based on chronology of Williams *et al.* (1988)

<sup>b</sup>TL ages of Huntley *et al.* (1993, 1994)

<sup>c</sup>AAR ages from the whole-rock method on aeolianites (Murray-Wallace *et al.*, 2001).

<sup>d</sup>Elevation estimates assume a +2 m APSL level for MIS 5e sea surface after Murray-Wallace and Belperio (1991) and a constant uplift rate of 0.07 mm yr<sup>-1</sup>.

Uplift corrected sea level may vary depending on the age uncertainty of the deposit. Uplift corrected sea level is based here on the average age of the deposit.

The well-preserved archive of interglacial highstands found on the Coorong coastal plain is of global significance. Few locations around the globe maintain such well-preserved morphological evidence of successive sea-level highstands, with many palaeo-shorelines only documenting the last interglacial sea level. As Australia lies in a far-field zone relative to Quaternary continental ice sheets, the Coorong coastal plain also yields a more closely defined eustatic sea-level curve. Detailed analysis of the facies architecture in the barrier shorelines on the Mount Gambier coastal plain, 120 km to the south-east, will aid in further recognising and constraining palaeo-sea level elevation and timing. This will assist in tuning the marine isotopic record and determining ice volume during past interglacials.

## 2.8 Conclusions

Sea-level estimations can constrain the timing of interglacials and glacials throughout the Quaternary. Sea-level highstands are found within a range of archives; from (presumably) continuous ice- and marine-cores which record the changing volumes of continental ice (and thus act as proxies for sea level), to geomorphological evidence recorded in shoreline deposits during times of elevated sea level, such as fossil coral reefs and uplifted shorelines. These sea-level indicators have both advantages and disadvantages. Marine- and ice-cores only provide proxies of global sea level, but also offer a continuous dataset throughout the Quaternary and can be derived from multiple locations throughout the world. Geomorphological evidence provides a direct record of palaeo-sea level but has not been continuous throughout the Quaternary and may be limited by restrictions in suitable dating techniques.

No single sea-level record can be representative of global sea level throughout the Late Quaternary. The response of sea level to the waxing and waning of Quaternary ice sheets varies locally depending on the distance of the coastline from formerly glaciated areas. For example, regions within the near-field to Quaternary ice sheets may experience a relative sea-level fall at the beginning of an interglacial as the continental landmass rebounds due to the reduced weight of the ice sheets on top of it (e.g. Lambeck *et al.*, 2012). The increased load upon the land surface as an ice sheet forms during glacials and the increased volume of water in the oceans during interglacials results in adjustment of the underlying crust and mantle. These effects vary from locality to locality and need to be accounted for before sea-level records can be directly compared. On the Mount Gambier coastal plain it might be expected that sea level would rise at the beginning of an interglacial due to an increase in ocean water volume, but may subside later in the interglacial due to warping of the crust and mantle beneath the continental shelf in response to the increased load of the overlying water. During



the present Holocene interglacial it is estimated that sea level around the Australian continent was approximately 1 m APSL approximately 7 ka. A similar scenario may have occurred in previous interglacials.

Much palaeo-sea level research has concentrated on the last interglacial *sensu stricto*, as more deposits associated with this interval have been preserved and suitable dating techniques commonly yield higher resolution within this episode than for previous interglacials. However, the vast body of research associated with the last interglacial has derived as many questions as it has answered. Sea level has been found to have been higher than present during MIS 5e, but the elevation is spatially variable. The timing of the start of the last interglacial has also been debated with certain records suggesting it was initiated by the Northern Hemisphere insolation maximum, while other studies indicate that it started well before then and demand other hypotheses into interglacial commencement. Research on the last interglacial begs the question if this was a particularly complex episode or whether our knowledge of previous interglacials is comparatively limited. This highlights the need for greater research into the interglacials prior to MIS 5e, to further aid in determining sea-level highstand elevation and interglacial duration. Further research could aid in determining whether or not there is a distinct pattern to previous interglacial cycles and which interglacial, if any, provides the best analogue to the present, Holocene, interglacial.

Further research in Australia on interglacial sea levels is therefore important for several reasons. As Australia is located in a far-field region from previous continental ice sheets any palaeo-sea level record will yield a more closely refined eustatic sea-level curve than from sites in the near and intermediate zones. The slowly uplifting Mount Gambier coastal plain has preserved previous interglacial shorelines, potentially as far back as MIS 19 (~ 790 ka). A continuous record of this length is rarely found in other geomorphological sites globally and provides the opportunity to constrain the timing and elevation of earlier sea-level highstands. In turn, analysis of the shoreline deposits on the Mount Gambier coastal plain may assist in refining the marine oxygen isotope record and quantifying global ice volume.



# Chapter 3

## **Stratigraphy of the Pleistocene Bridgewater Formation on the Mount Gambier coastal plain, southern Australia**

### **3.1 Introduction**

This chapter provides a stratigraphic framework for deposits across the Mount Gambier coastal plain, with which results of geochronological analyses (Chapter 5) are combined to allow for construction of a chronostratigraphy (Chapter 6) and greater understanding of coastal evolution within the region. This chapter presents an overview of temperate carbonate sedimentation, carbonate platforms, carbonate terminology and classification systems before relating these to carbonate deposition on the Mount Gambier coastal plain. The first half of the chapter also identifies common sedimentary structures found within aeolian and beach facies and methods of identifying between the two separate depositional environments. The preservation potential of both these facies types is discussed as well as the effects of subaerial exposure. The stratigraphy and carbonate setting of a range of global studies is then briefly presented and used to identify differing depositional environments.

Building upon the framework of calcarenite literature discussed in the first half, the second half of the chapter examines the stratigraphy of the Pleistocene Bridgewater Formation within a range of exposures on the Mount Gambier coastal plain. Stratigraphical methods used throughout this study are presented, as are the location of each of the study sites and the basis for their selection. Each of the study sites is described sequentially from the modern shoreline landward. Stratigraphical features and the identification of macro- and micro-fossils at each of the study sites aid in reconstructing the palaeo-depositional environment at each location. The identification of such settings will be of use later in the thesis (section 6.3) when a numerical age of each site has been determined and relative palaeo-sea level can be inferred.

### **3.2 Temperate carbonate sedimentation**

The continental margin of southern Australia is the largest area of active modern temperate carbonate production in the world (James *et al.*, 1997). This extensive production zone provides the material for onshore deposition by strong southerly winds along the southern

coastline of Australia. The following discussion outlines the carbonate production zones, identifies what encompasses temperate carbonate production zones and introduces the development of carbonate terminology and its use within this study.

### **3.2.1 Carbonate platforms**

A carbonate platform may be defined as a shallow-water carbonate succession and may be found in the form of ramps, rimmed- and open-shelves, and isolated platforms (Tucker and Wright, 1990). A carbonate shelf is a form of carbonate platform that has developed a recognisable relief above the surrounding sea floor with a distinct break in slope of its depositional surface (Fornos and Ahr, 1997). While rimmed shelves contain carbonate accumulations along the shallow outer margin, open shelves lack a distinct rim and are bounded by a less obvious break in slope (Fornos and Ahr, 1997). Carbonate ramps experience no apparent break in slope and extend from the shoreline to the basin without any abrupt change in facies. Different carbonate platforms styles can yield differences in onshore sedimentation dynamics and affect the chronology of deposition.

### **3.2.2 Cool-water platforms**

Traditionally, it was suggested that carbonate production occurred primarily in warm, tropical waters (Rodgers, 1957). The work of Chave (1967) and Lees and Buller (1972), however, recognised that latitude and water temperature do not restrict carbonate production, and identified several areas of carbonate sedimentation in cool-water, high-latitude provinces such as southern Australia and north-western Europe.

More recently, shelf carbonates have been suggested to be found in abundance in areas of low terrigenous-clastic sediment input (Brooke, 2001). Therefore, fluvial discharge is illustrated as the primary limiting agent of carbonate distribution rather than water temperature or salinity (Chave, 1967). This is particularly evident when comparing the location of carbonate production zones in the Northern and Southern Hemispheres (James, 1997). Widespread glaciations experienced throughout the Pleistocene in the Northern Hemisphere resulted in large volumes of terrigenous sediment being transported to continental shelves, causing significant carbonate production zones to be limited to the outer margins. In the Southern Hemisphere, where Pleistocene glaciation was manifested by significantly smaller ice volumes, widespread areas of Quaternary cool-water carbonate deposits are found, such as in Australia, New Zealand and South Africa (James, 1997). In addition, carbonate sediments are abundant on or around islands, where fluvial systems are small or not well-developed.

Water temperate has been identified as having some impact on carbonate production, with production rates being much higher in warm-water species than in cooler waters (Rao, 1996). Major ocean currents can therefore influence where carbonates are distributed; with warm ocean currents, such as the Gulf Stream in the western Atlantic and the Leeuwin Current in the eastern Indian Ocean, resulting in warm water carbonate-producing species being located at higher latitudes than expected (e.g. James, 1997).

Temperate (or cool-water) carbonates can be defined as sediments that accumulate in marine waters that have a mean temperature of less than 20°C (James, 1997). Nelson (1988) noted four important attributes of these temperate sediments: 1) they contain little or no lime-mud; 2) marine cementation is minor and patchy; 3) they are dominated by calcite mineralogy; and 4) deposition processes result in ramps and open shelves.

Lees and Buller (1972) attempted to distinguish between the different groups of organisms found within temperate and tropical carbonate provinces. Within temperate-water carbonate environments, faunal associations are composed of molluscs, benthic foraminifers, echinoderms, bryozoan, barnacles, ostracods, sponges (calcareous spicules) and worms (Lees and Buller, 1972). Ahermatypic corals are rarely recorded in temperate provinces and floral associations are primarily composed of calcareous red algae. Lees and Buller (1972) also noted that tropical water floral and faunal associates may include many of the components described in temperate climates, yet the following differences were observed: warm-water associations contained significant contributions from corals and/or calcareous green algae and barnacles and bryozoans do not appear to contribute significantly to sediment in warm-water associations.

### **3.2.3 Carbonate terminology**



The term Chlorozoan Association (from Chlorophyta + Zoantharia) was proposed by Lees and Buller (1972) to be used to describe sediments found in warm or tropical water, while the term Foramal Association is used for temperate carbonates where foraminifera and molluscs are commonly present. In 1997, James suggested new definitions were required to reflect modern thinking and the increased understanding of carbonate sedimentation throughout the geological record. James (1997) stated that the term Association refers to a group of sedimentary particles occurring together under similar environmental conditions and having a uniform or distinct aspect. James replaced the term Chlorozoan with Photozoan Association, suggesting that it better reflected the shallow, warm-water, benthic calcareous communities and their resultant sediments within warm-water carbonate provinces, while also emphasising

the light-dependent nature of the major biotic constituents. James (1997) criticised the term Foramal Association for its use of taxa in its name, noting that in areas where foraminifera and molluscs are not dominant other terms are commonly used. James (1997) suggested that to aid in simplification and ease of communication the term Heterozoan Association (from the Greek *Heteros* meaning other/different) be used to describe temperate-carbonate provinces.

### 3.2.4 Carbonate classification

Sedimentary carbonates were commonly grouped according to their presumed depositional environments before the publication of carbonate classification schemes by Folk (1959; 1962) and Dunham (1962). Previous classification schemes failed to distinguish clearly between carbonate grains and carbonate mud, or to emphasise the difference between a variety of carbonate grain types (Boggs, 2001). The most widely used classification schemes are based on the concept of textural (fabric) maturity, whereby the fabric is suggested to relate to the level of energy experienced during deposition (Tucker and Wright, 1990). The primary parameters used in carbonate classification are concerned with the types and carbonate framework grains and the grain/micrite ratio (Boggs, 2001).

Folk's (1959) classification (Figure 3.1, Table 3.1), is based on the relative abundance of three major components: carbonate grains or allochems; microcrystalline carbonate mud; and sparry calcite cement. Classification is made through determining the relative abundance of the total allochems versus micrite plus sparry calcite cement. Subdivision is then determined by the abundance of different types of carbonate grains and the relative abundance of micrite compared with sparry calcite cement (Boggs, 2001).

Percent allochems	Over two thirds mud matrix				Subequal spar and lime mud	Over two thirds spar cement		
	0-1%	1-10%	10-50%	Over 50%		Sorting poor	Sorting good	Rounded and abraded
Representative rock terms	Micrite and dismicrite	Fossiliferous micrite	Sparse biomicrite	Packed biomicrite	Poorly washed biosparite	Unsorted biosparite	Sorted biosparite	Rounded biosparite
Terminology								
	Micrite and Dismicrite	Fossiliferous Micrite	Biomicrite		Biosparite			
Terrigenous analogues	Claystone		Sandy claystone	Clayey or immature sandstone	Submature sandstone	Mature sandstone	Supermature sandstone	

Lime mud matrix

Sparry calcite cement

**Figure 3.1:** Textural classification of carbonate sediments on the basis of lime mud matrix and sparry calcite cement on the abundance and sorting of carbonate grains (after Folk, 1962).

Dunham's (1962) classification of carbonates (Table 3.2) describes the original depositional texture of carbonates and distinguishes between carbonate rocks in which the grains are touching or are tightly packed with those in which the grains appear to float within a carbonate matrix. The scheme assesses whether the grains were bound together at the time of deposition, such as within a calcareous mat (Blatt *et al.*, 1980; Boggs, 2001). Dunham's (1962) scheme attempts to separate components that were not bound together at the time of deposition into those that contain lime mud and those in which lime mud is lacking. The three main divisions within Dunham's (1962) classification are between limestones which are matrix-supported (lime mudstones and wackestones), grain-supported (packstones and grainstones) and those that are biologically bound (boundstones) with a fourth category; crystalline limestones, also recognised. Boggs (2001) noted that Dunham's classification scheme does not consider the identity of the carbonate grains and that it is therefore desirable to also use other classification schemes.

Criticism has been directed at each of the classification schemes. Recognition of certain categories and their interpretation has been identified as a problem, specifically when studying limestones in thin section as many grains are not in contact but appear to float, resulting in difficulty determining between wackestone and packstone (Tucker and Wright, 1990). Blatt *et al.* (1980) emphasised that previous studies have often failed to recognise that the classification schemes are not the source of a conclusion but a tool for organising information.

**Table 3.1:** Folk's (1959; 1962) Classification of carbonates

Table 6.12. Folk's (1955, 1962) classification of carbonates									
		Limestones, partly dolomitized limestones,					Replacement dolomites		
		>10% Allochems Allochemical rocks		<10% Allochems Microcrystalline rocks					
		Sparry calcite cement > microcrystalline ooze matrix	Microcrystalline ooze matrix > spars calcite cement	1-10% Allochems	<1% Allochems	Undisturbed bioherm rocks	Allochem ghosts	No allochem ghosts	
		Sparry allochemical rocks	Microcrystalline allochemical rocks						
		Intrasparrudite	Intramicrodite						
		Intrasparite	Intramicrorite						
		Oosparrudite	Oomicrodite						
		Oosparite	Oomicrorite						
		Biosparrudite	Biomicrodite						
		Biosparite	Biomicrorite						
		Biopelsparite	Biopelmicrorite						
		Pelsparite	Pelmicrorite						



### **3.2.5 Carbonate sedimentation on the Mount Gambier coastal plain**

As previously mentioned, the southern continental margin of Australia is the largest area of modern temperate carbonate deposition on the globe (James *et al.*, 1997). Extensional basins along southern Australia were formed during the rifting of Australia from Antarctica in the Cretaceous (Veevers, 1986). The rapid movement of Australia combined with increased ocean circulation during the Eocene resulted in the formation of a Cenozoic carbonate shelf above the older terrigenous-clastic margin (Boreen *et al.*, 1993). The resulting carbonate shelf along the coast of southern Australia is wide: up to 200 km in the Great Australian Bight, with water depths up to 50 m. Farther to the east, the shelf is narrower and relatively steep (Gostin *et al.*, 1988).

The Otway carbonate platform comprises an eastern portion of the southern Australian continental margin in the form of a narrow open shelf with an average depth of 180 m (Boreen *et al.*, 1993). The Otway shelf lies between 37° and 40°S and is approximately 400 km in length. The shelf is at its narrowest point at Portland where it is 35 km wide, but broadens progressively westwards, measuring 60 km wide at Robe and 80 km at Warrnambool (Boreen *et al.*, 1993). The modern Otway Shelf comprises carbonate-generating organisms of a cool temperate bryomol assemblage (Nelson, 1988). The assemblage is distinguished by an abundance of non-phototrophic organisms consisting of bryozoa, with accessory molluscs, foraminifera, coralline algae and echinoderms (James and von der Borch, 1991; Boreen *et al.*, 1993). The Otway margin is fundamentally different from tropical margins in its lack of reef-building coral. The Mediterranean climate experienced along much of the southern Australian continental margin, combined with the generally low relief and lack of perennial streams results in a limited volume of silicate-dominated terrigenous sediment reaching the South Australian coastline. This permits the growth of carbonate-secreting organisms and results in bioclastic sedimentation being prevalent over much of the continental margin (Gostin *et al.*, 1988).

### **3.3 Sedimentary structures of aeolian and beach environments**

Throughout this thesis deposits of the Bridgewater Formation are referred to as calcarenite, which describes sand-sized sediment primarily composed of calcareous material. This term is commonly used as it does not imply the mode of sediment transportation. Where it is possible to identify that transportation was by wind, the sediment may instead be referred to as aeolianite.

The sands comprising the Bridgewater Formation on the Mount Gambier coastal plain are primarily calcareous and consist of aeolian, sub-aqueous and lagoonal facies. Identifying each of these separate facies sometimes proves challenging as they commonly yield similar bedforms. The following discussion describes the principal facies used to identify distinct modes of sediment transport and infer sea-level highstands. The stratigraphical terminology adopted in this study is presented alongside the depositional structures found within aeolian and sub-aqueous structures. Finally, previous studies that have used the identification of calcareous deposits to aid in determining sea-level highstands are discussed in order to provide a premise for identifying sea-level highstand deposits on the Mount Gambier coastal plain.

### **3.3.1 Stratigraphical terminology**

Structural terms used throughout this study are based on that of the North American Commission on Stratigraphical Nomenclature (NASCN, 1983) and the Field Geologist's guide to Lithostratigraphic Nomenclature in Australia (Staines, 1985). This section defines the structural terms used throughout this research and aids in describing possible bedding structures found within calcarenite of the Bridgewater Formation (Table 3.3).

Beds may be defined as tabular layers of sedimentary rock that have lithological, textural or structural unity that distinguishes them from the layers above or below (Boggs, 2001). Beds thicker than 1 cm are commonly classed as strata, while layers less than 1 cm may be described as lamina. The geometry of a bed is dependent on the relationship between the bedding surfaces and geometric forms and may include uniform-tabular, curved-tabular, wedge-shaped and irregular (Boggs, 2001). Where laminae within a bed are parallel to the bedding planes the bedding may be described as parallel or laminar. Where laminae are deposited at an angle to the principal bounding surfaces the term cross-bedding will be used. These structures are illustrated in the internal morphology of a dune (Figure 3.2).

**Table 3.3:** Structural terms used throughout this study

TERM	DEFINITION
<b>Lithostratigraphic unit</b> <sup>(1,2)</sup>	A body of rock strata which is distinguished on the basis of observable physical features in lithic characteristics and stratigraphic position.
Group	A sequence of two or more neighbouring formations that contain significant unifying lithological features in common.
Formation	The primary unit of lithographic classification consisting of a body of rock strata with a characteristic lithology.
Member	A named entity within a formation which possesses lithologic characteristics which distinguish it from other parts of the formation.
Bed	The smallest formal lithostratigraphic unit within a stratified sequence of rocks, consisting of lithologically distinctive layers several centimetres to a few metres in thickness
<b>Allostratigraphic unit</b> <sup>(3)</sup>	A mappable stratiform body of sedimentary rock defined and identified on the basis of its bounding discontinuities..
Alloformation	The fundamental unit in allostratigraphic classification, may be divided into allomembers.
Allomember	The formal allostratigraphic unit next in rank below an alloformation.
<b>Structural Terms</b> <sup>(3)</sup>	
<b>Bed</b>	A tabular or lenticular layer of rock that has lithological, textural or structural unity that distinguishes it from layers above or below. Beds are separated from one another by bounding surfaces.
Lamina	Layer of sediment < 1 cm thick <sup>(4)</sup> .
Stratum	Layers of sediment > 1 cm thick.
Bedset	A group of similar beds or cross-beds, representing a continuous period of sedimentation.
Coset	Two or more bedsets in a vertical sequence that contain similar structure and composition.
<b>Bed dip</b>	
True Dip	The angle the bed dips from the horizontal, taken perpendicular to the strike of the bed
Apparent Dip	The dip seen at a particular cross-section. Always less than the true dip
Gentle (low angle)	3-18°.
Moderate	19-25°
Steep (high angle)	26-35°
<b>Bedding types</b> <sup>(8)</sup>	
Foreset bed	The cross-laminae or strata found on the steep leeward side of a dune. Formed by grainfall and grain flow.
Topset bed	Low angle ripple laminations in the crest of the dune.
Backset bed	Low angle ripple laminations on the stoss (windward) side of the dune.
Bottomset bed	Low angle, leeward dipping, fine-grained strata. Formed beyond the downward limit of the slip face. Buried as the dune advances landwards.
<b>Internal bed characteristics</b>	
Parallel bedding	Beds that do not contain internal dipping laminae and are bounded by nearly planar surfaces that are in effect parallel to one another
Cross bedding	Strata or laminae that have an apparent dip
Tabular cross-bedding	Cross-bedded units that are laterally extensive and have essentially planar bounding surfaces. Formed mainly by the migration of large scale ripples and dunes (lower flow regime conditions)
Trough cross-bedding	Cross-bedded units where one or both bounding surfaces are curved, concave up strata. Small scale trough cross-bedsets are formed by migration of small current ripples, where by the migration of large-scale ripples may create trough cross-bedsets that range from 1 to 4 m in width, and a few tens of centimetres in thickness
Hummocky cross-stratification <sup>(5,10)</sup> (HCS)	Characterised by undulating sets of cross-laminae that are both concave upwards (termed 'swales') and convex upwards (termed 'hummocks'). The cross-beds gently cut into each other with curved erosion surfaces.
Swaley cross-stratification <sup>(6,7)</sup> (SCS)	Associated with HCS. Commonly flat bedded. Bedsets may be of substantial thickness. Suggested to be almost continuous rather than episodic though still associated with storm wave conditions. Probably formed in shallower water such as that found in the lower shoreface
Washover-deposits <sup>(9)</sup>	Storm driven waves cut through and overtop barriers, washing lobes of beach sediment into the back-barrier lagoon. Deposits are generally composed of fine- to medium-grained sand with thin to flat laminated beds. Scour pits may be present formed in the lee of any detritus.

<sup>1</sup>NASCN (1983); <sup>2</sup>Staines (1985); <sup>3</sup>Boggs (2001); <sup>4</sup>McKee and Weir (1953); <sup>5</sup>Harms *et al.* (1975); <sup>6</sup>Leckie and Walker (1982); <sup>7</sup>Tucker and Wright (1990); <sup>8</sup>Pye and Tsoar (1990); <sup>9</sup>Barwis and Tankard (1983); <sup>10</sup>Greenwood and Sherman (1986)

### 3.3.2 Lithostratigraphy and allostratigraphy

Ready identification of beach and dune facies aids in understanding depositional processes and coastal evolution at a given site. The use of allostratigraphy and lithostratigraphy can further assist in the interpretation of these sedimentary deposits.

The North American Commission on Stratigraphic Nomenclature (NASCN, 1983) defines a lithostratigraphic unit as a body of sedimentary, extrusive igneous, metasedimentary or metavolcanic strata that is distinguished on the basis of its lithic characteristics and stratigraphic position. Lithostratigraphic units may conform to the law of superposition which states that in any succession of strata not disturbed since deposition, younger sediments will lie above older sediments. Separate lithostratigraphic units may be recognised by observable rock characteristics, with boundaries placed at the positions of lithic change (NASCN, 1983). Different lithological units may be separated from one another by contacts, which are planes or irregular surfaces between rocks of different types (Boggs, 2001). These contacts may be conformable or unconformable. Conformable strata are found where there are unbroken depositional assemblages whereby layers have been deposited upon one another through essentially uninterrupted deposition (Boggs, 2001). Unconformities are surfaces of erosion or non-deposition that separate younger strata from older strata and represent a significant hiatus or interruption in the continuity of the geological record.

An allostratigraphic unit may be defined as a mappable stratiform of sedimentary rock that is defined and identified on the basis of its bounding discontinuities (NASCN, 1983). Walker (1992, pg 9), suggested that this definition required alteration to read ‘... bounding discontinuities and their correlative conformities’. Walker (1992) stated that the intent of allostratigraphy is not to replace lithostratigraphy, but that it should be used as a parallel scheme that emphasises bounding discontinuities which highlight important changes in depositional conditions. Allostratigraphy is therefore particularly useful in identifying structural forms within aeolianites as they are monolithological features. Bounding discontinuities define allostratigraphic units in which depositional conditions were either similar or changed progressively without breaks. They are therefore more natural subdivisions of the geological record in terms of interpretative purposes as opposed to lithostratigraphical units (Walker, 1992). The classification of allostratigraphic units is of value when studying Quaternary stratigraphic successions of compositionally similar sediment that are products of different processes and may demonstrate different ages (Brooke *et al.*, 2003).

The recognition of separate lithostratigraphic or allostratigraphic units identifies that there has been a change in the sediment deposition regime. This may be in the form of a period of non-deposition, or a change in deposition style such as sub-aqueous to aeolian.

### **3.3.3 Aeolian environments**

The term aeolianite was first used by Sayles (1931) to describe any sediment deposited by the wind and subsequently lithified. As it has come to be used in the geological community, aeolianite is predominantly a coastal limestone that has the potential to record the reworking of marine carbonate sediment into coastal dunes (Brooke, 2001). Aeolianite is most commonly found as calcium carbonate cemented dune rock deposited in coastal environments (Fairbridge and Johnson, 1978), though the term has expanded to also encompass shallow marine and terrestrial facies (Brooke, 2001).

In a review of the global distribution of aeolianite, Brooke (2001) correlated the occurrence of temperate Hertzogian Association carbonates with the distribution of aeolianite. However, no significant relationship was identified between aeolianite and the distribution of reefal carbonates (Brooke, 2001). Major aeolianite tracts were found to be located along the coastal margins of carbonate shelves in the Southern Hemisphere which received little terrigenous sediment due to the limited extent of Pleistocene glaciations in this region (James, 1997) and the lack of silicate input from other terrestrial sources. The ultimate control on the formation of aeolianite is suggested to be carbonate production on shallow shelves and banks (Brooke, 2001). McKee and Ward (1983) suggested that requirements for the development of aeolianite include a warm climate favouring the production of calcium carbonate sediments and onshore winds providing a transport mechanism of coastal carbonate to inland areas of deposition. On the Mount Gambier coastal plain both of these criteria are met through the (cool but) highly productive Otway carbonate shelf, and strong southerly winds.

Brooke (2001) also noted that coastlines that preserve aeolianite morphologies commonly form elongate, shore-parallel sediment bodies deposited as transverse ridges. The elongated dune ranges of the Bridgewater Formation on the Mount Gambier coastal plain are a classic example.

Assessment of sedimentary structures present within aeolianite (and calcarenite) can aid in palaeo-reconstruction of its depositional environment. Several studies investigating the shoreline barriers on the Coorong coastal plain in southern Australia identified composite barrier formation (Schwebel, 1978; Murray-Wallace *et al.*, 1999) and noted distinct facies

within these barriers indicative of different depositional sub-environments. For example, in an assessment of the facies architecture of the Woakwine Range, Murray-Wallace *et al.* (1999) noted a distinctive layer of landward migrating dunes overlying a lagoonal facies. Familiarity with the range of possible facies and their terminology allows for more accurate palaeo-environmental reconstruction of the depositional setting.

#### **3.3.4 Internal dune morphology**

Initial stages of dune formation along a coastal area consist of the transfer of beach sand by onshore winds to form parallel ridges along the coast (McKee and Ward, 1983). When sand is transported by wind, bedforms will develop. Within a few minutes of aeolian transport small ripples form, while dunes will develop after a more considerable period of time; between several hours to thousands of years (Kocurek, 1996). The stoss (or windward) slope of a dune is typically found at a lower angle (10° to 15°) than the lee slope, which is commonly at the angle of repose for dry sand, ~33°. As wind flows over the dune, the flow must accelerate over the inclined stoss slope, resulting in an increased rate of transport and erosion on this face. Deposition, therefore, dominantly occurs on the lee face (Kocurek, 1996).

Stratification within an aeolian deposit results from the migration of bedforms as they climb at various angles and directions over one another. Yet, bedforms of moving sand are rarely simple and can be affected by the presence of existing structures (Brookfield, 1992). Hunter (1977) identified the thinnest recognisable strata within aeolian dune systems and grouped them into; plane-bed laminae, ripple-form laminae, ripple-foreset cross-laminae, climbing translational strata, grainfall laminae, and sandflow cross-strata. Hunter (1977) outlined the characteristics of basic types of aeolian stratification and these are presented in Table 3.4.

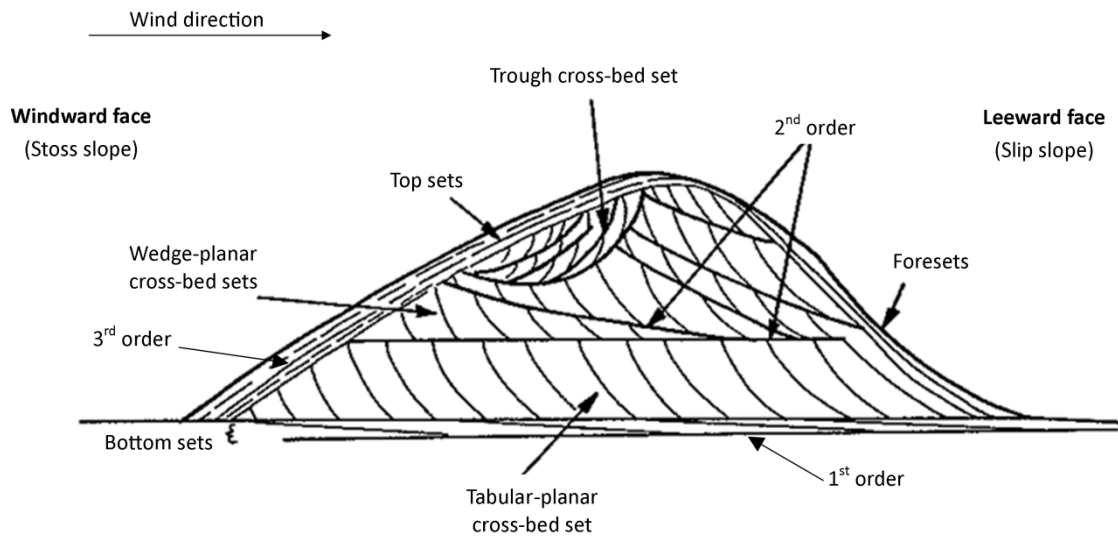


**Figure 3.2:** Schematic diagram of the internal stratification features in an 'ideal' simple dune (modified from Pye and Tsoar, 1990).

Where tractional processes are dominant on the dune face, wind ripples occur and result in wind-ripple laminae, while on slopes where gravity processes dominate grainfall laminae and sandflow strata are more common stratification types (Kocurek, 1996). Wind-ripple laminae (also termed climbing translational stratification) are thin (a few mm thick) and closely packed, with foresets generally not apparent. Wind ripple laminae are commonly of low angle and are produced on both the stoss and lee sides of the dune. Inverse grading is common in these laminae, reflecting grain segregation on the wind ripples (Kocurek, 1996). Grainflow laminae develop on the leeward face of the dune where flow separation occurs (Hunter, 1977). As the airborne grains fall onto the foreset slope, they form relatively high angle, uniform laminae that pinch out towards the base of the slope. The dramatic variation in grainfall laminae thickness has been attributed to wind duration (Fryberger and Schenk, 1981). Grainfall deposits tend to show intermediate packing, are indistinctly laminated and are generally less well-preserved in subaqueous settings (Kocurek, 1996). Sandflow occurs when the wedge of sand formed through grainfall processes avalanches as the grainfall strata steepens above the angle of repose (Hunter, 1977; Fryberger and Schenk, 1981). Sandflow cross-strata are, however, well-sorted and internally structureless due to loose packing and appear as tabular, upward tapering wedges (Kocurek, 1996).

Hunter (1981) suggested that the size of the aeolian deposit may affect the percentage of each stratification type found within the unit. Hunter (1981) observed that in relatively

large dunes sandflow cross-strata are more dominant, while in smaller dunes wind climbing ripple stratification and grainfall laminae are more common. This hypothesis is supported by the findings of Loucks and Ward (2001) who found that in relatively small dune sets on the Cancun deposits, Mexico, stratification was composed primarily of climbing ripple structures (57%), and grainfall lamination (36%), while sandflow strata only comprised a minimal amount (7%) of the aeolian stratification.

Bounding surfaces (or unconformities) may be defined as an erosional surface within or between sets of cross-strata (Kocurek, 1996). Bounding surfaces can be recognised at three distinct scales (Brookfield, 1977, 1992; Collinson and Thompson, 1989; Kocurek, 1996). Third-order bounding surfaces are the smallest recognised scale and separate bundles of foreset laminae within the same set and are suggested to record short-term fluctuations in wind strength and direction. These are most commonly found in the upper parts of sets and usually form a convex-upwards shape. Second-order bounding surfaces may be either horizontal or dip at angles up to 20°. These reactivation surfaces are suggested to reflect a pause in dune migration which may have been caused by plant colonisation on the dune or a modification of the slip face by varying wind strengths. First-order bounding surfaces are more difficult to recognise and their presence may commonly only be noted where they clearly truncate or are overlain by second-order surfaces. First-order bounding surfaces are characterised by their large lateral extent and low angles of inclination. These discontinuities reflect an erosional break or the migrating face of a dune deposit and represent the climbing face of a dune. Recognisable bounding surfaces within the sedimentary structures of a dune are illustrated in Figure 3.2 at various scales. Figure 3.3 also highlights a range of bedding types commonly found in aeolian sediments within South Australia.



**Table 3.4:** Characteristics of basic types of aeolian stratification (Hunter, 1977)

Depositional Process	Character of depositional surface	Type of stratification	Dip angle	Thickness of strata and Sharpness of contacts	Segregation of grain types Grain sizing	Packing	Form of strata
Tractional deposition	Rippled	Subcritically climbing translent stratification	Stratification: low (typically 0-20°, maximum 30°). Depositional surface: similarly low	Thin (typically 1-10mm, max. ~5cm). Sharp, erosional contact.	Distinct inverse	Close	Tabular, planar
		Supercritically climbing translent stratification	Stratification: variable (0-90°) Depositional surface: intermediate (10-25°)	Intermediate (typically 5-15 mm). Gradational contact.	Distinct inverse except in contact zones	Close	Tabular, commonly curved
		Ripple-foreset cross-lamination	Relative to translent stratification: intermediate (5-10°)	Individual laminae: thin (typically 1-3 mm). Sharp or gradational, non-erosional contact.	Individual laminae and sets of laminae: indistinct, normal and inverse, neither greatly predominating	Close	Tabular, concave-up or sigmoidal
		Rippleform lamination	Generalized intermediate (10-25°)			Close	Very tabular, wavy
Largely grainfall deposition	Smooth Smooth	Planebed lamination	Low (typically 10-25°)	Sets of laminae: intermediate (typically 1-10 cm). Sharp of gradational, non-erosional contact		Close	Very tabular, planar
		Grainfall lamination	Intermediate (typically 20-30°, min. 0°, max. ~40°)			Intermediate	Very tabular follows pre-existent topography
Grainfall deposition	Marked by avalanches	Sandflow cross-stratification	High (angle of repose) (typically 28-34°)	Thick (typically 2-5 cm). Sharp, erosional or non-erosional contact.	Distinct to indistinct, inverse except near toe	Open	Cone-shaped, tongue-shaped, or roughly tabular



**Figure 3.3:** Bedding within aeolianite deposits from the River Murray mouth region South Australia. **A:** Tabular cross-bedding, Surfers Beach. **B:** Tough-cross bedding, Knights Beach, Port Elliot. **C:** Planar bedding, Boomer Beach, Port Elliot (geology hammer is 28 cm long)

### 3.3.5 Beach environment

When reconstructing palaeo-shoreline environments familiarity with the facies of the beachface can aid in depositional interpretations. The beachface environment can be categorised into a number of different zones. Within these zones common sedimentary structures may differ as illustrated in Figure 3.4.

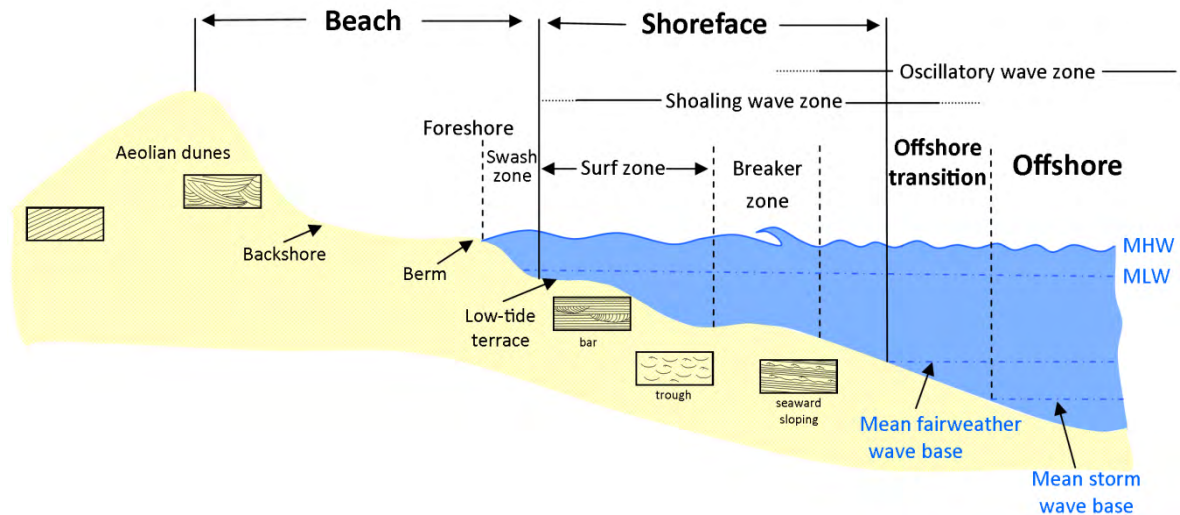


**Figure 3.4:** Generalised cross-sectional profile of the beach and nearshore identifying principal zones of wave activity (modified from Boggs, 2001). Note, MHW = mean high water level, MLW = mean low water level.

The backshore extends landwards from the beach berm above the high tide level and may commonly include back-beach deposits. The backshore is only inundated by seawater during higher energy conditions such as storms. This zone is, therefore, primarily dominated by aeolian processes and storm-wave deposition in the form of washover facies.

The foreshore encompasses the intertidal zone between the high and low tide levels. Sedimentation is dominated by swash processes and structures within this zone are predominantly gently ( $2-3^\circ$ ) seaward dipping, parallel laminae.

The shoreface extends from the low tide level to the transition between beach and shelf sediments (also known as the fair weather wave base, which is the depth below which waves in normal climatic conditions do not interact with the sea floor). The shoreface may be further divided into three zones; upper, middle, and lower. The upper shoreface includes the surf zone and is dominated by strong bidirectional waves and longshore currents. Sedimentary structures within this zone consist of multi-directional cross-bedding, but may also include low-angle bidirectional cross-beds. The middle of the shoreface encompasses the breaker zone and is thus also dominated by high energy conditions in the form of breaking waves and

rip currents. Sedimentary structures within the middle shoreface may be highly complex depending on the presence of onshore bars, but may include both landward and seaward dipping trough-cross-beds as well as sub-horizontal planar lamination. The lower shoreface, or outer shoaling zone, is composed of sediments deposited in low energy conditions and thus nearly horizontal laminated bedding is the primary sedimentary structure within this zone. During stormy conditions, however, hummocky and/or swaley cross-bedding may develop as the wave base interacts with the sea floor.

The offshore zone extends seaward from the fair-weather base and sedimentary deposits here are generally fine-grained and massive, with asymmetric ripples forming as a result of oscillatory wave currents.

**Table 3.5:** Sedimentary structures of the beach environment

STORM DOMINATED – HIGH ENERGY ENVIRONMENT				
Zone of Deposition	Sedimentary Structure	Dip Direction	Dip Angle	Bedding thickness
<b>Backshore</b> <sup>(1)</sup> Seaward of beach barrier	<b>Overwash deposits</b> – horizontally bedded alternating layers of terrigenous sand, shell fragments and heavy minerals. Onshore directed cross-bedding	Landwards	Gentle: 1-4°	
<b>Lower Foreshore</b> <sup>(2,3)</sup> Extends to storm wave breaker zone	<b>Swaley cross-stratification</b> - staked swales preserved	Variable/Flat	Gentle: relatively flat	Substantial thickness (several metres)
<b>Offshore</b> <sup>(3,4,5,6)</sup> Between fair-weather wave base (FWB) and storm wave base (SWB)	<b>Hummocky cross-stratification</b> - gently curved low angle bedding	Variable	<10-15°	< 2 m
MODERATE ENERGY – BARRED BEACH				
Zone of Deposition	Sedimentary Structure	Dip Direction	Dip Angle	Bedding thickness
<b>Upper shoreface</b> <sup>(8)</sup>	Alongshore bars – parallel lamination	Seaward dipping		
<b>Lower shoreface</b> <sup>(3,7,9)</sup>	Rip channels – cross-bedding associated with rip currents and migrating ripples	Seaward dipping	Steep	0.5-1.5m
MODERATE ENERGY – NON BARRED BEACH				
Zone of Deposition	Sedimentary Structure	Dip Direction	Dip Angle	Bedding thickness
<b>Foreshore</b> <sup>(7,10,11)</sup> – swash zone	Parallel laminations (laminae, 1-2 cm thick, coarsen upwards)	Seaward	Gentle	
<b>Upper shoreface</b> <sup>(7)</sup> Breaker zone	Cross-bedding generated by shoaling waves. Pebbles lags concentrated by breaking waves in upper section	Seaward		
<b>Lower shoreface</b> <sup>(9,10)</sup>	Asymmetrical ripple lamination – shoreward inclined ripple cross-lamination	Landwards		
<b>Offshore</b> – <sup>(10)</sup> between FWB and SWB	Symmetrical ripple lamination			
<b>Offshore</b> – below FWB <sup>(7,12)</sup>	Flat parallel laminations – bioturbated sand	Flat	Flat	
LOW ENERGY ENVIRONMENTS				
Zone of Deposition	Sedimentary Structure	Dip Direction	Dip Angle	Bedding thickness
<b>LOW WAVE ENERGY BEACH</b>				
<b>Foreshore</b>	Parallel laminated sand, small-scale ripple lamination	Flat	Flat	2 m
<b>Upper shoreface</b> <sup>(12)</sup>				
<b>TRANSGRESSIVE LAGOONAL BARRIER</b> <sup>(13,14,15)</sup>				
<b>Upper sequence</b>	Medium barrier sand with thin clay lenses		Finely laminated, flat. May be structureless due to bioturbation	7 m
<b>Middle of sequence</b>	Lagoonal facies: a shell-rich layer composed of clay and silt			8 m
<b>Lower sequence</b>	Medium to coarse marine sand underlies lagoonal facies			
<b>PROGRADING LAGOONAL BARRIER</b> <sup>(13)</sup>				
<b>Upper shoreface</b>	Medium-grained, laminated sand			4 m
<b>Middle Shoreface</b>	Fine to medium sand with clay and silt lenses			5 m
<b>Lower shoreface</b>	Shell-rich clay and silt			2.5 m

<sup>1</sup>Sedgwick and Davis (2003); <sup>2</sup>Leckie and Walker (1982); <sup>3</sup>Tucker and Wright (1990); <sup>4</sup>Dott and Bourgeois (1982); <sup>5</sup>Walker *et al.* (1983);

<sup>6</sup>Harms *et al.* (1975); <sup>7</sup>Elliot (1986); <sup>8</sup>Hunter *et al.* (1979); <sup>9</sup>Short and Hesp (1999); <sup>10</sup>Clifton *et al.*, (1971); <sup>11</sup>Clifton (1969); <sup>12</sup>Howard and Reineck (1981); <sup>13</sup>Kraft and Chrzastowski (1985); <sup>14</sup>Reading (1996); <sup>15</sup>Murray-Wallace *et al.* (1999).

### **3.3.6 Coastal barriers**

Coastal shoreline barriers may be defined as elongated, shore-parallel sand bodies that extend above sea level (Roy *et al.*, 1994). Coastal barriers form through vertical accumulation of sand which has been transported onshore. Barriers are most commonly found on wave-dominated coasts, where waves influence the shape of the barrier and its seaward shore with episodic washover of barriers resulting in saline, lagoonal waters landward of the barrier (Woodroffe, 2003). Coastal dunes may accumulate above the barrier. Transgressive barriers, where barriers are in dynamic equilibrium with rising sea level by transferring sediment landwards, most commonly form on high-energy coasts where sand is supplied by high-energy waves in large quantities (Roy *et al.*, 1994). In these conditions, transgressive barriers may be 15-25 m thick and 2-3 km wide (Thom, 1984), though volumes will vary depending on sediment supply. In eastern Australia, transgressive dunes occur in the most exposed locations; usually downdrift in terms of longshore transport (Woodroffe, 2003). While coastal barriers are a common feature on many modern coastlines, a much lower number are preserved in the geological record as they are often eroded by successive sea-level highstands or subaerial processes. Barriers composed of siliceous sands may be more extensive, but carbonate dunes cemented to form aeolianite more commonly preserve a more detailed archive of dune activity (Woodroffe, 2003).

On the Mount Gambier coastal plain, coastal barriers are comprised predominantly of carbonate-skeletal sands, transported onshore from the Bonney Shelf. The high-energy, wave-dominated shoreline of the coastal plain promotes the development of these features. Barriers are of a similar size as the size of transgressive barriers proposed by Thom (1984), and their overall morphology including a back-barrier lagoon, fits the conceptual model of coastal barrier development well. The barriers on the Mount Gambier coastal plain are well-preserved due to the steady tectonic uplift of the region which essentially removes each barrier from successive sea-level highstands, and the semi-arid climate which promotes pedogenesis and the formation of protective calcrete horizons which preserve the overall morphology of the barriers.

### **3.3.7 Distinguishing between aeolian and sub-aqueous deposition**

Aeolian and subaqueously formed sedimentary structures are commonly similar in their visual characteristics and thus distinguishing between the two modes of deposition can be challenging when they are similarly cross-stratified (McKee and Ward, 1983; Brookfield, 1992). Loope and Abegg (2001) noted that aeolianites are commonly found to contain grains that

have been generated in sub-aqueous environments further complicating the distinction between aeolian and sub-aqueous deposition.

McKee and Ward (1983) noted the difficulty in confidently confirming the depositional environment of calcareous aeolianite and suggested that a diagnostic feature common to aeolian limestone and calcareous dunes is the presence of rhizoliths or root casts which are rarely found in marine or beach deposits. Trace fossils such as rhizocreations, root-hair sheaths and the micro-boring of certain plant root systems can also aid in identifying aeolian deposition (McKee and Ward, 1983).

While Hunter (1977) cautioned that the basic types of stratification found within dry aeolian deposits may also be found within water-lain sands, stratification may also be used to distinguish between depositional environments when used attentively. McKee and Ward (1983) identified stratification within aeolian deposits as alternating between fine and coarse laminae, generally highly cross-stratified on a large scale, and with high-angle foresets dipping predominantly landwards if coastal. Hunter (1977) noted that there is a distinct difference in the climbing-ripple structures, with sub-aqueous current ripples generally being well graded and having distinct ripple-foreset cross-lamination. Loope and Abegg (2001) suggested that this is the only commonly occurring, reliable diagnostic criteria for distinguishing an aeolian mode of deposition. However, Kindler and Davaud (2001) noted that wind-ripple strata may be poorly defined in well-sorted carbonate aeolianites that are lacking detrital quartz. Other differences between climbing ripple-structures in aeolian and sub-aqueous environments include variations in height-to-spacing ratios and the plan form of ripples (Hunter, 1977).

Table 3.6 compares aeolian and subtidal stratification patterns. However, it must be cautioned that some of the criteria are reliant on a lack of features and it is sometimes challenging to be confident these features are definitely not present.

**Table 3.6:** Comparison of aeolian and subtidal stratification patterns (from Loope and Abegg, 2001)

<b>Aeolian</b>	<b>Subtidal</b>
Climbing translational stratification	Subaqueous climbing ripples
Grainfall	Grainfall
Grainflow	Grainflow
Well to very well sorted	Moderate sorting
Typically very fine to medium sand grains > 4 mm extremely rare	Grains > 4 mm common
Well-rounded and abraded allochems	Rounding variable
Large-scale (>1 m) cross strata common	Large-scale cross strata rare
Tangential foresets	Tangential foresets less common
Straight-crested, low amplitude ripples (high ripple indices)	Sinuuous, high-amplitude ripples (low ripple indices)
Trace fossil diversity low	Trace fossil diversity high
Adhesion ripples present	Adhesion ripples absent
Calcrete (scattered rhizoliths, alveolar texture) within or immediately below aeolianites	Calcrete only present immediately beneath exposure surfaces
Vadose cements (scattered pendant meniscus)	Vadose cement present below exposure surfaces

Frebourg *et al.* (2008) analysed thin section samples of aeolianite from a range of global locations and concluded that with the exception of pinstripe laminated facies there was no other clearly distinguishable evidence of aeolian deposition within the samples. Frebourg *et al.* (2008) suggested that aeolian sedimentary structures, such as leeward-dipping foresets, grainflow and pinstripe lamination, are more easily distinguishable at the outcrop scale.

Distinguishing between aeolian and sub-aqueous deposits is even more challenging in carbonate environments. Within siliciclastic sands the recognition of aeolian origins is reliant on the presence of diagnostic structures. However, within carbonate-rich aeolian deposits sedimentary structures are less easily detectable due to a lack of grain size contrast (Frebourg *et al.*, 2008), the diversity of shapes, and the densities of carbonate particles which lowers the critical shear velocity of the sediment and thus blurs the sedimentary structure record (Jorry *et al.*, 2006).

In an investigation into the Pleistocene history of Bermuda, Land *et al.* (1967) adopted a range of criteria to differentiate between marine and aeolianite deposits. The criteria incorporated; colour, texture, structure, and fossil presence into the diagnosis. Land *et al.* (1967) suggested that on Bermuda, aeolianites were medium- to fine-grained in texture and well- to moderately-sorted, while marine deposits were coarse- to medium-grained and sands were poor- to moderately-well-sorted. In terms of structure, Land *et al.* (1967) proposed that the Bermudian aeolianites displayed steep foreset bedding with windward stratification and the presence of burrow and root structures, while marine sediments displayed shallower dipping beach stratification with rare festoon or tabular cross-bedding. Land *et al.* (1967) also



noted fossils within aeolianite were predominantly terrestrial while marine molluscs were present within the marine deposits.

In summary, while it is difficult to distinguish between sediments deposited within aeolian and subaqueous environments, there are several features that may be used to identify depositional settings. Commonly, sediment that has been deposited by the wind may produce thicker sets of cross-beds at a larger scale than those formed in sub-aqueous or beach settings. The dip-angle of the beds within an aeolian deposit may also be steeper than on a beach face, with beach facies commonly of a gentle angle as a result of swash and backwash processes. The ripple index of wind ripples, where preserved, is higher than that of sub-aqueous deposits. The presence of rhizolith/root cast features are also indicative of aeolian deposits and are rarely found in preserved beach facies. In sandy sediments it is hard to distinguish between aeolian and subaqueous settings based on structures alone and interpretations can be aided by data on the sediment size and surface textures. Large clast sizes, such as a gravel lag, are indicative of a beach environment as would be too large to have been entrained by aeolian processes. Identification of these separate facies will prove useful for palaeo-environmental reconstruction on the Mount Gambier coastal plain, where shoreline barriers are likely to consist of both subaqueous and aeolian facies.

### **3.3.8 Preservation potential of carbonate sand deposits**

Palaeo-environmental reconstruction of facies within shoreline successions on the Mount Gambier coastal plain will be further aided by knowledge of the preservation potential of varying facies. The preservation potential of certain facies within the aeolian and subaqueous environments is dependent on a range of factors. This section addresses what these factors are and discusses which facies may be preferentially preserved.

#### **Aeolian deposits**

Carbonate aeolianites may be preferentially preserved in areas subjected to rapid pedogenesis and the resultant formation of calcrete palaeosols which aid in protecting the underlying sedimentary structures. In comparison with siliciclastic aeolian deposits, which lack significant early cementation, the meteoric cementation and presence of well-lithified calcrete profiles improves the preservation potential of carbonate aeolianite (Abegg *et al.*, 2001). On the Mount Gambier coastal plain the development of calcrete profiles have aided in preserving the barrier successions of the Bridgewater Formation.

Unlike many other systems, in aeolian environments accumulation of sediment may occur well above the baseline of erosion yet have little preservation potential. Kocurek (1996)



stated that there are two factors which promote the preservation of aeolian deposits; subsidence, and a rise in the water table. Loope and Abegg (2001) proposed that the preservation of aeolianite is more likely if the dune strata are beneath the water table and if the structure is lowered beneath the wave base of subsequent sea-level transgressions through subsidence. Subsidence may occur through tectonism or loading and compaction, while a rise in the water table may be associated with a change to a more humid climate, subsidence through a water table or sea-level rise (Kocurek, 1996). Aeolianites that are deposited at a time of regressing sea level may have a greater likelihood of preservation as opposed to those deposited during transgressive sea level, as they are potentially subjected to a longer period of cementation (Abegg *et al.*, 2001). Within the Wilderness Barrier system in South Africa, Bateman *et al.* (2011) suggest that during MIS 1, only late Holocene dunes are preserved, as they formed during sea-level regression.

The preservation of dune deposits is suggested to be enhanced by cementation of the dunes or if dunes climb during migration, thus burying strata below the interdune surface. The importance of the transfer of sand from the bedforms to the storage space below the interdune surface is also stressed by Kocurek (1996), who stated that this transfer may occur as the wind power decelerates over time.

The angle and thickness of aeolian bedforms also aid in preserving the original sedimentary structure (Rubin and Hunter, 1982; Mountney and Howell, 2000). For bedforms of a given morphology and size the angle of climb is a key parameter in determining the thickness of the set that accumulates after the passage of bedforms, with thicker and larger bedforms preserving thicker sets (Mountney and Howell, 2000). Where climbing is of a low angle (subcritical) the basal position of the original bedform will only be partially preserved. It is the lower portions of foresets that commonly accumulate material and, therefore, the preserved lower set only provides a record of basal lee processes (Kocurek, 1996).

Climate is another critical factor contributing to the preservation of carbonate aeolianites. Climate can influence how quickly a dune is cemented and can affect the rate and distance of inland dune migration (Abegg *et al.*, 2001). In humid climates carbonate aeolianites are more readily case-hardened which aids in stabilisation of the dune (Budd, 1988; Dravis, 1996). Climate also influences diagenesis which can lead to calcrete formation. Calcrete formation is favoured by arid to semi-arid conditions, and can act as a protective covering to carbonate deposits. Calcrete formation and its use in palaeo-environmental reconstruction is further addressed later in the chapter (section 3.3.8).

Vertebrate trackways are useful in the recognition of carbonate aeolianite, but are rarely preserved (Loope and Abegg, 2001). Preserved elephant footprints have been recognised within a Pleistocene aeolianite exposure at Still Bay, South Africa, and are thought to have been made during MIS 5e to MIS 5b (Roberts *et al.*, 2008). The preservation of the footprints at Still Bay was dependent upon factors such as substrate consistence, substrate slope and the time elapsed between making and burial of the footprints (Roberts *et al.*, 2008). It is proposed that sand was moistened by rain or dew in order to provide the necessary cohesion to preserve the anatomical detail of footprints (Roberts and Berger, 1997). Trackways of the ruminant goat *Myotragus balearicus* preserved in late Pleistocene aeolianite on the southern coast of Mallorca are suggested to have also been deposited while the sediment was wet, aiding in their preservation (Fornos *et al.*, 2002). The high carbonate content of the coastal dunes is also suggested to aid in the preservation of footprints as it promotes rapid calcification by groundwaters. On the eastern side of Clare Bay, South Australia, Belperio and Fotheringham (1990) described a set of kangaroo prints on a prograding beach bar exposed through coastal erosion. Belperio and Fotheringham (1990) also suggested that these footprints were preserved due to the moist nature of the sand at their time of formation and to the fortuitous timing of overwash processes.

### **Beach Facies**

A range of factors can determine the preservation potential of certain beach facies. Local factors include: sediment supply, pre-existing topography, wave energy, tidal range, depth of erosion, erosional resistance and the rate of sea-level change (Belknap and Kraft, 1981; Billeaud *et al.*, 2007). Rapid sedimentation can aid in preservation of facies (Clifton *et al.*, 1971), and therefore certain beach facies found lower in a sequence may potentially be preferentially preserved. For example, within prograding systems the swash zone, rip channel and nearshore facies may be favourably preserved over a bar sequence (Davidson-Arnott and Greenwood, 1976; Hunter *et al.*, 1979). Belknap and Kraft (1981) commented upon the effect of erosion depth on preservation of beach facies. They suggest that where erosion depth is greater preservation will be limited. They then relate this to rate of sea-level change and noted that in the early stages of a transgression, where the rate of sea-level rise is rapid the depth of erosion will be less and thus preservation potential of facies is increased. Where sea-level rise and coastal erosion are slower, however, the depth of erosion is greater and potential for facies preservation is reduced (Belknap and Kraft, 1981).

Short and Hesp (1982) noted that the climatic regime experienced in a region can also aid in the preservation of beach facies, and specifically noted the semi-arid climate of South Australia which promotes the formation of hard calcrete horizons.

### **Summary**

A range of factors may influence the preservation potential of both aeolian and beach facies. The mineralogy of the material can aid in preservation with carbonate sands promoting the formation of hard calcrete horizons as opposed to siliceous sediment. The climate of the region can also aid in calcrete formation, while the climate at time of deposition, can aid in preserving certain features such as animal trackways in dunes in wet sediment. Rates of sea-level change can also promote faster or slower rates of erosion, and in turn influence the preservation potential of facies.

Higher rates of sedimentation can aid in preserving facies lower in a sequence and thus these facies are preferentially preserved. In the beach environment these include offshore and nearshore facies, while in an aeolian system preserved facies are found towards the base of the dune, such as basal sets. Accurate interpretation of facies architecture in regards to regressing or transgressing sea levels and knowledge of preferentially preserved deposits will enhance palaeo-environmental reconstructions.

### **3.3.9 Subaerial alteration**

Periods of subaerial exposure of the upper bounding surface of sediment or rock can aid in identifying significant breaks in sedimentation. To recognise these subaerial exposure surfaces the sediment must be exposed long enough for subaerial diagenetic processes to modify or remove pre-existing material. Major subaerial exposure events in coastal environments may include episodes of global sea-level fall associated with glacials or tectonic uplift, and can be present in both sub-tidal and aeolian sedimentary surfaces (Harrison, 1977; Loope and Abegg, 2001). Indicative features of subaerially exposed surfaces include calcrete horizons, palaeosols and protosols, and karstic features such as rhizoliths and solution pipes.

### **Calcrete**

Karst and soil surfaces are commonly the result of diagenesis of carbonate sediments due to subaerial exposure and involve the mobility of calcium carbonate. Soil facies are less commonly preserved intact prior to subsequent erosion. Esteban and Klappa (1983) suggested that the formation of a calcrete (or caliche) facies, whereby soil products are lithified before erosion or the deposition of new sediment, acts as an exception to this rule and provides a useful indicator of sub-aerially exposed surfaces. Calcrete can be described as a fine-grained,

chalky to well-cemented deposit which is low in magnesium calcite and has formed in pre-existing sediments (Esteban and Klappa, 1983). The term calcrete (or caliche) refers to secondary calcareous material that has accumulated as hard beds or within a recognisable soil horizon at the surface (Warren, 1983).

Climate and surrounding soil cover commonly determine calcrete development. Calcretes can be found within semi-arid climates; where moisture availability is not too great as to result in net solution and karst topography, but not limited either in which case only a superficial case-hardened surface may develop (Harrison, 1977). Esteban and Klappa (1983) suggested that calcrete horizons are restricted to areas experiencing less than 500 mm rainfall per annum and where evaporation rates exceed precipitation. In southern South Australia, Warren (1983) proposed that the semi-arid Mediterranean climate, where little surface runoff is experienced and the water infiltrated into the dunes is quickly returned to the atmosphere by evapotranspiration, is a primary factor in the formation of pedogenic calcretes in this region. As well as climate, the available soil cover present can influence calcrete formation. Harrison (1977) noted three ways in which soil cover can influence calcrete development: 1) soil cover can determine the downward flow of meteoric water and ultimately affect the moisture balance, 2) the soil environment may affect the water chemistry and in turn weathering of the underlying substrate, and 3) the soil may serve as a source of calcium carbonate.

Calcrete formation in coastal carbonates has been noted to be associated with the near surface soil zone of intense plant root growth and plentiful soil biota (Warren, 1983). Rates of calcrete formation may also be affected by rainwater and groundwater chemistry and this is discussed further in Chapter 4 (section 4.2). Harrison (1977) described the formation of calcrete (caliche) profiles as encompassing four stages. 1) Initiation – the carbonate sediment becomes subaerially exposed and subjected to dissolution by meteoric water, through tectonic uplift or perhaps a fall in relative sea level. A calcrete profile will be initiated if most of the water for evaporation is held at or near the subaerial surface resulting in calcium carbonate taken into solution and reprecipitated close to the subaerial surface. 2) Development of a seal – over time the continued dissolution of source calcium carbonate and associated reprecipitation will result in the development of enough secondary calcium carbonate to accumulate and effectively seal against the downward percolation of meteoric waters. 3) Aggrading accumulation of carbonate – the development of an impermeable horizon will limit the subsequent precipitation of calcium carbonate to higher positions within the calcrete

profile, continuing until the source of calcium carbonate is depleted. 4) Destruction of the original profile – at the terminus of stage 3 the continuation of calcrete formation can only occur at the expense of the upper portion of the earlier formed calcrete. Resultant *in situ* calcrete evolution is thus self-limiting and will reach a critical stage beyond which the profile thickness will not increase, despite continued subaerial exposure (Harrison, 1977).

Calcreted surfaces are not always uniform in appearance. As mentioned previously, the calcrete profile will reach a certain thickness beyond which it cannot increase, and thus its extent is ultimately controlled by the moisture balance, the porosity and permeability of the underlying substrate, and the availability of a source of calcium carbonate (Harrison, 1977). Calcrete horizons may be laminar in appearance, in which case they have formed as water perched on top of a surface is affected by evapotranspirative processes and thus deposit laminations (Warren, 1983). Calcrete may also appear rubbly or brecciated in character, whereby sub-angular to rounded fragments of the host structure are found floating within micritic carbonate (Harrison and Steinen, 1978). In South Australia, Warren (1983) noted brecciated surfaces consisting of fragmented earlier dune calcretes was the result of erosion and disaggregation of calcreted dune surfaces. Warren (1983) described regions whereby subsequent deposition of dune sand may occur above the brecciated surface, and then subsequent lowering of this sediment by deflation processes to expose the breccia once more, which may then become incorporated and cemented into a new calcrete. Brecciated calcretes may thus be indicative of a re-worked calcrete.

Calcreted surfaces have been used in several studies to determine episodes of subaerial exposure and a hiatus in sediment deposition. Harrison and Steinen (1978) described multiple brecciated micritic carbonate horizons within carbonate sands in Barbados and Kentucky, USA. They were able to trace the calcreted surface from one outcrop to the next and stated they were relatively planar. The horizons were interpreted to be of diagenetic origin, forming through the exposure of carbonates to subaerial conditions resulting from relative sea-level falls in the regions (Harrison and Steinen, 1978). Warren (1983) noted that cliff facies within coastal dunes in southern South Australia were composed of cross-bedded dune sand separated by calcrete horizons. He associated the deposition of dune sands to interglacials, and calcrete formation to occur as the sediment is exposed prior to the next episode of dune deposition. Also within South Australia, Milnes and Ludbrook (1986) described laminar carbonate crusts commonly found on top of individual beds. Barwis and Tankard (1983) interpreted calcrete development to have occurred as the underlying seaward-

dipping sandstone in False Bay, South Africa, was subaerially exposed during a sea-level lowstand of the last interglacial.

### Palaeosols and protosols

Soil formation is also a diagenetic response to subaerial exposure of carbonate sediments. Red soils have been recognised as forming during glacials on the island of Bermuda (e.g. Bretz, 1960) and are proposed to represent solutional unconformities formed during extensive time intervals of essentially no bioclastic deposition (Land *et al.*, 1967). Land *et al.* (1967) also suggested that the percolation of fresh water during glacials resulted in the formation of soils at the land surface and induced diagenesis in the underlying rocks.

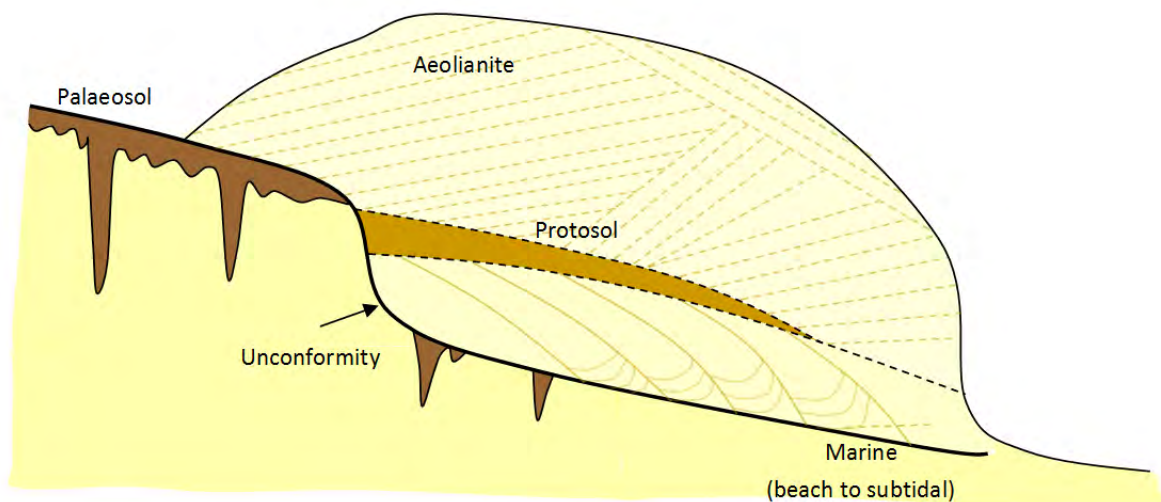


**Figure 3.5:** A model of the formation of a succession of littoral deposits, aeolianite and protosols on Bermuda modified from Hearty *et al.* (1992).

Figure 3.5 illustrates multiple facies of limestones separated by *terra rossa* palaeosols. The formation of these palaeosols on Bermuda is suggested to relate to accumulations of atmospheric dust (Bricker and Mackenzie, 1970) and volcanic impurities (Muhs *et al.*, 2012b).

On the island of Bermuda, red *terra rossa* soils were originally viewed as glacial-age deposits (Bretz, 1960; Bricker and Mackenzie, 1970) while light coloured (tan, brown or yellow) soils are commonly interpreted as interstadial/interglacial soils or 'protosols' (*sensu* Vacher and Hearty, 1989). A similar interpretation is observed on the Bahamian islands where low stands of sea level during glacials are marked by *terra rossa* palaeosols developed on limestone deposits. Hearty (1998) suggested that the colour and texture of palaeosols on Eleuthera Island, the Bahamas, can act as a qualitative indicator of the relative ages of stratigraphic units; becoming redder with increased age.

Three types of palaeosol have been recorded interbedded between aeolianite units on the Nepean Peninsula, Victoria, Australia (Zhou *et al.*, 1994). Calcrete horizons and *terra rossa* soil formation are attributed to groundwater fluctuations. A thermoluminescence age of  $16.6 \pm 1.2$  ka for a *terra rossa* palaeosol on the Nepean Peninsula suggests that the palaeosol formed towards the end of the last glacial (MIS 2) when the regional climate was cold, dry and windy (Zhou *et al.*, 1994).

Where palaeosols are well-developed, they can be used to identify significant hiatuses in sediment deposition. Protosols are less well developed soil horizons, representing shorter breaks in sediment deposition. Vacher *et al.* (1995) described protosols as bounding surfaces that have been vegetated but lack the features of a mature soil profile. Protosols may reflect relatively brief interruptions or reductions in carbonate sand deposition as a result of minor sea-level regression or ecological stability. Occasionally protosols can be used to identify breaks in sedimentation within an isotopic substage event, thus constraining their formation from a few hundred to a few thousand years (Hearty *et al.*, 1992; Vacher *et al.*, 1995; Hearty, 1998). Vacher *et al.* (1995) proposed that where protosols are located between an underlying marine unit and an overlying aeolianite unit they mark the transition from an erosional coastline to a depositional one during a sea-level highstand and only represent a time-slice of a few thousand years. Unlike palaeosols, there is no significant karstification (such as solution pipes) of underlying limestone associated with the formation of protosols, though a thin calcrete profile may be present.

However, it is suggested that interbedded palaeosol units be interpreted with caution. Hearty (1998) warned that while red palaeosols are generally associated with periods of sub-aerial alteration and reduced deposition during glacial lowstands, they may have also formed during periods of prolonged emergence within interglacial stages (Hearty and Vacher, 1994), and therefore, cannot be used exclusively for defining full glacial cycles.

Carew and Mylroie (2001) also warned of the potential difficulty in using palaeosols to mark aeolianite depositional episodes due to the mobility potential of the soil. Surface *terra rossa* palaeosols may infiltrate into karst features, such as solution pipes, that penetrate the rock at various depths. Carew and Mylroie (1991) highlighted the potential confusion that may be experienced when taking core samples through aeolianite to analyse periods of carbonate deposition based on palaeosol boundaries. Figure 3.6 illustrates how palaeosols may infiltrate into lens cavities within karstic environments and appear as distinct horizons of sub-aerial alteration. In other instances palaeosols may bifurcate and appear to split into two

palaeosols, or two palaeosol horizons may merge into one, complicating aeolianite deposition interpretation (Carew and Mylroie, 1991).

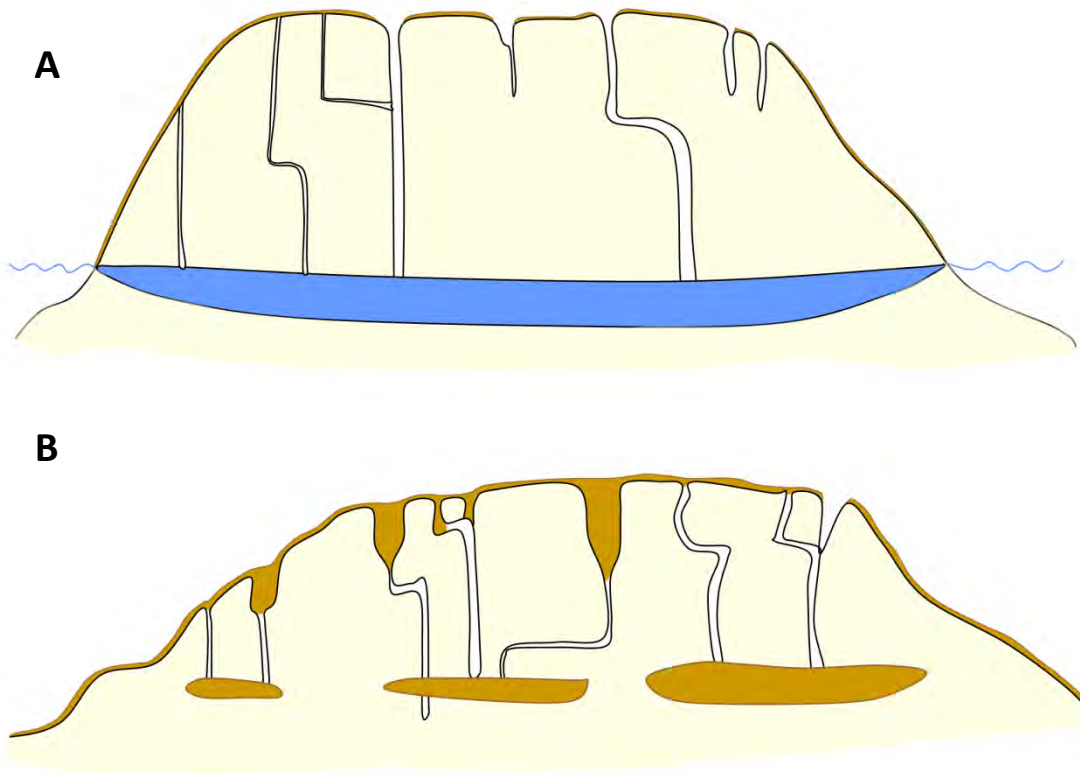


**Figure 3.6:** The potential effects of soil infiltration into karst features (modified from Carew and Mylroie, 1991) **A:** A fresh water lens has perched on marine groundwater during a sea-level highstand. Sinks and solution pipes develop in the aeolianite and allow transportation of water down to the lens. Caves also form at the bottom of the lens through dissolution. **B:** During a sea-level lowstand the water level in the phreatic caves has drained. Soil from the surface has then infiltrated down into the karst features, and these horizons may be mistaken for subaerially exposed surfaces.

Failure to interpret palaeosols and protosols correctly can also lead to inaccurate conclusions in the length of time surfaces have been subaerially exposed. Carew and Mylroie (2001) used the calcarenite protosols formed on the Bahamian islands as an example; these protosols represent a 100 to 1000 year pause in sea-level highstand carbonate deposition, and incorrectly interpreting these as palaeosol deposits would suggest a much longer period of non-deposition (~100,000 years).

### Karstic features

The presence of karstic features within the topography can also indicate intervals of subaerial exposure. Rhizoliths (or root casts) are formed where carbonate allochems are dissolved and calcite is reprecipitated around plant roots that may have grown within soil horizons overlying carbonate sands (Loope, 1988). Loope (1988) suggested that in semi-arid regions experiencing a negative water balance, calcification can keep pace with decomposition allowing root cast



structures to form. He related their abundance in Quaternary coastal dunes in western USA to glacio-eustatic sea-level fluctuations. Loope (1985) described abundant burrows and rhizoliths preserved in aeolian sandstones in the Permian Cedar Mesa sandstone, Utah, and stated they are indicative of deflation surfaces that were stable for considerable lengths of time.

Other karstic features in subaerially exposed carbonate surfaces include solution pipes. Warren (1983) suggested that as a calcrete develops in the near-surface region, infiltrating rainwater will collect in depressions within the hard surface. The concentration of fresher water will lead to a localised redissolution of the calcrete until the water breaks through the calcrete horizon to form near-vertical solution pipes (Warren, 1983). On a reef tract in Belize, Esteban and Klappa (1983) commented upon drowned cenotes that have floors 120 m below present sea level and suggested that they are evident of karstification during glacial sea-level lowstands.

### **3.4 Calcarenite deposition and its role in identifying sea level**

This section addresses the use of identifying calcarenite depositional environments in determining palaeo-sea level. Debate (e.g. Brooke *et al.*, 2001 and references therein) has focused on whether aeolianite, specifically, is deposited during sea-level highstands associated within interglacials, or during glacial lowstands as discussed previously by Frebourg *et al.* (2008).

The following discussion presents a range of studies on coastal calcarenite deposits from around the world and evaluates their potential use in determining Quaternary palaeo-sea levels. The carbonate platform type at each of these localities is discussed in conjunction with significant stratigraphical structures that aid in determining sea-level height.

#### **3.4.1 Perth Basin, Western Australia**

Carbonate aeolianite deposits stretch along the Western Australian coastline for over one thousand kilometres from Shark Bay to the southern coast, and are termed the 'Tamala Limestone' (Playford *et al.*, 1976). The source of aeolianite material along the coastline in this region is attributed to the highly productive offshore carbonate shelf, where warm waters are transported southwards along the coast by the Leeuwin Current, and continental aridity prevents large volumes of terrigenous material from reaching the coast (Hearty and O'Leary, 2008). The Tamala Limestone encompasses aeolianite composed of abraded molluscan shell fragments, calcareous red algae, foraminifera, echinoderm fragments and mixed quartz (~20%), with palaeosols and well-indurated calcrete horizons found throughout the deposit (Playford, 1997; Playford and Leech, 1977; Kendrick *et al.*, 1991). Hearty and O'Leary (2008)

suggested that the soils found capping the Tamala Limestone increase in richness, hue and chroma (yellows and browns to reddish browns and reds) with increased age.

Rottneest Island is the largest in a chain of limestone islands located on the shallow continental shelf, approximately 18 km west of Perth (Playford and Leech, 1977). The Tamala Limestone is the most prominent geological unit on Rottneest Island, and is recorded as 150 m thick in certain localities and characterised by large-scale aeolian cross-bedding (Playford, 1997). Calcrete horizons are found within coastal areas on the island and overlie softer limestones containing abundant rhizoliths, which may in turn be overlain by grey-brown soils (Playford, 1997). Solution pipes up to 50 cm in diameter indicate intervals of non-deposition alongside the calcrete profiles and rhizoliths. Playford (1997) suggested that salt lakes found in the centre of Rottneest Island mark former blue holes and are indicative of karst development during sea-level lowstands. Through studies of the sedimentary structures within coastal Western Australian aeolianites, Hearty and O'Leary (2008) identified that most aeolianites generally displayed large-scale festoon bedding on windward dune faces, and planar cross-bedding on the leeward sides.

There is debate over whether deposition of aeolianite sands along the Western Australian coastline occurred during times of high or low sea level (Kendrick *et al.*, 1991; Hearty and O'Leary, 2008). This debate is not specific to WA but has been questioned globally. It was originally suggested that the coastal sand dunes in WA were deposited onshore during times of lower sea level throughout the Quaternary and early Holocene, when widespread areas of continental shelf would have been exposed (Fairbridge and Teichert, 1953; Playford, 1997). However, Hearty and O'Leary (2008) have since proposed that the aeolian sediments were deposited during times of Quaternary sea-level highstands because of several factors: abundant taxa comprising the biosediment are warm-water species associated with interglacial highstands; facies appear to shallow upwards in a similar fashion to the facies of the present highstand and; coarse grain sizes prominent throughout the deposits are indicative of high energy environments associated with highstands. Nevertheless, these factors may not be uniquely interglacial as, for example, fragments of warm-water species can remain on a source shelf as a remnant of previous interglacials.

Price *et al.* (2001) conducted thermoluminescence (TL) dating of aeolianite deposits on Rottneest Island and the Fremantle coastline. They suggested that aeolianites were deposited during both sea-level highstands and lowstands, as TL analysis yielded dates of aeolianite deposition during both the Last Glacial Maximum (LGM) and the last interglacial. Price *et al.*

(2001) proposed that deposition could have occurred during both high and low sea level due to the substantial volume of sediment available on the shallow platform at both times.

### **3.4.2 Bermuda**

The carbonate platform surrounding the island of Bermuda is the site of the northern-most coral reefs in the Atlantic (Vacher and Rowe, 1997). Bermuda is located at a latitude of 32°20'N, but hosts a subtropical climate due to the warm waters of the Gulf Stream flowing to the west and north of the island.

Carbonate Pleistocene rocks on the island of Bermuda were first recognised as aeolianite by Sayles (1931). He proposed that the aeolianite and soils, which were commonly found capping the deposits, were products of glacial and interglacial periods respectively. Sayles (1931) suggested that aeolianites were deposited during glacials, when a lower sea level exposed sources of sand on the continental shelf which were then blown shoreward by strong winds. While during interglacials the higher sea level resulted in a cut-off of the sediment supply and formation of soil deposits. Bretz (1960) later analysed Sayles' (1931) findings and accepted that the aeolianite-soil couplets were eustatically controlled yet suggested that the aeolianites were coastal dunes, not desert dunes as Sayles had previously proposed. Bretz (1960) indicated that the source of the sediment of the Bermuda aeolianites was derived from the beach and thus correlated the deposition of the coastal dunes with interglacials.

The stratigraphy of the Bermuda limestone has since been studied in greater detail. Vacher and Rowe (1997) noted that the limestone units are composed of an assemblage of five marginal facies, two of which are coastal-terrestrial deposits and three are coastal-marine. The aeolian facies are commonly located in hillocky mounds and shore-parallel ridges up to tens of metres above the source beaches (Vacher *et al.*, 1995; Vacher and Rowe, 1997). Large sets of conformable foresets are a common occurrence and can remain uninterrupted by soils or bioturbation for tens of metres, suggesting that sediment was deposited in large volumes relatively quickly, such as by large storm events (Vacher and Rowe, 1997). The essential marine units were deposited in erosional, depositional, and protected coastal environments as indicated by the varying bioconstituents of the deposits. Depositional coastline deposits consisted of shore-parallel wedges, generally of bioclastic grainstones, typically laterally grading into an aeolianite deposit. Where found, protected beach deposits were distinguished by the presence of whole and well-preserved marine shells (Vacher *et al.*, 1995).

### 3.4.3 Bahamas

Coral reefs surrounding the islands of the Bahamas indicate that the related carbonate factory is a tropical one. The carbonate shelf in this region, the Bahamas Banks, is a steep carbonate platform. The Quaternary stratigraphy of the Bahamas, similar to the aeolianite sequences on Bermuda, is composed of a succession of interglacial limestone facies separated by *terra rossa* soils, with younger deposits superimposed onto older ones (Carew and Mylroie, 2001). Aeolianite ridges on the Bahamian Islands range from only a few metres in height to over 63 m in some locations, though the average elevation of these ridges is 20 to 30 m APSL (Carew and Mylroie, 2001).

The carbonate sedimentary facies (formed in dune, beach and subtidal environments) are interpreted to have been deposited during interglacial highstands, while *terra rossa* palaeosols (of a reddish silty/clayey nature) are thought to depict times of lower sea level (Hearty and Kindler, 1993, 1997; Hearty, 1998; Hearty *et al.*, 1999; Hearty and Kaufman, 2000). Carew and Mylroie (2001) noted that the steep morphology of the Bahama Banks carbonate platform results in aeolianite deposition only occurring when sea level is within ten metres of its present position. Hearty (1998) was able to identify beach deposits within aeolianite bodies due to the laminar bedding associated with beach facies. Garrett and Gould (1984) suggested that the presence of air pockets known as keystone vugs or fenestrae (indicative of a beach zone whereby wave action traps air into underlying sediment) could be used to estimate sea level throughout New Providence. This technique was also later used by Kindler and Hearty (2000) throughout the Bahamas.

Unlike the aeolian deposits on Bermuda, which are thought to be predominantly regressive (Vacher and Rowe, 1997), aeolianite successions of the Bahamas are suggested to have formed during sea-level transgressions, still stands, and regressions (Carew and Mylroie, 2001). The narrow coastal range of aeolianite deposition due to the steep carbonate shelf results in pre-existing aeolianite and coral reef deposits acting as an anchor for subsequent aeolianites (Carew and Mylroie, 2001). Hearty (1998) described the stratigraphy of aeolianite on Eleuthera Island, and through amino acid racemisation (AAR) dating and the identification of interbedded palaeosols suggested that aeolianite deposits related to subsequent sea-level highstands from the Holocene to MIS 13/15. Calcareneite protosols and abundant land snails, as well as palaeosols, are common throughout the deposits and represent pauses in deposition of carbonate material on a scale of hundreds to thousands of years (Carew and Mylroie, 2001).

#### 3.4.4 Mallorca, Western Mediterranean

The Mediterranean carbonate platform is temperate but poorly protected. The Balearic Ramp, located off the islands of Menorca and Mallorca, is an isolated platform with an average width of ~15 km and an average depth of 15 m. The Balearic Ramp differs from other present day temperate carbonate platforms which are primarily high-energy open shelves (Fornos and Ahr, 1997).

Clemmensen *et al.* (1997) divided the Pleistocene succession of calcarenites on the island of Mallorca into six basic sedimentary cycles, each composed of beach and aeolian deposits. Butzer and Cuerda (1962) analysed these deposits and suggested that the cycles were related to Pleistocene glacio-eustatic sea-level variations with aeolianite deposited during glacial episodes characterised by low sea levels and strong winds. Hearty (1987) later described coastal deposits in more sheltered localities such as the Bay of Palma on the island of Mallorca, and noted that the coastal deposits are characterised by alternating sequences of marine and aeolian sand and continental *terra rossa* soils. Hearty (1987) used uranium-thorium and AAR dating to indicate that several of the marine units in this region were deposited during sea-level highstand events during MIS 5, 7, and 9.

On the north-eastern coast of Mallorca, Fornos *et al.* (2009) used optically stimulated luminescence (OSL) analysis to suggest that episodes of aeolian transport and dune formation occurred during glacial sea-level lowstands. A lower sea level within the Mediterranean during glacials would have exposed marine carbonate sediment within Alcudia Bay, and combined with stronger winds and reduced vegetation cover during this time onshore aeolian transportation is suggested to have been enhanced (Fornos *et al.*, 2009). Muhs *et al.* (2010) also describe landward-dipping foresets within aeolianite sea cliffs at S'Estret d'es Temps, in the southeast of Mallorca, which indicate formation when sea level was lower than present.

Cliff front dunes were also described in southern Mallorca by Fornos *et al.* (2002). They stated that the dunes are composed of bioclastic sand containing red algae, molluscan fragments, echinoid spines, benthic foraminifera and bryozoan, thought to originate from the nearest shallow marine carbonate platform. Fornos *et al.* (2002) suggested that the coarse, well-sorted, aeolian sediment deposited in laminae 2-5 mm thick coupled with finer sand laminae represents pinstripe lamination formed by wind ripples.

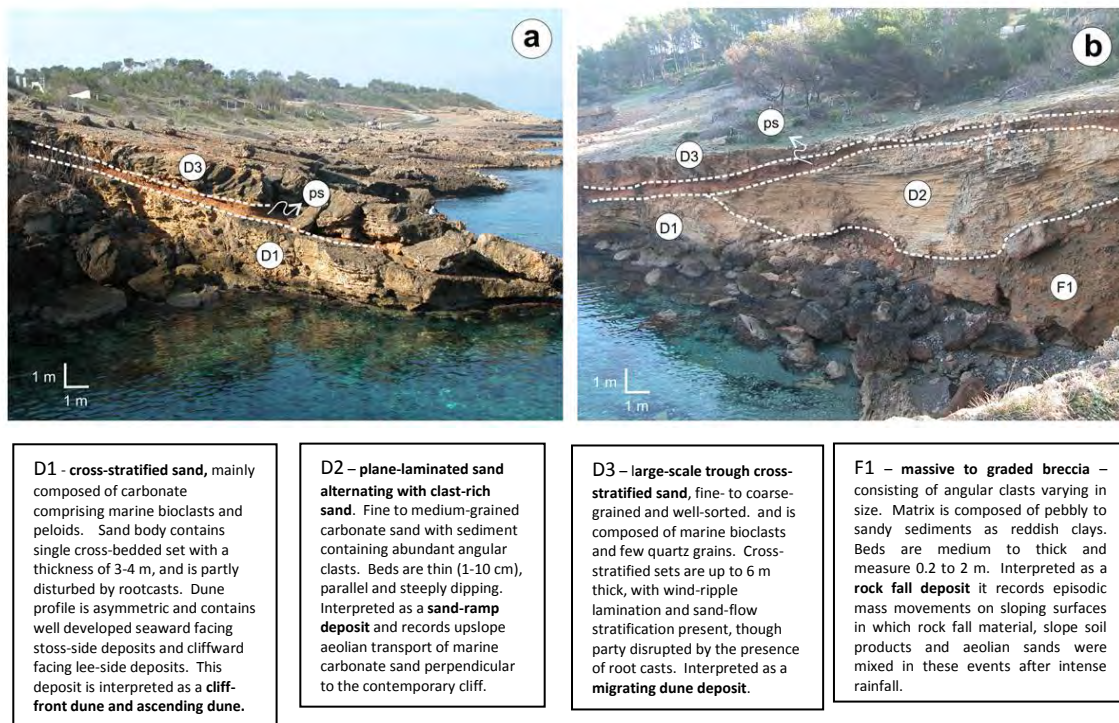


**Figure 3.7:** Stratigraphy of calcareous aeolianite deposits at Pollenca Bay, Mallorca (Fornos *et al.*, 2009).

Stratigraphical features of aeolian facies at Pollenca Bay, Mallorca are indicated by Fornos *et al.* (2009) in Figure 3.7. These facies include basal coastal cliff-toe deposits which are overlain by a well-developed palaeosol and second cliff-front dunes. Basal cliff-front dune deposits are composed of fine- to coarse-grained marine carbonate sand and characterised by a single cross-bedded set 3-4 m thick. Dune cross-stratification is generally comprised of well-developed topsets and foresets indicating the asymmetric dune was moving landwards (Fornos *et al.*, 2009).

### 3.4.5 South Africa

The Agulhas Bank, located at the southern-most tip of Africa, is now a submerged continental shelf area, and is both wide and deep in comparison to worldwide averages (Birch, 1977). This is a temperate carbonate province due to the dominantly cool waters on the surrounding shelves.

The aeolianite deposits located on the tectonically stable southern and eastern coasts of South Africa represent the largest continental record outside of Australia in the Southern Hemisphere (Brooke, 2001). On the southern coastline of the Western Cape Province a wide range of aeolian deposits are exhibited including large-scale (>200 m) barrier dunes and extensive aeolianites (Carr *et al.*, 2007). While aeolianites of interglacial age have been

reported on the coastal plain it is suggested that aeolianite is continually forming in glacial also but only highstand deposits are preserved (Bateman *et al.*, 2011). The Pleistocene Waenhuiskrans Formation, found on the Southern Cape coast, is sandy, semi-consolidated, and contains large scale (up to 3 m) trough cross-bedded aeolianite units. The aeolianite consists of very coarse, well-rounded grains, with scatterings of terrestrial and marine shells and foraminifera (Bateman *et al.*, 2004). The mineralogy of the aeolianite is approximately 75% silica and 25% carbonate (Bateman *et al.*, 2004). Aeolianite formation is reliant on conditions which favour the transportation and deposition of calcareous sand as well as conditions favourable to cementation of the deposit. It is therefore suggested that the aeolianites on the southern Cape coast of South Africa were deposited in post-interglacial periods (interstadials) where sea levels fluctuated and climatic conditions were cooler and wetter and more preferable for preservation than during interglacial highstands themselves (Bateman *et al.*, 2004). Figure 3.8 shows high angle cross-bedding within the aeolianite in the Wilderness deposit and the formation of a palaeosol indicative of subaerial exposure.

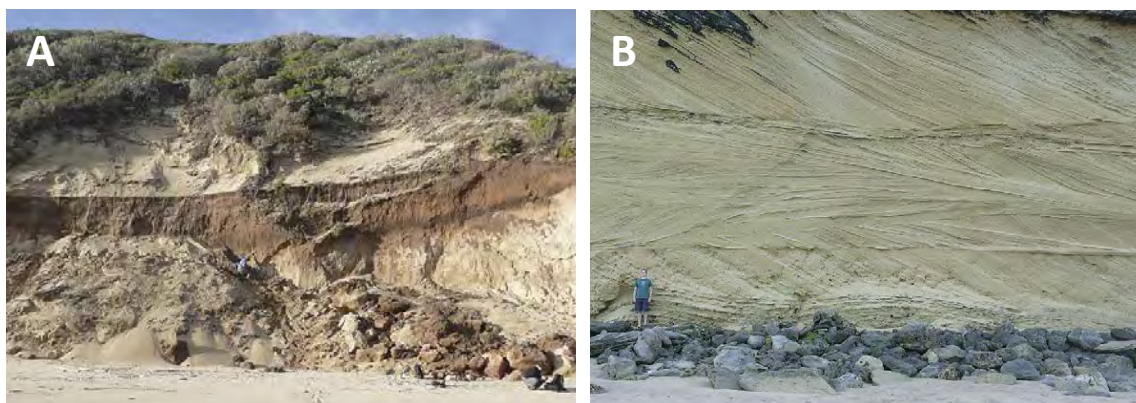


**Figure 3.8:** Exposure of aeolianite units in the Wilderness seaward barrier, South Africa, highlighting (A) the development of a *terra rossa* palaeosol above aeolianite and capped by aeolian dunes and (B) the complex internal architecture of aeolianite within the Seaward barrier as exposed by sea cliffs (from Bateman *et al.*, 2011).

### 3.4.6 Hawaii

On the southeast coast of the island of Kaua'i, Hawaii, exists an extensive succession of Pleistocene and Holocene carbonate aeolian units (Blay and Longman, 2001). Blay and Longman (2001) suggested that the aeolianite units were deposited within the last 0.5 Ma and were derived from shallow marine organisms including coralline red algae, corals, molluscs, echinoderms and foraminifers transported by trade winds during sea-level highstands. Red palaeosol and light grey calcrete horizons are observed to vertically separate the aeolian units and are proposed to have developed during sea-level lowstands (Blay and Longman, 2001). Large-scale cross-beds, commonly 2-5 m thick, are found within the carbonates sands, with older units found to be stabilised by calcite cements. Within the older units subaerial exposure

is evident through karst features such as sink holes and rhizoliths, and bioturbation such as animal burrows and root mottling.

Through the use of amino acid racemisation (AAR) dating of aeolianite on the Hawaiian island of O'ahu, Hearty *et al.* (2000) suggested that the aeolian dunes formed during interglacials MIS 1 and MIS 5e due to similar D/L ratios as those found in last interglacial deposits on Bermuda and the Bahamas. However, it is likely that thermal histories were different in these geographically varied locations and that racemisation rates would have varied between whole-rock samples composed of skeletal fragments from differing species. Comparison between the D/L values of these sites should thus be taken with caution.

On the island of Moloka'i, Fletcher *et al.* (2005) examined a succession of two distinct aeolianite units and an associated caliche palaeosol. Again, through the use of AAR analysis, Fletcher *et al.* (2005) concluded that these aeolianite units formed at times of higher sea level, during the later stages (a-d) of MIS 5.

#### **3.4.7 Lord Howe Island**

Lord Howe Island is a remote composite volcanic and carbonate island located in the south-western Pacific Ocean, east of the Australian coast and positioned at the southern limit of reef-forming seas (Woodroffe *et al.*, 2006). The island is surrounded by a shallow submarine platform as a result of marine erosion and carbonate deposition. The central portion of the island is covered by calcarenite, deposited primarily as aeolianite (Figure 3.9) but with isolated, interbedded beach units (Woodroffe *et al.*, 2006). The aeolianites consist of two lithostratigraphic formations, the Searles Point Formation and the Neds Beach Formation. The Searles Point Formation comprises pale brown to yellow, moderately- to heavily-cemented skeletal grainstone deposited as thick dune topset and foreset beds with bounding unconformities marked by clay-rich palaeosols (Brooke, 1999; Brooke *et al.*, 2003). Brooke *et al.* (2003) identified the palaeosols and clay-pot pedogenic structures to be indicative of substantial periods of subaerial exposure and diagenesis. The Neds Beach Formation comprises white to yellowish brown, lightly- to moderately-cemented skeletal carbonates deposited in both dune and beach environments (Brooke, 1999; Brooke *et al.*, 2003). Less well-developed protosols interbedded throughout the Neds Beach Formation are records of minor pauses in carbonate deposition (Brooke *et al.*, 2003).





**Figure 3.9:** Photomosaic of cliffed exposures of dune bedsets in the shorelines at the northern end of Johnsons Beach, Lord Howe Island from Brooke (1999). Three beds are evident in the outcrop (jb1, jb2, jb3) and each separated by a protosol (pr1, pr2, pr3). The staff is 2 m long.

**jb1** – very pale brown, weakly to moderately cemented grainstone. Low angle cross-bedding up to 3 m thick, dipping seaward (240°).

**jb2 and jb3** – thick sets (up to 12 m) of steeply-dipping foresets, composed of weakly cemented, very pale brown grainstone. These beds were deposited as climbing dunes, and measurements of bedding indicate they were mobilised by southerly winds.

**p1** – subtle protosol horizon indicated by dark colouration and the occasional rhizoliths, exhibited from unit jb1.

**p2** – a well-developed clayey-sand protosol, up to 1 m thick, caps the cross-bedded unit jb1a/jb2a. Contains *Placostylus* and *Guedoconcha* as well as snails, bird bones and rhizoliths.

**p3** – a weakly developed sandy protosol, approximately 0.3 m thick, containing land snails and small rhizoliths. A weak podzolic soil profile overlies this.

Previous studies of aeolianite deposits on Lord Howe Island have suggested the sediment was deposited during glacial sea-level lowstands (McDougall *et al.*, 1981) as the aeolianite outcrops extend below present sea level and radiocarbon ages indicate certain units are last glacial in age (Squires, 1963). More recently, however, thermoluminescence (TL) dating of the aeolianite deposits has suggested that the units were primarily deposited during or shortly after interglacial sea-level highstands (Price *et al.*, 2001).

### 3.4.8 Discussion of international calcarenite deposits

Globally, aeolianite deposits are primarily formed as large tracts along the coastal margins of extensive carbonate provinces, with carbonate production on shallow shelves serving as the ultimate control on the formation of aeolianite (Brooke, 2001). The bulk of carbonate within aeolianite deposits has been found to be Heterozoan and produced in regions of low terrigenous sediment input (Brooke, 2001).

Through a brief comparison of a range of global calcarenite units it is evident that these deposits are not solely formed during interglacial or glacial episodes alone. Studies of carbonate successions on Bermuda and the Bahamas have revealed similar sea-level highstand calcarenite deposits since the middle Pleistocene (Hearty *et al.*, 1999). It is suggested that the palaeosols found capping these deposits are indicators of intervals of non-carbonate deposition during glacials or interstadials (e.g. Bretz, 1960). Calcarenite deposits are also

recognised as being deposited during interglacials on several Hawaiian Islands (Hearty *et al.*, 2000; Blay and Longman, 2001) and on Lord Howe Island (Brooke, 1999; Price *et al.*, 2001). On the island of Mallorca, OSL analysis indicated that aeolian transport and dune formation occurred at time of lower sea level when carbonate material was exposed on the surrounding shelf (Fornos *et al.*, 2009). Aeolianite deposits identified on the Southern Cape of South Africa are suggested to have been deposited during interstadial periods (Bateman *et al.*, 2004), while on the coast of Western Australia, through TL dating, Price *et al.* (2001) suggested that aeolianite was deposited during times of both high and low sea level.

Through this brief examination of calcarenite deposits it has been illustrated that the type of carbonate platform can influence calcarenite deposition. The Bahamas Banks, for example, are extremely steep meaning that when sea level falls below ten metres of its present position there is no available beach source from which aeolianites can form (Carew and Mylroie, 2001). The situation is also similar for the carbonate platform surrounding Bermuda, and thus calcarenite can only be deposited in times of higher sea level. On carbonate ramps, however, deposition of calcarenite can occur at any time during a sea level cycle as carbonate production is continuously occurring (Carew and Mylroie, 2001). The Balearic Ramp in the Mediterranean is an example of this, as is the shallow carbonate platform surrounding Rottnest Island, Western Australia.

Reconstruction of the facies architecture of calcarenite deposits may aid in identifying palaeo-sea-level elevations. To determine whether deposits were formed during highstands or lowstands a thorough understanding of the tectonic history of the region is required and suitable material for geochronological analyses. The following half of the chapter presents the stratigraphy of the Bridgewater Formation shoreline barrier successions on the Mount Gambier coastal plain. The presented stratigraphy will then be compared with global calcarenite deposits discussed in this chapter and later in the thesis when the chronostratigraphy of the Bridgewater Formation on the Mount Gambier coastal plain has been developed (section 6.2).

### **3.5 Stratigraphy of the Bridgewater Formation on the Mount Gambier coastal plain**

The following discussion outlines the stratigraphical setting and general characteristics of the Pleistocene Bridgewater Formation in the Mount Gambier region, southern Australia. The stratigraphical methods are described, the location of each of the sample sites is presented and reasoning for their selection is discussed. Descriptions of fieldwork observations and field measurements are presented. Fieldwork observations include the description of sedimentary features present within the calcarenite and the presence of any fauna within the deposits. This evidence is then used to aid in reconstruction of depositional and climatic environments for each of the sites.

### **3.6 Stratigraphical methods**

In the field, stratigraphical units were identified and sedimentary structures recorded where access permitted mapping the extent of each unit using tape measures. Multiple high resolution photographs were taken at all study sites to aid in sketching exposures of Bridgewater Formation calcarenite and the interpretation of facies architecture. Measuring staffs were used to determine the thickness of stratigraphical units where accessibility was limited. Measurements were recorded in the form of stratigraphical sketches and included unit thickness, sediment colour, bedding characteristics and observable karst development which was measured in terms of size and abundance. Where visible and accessible, bedding dip and dip direction were recorded using a Brunton Compass to determine palaeocurrent directions. At certain localities, where Australian Height Datum (AHD) data had not been previously published, the elevation of the site was surveyed using an electronic Dumpy Level. Site locations were recorded with a handheld GPS device. Depositional environments were reconstructed by facies architecture interpretation and comparing these observations with characteristic bedding types as detailed in previous studies and discussed in section 3.3.7.

### **3.7 Location of study sites**

Sample sites were commonly road and rail cuttings, or small quarries, through barrier shorelines exposing Bridgewater Formation calcarenite. The locality and spread of the study sites was primarily based on the accessibility of these exposures and on previous knowledge of the area by local residents.

Ideally, sample sites would be located across each of the barrier shoreline successions and would extend into the previously unexamined older dune ranges. However, locating suitable sampling locations was more successful in some barriers than in others and was

dependent on the location of previously established cuttings. For example, the Gambier Range, which trends sub-parallel to the modern shoreline and seaward of the town of Mount Gambier, appears as an area of significant raised elevation (Figure 3.11). However, road cuttings through the range were commonly overgrown and accessible quarries into the structure were limited. The extent of urban development also restricted locating suitable study sites.

Figures 3.10 and 3.11 show the location of the study sites examined in this research. Figure 3.12 highlights the elevation of the Mount Gambier coastal plain from Shuttle Radar Topography Mission (SRTM) data collected by the Space Shuttle Endeavour in 2000, and provides elevation data accurate to ~30 m resolution. The dune ranges (represented by linear strands of elevated terrain) extend sub-parallel to the shoreline. SRTM data are also used to examine the height and width of each of the barrier shorelines and this data is presented as each dune range is discussed in turn. Where possible each of the shoreline barriers was sampled at multiple locations along its extent within the region to yield a representative sample distribution.

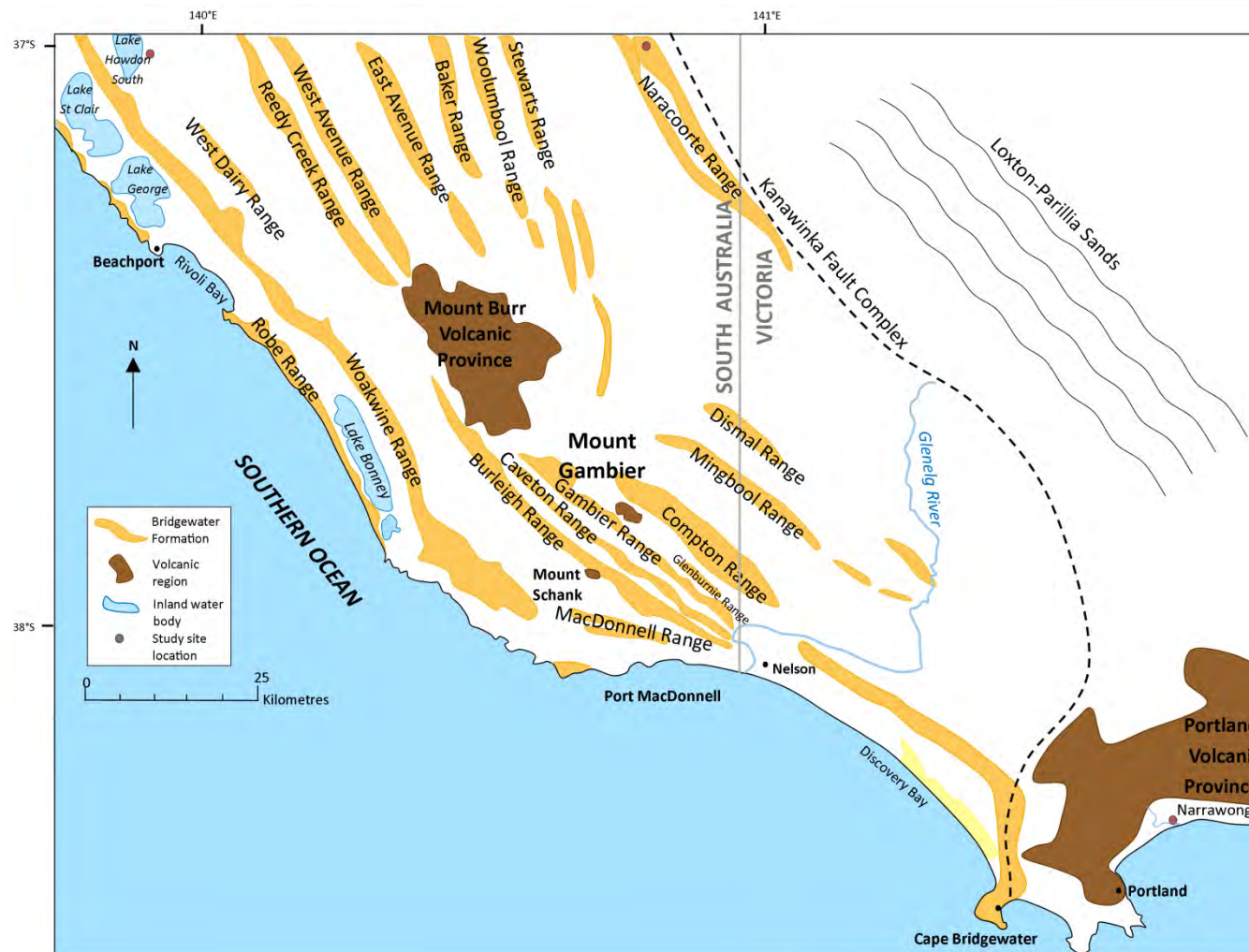


**Figure 3.10:** Map of shoreline barrier deposits of the Bridgewater Formation and sample sites across the Mount Gambier coastal plain. Red dots mark sample sites at Lake Hawdon South, Henschke Quarry in Naracoorte and Narrawong. (See Figure 3.11 for sample sites in the Mount Gambier region).

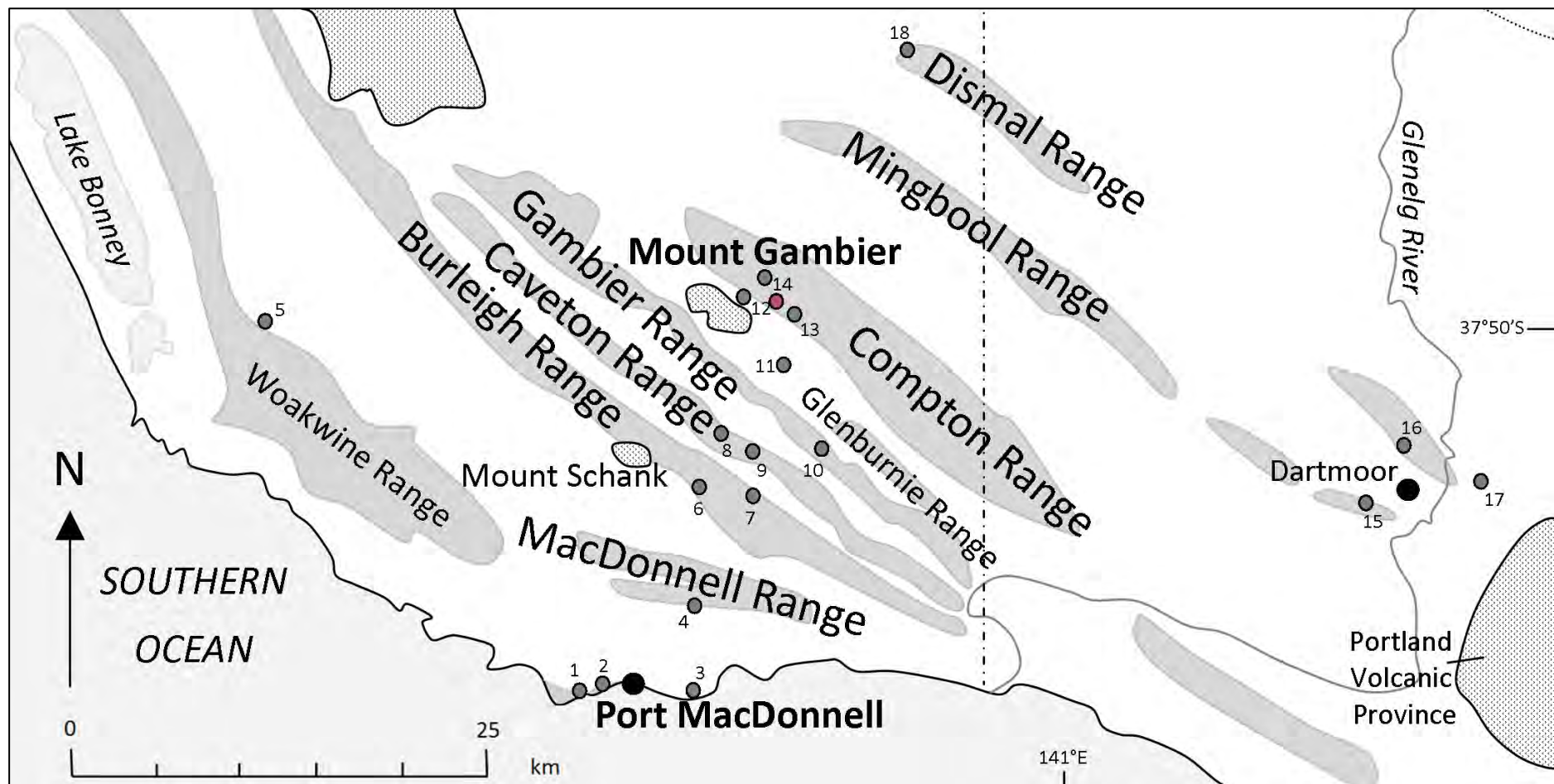


**Figure 3.11:** Map of sample sites across the Mount Gambier region. 1=Shelly Beach; 2=Port MacDonnell Beach, 3 = Racecourse Bay, 4 = Swarts Road sand quarry; 5 = German Creek shell bed; 6= Rabbitors Road cutting; 7= Laslett Road cutting; 8= Caveton Range on Rabbitors Road; 9 = Bucks Hill; 10= Gooch Road, 11 = Caroline Main Road; 12 = Road cutting through Grey St; 13 = Heritage Industries; 14 = Baxter's Quarry; 15 = Don's Quarry, Mumbannar; 16 = Dartmoor Cemetery; 17 = Fort O'Hare Quarry; 18 = Small quarry near Mingbool village; Red circle = siliceous sands site.



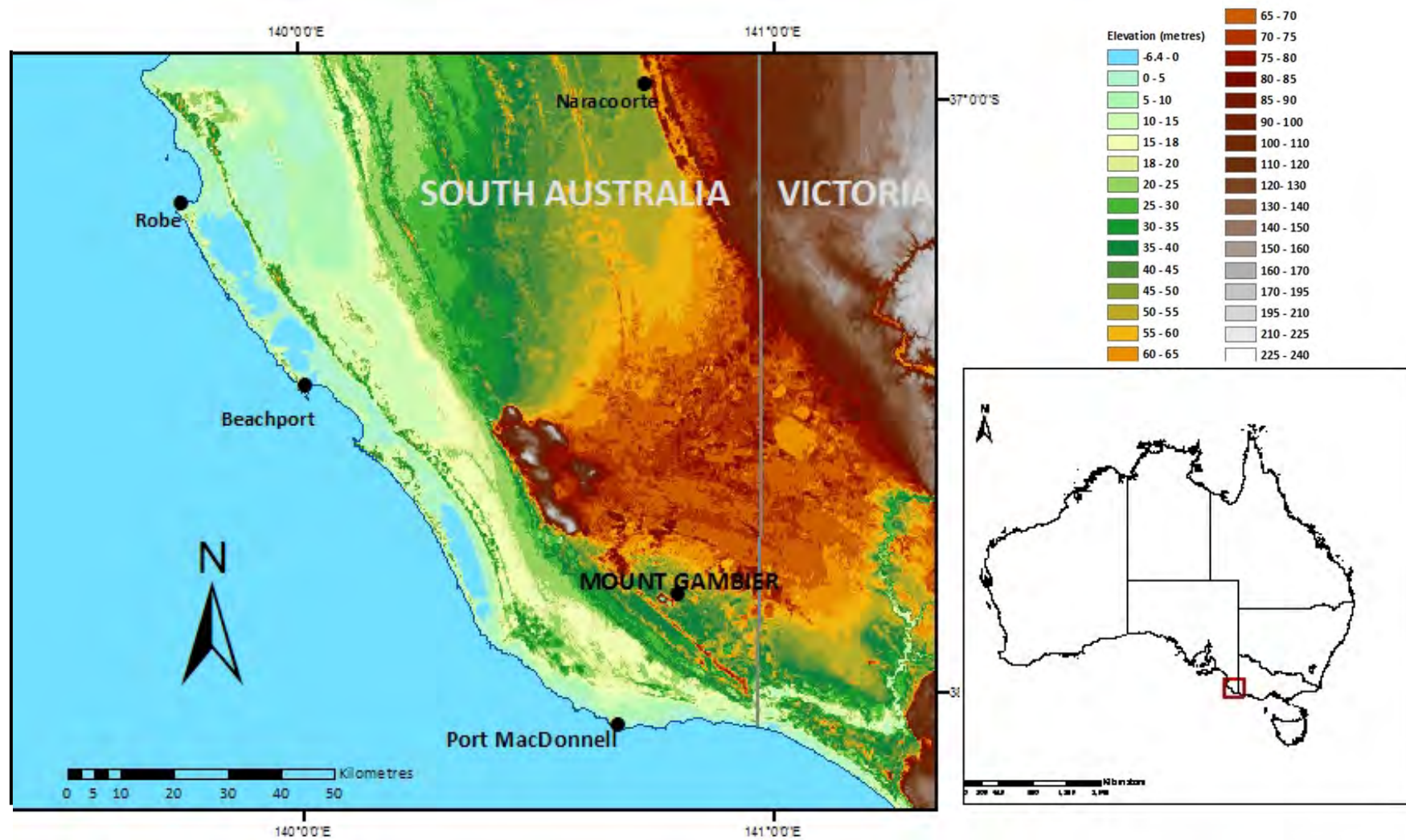


Figure 3.12: SRTM image highlighting the topography of the Mount Gambier coastal plain. Datum used is WGS 84 54.

### 3.8 Shoreline barriers of the Bridgewater Formation, Mount Gambier coastal plain

Bridgewater Formation deposits are composed of calcareous sands of middle to late Pleistocene age and were first defined at Bridgewater Bay, western Victoria, by Boutakoff (1963). Belperio (1995) suggested that five sediment facies associated with deposition of Bridgewater Formation sands are exposed in a range of cuttings across the Mount Gambier coastal plain. These facies comprise skeletal calcarenite deposited in shallow subtidal, littoral, dune, lagoonal and ephemeral lacustrine environments. Belperio (1995) suggested that only the first three of these facies comprise the Bridgewater Formation *per se*, and that no formal nomenclature describes the lagoonal facies, other than last interglacial Glanville Formation defined landward of the Woakwine Range. Ephemeral lacustrine environments have been defined separately as the Padthaway Formation.

Belperio (1995) also noted the common stratigraphical components of each of these five facies. Shallow subtidal facies of the Bridgewater Formation may comprise seaward-dipping, coarse carbonate sands and include abundant marine shell fragments. Littoral zone sediments may be found as well-sorted, medium- to coarse-grained skeletal carbonates, deposited in narrow lateral bodies, sub-parallel to the modern coastline. These sediments may display distinctive bidirectional trough cross-bedded strata and extend into the core of the ranges. Belperio (1995) indicated that the bulk of the visible deposits are composed of transgressive dune aeolianite, composed of weakly cemented, fine- to medium-grained skeletal sand. Reactivation surfaces, identifiable by palaeosols, protosols and rhizolith concentrations, commonly separate aeolianite units of landward dipping, large-scale cross-beds. On their lee side, these aeolian facies may overlie or interfinger with lagoonal facies. Lagoonal facies, preserved in interdune corridors, are typically composed of shelly and muddy calcarenite. Large, articulated intertidal to subtidal bivalves are commonly found within these facies and include the genera *Anadara*, *Katelsia* and *Ostrea*. Padthaway Formation lacustrine sediments are also deposited in interdune corridors but are not necessarily coeval with the Bridgewater Formation barriers, and consist of dense, white, calcitic mudstone, commonly 1-2 m thick.

The Glanville Formation refers to peritidal and shallow marine sediments deposited during the last interglacial maximum (MIS 5e). These deposits are characterised by elements of warmer water fauna no longer found living in southern Australia waters. These fauna include the cockle *Anadara trapezia* and the large foraminifer *Marginopora vertebralis*



(Howchin, 1935; Ludbrook, 1976). However, the bulk of Glanville Formation deposits are similar to that found in modern peritidal environments and include bivalves such as *Katelysia rhytiphora*, *K. scalarina*, *Ostrea angasi*, *Chlamys (Equichlamys) bifrons*, *Fulvia tenuicostata*, *Brachidontes rostratus* and gastropods such as *Batillaria (Zeacumantus) diemenensis*, *Niotha pyrrhus*, and *Bulla botanica* (Belperio, 1995).

The Bridgewater Formation overlies the Miocene-Oligocene Gambier Limestone. As mentioned in Chapter 1, the Gambier Limestone is a muddy to grainy bryozoan calcarenite and marl, rich in foraminifers and echinoid spines. Gambier Limestone was exposed to extensive karstification during sea-level lowstands within the Late Miocene (James and Bone, 1989). During the late Pliocene to early Pleistocene a sea-level highstand is suggested to have reached the base of the Kanawinka Escarpment (James and Bone, 1989) and the ocean would have covered the Gambier Limestone during this episode, likely resulting in some dissolution of the surface of this geological unit. The rise and fall of sea level across the Gambier Limestone has resulted in a karstified and marine-abraded erosion surface. Dissolution features are evident in the form of dolines, cenotes and collapsed dolines. The ability to detect the surface of the Gambier Limestone will allow for identification of the base of Quaternary successions of the Bridgewater Formation and the Glanville Formation.

### **3.8.1 Previous studies**

Several studies have examined the Quaternary raised beach successions of the Mount Gambier coastal plain. Crocker and Cotton (1946) described several of the raised palaeo-shorelines and their marine fossil assemblages and were the first to assign separate names to the dune ranges of the southeast, using the terms Burleigh Range and Caveton Range as correlatives to the Reedy Creek and West Avenue Ranges farther north. Hossfeld (1950), however, suggested that alternative names for the dune ranges of the southwest were unnecessary and produced a map outlining the dune ranges across the Coorong coastal plain. Sprigg (1952) also published a more detailed map of the dune ranges on the Mount Gambier coastal plain (Figure 3.13) and assigned each of the dune ranges to interglacial sea-level highstands within the framework of the Milankovitch hypothesis (in this thesis the names of the barriers as described by Sprigg (1952) are adopted). More geochronological evidence is required to demonstrate a time-equivalence with the barrier successions farther north on the Robe-Naracoorte coastal plain and with successive interglacial sea-level highstands. Sprigg (1979) re-assessed the stratigraphy of the dune ranges closest to the present shoreline and suggested that they were in fact glacial in age. He did not, however, address the issue of preservation potential of the

dune ranges nearest to the sea, which would have been submerged during successive sea-level transgressions (Murray-Wallace and Cann, 2007). More recently, Murray-Wallace *et al.* (1996) assessed the neotectonic setting of the region and in doing so conducted amino acid racemisation (AAR) analyses on two of the shoreline barriers; the Burleigh and Caveton Ranges. These sites are re-visited in this study and the exposed facies detailed to a greater extent. This research aims to build upon the work of these previous studies and to further investigate the more inland barrier successions that have been described only briefly (e.g. Sprigg, 1952).



Figure 3.13: Barrier shorelines of the Mount Gambier coastal plain, from Sprigg (1952).

Several studies have described the timing of barrier shoreline development applying a variety of geochronological methods. Cook *et al.* (1977) and Idnurm and Cook (1980) identified the Brunhes-Matuyama palaeomagnetic boundary between the East and West Naracoorte Ranges, and that all the dune ranges to the west, including the West Naracoorte Range, were younger than 780 ka. AAR was first applied to fossil molluscs on the dune ranges

near to Robe by von der Borch *et al.* (1980) who analysed amino acids from the cockle *Katelysia* situated in the back barrier facies of the Woakwine Range. They concluded that the bulk of the Woakwine Range had been deposited during the last interglacial maximum (MIS 5e). AAR analysis has since been conducted on several of the shoreline barriers on the Coorong coastal plain and the younger barriers on the Mount Gambier coastal plain (e.g. Murray-Wallace *et al.*, 1996; 2001). TL analysis was conducted on samples from several of the dune ranges between Robe and Naracoorte by Huntley *et al.* (1993a; 1994) and more recently OSL analysis by Banerjee *et al.* (2003). These studies largely support the hypothesis that the palaeo-shorelines were deposited during interglacial sea-level highstands.

The dune ranges of the Mount Gambier coastal plain are suggested to be correlative with those farther north near Robe (e.g. Crocker and Cotton, 1946; Hossfeld, 1950). Murray-Wallace *et al.* (1996) analysed neotectonism associated with the Mount Burr and Mount Gambier volcanic provinces and found that rates of uplift varied across the Coorong coastal plain. Uplift is greatest close to the volcanic provinces and thus the barrier shorelines are spaced farther from one another in the Mount Gambier area and coalesce towards the River Murray mouth region. Boutakoff (1963) also noted that in western Victoria the dune ranges appear to coalesce again towards the Portland region. The presence of the Kanawinka Fault and the increased distance from the centres of eperiogenic uplift at this locality are likely reasons for this observation.

Previous studies have primarily concentrated on the shoreline barriers inland of Robe where areas of relative elevation reflect palaeo-barrier shorelines and low-lying areas are indicative of back-barrier flats. Farther south, near Mount Gambier, while the dune ranges are spaced farther apart, the underlying limestone geology of the region can create difficulties in identifying their exact extent. Resultant sinkholes and dolines formed as karst within the Gambier Limestone may be incorrectly identified as inter-dune depressions or previous back barrier lagoons. Figure 3.14 highlights the subtlety needed to identify the dune ranges within the Mount Gambier landscape.



**Figure 3.14:** View looking southward from Centenary Tower, Valley Lake, Mount Gambier indicating the subtlety of the landscape and potential difficulties in identifying barrier sequences.

The following section describes stratigraphical features observed at each of the study sites within the shoreline barriers. Each shoreline barrier is addressed in turn starting from the modern coastline and traversing inland.

### **3.8.2 Modern shoreline of the Mount Gambier coastal plain**

The modern shoreline of the Mount Gambier coastal plain differs from that farther north on the Coorong coastal plain in that it lacks significant coastal dunes. The Holocene dunes of the Younghusband Peninsula are laterally persistent, for approximately 300 km, shoreward of the Coorong lagoon between Goolwa and Robe, but do not extend to the Mount Gambier coastline. Large coastal dune fields are also found east of the Mount Gambier coastal plain in Discovery Bay, western Victoria (Figures 3.10 and 3.18g). The lack of coastal dunes in this region highlights how dramatically the shoreline can change over a short distance and may be a result of differing energy regimes or sediment supplies to the area. Present conditions at Port MacDonnell may therefore not provide a good analogue of interglacial coastal aeolianite deposition in the past.

The small coastal town of Port MacDonnell (S38°03'29.6", E140°40'23.6") lies directly south of Mount Gambier. The coastline in this region is dominated by dissipative beaches where waves break up to 100 m offshore and the predominant wind and wave direction is from the southwest. Bryozoan-rich Miocene Gambier Limestone forms a modern abrasion surface at the shore face (Figure 3.18c) and thick lenses of flint are evident, having formed through the re-precipitation of sponge spicules within the limestone (Figure 3.18f). Several beaches in this region are dominated by flint clasts which are formed through the physical breakup of flint lenses. Flint is not found farther north on the Robe coastal plain as Gambier Limestone does not outcrop in this region.

The abrasion surface at Port MacDonnell is backed by a (proposed) Holocene beach deposit consisting of coarse sand, sub-angular flint cobbles and fossil shells (Figures 3.18d-e). The shell assemblage is primarily composed of *Turbo undulatus* shells and opercula, indicative of a high-energy, rocky beach environment (Ludbrook, 1984). The Holocene beach deposit is approximately 1 m high and has been pedogenically altered along its upper surface where a 20 cm thick soil layer has formed and infiltrated deeper into the profile in certain locations. This deposit is likely Holocene in age due to its proximity to the present shoreline, the presence of well-preserved shells and its elevation 1 m above the present tidal zone which indicates deposition may have occurred when sea level was higher than present. Lewis *et al.* (2013) suggested that the Holocene sea-level highstand varied around the Australian coastline

and that in South Australia the present sea level was attained between 8000 and 7500 cal. yr BP. Belperio *et al.* (2002) indicated that Holocene sea level could have been as high as +3 m APSL in Spencer Gulf, ~500 km northwest of Mount Gambier.

In more sheltered sections along the beach at Port MacDonnell, light gray (2.5 Y 7/2), medium sand is deposited on a low gradient. Foraminifera were identified within this sediment and were dominantly *Elphidium crispum*, *Ammonia beccarii* and *Discorbis dimidiatus*. Flint cobbles are also deposited in certain localities along the shoreline and rest on top of the limestone abrasion surface and affront the Holocene beach deposits. Common species of modern molluscs found at Port MacDonnell Beach include *Turbo undulatus*, (which are particularly abundant) and *Thyas orbita*, the presence of which is indicative of a high-energy, rocky environment.

To the west of Port MacDonnell (S38°03'29.6", E140°40'20.8") above a pedogenically altered Holocene beach deposit rests a distinct layer of large shells. This shell layer is overwhelmingly dominated by the gastropod *Turbo undulatus* and their opercula (Figure 3.18a). Shells are largely well-preserved but fragmented or chipped in some instances. The shell layer is monospecific and is exposed for approximately 2 m in width. The shells appear to rest only on the surface of the deposit and are not buried within the soil or deposited in any specific order. This deposit is likely an aboriginal midden similar to those described by Cann *et al.* (1999) in the Robe region.

At Racecourse Bay (S38°03'22.5", E140°45'52.0"), 5 km to the east of Port MacDonnell, the coastline is dominated by flint cobbles, derived from the physical break-up of flint layers within the Gambier Limestone. The flint cobbles comprise a steeper gradient shoreface than at Port MacDonnell and likely reflect a higher energy environment. Three transects were taken within a 500 m wide embayment at Racecourse Bay (Figure 3.15) to provide a modern analogue of beach profiles and sediment supply in relation to current wave direction and wave action. Each transect was taken at low tide and the cross-sections are illustrated in Figures 3.16a, b and c. Transects were conducted in areas where human influence on the coastline was minimal and at several localities around the embayment to establish the effects of wind and wave direction and strength on the beach profile.

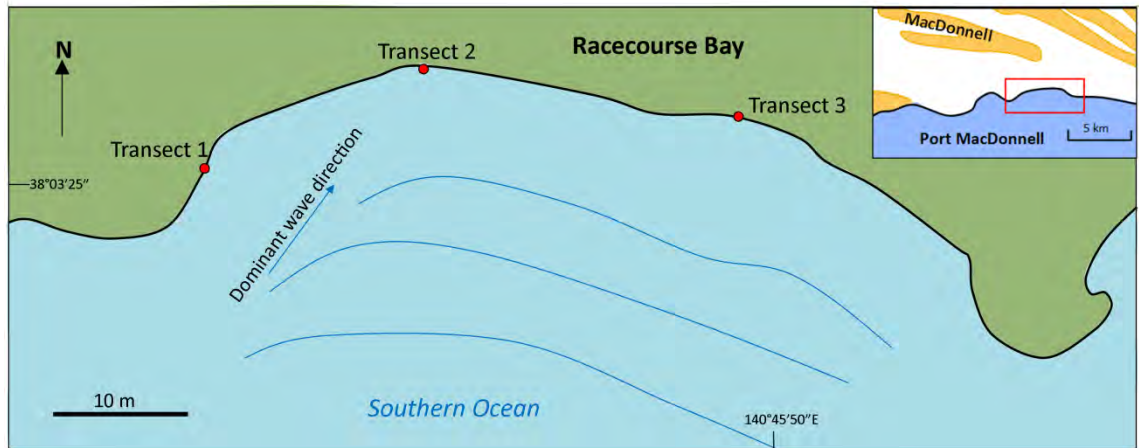


**Figure 3.15:** Location of beach transects within Racecourse Bay.

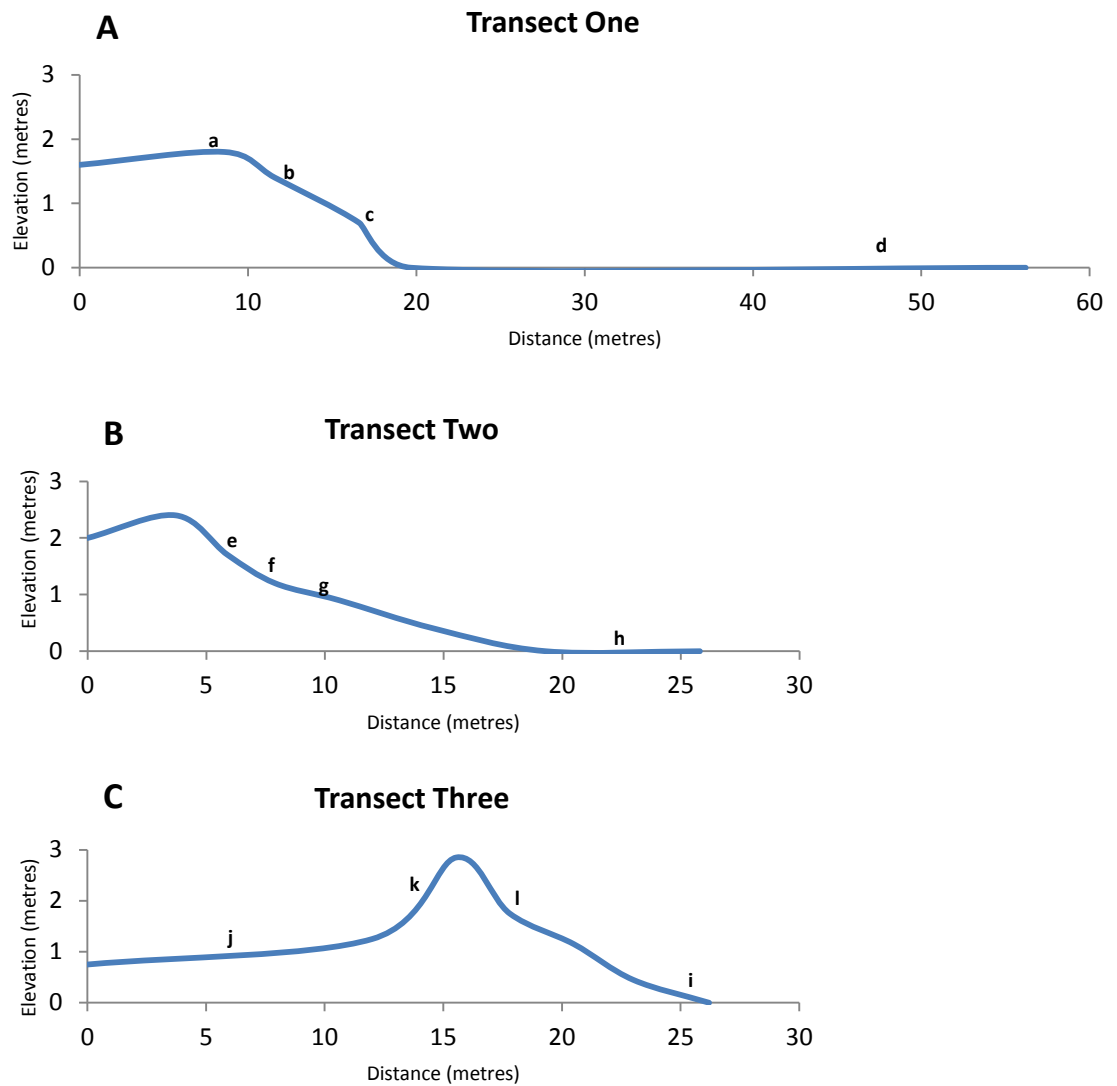


**Figure 3.16:** Transects across Racecourse Bay; **A:** Locality 1, **B:** Locality 2, **C:** Locality 3 (lower case letters a-l correspond with the photographs in Figure 3.17 and identify their location on the transect)





**Figure 3.17:** Photographs from transects across Racecourse Bay: **A-D** = transect 1; **E-H** = transect 2; **I-L** = transect 3. Location of photographs within transect are located in Figure 3.15. **A:** Top of beach ridge crest, looking eastwards across Racecourse Bay, **B:** Large flint cobbles and seaweed indicating high-tide mark, **C:** Flint cobbles at base of beach ridge (hammer is 28 cm long). **D:** 30 m wide shore platform scattered with flint cobbles, **E:** Transect 2 looking westwards. Beach is sandier at this location landward of shore platform; **F:** Large flint cobbles deposited on top of sand beach ridge, **G:** Seaweed marks high tide, **H:** Flat, sandy shore platform landward of flint cobble dominated platform, **I:** Transect 3, flint cobble dominated ridge looking eastwards, **J:** Extensive shrub vegetation landward of ridge, **K:** Landward side of beach ridge, **L:** Steep step in seaward side of beach ridge.



### **Transect One**

The first transect (S38°03'24.8", E140°45'37.2") was recorded on the western side of the embayment, where the beach faces southeast. At this location waves were breaking obliquely to the shore. The beach face was fronted by a wide (>30 m) shore platform, or abrasion surface, littered with large ( $\bar{x}$  = 25 cm long axis) and very angular flint cobbles (Figure 3.17d), perhaps indicative of deposition during high energy settings, but not of persistent wave action whereby cobbles may appear more rounded. The beach ridge is approximately 1.7 m high at its tallest point. Flint cobbles trend towards a smaller size at the ridge crest but still remain angular in shape. The beach face itself is steepest at the toe of the beach profile where a berm feature is potentially indicative of continual sediment removal by wave action. Above the berm the gradient is gentler and relatively uniform to the ridge crest. Cobbles become sparse and vegetation becomes denser on the leeward side of the crest. Vegetation is first visible approximately 20 cm below and seaward of the beach ridge crest and possibly marks mean maximum sea level height.

### **Transect Two**

The second transect was taken in the centre of the embayment where the beach faces south-east and was the only section in the embayment significantly covered by sand. As in transect one, a wide shore platform littered with flint cobbles fronts the beach. At the time of measurement this platform was covered in water and deemed unsafe to measure. The protective shore platform may result in the dissipation of wave energy before it reaches the beach and result in a lower energy environment depositing a greater volume of sand than found anywhere else in the embayment. The beach face also forms a ridge-like structure at this location and its crest is 2.5 m high at the tallest point. The ridge is fronted by a sand flat of medium sand, 6.5 m in width, with few sub-rounded flint cobbles deposited on its surface (Figure 3.17h). Landward of the sand flat, smaller (~3 cm in length), rounded flint cobbles are deposited and intermixed with larger flint clasts. The sand deposit becomes steeper towards the beach ridge crest. Approximately 10 m from where the slope gradient began a distinct laterally extensive band of seaweed likely represents mean sea level as the sediment beneath was still found to be wet from the high tide earlier that morning (Figure 3.17f).

Sand remains the dominant sediment throughout the profile, while the size of dispersed flint clasts varies. Flint clasts are smaller at the seaward extent of the beach ridge, with bivalves and gastropod fragments (species unidentifiable) also present. As the gradient increases towards the crest of the profile larger (~20 cm long) flint clasts are visible and shrub-like vegetation is evident, suggestive of sediment deposition during high-energy events such as

storms. Shrub-like vegetation is prominent at the ridge crest and may have aided in stabilisation of this feature. As found at transect one, the landward side of the profile is gentler in gradient than the seaward side and vegetation is dense within 4 m landwards of the ridge crest.

### **Transect Three**

A final transect (S38°03'22.7", E140°45'52.0") was taken on the eastern edge of the embayment where the beach faces southwest and into the dominant wave breaking direction. At the time the transect was conducted (low tide) waves were breaking at the base of the beach ridge, covering any shore platform that may have been present (Figure 3.17i). The beach ridge crest at this locality reaches almost 3 m in height, and is considerably higher than the crest height recorded in transects one and two, possibly reflecting a higher energy environment at this locality where breaking waves push a greater volume of sediment landwards. The beach ridge is also steeper at this locality, possibly for similar reasons.

Two small berm-like features are located within the beach ridge. The first is 3.2 m from the shoreline (45 cm above water level) and a distinct band of seaweed at this location likely reflects mean sea level. The first berm is 2.5 wide and 70 cm in height. Another berm-like feature is found 2.7 m landwards of the previous berm and is possibly indicative of a high neap-tide or storm berm.

Flint clasts are the dominant sediment type at this locality. At the shoreline pebbles are medium in size (~15 cm in length) and become smaller (~5 cm) and more rounded towards the base of the first berm, likely as a result of continued mechanical abrasion in the swash zone. Towards the beach ridge crest flint clasts become larger in size (~20 cm) and more angular, perhaps evident of higher energy storm events where larger clasts can be entrained to the back of the beach face.

The landward side of the berm is also steeper than found in transects one and two. Vegetation is not apparent until ~10 m landwards of the ridge crest, so is unable to stabilise the beach ridge structure and therefore washover events may result in the erosion of the landward side of beach deposit. The steeper landward side may also be a factor of the larger beach ridge size at this locality.

### **Summary**

Field observations highlight that the beach ridge at Racecourse Bay varies in profile, clast size, clast roundness and dominant sediment type depending on its position relative to dominant

wind and wave direction around the embayment. The beach face at Racecourse Bay is reflective and composed predominantly of coarse sediment; it varies from the dissipative beach face of Port MacDonnell, where fewer flint cobbles are found. This may be indicative of variable volumes of flint sources along the coastline and/or differing energy levels. A comparison of two beaches in close proximity to each other, as well as the observation of a lack of Holocene dunes in the area compared to regions east and west of Port MacDonnell, highlights that the coastline can change dramatically within a few kilometres. Recognition of this variation will be of use when assessing potential palaeo-shorelines on the coastal plain and in deciphering whether the modern coastline is necessarily analogous to that of previous shorelines.

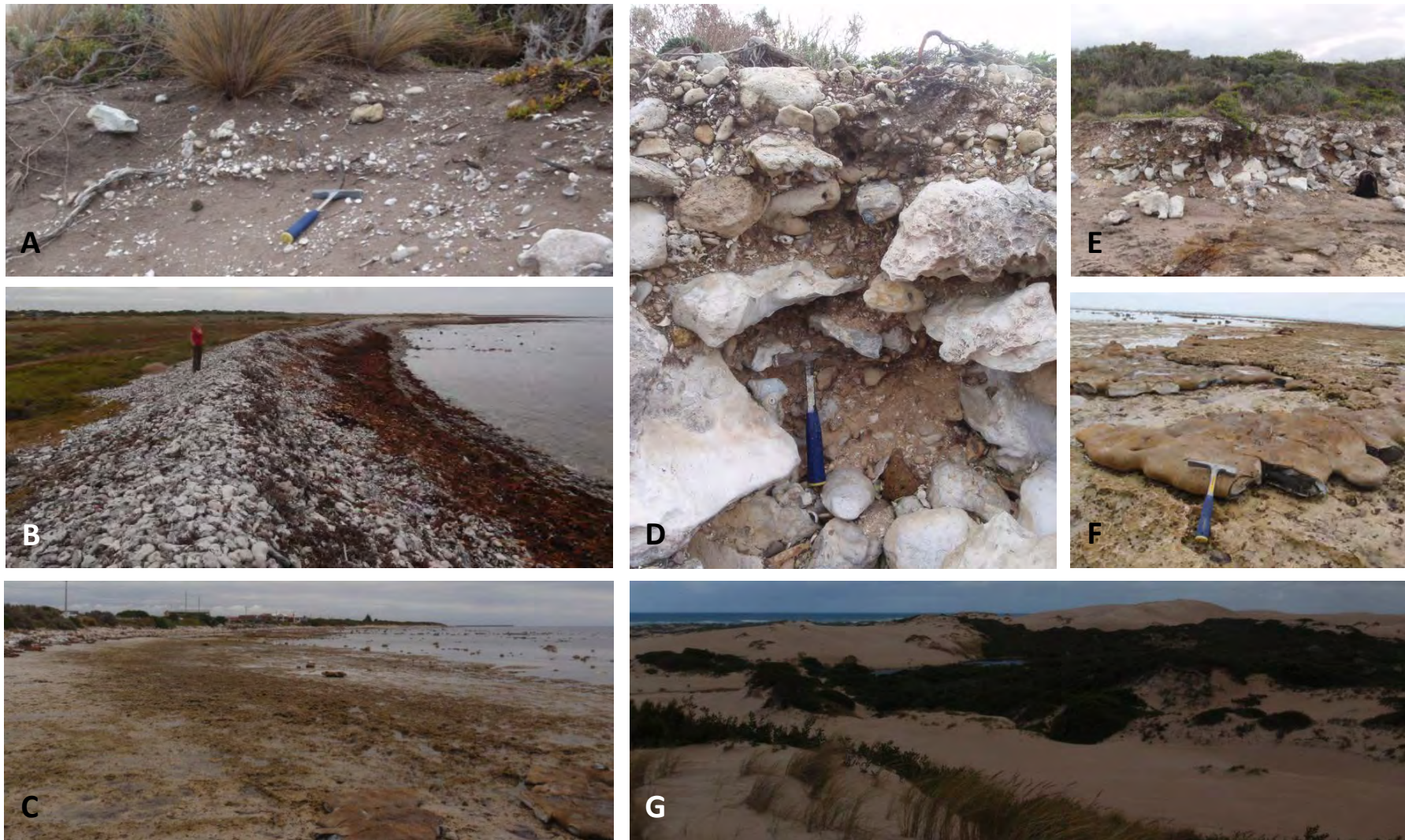


**Figure 3.18:** Photographs of the modern shoreline along the Mount Gambier coastal plain. **A:** Aboriginal midden, Port MacDonnell; **B:** Flint cobble beach, Racecourse Bay, **C:** Gambier Limestone marine abrasion surface, Port MacDonnell; **D and E:** Holocene beach deposit, Port MacDonnell; **F:** Flint lens in Gambier Limestone; **G:** Large coastal sand dunes, Discovery Bay, western Victoria (coastline is ~1 km from where photograph is taken). Geology hammer is 28 cm long.

### 3.8.3 Robe Range

Steep aeolianite cliffs at the western extent of Port McDonnell Beach are composed of two clearly distinct units separated by a 75 cm thick calcrete palaeosol. These aeolianite units are suggested to form part of the Robe Range, the youngest Pleistocene barrier on the Mount Gambier coastal plain, due to the proximity of the barrier to the coastline and the presence of two separate, stacked aeolianite units. Robe Range has previously been described near the township of Robe by Schwebel (1978; see Figure 3.20b). Schwebel (1978) identified unconformities within the Robe barrier and suggested the dune had been deposited during three separate highstands; aeolian sands capping the dune were deposited during the Holocene and named Robe I, while Robe II refers to sands deposited during MIS 5a (~82 ka) and Robe III reflects sands deposited during MIS 5c (~105 ka).

Robe Range does not appear to be as laterally extensive as some of the older Pleistocene barriers along the Coorong coastal plain. Robe Range has been mapped between Beachport and Robe but is not identified farther north of Robe, or farther south of Beachport until Cape Northumberland. North of Robe the Younghusband Peninsula closely extends along the coastline and these Holocene sands may have obscured underlying units of Robe Range.

#### **Western extent of Port MacDonnell Beach**

While aeolianite cliffs are not found at the shoreline to the east of Port MacDonnell, at the western extent of the beach aeolianite cliffs tower up to 13 m above the sea surface, and extend to Shelly Beach and Cape Northumberland, approximately 1 km farther west (Figure 3.19a). The upper aeolianite unit, above a palaeosol calcrete unconformity, is approximately 8 m high at Port MacDonnell and displays low angle (13-17°) trough cross-bedding dipping eastwards before flattening out (Figure 3.19c). This upper aeolianite unit is capped by a rubbly calcrete approximately 75 cm thick, with dense vegetation growing above that. The unit is composed primarily of coarse, very pale brown (10YR 8/13) sand. Foraminifera are not abundant within the sediment, but *Elphidium crispum* and *Discorbis dimidiatus* are identified.

The lower aeolianite unit at the western extent of Port MacDonnell Beach has been well cemented on its exposed face and a blackened weathering crust coats the deposit. Beneath the weathering crust the unit comprises medium, very pale brown sand (10YR 7/4). Some laminar bedding is still evident within this lower unit but was inaccessible to strike and dip measurements due to the presence of larger aeolianite boulders that have fallen to the base of the cliff.

The palaeosol unit separating the two aeolianite units at this location is approximately 50 cm thick and is covered by a calcrete layer approximately 25 cm thick which comprises laminar calcrete below and rubblier calcrete above. The contact between the calcrete unconformity (atop the palaeosol) and the upper aeolianite unit is sharp and extends laterally around the headland as far as is accessible to follow. The size and extent of this unit suggests a significant hiatus in aeolianite deposition and a lengthy period of subaerial exposure prior to the deposition of the upper aeolianite unit.

### **Shelly Beach**

At Shelly Beach, approximately 300 m west of Port MacDonnell Beach, a distinct unconformity also separates two aeolianite units in cliffs directly landward of the beach (Figure 3.19d). The upper aeolianite unit is approximately 4 m thick and composed of yellow (10YR 7/6), angular, medium-grained sand. Cross-bedding is evident within this unit and beds dip northward into the cliff. Farther west along Shelly Beach this unit displays distinct trough cross-bedding, where steeply dipping beds are capped by shallower dipping beds suggesting a change in dominant wind direction (Figure 3.19d). The upper aeolianite unit is also capped by a 1 m thick calcrete, which is massive in the cliffs to the back of Shelly Beach but rubblier and with numerous rhizoliths farther west. *Discorbis dimidiatus* is the prominent foraminiferal species within this deposit accounting for 70% of the 200 tests counted. *Elphidium crispum*, *E. macelliforme* and *Ammonia beccarii* were also found within the deposit comprising 26.5, 2 and 1.5 % of the counted test respectively.

The lower aeolianite unit is approximately 3 m thick and composed of brownish-yellow (10YR 6/6), medium-grained, sub-angular sand. Cross-bedding is also evident within this lower unit and dips towards the southeast. Foraminifera are identified within the deposit though these tests appear more weathered, with many tests cemented and in some cases rounded so much that any identifiable ornamentation has been removed. *Elphidium crispum* are the dominant species of foraminifera of those identified. The unconformity separating the two units is laterally extensive along Shelly Beach (some 50 m) but is not as thick as at Port MacDonnell and is marked by an undercut surface, at which no palaeosol or calcrete is visible and has perhaps been eroded.

Large (~4 m in diameter) aeolianite boulders are also found at the base of the cliffs at this locality. Directly south of Shelly Beach, an island of aeolianite is visible approximately 50 m offshore. This aeolianite island is approximately 40 m wide and 6 m high and has two separate undercut unconformities extending laterally within it. Three aeolianite islands are

present at Cape Northumberland, 500 m west of Shelly Beach. The presence of these aeolianite islands and the large boulders at the base of the coastal cliffs indicates that Robe Range once extended at least 50 m farther south (and likely farther) and that the shoreline has retreated due to erosion during the present sea-level highstand. This also indicates the reduced preservation potential of the dune range in the larger geological record as subsequent sea-level highstands erode the structure.

#### **Cape Northumberland**

At Cape Northumberland aeolianite cliffs at the coastline, and within three offshore islands, are steep and unfortunately inaccessible for sampling. The cliffs are approximately 15 m tall and multiple sets of cross-bedding are visible within them. Interestingly, at this locality aeolianite units are not separated by one distinct unconformity but several. Up to five undercut surfaces within the aeolianite cliffs (Figure 3.20) are perhaps indicative of periods of subaerial exposure and may represent palaeo- or protosols that have been eroded. These unconformities may represent episodes of relative sea-level fall while the multiple aeolianite units may be a reflection of sudden sea-level rise resulting in sediment from the shelf to be entrained landwards by winds. However, unconformities do not necessarily coincide with chronological boundaries and the timescale for palaeosol formation may be unclear (Leighton *et al.*, 2013).

#### **Relict beach deposit, Port MacDonnell Beach**

Traversing the shoreface to the east of the aeolianite cliffs at the western extent of Port MacDonnell Beach, a weathered aeolianite unit is evident on the beach face. Deposits of this unit are coated in a dark weathering crust similar to that coating the lower aeolianite unit previously described within the cliffs. The aeolianite unit on the beach face may, therefore, represent remnant deposits where the lower aeolianite unit once covered the beach but has since been eroded. Approximately 100 m east of the aeolianite cliffs a flint conglomerate unit is present in sporadic outcrops. The flint conglomerate unit is composed predominantly of abraded flint cobbles, derived from flint lenses which have precipitated from the outcropping Gambier Limestone, and shell fragments deposited within a lime matrix. Molluscs within the deposit are primarily of the gastropod family and include species such as *Turbo undulatus* and *Thyas orbita*, and bivalves such as *Katelsysia*. These species are similar to those found on the modern beach at Port MacDonnell. The flint conglomerate rests stratigraphically above the Gambier Limestone abrasion surface and below the weathered outcrops of aeolianite.

The flint conglomerate unit may represent a cemented palaeo-beach unit, deposited before the lower aeolianite unit in the coastal cliffs. The gastropod species and abraded flint cobbles within the unit are indicative of a high-energy, rocky coastal setting at the time of deposition. Figure 3.21 illustrates a composite cross-section of how the beach may have looked before erosion of the aeolianite.

### **Summary**

Thick aeolianite units west of Port MacDonnell are suggested to comprise part of Robe Range. A laterally extensive (~500 m) unconformity represented by a calcrete palaeosol and undercut surface separates two aeolianite units and indicates that a significant hiatus in aeolianite deposition has occurred. The two aeolianite units may have possibly been deposited during subsequent sea-level highstands as suggested by Schwebel (1978) for Robe Range in the Robe region. Multiple undercut surfaces seen in aeolianite units at Cape Northumberland may represent eroded protosols formed during relative drops in sea level. The presence of large aeolianite islands south of the coastline indicate that the Robe Range was once much wider than today and has retreated through coastal erosion during the present sea-level highstand. The flint conglomerate may represent a relict beach facies deposited before the deposition of the lower aeolianite unit. The conglomerate may have been deposited during the same sea-level highstand as the aeolianite which may have blanketed the beach unit as sea level regressed.

Geochronological analysis is necessary to determine the time of deposition of these deposits and will be discussed further in Chapter 5. If the aeolianite units correlate to those described by Schwebel (1978) farther north and are indeed of last interglacial, interstadial age, the flint conglomerate unit may be significant as it is the first subaqueously deposited interstadial coastal strata found above present sea level in Australia.



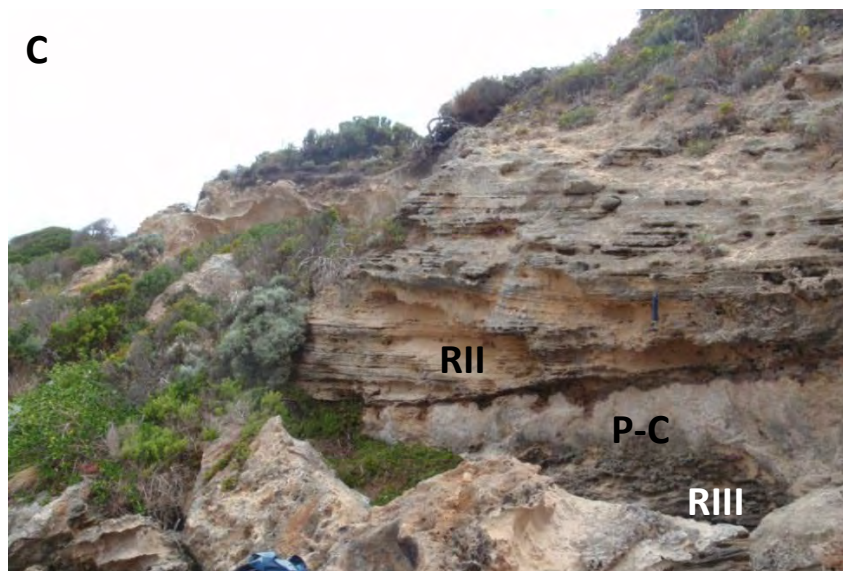


**Figure 3.19:** Aeolianite of Robe Range equivalent in the Port MacDonnell region, South Australia. **A:** Plan view sketch of aeolianite outcrops at the coast on the Mount Gambier coastal plain; **B:** View eastwards towards Shelly Beach from Cape Northumberland (note, offshore islands of aeolianite); **C:** Aeolianite units separated by palaeosol at Port MacDonnell (RII= Robe II equivalent after Schwebel (1978), P-C = palaeosol/calcrete, RIII = Robe III equivalent); **D:** Aeolianite units at Shelly Beach (note, unconformities (U) within aeolianite cliffs at this site are represented by undercut units).

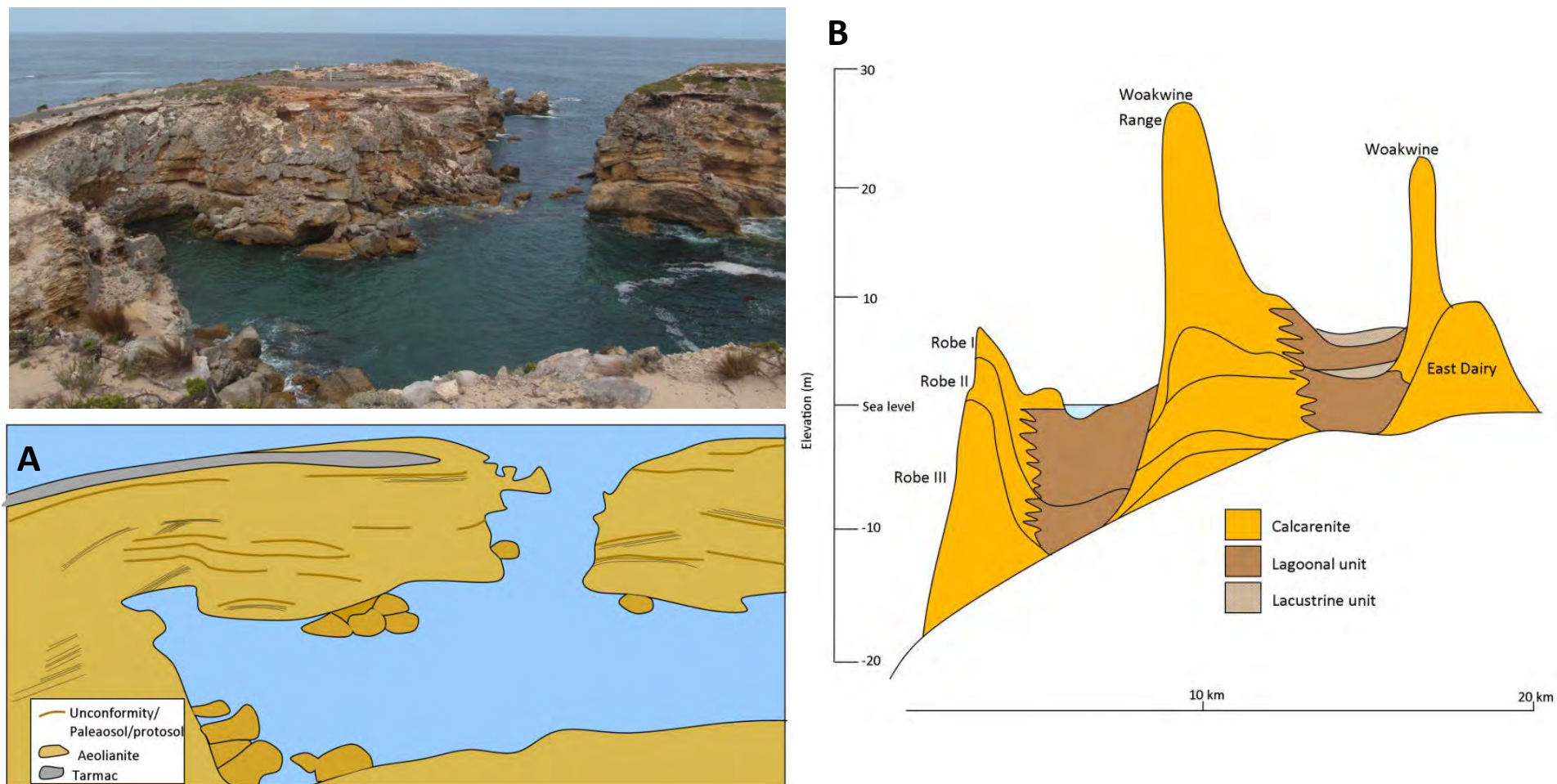


**Figure 3.20:** Multiple unconformities within aeolianite of Robe Range. **A:** Aeolianite cliffs at Cape Northumberland display multiple undercut units potentially indicative of former protosols (cliffs are approximately 10 m high), **B:** Composite barriers of Robe Range and Woakwine Range as identified near Robe (modified from Schwebel, 1984), note black lines refer to unconformities. Note that vertical scale is exaggerated.



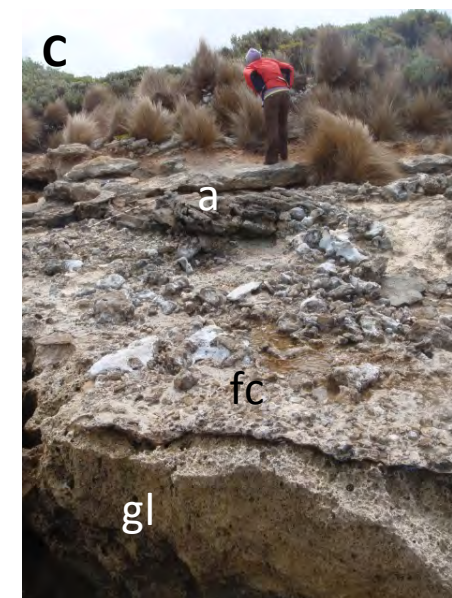
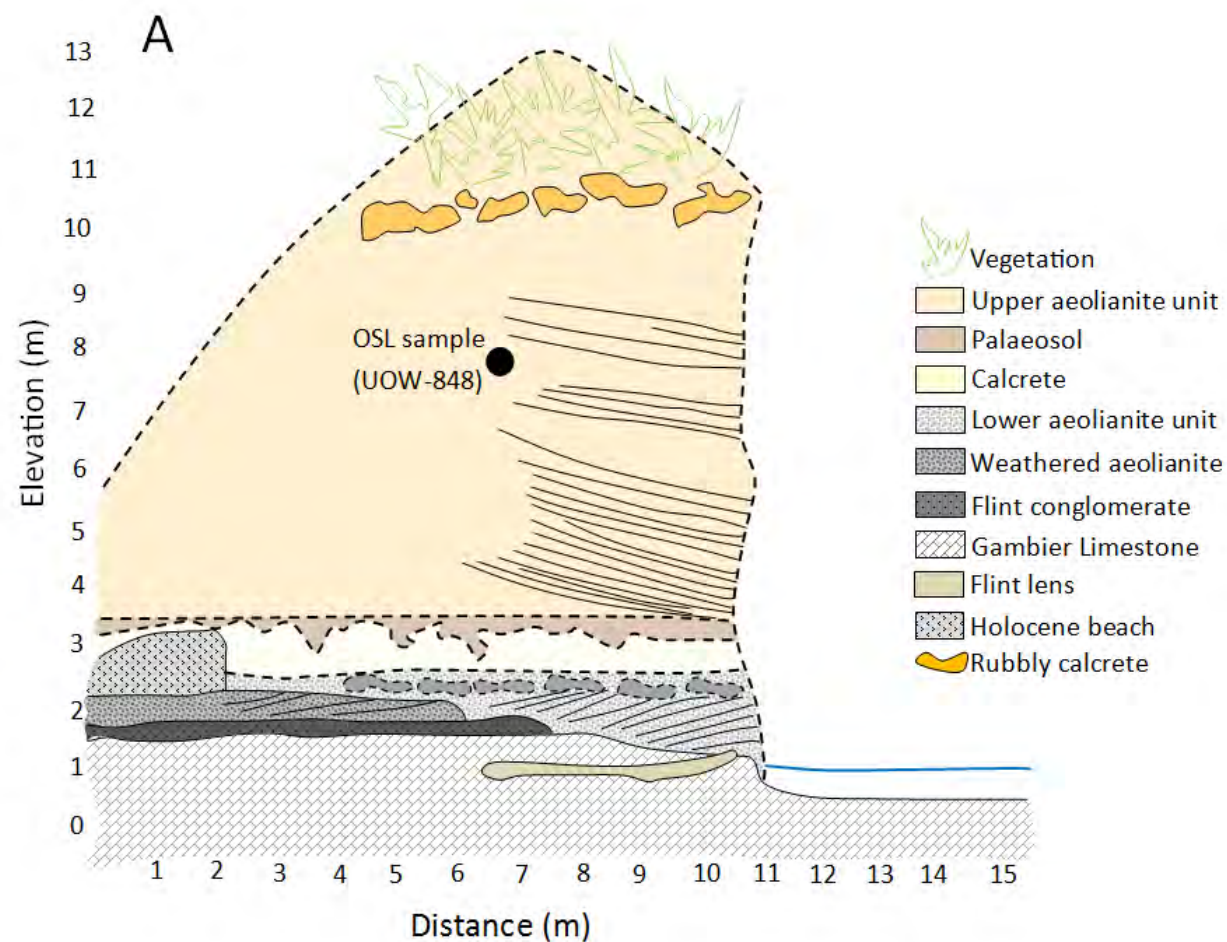


**Figure 3.21:** Composite stratigraphical cross-section illustrating where units of the Robe Range may have lain above the flint conglomerate at Port MacDonnell prior to coastal erosion (**A**). Solids lines indicate the actual cross-section drawn from Port MacDonnell modern beach face while the dashed lines represent the aeolianite cliffs to the west of Port MacDonnell beach and are placed above the original cross-section for illustration purposes. **B:** Port MacDonnell beachface indicating stratigraphical setting with weathered aeolianite (a) overlying the flint conglomerate (fc) which in turn rests upon the Gambier Limestone (gl). **C:** Small cove at Port MacDonnell Beach illustrating stratigraphical relationship between Gambier Limestone, flint conglomerate and weathered aeolianite.

### **3.8.4 MacDonnell Range**

The next shoreline barrier inland from the Robe Range aeolianite at Port MacDonnell is the MacDonnell Range, found 7 km landward of the present coastline. The map of Sprigg (1952) (Figure 3.13) and transects across the MacDonnell Range (Fig 3.22a,b) highlight that it is a two-armed structure trending for approximately 15 km and ending just to the west of Allendale East. Following the north-westward trend of the modern coastline the MacDonnell Range aligns with the Woakwine Range, which is laterally extensive for 300 km landward of the Coorong Lagoon and 5 km landward of the coast. The MacDonnell Range reaches up to 45 m above sea level at its highest point, and stands up to 20 m above the coastal plain as shown by a transect along the top of the dune range (Figure 3.22a). Transects across the width of the structure (Figure 3.22b) highlight the two arms of the dune range and indicate that the inland arm is the taller of the two.

#### **Sand quarry, Swarts Road**

A suitable sampling location was found in the form of a small sand quarry within MacDonnell Range. Within this exposure the sediment comprises mostly free-flowing, pale yellow (2.5Y 8/2), medium sand. In two locations within the quarry, sand is semi-consolidated and laminar cross-bedding is evident (Figure 3.22g). Beds are found to dip 14° southward and may represent the stoss side of a dune structure. Beds within the consolidated outcrops are approximately 2 cm thick, becoming thinner (3 mm thick) towards the top of the outcrop. The angle of cross-bedded units and the absence of fossil shells within the exposure suggest that this is an aeolian deposit. A lack of fossil shell beds within the MacDonnell Range region may be a result of the large volumes of landward transgressing dunes overlying any remnants of beach or lagoonal facies.

The sand quarry has been capped by a 30 cm thick dark brown soil layer. Rubbly calcrete is also present within this pedogenically altered layer but has been weakly developed. Stratigraphically beneath the soil unit, a 1 m thick layer of rhizoliths is indicative of past vegetation that would have grown on the dune surface. The presence of the soil, calcrete and a thick rhizolith layer (Figure 3.22f) indicate that the dune structure has been subaerially exposed for a substantial period of time.

#### **German Creek**

Other suitable sample locations within the dune range were difficult to find. A shell deposit was identified north of Kongorong near to the settlement of German Creek, approximately 30 km northwest of the sand quarry at Allendale East. The shell deposit is found on the

ground surface and had likely been exposed through the removal of overlying sediment, perhaps in the construction of the nearby dirt road or as part of land clearing for the adjacent forest. The shells are found in a 20 m radius at the side of the road and consist primarily of the bivalve *Katelsia rhytiphora* (Figure 3.22e). Individuals are well-preserved, generally large in size and many are articulated. The shell unit is located in a topographic low 16 m APSL (from SRTM data), in the lee of Woakwine Range, and the bivalves may represent remnants of a lagoonal deposit that formed during the last interglacial (~125 ka).

### **Erosional history**

Between the present coastline at Port MacDonnell and MacDonnell Range no other remnants of aeolianite are observed. In fact, on both the landward and seaward sides of MacDonnell Range, Gambier Limestone crops out at the ground surface and represents a marine abrasion surface. This differs from coastal plain surrounding the Woakwine Range farther north where Gambier Limestone does not outcrop at the surface. South of the base of the sand quarry, ridges within the Gambier Limestone extend for approximately 500 m seawards. These ridges are approximately 2-3 m in height and approximately 50 m from crest to crest and are indicative of coastal scouring by previous sea-level highstands, likely most recently during the last interglacial (Figure 3.22h).

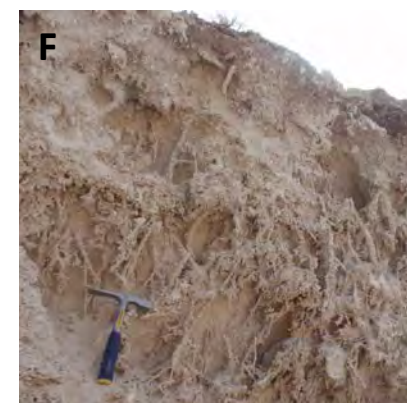
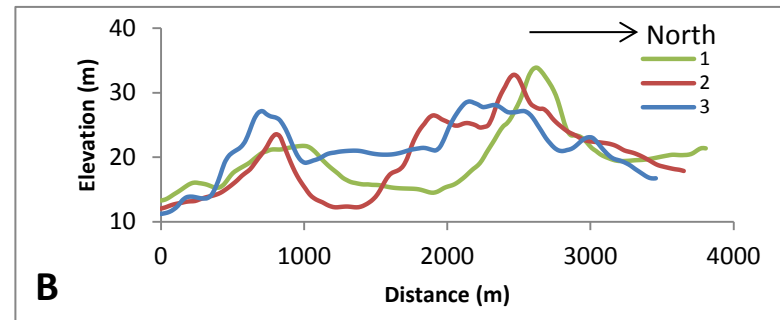
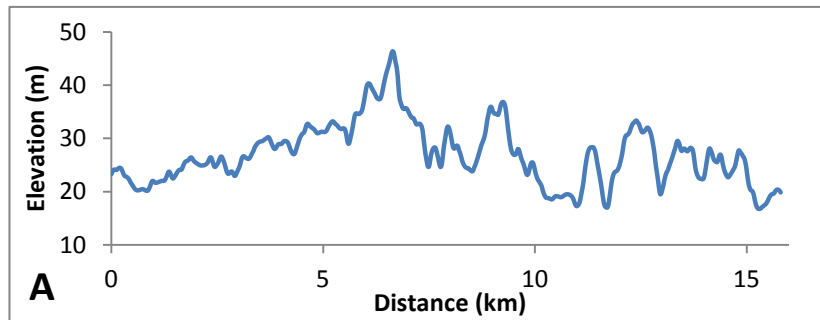


**Figure 3.22:** Images of MacDonnell Range.  
**A:** Lateral transect along the crest of MacDonnell Range, derived from SRTM data,  
**B:** Transects across the width of MacDonnell Range, **C:** Location of transects taken on MacDonnell Range (scale bar is 5 km), **D:** Sand quarry at Swarts Road, **E:** *Katelaysia* shell bed at German Creek, **F:** Rhizoliths and soil profile within exposure at Swarts Road, sand quarry, **G:** Laminated cross-bedding in consolidated sand within Swarts Road sand quarry, **H:** Last interglacial beach ridges scoured into Gambier Limestone seaward of sand quarry, represent a marine abrasion surface. The fence line highlights the undulating surface.



### Lake Hawdon South

As previously mentioned, identifying suitable sample sites within the MacDonnell Range proved challenging. A thick shell bed was identified in a drain cutting within a topographic low, landward of the Woakwine Range, near Lake Hawdon South, 90 km north-west of Mount Gambier. Sediments from the Woakwine Range have been determined to be last interglacial (~125 ka) in age (e.g. U-series dating by Schwebel, 1978; 1984), as have shells from a separate exposure approximately 6.5 km southwest of the Lake Hawdon sample site (Belperio *et al.*, 1995). Molluscan species were sampled from this deposit to use as calibration points for AAR analysis, as they could confidently be determined to be last interglacial in age.

Approximately 25 km to the southeast of Robe, directly east of Lake Hawdon South, a lagoonal facies is exposed in Biscuit Flat drain (S 37°13'53.4", E 140°01'14.5"). The exposure is 1.25 m high and is blanketed by a 30 cm thick massive calcrete. At the base of the cutting a 25 cm thick shell bed is evident. Species within this shell bed include *Brachidontes rostratus*, *Chlamys bifrons*, *Katelysia rhytiphora*, *Anadara trapezia*, *Fulvia tenuicostata*, *Spisula* (*Notospisula*) *trigonella*, *Tellina deltoidalis* and *Pleuroploca australis* (Figure 3.23b). The base of the shell layer is dominated by a laterally persistent layer of *Ostrea angasi*. The species present are indicative of sub-littoral or lagoonal environments (Ludbrook, 1984). Individuals are commonly found articulated and well-preserved, suggesting that the shell assemblage was deposited in a low-energy environment and has not been transported far (if at all) from its life assemblage position. Directly above the shell layer is a unit of finer shell fragments that has not been affected by fluctuating water levels within the drainage canal. A layer of fine clay-rich mud overlies the finer shell layer and is suggestive of pedogenic alteration, which in turn is overlain by a thin calcrete layer (Figure 3.23a,b).

The diverse range of species within the lower shell bed aids in reconstructing the palaeo-depositional environment. The presence of *Anadara trapezia*, a bivalve no longer found living within South Australian waters, is suggestive of deposition during times of warmer sea surface temperatures, such as during the previous interglacial (Cann and Clarke, 1993). While up to eight coastal deposits across Australia have been identified to contain *Anadara trapezia* of MIS 7 age, over 50 sites have been reported to contain *Anadara trapezia* of MIS 5e age and it is thus suggested MIS 5e provided optimal growth conditions (Murray-Wallace *et al.*, 2000). Murray-Wallace *et al.* (2000) suggested that an enhanced Leeuwin Current during MIS 5e could have brought warmer waters to the South Australian coastline and provided a habitat for *A. trapezia*. The presence of this species within the lagoonal deposit aids in confining the age of this deposit to MIS 5e and identifies this deposit as part of the Glanville Formation.

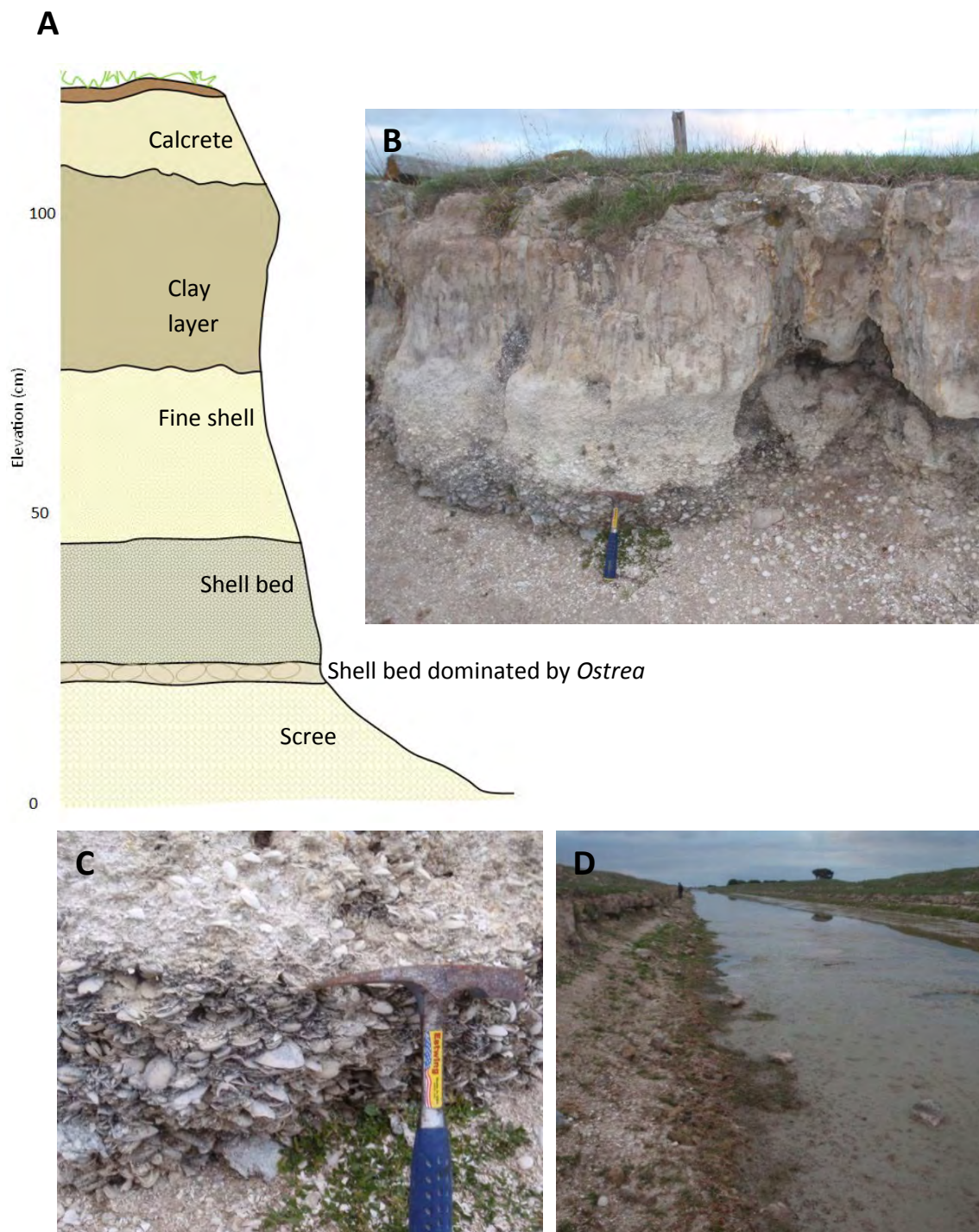


**Figure 3.23:** Exposure of lagoonal facies within Biscuit Drain, Lake Hawdon South, South Australia. **A:** Cross-sectional schematic sketch of the exposure; **B:** Channel bank at Biscuit Drain; **C:** Densely packed shell within channel bank; **D:** Looking northward along Biscuit Drain.



*Ostrea angasi*, a marine bivalve, found near the bottom of this exposure, is commonly found in deeper water (up to 30 m below the sea surface; Ludbrook, 1984) and attest to a previous connection with the open sea. The sediment size within the deposit becomes increasingly finer towards the top of the exposure, further suggesting that this is a shoaling (or shallowing) upwards deposit. Cann *et al.* (1999) described a similar assemblage of molluscs beneath surficial sediment of Lake Robe, approximately 20 km west, deposited during the flooding of the Robe-Woakwine corridor during the Holocene sea-level highstand.

### **Narrawong, Victoria**

The shoreline barriers coalesce towards the Portland region as rates of uplift reduce with increased distance from the Mount Burr and Mount Gambier volcanic provinces. To constrain the rate of uplift in this region, a site in Narrawong, Victoria, previously determined to be last interglacial in age by uranium-series and AAR analysis by Sherwood *et al.* (1994) was revisited. Sherwood *et al.* (1994) described a shell bed on the bank of the River Surry as it crosses the Princes Highway. On a visit to the site, however, the water level was high, covering any shell beds present. A 1 m high road cutting (38°15'24.6", E141°41'40.2") directly west of the river revealed a small amount of calcarenite, and from this a sediment sample was collected. This sediment is brownish yellow (10YR 6/8) medium sand, and pristine samples of the foraminifera *Elphidium crispum* and *Discorbis dimidiatus* are identified within it. Two shell fragments were found within the sand; one oyster fragment and a bivalve, possibly a *Spisula*. No bedding was apparent within the sand and it had likely been modified by road works.



**Figure 3.24:** Calcarenite within road cutting, Princes Highway, Narrawong.

### 3.8.5 Burleigh Range

Burleigh Range is the next major barrier inland from MacDonnell Range and is approximately 13 km from the present shoreline. Burleigh Range follows the direction of the modern coastline and trends north-westerly joining Reedy Creek Range northwest of the Mount Burr volcanic province. Burleigh Range and Reedy Creek Range form one of the most lateral shoreline deposits on the Coorong coastal plain, spanning several hundred kilometres. At its highest point, the Burleigh Range reaches 47 m APSL, and approximately 15 m above the surrounding coastal plain as highlighted by a lateral transect along its crest (Figure 3.26a). At its widest point the range stretches approximately 2 km and is essentially a one-armed structure as shown by multiple transects across its width (Figure 3.26b).

Australia's youngest volcano, Mount Schank, erupted through the eastern edge of the Burleigh Range approximately  $4930 \pm 540$  ka (Smith and Prescott, 1987). In certain localities basaltic pyroclastics from the volcanic centre can be found overlying the dune range (Murray-Wallace *et al.*, 1996).

#### Rabbitors Road cutting

Approximately 2 km east of Mount Schank, a road cutting trending north-south along Rabbitors Road (S37°23'17.7", E140°46'06.9") cuts obliquely through Burleigh Range, revealing the internal structure of the barrier sequence. The road cutting exposes three lens-shaped gravel beds, separated by finely bedded, pale yellow (2.5Y 8/4) medium-grained sand. At the top of the road cutting, above the gravel lenses, calcarenite displays higher angle cross-bedding. The gravel lenses are composed of flint cobbles similar to those found at the modern shoreline, as described at Racecourse Bay. The exposed x and y axes of flint cobbles were measured from the gravel lenses and compared with those at Racecourse Bay where 100 cobbles were measured (for x, y and z axes). The cobbles within Burleigh Range were found to be more rounded and almost uniformly smaller in size (Figure 3.25). These results suggest that the cobbles in the Burleigh Range likely experienced more erosion than those found at the shoreline presently. Flint cobbles are not found in the barrier shorelines farther north on the Coorong coastal plain as the Gambier Limestone does not outcrop at the surface in that region.

The three flint lenses are visible on both sides of the road cutting and their size and characteristics are described in Table 3.7. The maximum height of the flint lenses appears higher on the eastern side of the road cutting and the exposed length of these facies is greater on the western side, both of which may be a product of the angle at which the road was cut. The overall shape of the lenses and the size and roundness of flint clasts within each facies are

also comparable. Beneath each flint lens finely bedded calcarenite is present and its low dip angle is indicative of beach sands. The presence of the three flint lenses in a north-south direction suggests that the shoreline at this locality was prograding as the clasts were deposited.

Shell fragments of the bivalve *Katelsia rhytiphora* and the clam *Chlamys bifrons* were found within finely bedded calcarenite. *Katelsia* is commonly found on sandy shores of lower littoral zones and sandy muds within estuaries, while *Chlamys* may be found on sandy floors 2-30 m below the surface (Ludbrook, 1984). The presence of fragments and the absence of a distinct shell bed suggest that these specimens may have been transported to this locality and are not life-assemblages.

The stratigraphical structures within Burleigh Range at the Rabbitors Road cutting were measured by dividing the western face of the road cutting into ten metre sections and measuring bedding and structural features where possible (Figure 3.27). Allostratigraphy was used to aid in identifying bounding discontinuities which can assist in the identification of sediment removal. The exposure is approximately 7 m high at its tallest point and becomes smaller to the north and south. The structure is capped by a thin layer of soil, and overgrown vegetation masks some of the stratigraphy in the upper exposure. The development of a dark weathering crust and the use of machinery to cut out the road have also prevented the description of stratigraphy throughout the entire exposure. Several solution pipes and rhizoliths are visible throughout the cutting, indicating significant subaerial exposure.

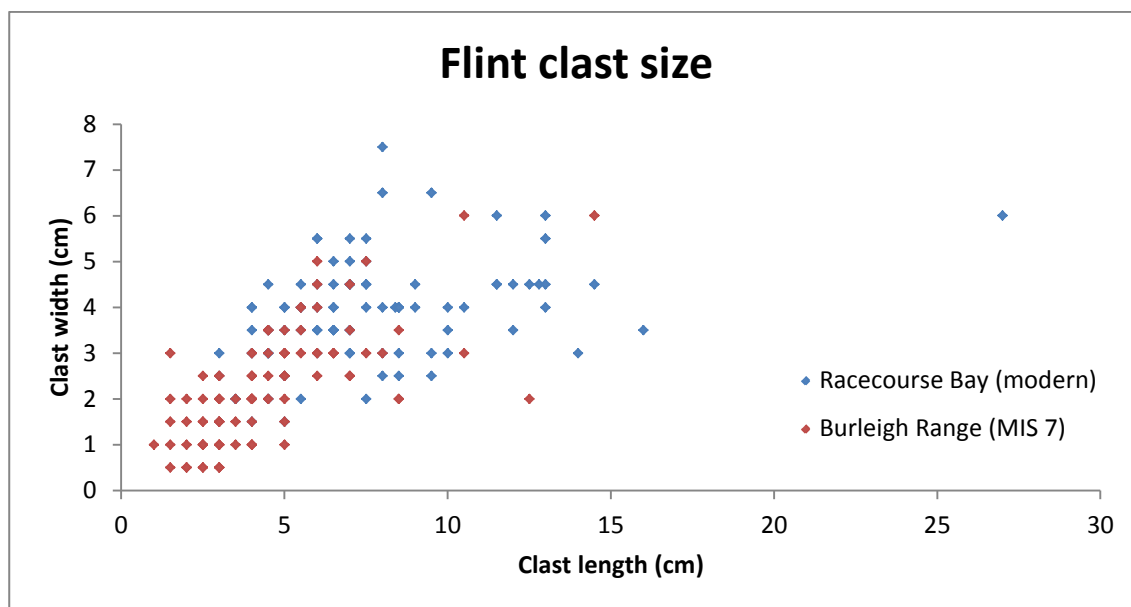


**Figure 3.25:** Scatter plot comparing flint cobbles sizes within Burleigh Range at Rabbitors Road with those on the modern shoreline at Racecourse Bay. \*Note, the two smallest axes of the clasts measured at Racecourse Bay are shown here only, to aid in a fair comparison with Burleigh cobbles, in case the longest axes within the gravel lenses are unexposed.

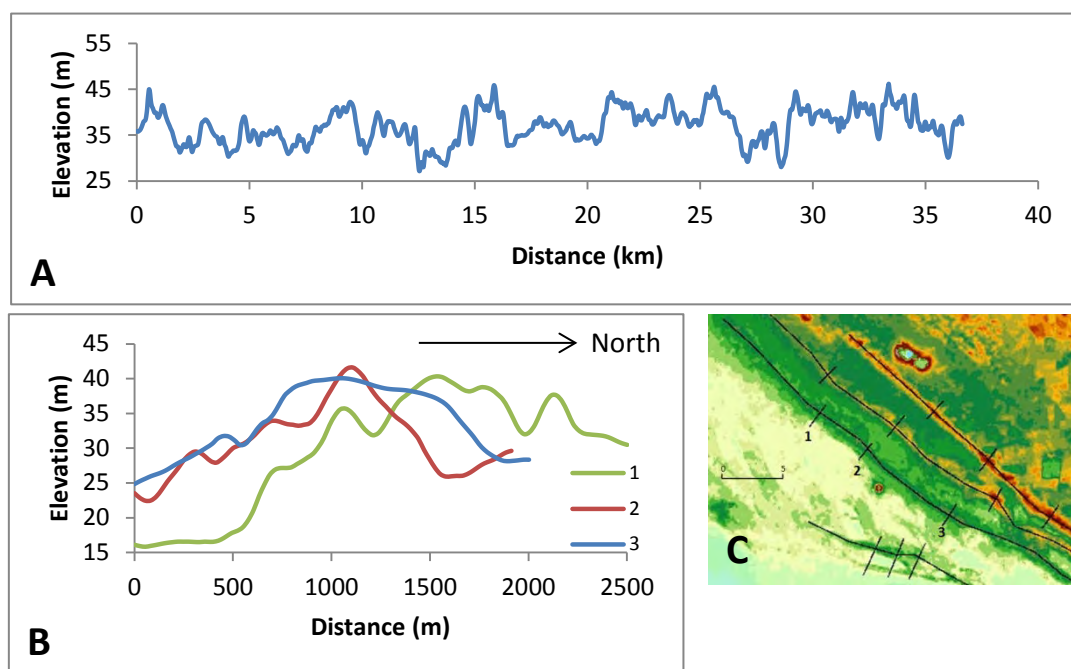


**Figure 3.26:** Transects along the Burleigh Range derived from SRTM data. **A:** Lateral transect along the crest of Burleigh Range, **B:** Transects across the width of Burleigh Range, **C:** Numbered location of transects (scale bar is 5 km).

**Table 3.7:** Comparison of features of the exposed flint lenses either side of Rabbitors Road cutting, Burleigh Range

Gravel lens	Length of ridge outcrop	Crest / maximum height of ridge outcrop	Flint pebble clast size	Additional notes
<b>Southern</b>				
East face	7.5 m	0.9 m	Predominantly medium, no large clasts evident	Only seaward side of beach ridge is visible
West face	9.5 m	1.3 m	Predominantly medium sized, with small to medium clasts more common towards seaward extent of structure	Only seaward side of beach ridge is visible
<b>Middle</b>				
East face	6 m	2.8 m	Medium to large. Medium sized at crest	Only seaward side of beach ridge visible
West face	12 m	1.7 m	Medium to large – more sparsely populated than on other beach ridges observed	Only seaward side of beach ridge visible
<b>Northern</b>				
East face	23.4 m	2.1 m	Predominantly medium in size, becoming smaller towards ridge crest	Laminated sands visible within beach ridge on landward side. Ridge steeper on seaward side
West face	34 m	1.5 m	Small to medium	Thinly laminated sands with slight landward dip within beach ridge to landward side. Ridge steeper on seaward side

Directly northward and beneath each of the gravel flint lenses, calcarenite is found to be finely bedded and laminar (Figure 3.28b). Above the flint lenses, and higher up into the structure, sand beds are more steeply dipping (up to 30° in places), dip in a range of directions (SE, NNE and W) and commonly form trough-cross beds (Figure 3.28a,c and d). The high angle and range of dip directions within these upper sands suggests they may have been deposited by winds of varying directions. It is therefore interpreted that the lower stratigraphical features within the cutting (flint gravel lenses and laminar, finely bedded calcarenite) were deposited in a beach environment, and were potentially capped by aeolian sands as sea-level regressed.

### Beach ridges

The flint gravel lenses visible in the road cutting may be relict beach ridges. Staport (1975) defined beach ridges as linear mound-shaped ridges that form parallel to the coast. The crest of a beach ridge has an elevation above mean tide, while the bottom of the ridge or adjacent trough is found near the mean low tide (Taylor and Stone, 1996). Beach ridges, therefore, originate in the inter- and supra-tidal zone and are primarily the product of marine processes, dominated by the swash (Carter, 1986; Otvos, 2000).

Discussions on Australian beach ridge form by several authors have concentrated on berm initiation and have mainly focused on sand ridges (Davies, 1957; McKenzie, 1958; Thom,

1964; 1965; Jenkin, 1968; Hesp, 1984). Through the study of beach ridges at Guichen Bay, near Robe, South Australia, Sprigg (1952) proposed two hypotheses for beach ridge formation. The first was concerned with minor variations in sea level which would result in oscillatory migrations of the strandline, forming a ridge and swale like topography. Sprigg's second, and favoured, hypothesis involved cyclic changes in the lunar orbit (18 to 61 year cycle), which would influence mean sea level by ~1.25 cm, and tidal range by 3%, enabling sand to be transported higher up the beach face and in greater quantities. Beach ridge formation appears as an unresolved issue in the literature. Beach ridge sediments commonly prove difficult to date accurately and thus determining a periodicity for beach ridge formation is challenging.

The flint gravel lenses within Burleigh Range have been capped by aeolian dunes. A similar setting has been described on the coast of Murlough, north-eastern Ireland, where multiple prograding Holocene gravel beach ridges have been covered by dune sands (Orford *et al.*, 2003). Orford *et al.* (2003) proposed two possible mechanisms for the depositional sequences observed at Murlough. The first mechanism, sequential sediment sourcing (SSS), specifies that the gravel ridges were deposited as a complete set, under a reflective morphodynamic regime and the overlying dune sands were deposited afterwards, once the gravel sediment source had been exhausted. The second mechanism, alternating sediment decoupling (ASD), is a form of synchronous deposition where each ridge and adjacent dune deposit were built sequentially as composite and related units, requiring multiple switches in sediment composition of the beach whereby either sand or gravel are the dominant sediment (Orford *et al.*, 2003).

In addition to differing beach sediment composition, gravel ridges and sand dunes also require different energy regimes and inter-tidal conditions. Gravel barrier beaches are essentially formed on high-energy, reflective coastlines (Carter and Orford, 1984), while dunes are more commonly deposited at the back of dissipative or low angle beaches. Orford *et al.* (2003) thus ask the question: how can two distinctive coastal settings, with greatly differing morphodynamic beach contexts, alternate to generate superimposed units of drastically different particle size?

While flint cobbles are found on the modern shoreline at Racecourse Bay, these units are not capped by aeolian sands, and thus are not directly analogous with the exposure of the Burleigh Range at Rabbitors Road. The presence of sandy deposits at the base of the beach berm as noticed in transect two in Racecourse Bay (section 3.8.2), may help to explain the finely bedded calcarenite found underlying each of the flint lenses within the Burleigh Range.

These finely bedded sands may have been deposited in more sheltered, lower-energy conditions, as seen at transect two. The overlying flint cobbles may then have been deposited if energy conditions increased and waves were able to entrain larger material, such as during a storm event. As the shoreline prograded the beach essentially moved southward, and the previous flint lens became a relict, with clasts perhaps being deposited here during high-energy, over-wash conditions. Rather than the alternating sediment decoupling mechanism suggested by Orford *et al.* (2003) the sequential sediment sourcing method may have occurred on this palaeo-shoreline. However, rather than an exhaustion of sediment resulting in changed sediment deposits, it may be suggested that the laminar sands were deposited during low-energy, or sheltered conditions and modified by wave and tidal action. The flint lenses may have been deposited on top of these during higher energy conditions, while the trough-cross-bedded sands overlying the gravel lenses were deposited by winds as the sea level transgressed towards the end of the interglacial highstand.

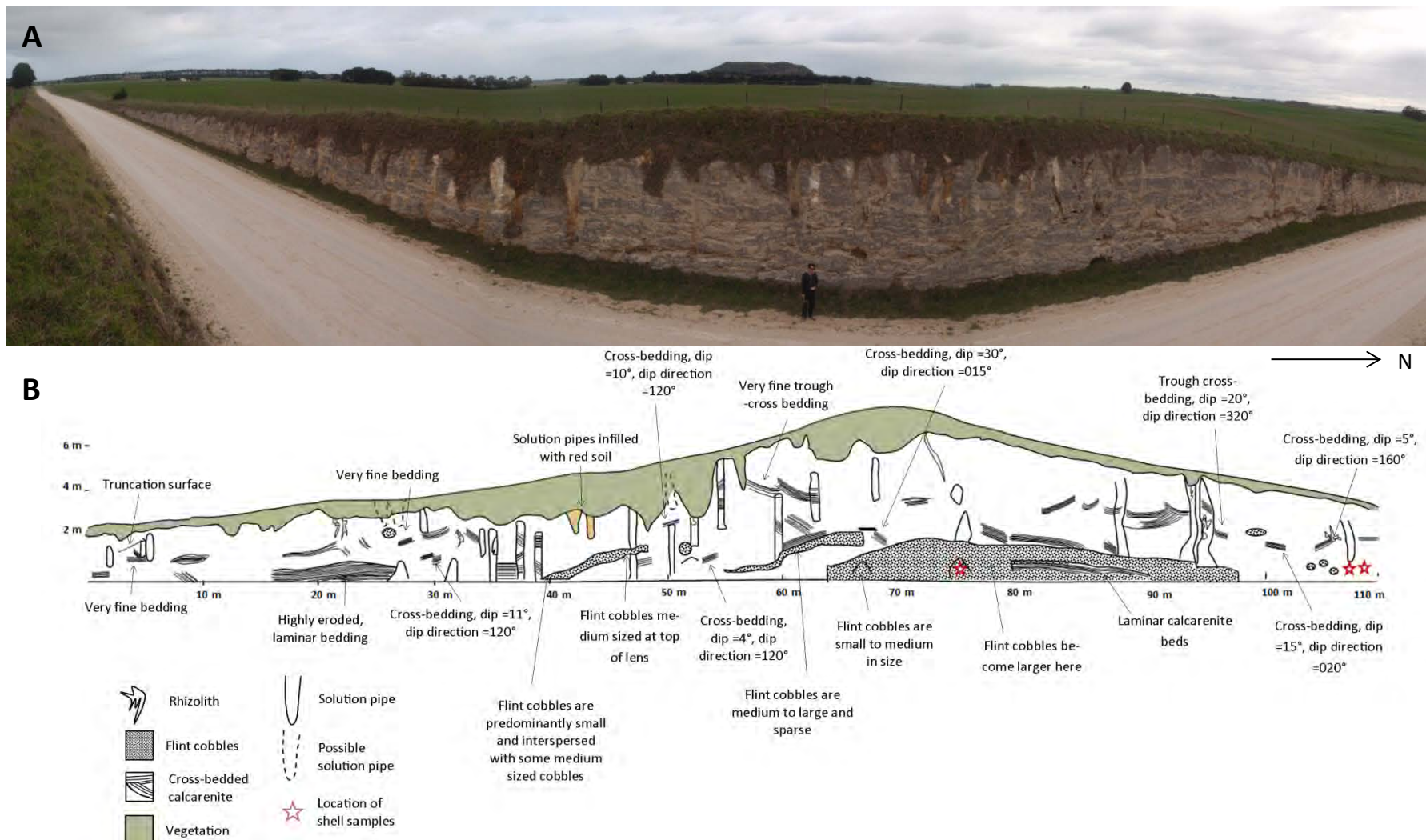
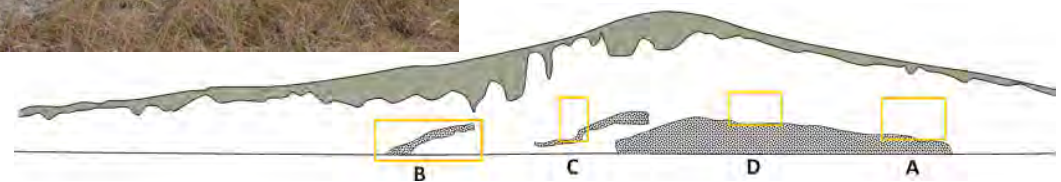


**Figure 3.27** Rabbits Road cutting through Burleigh Range, South Australia. **A:** Western side of road cutting with Mt. Schank in the distance (note, person for scale and image is distorted by panorama; road is actually straight and trends in a north-south direction). **B:** Interpretive sketch of stratigraphical facies observed in western face of road cutting, with flint cobble beach facies indicating a prograding shoreline capped with aeolian sands deposited as sea level regressed.





**Figure 3.28:** Photographs of stratigraphical features exposed in Burleigh Range at Rabbitors Road, **A:** Trough cross-bedding landward of northern gravel lens, **B:** Laminar sands beneath most southerly flint lens, **C:** High angle cross-bedding in solution pipe above middle gravel lens, **D:** High angle cross-bedding above middle beach ridge. (Note, staff is 2 m in length, with divisions every 20 cm for the first metre then every 10 cm for the following metre).



### Laslett Road cutting

Laslett Road extends eastward and perpendicular to Rabbitors Road. The road also cuts through and exposes a section of the Burleigh Range (S37°56'30.9", E140°47'42.7"), landward of that observed within Rabbitors Road. The exposure is approximately 4 m tall and is covered by a fine soil layer in which grass has grown. There is no evidence of a calcrete deposit at the surface. A weathering crust has developed on the exposed calcarenite making a complete stratigraphical description of the exposure challenging. Where exposed, calcarenite displays very fine, predominantly laminar bedding within pale yellow (2.5Y 8/2), fine sand. Marine shell fragments as well as whole individuals are found sporadically along the length of the cutting, and were commonly lodged into the sediment approximately 1 m above the road surface. Shells are commonly well preserved, but are not in a life-assemblage as no articulated pairs were recorded. Thus, transport occurred in low energy conditions *post-mortem*. Molluscs are predominantly bivalves and include genera such as; *Macra* sp. which are common in sandy and muddy environments (Ludbrook, 1984); and *Brachidontes* sp. which are common to the middle and upper littoral zones. The benthic foraminifer *Elphidium crispum* is found in pristine condition within the sediment, but uniformly small in size. In the lowest metre of the exposure fine calcareous nodules or tubes appear within the sediment (Figure 3.29d) and are perhaps indicative of bioturbation caused by burrowing organisms within oxygen-rich sediment.

The presence of well-preserved shells, bioturbation burrows and fine sands deposited within laminar beds suggests this is a lagoonal setting, formed on the leese side of the Burleigh Range.



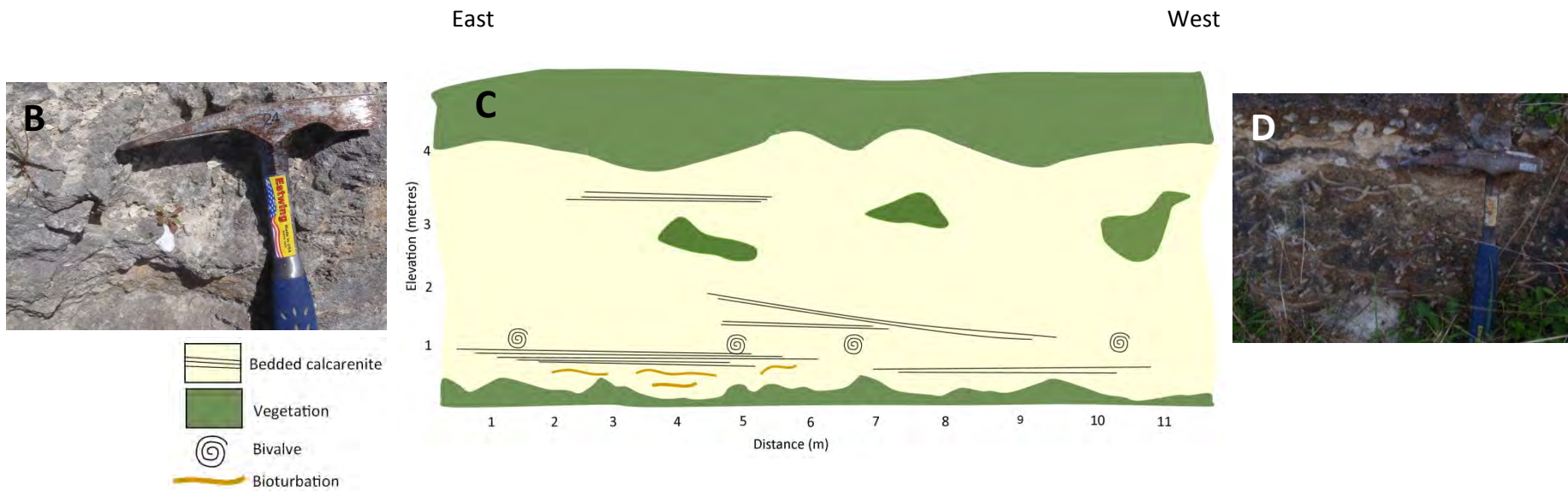


**Figure 3.29:** Laslett Road cutting within Burleigh Range, South Australia. **A:** Southern side of Laslett road cutting indicating laminated bedding, **B:** Bivalve shell within calcarenite, **C:** Stratigraphical interpretive sketch of Laslett Road cutting, **D:** Bioturbation burrows in lower portion of road cutting.

### 3.8.6 Caveton Range

Caveton Range is the next major barrier shoreline inland and is approximately 2 km northeast of Burleigh Range. Caveton Range trends in a north-westerly direction sub-parallel to the modern coastline. Depicting the extent of the barrier shoreline through the Mount Burr volcanic province is challenging, but northwest of this region the Caveton Range becomes the West Avenue Range as it trends along the Coorong coastal plain. At its highest point on the Mount Gambier coastal plain, Caveton Range reaches nearly 80 m APSL but on average is 45-50 m APSL and 20 m above the surrounding land. A lateral transect along the crest of the barrier (Figure 3.30a) reveals it becomes slightly taller towards the southeast. Transects along the width of the structure (Figure 3.30b) indicate it is also a one-armed structure and extends approximately 2 km at its widest point.

### Rabbitors Road # 2

Approximately 2 km farther north along Rabbitors Road from the road cutting through the Burleigh Range, a silage pit within a farmer's field (S37°54'06.2", E140°46'18.5") exposes laminated, fine, calcareous sands. In total 11, separate units are identified and are laterally persistent throughout the 25-m-long exposure (Figure 3.31). Each unit was identified based on colour and sedimentary structures, the presence or absence of certain fauna, and the degree of resistance of the unit (the presence or absence of undercutting). Multiple marine molluscan species are evident throughout the exposure, including; *Tellina deltoidalis*, *Katelysia rhytiphora*, *Niotha pyrrhus*, *Fulvia tenuicostata*, *Anapella cycladea* and *Modiolus areolatus*. Many of these individuals are found articulated and commonly well-preserved. Several of these genera have very fragile shells (e.g. *Tellina* and *Fulvia*), and therefore their high degree of preservation and the identification of articulated pairs suggests that they have not been subjected to turbulent conditions. Sands are very fine at the bottom of the exposure and became slightly coarser towards the top of the exposure. Foraminifera are found to be abundant throughout the deposit, and commonly consist of the benthic species *Ammonia beccarii* and small tests of *Elphidium crispum*. All foraminifera are well preserved and indicative of limited transportation. *Ammonia beccarii* are ubiquitous within the modern Coorong lagoon (Lower *et al.*, 2013), and their presence is indicative of a lagoonal deposit. Multiple bulbous features are evident throughout the layered sequence and are indicative of bioturbation within a back-barrier lagoon. Several laminar hardgrounds are found in certain layers, suggestive of episodes of subaerial exposure on the lagoonal surface. The exposure is capped by a thick and well-developed soil. A rubbly calcrete layer lies directly beneath the soil,

and suggests an extensive period of subaerial exposure. No cross-bedding within the sand is evident, suggesting that no sediment was transported by aeolian processes in this deposit.

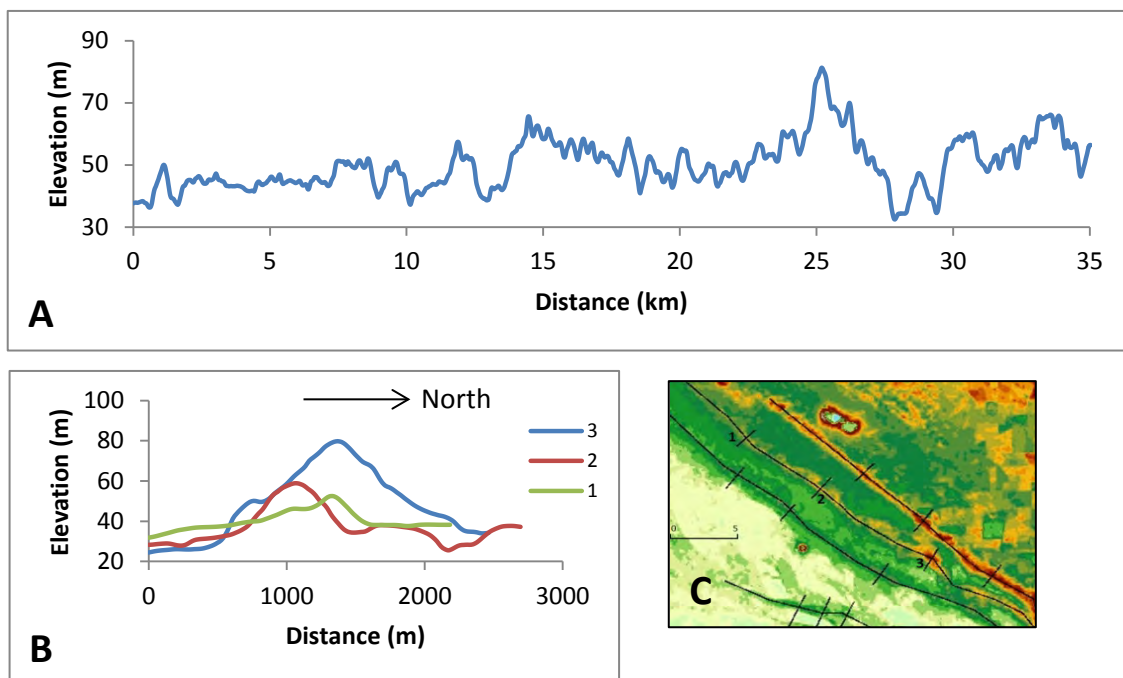
Unit 1, the lowest layer within the exposure contains nodular, bulbous features indicative of bioturbating organisms within oxygen-rich sediment. Above this, unit 2 consists of a laterally persistent shell bed, found 60 cm from the ground surface (Figure 3.32a). Many of these shells are articulated and well preserved. Those that are disarticulated, however, commonly lie facing convex down, suggestive of some transportation from their life-assemblage environment. Abundant species within this layer include the bivalves; *Katelysia rhytiphora*, *Tellina deltoidalis* which are common in the middle littoral zone in estuarine and sheltered environments, and occasional *Fulvia tenuicostata*, which are also indicative of low energy, sandy and muddy locations (Ludbrook, 1984). Shells are found within light gray (2.5Y 7/2), very fine sands.

Unit 3 is massively bedded, and lacks any distinctive sedimentary structures (Figure 3.32b), suggestive of quickly deposited sediments. Molluscan fauna are absent within the light gray (2.5Y 7/2), very fine sands. Unit 4 is again composed of very fine, light gray (2.5Y 7/2) sands. Bulbous, bioturbation nodules are present within this 15 cm thick unit. Unit 5, directly above, is a persistently undercut layer, and suggests that unit 4 is relatively more resistant and may represent a once subaerially exposed hard ground (Figure 3.32c). Unit 5 is composed of pale yellow (2.5Y 8/2), very fine sand which contains a high proportion of silt, suggestive of a very low-energy depositional environment. Few shells were found throughout this unit.

Unit 6 is 35 cm thick, and similar in appearance to the unit below, but contains several fine, laminar beds within the fine, white (2.5Y 8/1) sand, perhaps indicative of several periods of deposition, such as a wash-over facies. Unlike unit 5, unit 6 is not undercut, which may be due to a lower proportion of silt within the deposit, making it less resistant to erosion. On the boundary between units 6 and 7 a distinct layer of disarticulated, and sometimes fragmented, *Modiolus areolatus* are present (Figure 3.32d). This mussel species is commonly found buried in medium, coarse-grained sand, in areas of good water movement, between 2 and 20 m deep (Ludbrook, 1984). Its presence within fine lagoonal muds suggests that it may have been deposited over the shoreline barrier as part of an over-wash event. The light weight of their shells means that they could have been transported a significant distance by waters of lower energy than other shells found in the littoral zone. Unit 7 is also composed of fine, white (2.5Y 8/1) sands, but hard laminar layers within the unit are indicative of episodic subaerial exposure, suggesting a slower rate of sediment deposition.

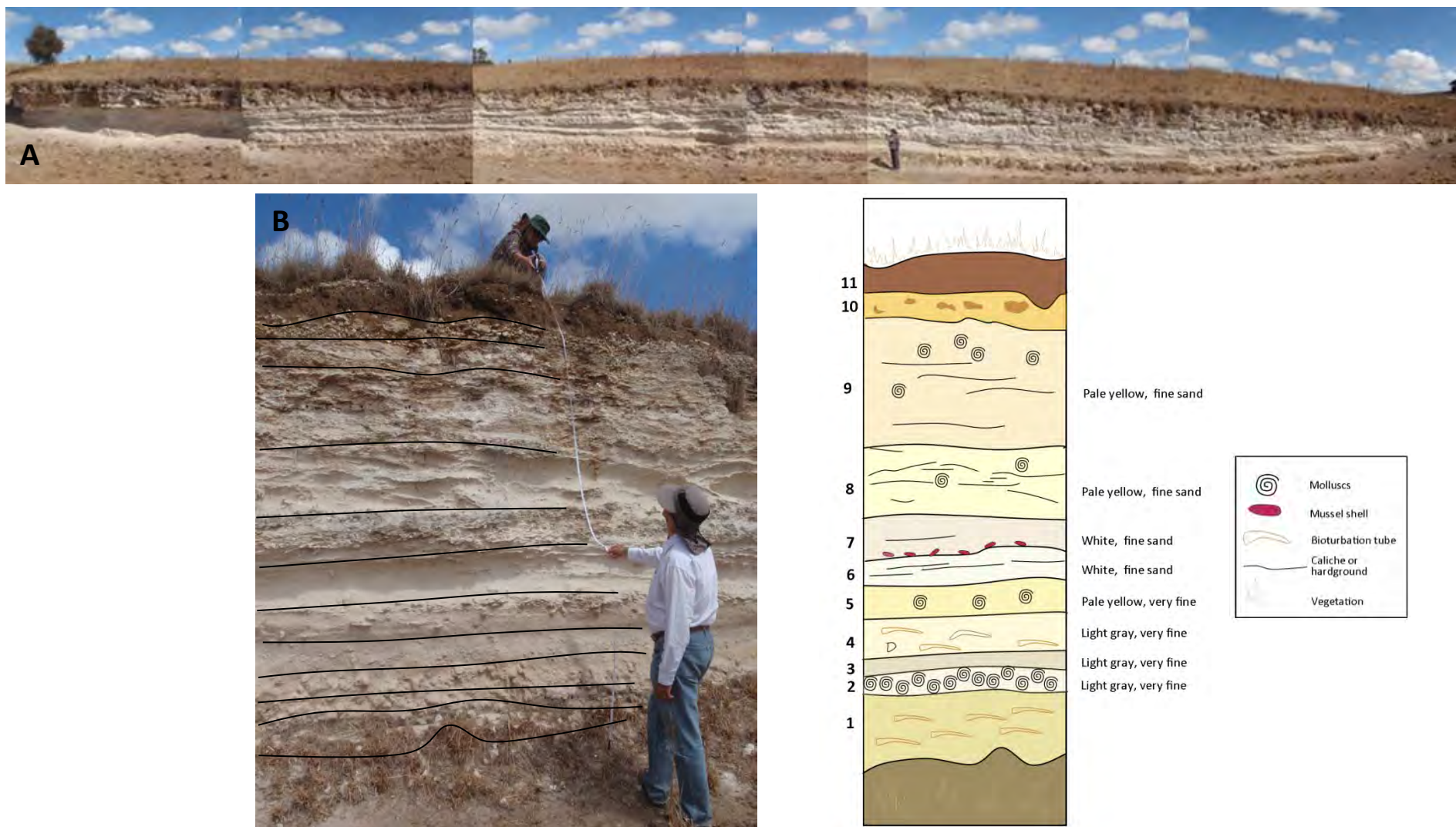
Unit 8 is 35 cm thick and consists of massively bedded, pale yellow, fine (2.5Y 8/2) sand. Thin, laminar caliche structures are evident within this unit as are a small number of fine-grained rhizoliths (Figure 3.32e), suggesting periods of subaerial exposure and pedogenic processes that have allowed soils supporting plant life to develop. The more resistant caliche layers have led to undercutting of sands directly beneath these structures. Disarticulated shells of juvenile *Anapella cycladea* are present but limited in abundance and indicative of estuarine and tidal inlet environments.

Unit 9 is significantly larger than lower layers at 85 cm thick, and has been significantly affected by pedogenic processes (Figure 3.32f). Distinct, laminar, calcrete layers are evident throughout the unit, indicative of several episodes of subaerial exposure followed by further sediment deposition. Shells of *Anapella cycladea* and *Katelsia rhytiphora* are abundant throughout the unit but have likely been transported upwards through reworking processes. Unit 10 comprises a 15 cm thick layer of rubbly calcrete, suggestive of lengthy subaerial exposure. The rubbly nature of the calcrete may have developed through weathering processes or pedogenic effects such as plant root growth causing physical break-up of a perhaps once laminar layer. A dark-reddish gray (2.5 YR 4/1) well-developed soil caps the exposure and supports abundant plant life.

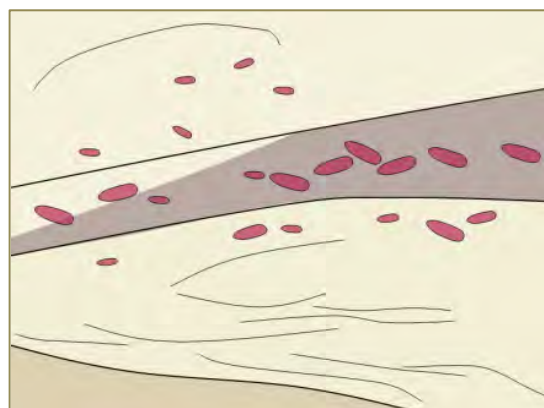
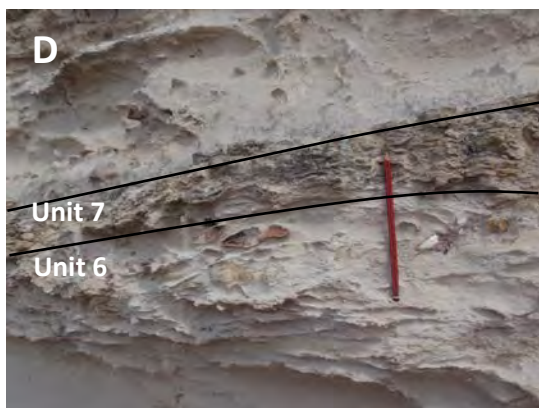
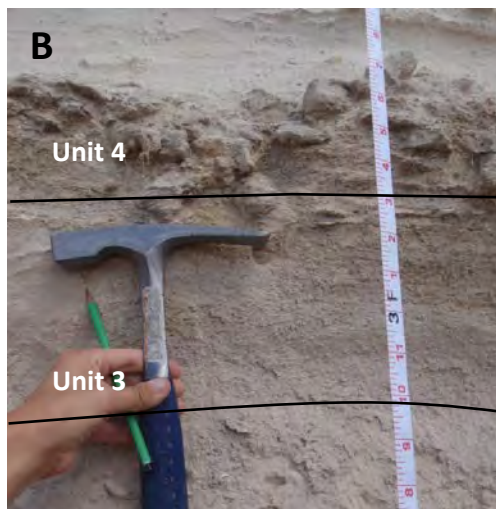


**Figure 3.30:** Transects across Caveton Range derived from SRTM data. **A:** Transect along the length of Caveton Range, **B:** Transects across the width of Caveton Range, **C:** Location of transects (note, transects are next to labelled numbers and scale bar = 5 km).





**Figure 3.31:** Exposure of lagoonal facies within Caveton Range, South Australia. **A:** Length of exposure, note person for scale. **B:** Separate units within the exposure, **C:** Stratigraphical sketch of different units and Munsell soil colour and sediment size.





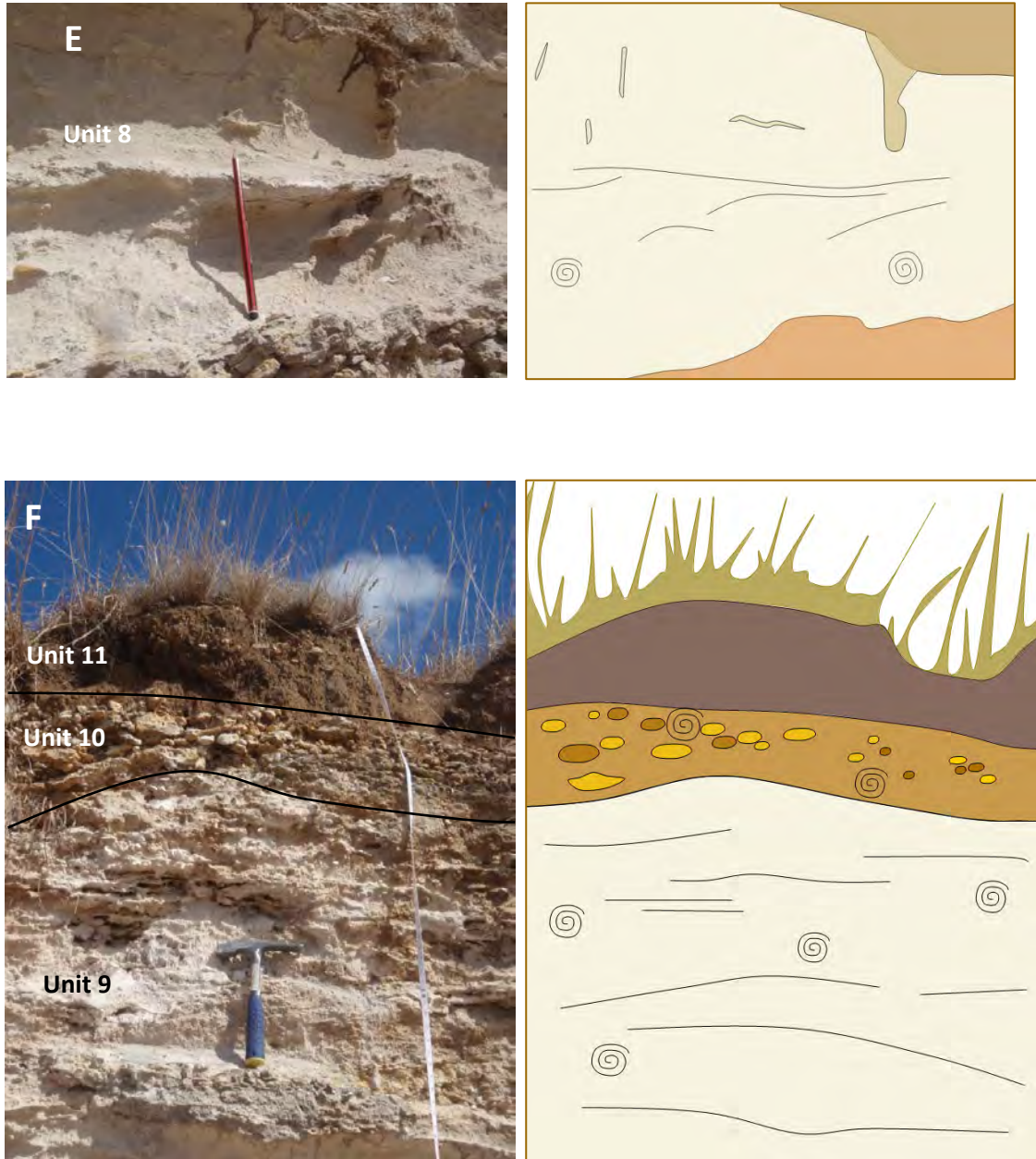


**Figure 3.32:** Interpretative sketches of different units within lagoonal facies of the Caveton Range (geology hammer is 28 cm long and pencil is 13 cm long). **A:** Laterally extensive shell bed within unit 2; **B:** Massively bedded unit 3 and nodular unit 4; **C:** Fine caliche and sporadic shells within unit 5; **D:** More resistant unit 6 with abundant caliche and *Modiolus aerolatus* between units 6 and 7; **E:** Caliche and bioturbation tubes within unit 8; **F:** Pedogenically altered units 9, 10 and 11.

**Table 3.8:** Sedimentological features, fauna and microfauna present within different units of lagoonal facies within Caveton Range, South Australia

Unit	Grain size		Clay (%)	Volume weighted mean (µm)	Sediment size <sup>#</sup>	Colour*	Foraminifera present <sup>(n)</sup>		Molluscan species present	Molluscs present	
	Sand (%)	Silt (%)					<i>Ammonia beccarii</i> (%)	<i>Elphidium crispum</i> (%)		Abundance, size and preservation of molluscs	Common environmental habitat of molluscan species
2	46.0	35.5	18.5	145.4	Very fine sand	2.5Y 7/2 Light gray	84.5	15.5	<i>Katelysia rhytiphora</i>	Abundant, mature in size, commonly articulated	Marine cockle, common to sandy shores of lower littoral zone <sup>(1)</sup> , and estuarine environments with good tidal exchange
									<i>Anapella cycladea</i>	Abundant, mature in size, sometimes articulated	Common in estuarine environments with good tidal exchange <sup>(1)</sup>
									<i>Tellina (Macomona) deltoidalis</i>	Very abundant, mature in size, commonly articulated	Commonly found in muddy sands within the mid-lower littoral zones of estuaries <sup>(1)</sup>
									<i>Fulvia tenuicostata</i>	Not common (only 2 found), mature size, not articulated	Common within sand mud and found between 2 and 30 m water depth <sup>(1)</sup>
									<i>Niothus pyrrhus</i>	Common, well preserved, mature in size	Found on sandy bottoms within the littoral zone <sup>(1)</sup>
3	37.1	37.9	25.0	71.5	Very fine sand	2.5Y 7/2 Light gray	74.5	25.5	None present		
4	45.9	34.9	19.2	124.8	Very fine sand	2.5Y 7/2 Light gray			None present		
5	60.8	26.8	12.4	95.8	Very fine sand	2.5Y 8/2 Pale yellow	35.5	64.5	<i>Tellina (Macomona) deltoidalis</i>	Much less abundant than unit 2, mainly disarticulated but several articulated pairs found	Commonly found in muddy sands within the mid-lower littoral zones of estuaries <sup>(1)</sup>
6	61.6	27.0	11.4	252.8	Fine sand	2.5Y 8/1 White			<i>Modiolus areolatus</i>	A few disarticulated shells and fragments of mature individuals found	Commonly found buried in sands where water level is 2-20 m deep
7	60.0	26.7	12.3	163.9	Fine sand	2.5Y 8/1 White	25.5	74.5	<i>Modiolus areolatus</i>	Abundant, mature individuals found at the base of the unit, commonly disarticulated, though several articulated pairs found	Commonly found buried in sands where water level is 2-20 m deep
8	87.9	7.8	4.3	168.6	Fine sand	2.5Y 8/2 Pale yellow	46	54	<i>Anapella cycladea</i>	Common, juvenile to mature in size, only disarticulated	Common in estuarine environments with good tidal exchange <sup>(1)</sup>
									<i>Katelysia rhytiphora</i>	Less abundant, mainly juvenile in size, disarticulated	Marine cockle, common to sandy shores of lower littoral zone <sup>(1)</sup> , and estuarine environments with good tidal exchange
									<i>Tellina (Macomona) deltoidalis</i>	Less abundant, mature in size, only disarticulated shells found	Commonly found in muddy sands within the mid-lower littoral zones of estuaries <sup>(1)</sup>
9	77.9	14.5	7.6	248.4	Fine sand	2.5Y 8/2 Pale yellow	84	16	<i>Anapella cycladea</i>	Abundant, juvenile in size, only disarticulated pairs found	Common in estuarine environments with good tidal exchange <sup>(1)</sup>

<sup>#</sup>Results derived using Mastersizer equipment and sizes classed using the Wentworth scale \*Based on Munsell soil colour, <sup>(1)</sup>Ludbrook (1984). Note, units 10 and 11 are modern soil horizons.

Changes in the molluscan assemblage towards the top of the exposure indicate a change in depositional environment towards more brackish conditions as shown in Table 3.8. These findings are similar to those of Murray-Wallace *et al.* (1996). This is indicated further by the slight coarsening of sediments and through a change in foraminiferal species. *Ammonia beccarii* are the dominant species in lower units, while *Elphidium crispum* dominates towards the top of the exposure, suggesting a more marine sediment source and a possible connection with the open sea.

The high degree of preservation of a lagoonal facies such as this deposit is not common on the coastal plain, and is not found farther along the Caveton Range, reflecting the poor preservation potential of lagoonal facies and other units deposited within a low energy environment. The relict lagoon at Rabbitors Road # 2 has potentially been protected from erosion by the thick calcrete unit that has formed at the top of the deposit.

#### **Bucks Hill**

Approximately 2 km northwest from the exposure of lagoonal facies at Rabbitors Road, a small quarry at Bucks Hill (S37°53'21.6", E140°44'37.7") reveals steeply dipping cross-beds within Caveton Range. The 1.5 m tall cutting exposes very pale brown (10 YR 8/3), sub-rounded, medium-grained sand. Beds are dipping near to the angle of repose for sand at 32° in a northward direction, suggesting that this is an aeolian deposit. No fossil shells are found within the exposure, and foraminifera are difficult to identify, appearing severely rounded and abraded, resulting in a lack of distinguishable markings. A dark-coloured weathering crust has capped the face of the exposure making identification of other sedimentary structures difficult. A fine soil layer has developed overlying the cutting, but there is no evidence of calcrete development.



**Figure 3.33:** Exposure of aeolian facies of Caveton Range at Bucks Hill, South Australia. Note geology hammer (28 cm in length).

### 3.8.7 Gambier Range

From SRTM imagery (Figure 3.12) Gambier Range appears as a prominent structure to the seaward side of Mount Gambier, 20 km landward of the present shoreline, and it trends north-westerly. At its highest point Gambier Range reaches 80 m APSL (Figure 3.34a), and 30 m above the surrounding landscape and is one of the most prominent barriers on the coastal plain. At its widest extent Gambier Range stretches 1.5 km wide and is a one-armed structure (Figure 3.34b). Towards the southeast extent of the dune range, it trends in a more southerly direction and merges with the more seaward Caveton and Burleigh Ranges near the Victorian border. Gambier Range is difficult to identify in the Mount Burr volcanic province but northwest of this region it joins East Avenue Range. East Avenue Range is less laterally extensive than the Woakwine, Reedy Creek and West Avenue Ranges seaward of it, and can be found as interconnected bodies of raised elevation, trending in a northwest direction.

#### Gooch Road, Myora Forest

Despite its prominence in the landscape, finding a suitable sampling location within Gambier Range proved difficult. A small cutting into calcarenite was identified south of Gooch Road within Myora Forest (S37°54'11.3", E140°51'25.9"). The 4 m high, 15 m wide, cutting exposed gently (4-6°), north-easterly dipping beds. Bedding throughout the exposure remains laminar and fine. No other cross-bedding is observed. Layers are well-cemented, with unconsolidated, brownish yellow (10YR 6/8) fine to medium sands found between cemented layers (Figure 3.35b). No fossil shell is found within the deposit. Foraminifera are abundant within the sediment, with *Elphidium crispum* comprising 66% of the 200 foraminifera tests counted, and *Discorbis dimidiatus* accounting for 33%, indicative of a marine source. A fine soil layer covers the top of the exposure, but no distinctive calcrete layer or other subaerial exposure indicators such as solution pipes or rhizoliths are observed.

#### Caroline Main Road

A 3 m deep cutting along Caroline Main Road, approximately 2 km north of the quarry on Gooch Road, exposes a facies of very fine sand. This sand unit is approximately 75 cm thick and lies directly beneath a 10 cm thick laminar calcrete, which in turn underlies a 30 cm deep soil profile. The sand is very well cemented and fine-grained. Laminar beds are observed within this layer. Stratigraphically beneath this lies a 50 cm thick unit of light gray (2.5 Y, 7/2), very fine sand. This unit has a muddier consistency to the layer above and chipping away at the face of the exposure reveals that this layer was packed with very small (5 mm), very friable gastropods that could not be identified (Figure 3.36c). A 3 cm thick dark brown unit laterally bisects this layer for the length of the exposure (Figure 3.36b), yet sediment above and below

this appear similar in colour, size and fauna present. The layer containing gastropods is undercut relative to the fine, laminar sands deposited above. Beneath the gastropod layer sediment appears similar to the laminar bedded sand above, but has been masked by slumped debris in places. Nodular, bulbous features are evident in these sandy layers above and below the gastropod layer and possibly indicate the once presence of burrowing organisms. The lower portion of the exposure is covered by sediment that has slumped, possibly during excavation of the road cutting.

Closer inspection of the sediment within this exposure indicates the presence of diatoms. The friable nature of the gastropods indicates they may be terrestrial. Along with the lack of foraminifera and other marine shells within the exposure, it may be suggested that this deposit formed as part of a fresh water interdune corridor, and sediments are not specifically related to interglacial sea-level highstands.

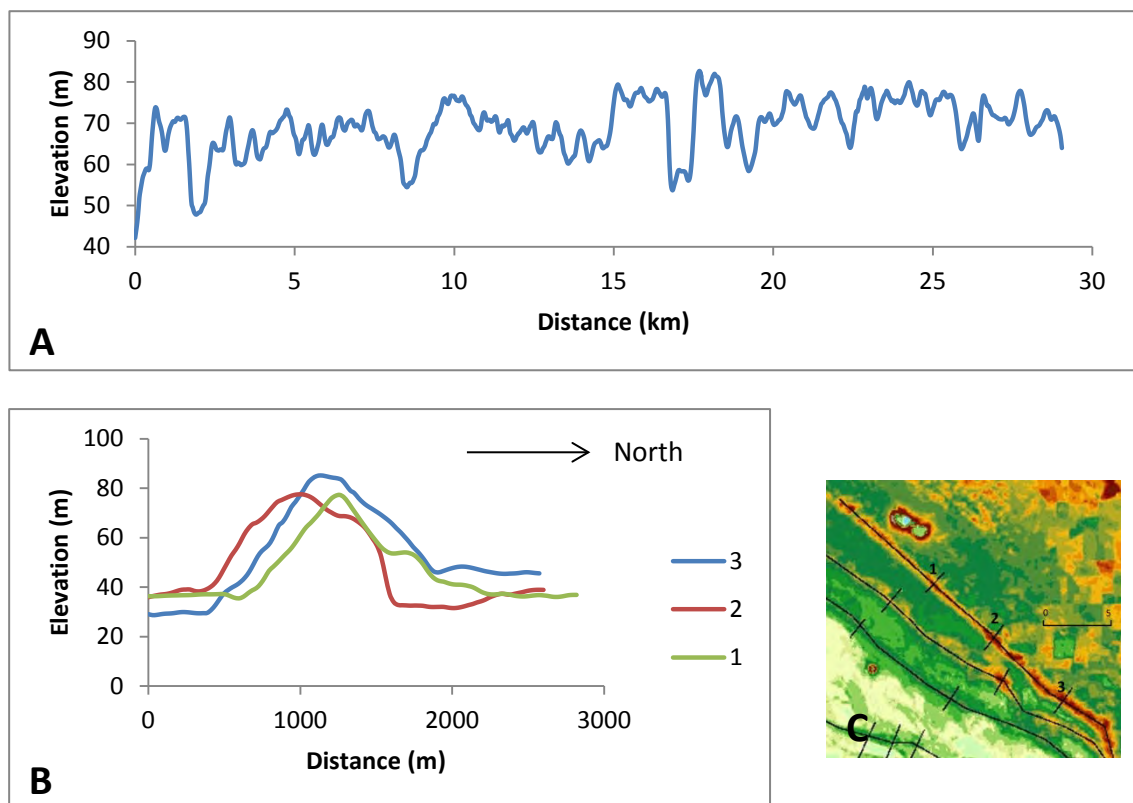


**Figure 3.34:** Transects across the Gambier Range derived from SRTM data. **A:** Lateral transect across the Gambier Range. **B:** Transects across the width of the Gambier Range. **C:** Location of transects taken (scale bar is 5 km).





**Figure 3.35:** Photographs of an exposure within Bridgewater Formation, Gambier Range, Myora Forest. **A:** Entire exposure, highlighting a lack of a distinct calcrete horizon. **B:** Well-cemented beds with unconsolidated sand between them, perhaps indicative of episodic wetting and drying or variances in permeability between the sand layers **C:** Low angle laminar cross-bedding within exposure. Note, geology hammer is 28 cm in length.



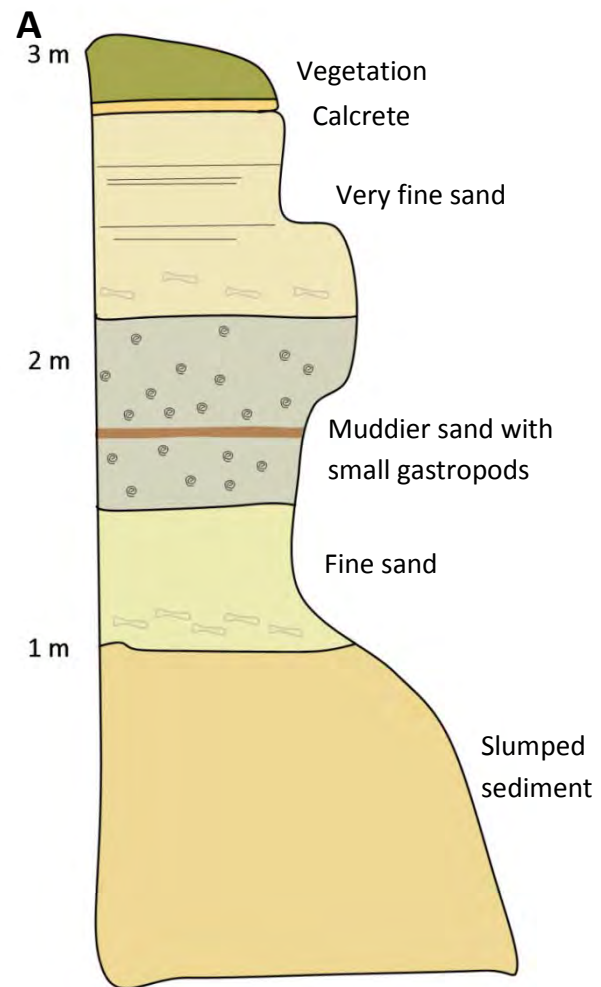


**Figure 3.36:** Very fine sand exposed in the interdune corridor landward of Gambier Range along Caroline Main Road, South Australia. **A:** Interpretative sketch of exposed facies. **B:** Laterally persistent dark brown layer within muddy sands, **C:** Muddy sands containing small gastropods with possible bioturbation burrows above, **D:** Photograph of entire exposure.

### 3.8.8 Compton Range

The extent of the Compton Range is perhaps the most difficult to determine of the barrier shorelines on the Mount Gambier coastal plain. Sprigg (1952) identified the range as a wide structure directly north of Mount Gambier township and tapering in width towards the northeast and southwest. From SRTM imagery (Figure 3.12), areas of raised elevation directly north of the town are present but sporadic, and tracing a lateral transect along the crest of the dune structure reveals rapid drops in elevation between these bodies of sediment (Figure 3.37a). The highest point of the barrier structure is approximately 68 m APSL, and on average the range is 20 m above the surrounding landscape. Compton Range correlates with the Baker Range north of the Mount Burr volcanic province, but this structure is also difficult to trace laterally, and is composed of isolated sediment bodies. Multiple transects across the width of the barrier reveal it is a two-armed structure, similar to MacDonnell Range, and that extends up to 3.5 km in cross-section (Figure 3.37b).

#### Grey Street, Mount Gambier

A small road cutting along the northward trending Grey Street, within the town of Mount Gambier, reveals cross-bedding within calcarenite of the Compton Range (S37°49'31.7", E140°43'14.3"). The cutting is approximately 2 m high and has been blanketed by ash from the eruption of Mount Gambier. A weathering crust has developed on the face of the structure in certain localities, making a complete stratigraphical analysis challenging.

Tabular, multi-directional cross-bedding is evident within the calcarenite, though the dip angle and direction were not accessible with a Brunton Compass, so were not measured. At lower sections within the exposure bedding appears to be at a relatively high angle, and is indicative of aeolian deposition (Figure 3.37d,e). Shell fragments are visible throughout the exposure, but no distinct shell bed is present and it is likely that shells were transported to this locality. Shells are disarticulated, commonly fragmented and fragile. Shell surfaces have been subjected to certain weathering processes and it was not possible to identify all of the species within the deposit. A couple of bivalve shells were found, but could not be further identified. Two mussel shells were also found within the deposit and may be of the genus *Modiolus*, which Ludbrook (1984) suggests is commonly found in areas of high water movement.



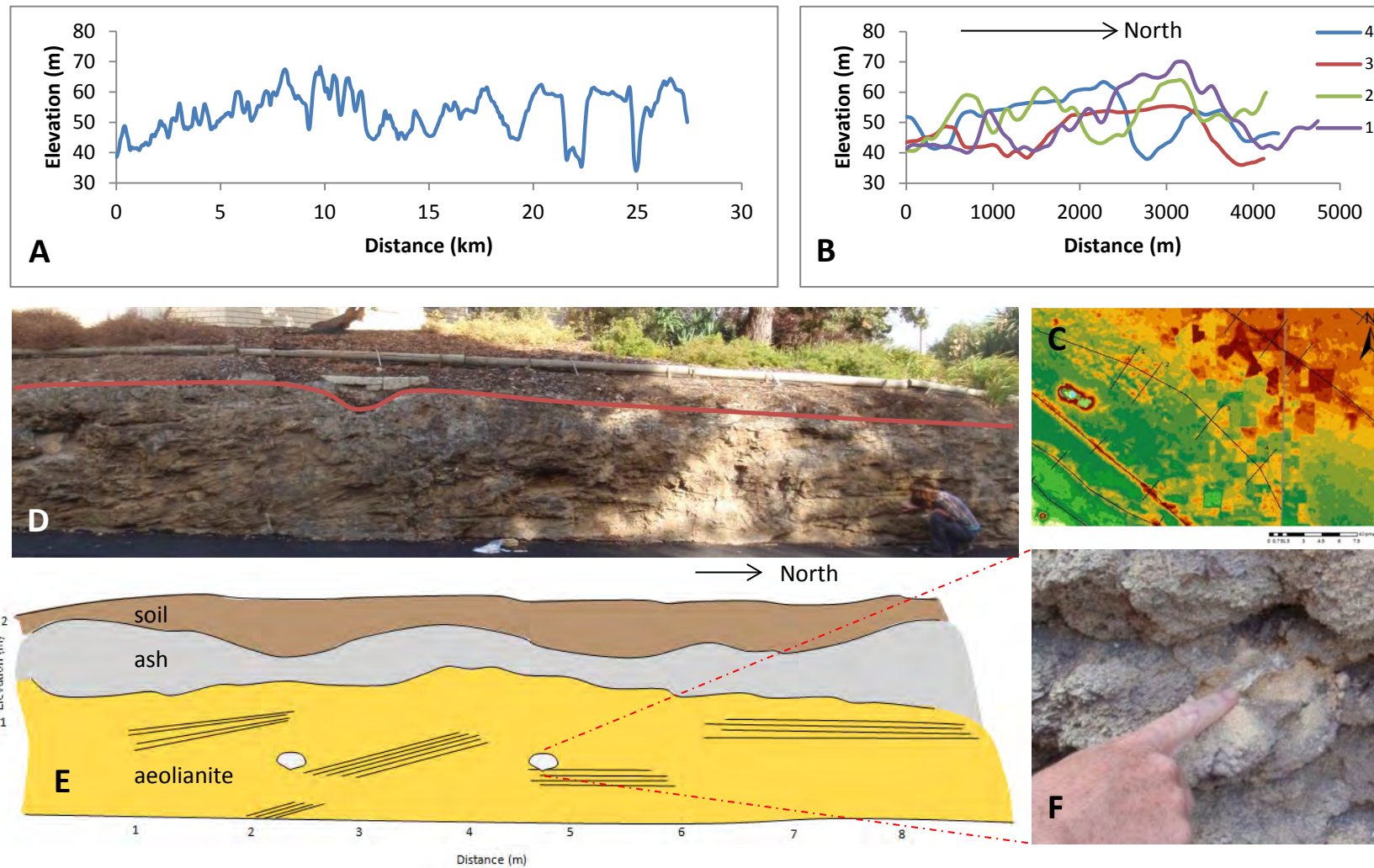


**Figure 3.37:** Images of Compton Range from SRTM transects and exposures at Grey Street, Mount Gambier. **A:** Transect across the length of Compton Range, **B:** Transects across the width of Compton Range, **C:** Location of transects (note scale bar is 5 km), **D:** Exposure of Bridgewater Formation at Grey Street, Mount Gambier: high angle cross-bedding within calcarenite (red line indicates *in situ* karstified surface). **E:** Interpretive sketch of exposure. **F:** Shell fragments found within calcarenite.

### **Baxter's Quarry, Mount Gambier**

Immediately to the north of Mount Gambier a north-facing wall within Baxter's Hire Quarry (S37°49'05.6", E140°47'20.4") reveals distinct cross-bedding within calcarenite of the Bridgewater Formation. From SRTM data and comparing the location to the map of Sprigg (1952) it is evident this cutting is within the Compton Range. The quarry wall is approximately 5 m high and 75 m long. A thick red soil profile has developed above the cutting and has infilled several of the large, abundant solution pipes, as have certain rhizolith structures (Figure 3.38a), indicating a significant period of subaerial exposure. The solution pipes within this cutting are larger than any identified in dune ranges seaward of this point (some solution pipes here are up to 75 cm wide and 350 cm deep; Figure 3.38b). The size of the solution pipes may correlate with the age of the structure and the length of subaerial exposure.

A range of cross-bedding styles is identified throughout the exposure. Most noticeable is a lateral unconformity that can be traced for the entire length of the cutting and is approximately 1 m from the top of the exposure. This unconformity is overlain by a bed approximately 15 cm thick that has been undercut relative to the surrounding calcarenite. The bed is reddish-orange in colour and may have once been a soil profile that has since eroded, possibly causing the visible undercutting. This unit indicates a significant hiatus in sand deposition. Most solution pipes begin at the top of the exposure and extend down through the unconformity, while others appear to start at the unconformity and extend downward. This may be a result of water travelling down through the solution pipe and traversing across the unconformity surface and eroding underlying calcarenite in a different location. Another possibility is that the underlying unit was subaerially exposed for a significantly long time to allow such large solution pipes to develop. The unconformity appears to separate two distinctively different bedding patterns. Overlying the unconformity beds are thicker and of high dip angle, while below the bedding is commonly finer and more laminar. Where accessible the observed sedimentary structures were mapped and a stratigraphic sketch was constructed (Figure 3.39a).

Approximately 20 m from the eastern side of the cutting, a steep, eastward-dipping bed is visible above the unconformity surface (Figure 3.39e), and possibly represents a dune foreset. The presence high angle bedding observed within the upper portion of the exposure, within very pale brown (10YR 7/4) medium sand, and a dune foreset indicate aeolian deposition. The unconformity may therefore represent a truncation surface and may be overlain by a bottom set to the dune structure.

Fine, laminar bedding present beneath the truncation surface is indicative of a subaqueous depositional environment. Multiple sets of low-angle trough cross-bedded units are visible within the calcarenite underlying the unconformity surface, and can be isolated from the primarily laminar bedding found throughout this lower section. Herringbone bedding, where foresets of successive sets dip in opposing directions, is also evident at several localities approximately 1.5 m from the bottom of the cutting. Leckie and Walker (1982) suggested that herringbone bedding may be indicative of reversing currents within a tidal environment. The opposing beds within the identified herringbone bedding are separated, within this exposure, by fine laminar beds (Figure 3.39f). This perhaps suggests a change in wave direction or energy regime within the tidal zone.

Shallow dipping beds to the western side of the cutting appear to form swale-like deposits. The ridge crests of these swales are approximately 3.05 m apart and beds are 20 cm thick (Figure 3.39g). Flat, laminar beds are visible above and below this structure. This undulating unit may represent swaley cross-stratification, which Leckie and Walker (1982) suggested may form as a result of sediment remobilisation during storm conditions on the continental shelf above the storm and fair weather wave base (Table 3.5). This further supports the hypothesis that calcarenite below the lateral unconformity within this exposure was deposited in subaqueous conditions, while overlying calcarenite was deposited by aeolian processes.

This exposure represents an upward shoaling sequence, with deposition occurring near to the fair-weather wave base on the continental shelf, as well as deposition in the intertidal zone evidenced by herringbone bedding, and aeolian deposition visible at the top of the cutting. Thus, this exposure may have formed during a regressive sea level phase. Sea level may have once been several metres above the swaley cross-beds and, following a fall in relative sea level, intertidal sediments were deposited above the deeper water sediment. There may have been a significant period whereby the calcarenite was exposed as sea level dropped farther, allowing for the formation of potential soil layer, which is now represented by an undercut unit, before aeolian sands capped the deposit. As sea level fell farther at the end of the interglacial highstand, aeolian deposition also ceased at this locality and subaerial exposure features developed.

No whole shells were found within the deposit though foraminifera are identified within the aeolian sands and found to be moderately well-preserved, though numerous individuals are well-cemented. Of the 200 tests counted, *Elphidium crispum*, *Discorbis*

*dimidiatus* and *Ammonia beccarii* were identified within the sample and found to comprise 48.5%, 14% and 37.5% respectively. *Elphidium* and *Discorbis* are known to be common on the modern shallow continental shelf near Robe (Li *et al.*, 1996), while *Ammonia* is ubiquitous with the modern Coorong Lagoon (Cann *et al.*, 1999; Lower *et al.*, 2013). This suggests that these aeolian sands were derived from a range of sources; potentially both from the continental shelf and lagoonal regions.

In addition to samples collected for AAR analysis, a sediment sample was collected for OSL analysis from this exposure. The OSL sample was collected from the aeolian facies at the eastern extent of the exposure and above the major truncation surface identified across the length of the deposit (Figure 3.39a). The sample was collected from within steeply dipping cross-bedded sands and approximately 50 cm below a minor truncation surface which potentially reflects a bottem set dune.

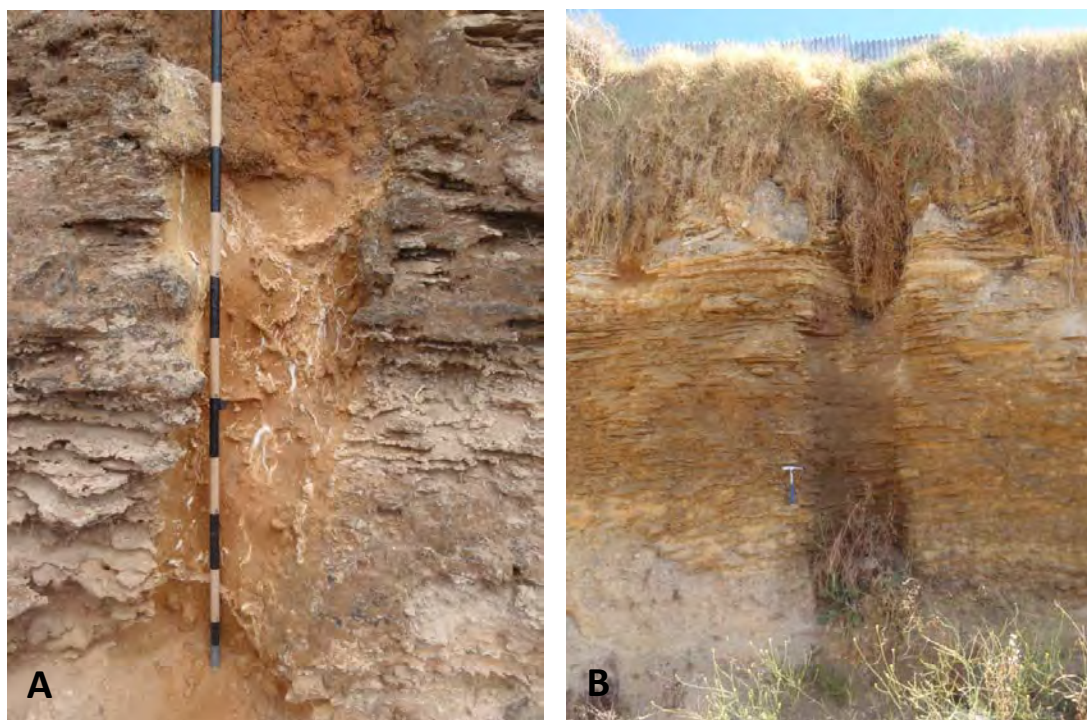


**Figure 3.38:** Subaerial exposure structures within Baxter's Quarry, Compton Range, South Australia. **A:** Solution pipe infilled with soil and rhizoliths (staff marks every 10 cm). **B:** Large solution pipe extending from the top of the exposure downwards (geology hammer is 28 cm in length).



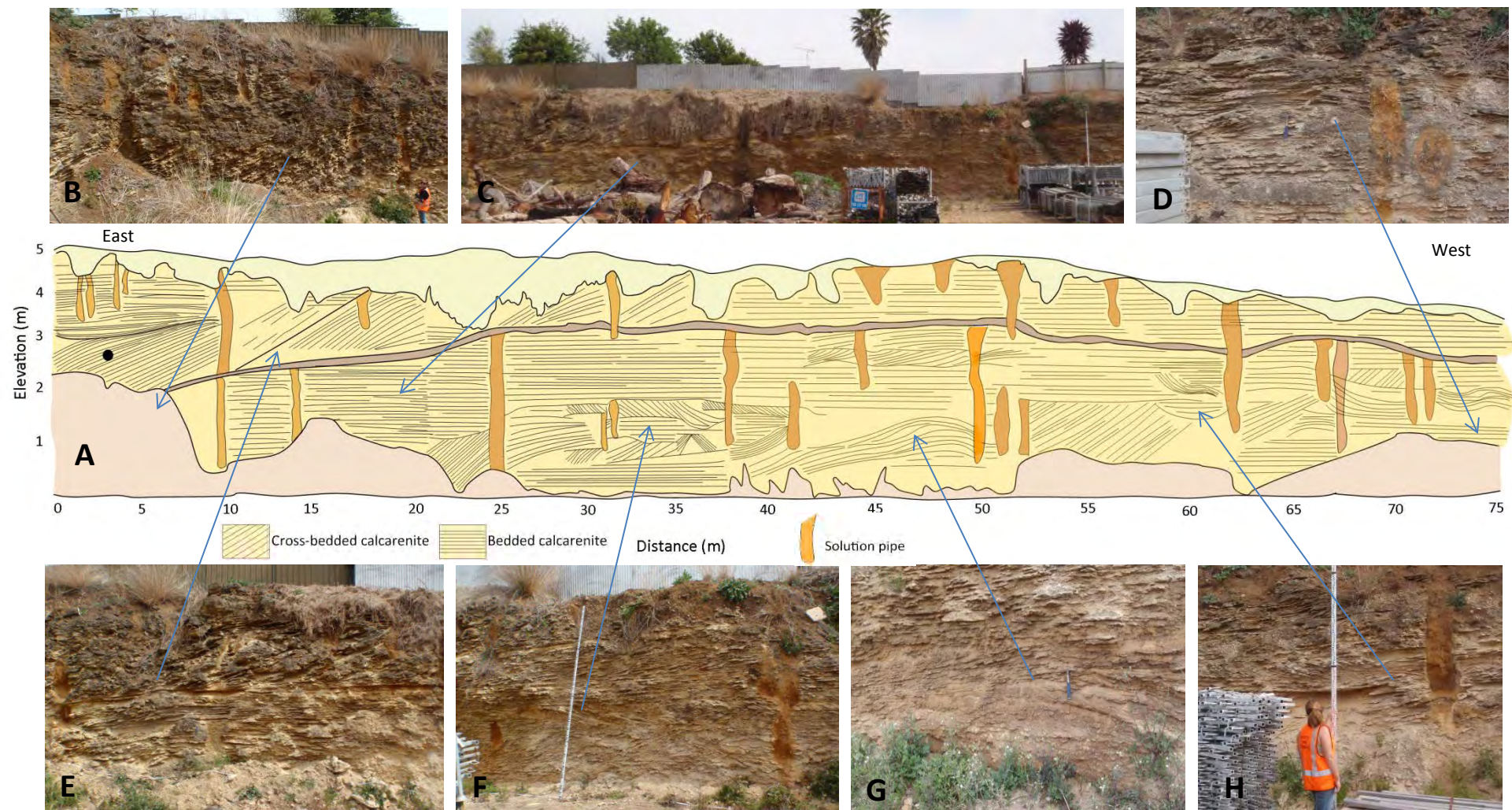


**Figure 3.39:** Exposed Bridgewater Formation within the Compton Range, Baxter's Quarry. **A:** Sketch of stratigraphical features within exposure (brown layer highlights the undercut unit above an unconformity surface and black circle indicates location of OSL sample: BaQu). **B:** High angle bedding on eastern side of exposure, **C:** Laterally extensive unconformity, **D:** Swale-like bedding, **E:** Dune foreset above unconformity, **F:** Multi-directional cross-bedding, potentially herringbone bedding, **G:** Swale-like crest within calcarenite, **H:** Fine cross-bedding and solution pipe.

### Heritage Industries

To the east of Mount Gambier, a south-facing cutting (S37°49'37.2", E140°47'55.2") within an old saw mill, now owned by 'Heritage Industries' reveals laminar and cross-bedded calcarenite of the Bridgewater Formation. When this location is plotted on Sprigg's (1952) map it suggests it is found in a region where it may form either part of the Glenburnie or Compton Ranges. From the map produced by Sprigg (1952) the Glenburnie Range does not appear to have a distinct boundary, and it is difficult to decipher this as a separate dune range from SRTM data. This study therefore, deems the Glenburnie Range to be an extension of the Compton Range.

A weathering crust has developed on the face of the exposure and sediment has slumped down from the top of the cutting, masking some of the sedimentary structures and making a complete measurement of stratigraphical features difficult. The exposure is approximately 16 m wide and 5 m tall (Figure 3.40). The top of the cutting is capped by a thick soil, supporting dense vegetation. The cutting does not occur at the top of the dune crest (as the dune crest slopes farther northward from this point) and it is difficult to decipher the true depth of the soil profile from this locality. Multiple solution pipes are evident throughout the exposure and are up to 1 m wide in places (Figure 3.41c). A cave-like structure at the eastern end of the exposure appears to be the lower portion of a set of solution pipes where their sides have been eroded. Some solution pipes are filled with thick, red *terra rossa* soil, while other pipe features are stained red indicating they too were once in-filled. The abundance and size of solution pipes at this locality reflects a sustained episode of subaerial exposure.

Bedding within the exposure is predominantly fine and laminar with some sets of low-angle cross-bedding also evident. Sediment is composed of pale yellow (2.5Y 8/3) medium-grained sand. Foraminifera are present within the sediment, with species *Elphidium crispum*, *Ammonia beccarii* and *Discorbis dimidiatus* all identifiable. At least three lateral bands of fossil shells are recognised within the exposure. Two lower bands of shells are found approximately 40 cm and 85 cm from the ground surface at the eastern end of the exposure and are dominated by the oyster *Ostrea angasi* (Figure 3.41d). A large shell of a fragmented gastropod was also found within this layer but was not identifiable at genus level. The shell bands are approximately 10 cm thick and *Ostrea* are not commonly articulated but generally whole, mature and found facing concave down. *Ostrea* are found throughout the shell band as are rounded pebbles. To the eastern end of the exposure the two shell bands appear to coalesce. Traversing farther west along the cutting individual *Ostrea* are also visible approximately 1 m above the ground surface but the shell bed is less identifiable.

A more laterally extensive shell bed is evident higher in the cutting, approximately 2.5 m from the ground surface (Figure 3.41a, b). This band is primarily composed of molluscan fragments and identification of specific species is challenging. Several whole bivalve shells are recognisable including *Katelysia* and *Placamen*, as well as juvenile and fragile gastropods such as *Batillaria*. *Ostrea* fragments are abundant, but no whole shells were found. Within this upper shell band, coarse, sub-rounded pebbles approximately 2 cm in diameter are also present.

The fine bedding consistently observed throughout the exposure, combined with the presence of large, whole oyster shells, and a laterally persistent layer of shell fragments and pebbles indicate that this was a subaqueous setting. The preservation of the *Ostrea* in the lower shell layers suggest they were transported by low energy waters. The fragmented nature of the upper shell layer is indicative of a higher energy setting and low angle cross-beds directly beneath this layer suggest this may have been a swash zone.



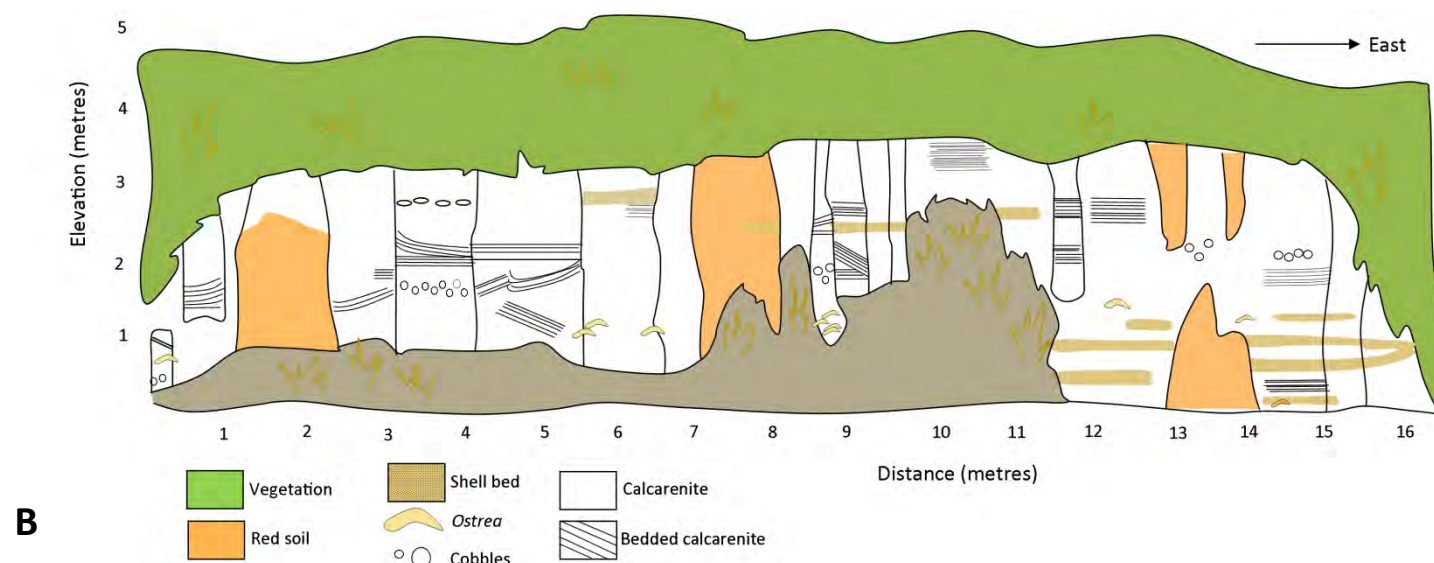


**Figure 3.40:** Exposure within the Compton Range at Heritage Industries, South Australia. **A:** Northern quarry wall at Heritage Industries. **B:** Interpretive sketch of stratigraphical features within exposure (Note, this sketch is not as detailed as that at Baxter's Quarry due to the volume of vegetation and slumped sediment obscuring the stratigraphy within this exposure).



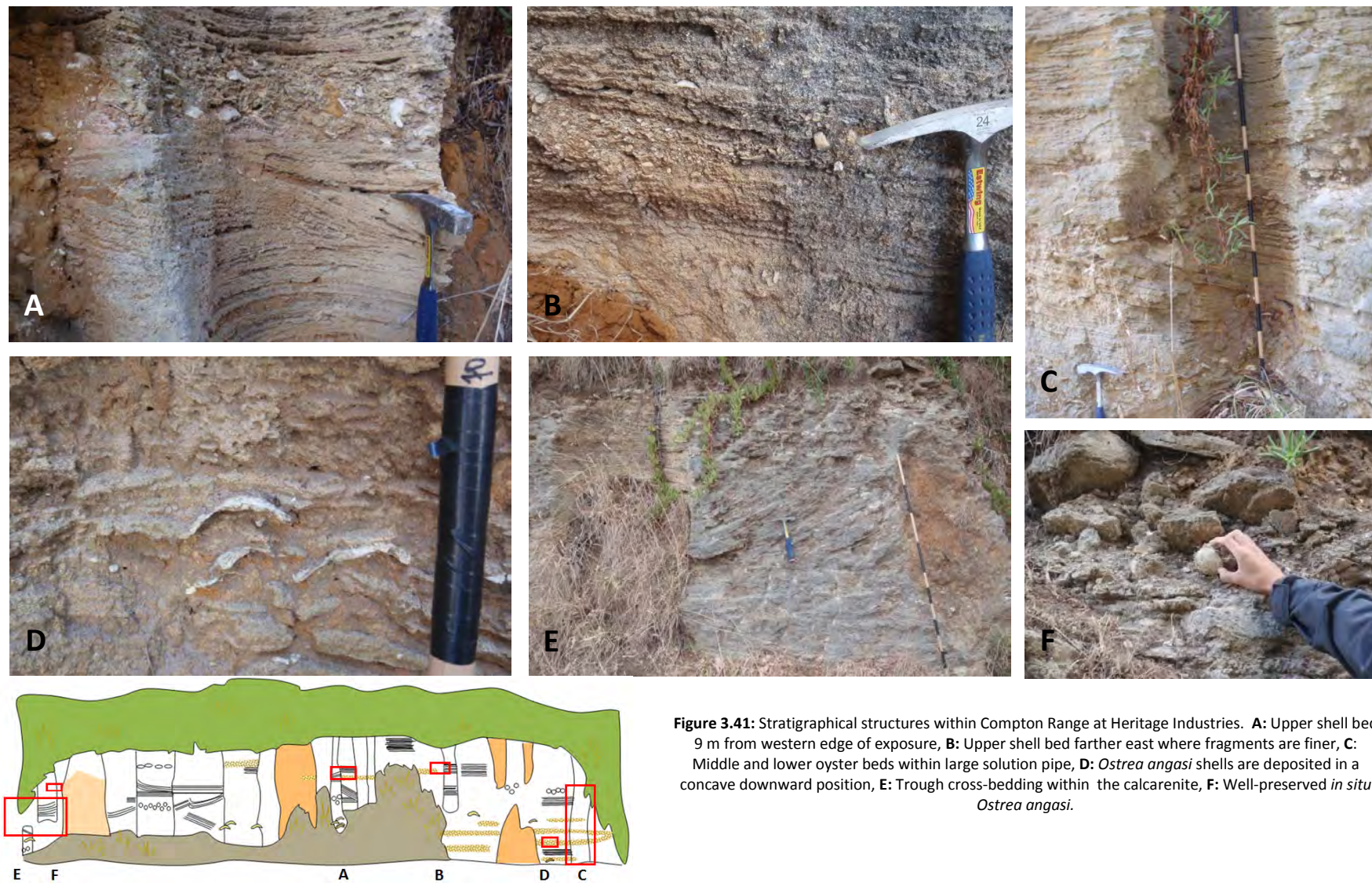


**Figure 3.41:** Stratigraphical structures within Compton Range at Heritage Industries. **A:** Upper shell bed 9 m from western edge of exposure, **B:** Upper shell bed farther east where fragments are finer, **C:** Middle and lower oyster beds within large solution pipe, **D:** *Ostrea angasi* shells are deposited in a concave downward position, **E:** Trough cross-bedding within the calcarenite, **F:** Well-preserved *in situ* *Ostrea angasi*.

### 3.8.9 Mingbool Range

Mingbool Range trends sub-parallel to the modern shoreline and is approximately 32 km from the coastline north of Port MacDonnell, but only 25 km from the coastline in western Victoria. The barrier shoreline extends from directly 10 km north of Blue and Valley Lake in Mount Gambier to the Glenelg River in Western Victoria. As the barrier trends farther eastward it follows a more southerly path, as does the Dismal Range farther inland, due to the influence of the Kanawinka Fault (Figure 3.10). Mingbool Range does not appear as laterally extensive in Western Victoria where the barrier elevation is not as prominent and the average height of the dune crest falls slightly before increasing again towards Mumbannar and west of the Glenelg River. Mingbool Range reaches approximately 80 m APSL north of Mount Gambier and falls to 50 m APSL in western Victoria (Figure 3.42a). Transects across the width of the barrier show a range of patterns; generally the feature is one-armed and can stretch up to 3 km wide, but farther south appears as two distinct arms and only 1.5 km wide (Figure 3.42b). Farther north Mingbool Range corresponds with Woolumbool Range, which is not very extensive laterally and persists as isolated bodies of higher elevation terrain trending in a north-westerly direction.

#### Don's Quarry

A small (approximately 30 m wide and 3 m deep) quarry (S37°54'41.9", E141°11'10.4") within farmland in Mumbannar, near Dartmoor in far-western Victoria reveals fine, laminar bedding within the Bridgewater Formation calcarenite. SRTM imagery reveals this is an exposure within the Mingbool Range. A thick layer of grass covers the top of the quarry walls and floor, leaving 1 m of the calcarenite within the walls exposed (Figure 3.43). Beds within the calcarenite are consistently laminar and are roughly 3 mm thick, within yellow (10YR 7/6), fine sand. A dark red weathering crust has developed on the face of the exposure, while behind this sediment is relatively unconsolidated. Foraminifera are abundant within the sediment in the quarry walls, but are relatively small in size. *Elphidium crispum* accounted for 67% of the 200 tests counted, while *Discorbis dimidiatus* and *Ammonia beccarii* comprised 24% and 9% respectively. A fine soil has developed and overlies the quarry walls, but there is no evidence of other subaerial exposure features such as rhizoliths or solution pipes.

Boulders of well-cemented calcarenite, approximately 1 m in diameter are found on the quarry floor and on top of the quarry walls. Overturning these boulders revealed whole and fragmented oyster shells of the species *Ostrea angasi*. Oyster shells are also evident within the top of the exposure in places, but determining where the shells originated from is difficult as they have been disturbed during excavation of the quarry. Moulds of other bivalves

are identified within other calcarenite boulders but it was not possible to determine the genus of the shell (Figure 3.44g). Some of the boulders were composed of coarser sediment and shell fragments, indicative of a higher-energy environment.

To the east of the quarry, boulders reveal what appear to be cemented, laminar beds of calcarenite. These beds are disjointed and in some places appear to have collapsed downward (Figure 3.44h,i). Oyster fragments are visible beneath these calcarenite beds and are well-cemented within the boulder. For the sediment to have cemented to form distinct beds the material must have been subjected to some subaerial exposure or perhaps formed as beach rock. The collapse of these beds may have occurred during a slumping event resulting from the presence of unconsolidated sediment underlying the beach rock/cemented calcarenite.

The fine size of the sediment and small foraminifera suggest that the calcarenite exposed within the quarry walls was deposited within a low energy environment. The fine, laminar bedding is indicative of a subaqueous environment as are the presence of *Ostrea angasi* which are commonly found on sandy bottomed surfaces in 2-30 m of water depth (Ludbrook, 1984).

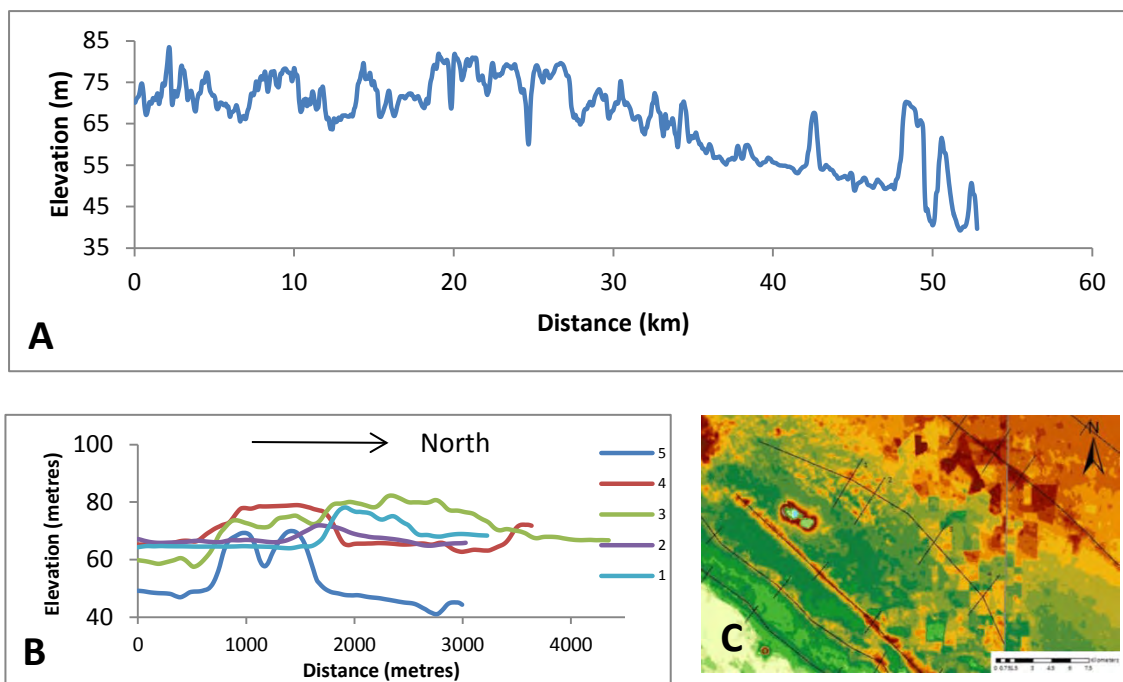


**Figure 3.42:** Transects across the Mingbool Range derived from SRTM data. **A:** Lateral transect across the crest of Mingbool Range. **B:** Transects across the width of the barrier shoreline. **C:** Locations of transects along Mingbool Range.

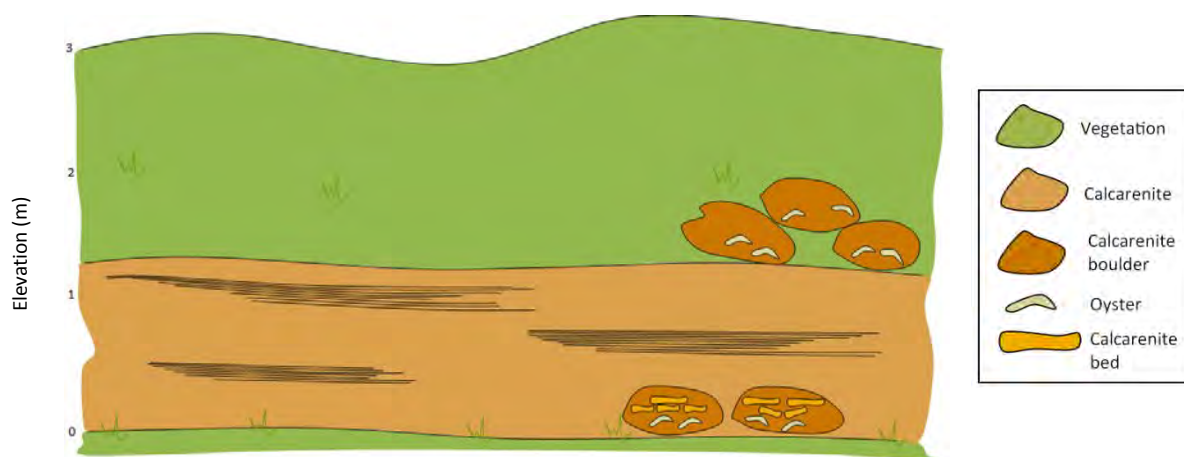


**Figure 3.43:** Interpretive sketch of exposed facies within the Mingbool Range at Don's Quarry, western Victoria.





**Figure 3.44:** Stratigraphical features exposed within Don's Quarry, Mingbool Range, western Victoria. **A:** Exposed quarry wall. **B:** Fine, laminar bedding within calcarenite. **C:** Oyster fragment at top of the quarry wall. **D:** Oyster fragments, **E** and **F:** Boulders of coarser sediment, **G:** Bivalve mould within calcarenite, **H:** Intraclasts of calcarenite beds reflecting dessication in an intertidal zone, **I:** Oyster fragments beneath brecciated calcarenite beds.

### **3.8.10 Dismal Range**

Dismal Range is not as laterally extensive as the barrier shorelines seaward of it, but can be identified as a northwest trending body of raised elevation extending for 10 km approximately 20 km northeast of Mount Gambier, and 8 km landward of Mingbool Range. At the Victorian border the barrier becomes very subdued, but following the direction of the shoreline farther southeast it becomes visible in the landscape once more near the town of Dartmoor, and extends to the eastern side of the Glenelg River. Trending east from the Mount Burr volcanic province the dune ranges curve in a more southerly direction, and the Dismal and Mingbool Ranges nearly coalesce near to the Glenelg River. In Victoria, this dune range is also referred to as Ardno Dune (Boutakoff, 1963), but in this thesis the South Australian names are adopted as that is where the majority of study sites are located. Towards the northwest the Dismal Range becomes the Stewarts Range and is also composed of a range of isolated bodies.

At its highest point, Dismal Range reaches 85 m APSL but only approximately 15 m above the coastal plain in the Mount Gambier region. In western Victoria as the dune range becomes more prominent in the landscape again, it reaches 60 m APSL west of the Glenelg River, and 70 m APSL east of the river (Figure 3.45a). Transects across Dismal Range indicate it is a predominantly one-armed structure, and narrower than other barrier shorelines on the coastal plain, being 1 km wide at its maximum extent (Figure 3.45b).

### **Dartmoor Cemetery**

Approximately 20 m west of Dartmoor Cemetery, far-western Victoria, a large excavation (S37°54'55.6", E141°14'54.0") 100 m in length and 6 m high, reveals laminar bedding within Bridgewater Formation calcarenite (Figure 3.46). While this locality is no farther north than the previously described site at Don's Quarry, and only 5.5 km west, it appears to be within a separate dune range; the Dismal Range. As previously mentioned the Dismal and Mingbool Range nearly coalesce in this region. The cutting at Dartmoor trends parallel to the dune range in a north-westerly direction.

The exposure is capped by a 1 m thick soil, though no calcreted unit is visible. Small solution pipes, approximately 1 m deep, at the top of the exposure indicate subaerial exposure, and have been filled with red soils in places. A dark weathering crust has developed on the face of the exposure and masks the underlying bedding in certain locations.

Bedding within the exposure is almost uniformly laminar and fine, with beds approximately 3-4 mm thick. Towards the western end of the exposure, low angle cross-bedding and trough-cross-bedding are evident within the fine, pale yellow (2.5Y 8/4) sand.

Individual shells are sporadically found approximately 1 m above the ground surface along the length of the exposure. Shells are commonly found whole but not articulated, though only fragments of the umbo region were found in places. Only two molluscan species were recorded; *Ostrea angasi* and *Pecten benedictus*. *Pecten benedictus* may bury itself completely within sand in water depths from 3-30 m deep, while *Ostrea angasi* is commonly found in sandy or muddy-bottomed estuaries and again may live up to 30 m below the water surface (Ludbrook, 1984). As no articulated pairs were identified the molluscs must have been transported from their life position. Foraminifera are abundant within the sediment and are dominated by the species *Elphidium crispum*, which comprised 56.5% of the 200 tests counted, while *Ammonia beccarii* and *Discorbis dimidiatus* accounted for 20 and 23.5% respectively. Tests were commonly found to be well-cemented and some of the shell fragments were recrystallised.

Towards the western end of the exposure, approximately 1 m below a set of low-angle trough-cross beds, a small unit (roughly 30 cm by 15 cm) of shell grit and shell fragments is evident. It was not possible to identify the species of shell fragments but directly below this deposit a single *Pecten* shell was found (Figure 3.47b). The presence of this coarser material indicates a higher energy depositional environment.

Bioturbation structures are present within the exposure and found approximately 1-2 m from the ground surface (these structures may also be higher up in the cutting, but this was inaccessible to examine). The presence of these features indicates that a degree of oxygen must have been present within the sediment to support such life, and that the sediment was soft and wet. As the identified bioturbation structures are low within the exposure they indicate that this is an upward shoaling deposit.

A small calcarenite boulder found at the base of the exposure contains molluscan shell fragments, including oyster fragments. Small holes, approximately 3 mm in diameter, are also evident within the boulder (Figure 3.47d) and may represent air pockets within the sediment formed in a swash zone setting. Garrett and Gould (1984) and Kindler and Hearty (2000) described similar structures as keystone vugs or fenestrate within calcarenite in Bermuda and the Bahamas.

All of these factors; the fine, low-angle bedding; fine-grained sands; the presence of bioturbating organisms; and molluscan species that are commonly found in sandy bottomed environments up to 30 m below the water surface, suggest that this was a subaqueous

environment. The presence of a shellgrit unit and potential keystone vugs are indicative of higher energy environments and may indicate a possible swash zone. This exposure potentially reveals a transgressive sea level, where further subaqueously derived sediment is deposited on top of the previous sea floor as relative sea level rises.

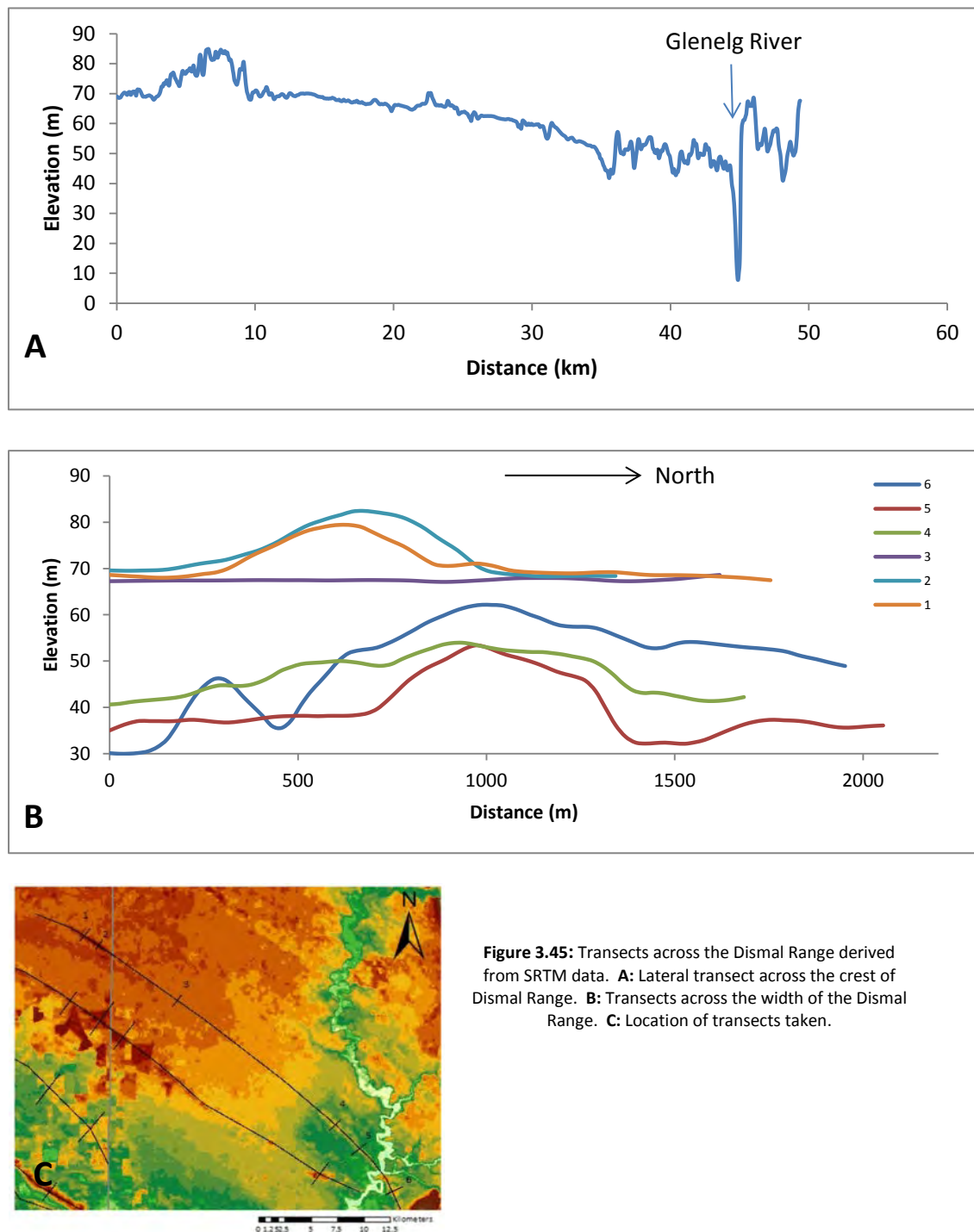


**Figure 3.45:** Transects across the Dismal Range derived from SRTM data. **A:** Lateral transect across the crest of Dismal Range. **B:** Transects across the width of the Dismal Range. **C:** Location of transects taken.



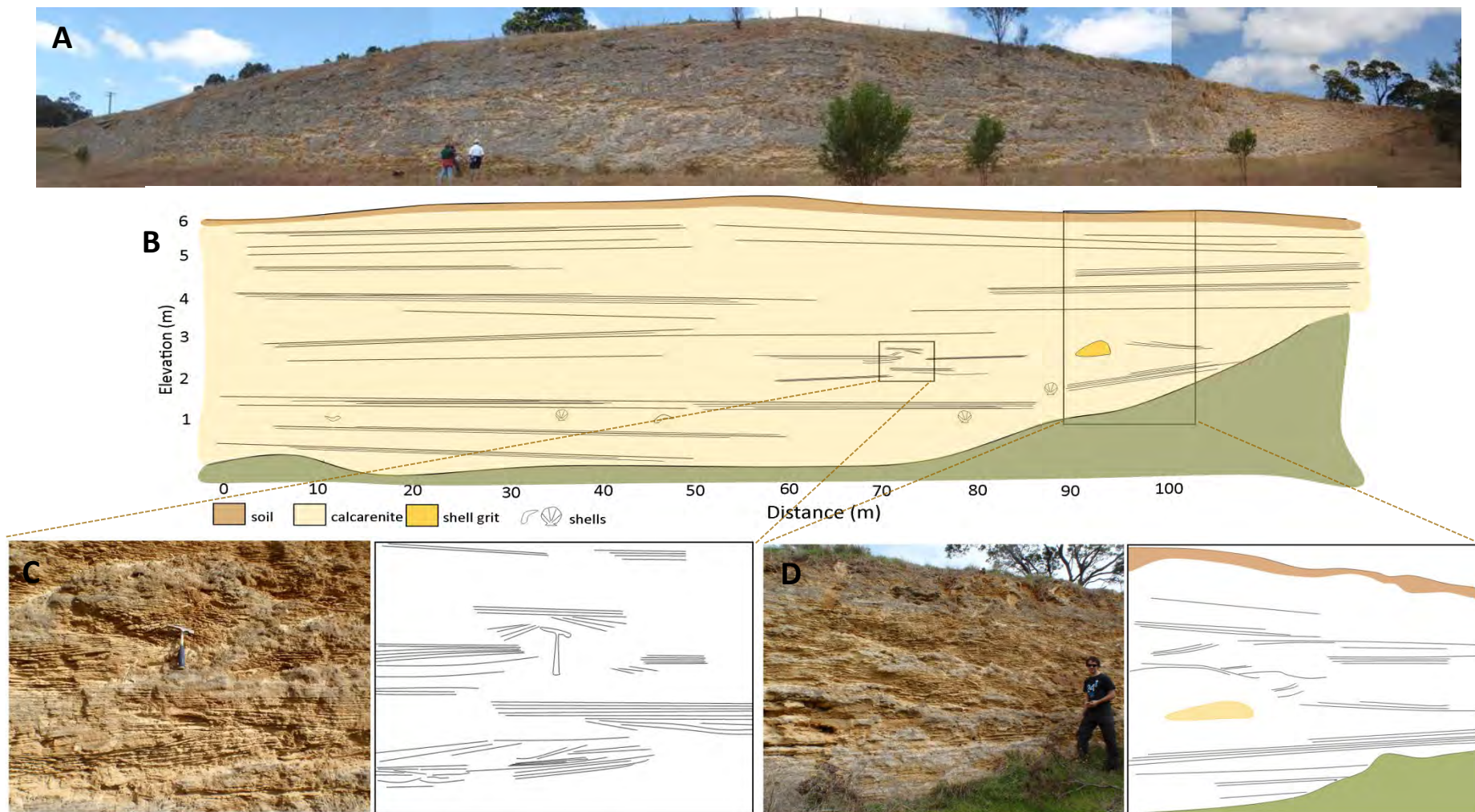


**Figure 3.46:** Exposure of calcarenite within Dismal Range, near Dartmoor Cemetery, western Victoria. **A:** Panorama of exposure. **B:** Interpretive sketch of facies within exposure. **C** and **D:** Close-up images and associated sketches of bedding patterns within exposure. Note the multi-directional bedding in Figure C, and the shell grit unit (yellow oval feature) in Figure D.





**Figure 3.47:** Stratigraphical features within exposure at Dartmoor Cemetery, Dismal Range. **A:** Bioturbation burrows near base of exposure. **B:** Shell grit and *Pecten* shell towards western end of exposure, **C:** *Pecten benedictus* ~1 m from cutting floor, **D:** Air pockets and *Ostrea* fragments within calcarenite boulder, **E:** Possible bioturbation burrow, **F:** Trough cross-bedding towards western end of exposure above shell grit (where pen is), **G:** Laminar bedding and *Pecten* shell, **H:** Bioturbation structures and/or rhizoliths causing slumping in bedding, **I** and **J:** *Ostrea* fragments within calcarenite.

### **Fort O'Hare rail cutting**

Approximately 1 km southeast of Dartmoor, a north-facing railway cutting through Fort O'Hare (S37°55'44.7", E141°17'15.3") reveals laminar bedding within what is likely the Dismal Range. The railway cutting is approximately 8 m high and trends in an east-west direction for approximately 150 m. At the western end of the cutting the ground surface is higher than at the eastern end, and thus, while observed structures within the exposure are predominantly laminar, they become increasingly higher from the ground surface from west to east (Figure 3.48). The exposure is capped by a thin soil layer supporting grass vegetation. No calcreted unit is visible at the top of the exposure and solution pipe features are generally not present within the cutting face. The cutting face, as seen from the ground surface, does not span the entire depth of the exposure. A later visit at the level of the railway, some 5 m below, revealed the cutting is approximately 15 m deep in total, and a laminar calcreted layer is visible at the top of this larger exposure beneath which calcarenite has been undercut (Figure 3.49i). The majority of the exposure is inaccessible and thus stratigraphical interpretations are solely presented from the central region of the exposure.

The central portion of the exposure reveals fine, predominantly laminar beds within pale yellow (2.5Y 7/4) to yellow (10YR 7/6) medium- to fine-grained sand. Foraminifera are present within the sediment but prove difficult to identify as they are well rounded and the surface ornamentation on tests is reduced. *Elphidium crispum* appear to dominate the sediment, accounting for 67% of the 200 tests counted. *Ammonia beccarii* and *Discorbis dimidiatus* were also identified and represented 22% and 11% respectively. However, due to the cemented nature of the deposit and the difficulty in identifying many tests, these results may better represent the durability of *Elphidium* in comparison with *Ammonia* and *Discorbis* rather than the true population of these species within the deposit. At the westerly end of the cutting a 75 cm thick, densely packed shell bed is observed and is dominated by the oyster *Ostrea angasi*. Shells are commonly found articulated, well-preserved, and large (up to 15 cm in size). The level of preservation indicates that the molluscs have not been transported far, if at all, from their original habitat. Stratigraphically below the oyster bed, bedding within the calcarenite is laminar but has been significantly weathered. Bedding directly above the shell bed is also laminar while approximately 15 cm above the shell bed a darker layer is present. This layer is approximately 10 cm thick and has been undercut relative to the calcarenite deposited above and below. This unit is stained brown, possibly by a former soil, and presently supports the growth of a fine moss layer. This layer potentially represents a hiatus in calcareous sand deposition long enough for the development of a weak soil profile, potentially

a protosol. Above the dark bed and unconformity, bedding is fine and laminar again. In places a dark weathering crust has developed on the face of the exposure. This higher unit, above the former protosol, was difficult to accurately assess for stratigraphical structures, due to accessibility issues, but from the ground surface no cross-bedding or shells are visible.

Traversing eastward it is evident the shell bed is an extensive feature and in fact extends for the entire length of the exposure, as does the dark, overlying bed. Bedding remains laminar above and below the shell layer and unconformity. Approximately 50 m from the eastern end of the exposure, a 1 m wide section is in-filled with dark red soil. This could potentially be a very large solution pipe feature that has exposed a weakness within the calcarenite and has been filled with overlying soil, but as no other solution pipe structures are present throughout the rest of the exposure, it is likely a remnant of the cutting excavation. Directly west of this soil-filled structure and approximately 1 m below the shell bed, the bedding within the calcarenite appears different to that previously observed. At this locality beds appear to be coarser and undulating. This unit of wavy bedding is approximately 75 cm thick, while beds below this are fine and laminar (Figure 3.49h). The undulating bedding may possibly have formed during a higher energy event such as a storm, which has caused a disruption to the sea floor above the fair-weather wave base. The disruption to the bedding pattern may have also formed from an increase in pressure above the sediment, such as a water deepening event, or it may simply be the result of preferential erosion within the exposure.

Approximately 20 m east of this, the shell bed is now approximately 6 m from the ground surface, and inaccessible. Large specimens within the shell bed are visible from the ground surface and indicate a change in molluscan species within the unit. Small calcarenite boulders, removed from the shell layer, are present at the base of the structure in this locality and allow for a closer examination of species present. Specimens within the shell layer in the exposure are mature, well-preserved and are commonly articulated, while those in the boulders are sometimes fragmented, likely as a result of the fall. In some instances the molluscs have been coated in a black crust as a result of weathering caused from exposure in the cliff face, but many still preserve their original colouring. Species within the shell layer at this locality include the clams *Pecten benedictus albus*, *Chlamys asperrima asperrima*, *Chlamys (Equichlamys) bifrons* and the oyster *Ostrea angasi*. This collection of species is indicative of a sandy or muddy sea floor, and may be found free-living or attached to the surface with *Pecten benedictus albus* commonly completely burying itself within the substrate (Ludbrook, 1984).

All of these species are common in low- to medium-energy environments and live between 2 and 30 m of water depth.

The stratigraphical structures present, including the consistently fine, laminar bedding within medium to fine sands, a unit of undulating bedding perhaps indicative of a storm event above fair-weather wave base, and the presence of well-preserved, commonly articulated clams and oysters associated with sandy-floored environments in 2-30 m of water depth, suggest this railway cutting exposes a subaqueous deposit. The lateral extent and dense packing of the shell bed suggest this was likely an assemblage of molluscs in growth position. The dark unit above the unconformity may be a remnant of a soil profile that may have formed during a brief period of exposure, possibly as sea level regressed. However, the fine laminar bedding seen above this unit is also indicative of a subaqueous environment, and if there was a relative fall in sea level followed by a subsequent sea-level rise it might be expected that any soil layer would be eroded or washed out. A further possible explanation is that this dark layer represents compaction during a water deepening event. This unit requires further re-examination to determine how it may have formed and under what environmental conditions.



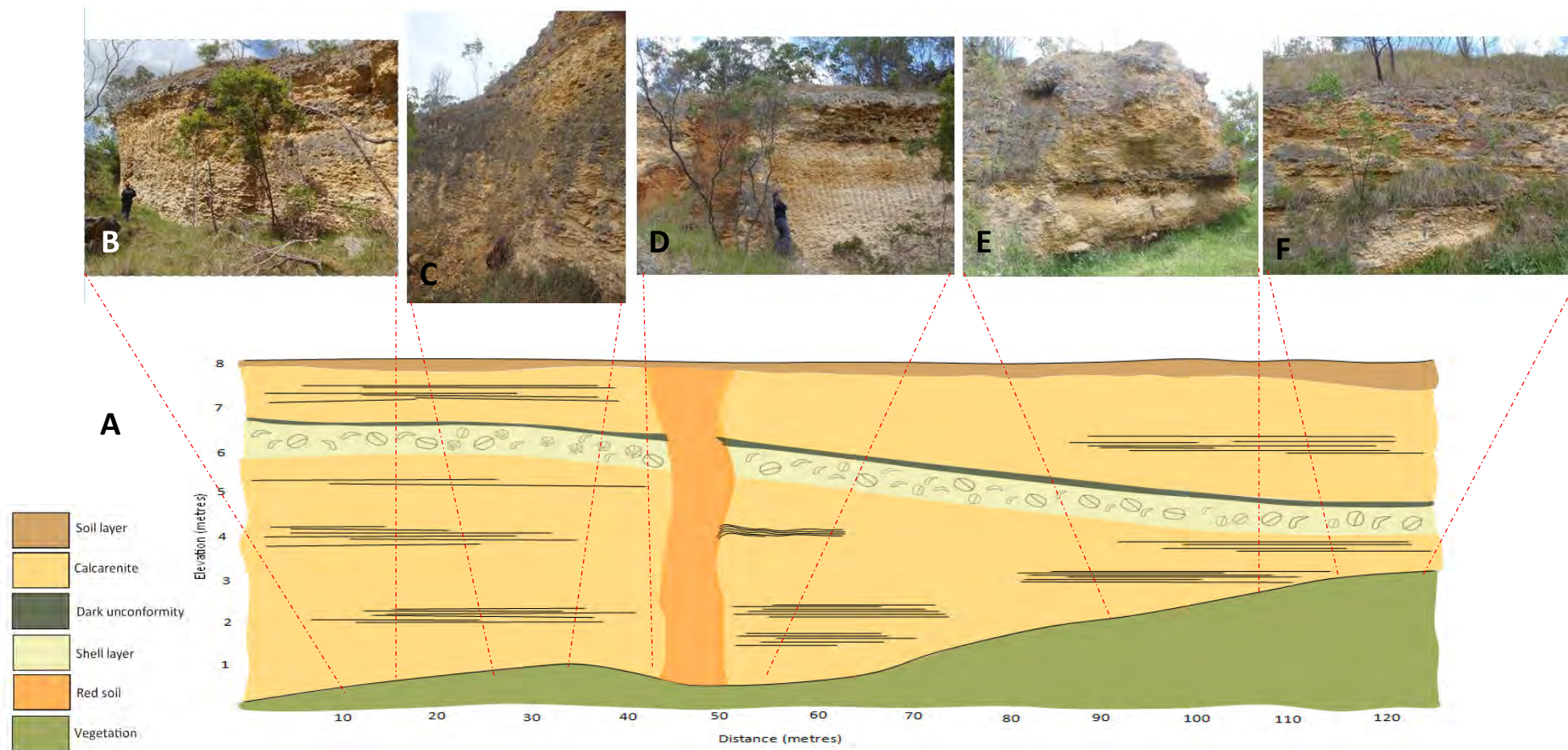


**Figure 3.48:** Exposure of Dismal Range calcarenite in Fort O'Hare rail cutting, western Victoria. **A:** Interpretive sketch of stratigraphical structures. **B:** Laminar bedding, western extent of exposure, **C:** Shell bed at this location contains clam species as well as oysters, **D:** Swaley bedding beneath shell bed, **E:** Dark layer beneath unconformity overlying shell bed, **F:** Eastern extent of exposure where shell bed is only 1 m from ground surface.



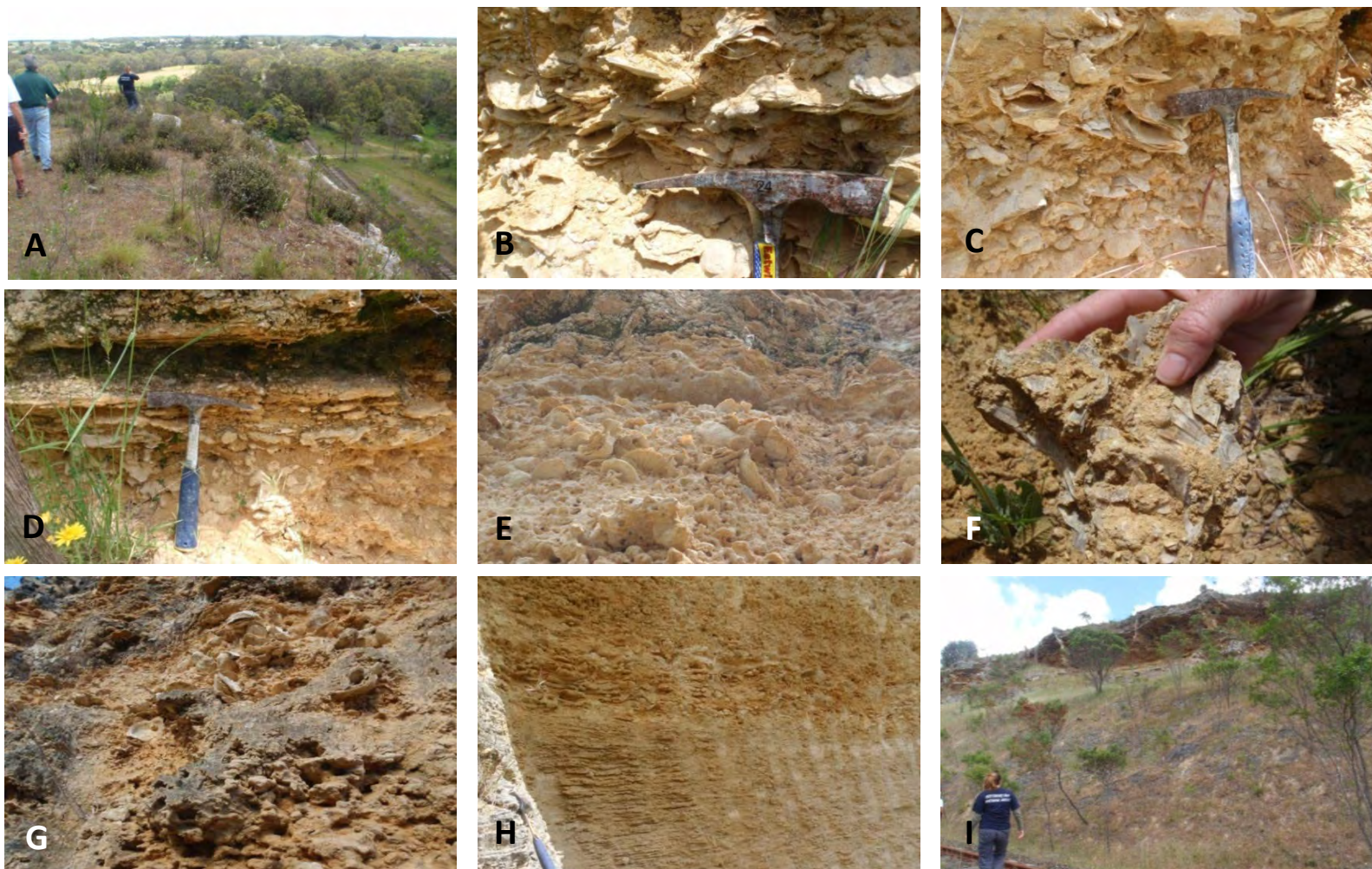


**Figure 3.49:** Stratigraphical features exposed within Fort O'Hare rail cutting. **A:** View to railway from top of exposure, **B** and **C:** Densely packed oyster bed at eastern end of exposure, **D:** Undercut darker layer above shell bed, **E:** Oysters and other clams within shell bed farther west in the cutting, **F:** *Pecten* within boulder fallen down from shell bed, **G:** Articulated oysters within shell bed, **H:** Wavy bedding within calcrenites beneath shell bed, **I:** View to cutting from railway, and calcrete cap to unit is visible.

### **Mingbool village**

A small quarry (S37°41'38.6", E140°54'30.5") approximately 18 km northeast of Mount Gambier and 5 km east of the settlement of Mingbool reveals low-angle bedding within Bridgewater Formation sediment. Geographical comparison of the site with SRTM data and Sprigg's (1952) map reveal the site is located within Dismal Range. The quarry walls within this exposure are of a gentle gradient and much material has slumped down obscuring large portions of the exposure. A thick red soil has developed at the top of the exposure, and this also slumps down over the quarry walls in locations.

Fine, low-angle, laminar- and cross-bedding are visible within the very pale brown (10YR 8/3) fine-grained sand at certain locations in the quarry walls. A case hardening has formed on the face of the exposure but sand is found to be free flowing beneath this. Foraminifera are abundant within the sediment and are commonly stained orange. Some foraminifera are also found recrystallised and/or chipped, but distinctive markings are still present. The benthic foraminifera, *Elphidium crispum*, dominates the deposit, accounting for 57% of the 200 tests counted while *Discorbis dimidiatus* and *Ammonia beccarii* represented 33% and 10% respectively, indicative of a predominantly marine sediment source.

Several shell fragments are visible within the calcarenite, but do not form a distinct shell bed. Numerous shells are found whole, but unpaired, though some are found to be fragmented. Identifiable shells include the oyster *Ostrea angasi* and *Pecten* which were unidentifiable to species level. These are similar to the molluscan species within the shell bed at Fort O'Hare and the exposure near Dartmoor Cemetery, some 50 km to the east of this location, which are also within the Dismal Range. Several rounded pebbles are present within the calcarenite near to the location of the oyster fragments, which is a similar observation to the rounded cobbles associated with oysters at Heritage Industries within the Compton Range. Oysters are sometimes found attached to substrate and these cobbles may have provided such a source.

The low-angle bedding, fine sediment size and presence of relatively deep-water molluscs indicate that this would likely have been a sub-aqueous environment. While the exposed stratigraphical features in this quarry reveal little about sea level at this locality (except that it was at least as high as this deposit), this site allowed for the collection of shell, foraminiferal and whole-rock material from the Dismal Dune for AAR analysis. The geochronology of this deposit will be discussed further in Chapter 5.



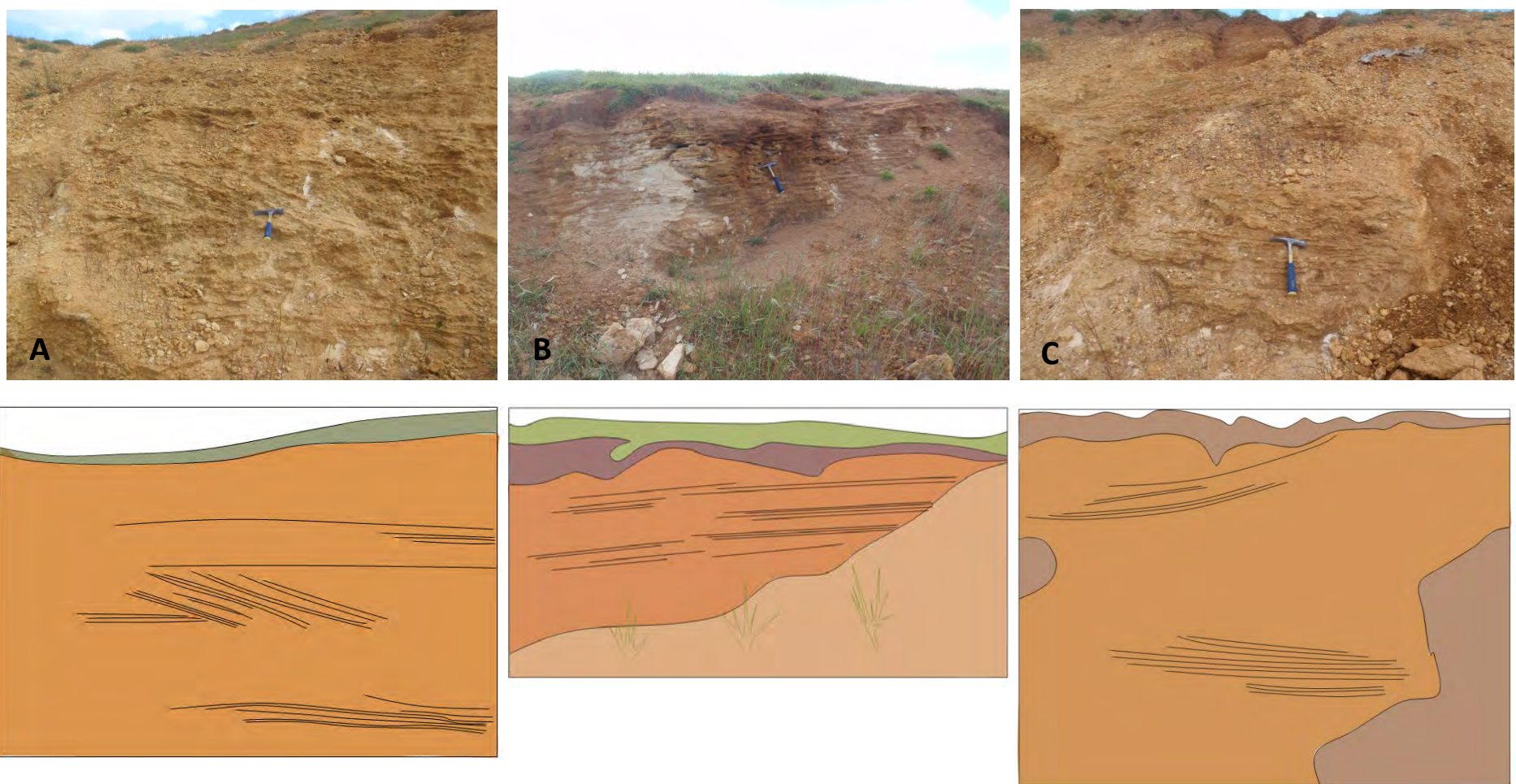


**Figure 3.50:** Photographs and associated sketches (to same scale as photographs) of bedding within small quarry within the Dismal Range near Mingbool village, South Australia. **A:** Cross-bedding within calcarenite on southern side of exposure, **B:** Laminar cross-bedding and thick soil profile on western side of exposure, **C:** Laminar bedding on eastern side of quarry walls. (Note, geology hammer for scale is 28 cm in length).





**Figure 3.51:** Stratigraphical structures within calcarenite at Mingbool village, Dismal Range. **A:** *Pecten* and *Ostrea* fragments within the calcarenite, **B:** Free-flowing sand beneath the weathering crust, **C:** *Ostrea* fragment and cobble within calcarenite, **D:** *Pecten* shell within calcarenite boulder.

### **Distinguishing between Bridgewater Formation and older limestones**

Within the Mount Gambier region the calcareous sands of the Bridgewater Formation rest upon the Gambier Limestone. In western Victoria, distinguishing between the Bridgewater Formation and the underlying deposits of Pliocene age is more challenging. Within the lower Glenelg River gorge, shallow, neritic sands and littoral calcarenites have been identified as Werrikoo Limestone (Singleton *et al.*, 1976). Due to foraminiferal assemblages within these deposits, Mallett (1977) has assigned the deposits to foraminifera zone N22/23 which is thought to straddle the Pliocene-Pleistocene boundary. Singleton *et al.* (1976) described the Werrikooian shell bed as consisting of abundant *Ostrea* and *Pecten*.

McLaren *et al.* (2011) identified facies of Werrikoo Limestone near Dartmoor railway station and within the cliffs of the Glenelg River near Dartmoor. These sites are in very close proximity (within 2 km) to the exposures described within this thesis at Fort O'Hare Quarry and at Dartmoor Cemetery. The site at Fort O'Hare Quarry has similar fauna as that described within the Werrikoo Limestone; within abundant *Ostrea* and *Pecten* and at Dartmoor Cemetery bioturbation tunnels are identified, similarly to those described by McLaren *et al.* (2011). Lacking within the Fort O'Hare Quarry site and Dartmoor Cemetery sites, however, are interbedded clays and brackish-water gastropods, typical of the Werrikoo Limestone as described by Singleton *et al.* (1976) exposed in cliffs adjacent to the Glenelg River. The laminar bedded sands at Fort O'Hare are also lacking in quartz pebbles as identified within the Werrikoo Limestone.

The Werrikoo Limestone underlies and grades upwards into Bridgewater Formation sediments in western Victoria (Holdgate and Gallagher, 2003). In the western Otway Basin, the contact between these two formations is conformable, while elsewhere it is unconformable (Cupper *et al.*, 2003). Identifying the two separate units is therefore challenging, as both are described as hosting similar faunas (e.g. abundant *Ostrea* and *Ammonia beccarii*) and similar sedimentary facies within calcarenite. McLaren *et al.* (2011) conducted strontium isotope analysis on brachiopods from the Werrikoo Limestone to constrain the age of this deposit and yielded ages extending from 0.484 to 1.377 Ma. These ages overlap the proposed age of Bridgewater Formation from the Dismal Range (MIS 17) and therefore do not confirm deposition during the Pliocene. AAR dating of sediment and fossil shell from this site may aid in constraining the age of the deposit further (Chapter 5).

Without extensive mapping, it is difficult to constrain the geographic limits of each deposit. Due to the location of the deposit within a north-westerly trending body of raised

elevation that appears to correspond with the Dismal Range described by Sprigg (1952) in South Australia, the deposits exposed at Fort O'Hare Quarry and Dartmoor are interpreted here to be the Bridgewater Formation. These exposures have also not been dissected by the Glenelg River, as have all other noted exposures of Werrikoo Limestone, and thus, may also be stratigraphically higher within the landscape. This is discussed further following the results of geochronological analysis of this deposit (Chapter 5).

### 3.8.11 Naracoorte Range

The Naracoorte Range has been divided into two separate palaeo-shorelines; East Naracoorte and West Naracoorte Ranges. Idnurm and Cook (1980) found that the East Naracoorte Range was of reversed magnetic polarity, and therefore suggested it must be older than 780 ka. The West Naracoorte Range and all barriers shoreward of this were found to be of normal magnetic polarity (Idnurm and Cook, 1980). The Naracoorte Range extends as a distinct linear shoreline for over 100 km (Murray-Wallace *et al.*, 1998) and as it trends farther southeast it follows the Kanawinka Fault. The Kanawinka Fault trends in a south-easterly direction, though more southerly as it extends into Victoria.

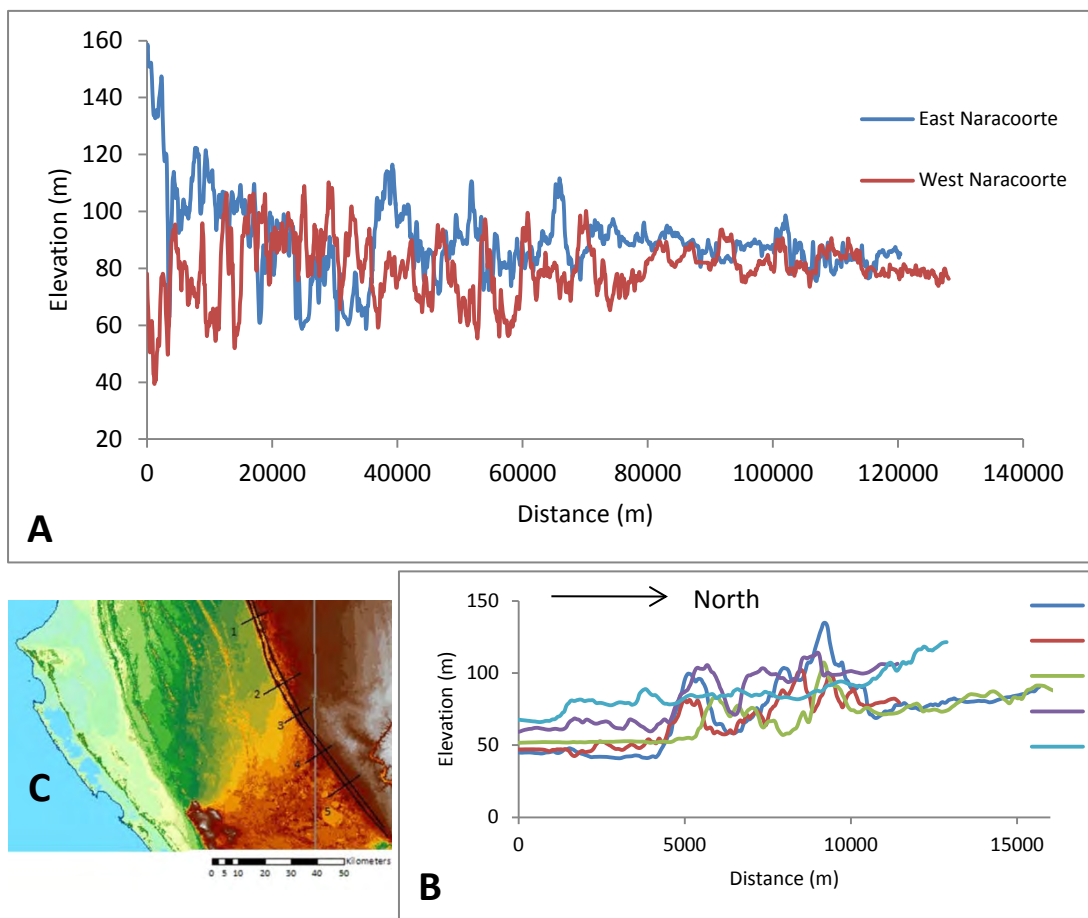


**Figure 3.52:** Transects of Naracoorte Range derived from SRTM data. **A** Lateral transects across the East and West Naracoorte Range; **B**: Transects across the width of the barriers; **C**: Location of transects.

SRTM imagery highlights that the East and West Naracoorte Ranges can be distinctly separated from one another farther northward, but as the barrier shoreline trends southward the distinction becomes blurred. This is also indicated by transects taken across the width of the structures. Transects 1, 2, and 3 taken farther north indicate two clearly separate structures, while transects 4 and 5, southwest of their extent, indicate more of a gradual incline.

### **Henschke Quarry**

Henschke Quarry, to the east of Naracoorte (S36°58'05.6", E140°45'59.0"), exposes a range of Pleistocene fossils in the quarry walls. On the eastern side of the quarry, exposed within the upper section of the wall is a distinct layer, approximately 15 cm thick, of marine shells. These shells are composed of both gastropods and bivalve genera, and individuals are up to 5 cm in length. Shells are moderately-densely packed within the layer, yet it is laterally persistent for over 10 m. The unidentified clam genera are well-preserved with distinctive markings still present on the shell and whole individuals largely intact, but are not articulated. Gastropod species appear to have been subjected to a greater amount of diagenesis and dissolution processes. Molluscs are well-cemented into the surrounding substrate.

Boulders of calcarenite that had fallen as a result of excavation of the quarry allow a closer examination of the sediment. The boulders revealed the presence of coral associated with the molluscan assemblages. The existence of coral within the deposit indicates that the sediment must have been deposited in warmer waters than found at the modern shoreline today. The fragments of coral were small, well-cemented and not possible to identify.

As the surrounding substrate was very well-cemented and no bedding was evident, it proved difficult to assess the timing of deposition of this unit; whether deposited as part of the Bridgewater Formation or older Neogene Limestone. Samples were collected for AAR analysis to constrain an age of the unit. Several other gastropod shells were also identified, and while their surfaces had been highly altered, masking distinctive markings (and their apertures are not preserved), they are possibly of the genus *Hartungia*. Ludbrook (1978) suggested that the presence of *Hartungia dennati chavani* is indicative of Early Pleistocene Bridgewater Formation. Ludbrook (1978) identified this species within the Naracoorte Range previously and correlated this deposit with the Point Ellen Formation on Kangaroo Island, as well as the Roe Calcarenite, a Plio-Pleistocene succession on the coastal margin of eastern Western Australia.



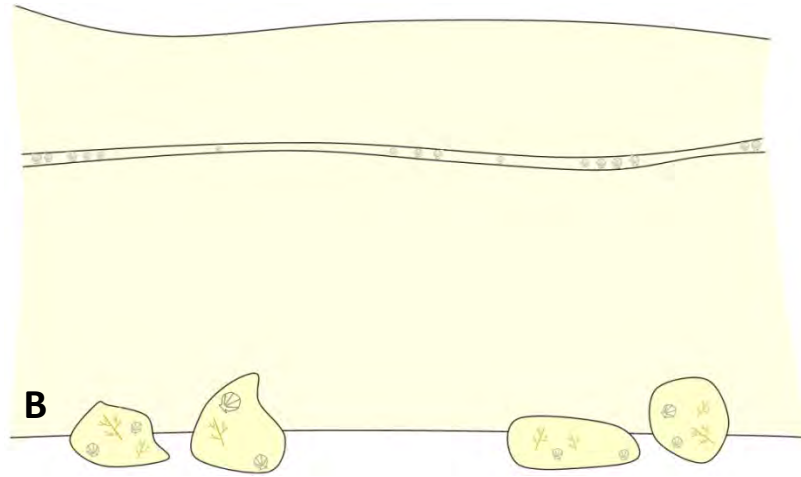
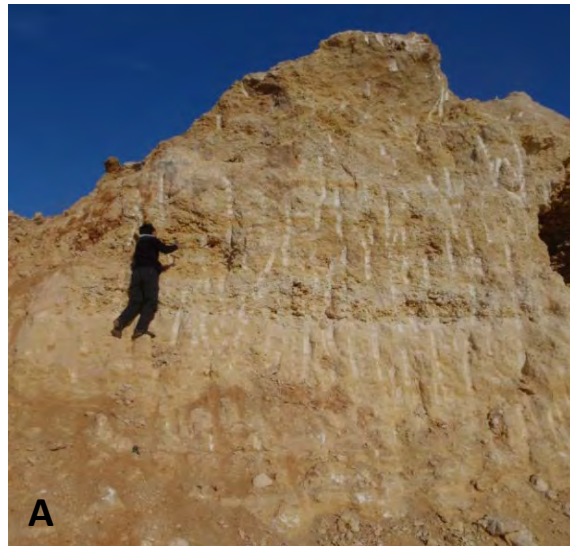


**Figure 3.53:** Calcarenite exposure within Henschke Quarry, Naracoorte, South Australia; **A:** Eastern wall of quarry - person's hand is at layer where shells were collected; **B:** Illustration of eastern wall and laterally extensive shell layer (exposure is approximately 7 m high); **C:** Calcarenite boulder at base of wall displaying shelly material and coral; **D:** Clam shell *in situ* (pen in 15 cm in length). Interpretations of stratigraphical features and bedding at this site were impeded by the scouring result of excavation works.

### **3.8.12 Summary of stratigraphy at sample sites of the Bridgewater Formation on the Mount Gambier coastal plain**

This work has further detailed previous investigations of the dune barriers on the Mount Gambier coastal plain. Previously, descriptions of facies architecture within the shoreline barrier complexes had been completed within both the Burleigh and Caveton Ranges along Rabbitors Road. This thesis has further detailed exposed facies and fauna present within these barriers at previously described and newly identified sites (Laslett Road and Bucks Hill) and gathered more samples in an attempt to further constrain the age of these deposits. This research documents previously undescribed deposits across the width of the Mount Gambier coastal plain including; palaeo-sea level beach facies at Port MacDonnell, a possible extension of the Robe Range previously only sampled from near Robe, and the MacDonnell Range which is correlated morphostratigraphically in this thesis with the last interglacial (MIS 5e) Woakwine Range. The barrier shoreline complexes inland of Caveton Range have not previously been sampled, but were briefly described by Sprigg (1952). This research presents descriptions of the facies architecture of these four farthest inland barriers (Gambier, Compton, Mingbool and Dismal) and samples have been collected for AAR analysis to aid in constraining their time of deposition.

From stratigraphical analysis of exposures within the Bridgewater Formation a range of depositional facies have been identified including beach, sublittoral lagoonal and aeolian units. The identification of these facies and their height above present sea-level within eight separate shoreline barriers will allow for palaeo-shoreline reconstruction once a chronostratigraphy and uplift history have been established.

In the younger, more seaward deposits a wider range of facies is evident. For example, aeolian deposits are found within Robe Range; lagoonal and aeolian facies are identified in the MacDonnell/Woakwine barrier complex; beach, aeolian and lagoonal facies are found in Burleigh Range; and exposures within Caveton Range display both lagoonal and aeolian facies. In the older dune ranges, such as Mingbool and Dismal Ranges only subaqueous deposits were observed, and the marine molluscs found in such locations suggest the exposed facies may have been deposited up to 30 m below the water surface. The lack of aeolian or lagoonal deposits, which would have been deposited above and at sea-level, may relate to the higher levels of erosion these barriers may have experienced since initial deposition. Any lagoonal or aeolian sediments deposited on top of subaqueous material as sea-level regressed may have eroded over time leaving only subaqueous facies. Transects across the barriers suggest this may also be true; with older barriers appearing more subdued



in their elevation. However, it may be that lagoonal and aeolian deposits from the older barriers do remain but were not found in this study due to a lack of adequate exposures. The subdued topography of these features therefore may be a result of a less intense interglacial (where temperatures may have been cooler and thus carbonate production on the offshore shelf was reduced) and a lower volume of initial sedimentation. Palaeo-shoreline reconstruction will therefore be more precise in the younger barrier shorelines where sea-level indicators are more constrained.

The use of SRTM imagery allowed analysis of the overall morphology and lateral extent of each of the barriers, which has not previously been detailed. The younger barrier shorelines were found to be more laterally extensive. MacDonnell Range extends into Woakwine Range farther north which trends along the coastline as far north as Lake Albert. Both Burleigh and Caveton Ranges are seen to extend farther north also, with their counterparts, Reedy Creek and West Avenue Ranges, both easily identifiable. However, the youngest Pleistocene barrier shoreline, Robe Range, is only found to extend for a couple of kilometres along the modern coastline at Port MacDonnell. It crops out again between the towns of Beachport and Robe but is not recorded other than this, which may be a result of variations in sediment availability along the coastline. Another possibility is that it is masked by the Holocene sands of the Younghusband Peninsula, which are laterally extensive from Cape Jaffa to Lake Albert.

Gambier Range, situated immediately seaward of the town of Mount Gambier, appears to be the most prominent barrier shoreline on the coastal plain. It reaches heights of 30 m above the surrounding land surface, and while its formation appears lost in the Mount Burr volcanic province, the corresponding East Avenue Range is clearly visible and laterally extensive northward. Compton Range, directly north of Mount Gambier, is one of the most difficult barrier shorelines to constrain with regards to its spatial extent. It appears as isolated landform fragments of higher relief, and has a much wider extent (4 km) than many of the other barriers ( $\bar{x}$  = ~2 km). The wide extent of this deposit may be suggestive of a longer interglacial, and the isolated high-relief fragments may be a result of greater erosion of the shoreline. The relationship between volume of the shoreline barriers and the proposed duration and intensity of interglacials is further discussed in Chapter 6 (6.6.3). Compton Range is not as laterally extensive as the younger barriers and it is difficult to isolate its counterpart, Baker Range, northward of the Mount Burr volcanic province, occurring as only isolated higher-relief fragments trending in a north westerly direction.

Mingbool and Dismal Range also occur as interconnected ridges, with isolated patches of higher elevation trending in a northwest direction with distances of up to 5 km recorded between areas of relief. These two barriers appear more extensive laterally than the Compton Range and their extent can be mapped as far east as the Glenelg River in Victoria. These two barriers are both seen to curve in a more southerly direction as they trend farther west due to the influence of the Kanawinka Fault, causing the two shorelines to nearly coalesce in western Victoria. The most inland barrier, Naracoorte Range, is more difficult to isolate in the Mount Gambier region. Farther to the northwest, directly inland from Robe, the Naracoorte Range can be clearly separated into the East and West Ranges, yet the barriers seem to coalesce north of Mount Gambier. As mentioned previously, the more subdued nature and limited lateral extent of the older barrier shorelines may be a result of increased exposure to erosional processes.

**Table 3.9:** Summary table of sedimentary structures and depositional facies identified at sample sites within exposures of the Bridgewater Formation on the Mount Gambier coastal plain

Dune Range	Sample site	Sediment colour Grain size	Sedimentary structures present	Elevation APSL (m)	Molluscs present			Foraminifera present	Facies
					Species	Abundance/preservation	Indicative environment		
Modern beach	PMB	Light gray, medium sand	Marine abrasion surface, with sheltered areas of sand and flint cobbles	0	<i>Turbo undulatus</i>	Abundant.	High-energy	EC, DD	Beach
	Racecourse Bay		Beach ridge with multiple berms, mostly comprised of flint cobbles	0					Beach
Holocene beach	Port MacDonnell		Beach deposit consisting of coarse sand and dominated by gastropod shells. No bedding evident	2-3	<i>Turbo undulatus</i>	Abundant	Rocky, high-energy	DD, EC	Beach
Robe Equivalent	PMB flint conglomerate	Coarse	Flint cobbles and shell fragments within a lime matrix	0-1	<i>Turbo undulatus</i> , <i>Thias orbita</i> , <i>Katelsysia rhytiphora</i>	Common. Fragmented and well cemented.	Rocky, high-energy		Beach
	Upper aeolianite, PMB	Very pale brown, CS	Tough cross-bedding, (13-17°), dipping eastwards. Capped by a rubbly calcrete	3-13				EC, DD	Aeolian
	Lower aeolianite, PMB	Very pale brown, MS	Well cemented. Laminar bedding. Overlain by a calcrete	1-3					Aeolian
	Weathered aeolianite, PMB	Yellow, FS	Very cemented. Similar colour weathering crust to that in lower aeolianite unit in Port MacDonnell cliffs	1-1.5					Aeolian
	Upper aeolianite, SB	Yellow, MS	Northwards dipping cross-beds of varying angles and capped by a calcrete.	3-12				DD, EC, EM, AB	Aeolian
	Lower aeolianite, SB	Brownish yellow, MS	South-east dipping cross-beds, capped by an undercut unconformity	1-3					Aeolian
	Swarts Road sand quarry	Pale yellow, MS	Sand largely free-flowing. Where consolidated southwards dipping cross-beds at 14°. Rubbly calcrete and rhizoliths present at top of exposure	16*				EC, AB	Aeolian
MacDonnell	Narrawong	Brownish yellow, MS	None present	4	Possibly a <i>Spisula</i>	Single disarticulated shell identified only		EC, DD	
	German Creek		Shells found on ground surface	16*	<i>Katelsysia rhytiphora</i>	Abundant, well-preserved, articulated	Lower littoral zone of sandy shores.		Lagoonal?
	Lake Hawdon South		Shoaling upwards. Deep-water <i>Ostrea angasi</i> lie below a thick shell bed of bivalve species, which is capped by finer shell fragments, which is in turn overlain by a pedogenically altered clay layer and a thin calcrete unit.	9*	<i>Chlamys bifrons</i> , <i>Katelsysia rhytiphora</i> , <i>Anadara trapezia</i> , <i>Fulvia tenuicostata</i> , <i>Spisula trigonella</i> , <i>Tellina deltoidalis</i> , <i>Pleuroploca australis</i>				Lagoonal – Glanville Formation
Burleigh	Rabbitors Road	Pale yellow, MS	Three prograding flint cobble lenses lie on top of finely bedded calcarenite. Higher in the unit steep angle trough cross-beds are evident. Solution pipes and rhizoliths are abundant.	34^	<i>Katelsysia rhytiphora</i> , <i>Chlamys (Equichlamys) bifrons</i>	Fragments	Lower littoral zones Sandy to silty floors, 2-30 m deep		Beach and aeolian
	Laslett Road	Pale yellow, FS	Fine laminar bedding. Bioturbation burrows	32*	<i>Spisula trigonella</i>	Whole, disarticulated, well-preserved.	Muddy or sandy-mud estuaries	EC	Lagoonal
Caveton	Rabbitors Road	Light grey to pale yellow, VFS to FS	Laterally extensive laminar units within very fine material. Abundant shell, bioturbation burrows and rhizoliths. Exposure capped by rubbly calcrete.	32^	<i>Katelsysia rhytiphora</i> , <i>Anapella cycladea</i> , <i>Tellina deltoidalis</i> , <i>Fulvia tenuicostata</i> , <i>Niothus pyrrhus</i> , <i>Modiolus aerolatus</i>	Abundant, whole, commonly articulated, very well preserved	Lower littoral zone, estuarine, sandy and muddy floors.	EC, AB	Lagoonal
	Bucks Hill	Very pale brown, MS	Steeply dipping (32°) cross-beds	45*					Aeolian
Gambier	Gooch Road	Brownish yellow to Yellow FS to MS	Gently (4-6°) north-easterly dipping cross-beds. Well cemented layers with free-flowing sand between.	55*				EC, DD	Aeolian
	Caroline Main Road	Light gray, VFS	Fine, laminar beds within fine sand overlying more clayey material containing small gastropods		Very small gastropods – likely terrestrial in origin	Very small, abundant in one layer	Perhaps a fresh water interdune corridor	None – but diatoms	Lacustrine (freshwater)
Compton	Grey St		High angle cross-beds	60*	<i>Modiolus</i>	In frequent, disarticulated, fragile	Good water movement 2-20 m deep		
	Baxter's Quarry	Very pale brown, MS	High angle cross-beds overlie laterally extensive unconformity. Below this bedding is finer and more laminar. Herringbone cross-bedding and swale-like features. Large solution pipes.	44.8-50"	None recorded			EC, AB, DD	Aeolian and subaqueous
Mingbool	Heritage	Pale yellow, MS	Very fine low-angle bedding. Three shell beds, two with large oysters present, one with multiple bivalves and shell fragments. Large solution pipes.	46.5-51"	<i>Ostrea angasi</i> , <i>Placamen</i>	Oysters fragmented. Some whole bivalves identifiable, but commonly hard to identify at species level	Water depths of 2-20 m, low-medium energy, sand within areas of high current flow		Subaqueous
	Don's Quarry	Yellow, FS	Very fine laminar bedding.	45*	<i>Ostrea angasi</i>	Common, some whole, many fragmented. Disarticulated.	Water depths of 2-20 m, low-medium energy	EC, DD, AB	Subaqueous
Dismal	Dartmoor Cemetery	Pale yellow, FS	Fine laminar bedding. Bioturbation burrows are present low in exposure. Shell grit and keystone vugs.	50*	<i>Ostrea angasi</i> , <i>Pecten benedictus albus</i>	Infrequent. Whole, disarticulated and sometimes recrystallised	2-30 m deep, low-medium energy. Completely buried in sand.	EC, DD, AB	Subaqueous
	Fort O'Hare Quarry	Pale yellow to Yellow, FS to MS	Laterally extensive shell layer of articulated deep-water marine shells, overlain by an undercut unconformity. Bedding is mostly fine and laminar	40*	<i>Ostrea angasi</i> , <i>Pecten benedictus albus</i> , <i>Chlamys asperrima asperrima</i> , <i>Chlamys (Equichlamys) bifrons</i>	Abundant within densely packed shell bed. Whole shells, commonly articulated, well preserved.	Commonly 2-30 m water depth on sandy to silty floors	EC, AB, DD	Subaqueous
	Mingbool village	Very pale brown, FS	Low angle laminar cross-bedding.	70*	<i>Ostrea angasi</i> , <i>Pecten benedictus albus</i>	Infrequent. Disarticulated, poorly preserved	Water depths of 2-20 m, low-medium energy	EC, DD, AB	Subaqueous
Naracoorte	Henschke Quarry		Laterally extensive layer of clams and gastropod shells. No bedding evident.	80*	Possibly <i>Hartungia</i>	Frequent, generally well preserved but highly cemented. Disarticulated.			

Derived from data collected by Murray-Wallace *et al.* (1996); Elevation refers to the elevation of each sampling site within the barriers in metres above present sea level \* Derived from SRTM data; ^ Derived from surveying with an electronic Dumpy level from a known AHD benchmark. Sediment size derived from a MasterSizer. Site abbreviations: PMB = Port MacDonnell Beach, SB = Shelly Beach. Sediment size abbreviations: VFS = very fine sand, FS = fine sand, MS = medium sand, CS = coarse sand. Foraminifera abbreviations: EC = *Elphidium crispum*, AB = *Ammonia beccarii*, DD = *Discorbis dimidiatus*, EM = *Elphidium macelliforme*

### 3.8.13 Siliceous sands

In addition to sediments of the Bridgewater Formation, sands of a differing origin and composition are also recognised on the Mount Gambier coastal plain. One such example is identified within a housing development north of Mount Gambier (S37°49'37.2", E140°47'55.2"). The lowest unit identified at this exposure is highly weathered Bridgewater Formation, within which very small shell fragments are evident. A thick (up to 75 cm in places), red (*terra rossa*) soil overlies the weathered Bridgewater Formation indicative of substantial subaerial exposure. Overlying the *terra rossa* soil is a one metre thick layer of light gray (10YR 7/11) siliceous sand (Figure 3.54). This sand differs from that as identified as Bridgewater Formation calcarenite in both composition and colour. Overlying the siliceous sand in turn is a 10 cm thick layer of ash, likely deposited following the Holocene eruption of Mount Gambier. A 50 cm thick brown soil has developed above the ash.

Previous studies have suggested that siliceous sands identified within the region comprise the Malanganee Sands (Boutakoff, 1963). The Malanganee Sands are proposed to have formed in Holocene to Pleistocene time and any bedding within the deposits is rarely recognised (Copper *et al.* 2003). It has been previously suggested that the Malanganee Sands are derived from Bridgewater Formation deposits, whereby calcareous sediments have been removed through dissolution processes and winnowing of siliceous grains has occurred (Boutakoff and Sprigg, 1953; Boutakoff, 1962; Kenley, 1971). In the River Murray mouth region, siliceous sands have been identified as glacial age deposits, formed at times of lower sea level and originating from inland sources deposited by strong winds during glacials (e.g. Murray-Wallace *et al.*, 2010). The Loxton-Parilla Sands are located inland from barrier successions of the Bridgewater Formation on the Mount Gambier coastal plain (Figure 3.10). These sands are also suggested to form arcuate palaeo-sea level shorelines composed of bioclastic carbonate sands and therefore potentially indicate that these are not the inland source of the identified siliceous sands unless they have been winnowed also. The Malanganee Sands are suggested to be equivalent to the Lowan sands within the Murray Basin (Crocker, 1946), though the Bridgewater Formation has been shown to not be the source of these sands (Pell *et al.*, 2001). Other potential sources of siliceous sands may include the exposed sea floor during sea-level lowstands and interdune corridors (Copper *et al.*, 2003). An OSL sample was obtained from the siliceous sands exposed at this site and the results of this analysis will be discussed in Chapter 5 to aid in constraining a time of deposition and a potential source of this sediment.



**Figure 3.54:** Siliceous sands overlying soil developed on Bridgewater Formation sediment, north of Mount Gambier. The contrast between the two deposits is striking and suggests a varying composition and source of sediment.

### 3.9 Comparison of stratigraphical features observed in the Pleistocene Bridgewater Formation on the Mount Gambier coastal plain with Pleistocene calcarenite elsewhere

Coastal aeolianites commonly form shore-parallel sediment bodies deposited as transverse dune ridges (Brooke, 2001). The laterally extensive barriers of the Bridgewater Formation are thus comparable in their overall morphology to many other coastal aeolianite bodies around the world; including those described in South Africa (Carr *et al.*, 2007; Bateman *et al.*, 2011), the Bahamas (e.g. Hearty, 1998), Bermuda (e.g. Land *et al.*, 1967), Hawaii (Blay and Longman, 2001), and Lord Howe Island (Brooke *et al.*, 2003).

The stratigraphy within exposed sections of the Bridgewater Formation on the Mount Gambier coastal plain can also be closely compared with other global coastal calcarenite bodies. For example, the capping and separation of stacked aeolianite units by palaeosols and calcrete, as exposed within Robe Range at Port MacDonnell and Shelly Beach, is similar to the aeolianite soil couplets described in Bermuda (e.g. Land *et al.*, 1967). The red palaeosols in Bermuda are suggested to have formed during glacials of lower sea level and relating to increased diagenesis of the underlying limestone by fresh water during this time (Land *et al.*, 1967) and to accumulations of atmospheric dust (Bricker and MacKenzie, 1970) and volcanic impurities (Muhs *et al.*, 2012b). Hearty (1998) also noted a similar relationship in the Bahamas, as did Zhou *et al.* (1994) on the Nepean Peninsula, Victoria, Australia, Brooke *et al.* (2003) on Lord Howe Island, and Blay and Longman (2001) in Hawaii. Palaeosols are essentially markers of significant hiatuses in calcarenite deposition.

Other indicators of significant periods of non-deposition include the presence of karst weathering features. On the Mount Gambier coastal plain these are most commonly found in the form of vertical solution pipes and rhizolith structures. Solution pipes are noticeably larger in the older structures including the Baxter's Quarry and Heritage Industries sites within Compton Range. Karst has also been associated with periods of subaerial exposure within calcarenite deposits in Hawaii in the form of sink holes and rhizoliths (Blay and Longman, 2001) and as solution pipes in Western Australia (Playford, 1997).

Distinct bedding patterns have also been used to identify palaeo-shorelines. On the Mount Gambier coastal plain, fine, laminar bedding is associated with subaqueous depositional environments, whereas high-angle cross-bedding was found to be indicative of aeolian entrainment. Loope and Abegg (2001) noted that large-scale cross-beds are common to aeolian deposits and rare in sub-aqueous environments. This was also noted by Land *et al.* (1967) in coastal calcarenite deposits on Bermuda, and laminar bedding was further associated with beach facies in the Bahamas by Hearty (1998).

Other indicators of beach deposits include the presence of well-preserved fossils. Shells commonly found within the Bridgewater Formation on the Mount Gambier coastal plain include bivalves (*Katelysia rhytiphora*, *Tellina deltoidalis*, *Anapella cycladea*, *Fulvia tenuicostata*, *Ostrea angasi*, *Pecten benedictus*) and gastropods such as *Turbo undulatus*, *Niothus pyrrhus* and *Thais orbita*. These genera indicate a range of depositional settings, from deep-water, subaqueous environments, as indicated by *Pecten* and *Ostrea*, to high-energy rocky environments indicated by *Turbo*, and lagoonal environments suggested by the presence of *Tellina*. In other locations shell deposits have been associated with sub-aqueous deposits, for example those described on the island of Bermuda (Vacher *et al.*, 1995). Other beach indicators include the presence of air pockets or keystone vugs. These were identified in boulders of calcarenite found at the foot of an exposure within the Dismal Range at Dartmoor Cemetery. Garrett and Gould (1984) and Kindler and Hearty (2000) identified similar features within calcarenite deposits on the Bahamas and suggested the air pockets were trapped in underlying sediment and were indicative of a swash zone environment.

These comparisons indicate that the stratigraphy recorded on the Mount Gambier coastal plain is highly comparable with other global coastal calcarenite deposits. Palaeo-sea level reconstruction derived from the Mount Gambier coastal plain will therefore prove valuable in comparing with records derived from those sites that lie at differing distances from former continental ice sheets.

### 3.10 Chapter Summary

This chapter has discussed the processes associated with temperate carbonate sedimentation and how these can lead to the onshore deposition of calcarenite on the Mount Gambier coastal plain. Common sedimentary structures within such deposits were then presented alongside indicators to differentiate between aeolian and sub-aqueous deposition. These sedimentary structures found within other global coastal calcarenite deposits were then discussed in relation to palaeo-shoreline reconstruction. The second half of the chapter presented the stratigraphical findings within exposures of the Bridgewater Formation on the Mount Gambier coastal plain. This research has built upon previous stratigraphical investigations (e.g. Crocker and Cotton, 1946; Hossfeld, 1950; Sprigg, 1952; Murray-Wallace *et al.*, 1996) and presented new descriptions and findings from the more inland barrier complexes not previously sampled from. Palaeo-shoreline reconstruction at each study site will be aided by identification of sedimentary structures outlined in the first half of the chapter. These indicators included differing bedding patterns, the presence of macro- and micro-fossils (such as marine molluscs and foraminifera) and sub-aerial exposure structures.

Morphological analysis using SRTM imagery allowed the identification of eight separate palaeo-shoreline barriers on the Mount Gambier coastal plain. Using SRTM data it was possible to assess the lateral extent of these structures as well as their width and changes in their height. Barriers appeared to coalesce as they extend south-easterly away from the Mount Burr volcanic province, and most could be seen to extend farther northwest from this location.

This chapter has described the facies architecture at multiple locations from each of the barrier shorelines on the Mount Gambier coastal plain. Stratigraphical analysis and identification of micro- and macro-fossils have aided in reconstructing past depositional environmental and will aid in constraining palaeo-sea level (section 6.3). Prior to determining the age of the deposits, the petrographic characteristics of the sediments are analysed (Chapter 4) to detect any diagenetic effects that may account for discrepancies within the geochronological dataset.



# Chapter 4

## **Sedimentary petrography of the Bridgewater Formation, Mount Gambier coastal plain, southern Australia**

### **4.1 Introduction**

This chapter examines the extent of carbonate diagenesis within deposits of the Bridgewater Formation on the Mount Gambier coastal plain in southern Australia and assesses whether this is directly comparable to the relative age of the calcarenite successions. The degree of sediment diagenesis was evaluated as a framework to assess the integrity of the geochronological results of this thesis. For example, samples that are highly cemented may yield lower D/L values suggestive of a younger age when analysed using amino acid racemisation (AAR; Murray-Wallace, 1993). Detailed descriptions of the texture and fabric of the sediment will also aid in determining components of whole-rock samples for AAR analysis and may aid in reasoning any outliers within data sets.

The chapter firstly addresses how diagenesis occurs in differing environments and how it might be identified within carbonate sediments. To assess diagenetic changes, sediments from the Mount Gambier coastal plain were analysed using X-ray diffraction (XRD) techniques to account for changes in the mineralogy of the calcarenite between deposits, thin section analysis and point counting of grains to determine the fabric and texture of the calcarenite and the development of inter- and intra-grain cements, an assessment of karst development within calcarenite to clarify larger-scale diagenesis of the exposure, and scanning electron microscope (SEM) photographs of foraminifera from representative deposits to determine whether there is a trend in the degree of diagenesis or textural changes to tests with proposed age of the deposit based on geographical location of the barrier shoreline. Results aid in determining both the original depositional environment of the sediment and the diagenetic environment in which sediments have been exposed.

### **4.2 Carbonate diagenesis**

Diagenesis encompasses the changes to the character and composition of sediments and can occur from the time of deposition up until materials are influenced by metamorphism (Larsen and Chilingar, 1979). The interaction between water and carbonate sediments is the primary force in carbonate diagenesis and therefore the composition of the fluids in the surface and

sub-surface zones is a critical factor (James and Choquette, 1989). Throughout time, carbonate sediments and rocks may be deposited, precipitated, buried, eroded, exposed and reburied and at each stage will be subjected to interactions with differing fluids. Fluids that may potentially interact with carbonate sediments include marine, meteoric or deep subsurface liquids and these fluids thus characterise separate diagenetic environments (Figure 4.1). The degree to which any carbonate may be altered within one of these settings is dependent upon the composition and flux of the fluid through the sediment and the length of time the carbonate sediment remains within that environment.

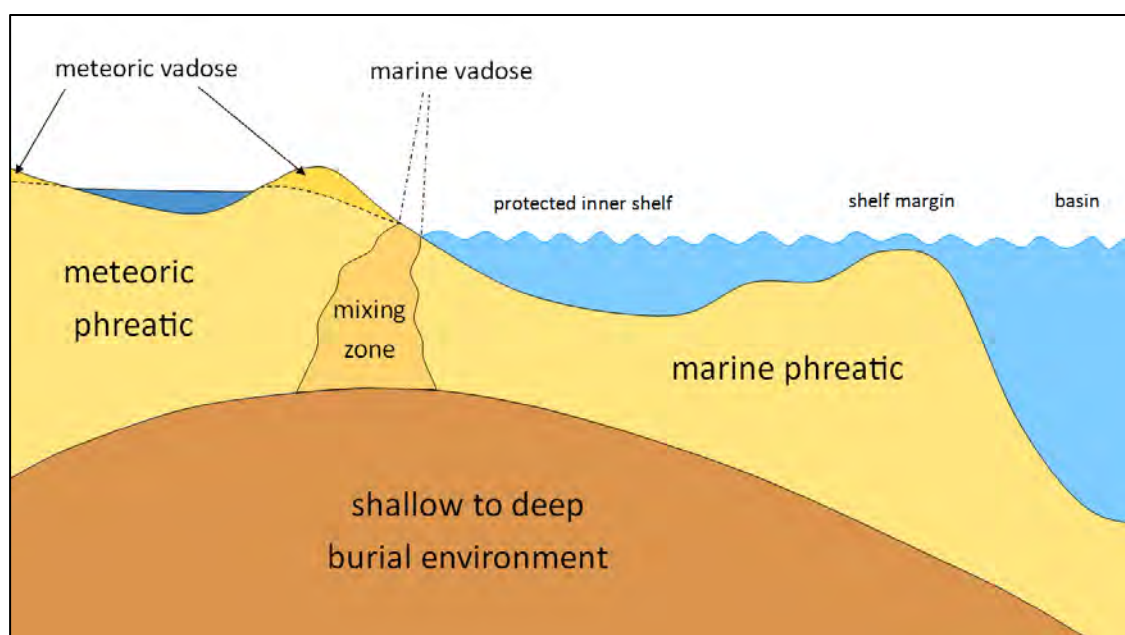


**Figure 4.1:** Diagenetic environments (modified from Tucker and Wright, 1990).

Diagenetic processes that may affect carbonate sediments and rocks include dissolution, cementation, compaction, neomorphism and the replacement of carbonate grains and matrices by non-carbonate substances (Flügel, 2004). Dissolution commonly occurs in the near-surface meteoric environment, but also acts during deep burial and in deep sea regions (Bathurst, 1972). The undersaturation of pore fluids with respect to carbonate results in dissolution of metastable carbonate grains and cements. Cementation occurs when there is a super-saturation in pore fluids with respect to carbonate minerals that leads to the precipitation of minerals in primary or secondary pores (Flügel, 2004). In the deep burial environment, sediments may be exposed to compaction by pressure from overlying sediments causing mechanical and chemical alterations. Neomorphism occurs extensively in the meteoric and deep sub-surface zones and refers to polymorphic transformations (e.g. the

inversion of aragonite to calcite) that occur in the presence of water (James and Choquette, 1989).

#### **4.2.1 Meteoric diagenesis**

The meteoric diagenetic environment may be divided into two zones; the vadose and the phreatic, which are separated by the water table. Within the vadose zone, pores periodically contain air, water or both. The meteoric vadose environment is greatly affected by changes in climate. Rainwater enters the meteoric vadose zone directly at the ground surface whereby water percolates through any soil profile present. Changes in rainfall and rates of evaporation can therefore directly alter the flux of fluid through the carbonate sequence. Climatic changes may also alter vegetation type or growth patterns and in turn alter the chemical composition of soil water as well as the soil profile itself. This may therefore alter the chemical concentration of water percolating into the carbonate sequence through the overlying soil profile.

Tucker (1990) suggested that dissolution, cementation and mineralogical transformation are the three main processes that operate on sediment particles in the meteoric zone. Products of meteoric diagenesis include dissolution features, which create porosity at a microscale, and karst when dissolution occurs to a greater extent. Meteoric cements are commonly composed of low magnesian (Mg)-calcite (Flügel, 2004). Significant chemical and textural changes are documented to occur within the meteoric diagenetic environment due to the conversion of high Mg-calcite and aragonite to low Mg-calcite and the addition of low-Mg calcite cement. Longman (1980) suggested that in the meteoric vadose environment solution processes may lead to the formation of vugs, molds and etched grains and that when water is saturated with calcite pendant, meniscus cements may commonly be found. In the phreatic zone, however, pores are filled with water continuously and therefore cement is distributed between all grains. Longman (1980) also proposed that cements in this environment may first nucleate around grain edges and grow outwards, producing a bladed isopachous calcite rim. Further cementation may result in coarsening crystal size towards the pore centre as permeability decreases.

#### **4.2.2 Karst development**

Karst development ensues when dissolutional processes occur on a greater scale, commonly within the meteoric vadose zone in areas affected by rain-sourced waters. Wright and Smart (1994) noted that while most palaeokarst features within the geological record are found

within such zones, significant dissolution of carbonates can also occur in areas affected by fluids other than meteoric waters.

Climate has a significant influence on the development of karst within carbonate landscapes. As previously mentioned, climate can control the flux and the chemistry of fluids entering the carbonate sequence and rates of karst denudation are commonly highest in regions where rainfall and the content of carbon dioxide within the soil is high (Wright and Smart, 1994), causing the production of carbonic acid which erodes the carbonate.

Karst structures may include the formation of solution pipes and cave systems and may indicate that surfaces have been subaerially exposed. Other subaerial exposure features include rhizoliths (carbonate-casts formed around root structures) and calcretes which are associated with calcium carbonate precipitation. Budd *et al.* (2002) attempted to quantify macroscopic subaerial exposure surfaces in the Suwannee Limestone, central Florida, with varying lengths of subaerial exposure of the limestone. They concluded that point counting of karstic subaerial exposure structures was not indicative of the duration of exposure of a surface and factors controlling the total variance of these structures included: changes in base-level; the abundance of vegetation; the  $p\text{CO}_2$  and availability of water. It is therefore suggested that the development of karst on the Mount Gambier coastal plain will vary locally depending on the above characteristics.

#### **4.2.3 Shallow marine diagenesis**

James and Choquette (1989) suggested that non biogenic carbonate precipitation is the dominant diagenetic process that occurs on the modern sea floor, occurring in the formation of ooids, hardening of soft grains, and the lithification of loose carbonate sediments to form marine limestones. Cementation is a common early diagenetic process within the shallow marine zone. Cements may initially be precipitated within the bioclasts of intraskeletal pores, shells and tests (Tucker, 1990). Precipitation of intergranular cements may lead to the formation of hardgrounds and crusts. Diagenetic processes will be dependent upon the energy regime. In areas of higher-energy, water flux is likely to be greater and thus cementation will occur more rapidly than in low-energy zones where water is more stagnant (Tucker, 1990). Longman (1980) suggested that isopachous fibrous cements are characteristic of the marine environment.

#### **4.2.4 Carbonate porosity**

Total porosity is the percentage of a rock that is occupied by interstices which may be isolated or connected, while effective porosity refers to the percentage of a rock body composed of

interconnected pores. Porosity in sedimentary rocks may be divided into primary and secondary porosity. Primary porosity forms during predepositional stages (such as porosity within foraminiferal tests) and depositional stages (such as intergranular porosity). Secondary porosity occurs during diagenesis any time after the deposition of sediment (Flügel, 2004). Secondary porosity may be generated by diagenetic processes such as dissolution, fracturing and brecciation. Flügel (2004) estimated that the average porosity of calcareous sand and mud is between 40 and 80% and largely of an interparticle nature, with only a minor intraparticle contribution.

Ward (1973) noted that calcarenites that undergo early diagenesis in arid climates may retain more intergranular porosity than calcarenites subjected to diagenesis in humid environments where higher rates of cementation may occur. Land *et al.* (1967) also suggested that porosity within aeolianite may remain high in later stages of diagenesis in the vadose zone, but porosity would be lower in the phreatic zone.

#### **4.2.5 Diagenetic models**

Several researchers have attempted to correlate stages of diagenesis with the age of carbonate sediment deposits and have accordingly suggested models of diagenesis (Land *et al.*, 1967; Reeckman and Gill, 1981; Hearty and O’Leary, 2008). On the island of Bermuda, Land *et al.* (1967) conducted extensive studies on Quaternary calcarenite and reported five grades of diagenesis within the deposits, with each succeeding grade representing a greater degree of diagenesis. Land *et al.* (1967) suggested that during stage 1 calcarenite was unconsolidated; during stage 2 calcarenite consisted primarily of skeletal material, Mg-calcite and aragonite and was commonly cemented by calcite at grain contacts; stage 3 was characterised by limestone consisting of only calcite and aragonite with grain-skin cemented grains in which Mg-calcites were replaced by calcite; during stage 4 limestone is in the process of losing aragonite by dissolution; and during stage 5 stabilised limestone consists only of calcite.

Through examination of Quaternary calcarenite deposits at Warrnambool, Victoria, Reeckman and Gill (1981) concluded that three stages of diagenetic evolution were evident. They related the end of each stage with a specific deposit age; stage 1 ends at <90,000 years and is marked by the disappearance of high Mg-calcite; stage 2 occurs between 400,000 and 700,000 years and is marked by the disappearance of aragonite; while the end of stage 3 is characterised by the complete infilling of pore space by low-Mg calcite. Reeckman and Gill (1981) used radiocarbon and U-series methods to date these interglacial calcarenites. Due to

the effects of diagenesis on subaerially exposed carbonate grains and the ease of grain mixing within deposits, these ages must be treated with caution and regarded as approximations only.

Hearty and O'Leary (2008) applied and adapted the diagenetic model suggested by Land *et al.* (1967) to calcarenite deposits on the West Australian coastline. Hearty and O'Leary (2008) modified the original diagenetic model (Land *et al.*, 1967) by suggesting that sediment hardness was a factor of diagenesis; with increased hardness being indicative of a greater degree of diagenesis. Hearty and O'Leary (2008) also suggested that the colour of the soil covering Western Australia calcarenite deposits was correlative with diagenetic grade, whereby soils with increases in hue (towards redder values) and chroma were indicative of a greater degree of diagenesis (Figure 4.2).

Through a study of early vadose diagenesis in a range of Quaternary aeolianite from Oman, South India, the Bahamas, Tunisia, and Mallorca, Gardner and McLaren (1994) suggested that the application of a model of progressive sequences of changes throughout carbonate diagenesis was unsuitable outside the region in which the model had been developed. Gardner and McLaren (1994) concluded that while the end point of diagenesis within the studied aeolianite appeared to be low Mg-calcite allochems with meniscus, rim- and pore-filling cements, this occurred at differing rates in different localities and through various diagenetic pathways. Therefore, while rates of diagenesis may be found to vary with the age of the shoreline barriers on the Mount Gambier coastal plain it is not suitable to directly apply diagenetic models, such as those derived by Land *et al.* (1967) and Reeckman and Gill (1981), to the Bridgewater Formation.

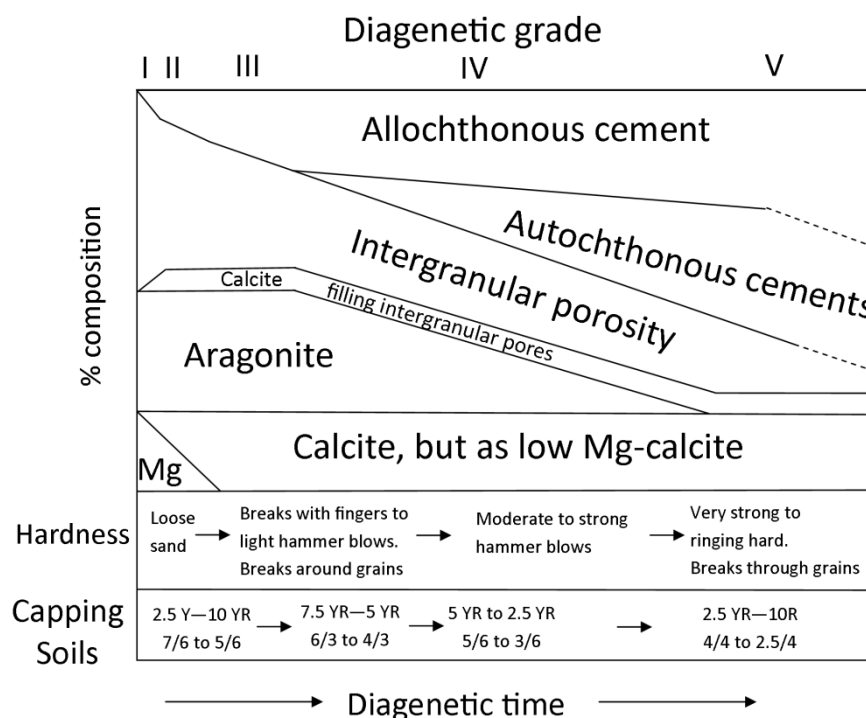


Figure 4.2: Varying diagenetic grades, modified from Hearty and O'Leary (2008).

### 4.3 Petrographic methods adopted within this study

In order to assess the degree of diagenesis within the Bridgewater Formation, a range of petrological methods were used as outlined in the section below.

#### 4.3.1 Thin section analysis

Thin sections of calcarenite were cut, where possible, perpendicular to laminae to aid in compositional assessment. Samples were ground optically flat to a thickness of 30  $\mu\text{m}$  and sealed on slides by glass cover slips. In several instances where sediment was weakly consolidated or not consolidated at all, samples were impregnated with resin. A total of 14 thin sections were analysed. At least one sample from each dune range was created, but the thin section from Don's Quarry was not clear enough to undertake point counting as the sediment was highly degraded and thus no sample was analysed from Mingbool Range. Samples were analysed by point counting methods as outlined by Flügel (2004). Within each slide 400 grains were counted and identified primarily on their microstructure and overall grain morphology (such as an elongate shape for molluscan fragments). Eleven separate categories (echinoid fragment, foraminifera, mollusc, algal fragment, bryozoan fragment, intraclast/lithoclast, quartz, opaque grains, void, cement/matrix, unknown) were identified



using criteria outlined in Appendix A. The proportion of grains in each class were then categorised following Brooke (1999) into dominant (>20%), major (15-20%), abundant (10-15%), common (5-10%), minor (2-5%) and rare (<2%).

Photomicrographs of thin section samples were also taken and used to analyse the type of cement (if present) between the framework grains. Cements were identified by their size and shape, as outlined by Flügel (2004) and are listed in Appendix A. Correct identification of framework grain proportions and cements between the grains may help determine the diagenetic environment of the sediment sampled.

#### **4.3.2 XRD analysis**

Powder X-ray diffraction (XRD) analysis was conducted on multiple sediment samples from sample sites within the dune ranges. The aim of this analysis was to determine and quantify the proportion of aragonite, high Mg-calcite, calcite and quartz within the dune ranges at each of the study locations. Any noticeable reductions in aragonite and high-Mg calcite with accompanying increases in calcite content may indicate a greater degree of diagenetic maturity of a sample. The CSIRO software package Siroquant was used to quantify XRD traces and these outputs determined mineralogical proportions.

The carbonate content of each of the sediment samples was also determined in order to assess whether there was an apparent trend between carbonate percentage and proposed age of the deposit. This was conducted by weighing each sample prior to the addition of 8M hydrochloric acid (HCl). HCl was continually added until the sediment was unreactive. The sample was then rinsed with distilled water and dried in a 110°C oven for two hours, before being weighed once more to determine the volume of carbonate dissolved by the acid. These results are discussed in comparison with other mineralogical characteristics in this chapter (see Table 4.2).

#### **4.3.3 Karst identification**

At each study site the degree of karst morphology was also readily noted. This included the structure and thickness of any calcrete units found capping the exposures at sampling sites. Size and number of solution pipes and rhizoliths were also noted systematically at each location. Certain karst features have previously been discussed at sample sites in their stratigraphical analyses (Chapter 3), but are summarised here and discussed in relation to diagenetic maturity of sample sites.

#### 4.3.4 SEM analysis of foraminifera

Foraminifera were hand-picked from sediment samples taken at each of the study sites. Foraminifera were then placed in glass test tubes, covered in Millipore water and sonicated for three minutes to remove any weak cements from the test surface. Tests were then dried and placed on carbon tabs which in turn were mounted on stubs with a 1 cm diameter. Stubs were then spray-coated with gold before being analysed under a scanning electron microscope (SEM).

Within each of the deposits *Elphidium crispum* tests were identified and were systematically used for AAR analysis (see Chapter 5). *Elphidium crispum*, therefore, was used preferentially for SEM analysis, though some *Discorbis dimidiatus* and *Ammonia beccarii* were also analysed in certain deposits to assess whether similar diagenetic textures were observed within different foraminiferal species. Assessment of varying textural surfaces, such as dissolution pits, recrystallisation of tests and the degree of cementation, was undertaken to evaluate differing diagenetic processes.

#### 4.4 Sediment texture and fabric of the Pleistocene Bridgewater Formation

The petrological characteristics of samples collected from exposures within the Bridgewater Formation on the Mount Gambier coastal plain are discussed in this section. Sample sites are shown in Figure 3.10. Figure 4.3 illustrates some of the bioconstituents found within sediment at the modern beaches. Bioclastic grains at the modern day Shelly Beach, Cape Northumberland, include bryozoan fragments, foraminifera, lithoclasts, and coralline algae. Images of the 250-500 µm fraction of sediment photographed with a 3D camera are presented (Figures 4.4, 4.5, 4.6). While viewing sediments at this size-fraction does not allow for analysis of the degree of sorting within a sample, this fraction is directly comparable to that used for whole-rock AAR analysis (Chapter 5).

Grain roundness is found to vary with sample sites, and is indicative of the varying energy regime and length of time sediments may have been exposed to such conditions. For example, grains from the modern beach are subangular, while grains from the Holocene beach deposit are more rounded, likely reflecting an extended exposure to high-energy beach conditions. Figures 4.4, 4.5, and 4.6 give a crude identification of the overall level of certain diagenetic features, for example cementation, visible in several of the samples. When comparing grains from different units within the Robe Range equivalent it is apparent that grains from the lower aeolianite unit at Port MacDonnell (Figure 4.4e) have retained more

cement than its proposed counterpart at Shelly Beach (Figure 4.4f) or the upper aeolianite unit at Port MacDonnell (Figure 4.4c). In contrast, sediment from the weathered aeolianite on Port MacDonnell Beach appears more highly cemented (Figure 4.4g). Comparisons of grains between sample sites from the MacDonnell Range also indicate varying energy environments. Samples from Swarts Quarry (Figure 4.4h) are duller in appearance than those from Narrawong (Figure 4.4i) which are well-rounded and very clear, perhaps indicative of less abrasion and a low energy depositional environment. Within more inland study sites (such as Dartmoor Cemetery, Figure 4.6a; and Fort O'Hare Quarry, Figure 4.6b) grains are commonly cemented together, perhaps indicative of diagenetic maturity, and have a sugary appearance suggestive of recrystallisation. While no direct diagenetic trends may be established from looking at these photographs alone they provide a good overall visual comparison of sediment changes observable with the naked eye and act as a reference point from which to compare more detailed assessments conducted later in the chapter.

Quartz grains were also studied to aid in determining the source origin of sediments. Kuenen and Perdock (1962) discussed how surface appearance of quartz grains varies between inland and coastal dunes. Quartz grains from inland dunes more commonly have a frosted, dull, opaque surface, while beach and fluvial quartz grains are more commonly polished in appearance, attributed to the mechanical action of waves and currents (Kuenen and Perdock, 1962).

The majority of quartz grains sampled from the Bridgewater Formation on the Mount Gambier coastal plain are clear and angular in appearance, reflecting a high-energy coastal origin. The original sources of this quartz are terrestrial environments and the quartz has likely been transported to the coast by the River Murray or the Glenelg River. Quartz grains from the modern Port MacDonnell Beach are rare but angular. Within the raised Holocene beach at Port MacDonnell grains are subangular, clear and have limited pitting on their surfaces, suggestive of continued abrasion. Within Robe Range aeolianite at Port MacDonnell and Shelly Beach, quartz grains are also subangular with a vitreous lustre, though they are duller in areas of pitting on the grain surface or where grains are more rounded. Quartz grains are subangular to subrounded and have a vitreous lustre at the Swarts Road sand quarry within the MacDonnell Range. At Narrawong, also within the MacDonnell Range grains are commonly clear, though frosted grains are also identified. Within Burleigh Range quartz grains vary; at Rabbitors Road, grains are generally angular and clear, reflecting coastal transportation, while those within the Laslett Road cutting are iron-stained and frosted,

suggesting that grains at this site have potentially been less affected by currents and waves. This supports the stratigraphical interpretation of the exposure at Laslett Road as a lagoonal deposit. Quartz grains at Rabbitors Road within Caveton Range are very small, duller and more frosted in appearance, again indicative of limited transport and supporting the stratigraphical interpretation of a lagoonal facies. Within Gambier Range at Gooch Road quartz grains are subangular and dull. Where grains are more rounded they are duller and more frosted in lustre. At Baxter's Quarry and Heritage Industries, within the Compton Range, quartz grains are small, angular and clear, indicating a coastal origin. Within Bridgewater Formation calcarenite exposed at Fort O'Hare Quarry, within the Dismal Range, quartz grains are sub-rounded to rounded and more frosted in lustre than other samples, indicating limited transportation. An exposure within Dismal Range at Mingbool village reveals quartz grains that are subangular and clear, indicative of a beach environment. Some quartz grains have been coated with *in situ* calcite cement indicative of diagenetic processes at this site.

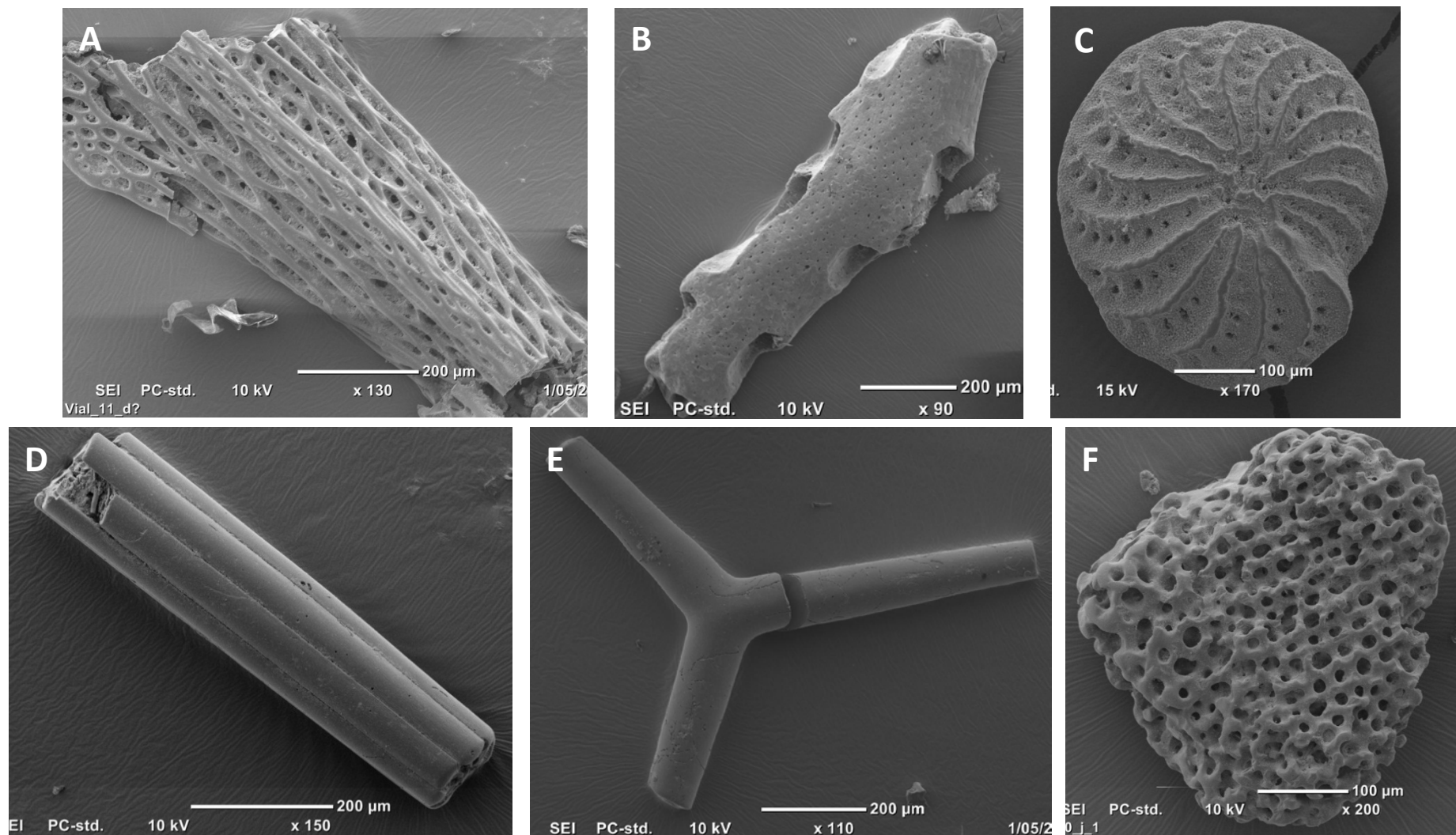


**Figure 4.3:** SEM image of bioconstituents from Port MacDonnell modern beach. **A** and **B:** Bryozoan fragments; **C:** Foraminifer (*Elphidium crispum*); **D:** Echinoid spine; **E:** Sponge spicule silica; **F:** Coralline algae.

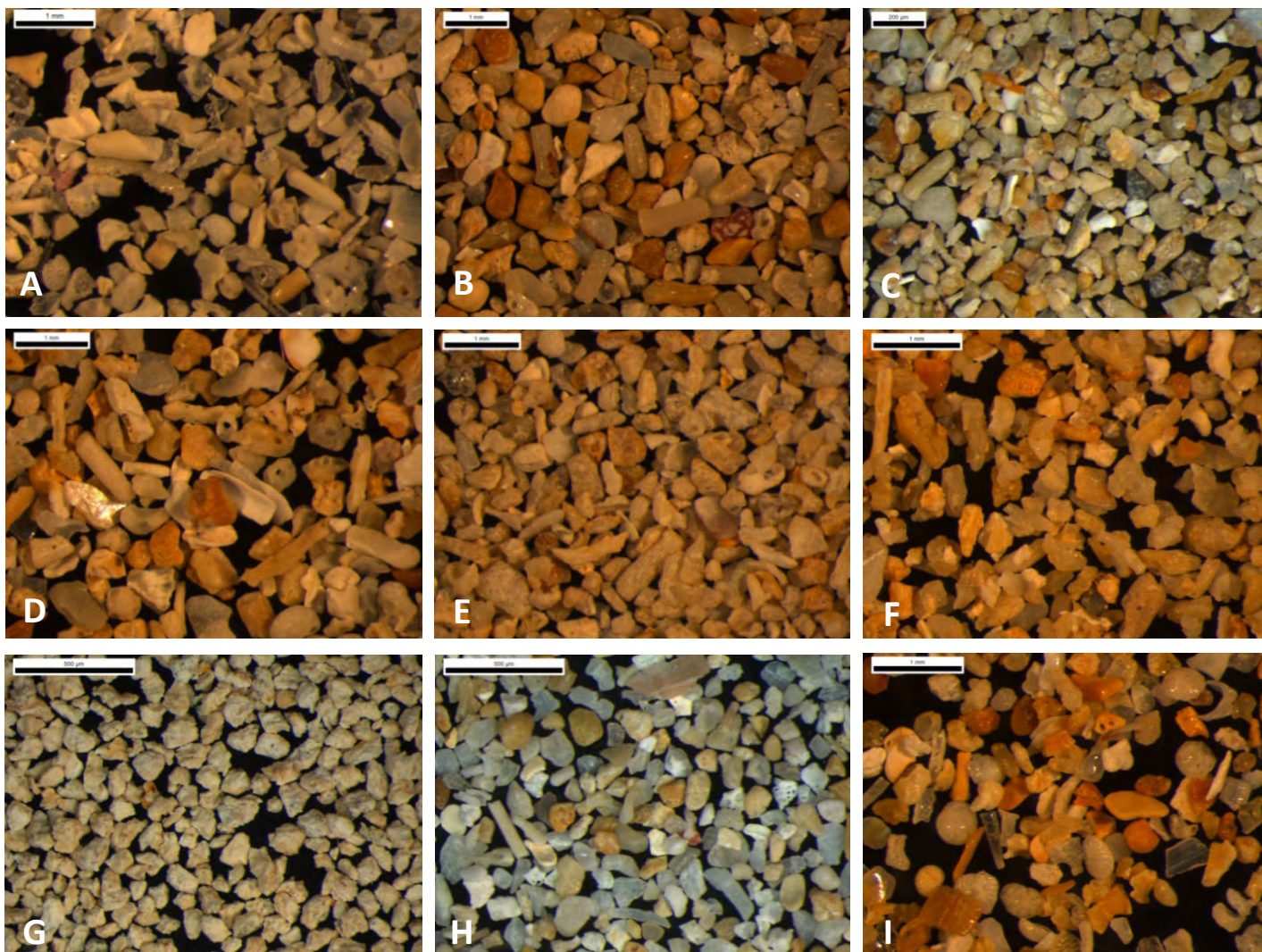


**Figure 4.4:** Images of the 250-500 µm fraction of samples of bioclastic sediment from the Mount Gambier coastal plain (generally increasing in relative age from A-I). **A:** Port MacDonnell Beach; **B:** Holocene back beach deposit, Port MacDonnell; **C:** Robe Range equivalent, upper Port MacDonnell aeolianite unit; **D:** Robe Range equivalent, upper Shelly Beach aeolianite unit; **E:** Robe Range equivalent, lower Port MacDonnell aeolianite unit; **F:** Robe Range equivalent, lower Shelly Beach aeolianite unit; **G:** Robe Range equivalent, weathered aeolianite Port MacDonnell Beach; **H:** MacDonnell Range, Swarts Road sand quarry; **I:** MacDonnell Range, Narrawong road cutting.



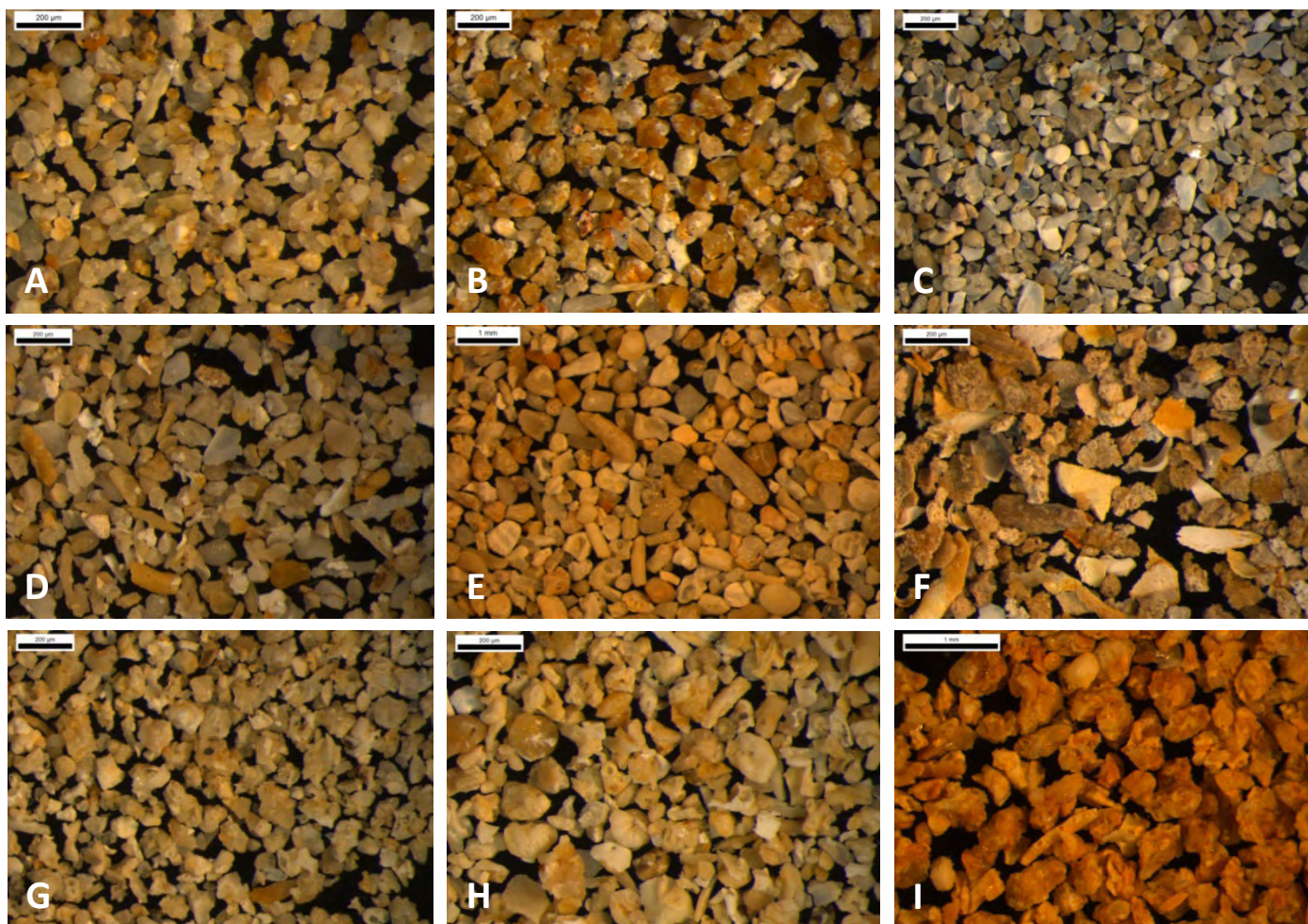


**Figure 4.5:** Images of the 250-500 µm fraction of samples of bioclastic sediment from the Mount Gambier coastal plain (generally increasing in relative age from A-I).  
**A:** Burleigh Range, Rabbitors Road; **B:** Burleigh Range, Laslett Road; **C:** Caveton Range, Rabbitors Road; **D:** Caveton Range, Bucks Hill; **E:** Gambier Range, Gooch Road;  
**F:** Gambier Range, Caroline Main Road; **G:** Compton Range, Baxter's Quarry; **H:** Compton Range, Heritage Industries; **I:** Mingbool Range, Don's Quarry.



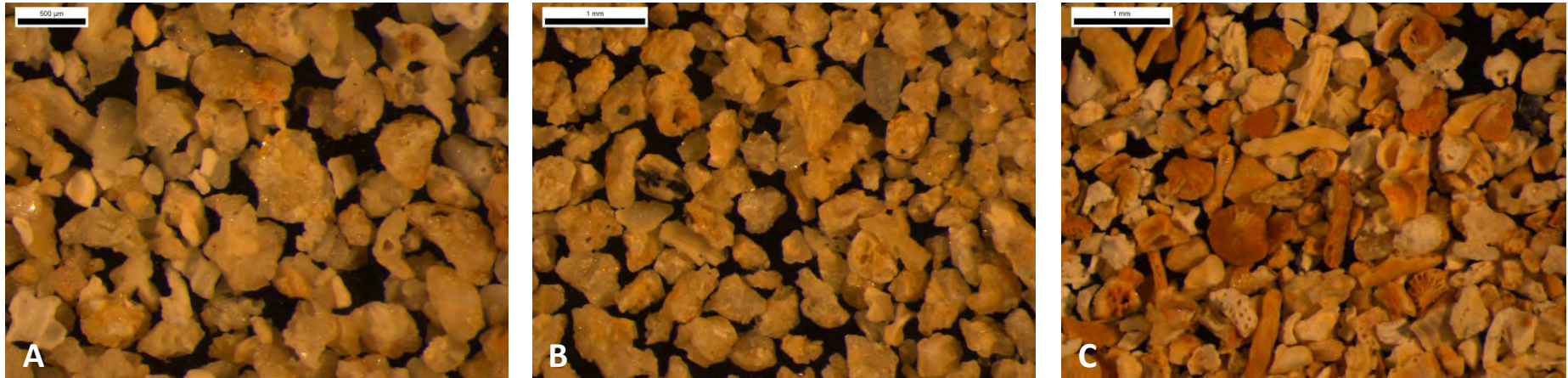


**Figure 4.6:** Images of the 250-500 µm fraction of samples of bioclastic sediment from the Dismal Range, Mount Gambier coastal plain. **A:** Dartmoor Cemetery; **B:** Fort O'Hare Quarry; **C:** Mingbool village.

The framework grains and cements (if present) within thin section samples are described to determine the depositional environment of the sample and to identify diagenetic processes. Samples are then compared with stratigraphical descriptions for each study site as presented in Chapter 3. Petrographic assessment of sediment samples may also aid in accounting for aberrant values obtained in AAR analysis of bioclastic sediments by the whole-rock method (Chapter 5); for example, samples that are highly cemented may yield lower values than expected due to the presence of younger cements.

Sediment for thin section analysis was sampled from representative sites across the coastal plain, with at least one sample compared from each dune range apart from Mingbool Range. Results from thin section point counting analyses are presented in Table 4.1 and sample locations are illustrated in Figure 3.11.

Increasing relative age  
↓

**Table 4.1:** Compositional data of thin sections derived from point counting 400 grains from representative samples across the Mount Gambier coastal plain

Dune Range	Sample site	Echinoid	Foraminifer	Mollusc	Algal fragment	Bryozoan fragment	Lithoclast	Quartz	Opaque grains	Void	Cement	Unknown	Coral	Total %
Modern Holocene	Shelly Beach*	5.75	0.25	18	10.75	1.25	43.5	0.75	4.75	N/A	N/A	15	N/A	100
	Port MacDonnell raised beach deposit*	10	5	36.6	4.3	4.5	30.8	3	3.8	N/A	N/A	2	N/A	100
Robe Equivalent	Port MacDonnell, upper aeolianite unit	4.75	1	21.5	3.75	3.75	19.5	3.5	9.25	14	11.75	7.25	N/A	100
Robe Equivalent	Port MacDonnell, weathered aeolianite	5.25	2	15.5	3.25	2	18.75	5.75	5	10.3	23.75	8.5	N/A	100
MacDonnell	Swarts Road sand quarry	10.5	0.25	30	7	4.75	21.75	10.5	3.25	0	0	12	N/A	100
Burleigh	Rabbitors Road*	17.25	5	22	4	13	4.5	21.75	8	N/A	N/A	4.5	N/A	100
Caveton	Rabbitors Road*	11.5	3.5	33	3	5.25	11.75	16.25	6.75	N/A	N/A	9	N/A	100
Caveton	Bucks Hill	12	9.5	17.25	2	12	3	2.5	5.5	21.8	4.25	10.25	N/A	100
Gambier	Gooch Road	6.5	2.75	13	2.75	2.5	9	22.75	2.75	0	33	5	N/A	100
Compton	Baxter's Quarry	7.25	1.5	15	2.75	3	10	12	3.75	13.5	25	6.25	N/A	100
Dismal	Dartmoor Cemetery	9.75	4.25	6	11.75	2.5	0.25	5.5	4	8.5	43.5	4	N/A	100
	Fort O'Hare Quarry	5.5	4.25	4.25	8	4.25	2.75	13.75	2.25	17.8	33.75	3.5	N/A	100
	Mingbool village	12.75	11.5	6.75	2	12.75	0.75	5	4.25	18	20.25	6	N/A	100
Naracoorte	Henschke Quarry	8.19	2.23	13.65	0	4.47	0	0.25	0.74	16.4	50.62	2.73	0.74	100

\*Denotes that sample was not consolidated when collected and thus was impregnated in blue resin to form a thin section

Proportion classes are based on that of Brooke (1999):

Dominant =  $\geq 20\%$ ; Major = 15 to 20%; Abundant = 10 to 15%; Common = 5 to 10%; Minor = 2 to 5%; Rare  $\leq 2\%$

#### **4.4.1 Modern beach, Shelly Beach**

Thin section analysis was conducted on the loose sediment collected from Shelly Beach so older samples could be compared with more recent sediment. This sample was impregnated in resin during thin section preparation. Carbonate grains are generally well-rounded to subrounded and reflect the high-energy beach environment of deposition. No cementation is observed around the edges of grains nor are there any signs of grain recrystallisation. Lithoclasts are the dominant component while molluscan fragments comprise a major proportion of grains. Algal fragments are abundant and echinoid grains are common (Figure 4.7a,b). Quartz grains are rare, which reflects a predominantly marine sediment source for this deposit. Foraminifers are also rare and this may be a result of the high energy beach environment which could potentially cause test destruction. Using Dunham's (1962) classification scheme (Table 3.2), which uses depositional texture to describe carbonates, this sediment sample may be classed as a grainstone.

#### **4.4.2 Holocene beach deposit, landward of Port MacDonnell Beach**

Fossil shell landward of Port MacDonnell Beach within a raised beach deposit thought to have been deposited during the Holocene sea-level highstand has been sampled for radiocarbon and AAR analyses (section 5.5.1). Loose sediment from this sample was impregnated with resin for thin section preparation. The grains are generally well-rounded to sub-rounded indicative of a high-energy beach environment, but are not as coarse as those found on the modern beach, perhaps indicating more sustained episodes of abrasion or a lower energy beach. The sample is dominated by molluscan grains and lithoclasts, while echinoid fragments and foraminifera are common confirming a marine source for this sediment. Algal and bryozoan fragments, quartz and opaque grains are minor components. Fine meniscus cement is present on the edges of grains, and some intra-pore regions (such as the pore-spaces of bryozoan fragments, Figure 4.7d) have developed a dog-tooth spar. More cement is present within this sample than observed at the modern beach and is perhaps suggestive of vadose weathering caused by minor wetting and drying through the overlying soil profile. The lack of mud within this sediment sample indicates that it may be classed as a grainstone after Dunham (1962).

#### **4.4.3 Robe Range equivalent, upper aeolianite unit, Port MacDonnell**

The upper aeolianite unit at Port MacDonnell, suggested to be an equivalent of Robe Range described in the Robe region by Schwebel (1984), was deemed to be a representative sample of this barrier succession. Sediment from this sample site was collected for both OSL and AAR analysis (Chapter 5) and thus assessment of petrological characteristics may prove useful.

Grains within this thin section are well-rounded and are indicative of aeolian transport. Mollusc fragments are the dominant framework grain, while voids are abundant indicating a moderate level of primary porosity. Lithoclasts are common, as is quartz. There is a notable increase in quartz content between the modern and Holocene beach samples compared with the Robe Range aeolianite. Echinoid and bryozoan fragments are minor components while foraminifers are rare. Cement is abundant between the framework grains and is predominantly micritic meniscus cement with some patches of blocky spar, whereby crystal size increases towards the centre of voids or chambers (Figure 4.7f). The presence of meniscus cement is indicative of a meteoric-vadose environment (Flügel, 2004). This sample may be defined as a grainstone due to the lack of mud within the sediment.

#### **4.4.4 Robe Range equivalent, weathered aeolianite, Port MacDonnell**

Geochronological analysis of Robe Range (presented in Chapter 5) will prove significant in constraining the age of a palaeo-beach stratigraphically below the aeolianite deposit. Petrological analysis of this deposit also allows direct comparisons with the aeolianite found in the cliff face 100 m farther west which, based on mapping, is stratigraphically equivalent. Grains within this deposit are mainly well-rounded (Figure 4.8a), suggestive of a high-energy environment such as aeolian transport, although quartz grains are subangular. Framework grains include echinoid fragments, quartz and opaque grains, which are common, while foraminifers, algal fragments and bryozoan are minor components. The sample is dominated by sparry calcite cement. A micritic rim has formed around grains and a dog-toothed spar has formed on this (Figure 4.8c). The crystal size of cements increases towards the centres of the voids similarly to drusy cement. Some echinoid fragments are filled with a blocky crystalline carbonate cement (Figure 4.8b), while foraminifera are generally in-filled with a finer micrite cement. This sample appears more cemented than in the upper aeolianite unit found in cliffs 100 m to the west, and is perhaps indicative of more frequent episodes of wetting and drying. A longer duration of wet periods may result in increased diagenesis. This aeolianite unit was found on Port MacDonnell Beach and is likely continually subjected to tidal influences which may account for the greater volume of cementation observed. The higher volume of cement within this sample means it may be classed as grain-supported packstone after Dunham (1962).

#### **4.4.5 MacDonnell Range, Swarts Road sand quarry**

Sediment collected from Swarts Road sand quarry was free-flowing and therefore impregnated with resin to allow a thin section to be created. This site was chosen to be representative of the MacDonnell Range (over the Narrawong sample site) as OSL analysis was undertaken on

sediment from this location. Grains in this deposit are subrounded indicating a high-energy depositional environment, potentially through aeolian transport, as indicated by steeply dipping beds (up to 14°) found in more consolidated sand at this site. Quartz grains are abundant (11%) within this sample, though smaller in size than other constituents. Lithoclasts dominate the deposit, while molluscan and echinoid fragments are abundant. Algal fragments are a common component, while bryozoan and opaque grains are minor and foraminifers are rare. The lack of foraminifers potentially reflects test destruction during long distance transport, or perhaps *in situ* leaching. Fine micritic meniscus cement (Figure 4.8e) is observed around many of the grains and is indicative of a meteoric-vadose diagenetic environment. Using Dunham's (1962) classification scheme this sample may be defined as a grainstone.

#### **4.4.6 Burleigh Range, Rabbitors Road**

Sediment collected for thin section analysis within this barrier was taken from the western face of the road cutting above the middle flint cobble lens (Figure 3.26). This thin section was made from an unconsolidated sample subjected to resin impregnation. Grains are sub-rounded to sub-angular and indicate a moderately high energy depositional environment. Grains are dominated by molluscan and quartz fragments. Quartz is a more dominant component in this sample than found in both the seaward MacDonnell Range, and the landward Caveton Range. Echinoid fragments comprise a major component, while bryozoans are abundant. Foraminifers and opaque grains are both common, while algal fragments and lithoclasts are minor constituents. Meniscus micrite cements are found between grains (Figure 4.9b) and suggest the sample has been above the water table where water has evaporated out of the system, indicative of a meteoric-vadose environment. The high volume of carbonate grains within this sample means that it may be described as a grainstone using the classification scheme of Dunham (1962).

#### **4.4.7 Caveton Range, Bucks Hill**

Consolidated sediment was analysed in thin section from Bucks Hill, an aeolianite deposit of the Caveton Range. Grains are subrounded indicating a moderately high-energy depositional environment. Voids are dominant and indicate high porosity of this deposit. Echinoid and bryozoan fragments are abundant, while molluscan fragments are a major constituent, indicating a primarily marine sediment source. Foraminifers and opaque grains are common, and algal fragments, lithoclasts and quartz comprise only a minor proportion of grains. Fine meniscus cement is observed between grains (Figure 4.9d) and indicates a vadose-marine environment. This sample is classed as a grainstone after Dunham (1962).

#### **4.4.8 Caveton Range, Rabbitors Road # 2**

Sediments of the lagoonal facies exposed within Caveton Range along Rabbitors Road were analysed in thin section to compare the petrological characteristics of this sample with the aeolianite at Bucks Hill within the same barrier, and with other barriers across the coastal plain. Sediment was unconsolidated when collected and therefore impregnated with resin to allow thin section preparation. Grains are subrounded to subangular and reflect a lower energy environment than observed in previously analysed deposits seaward of Caveton Range. Grains appear fine in thin section, which is confirmed by MasterSizer results (Table 3.9), and also indicates a low energy environment. Molluscan fragments dominate the deposit and quartz is also a major component. Echinoid fragments and lithoclasts are abundant while bryozoan fragments and opaque grains are common. Foraminifera and algal fragments are also identified and comprise minor proportions of the total grains counted. Micritic meniscus cement is found on the outside of grains and fine dog-tooth spar (Figure 4.9f) has developed within intra-pore regions. Cements are indicative of a meteoric-vadose diagenetic environment. The high volume of mud within this sample indicates that it can be described as a grain-supported packstone.

#### **4.4.9 Gambier Range, Gooch Road**

An exposure of Bridgewater Formation within Gambier Range along Gooch Road exposes a laminar bedded unit of calcarenite. Cemented laminar beds are interbedded with unconsolidated sands, and a sample from the cemented beds was analysed in thin section. The interbedding of consolidated and unconsolidated sands may indicate episodic wetting and drying or permeability variations with the unconsolidated sands draining more rapidly allowing more cement to be precipitated in the less permeable units. Grains are predominantly sub-rounded, though quartz grains are sub-angular. Quartz is a dominant component. Molluscan grains are abundant, while echinoid fragments are common indicating a primarily marine sediment source. Foraminifera, opaque grains and bryozoan fragments are minor constituents. Spar cement dominates this sample and no voids are identified by point counting, indicating limited porosity in this sample. Fine micrite cement is recognised on the edge of grains, upon which dog-toothed spar has developed. This spar cement becomes blocky towards the centre of inter-grain pore spaces (Figure 4.10b). Grain boundaries between carbonate crystals are compromised and yield a drusy mosaic, indicative of a near-surface meteoric or marine environment. This sample is also a grain-supported packstone after Dunham (1962).



#### **4.4.10 Compton Range, Baxter's Quarry**

Consolidated sediment from Baxter's Quarry was considered a representative sample from the Compton Range for petrological analysis as samples for AAR and OSL analyses were collected from this exposure (Chapter 5). The sample analysed in thin section was collected below the unconformity surface approximately 15 m from the eastern side of the exposure (Figure 3.38). Beds within this unit are laminated and finely deposited and are suggested to have been deposited in a subaqueous environment (section 3.8.8).

Grains are subrounded in shape. Molluscan fragments are a major framework grain in this cement-dominated thin section. Lithoclasts (predominantly of fragmented carbonate clasts) and quartz grains are abundant, while echinoid fragments are common. Opaque grains, bryozoan and algae are minor components while foraminifers are rare. While voids are abundant, grains are tightly packed. This sample is a grain-supported packstone after Dunham (1962). Micritic cements are present on the edges of grains (Figure 4.10d). Blocky spar cement has developed on top of this and fills pore spaces (Figure 4.10d). This later development of blocky sparite may be suggestive of a change from an exposed setting to a deeper, wetter environment below the water table. This would be consistent with the interpretation of this unit as a subaqueous deposit and is perhaps indicative of a sea-level transgression.

#### **4.4.11 Dismal Range, Dartmoor Cemetery**

A sample of consolidated sediment was collected from the exposure of Bridgewater Formation near to Dartmoor Cemetery. Grains appear subrounded and in places have been fragmented, possibly by dissolution processes, with some recrystallised pellets also identified. Echinoid and algal fragments are abundant in this sample, while molluscan and quartz grains are common. Voids are also common and indicate moderate porosity within the deposit. Bryozoan fragments, foraminifers and opaque grains are identified in minor proportions. The sample is dominated by calcite cement. A micritic rim has formed around grain edges, upon which a dog-tooth spar has developed, as has a blocky spar with larger crystals which fills pore spaces (Figure 4.10f). This sample is indicative of a marine environment similar to that observed at Gooch Road, Gambier Range. Using Dunham's (1962) classification scheme this sample can be described as a wackestone.

#### **4.4.12 Dismal Range, Fort O'Hare Quarry**

The sample of consolidated calcarenite analysed in thin section from Fort O'Hare Quarry was collected approximately 3 m beneath the unconformity that trends the length of the deposit

(Figure 3.47). Grains are sub-angular and suggest a lower energy depositional environment. Quartz grains are an abundant component, while echinoid and algal fragments are common framework grains. Foraminifers and bryozoans are identified in minor proportions and are further indicative of a primarily marine source. Voids are a major component and indicate moderate porosity. Calcite cement dominates the sample and is seen as a micrite cement on grain edges upon which clear dog-tooth spar has developed (Figure 4.11b,c,d), indicative of a meteoric or marine phreatic environment (Flügel, 2004). Drusy spar calcite has further infilled pore spaces, where calcite grains increase in size towards the pore centre. Similarly to the Dartmoor sample, this sample may also be described as a wackestone.

#### **4.4.13 Dismal Range, Mingbool village**

Consolidated sediment was collected from a small quarry near to the settlement of Mingbool for thin section analysis. Grains within the sample appear much redder in colour than previously analysed samples and suggest some iron staining of the sediment. Grains are subrounded and suggest a moderately high-energy depositional environment. Framework grains include echinoid, bryozoan fragments and foraminifers which are abundant and indicative of a primarily marine sediment source. Molluscan and quartz grains are common components, while algal fragments and opaque grains are identified in minor proportions. Meniscus micritic cements are found on grain edges, upon which isopachous dog-tooth spar has developed (Figure 4.11f). In certain pores, such as the chambers of foraminifers or intra-grain regions in bryozoans, drusy spar has developed (Figure 4.11e, 4.12a). Syntaxial overgrowth cements are also identified over certain echinoid grains (Figure 4.12b), indicative of a near-surface marine or vadose-marine environment (Flügel, 2004). This suggestion compliments the stratigraphical interpretation of this deposit (section 3.8.10) as a subaqueous depositional environment. This sample is not as mud-rich as those from Fort O'Hare and Dartmoor and may be described as a grain-supported packstone.

#### **4.4.14 Naracoorte Range, Henschke Quarry**

A thin section sample was collected from a consolidated calcarenite within Henschke Quarry, Naracoorte. It was hoped that petrological analysis of this deposit in thin section might help to identify whether this sample is from the Bridgewater Formation or the underlying Gambier Limestone. Grains are subrounded indicating a moderate energy depositional environment. Molluscan fragments are abundant, while echinoid fragments are common, suggestive of a primarily marine source. Foraminifers and bryozoan fragments are minor components while quartz is rare. The presence of coral, though rare, further indicates a marine sediment source. Coral has not previously been identified in the other seaward deposits and perhaps indicates a

difference in palaeoclimate at the time of deposition. This sample is dominated by calcite cement. Micritic cement is more abundant than seen in previous samples (Figure 4.12 c,d,e). Spar calcite is also present and is similar in character to that seen in many of the other deposits, with crystal size increasing towards the centre of pores. Thin section analysis suggests that while this sample is well-cemented, it is not significantly different from other Bridgewater Formation sediments previously analysed. The high mud content within this sample means that using Dunham's (1962) classification scheme this sample may be defined as a wackestone.

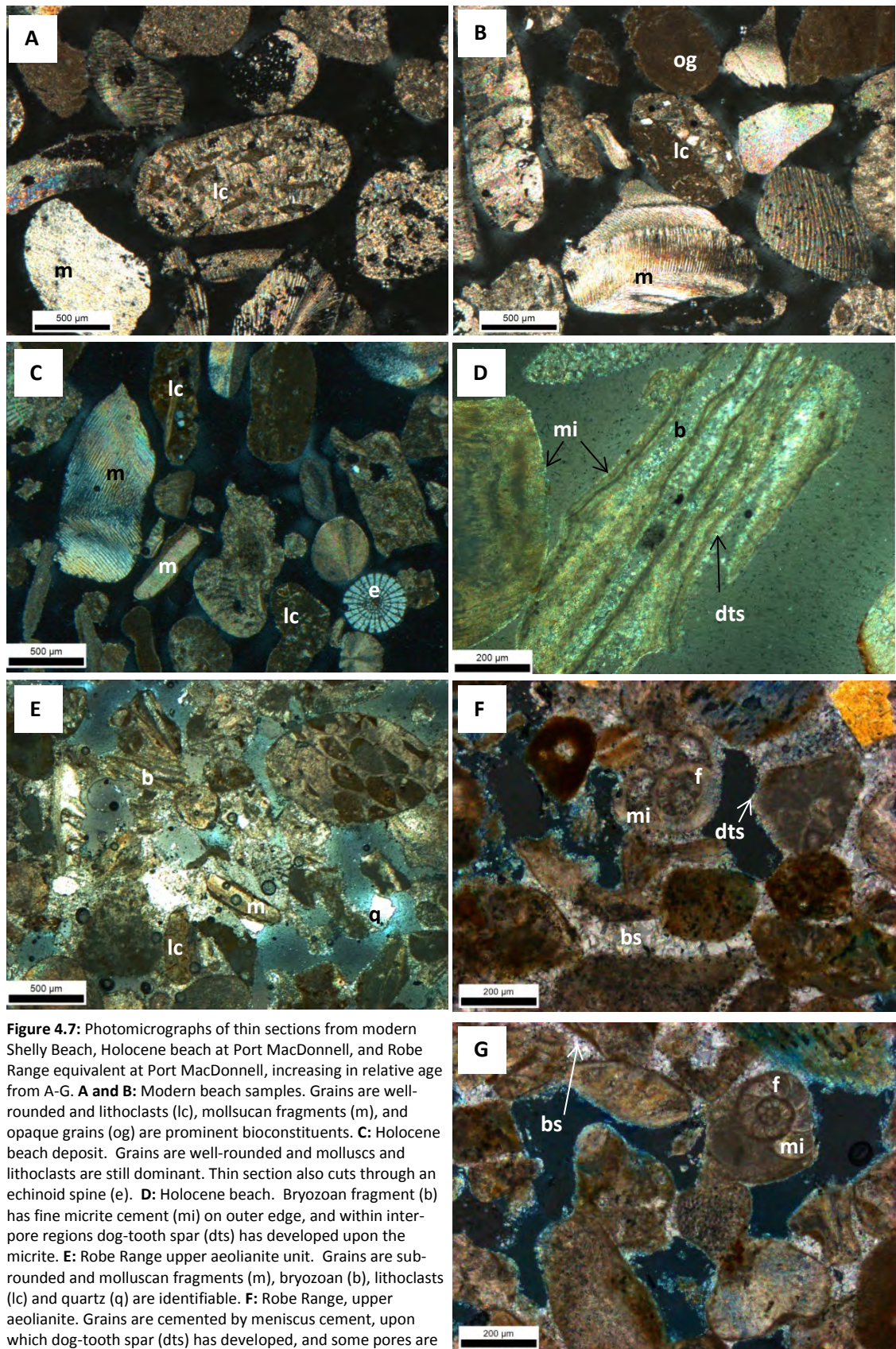


**Figure 4.7:** Photomicrographs of thin sections from modern Shelly Beach, Holocene beach at Port MacDonnell, and Robe Range equivalent at Port MacDonnell, increasing in relative age from A-G. **A and B:** Modern beach samples. Grains are well-rounded and lithoclasts (lc), molluscan fragments (m), and opaque grains (og) are prominent bioconstituents. **C:** Holocene beach deposit. Grains are well-rounded and molluscs and lithoclasts are still dominant. Thin section also cuts through an echinoid spine (e). **D:** Holocene beach. Bryozoan fragment (b) has fine micrite cement (mi) on outer edge, and within inter-pore regions dog-tooth spar (dts) has developed upon the micrite. **E:** Robe Range upper aeolianite unit. Grains are sub-rounded and molluscan fragments (m), bryozoan (b), lithoclasts (lc) and quartz (q) are identifiable. **F:** Robe Range, upper aeolianite. Grains are cemented by meniscus cement, upon which dog-tooth spar (dts) has developed, and some pores are filled by blocky spar (bs). **G:** Robe Range, upper aeolianite, also shows dog-tooth meniscus cement and blocky spar in intra-pore areas. Micrite cement (mi) is identified within foraminiferal chambers (f).



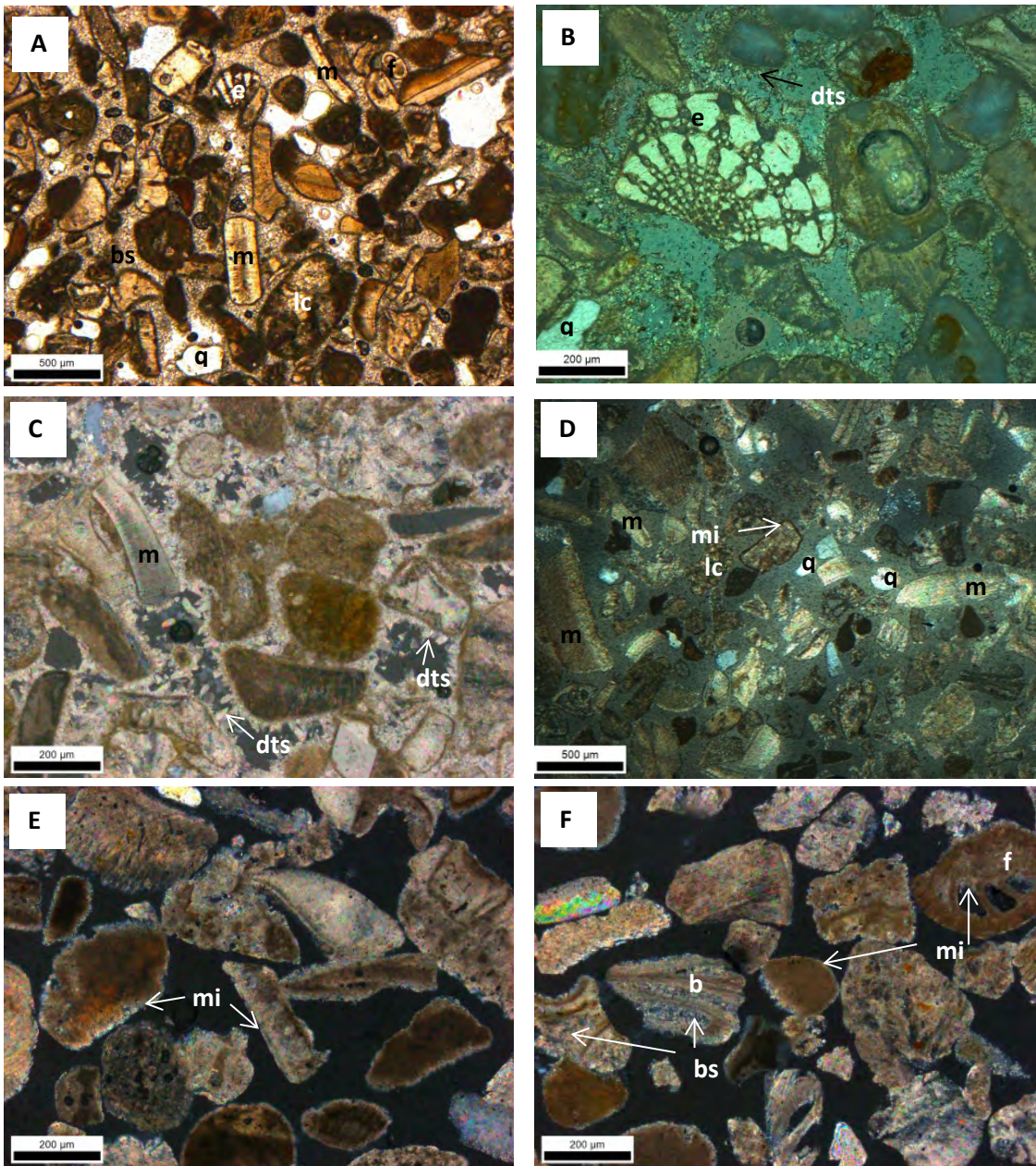


**Figure 4.8:** Photomicrographs of thin sections from the weathered aeolianite outcrop (A-C) on Port MacDonnell Beach and the MacDonnell Range (D-F) exposed at Swarts Road sand quarry. **A:** Grains are more cemented in this weathered outcrop than in the upper aeolianite unit 100 m west. Pore spaces are commonly filled by a blocky spar (bs) and common framework grains include molluscan fragments (m), foraminifer (f), echinoid fragments (e) and quartz (q) which is more frequently observed than in the modern and Holocene beach units. **B:** Meniscus cement is also identified and is commonly visible as dog-tooth spar (dts) that has developed upon a finer micrite. An echinoid (e) spine has filled with blocky carbonate spar cement. **C:** Dog-tooth spar (dts) is evident between grains in this sample. **D:** Unconsolidated sample from MacDonnell Range indicates grains are subrounded. Molluscan fragments (m), lithoclasts (lc) and quartz (q) are among the identifiable framework grains. **E:** Meniscus micrite cement (mi) is visible around grains. **F:** Again indicates the meniscus cement present around grains and for example, within foraminiferal (f) chambers. In some instances, such as between bryozoan fragments (b), a better developed blocky spar (bs) is identifiable. Grains are also highly corroded in this thin section.



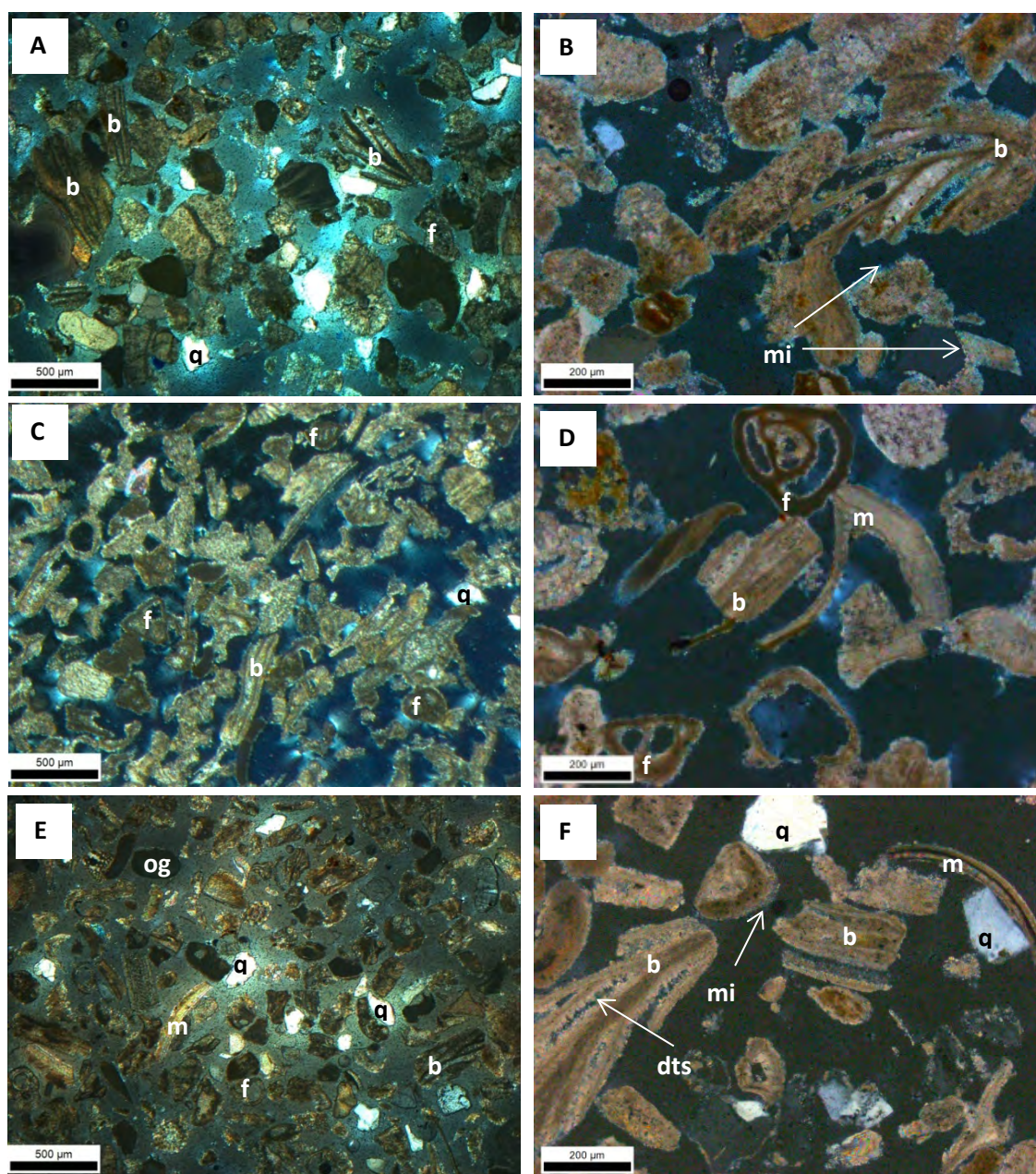


**Figure 4.9:** Photomicrographs of thin sections from Burleigh Range at Rabbits Road (A, B) and Caveton Range exposed at Bucks Hill (C, D) and Rabbits Road (E, F). **A:** Grains from Burleigh Range are subrounded to subangular indicating a high energy depositional environment. Identifiable framework grains include quartz (q), bryozoan fragments (b) and foraminifers (f). **B:** Grains are held together by a fine micritic meniscus cement (mi) indicating a meteoric vadose diagenetic environment. **C:** Framework grains from Bucks Hill are subrounded and include foraminifers (f), bryozoan (b) and quartz (q). **D:** Grains are connected by fine meniscus cement, which is also visible in intra-grain pores such as foraminiferal chambers. **E:** Grains within an exposure of Caveton Range at Rabbits Road are subangular in shape and indicate a lower energy environment. Framework grains include molluscan fragments (m), bryozoan (b), quartz (q) and foraminifera (f). **F:** While this sample was unconsolidated micritic meniscus cements (mi) are visible on the outer margins of grains. Within intra-grain pore spaces, such as within bryozoan fragments (b), dog-tooth spar (dts) is also visible.



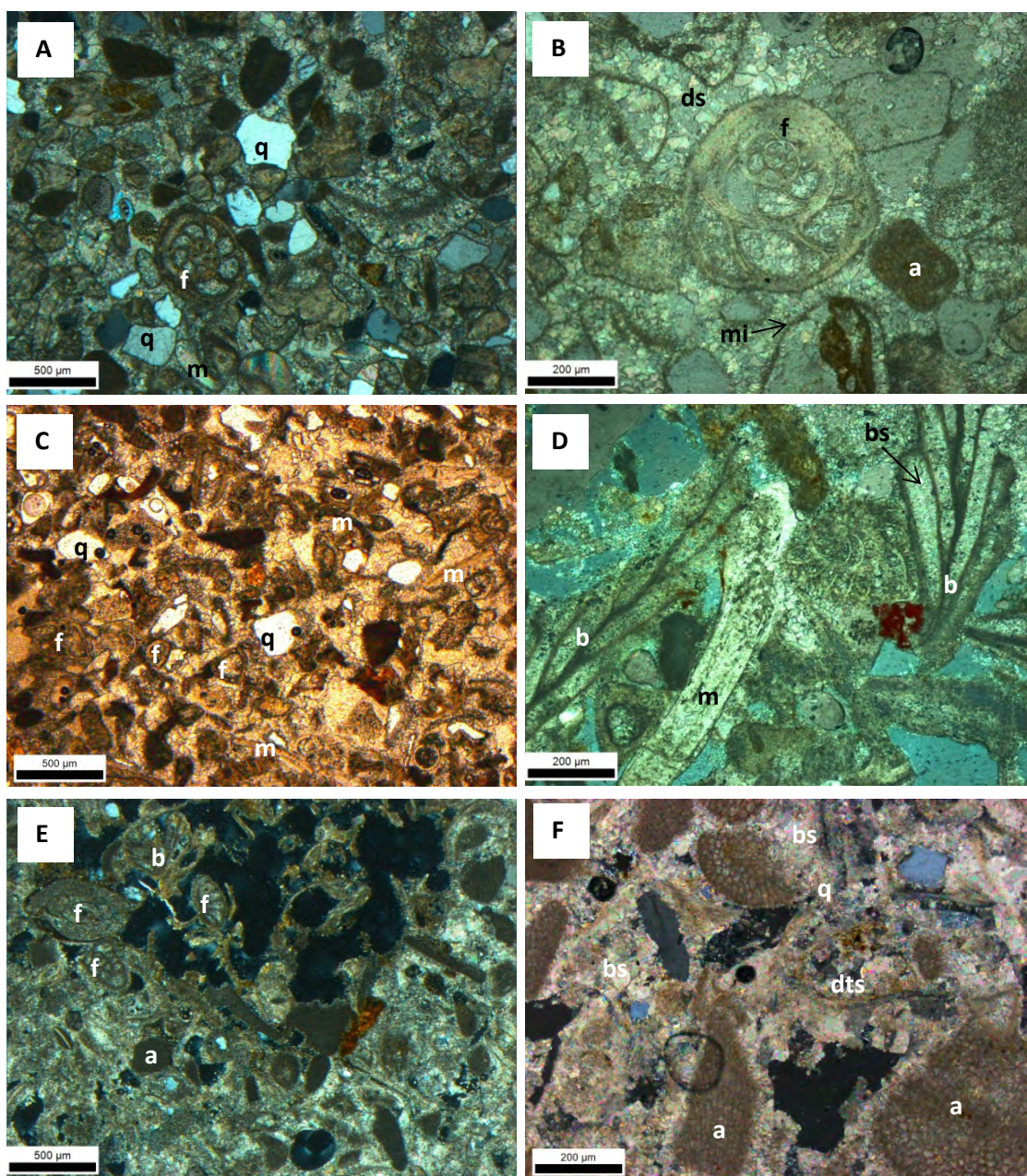


**Figure 4.10:** Photomicrographs of thin sections from Gambier Range at Gooch Road (A, B), Compton Range at Baxter's Quarry (C, D) and Dismal Range near Dartmoor Cemetery (E, F). **A:** Grains are subrounded and appear well-preserved. Foraminifera (f) exhibit all chambers intact, suggesting a lower energy environment. Other framework grains include molluscan fragments (m) and quartz (q). **B:** Voids were not observed in point counting, and grains are well-cemented. Fine micrite cement (mi) is observed on the outside of grains, upon which dog-tooth spar has developed. Towards the centre of pores the crystal size increases into drusy spar (ds). **C:** Grains within Baxter's Quarry thin section are well-rounded and tightly cemented. Framework grains include foraminifera (f), molluscan fragments (m) and quartz (q). **D:** A micritic rim has developed on grain edges. Blocky spar (bs) has developed later and infills many pore spaces. **E:** Grains are sub-rounded and highly cemented. Framework grains include bryozoan fragments (b), foraminifer (f), and algal fragments (a). **F:** A micritic rim coats grains upon which coarse dog-tooth spar (dts) has developed. Inter-pore spaces are filled with blocky spar (bs).



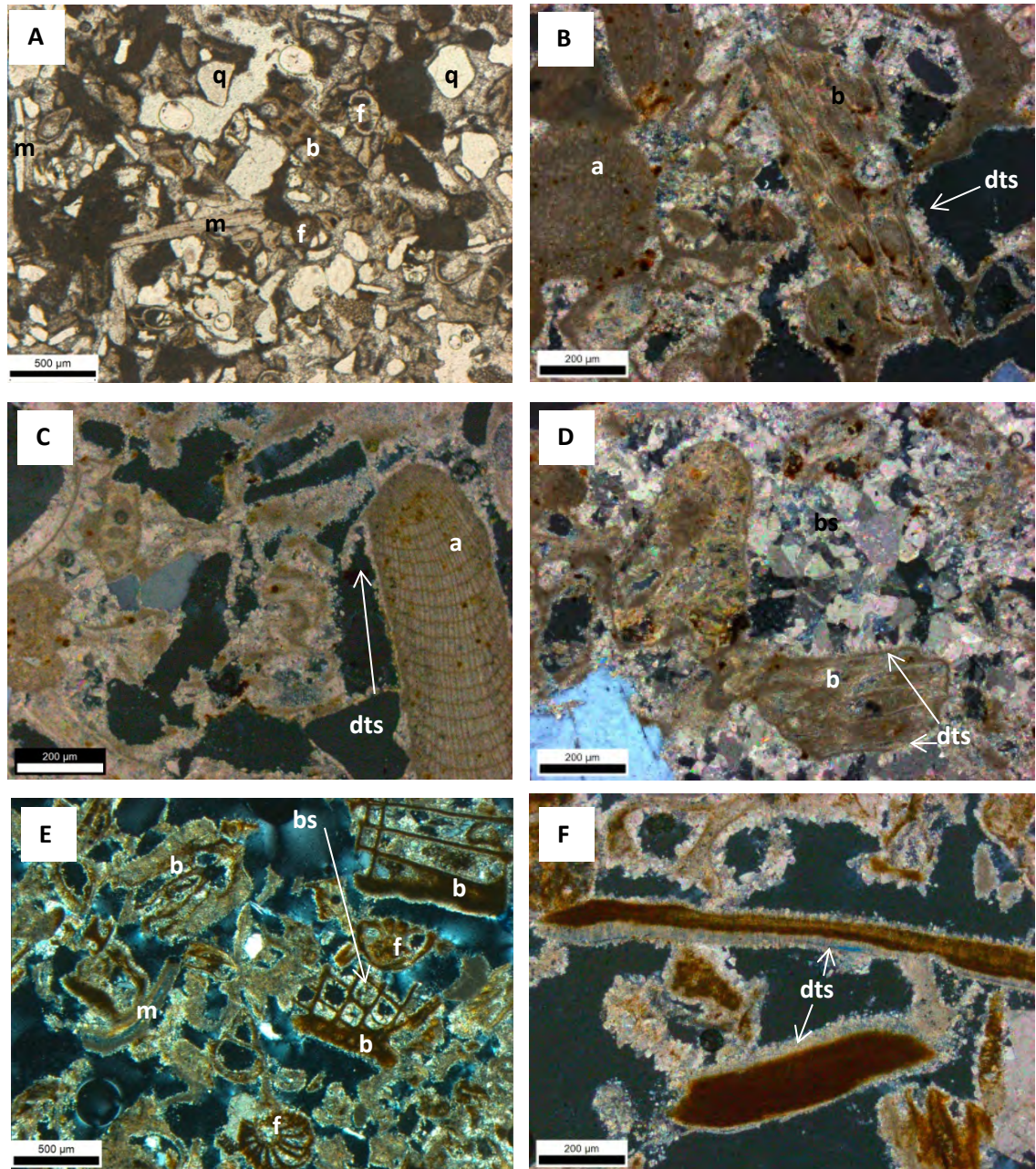


**Figure 4.11:** Photomicrographs of thin sections from Dismal Range exposed at Fort O'Hare Quarry (A-D) and Mingbool village (E, F). **A:** Grains are sub-rounded and tightly packed. Framework grains include molluscan fragments (m), bryozoan (b), quartz (q) and foraminifera (f). **B and C:** Dog-tooth spar (dts) has visibly formed as a meniscus around grains including algal fragments (a) and bryozoan fragments (b). **D:** Blocky spar (bs) has filled many inter-pore spaces. **E:** Grains are sub-rounded and in places grains appear fragmented as if affected by dissolutional processes. Framework grains include bryozoan fragments (b), foraminifers (f) and molluscan fragments (m). **F:** Grains are connected by meniscus cement. Fine micrite coats grains' outer surfaces and upon this isopachous dog-tooth spar (dts) has formed.



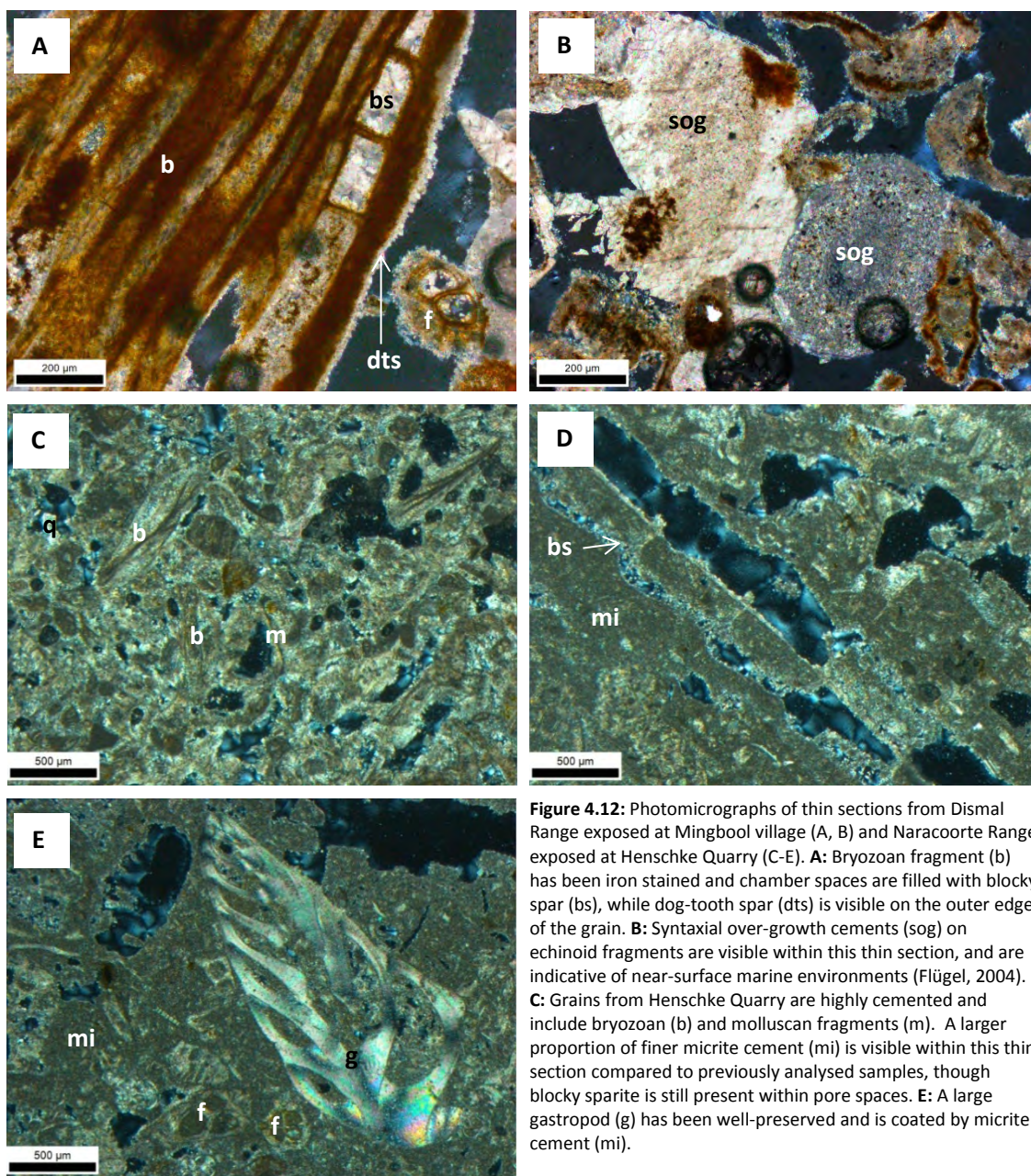


**Figure 4.12:** Photomicrographs of thin sections from Dismal Range exposed at Mingbool village (A, B) and Naracoorte Range exposed at Henschke Quarry (C-E). **A:** Bryozoan fragment (b) has been iron stained and chamber spaces are filled with blocky spar (bs), while dog-tooth spar (dts) is visible on the outer edge of the grain. **B:** Syntaxial over-growth cements (sog) on echinoid fragments are visible within this thin section, and are indicative of near-surface marine environments (Flügel, 2004). **C:** Grains from Henschke Quarry are highly cemented and include bryozoan (b) and molluscan fragments (m). A larger proportion of finer micrite cement (mi) is visible within this thin section compared to previously analysed samples, though blocky sparite is still present within pore spaces. **E:** A large gastropod (g) has been well-preserved and is coated by micrite cement (mi).

#### 4.4.15 Summary

Grains from each of the thin sections analysed vary in roundness; samples from the modern beach and Holocene beach are very rounded, indicating a high-energy environment. Other samples, such as those from Caveton Range exposure along Rabbitors Road and the exposure of Gambier Range at Gooch Road are less rounded and their more angular appearance potentially reflects diagenetic corrosion of test surfaces. Petrological examination of cements between framework grains can aid in determining the diagenetic environment of sediments. However, it is with caution these diagenetic trends are associated with sample age as diagenesis will vary depending on where within the deposit the sample has been collected. For example, samples collected near an exposed surface may have been subjected to more frequent wetting and drying episodes or more intensive diagenesis, which may have caused an increase in cementation within that sample.

Modern beach samples show no sign of cementation on grain peripheries, while fine meniscus cements are present on grains from the Holocene beach. This fine meniscus cement may have formed as water percolated down through the profile from the soil layer above. Consolidated sand from the upper aeolianite unit of the Robe Range equivalent at Port MacDonnell displays micrite meniscus cement with patches of blocky spar and indicates a meteoric-vadose diagenetic environment. The weathered aeolianite on Port MacDonnell Beach is highly comparable in the proportion of framework grains to the upper aeolianite, with a slight increase of quartz in this sample. The weathered aeolianite on the beach face is also more cemented than the upper aeolianite unit in the nearby cliffs and this is likely due to the exposure of the weathered unit to modern tidal forces on the beach face. Blocky spar cement within this unit is also indicative of a meteoric-vadose environment. Unconsolidated samples from MacDonnell Range indicate the presence of meniscus micritic cement, as do consolidated samples within Burleigh Range and Caveton Range, also indicating a meteoric vadose environment. Thin section analysis of sediment from Gambier Range at Gooch Road reveals a highly cemented unit, in which framework grains are filled with drusy spar cement, indicative of a near-surface meteoric or near-surface marine environment, consistent with its morphostratigraphic context (section 3.8.7; i.e. a subaqueous deposit). Cements between framework grains in Baxter's Quarry are visible as fine micrite upon which more blocky cement has developed and perhaps indicate periodic rise of groundwater or long-term submersion of this unit below the water table. Samples exposed within Dismal Range at Dartmoor and Fort O'Hare Quarry indicates the coating of grains with fine micrite, followed by the development of dog-toothed spar and blocky calcite cement. A similar pattern is visible within the exposure

near Mingbool village. Also present at this latter site are syntaxial overgrowth cements over echinoid grains which are indicative of a near-surface or vadose-marine environment. At Henschke Quarry, analysis of samples in thin section confirms that sediment from this locality is not significantly different from other samples of Bridgewater Formation collected across the Mount Gambier coastal plain.

In a study of coastal dune sequences in South Australia, Warren (1983) identified similar petrographic characteristics within Pleistocene sands. Warren (1983) found that individual sand grains were commonly coated in a micritic envelope and suggested this was formed by variations in the rate of water percolation and chemistry in a film of water surrounding the grains. Murray-Wallace *et al.* (2001) also noted similar petrographic characteristics when sampling sediments from the Coorong coastal plain. They found that the dominant framework grains included red algal, bryozoan and molluscan fragments and foraminifers, which are very similar to the dominant grains found on the Mount Gambier coastal plain, indicative of similar source and depositional environments. Coorong coastal plain grains were sometimes also found partially micritised with foraminiferal chambers and bryozoan pores commonly were infilled with micrite and micro-sparite (Murray-Wallace *et al.*, 2001). In general, there is an increase in cement content in samples on the Mount Gambier coastal plain that are presumed to be older based on their geographic position in relation to the modern shoreline. This may not necessarily relate solely to the age of the deposit but could be a function of the diagenetic environment to which the sediment has been exposed.

Volumes of quartz within sediment samples have also been identified to vary across the coastal plain (Figures 4.13, 4.14 and 4.15). Quartz is a minimal component in modern beach samples and from sites close to the present shoreline, while farther inland quartz comprises a larger proportion of the sediment sample. Four potential reasons for this variation in quartz content are proposed: 1) carbonate productivity has varied throughout interglacials within the Mid-Pleistocene with barrier successions with greater quartz volumes indicating reduced carbonate production during their corresponding interglacial; 2) sediment within barrier successions where quartz is a more dominant component may have been subjected to greater distances of transport, or higher energy entrainment which has resulted in greater abrasion of carbonate grains in relation to more resistant quartz; 3) barrier successions containing greater volumes of quartz may have been subjected to greater diagenesis, resulting in dissolution of a higher proportion of carbonate grains; 4) as the coast progrades with successive interglacials each ridge is farther from the inland sources of quartz.

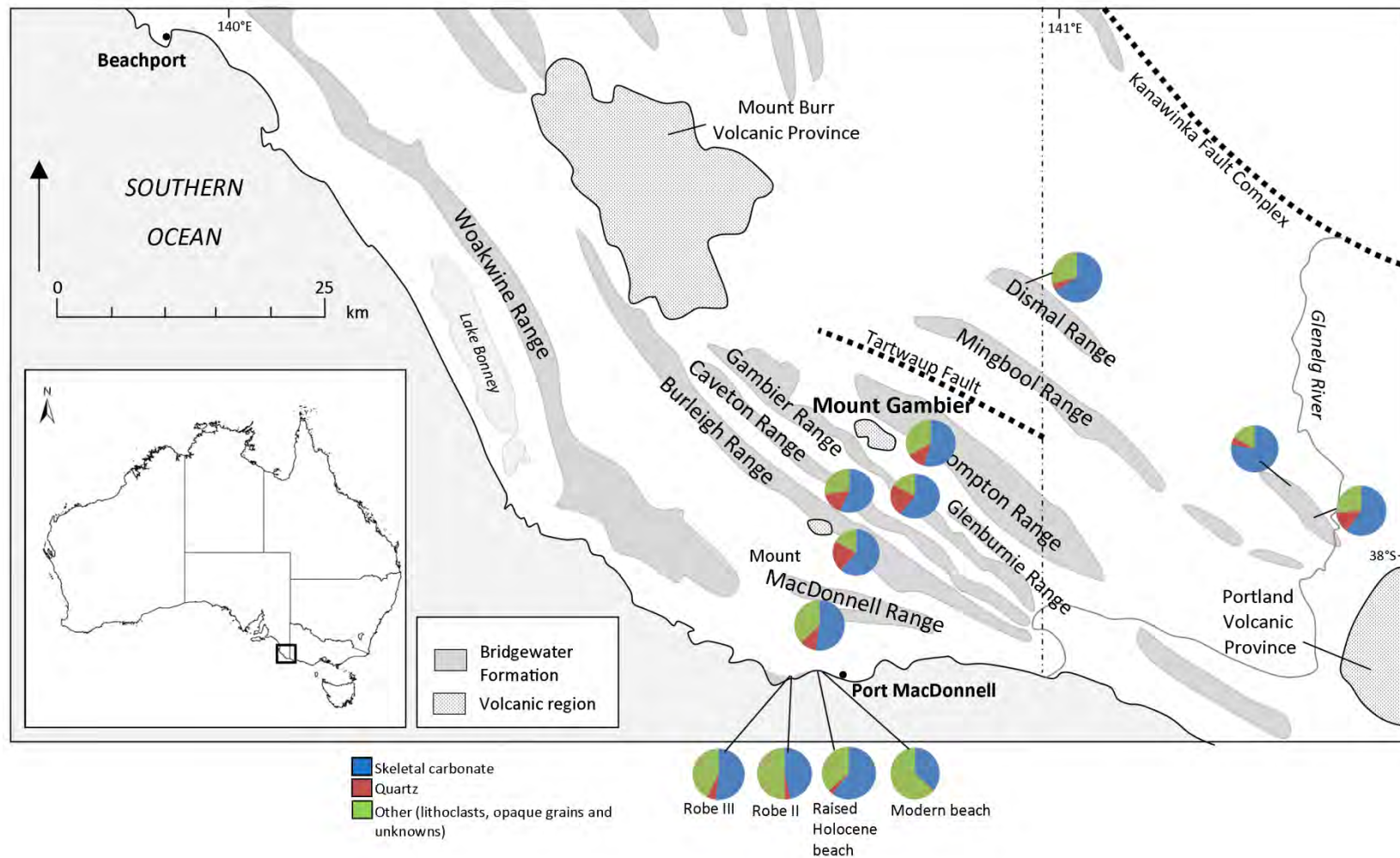


**Figure 4.13:** Pie charts illustrating the percentage of skeletal carbonate and quartz within sediment samples across the Mount Gambier coastal plain. Percentages are derived from point counting 400 grains in thin section. Quartz grains are rare from sample sites close to the present coastline, and are more abundant in some farther inland sites potentially reflecting dissolution of carbonate grains within these presumably (based on geographic location) older samples.

#### **4.5 Mineralogy of sediments on the Mount Gambier coastal plain**

Results from powdered XRD analyses of the proportions of aragonite, high and low Mg-calcite (referred to as calcite here) and quartz are reported in Table 4.2. Figure 4.14 is an area plot of these results and graphs the mineralogy of each sample in increasing (proposed) age order, reading from left to right, based on the geographical location of the barrier in relation to the present coastline. Figure 4.15 also displays results in a plot with mineralogy plotted against the proposed MIS of each barrier. Results indicate a low percentage of quartz in younger samples, consistent with the thin section grain counts. Quartz proportions increase in (proposed) late Pleistocene samples followed by a gradual decrease and plateau observed in middle Pleistocene samples. This increase in quartz could be a reflection of reworking from non-marine sourced sediments in older ranges or dissolution of carbonate grains within the deposit, as discussed earlier. There is an obvious decrease in percentages of aragonite from younger to older samples, which appears to have been replaced by calcite. This trend is also observed in decreases in high-Mg calcite with relative age, where high-Mg calcite has been replaced by low-Mg calcite. These mineralogical changes may reflect the diagenetic maturity of the samples.

The ternary plot (Figure 4.16) also demonstrates this trend, with younger samples containing greater proportions of high-Mg calcite and aragonite, and older samples clustering towards areas of abundant low-Mg calcite and low percentages of aragonite and high-Mg calcite.



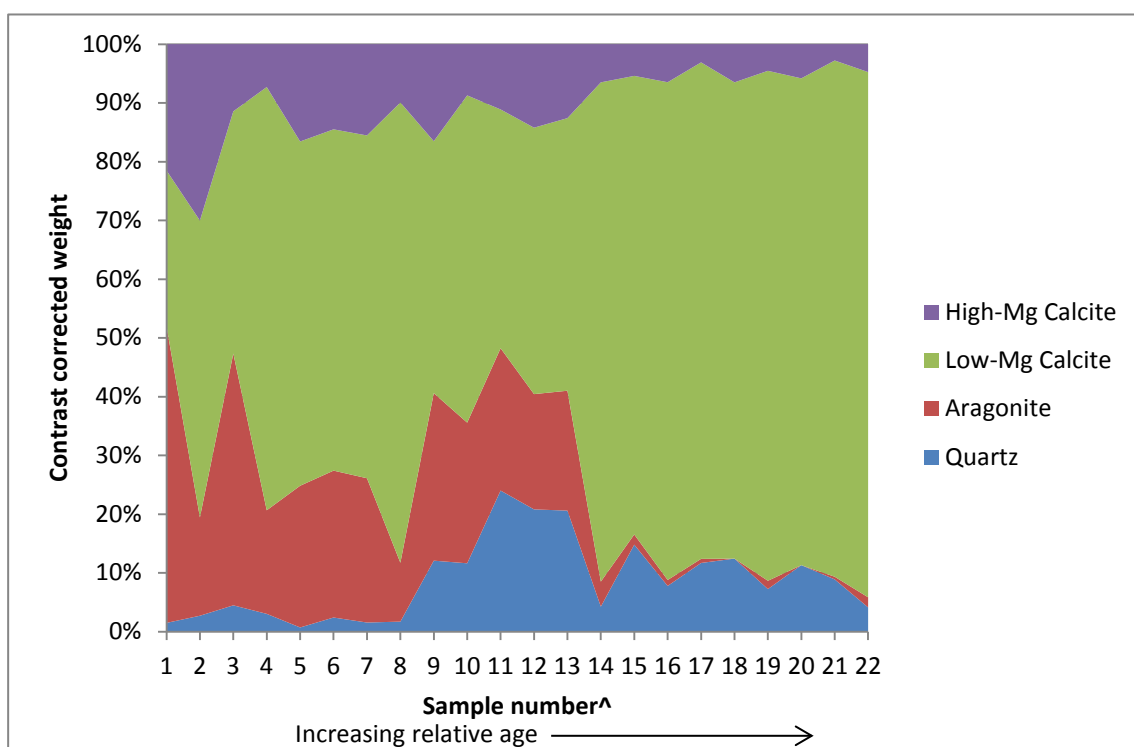


**Figure 4.14:** Area graph highlighting the mineralogical change in sediments from the Bridgewater Formation on the Mount Gambier coastal plain with increasing distance inland and proposed age from right to left (^denotes that the sample number correlates with that in Table 4.2).

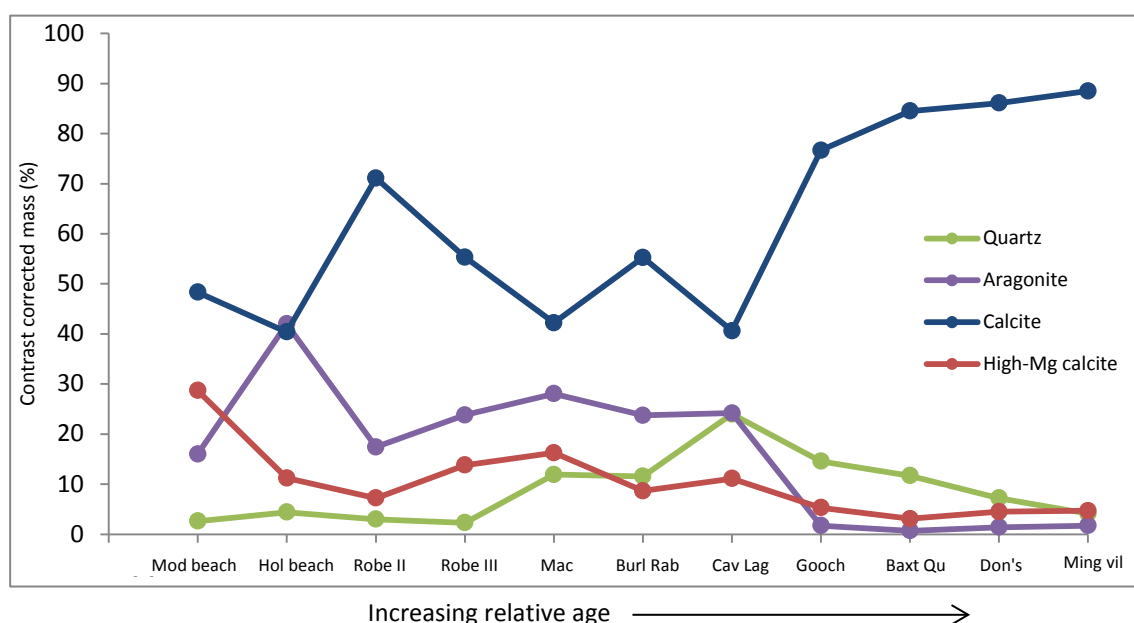


**Figure 4.15:** Plot identifying trends in mineralogy of sediment samples across the Mount Gambier coastal plain plotted against proposed MIS based on geographical position of barrier successions in relation to the modern shoreline. [Mod beach = Port MacDonnell, Hol beach = Holocene beach, Port MacDonnell, Robe II and Robe III = Robe Range equivalent at Port MacDonnell, Mac = Swarts Road, MacDonnell Range, Burl Rab = Burleigh Range at Rabbitors Road, Cav Lag = Caveton Range lagoonal facies unit 2, Gooch = Gambier Range at Gooch Road, Baxt Qu = Baxter's Quarry, Compton Range, Don's = Don's Quarry, Mingvil = Mingbool village, Dismal Range].



**Table 4.2:** Mineralogical composition of representative samples across the Mount Gambier coastal plain derived by powdered XRD analysis

Dune Range	Sample site	Contrast corrected mass				Sample number <sup>^</sup>	% CaCO <sub>3</sub> determined by HCl
		Quartz	Aragonite	Calcite	High-Mg calcite		
Modern	Shelly Beach	1.5	50.5	26.5	21.5	1	99
	Port MacDonnell Beach	2.6	16	48.3	28.7	2	99
Holocene	Port MacDonnell back beach deposit	4.4	42	40.4	11.2	3	99
Robe Equivalent	Port MacDonnell, upper aeolianite unit	3	17.4	71.1	7.2	4	99
	Shelly Beach, upper aeolianite unit	0.7	23.3	56.6	16	5	99
	Port MacDonnell, lower aeolianite unit	2.3	23.8	55.3	13.8	6	99
	Shelly Beach, lower aeolianite unit*	4.55	15.45	67.7	8.85	7	98
	Weathered aeolianite, Port MacDonnell Beach	1.8	10.5	82.1	10.4	8	99
MacDonnell Range	Swarts Road, Allendale East*	11.9	28.05	42.2	16.25	9	97
Burleigh Range	Rabbitors Road*	11.55	23.75	55.25	8.65	10	93
Caveton Range	Rabbitors Road, Unit 2	24	24.2	40.6	11.1	11	87
	Rabbitors Road, Unit 4	20.8	19.6	45.3	14.2	12	92
	Rabbitors Road, Unit 8	20.3	20.1	45.7	12.4	13	
	Bucks Hill	4.2	4.2	83.7	6.4	14	97
Gambier Range	Gooch Road*	14.55	1.7	76.65	5.3	15	88
Compton Range	Grey St, Mount Gambier	7.7	1	83.7	6.4	16	
	Baxter's Quarry	11.7	0.7	84.5	3.1	17	66
	Heritage Industries*	12.35	0	80.45	6.45	18	90
Mingbool Range	Don's Quarry	7.2	1.4	86.1	4.5	19	96
Dismal Range	Dartmoor Cemetery	11.1	0	81.2	5.7	20	96
	Fort O'Hare Quarry*	8.8	0.45	86.85	2.75	21	75
	Mingbool village	4.1	1.7	88.5	4.7	22	99
N/A Siliceous sands	North of Mt. Gambier	88.1	2.4	0.4			

\*Denotes that values for this site are an average of two whole-rock samples taken from within the same facies. <sup>^</sup>Denotes the sample number in relation to the x-axis in Figure 4.14

Note that calcium carbonate percentages as determined by HCl vary from the percentage of carbonate grains counted in thin section analysis. This may be a result of inaccuracies in sample weighing or the number of voids counted within thin sections that are not accounted for in HCl digestion.

Note, the remaining 8 % within the siliceous sand sample was comprised of hornblende, biotite and muscovite.

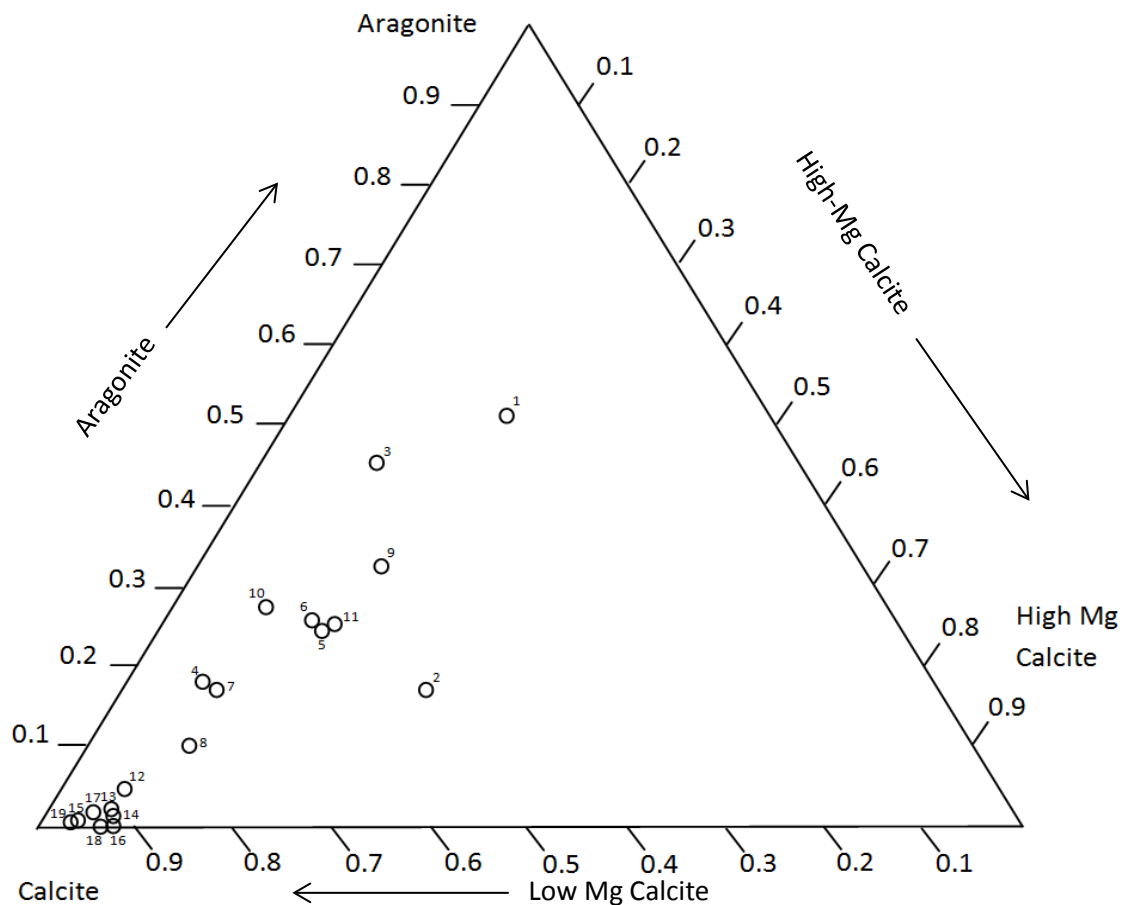


**Figure 4.16:** Ternary plot of XRD results from samples within Bridgewater Formation across the Mount Gambier coastal plain. **1:** Modern beach, Shelly Beach; **2:** Modern beach, Port MacDonnell; **3:** Holocene beach deposit; **4:** Upper aeolianite unit Port MacDonnell; **5:** Upper aeolianite unit Shelly Beach; **6:** Lower aeolianite unit Port MacDonnell; **7:** Lower aeolianite unit Shelly Beach; **8:** Weathered aeolianite Port MacDonnell Beach; **9:** MacDonnell Range, Swarts Road; **10:** Burleigh Range, Rabbitors Road; **11:** Caveton Range, Rabbitors Road; **12:** Caveton Range, Bucks Hill; **13:** Gambier Range, Gooch Road; **14:** Compton Range, Grey Street; **15:** Compton Range, Baxter's Quarry; **16:** Compton Range, Heritage Industries; **17:** Mingbool Range, Don's Quarry; **18:** Dismal Range, Dartmoor Cemetery; **19:** Dismal Range, Fort O'Hare Quarry; **20:** Dismal Range; Mingbool village

Calcium carbonate contents were also approximately analysed by adding 8 M HCl to sediment samples. These results (Table 4.2) indicate carbonate contents vary between 66% and 99% for each of the sample sites, and therefore non-carbonate grains are generally minimal. Huntley *et al.* (1993a) and Murray-Wallace *et al.* (2001) found carbonate contents on the Coorong coastal plain to range between 60 and 80%. Sources for the quartz and other non-carbonate material have been suggested by several authors. Sprigg (1979) suggested that quartz may have been transported down the River Murray and therefore the quartz content of the dune ranges would decrease with increased distance from the river mouth. Blackburn *et al.* (1965) proposed that quartz within the older dune ranges may have been deposited by drainage from the Grampian Mountains by the Glenelg River. Huntley *et al.* (1993a) suggested that some quartz may be derived from the reworking of older sediments such as the Late Miocene - Early Pliocene Loxton-Parilla Sands.

Warren (1983) also found similar trends in mineralogy when examining X-ray results from Holocene and Pleistocene calcarenites in South Australia. Warren (1983) suggested that Pleistocene dune sands were depleted in aragonite and high-Mg calcite while enriched in low-Mg calcite compared with their Holocene counterparts. James *et al.* (2005) analysed shelf sediments from the Great Australian Bight and Lacepede shelves and suggested that aragonite may be lost before sediments have even exited the marine diagenetic environment. James *et al.* (2005) suggested that the loss of aragonite may be due to dissolution in the shallow subsurface as a by-product of the degradation of bacteria within organic matter.

In summary, XRD analysis from sediment samples on the Mount Gambier coastal plain indicates that samples that are a greater distance inland, and presumed to be older in age, have a greater diagenetic maturity due to the decrease in aragonite and high-Mg calcite, and an increased proportion of low-Mg calcite. The increase in low-Mg calcite in older samples also compares well with thin-section analysis, which indicates an increase in cementation in older samples and thus an increase in the proportion of sparry calcite between pores.

#### **4.6 Karst development**

The size and number of karst features within exposures of the Bridgewater Formation are found to vary and do not appear to correlate with the proposed age of the deposit based on the geographical location of successions to the present coastline. Common karst features recognised include solution pipes, while secondary carbonate features such as calcrete horizons and rhizoliths are indicative of subaerial exposure. Table 4.3 compares the size and frequency of these features observed at representative sample sites across the Mount Gambier coastal plain.

Table 4.3: Summary of karst features found at sample sites across the Mount Gambier coastal plain						
<div>Increasing relative age</div> <div>↓</div>	Sample site	Karstic features present	Secondary carbonate features	Thickness/size of feature	Density/frequency of feature within exposed unit	Further notes and descriptions of feature
	Port MacDonnell modern beach		None identified			
	Holocene beach deposit, Port MacDonnell		None identified			
	Upper aeolianite unit, PMD		Calcrete horizon	75 cm thick		Rubbly calcrete
	Upper aeolianite unit, SB		Calcrete horizon	1 m thick		Massive to rubbly in places
	Lower aeolianite unit, PMD		Calcrete horizon	75 cm thick		Massive
			Palaeosol above this	10 – 30 cm thick		<i>Terra rossa</i> soil has sharp contact with overlying aeolianite
	Lower aeolianite unit SB		Potentially eroded palaeosol	25 cm thick		An undercutting between the two aeolianite unit perhaps represents an eroded palaeosol
	MacDonnell Range – Swarts Road quarry		Calcrete horizon	30 cm thick	Both rhizolith unit and calcrete is found across the 10 m width of the exposed upper surface of the sand quarry	Rubbly calcrete
			Rhizoliths	Unit of rhizoliths 1 m thick. Individual rhizoliths are on average 1 cm wide and up to 30 cm thick		Rhizoliths are extensive and very dense with up to 30 root cast features within a 1 m wide section
	Woakwine Range – Lake Hawdon South		Calcrete horizon	30 cm thick	Extends length of exposure	Massive calcrete
	Burleigh Range – Rabbitors Road		Rhizoliths	Rhizoliths are up to 1 m high and 30 cm wide	Not abundant but recognised in 4 or 5 isolated regions	
		Solution pipes		Solution pipes range from 50 cm to 3 m high and from 15 to 40 cm wide.	21 solution pipes identified in a 110 m exposure on western side of the road. Solution pipes yield a cumulative width of 2.6 m (2.4%) within the exposure.	Some solution pipes are infilled with terra rossa soils and rhizoliths. Others are stained orange indicating the former presence of soils.
	Burleigh Range – Laslett Rd		None identified			
	Caveton Range – Rabbitors Road		Calcrete horizon near top of exposure	15 cm thick	Recognised through the 25 m wide exposure	Rubbly calcrete
	Caveton Range – Bucks Hill	None identified				
	Gambier Range –Gooch Rd	None identified				
	Compton Range – Baxter’s Quarry	Solution pipes		Solution pipes vary in width from 20 cm to 1 m, and in height from 3m to 20 cm.	27 solution pipes are identified above and below unconformity, within 75 m wide exposure. Solution pipes yield a cumulative width of 4.54 m (6%)	Some solution pipes are infilled with <i>terra rossa</i> soils. Some solution pipes extend down from the unconformity surface while others extend from the upper surface of the exposure. 3 solution pipes have extended from this upper surface down past the unconformity surface.
	Compton Range – Heritage Industries	Solution pipes		Range from 30 cm to 1 m in width, and up to 3 m in height, though full extent not visible due to overlying vegetation.	13 solution pipes within a 13 m wide exposure. Solution pipes yield a cumulative width of 8.2 m (51%)	Solution pipes are very wide and in some cases have been filled with red-orange <i>terra rossa</i> soils. In places multiple solution pipes have merged.
	Mingbool Range – Don’s Q		None identified			
	Dismal Range – Dartmoor Cemetery	Solution pipes		Solution pipes range from 30 cm to 1 m high and from 10 to 30 cm wide.	~18 solution pipes are identified within the 120 m exposure.	Solution pipes are concentrated towards the western end of the exposure. Some have infilled with <i>terra rossa</i> soils.
	Dismal Range – Fort O’Hare Quarry	Potential solution pipe	Calcrete horizon	1 m thick 1.5 m wide, >6 m high	Recognised where top of exposure is visible Only 1 solution pipe evident within a 150 m wide exposure	Laminar calcrete Solution pipe is completely filled with red <i>terra rossa</i> soil
	Dismal Range –Mingbool v		None identified			

Solution pipes are not observed in the most landward barriers (Mingbool and Dismal Range) and are not recognised seaward of the Burleigh Range exposure along Rabbitors Road. No solution pipes are identified in exposures of Caveton or Gambier Ranges. Solution pipes are largest in size and greatest in frequency within exposures of Compton Range at Baxter's Quarry and Heritage Industries. A large solution pipe is potentially exposed at Fort O'Hare Quarry but no other solution pipes are visible within Mingbool or Dismal Ranges. This distribution of solution pipes across the coastal plain may relate to the age of the deposits to some extent, with the youngest deposits, such as those exposed within the MacDonnell Range and Robe Range, displaying no solution pipes as they have perhaps not been subaerially exposed long enough for them to develop. The large size of the solution pipes within Compton Range may be related to lengthier episodes of subaerial exposure allowing greater solution pipe development. XRD and petrological analyses of the Bridgewater Formation reveal that sites farther inland from the present coast have been more diagenetically altered, with the presence of greater proportions of low-Mg calcite and greater cementation between grains. It is therefore probable that greater dissolution has occurred within these more diagenetically mature barriers which may resulted in the formation of larger and more abundant solution pipes.

However, the abundance of solution pipes does not increase proportionally with distance from the coast. The distribution of solution pipes may also be related to the depositional environment of the deposit. Limited solution pipes have been recognised within facies identified as subaqueous; for instance the Gambier Range exposure at Gooch Road; Dismal Range exposures at Dartmoor Cemetery; Fort O'Hare Quarry and Mingbool village. The limited number and size of solution pipes found within these sites may be due to the fact that these deposits could have been previously covered by other material, such as aeolian dunes which, over time, have eroded. This notion is further supported by the lack of overlying calcrete horizons at these sample sites. Therefore, the length of time the sediment at these sample sites has been subaerially exposed may not necessarily correlate with the age of the deposit.

Solution pipe distribution may also relate to changes in base-level; vegetation abundance and the availability of water, which have been identified as factors by Budd *et al.* (2002). Herwitz (1993) suggested that clusters of solution pipes within aeolianite in Bermuda may have formed from stemflow that was more acidic and transported to the underlying soil in greater volumes by certain plant species. In conclusion, karst features within the Bridgewater

Formation on the Mount Gambier coastal plain may not directly relate to the age of the deposit but may be dictated by local climatic factors, the carbonate content of sediment, the elevation of the site with respect to the water table and localised water pathways.

#### **4.7 Surface textures of foraminifera**

As foraminifera are identified within nearly all sediment samples within the Bridgewater Formation calcarenite, the following section examines the textural surface of individual tests to determine if there is any relation between the relative age of sedimentary units and the degree of diagenesis. Firstly, the foraminiferal assemblages recognised on the Lacepede and Bonney shelves to the south of Mount Gambier are presented, as described from previous studies by Li *et al.* (1996, 1998). Comparing offshore and onshore assemblages from study sites can aid in determining the *post-mortem* taphonomic processes that have affected these assemblages. A review of the literature concerning *post-mortem* and taphonomic processes aids in establishing how certain features on foraminiferal tests are formed and acts as a guide for comparing foraminiferal tests from the Bridgewater sediments on the Mount Gambier coastal plain. Finally, images of selected foraminifera from sample sites analysed with a scanning-electron microscope (SEM) are presented. The features shown on these photographed tests are compared with those described in the literature to try and determine what *post-mortem* processes have occurred.

Analysing foraminiferal tests in detail may aid in confirming the depositional environment of the surrounding sediment and thus further strengthen stratigraphic interpretations made in Chapter 3. Assessment of the diagenetic properties of the foraminifera may also aid in identifying if tests are suitable for dating using amino acid racemisation (AAR), and may account for discrepancies in these data sets that will be presented in Chapter 5.

##### **4.7.1 Foraminiferal assemblages on the Bonney Shelf**

As described in Chapters 1 and 3, the Bonney Shelf is the narrow (50 km wide), eastern extension of the Lacepede Shelf (Li *et al.*, 1998), and extends from Robe to Portland. Li *et al.* (1998) analysed 94 dredge samples, 46 from the Lacepede Shelf and 48 from the more northern Lincoln Shelf, to assess differences in assemblages between the two areas which are separated by Kangaroo Island, south of Gulf St. Vincent.

Analyses of dredged sediments confirmed that common foraminiferal species on the Lacepede Shelf included *Discorbis dimidiatus*, *Ammonia beccarii*, *Elphidium macelliforme*, *Elphidium crispum* and *Parrellina imperatrix*. Li *et al.* (1998) recognised eight separate

assemblages, influenced predominantly by the interaction of differing current systems. Through comparison of the northern Lincoln and southern Lacepede Shelves Li *et al.* (1998) found fewer warm-water planktonic species and the lack of relict *Marginopora* on the Lacepede Shelf, and associated this with a weaker Leeuwin Current in this area, possibly due to Kangaroo Island acting as a barrier to the current.

Li *et al.* (1998) identified that relict and reworked specimens are more prevalent on the Bonney Shelf. The narrowing of the shelf in the Bonney region to only 50 m wide, from 200 km wide in the Great Australian Bight, acts as a constricting corridor for the south-easterly flow of water. The resultant stronger current may prevent the accumulation of modern sediment and thus expose more relict specimens on the shelf. Radiocarbon analyses on Lacepede and Bonney Shelf samples conducted by James *et al.* (1992, 1997) revealed that relict bryozoan and bivalves are between 13,000 and 25,000 years old. However, these are suggested to represent a minimum age of the sample only as analyses are a composite of the age of the test/skeleton and clay/oxide infill material. James *et al.* (1992) suggested that this demonstrates that the tests are of Pleistocene age rather than any earlier in the Cenozoic. This is significant in that foraminiferal tests on the shelf may be of a similar age before they are even transported landwards and deposited as part of beach and dune material, and may be significant when interpreting AAR derived numeric ages from Bridgewater Formation foraminifera (Chapter 5).

It was also noted by Li *et al.* (1998) that the relict foraminiferal assemblage on the Lincoln and Lacepede Shelves comprises predominantly lagoonal taxa, and suggest that these may be relicts from when shallow lagoons covered this region during sea level lowstands associated with glacial episodes. Foraminiferal biofacies on the open shelves of the South Australian coastline have been suggested to be the result of terrigenous-clastic input from inland areas and carbonate diagenesis during lowered sea levels, the reworking of strandline deposits during sea level cycles and, and seafloor sediment production during the Holocene (Li *et al.*, 1998).

### **Summary**

Foraminiferal tests identified within deposits of the Bridgewater Formation on the Mount Gambier coastal plain (see Table 3.9) are similar to those identified by Li *et al.* (1998) on the Bonney Shelf. Li *et al.* (1998) have shown that foraminiferal assemblages on the Bonney Shelf may reside there for some time after death and that sediment deposited during previous highstands may be reworked on the shelf. This residence time should be accounted for when



using foraminifera to determine the age of a deposit, but also when accounting for any diagenetic features present within the tests.

#### **4.7.2 Taphonomic processes affecting foraminiferal tests**

Fossil assemblages of foraminifera are not always equivalent to living assemblages and vary due to a range of taphonomic processes resulting in changes to the composition and preservation of communities. Murray (2006) lists these taphonomic processes as including: life processes, affecting the contribution of tests to the sediment; *post-mortem* processes, which alter the proportion of species within the taphonomically active zone (TAZ) where tests are potentially influenced by macrofaunal bioturbation; diagenetic effects that may alter faunal compositions when they are below the TAZ; and weathering effects within an outcrop.

Diz and Francès (2009) noted that recorded assemblages of living foraminifera only reflect a time slice of populations and may not be representative of longer intervals, whereas fossil assemblages are time-averages of multiple generations which are potentially biased by *post-mortem* processes. In Chapter 3, fossil assemblages within the calcarenite were established by counting 200 tests from multiple samples. These assemblages do not reflect the living assemblage of foraminifera, as *post-mortem* processes will have affected species proportions.

Shroba (1993) suggested that taphonomic damage of tests can be separated into both destructive and constructive agents. She noted that destructive features may include the breakage, pitting, boring, scratching and exfoliation of test surfaces while constructive features are associated with pyritization and encrustation by algae. In addition, tests may also be encrusted through the growth of carbonate cements. The following section assesses the *post-mortem* processes that may have resulted in these features within foraminiferal tests. Such features are then identified in tests from the Bridgewater Formation, and processes that may have caused them are determined.

#### **Dissolution**

Dissolution of calcareous tests may occur in waters that are under-saturated with calcium carbonate (Murray, 1989). The oxidation of organic matter in the top few centimetres from the sediment surface and the associated production of carbon dioxide may further promote dissolution (Peebles and Lewis, 1991; Murray and Alve, 1999; Walker and Goldstein, 1999; Buzas-Stephens and Buzas, 2005). Shroba (1993) suggested that dissolution may be enhanced on abraded foraminiferal tests.

Dissolution of tests may result in a range of features. Herrero and Canales (2002) extensively reviewed the literature and suggested that commonly described dissolution features on foraminiferal tests included: dull, pitted and etched surfaces; the breakage and loss of the last chamber; the enlargement and coalescence of pores; and the selective dissolution of outer layers resulting in reduced ornamentation of the test surface. Murray (1989; 1991) suggested that etching of the test initially results in a dull texture and opaque surface. Progressively the test becomes pitted and the last chamber will break. The test is then prone to further breakage and may finally result in total destruction (Murray, 1989; 1991). Dissolution textures have been indicated to be coarser than abrasion textures due to the etching of crystallites and removal of outer wall layers (Peebles and Lewis, 1991).

In a controlled laboratory experiment, Peebles and Lewis (1991) placed tests in formic acid. After 20 minutes they found that all fine particles had been removed from test surfaces, but that after 80 minutes the outer layer of oriented calcite laths had been completely removed, resulting in the exposure of unoriented calcite crystallites beneath. In the Moneva section of Jurassic sandstone, Spain, Herrero and Canales (2002) found that foraminifera tests commonly displayed an opaque, dull and white appearance and that sometimes wall surfaces were corroded which they related to exposure of tests to acid interstitial fluids during late meteoric diagenesis. The much older age of these Jurassic tests indicates the preservation potential of certain foraminiferal species, and while these tests are significantly older than those from the Quaternary Bridgewater Formation they provide examples of the effects of differing diagenetic processes. Murray and Wright (1970) studied the effects of dissolution on the benthic species *Ammonia beccarii*. They found that when etched the test surface became uneven and that etching preferentially attacked pores due to the large surface area of their walls, resulting in pore enlargement and elongation. Murray and Wright (1970) found that etching was most pronounced on topographically high areas of tests and chambers.

Dissolution has been found to affect certain foraminiferal species differently (e.g. Corliss and Honjo, 1981). Rates of dissolution can depend on wall thickness, wall microstructure, chemical composition, ornamentation, size and surface to volume ratio (Peebles and Lewis, 1991; Herrero and Canales, 2002). As well as differences in individual test properties, dissolution may vary due to the sedimentary and diagenetic environments that a test is deposited in, as tests are subjected to dissolution both prior to and after burial (Herrero and Canales, 2002). These factors were considered in the study of foraminiferal assemblages in the calcarenite of the Bridgewater Formation.

### **Abrasion**

Abrasion of tests commonly occurs during transportation when exposed to other moving sedimentary particles. Intense abrasion can occur in intertidal areas under the influence of nearshore waves, currents and tides. Abrasion may also occur in long distance aeolian transport. Goudie and Sperling (1977) found foraminifera in Quaternary dunes of the Thar Desert, India, some 800 km from the coast indicating how susceptible tests are to transport.

Shroba (1993) described the abrasion textures formed through pitting, scratching and exfoliation. She suggested pitting occurs through the impact of tests with other sedimentary grains and results in pits commonly 10  $\mu\text{m}$  in diameter, with steep walls, floored by broken test-wall material. Scratching may occur through grinding against other grains and produces linear excavations within the outer chamber wall (Shroba, 1993). Exfoliation may result from the combination of abrasion and solution (termed corrasion by Brett and Baird, 1986), and leads to irregular topography on the test surface (Shroba, 1993). Shroba (1993) also noted that abrasion can vary depending on the composition of different sedimentary grains and found that in siliclastic environments tests are not polished but stripped of their outer walls. Herrero and Canales (2002) recognised that the most common abrasion features described in the literature included erosional features such as impact depressions, scratches, smooth and polished surfaces, a loss of surface ornamentation, scalloped edges of test peripheries, and the breakage and loss of final chambers. Abrasion may result in small, shallow holes whereas dissolution may be associated with deep holes with smooth outer edges (Cottey and Hallock, 1988).

Through laboratory experiments, Peebles and Lewis (1991) concluded that abrasion textures in *Milionina* and *Rotaliina* were characterised by polished surfaces with scattered scratches, pits and broken edges. They concluded that unlike dissolution, damage to the test caused by abrasion increased over time and test genera became increasingly difficult to identify. After 64 hours of tumbling (the equivalent of 1-3 km of transportation), Peebles and Lewis (1991) noted small breaks and polishing around the aperture region of tests. After 376 hours of tumbling (6-18 km) they noted that 72% of tests were visibly damaged, with elevated portions of the test exhibiting the most damage, including flattened ornamentation, missing chamber walls, broken apertures, scratches and a loss in surface detail. In Jurassic sandstone foraminifera from the Basque-Cantabrian Basin, Spain, Herrero and Canales (2002) noted that corrosion features on foraminifera included the pitting and etching of tests resulting in holes on the test surface of irregular size and shape. Abrasion features included polished edges and ribs, scalloped peripheries, breakage of peripheral keels and the loss of last chambers.

The influence of abrasion on test structure has been found to vary depending on both the structural properties of the test and the depositional environment. Peebles and Lewis (1991) suggested that test size influences the effects of abrasion, with larger tests proving more resistant to abrasion, and found *Discorbis* were more likely to be preserved than other species they studied. Franceshini and Compton (2007) suggested that abrasion was a selective process and that within taxa the form and structure of the test would influence the resistance to its mechanical breakdown. Certain test characteristics may result in differing preferential transportation modes. Martin and Liddell (1991) suggested that tests that are robust, lenticular and have thick-walled shells are more commonly transported as bedload, which may result in greater test abrasion (Murray, 1991). Tests that are flattened, elongated, small and have a thin concoidal shell are more likely to be transported as suspended load, reducing the effects of abrasion and resulting in increased preservation (Murray, 1991).

### **Recrystallisation**

Sedimentary infilling of tests has been suggested to occur during biostratinomic stages, while cementation occurs mainly during early stages of fossil diagenesis (Herrero and Canales, 2002). Recrystallisation may include micritic infilling and the formation of pyrite and sparite cements. Herrero and Canales (2002) noted that pyrite textures include; framboidal, clustered, aggregated, bladed and equant pyrite forms. Within the Jurassic sandstone foraminifera in Iberian and Basque regions of Spain, Herrero and Canales (2002) found that calcitic crusts covered many of the foraminiferal tests. Some crusts were composed of small and regular calcite crystals on the outer surface, others displayed small and regular crystals accompanied by larger rhombic crystals on inner and external chamber surfaces, while some calcitic crusts were found to cover the whole test, obscuring morphological features and preventing accurate identification of test species. Therefore, in some cases tests may be so covered in crystals it is not possible to determine the genera they belong to and to accurately determine fossil assemblages. On the other hand, reinforcing a test's hard parts through filling of chamber cavities may increase the preservation potential of an individual.

### **Bioerosion**

Peebles and Lewis (1988) suggested that bioerosion, where organisms such as algae, sponges, bacteria and other predators, destroy the outer surface of tests has a greater occurrence in shallower waters as bioeroders require light. Bioerosion may result in interweaving of trails that randomly penetrate the test surface (Peebles and Lewis, 1988).

### Summary

A range of taphonomic processes change the foraminiferal assemblage between living and fossil populations. *Post-mortem* processes can commonly be determined through identification of textures on the test surface. It has been shown that different foraminiferal species will tolerate these *post-mortem* processes differently depending on properties such as size, wall microstructure, ornamentation and surface to volume ratio. Therefore, fossil assemblages may reflect a higher preservation potential of these species rather than a higher abundance in their living assemblage. Palaeo-environmental reconstruction using fossil assemblages must therefore account for these processes.

Physical changes to a test's surface may not necessarily relate to the age of a test. It has been shown that the depositional environment and degree of transport that a test has experienced may result in varying degrees of test destruction. Tests that have travelled farther have been shown to be more highly abraded while those deposited within the TAZ may experience greater levels of dissolution. Davaud and Septfontaine (1995) found that along Jerba Island, on the Tunisian coastline, dead tests of foraminifera were abundant in backshore and foreshore areas, but poorly preserved on the shoreface. They attributed this distribution to tests being easily removed within suspended load in storm-generated currents on the beach environment. Walker and Goldstein (1999) noted that the preservation of foraminifera depends on the microhabitat and biogeochemical conditions of the sediment as well as test composition. Martin and Liddell (1991) suggested that burial-exhumation history of a test will play a considerable role in the preservation of the test, with those that are well-buried being better preserved. Martin *et al.* (1995) proposed that the surface condition (or taphonomic grade) of a test was not a reliable indicator of test age, and that the degree of alteration of a test more likely reflects the residence time the individual has been within the sediment-water interface or TAZ. Identification of *post-mortem* processes through recognition of tests surfaces of foraminifera from calcarenite deposits on the Mount Gambier coastal plain may therefore be a better reflection of the depositional environment, or the degree of transportation a test has experienced, rather than the age of the test.

#### **4.7.3 Surface textures on foraminifera from deposits within calcarenite on the Mount Gambier coastal plain**

Foraminifera are identified in the majority of sediment deposits within the Bridgewater Formation on the Mount Gambier coastal plain, and have been used for single grain AAR analysis (Chapter 5). Selected tests were then analysed under a SEM to determine any differences on the surface of tests caused through diagenesis or *post-mortem* processes.

Where possible, tests were picked at random from the sample however; there is some subjectivity in this process as only tests that were recognisable at genera level were selected.

The photographs in the following section are a representative sample, from the many images that were taken, showing common textural differences on the tests from a variety of the sample sites within the barrier shorelines on the Mount Gambier coastal plain.

#### **Modern Beach**

Samples from Port MacDonnell Beach generally show well-preserved ornamentation on the test surface (Figure 4.17a,c,e). Foraminifera are commonly translucent, reflecting their young age. Microbial boring was common on the test surfaces (Figure 4.17b,g,i), which are otherwise generally smooth, and show no signs of cementation or recrystallisation associated with diagenesis and may be indicative of residence time in a subaqueous environment. Scalloping of the outer edges (Figure 4.17a,e), shallow pits filled with broken fragments of the test wall (Figure 4.17f), and scratches (Figure 4.17j) are also common and are associated with abrasion that tests would have been subjected to in the high-energy beach environment.

#### **Robe Range equivalent, upper aeolianite unit, Port MacDonnell**

Tests show a reduced ornamentation compared with those described on Port MacDonnell Beach which may be associated with polishing of the test surface through abrasion processes (Figure 4.18a,b,c,e,h). Tests also display scalloping of the outer edges, shallow abrasion pits (Figure 4.18b), and scratches (Figure 4.18f) on the test surface, which are likely to be associated with abrasion during beach or aeolian transportation. Small calcite crystals and micrite cements are found to partially cover parts of the test surfaces (Figure 4.18d,e,g) unseen in the modern beach samples, and are indicative of diagenetic processes.

#### **Robe Range equivalent, upper aeolianite unit, Shelly Beach**

Tests from Shelly Beach upper aeolianite unit are similar to those within the (proposed) same unit at Port MacDonnell in that they display scalloping of the test edges and abrasion pitting (Figure 4.18i,k,o), probably associated with transportation. However, the test ornamentation is not reduced as much as identified on tests within Port MacDonnell aeolianite samples. Exfoliation of the test surface is more prevalent (Figure 4.18l), where the outer test layer has been removed through dissolution processes. This is shown clearly in Figure 4.18n where the *Discorbis* shows the unorientated crystal matrix beneath this outer surface, and elongated aragonite crystals. Greater subjection to dissolution processes within this deposit may have resulted from exposure to more acidic pore waters, perhaps associated with overlying soil profiles.

**Robe Range equivalent, lower aeolianite unit, Port MacDonnell**

Foraminifera from the lower aeolianite unit at Port MacDonnell display evidence of abrasion processes evident as scalloping of outer edges (Figure 4.19a), polishing (Figure 4.19b,i), pitting (Figure 4.19g) and a reduced ornamentation of test surfaces (Figure 4.19c,d). Dissolution processes are also evident to a minor extent in the form of pitting and exfoliation around pore features (e.g. Figure 4.19b,e). The effects of bioerosion are also present on some test surfaces (Figure 4.19i) while cementation is minor to rare on test surfaces. These features are indicative of tests that have been transported a considerable distance, potentially by aeolian processes. Tests appear more abraded than those from the modern beach but are not significantly different from those of the upper aeolianite unit in this locality. The main difference in tests either side of the calcrete palaeosol at Port MacDonnell is the more significant reduction in ornamentation found in tests from the upper unit, indicative of a greater transportation distance.

**Robe Range equivalent, lower aeolianite unit Shelly Beach**

Tests from this deposit display a reduced ornamentation (Figure 4.19j,m) and edges are scalloped, indicative abrasion processes. In cases where abrasion has been more severe some edges have been removed completely (Figure 4.19n). Micritic cements partially cover several of the test surfaces (Figure 4.19k,l,p), in some instances complicating species identification. Crystals within calcite cements are found to vary in size from 5 to 20  $\mu\text{m}$ , and preferentially grow in areas of low relief such as sheltered pore cavities. On an *Elphidium* test (Figure 4.19o) cracks were found connecting pores and may reflect a combination of impact processes with dissolution. On the upper surface of the same test small (2  $\mu\text{m}$ ) crystals are found on the test surface. Crystal growth suggests that diagenesis occurred within this deposit and may relate to the proximity to the overlying unconformity and wetting and drying of sediment associated with a hiatus in sediment deposition.

**MacDonnell Range, Swarts Road sand quarry**

Within MacDonnell Range a presumed correlative of the last interglacial Woakwine Range, tests display evidence of severe abrasion. Tests have scalloped edges, and in some cases edges have been removed completely (Figure 4.20a). Ornamentation of test surfaces is commonly reduced (Figure 4.20f) and scratches and grazes are frequently observed (Figure 4.20g,h). Test surfaces are sometimes found to be polished (Figure 4.20c,g), and microbial borings are also present, which potentially formed prior to abrasion (Figure 4.20e). These tests are indicative of a high energy transportation environment, and have potentially been



transported for a considerable distance. Bedding within the quarry was found to be steeply dipping, so transportation was likely by aeolian processes.

#### **MacDonnell Range, Narrawong road cutting**

Tests photographed from Narrawong road cutting (also presumed to be MIS 5e in age due to dating of this site by Sherwood *et al.* 1994) are better preserved than those from the sand quarry on Swarts Road, illustrating not just an age function, but also the influence of local palaeoenvironmental factors during diagenesis. Tests from Narrawong road cutting commonly display minimal signs of abrasion, with edges only slightly scalloped. Where tests are scalloped it may have been through dissolution processes rather than impact forces. Bioerosion in the form of microbial boring is common on several of the test surfaces, and in places where it is found to be extensive (Figure 4.20k,n) the burrows appear to have enhanced solutional processes, resulting in a honeycomb-like appearance to the test surface. In other tests, dissolutional processes are identified in the form of small solutional pits (Figure 4.20p) and exfoliation of test surfaces (Figure 4.20q). Tests from Narrawong road cutting appear to not have been as severely abraded as those from Swarts Road, and are thus indicative of a lower energy environment. Dissolution processes are more prevalent and suggest tests were possibly within a TAZ beneath the surface in which acidic pore water may have caused the textural features observed on the tests.

#### **Burleigh Range, Rabbitors Road**

Foraminiferal tests from Burleigh Range exposure along Rabbitors Road show a high level of destruction. Tests have scalloped edges (Figure 4.21d) and in some cases outer edges have been totally removed (Figure 4.21a,e,f). Ornamentation has been severely reduced (Figure 4.21g) and in some tests, surfaces have been polished (Figure 4.21h). These textural features are indicative of abrasion processes potentially caused during transportation. Some tests show calcite cements have formed on the test surface indicating diagenetic processes have occurred. Tests within this exposure have been subjected to high levels of abrasion and have potentially been transported great distances or reworked several times.

#### **Burleigh Range, Laslett Road**

Tests from Laslett Road cutting exhibit a greater level of preservation than those from Rabbitors Road. Tests have been subjected to limited abrasion, and their outer edges show minimal scalloping. Abrasion pits were not observed on surfaces and ornamentation is generally well-maintained. Small calcitic crystals were found in protected areas of low relief (Figure 4.21j,n) and cements are found on small areas of the test surfaces (Figure 4.21l,m). Small solutional pits were also occasionally identified on test surfaces (Figure 4.21n). The

preservation of the foraminifera from Laslett Road is indicative of a low-energy environment and corresponds well with stratigraphical interpretation of this exposure as a lagoonal facies.

#### **Caveton Range, Rabbitors Road # 2**

From the lagoonal facies of Caveton Range tests show limited effects of abrasion. Tests have maintained their overall structure well, with only minor scalloping of edges and ornamentation is well-preserved (Figure 4.22a). Test surfaces are generally smooth and show limited cementation in low relief areas (Figure 4.22d) with only minimal cement found on test surfaces. Microbial borings are also common on test surfaces. Dissolution appears to be the dominant taphonomic process, with deep and rounded pits common on surfaces (Figure 4.22b) and enlargement and coalescence of pores (Figure 4.20g). Test surface textures are indicative of a low energy environment and support the stratigraphical interpretation that this is a lagoonal deposit.

#### **Gambier Range, Gooch Road**

Foraminiferal tests within Gooch Road appeared well-preserved under a petrological microscope. SEM imagery confirms that tests have maintained their original structure well, with minimal abrasion features observed. Some tests have maintained original ornamentation well (Figure 4.22h), whilst others are slightly reduced (Figure 4.22k,l). Solutional pitting and exfoliation are common on test surfaces (Figure 4.22i,j) and cementation is rare. Tests from this deposit appear to have experienced limited transportation and indicate a low-energy depositional environment. Dissolution is the primary taphonomic process affecting foraminifera at this locality.

#### **Compton Range, Baxter's Quarry**

Foraminiferal tests within Baxter's Quarry commonly yield thick calcitic cement which sometimes covers the entire test surface (Figure 4.23c,d). In some instances, it was difficult to assess other taphonomic processes due to this thick cement. Abrasion appears to have had a minor effect on some tests, with cracking (Figure 4.23a) and some scalloping evident at test peripheries (Figure 4.23e). Ornamentation is also evident on some tests where cement did not cover the entire surface (Figure 4.23d). Dissolution processes are evident in the form of extensive test surface exfoliation (Figure 4.23b).

#### **Compton Range, Heritage Industries**

Tests from the exposure of Bridgewater Formation at Heritage Industries display a greater degree of abrasion than tests within Baxter's Quarry. Abrasional features include scalloping of edges (Figure 4.23h,k) and in some cases complete removal of outer edges (Figure 4.23g).

Grazes (Figure 4.23j) and scratches (Figure 4.23n) are also indicative of abrasion processes. Dissolution has also been an active taphonomic process with the removal of weaker areas in some tests, such as the central umbilical region (Figure 4.23l,m). Cementation has also occurred on some tests in more protected regions. Test textures are indicative of a high-energy environment and indicate tests have been subjected to some diagenesis since deposition. These findings complement the stratigraphical interpretation of this exposure as a beach environment.

#### **Mingbool Range, Don's Quarry**

Foraminifera analysed from sediment samples taken from Don's Quarry generally yield a well-preserved overall shape. Many tests show limited abrasion and scalloping to outer margins and original ornamentation of test surfaces has commonly been maintained (Figure 4.24 c,k). Dissolution appears to be the dominant destructive process. The majority of tests are coated in a calcite crust that covers much of the test surface (Figure 4.24a,b,d,e,h,l,j). Some solutional pitting is evident where tests are not completely coated in the cement crust (Figure 4.24g,m). Examination of textural surfaces of foraminifera suggests that the tests within sediment from Don's Quarry have not been transported far, but have been subjected to dissolution processes, and compare well with the stratigraphic interpretation that this is a subaqueous deposit (section 3.8.9).

#### **Dismal Range, Dartmoor Cemetery**

Tests within the exposure of Bridgewater Formation near Dartmoor Cemetery are generally poorly preserved. Tests are commonly missing outer edges (Figure 4.24o,q,s) and this may be a product of abrasion or severe dissolution. Solutional pitting and exfoliation of test surfaces are common, as well as greater cementation on the outer test layer.

#### **Dismal Range, Fort O'Hare Quarry**

Foraminifera recovered from calcarenite exposed at Fort O'Hare Quarry are poorly preserved. Tests do not show significant signs of abrasion as outer margins are not extensively scalloped (Figure 4.25d,e,i,m). Where test edges are missing (Figure 4.25g) it is likely this has been as a result of severe dissolution rather than abrasion due to the lack of other features. Tests are commonly coated in a thick micrite crust (up to 30  $\mu\text{m}$  thick in some places; Figure 4.25j), where calcite crystals range from 2  $\mu\text{m}$  to 20  $\mu\text{m}$  in length. On some tests, the crust covers the majority of the surface preventing inspection of the test for other taphonomic features (Figure 4.25a,b,c). Dissolution features are also common. On the surface of one *Ammonia beccarii* specimen, dissolution appears to have been concentrated on deepening natural joins in the test surface (Figure 4.25e), with solutional pitting found in the test centre (Figure 4.25f). Upon

the surface of a *Discorbis dimidiatus* specimen, dissolution processes appear to have eroded the outer test, leaving a more resistant central portion (Figure 4.25m,n). Foraminifera from this deposit show limited signs of transport and are again indicative of a lower-energy environment, complementing the interpretation of a subaqueous setting (section 3.8.10). Tests in this deposit are the most cemented of any other samples analysed and may reflect an older age of the deposit or at least one that has been subjected to a greater degree of diagenesis.

#### **Dismal Range, Mingbool village**

Tests from a small quarry near to the settlement of Mingbool in the Dismal Range show some limited alteration of test edges, perhaps scalloped through abrasion (Figure 4.25o,q,s). Some test surfaces are missing, though this appears to be a result of dissolution rather than abrasion as test edges are not sharp (Figure 4.25r). In some instances, dissolution processes are visible in the enlargement of test pores (Figure 4.25t) and the exfoliation of test surfaces, exposing underlying layers of the test (Figure 4.25v). Calcite cements are found on the surfaces of the majority of tests in the form of rhombic calcite crystals, but are not as extensive as those found on tests from Fort O'Hare Quarry. Foraminifera from this deposit suggest sediment may have been deposited in a lower-energy environment, perhaps a subaqueous setting, where tests may have experienced low-energy interaction with the seafloor.

#### **Summary**

Examination of foraminiferal tests from a selection of deposits within the Bridgewater Formation on the Mount Gambier coastal plain reveals that tests exhibit variation in their degree of preservation. These differences are summarised in Table 4.4. In conclusion, it appears that taphonomic processes, which are dictated primarily by depositional environment, have resulted in the most dramatic changes to test surface textures, and that these may not necessarily correlate with the proposed age of the deposit. Different textures are observed in tests that have been deposited in aeolian environments compared to subaqueous or lagoonal environments. Tests found within aeolianite deposits, such as Robe Range equivalent and MacDonnell Range, display scalloped edges and reduced surface ornamentation. Tests within lagoonal environments, such as Caveton Range at Rabbitors Road are generally well-preserved showing signs of limited *post-mortem* transportation.

In conclusion, the degree of test preservation was not found to be related to the age of the deposit, but rather to the depositional environment and taphonomic processes that had affected that test. For example, tests within Gambier Range exposed at Gooch Road exhibit a

greater degree of preservation than those within the Burleigh Range exposure at Rabbitors Road, located 9 km seaward and presumably younger. Tests at Gooch Road are generally still well-rounded and maintain much of their original ornamentation, while tests within Burleigh Range at Rabbitors Road commonly display cementation of the test surface and multiple abrasion features such as scalloped peripheries or complete removal of edges. Test surfaces within the same dune range are also found to alter dramatically, depending on their depositional environment. For example, tests at Rabbitors Road within the Burleigh Range, as previously mentioned, are highly abraded, while those found at Laslett Road, also within the Burleigh Range, exhibit greater preservation. This corresponds with the stratigraphical interpretations of these sites as beach and lagoonal facies respectively.

Cementation of test surfaces was perhaps the only textural trait that could be weakly associated with age. Tests from more landward deposits such as Fort O'Hare Quarry and Dartmoor Cemetery display a higher degree of cementation on the test surface than younger deposits such as those found within Caveton or Robe Range, or the modern beach where no cementation is observed on tests.

While the textural surface of foraminiferal tests may indicate more about the environment of deposition than the age of the deposit, it is still of value to examine these surfaces as differing textures may lead to variable geochronological results. Highly abraded cavities may retain cements in their exposed chambers potentially contaminating results and (depending on the age of the cement) may yield significantly different geochronological results. Cementation is potentially the biggest threat to determining accurate geochronological results. Cementation on the test surface is not always visible on surfaces under a petrological microscope and thus cemented tests may not necessarily be originally discarded from geochronological analysis. Cemented tests will likely yield younger ages and not reflect the true time of protein synthesis cessation within foraminifera, thus skewing results. However, by analysing the textural surfaces of a range of tests across the study sites, deposits where foraminifera are more prone to cementation can be identified and geochronological results from these regions more thoroughly scrutinised for any younger outliers.

**Table 4.4:** Surface texture characteristics of foraminifera from sediment samples across the Mount Gambier coastal plain

Dune Range	Sample site and depositional facies	Abrasion features	Dissolution features	Cementation	Bioerosion	Concluding remarks
Modern	Port MacDonnell Beach	Very slight scalloping of peripheries	Negligible	Negligible	Microbial tunnels are common.	Test walls are generally smooth, no signs of dissolution or recrystallisation. Scalloping indicative of a higher energy environment
Robe (MIS 5a/c)	Port MacDonnell, upper aeolianite	Very reduced ornamentation. Outer edges slightly scalloped. Scratches and abrasion pits common	Negligible	Cementation present on some tests in pores and low relief areas.	Negligible	Indicative of high level of transport likely by wind as found in aeolianite deposit by bouncing of grains against test causing reduced ornamentation, pitting and scratches. Cementation indicative of an older age than modern beach.
	Shelly Beach, upper aeolianite	Minor scalloping, slightly reduced ornamentation. Abrasion pits infilled with broken walls. Cracking between pores.	Some deep and rounded solutional pits. Removal of outer layer shows unorientated crystals beneath.	Negligible	Negligible	Indicative of high energy environment. Severe abrasion indicates transportation.
	Port MacDonnell, lower aeolianite	Scalloping to outside of tests. Reduced ornamentation. Smooth tests may indicate polishing. Impact grazes and pits	Minor dissolutional pits are visible on surface. Possible enlargement of pores. Exfoliation of test surface		Microbial tunnels are common.	High energy environment, transported a considerable distance. Dissolution features are suggestive that deposit has been exposed to diagenetic processes perhaps episodic wetting and drying.
	Shelly Beach, lower aeolianite	Reduced ornamentation. Severe abrasion. Parts of test missing, cracking features common	Hard to detect beneath thick calcitic crust.	Tests coated in thick calcitic cement. Crystals vary in size and in pores.	Hard to detect beneath thick calcitic crust.	High energy environment and considerable transport as indicated by moderate abrasion of tests. Thick cements are indicative of wetting and drying, perhaps in exposure of the cliff face, or associated with formation of palaeosols and calcrete above.
MacDonnell (MIS 5e)	Swarts Road, sand quarry, aeolianite	Severe abrasion to some tests – large, irregular shallow pits. Reduced ornamentation. Scratches. Grazes. Scalloping of outer edges.	Negligible	Negligible	Microbial tunnels potentially formed prior to abrasion.	High energy environment and distance of transport.
	Narrawong, road cutting	Minor scalloping of outer edges	Primary destructive process. Enlargement of pores. Well-rounded solutional pits, enhanced by boring.	Negligible	Extensive microbial boring.	Suggests limited transportation of test <i>post-mortem</i> . High level of dissolution may be indicative of increased age, or perhaps tests have remained in TAZ for a considerable time.
Burleigh (MIS 7)	Rabbitors Road, road cutting, beach/aeolian	Severe abrasion. Strong scalloping of outer edges. Parts of tests missing in places. Pitting is common.		Thick calcitic crusts commonly complicate species identification	Microbial boring is common.	High level of abrasion suggests a considerable distance of transport. Thick calcitic crusts may indicate a greater age of test, and are potentially suggestive of sediment reworking in this deposit.
	Laslett Road, lagoonal facies	Only minor scalloping to edges. Slightly reduced ornamentation.		Crystals commonly found in protected areas		Limited transportation, though ornamentation indicates some abrasion has occurred. Crystallisation is perhaps indicative of age of test.
Caveton (MIS 9)	Rabbitors Road, lagoonal facies	Negligible	Deep, rounded pits are common. Coalescence and enlargement of pores.	Negligible	Microbial boring is common.	Tests have not been transported far from site of original deposition. High level of dissolution suggests tests have been altered within the TAZ, perhaps as lagoonal muds were oxidised by microfauna in the deposit.
Gambier (MIS 11)	Gooch Road, subaqueous deposit	Negligible	Exfoliation of test surface and small solutional pitting.	Negligible	Negligible	Limited transportation is indicated by lack of abrasion features. High degree of dissolution perhaps indicates oxidation of sediment near surface.
Compton (MIS 13)	Baxter's Quarry, subaqueous deposit			Thick calcitic crusts.	Negligible	
	Heritage Industries, beach facies	Well-abraded. Some tests show severe breakage. Scratches. Scalloping of outer edges.	Deep, rounded solutional pits are common.		Negligible	High level of transportation, perhaps associated with the swash zone. Solutional pitting may have been enhanced by initial abrasion and sediments may have been oxidised by microfauna.
Mingbool (MIS 15)	Don's Quarry, subaqueous facies	Abraded outer edges on selection of tests.	Surface exfoliation and solutional pitting are common.	Calcitic crystals cover much of test surfaces.	Negligible	Some level of transportation, but high degree of dissolution indicates a substantial time in TAZ. Cementation may relate to age of test.
Dismal (MIS 17)	Dartmoor Cemetery, subaqueous deposit	Few tests show slightly scalloped edges	Severe exfoliation of upper surfaces of some tests. Deep solutional pits	Highly cemented	Negligible	Limited transportation. High levels of dissolution and cementation may relate to age of tests.
	Fort O'Hare Quarry, subaqueous deposit	Scalloping is uncommon.	Dissolution dominant.	Highly cemented. Thick calcitic crusts.	Negligible	Limited transportation. High levels of dissolution suggest tests were once in an oxidated setting. Calcitic crusts may be indicative of age.
	Mingbool village, subaqueous facies	Minor abrasion features	Severe surface exfoliation.	Thick calcitic crusts are common	Negligible	Limited transportation. High levels of dissolution suggest tests were once in an oxidated setting. Calcitic crusts may be indicative of age.

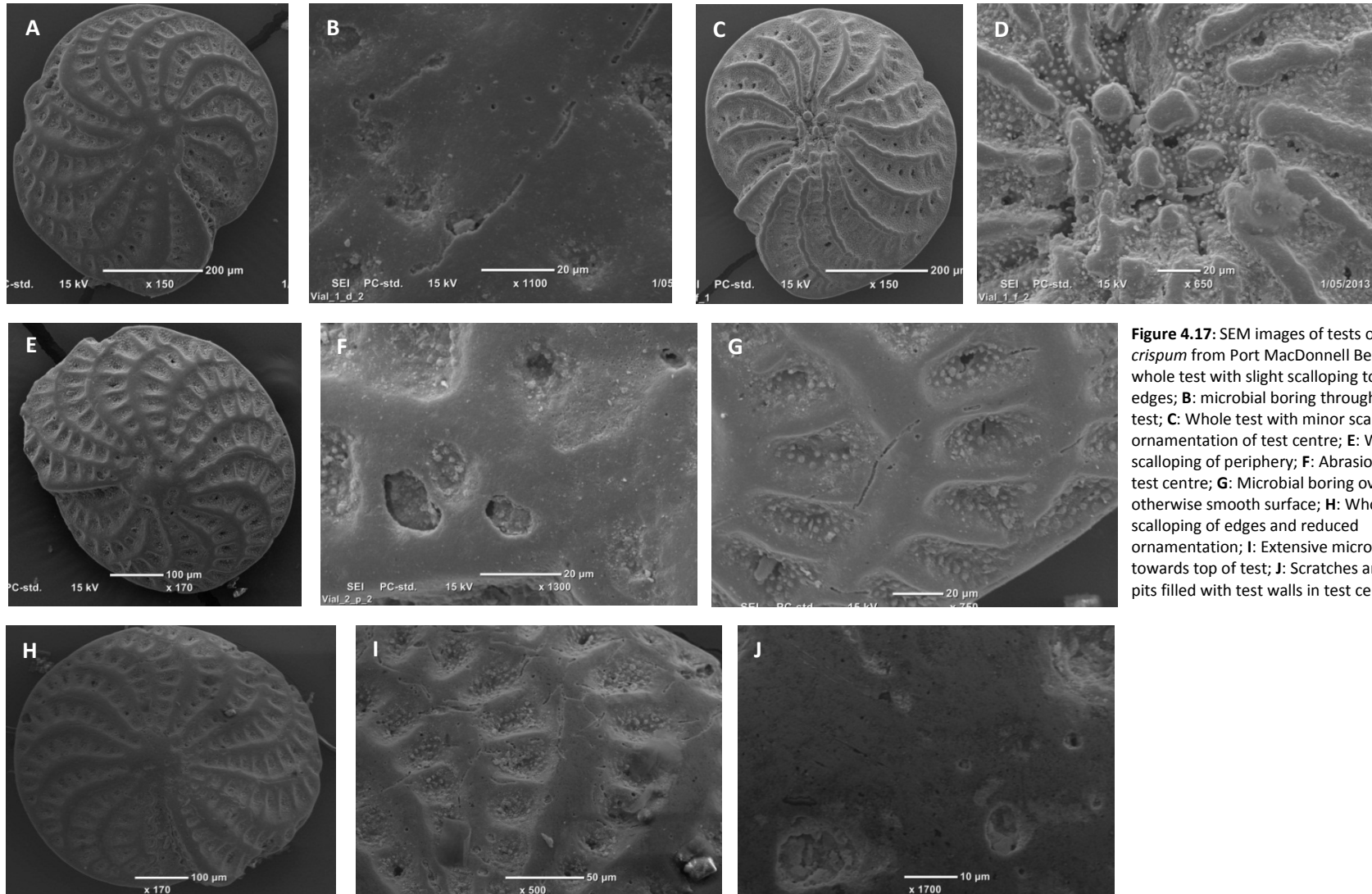


**Figure 4.17:** SEM images of tests of *Elphidium crispum* from Port MacDonnell Beach. **A:** whole test with slight scalloping to outer edges; **B:** microbial boring through centre of test; **C:** Whole test with minor scalloping; **D:** ornamentation of test centre; **E:** Whole test, scalloping of periphery; **F:** Abrasion pits on test centre; **G:** Microbial boring over an otherwise smooth surface; **H:** Whole test, scalloping of edges and reduced ornamentation; **I:** Extensive microbial boring towards top of test; **J:** Scratches and abrasion pits filled with test walls in test centre



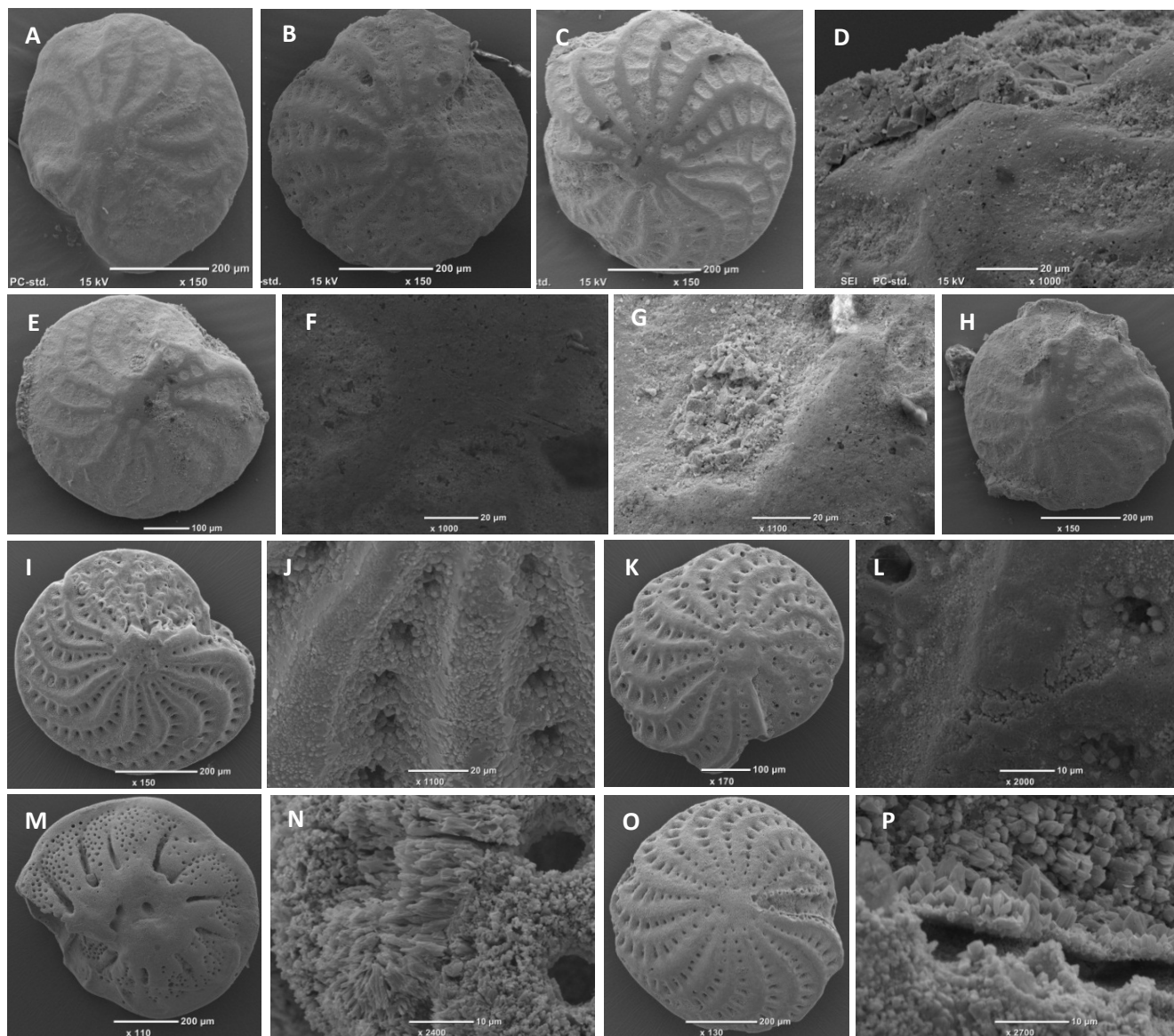


**Figure 4.18:** SEM images of foraminifera from upper aeolianite units at Port MacDonnell (A-H) and Shelly Beach (I-P). **A, B, C:** *Elphidium crispum* tests showing severely reduced ornamentation and minor scalloping of peripheries, both possibly caused by abrasion through aeolian transportation; **D:** Calcitic crust found on upper edge of test shown in C; **E:** *Elphidium crispum* indicating reduced ornamentation, and calcitic crusts at edges and in centre; **F:** Scratches in centre of test E; **G:** Calcite crystals formed preferentially in lower relief areas of test E; **H:** *Elphidium* displaying a flattened test surface and crusts forming at outer edge; **I:** *Elphidium crispum* displaying preferential of top half by dissolution processes, but overall test is well-preserved, with only minor scalloping of periphery and well-maintained orientation; **J:** Sheet-like crystals formed on lower half of test; **K:** *Elphidium crispum* showing scalloping of outer edges and round pits across much of the test; **L:** Dissolution over an otherwise smooth surface; **M:** *Discorbis dimidiatus* showing some abrasion of outer edge, **N:** Dissolution of upper surface, removal of outer layer revealing unorientated crystals underneath and growth of elongated crystals; **O:** *Elphidium crispum*, whole test has preserved much of original structure; **P:** Crystal growth around the aperture region.

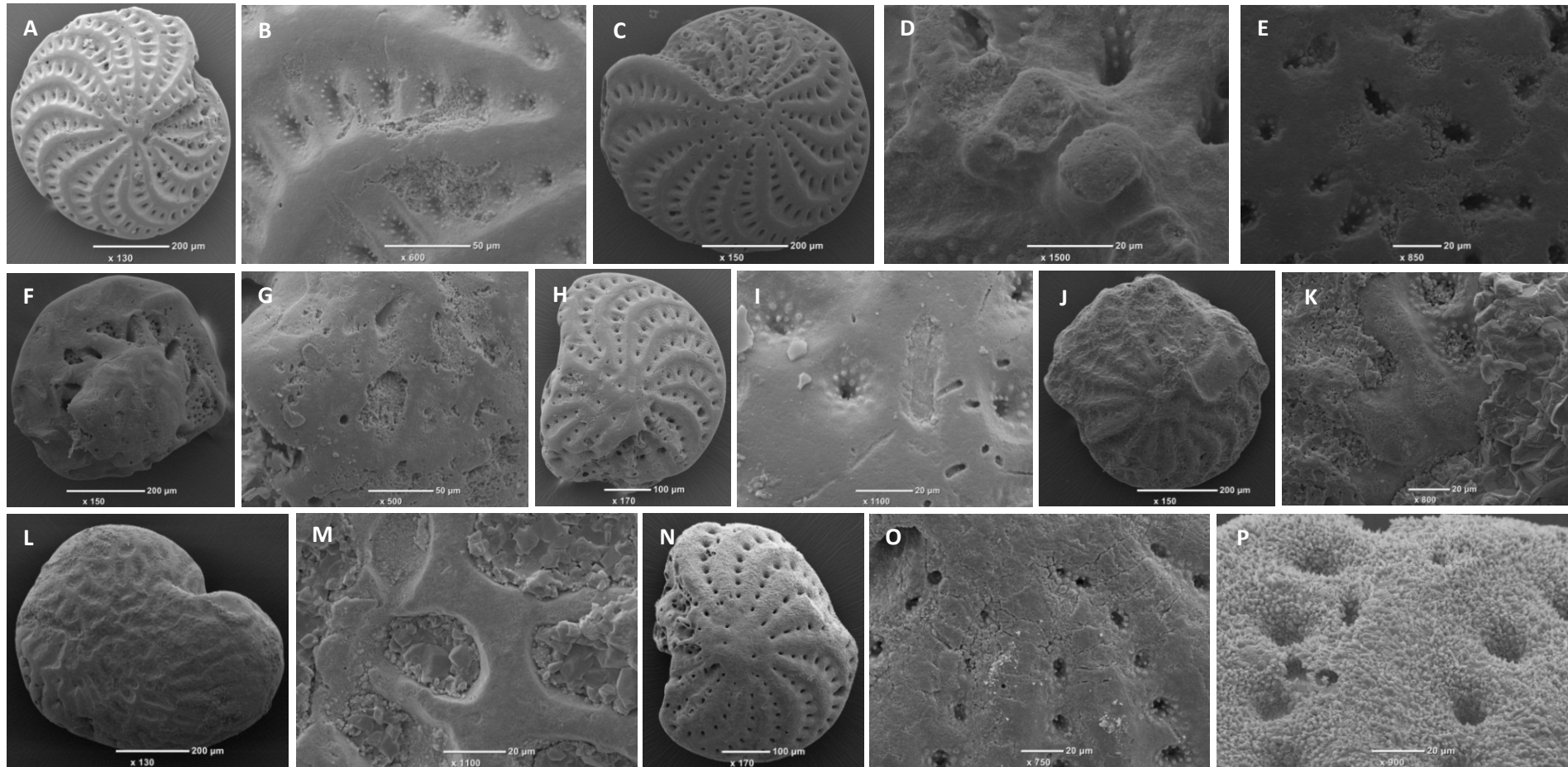


**Figure 4.19:** SEM images of foraminifera from the lower aeolianite units at Port MacDonnell (A-I) and Shelly Beach (J-Q). **A:** *Elphidium crispum* displaying minor scalloping to outer edge; **B:** Abrasion features on a polished test surface; **C:** *Elphidium crispum* showing a well-preserved test, with preferential erosion of upper half of test; **D:** Reduced ornamentation; destruction of a high relief region; **E:** Dissolutional pitting around pore margins; **F:** *Discorbis dimidiatus* with relative preservation of central region; **G:** Shallow abrasion and solution pits on tests surface; **H:** *Elphidium crispum* with abraded lower edge and polished surface; **I:** Microbial boring and a graze on test surface; **J:** Heavily cemented *Elphidium*; **K:** Micrite cement forming covering polished test surface with small solutional pits on high relief areas of test; **L:** Possibly an *Elphidium* – cement and abrasion have obscured ornamentation; **M:** Crystals preferentially growing in pore areas; **N:** Abraded *Elphidium crispum*; **O:** Cracking features between pores possibly associated with a combination of abrasion and solutional processes; **P:** Recrystallisation of test surface.

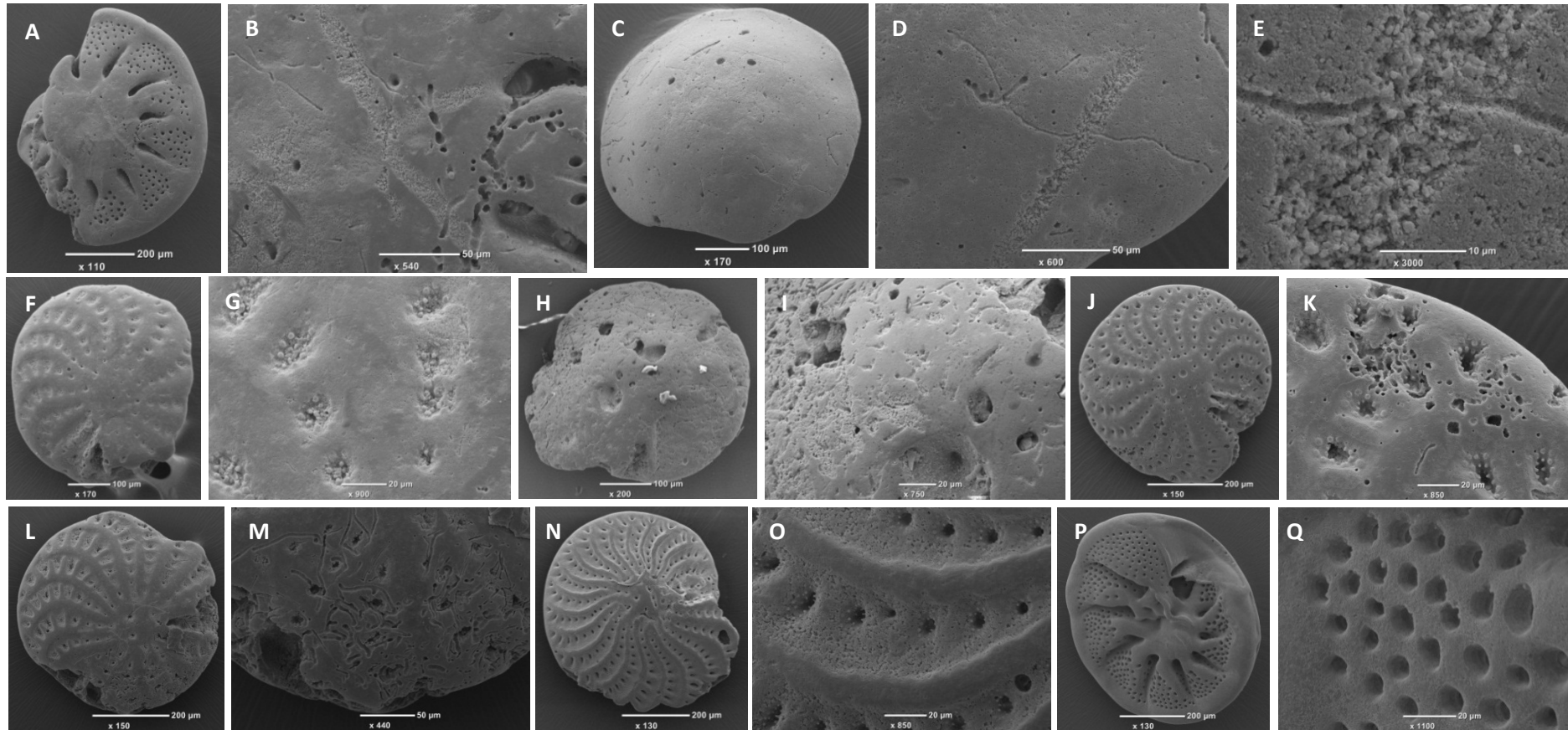


**Figure 4.20:** SEM images of foraminifera from the MacDonnell Range at Swarts Road sand quarry (A-I) and Narrawong (J-Q). **A:** Highly abraded *Discorbis dimidiatus*; **B:** Microbial boring and graze on test surface; **C:** *Discorbis dimidiatus* dorsal view showing scratching and pitting of test surface; **D:** Microbial boring and grazing on test surface; **E:** Close up of D showing graze possibly occurring after bioerosion; **F:** *Elphidium crispum* showing flattened and polished surface; **G:** Reduced ornamentation on test surface; **H:** Highly abraded *Discorbis dimidiatus* with microbial boring, abrasion pits and severe scalloping of peripheral edges; **I:** Close up of test surface showing abrasion pits filled with test walls and scratches on test surface; **J:** *Elphidium crispum* displaying minimal abrasion to outer edge, but a slightly polished surface; **K:** extensive microbial boring on test surface which has resulted in preferential dissolution in these areas causing a honeycomb-like appearance; **L:** *Elphidium crispum* showing a smooth test surface, a possible abrasion feature to outer edge and extensive microbial boring on lower half of test; **M:** Microbial boring on lower test; **N:** *Elphidium crispum* with a well-preserved test, disruption to outer edge may be caused by etching as is not scalloped as associated with abrasion features; **O:** Solutional pitting in low relief areas on test surface; **P:** Well-preserved *Discorbis dimidiatus*; **Q:** Slight solutional pitting around pores.

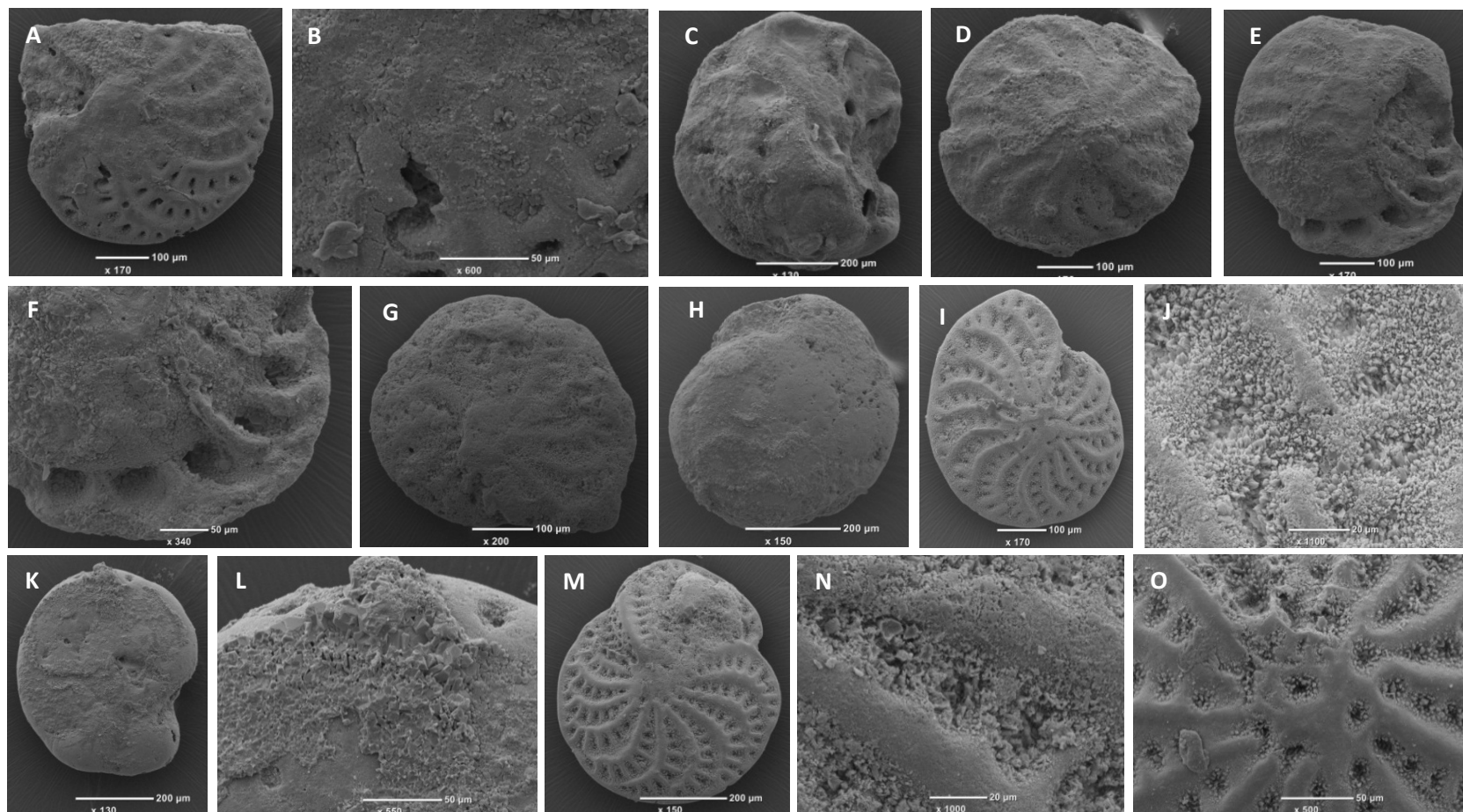


**Figure 4.21:** SEM images of foraminifera from the Burleigh Range exposures at Rabbitors Road (A-H) and Laslett Road (I-O). **A:** *Elphidium crispum* that has had part of the test removed, possibly through abrasion; **B:** Pit and crack associated with impact to the test surface. **C:** Possibly a *Discorbis* that has been highly altered through *post-mortem* processes; **D:** *Elphidium* with scalloped periphery and reduced ornamentation, possibly through abrasion processes; **E:** *Elphidium* with part of outer edge remove; reduced ornamentation and cement on outer surface; **F:** Close up of bottom of test, showing preferential crystal growth in exposed part of test; **G:** *Elphidium* with a scalloped edge, and reduced ornamentation possibly through abrasion during aeolian transport; **H:** *Discorbis* with a polished surface, random, deep pits and patches of cement; **I:** *Elphidium crispum* showing a well-preserved periphery and ornamentation; **J:** Close up reveals small crystal structures growing in areas of low relief; **K:** *Discorbis* illustrating a reduced ornamentation and patches of a calcitic crust; **L:** calcitic crust at top of test, with crystals of varying sizes; **M:** Well-preserved *Elphidium crispum*; **N:** Solutional pitting in areas of high relief and crystal growth in areas of low relief; **O:** Centre of test is generally smooth.



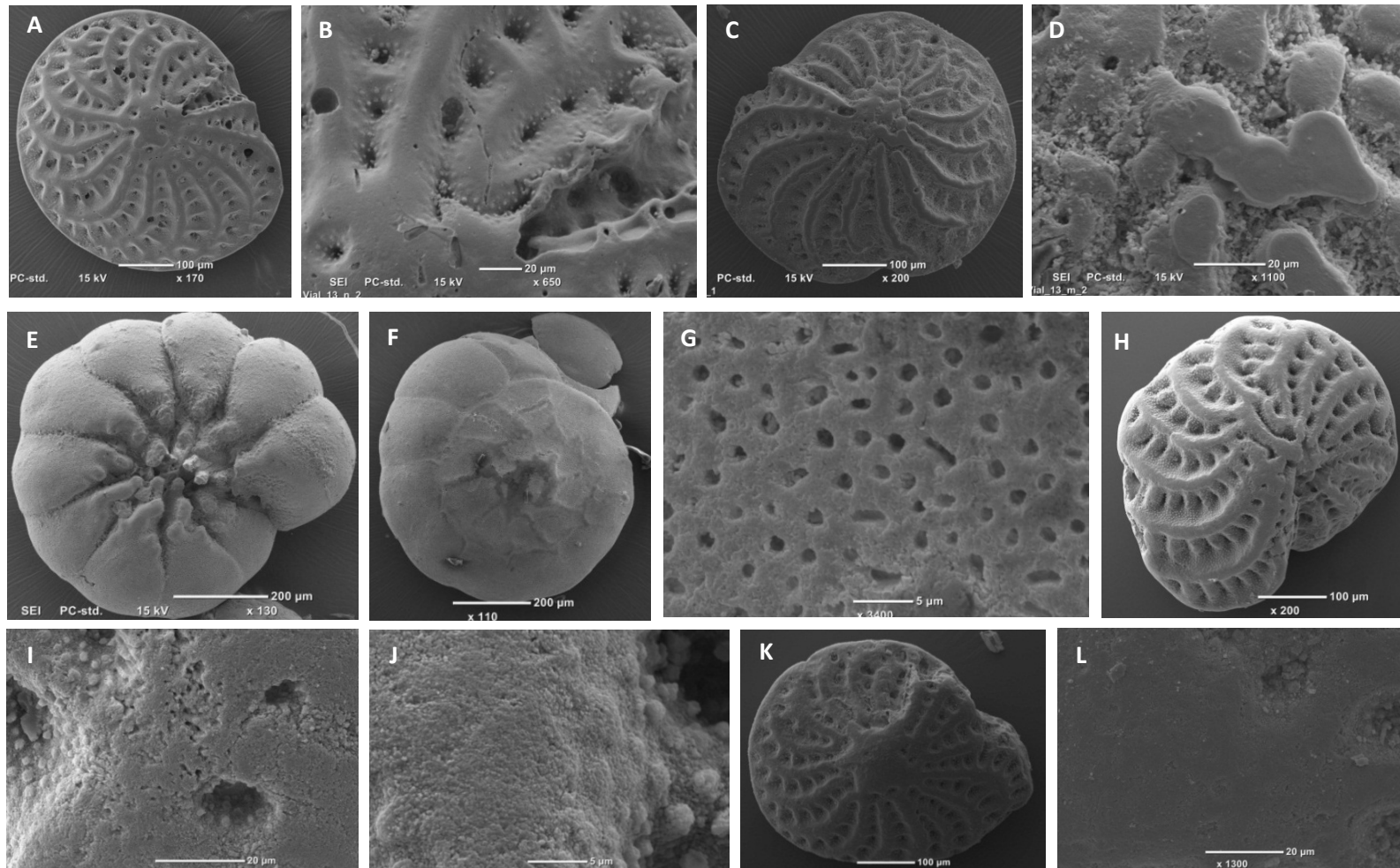


**Figure 4.22:** SEM images of foraminifera from Caveton Range lagoonal facies (A-I) and Gambier Range (J-N). **A:** Well-preserved *Elphidium crispum*, **B:** Microbial boring on a generally smooth test surface with spores around pore region; **C:** *Elphidium crispum* with well-preserved ornamentation; **D:** Ornamentation of test centre; **E** and **F:** Umbilical and dorsal view of *Ammonia beccarii* showing a well-preserved surface and preferential dissolution in test centre; **G:** Pore enlargement and coalescence indicative of dissolution processes; **H:** *Elphidium crispum* with deep rounded solutional pits and a smooth test surface; **I:** Smooth surface with micro-exfoliation; **J:** Pitted test surface and micro-exfoliation through dissolution **K:** Well-preserved *Elphidium crispum* with a smooth test surface and slight abrasion to periphery; **L:** micro-exfoliation of test surface.

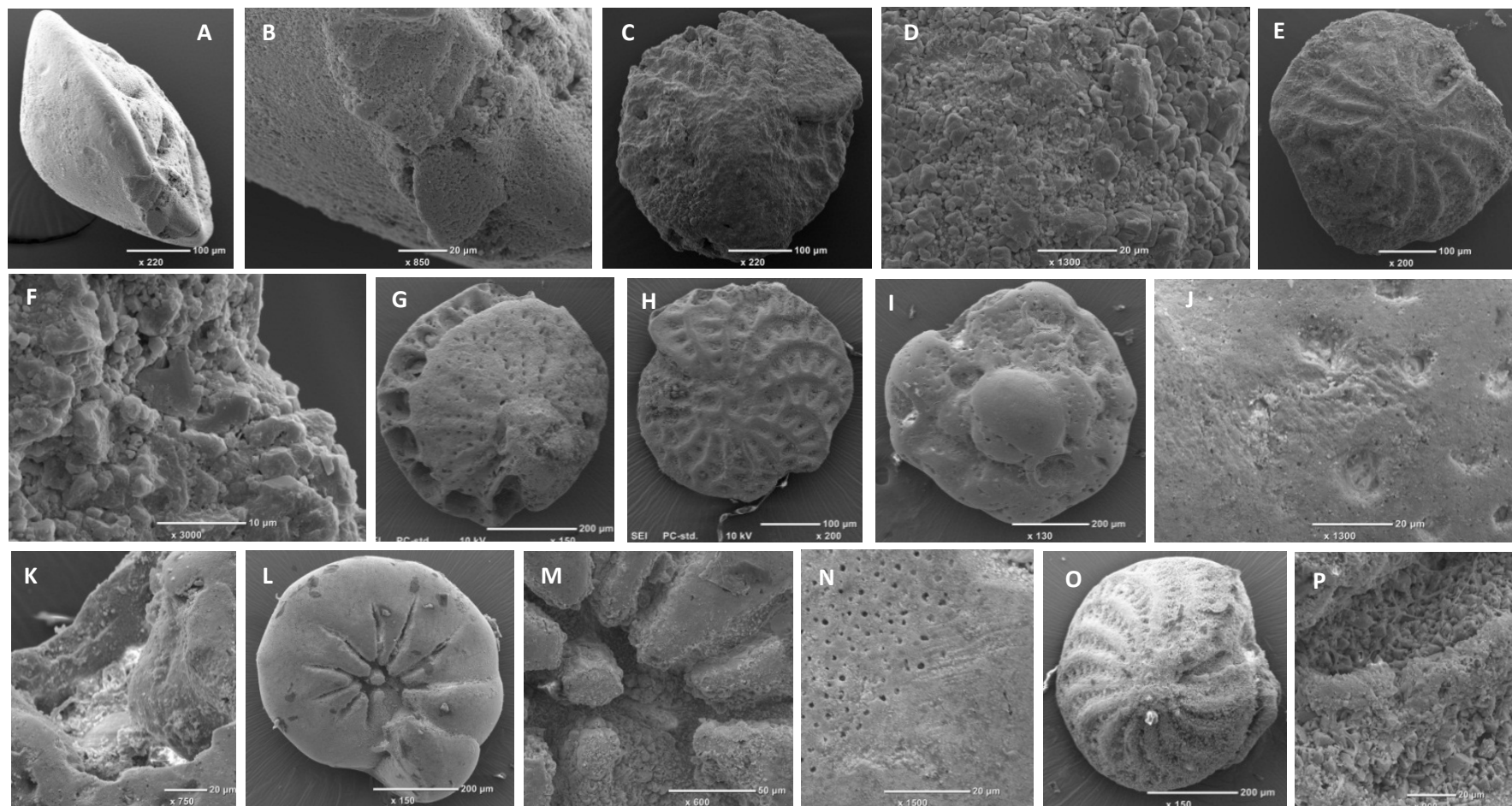


**Figure 4.23:** SEM images of foraminifera from Compton Range at Baxter's Quarry (A-F) and Heritage Industries (G-P). **A:** Side view of *Discorbis dimidiatus* showing abrasion to periphery and solution pitting to outer surface; **B:** Small solution pits and exfoliation to outer surface; **C:** Possibly an *Elphidium* coated in a thick calcitic cement; **D:** Rhombic crystals within cement; **E:** Highly abraded *Elphidium crispum* with reduced ornamentation; **F:** Recrystallisation of outer test surface; **G:** Removal of outer edge of *Elphidium*, possibly through abrasion processes associated with transportation; **H:** *Elphidium crispum* with scalloped edges, reduced ornamentation and polished surface in places; **I:** Abraded *Discorbis dimidiatus* highlighting preservation of more resistant central region; **J:** Abrasion feature on outer test surface; **K:** Scalloping of outer edge; **L:** *Ammonia beccarii* showing a generally well-preserved test structure; **M:** Preferential dissolution of umbilical region; **N:** Pore enlargement and scratches associated with abrasion on test surface; **O:** *Elphidium crispum* with highly recrystallised outer surface; **P:** Small calcitic crystals growing in areas of low relief.

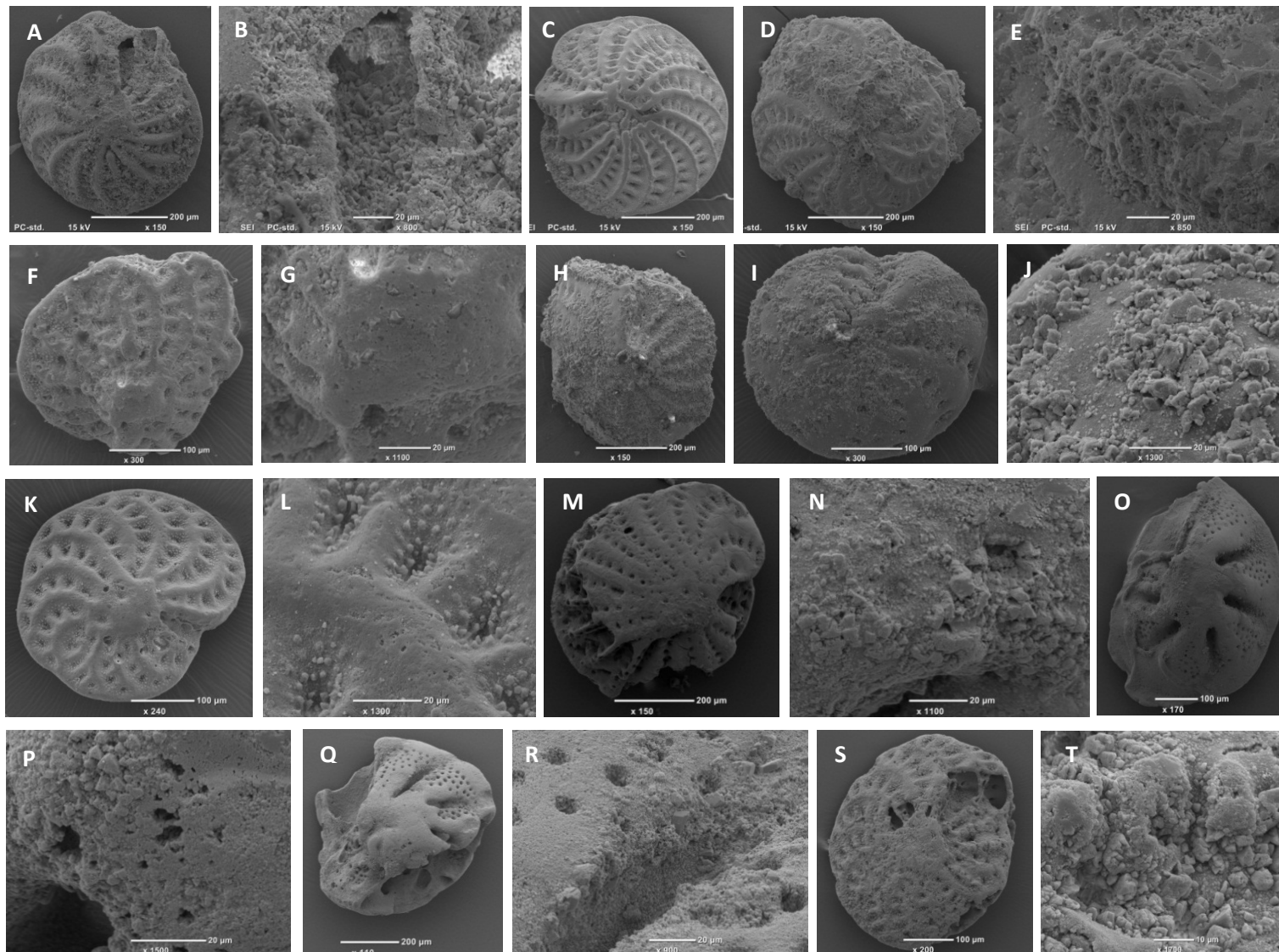


**Figure 4.24:** SEM images of foraminifera from Don's Quarry, Mingbool Range (A-L) and Dartmoor Cemetery, Dismal Range (M-T). **A:** Highly weathered *Elphidium crispum*; **B:** Recrystallisation around aperture area; **C:** Well-preserved *Elphidium crispum* with minimal signs of abrasion; **D:** *Elphidium crispum* with scalloped periphery and a thick cement on test surface; **E:** Cement is approximately 50  $\mu\text{m}$  thick; **F:** Highly eroded *Elphidium crispum* with scalloped edges and a central area more resistant to weathering; **G:** Pitting on the centre of the test; **H:** Recrystallised *Elphidium crispum*; **I:** *Elphidium* with a well-maintained shape; **J:** Crystals growing on an otherwise smooth surface; **K:** *Elphidium crispum* shows no signs of abrasion; **L:** Test is generally smooth with a lack of recrystallisation and some slight solution pitting in high areas of relief; **M:** Highly abraded *Elphidium crispum* showing removal of outer edge; **N:** Different sized crystals growing on test surface; **O:** *Discorbis dimidiatus* missing half of test; **P:** Signs of solutional pitting, exfoliation and recrystallisation on test surface; **Q:** *Discorbis dimidiatus* with removed outer edges, perhaps due to severe dissolution; **R:** Exfoliation surrounding pores and crystal growth in natural cavities; **S:** *Elphidium crispum* with large sections of test missing possibly through dissolution, and slight scalloping of the outer edge; **T:** Large crystals growing on test surface.



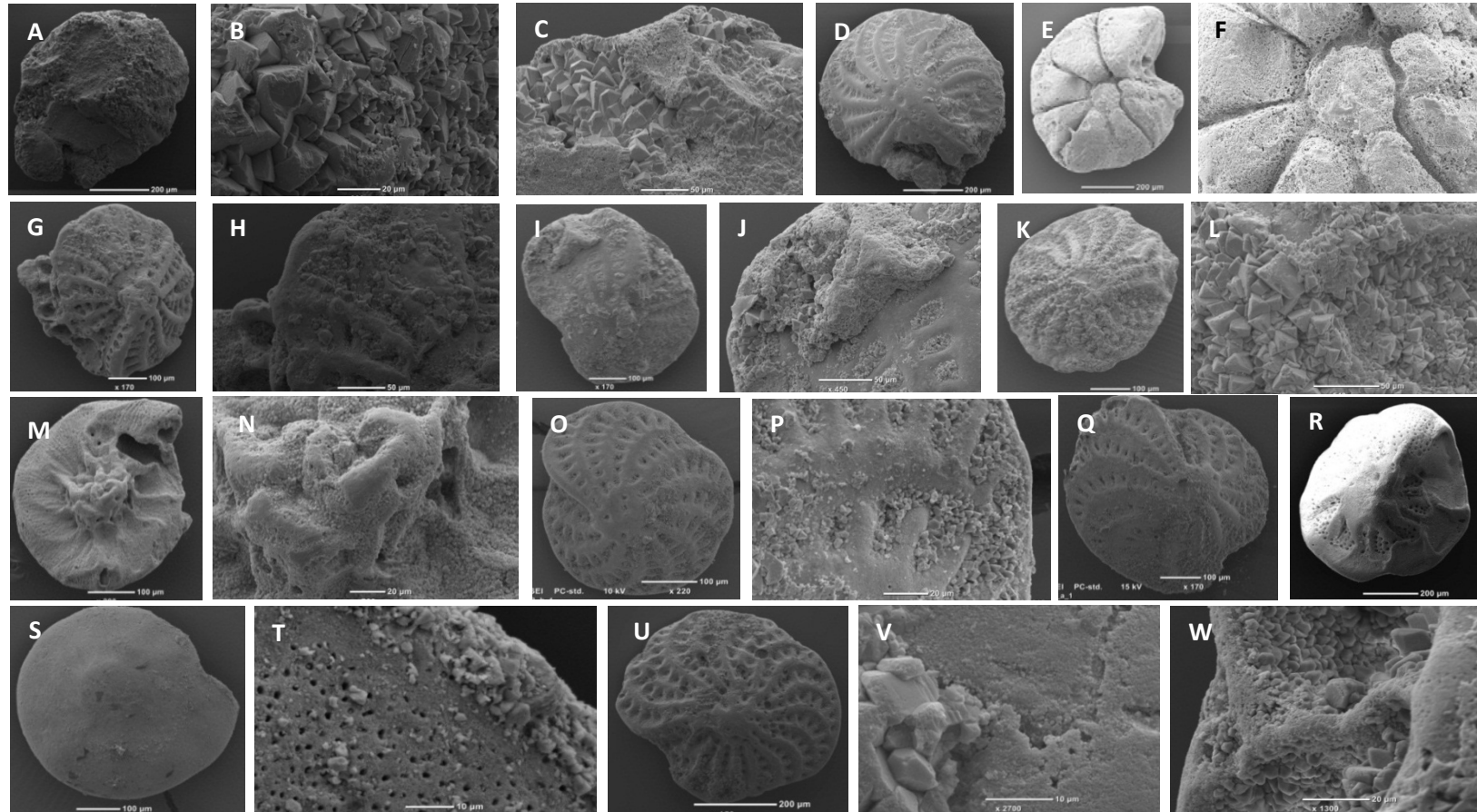


**Figure 4.25:** SEM images of foraminifera from Dismal Range at Fort O'Hare Quarry (A-N) and Mingbool village (O-W) **A:** Possibly an *Elphidium* coated in a thick calcitic cement; **B:** Micrite cement with crystals varying from 20  $\mu\text{m}$  to 5  $\mu\text{m}$  in size; **C:** Calcitic crystals on test surface also coated with a finer cement; **D:** *Elphidium crispum* showing reduced ornamentation; **E:** *Discorbis dimidiatus* umbilical view displaying effects of moderate dissolution; **F:** Dissolution of centre of test resulting in small, deep, pits; **G:** *Elphidium crispum* in partial destruction, removal of outer edge exposes inner chambers; **H:** Cement has formed on the upper half of test; **I:** *Elphidium* showing reduced ornamentation and a thick cement on test surface in place; **J:** Cement rind is approximately 30  $\mu\text{m}$  thick; **K:** *Elphidium crispum* with a micrite cement; **L:** Range of crystal sizes within the cement; **M:** *Discorbis dimidiatus* showing signs of dissolution – troughs radiate from test centre and pits are visible; **N:** More resistant central portion of test showing signs of dissolution; **O:** *Elphidium crispum* maintains overall shape well; **P:** Smooth surface of test with small rhombic crystals preferentially growing in areas of low relief; **Q:** *Elphidium crispum* showing removal of outer edge, reduced ornamentation and cementation on test surface; **R:** *Discorbis dimidiatus* umbilical view showing dissolution of outer margin and resistance of central portion to erosion; **S:** *Discorbis dimidiatus* dorsal view shows a rounded outer edge; **T:** Pore enlargement and a calcitic crust forming on outer margin; **U:** *Elphidium crispum* with slightly scalloped edges, pits across test surface; **V:** Calcite crystals and evidence of dissolution which has removed an outer layer of the test surface; **W:** Calcite crystals growing within a more protected region on test surface.

#### **4.8 General petrographic characteristics of the Bridgewater Formation on the Mount Gambier coastal plain - a summary**

Petrographic assessment from a range of representative study sites across the Mount Gambier coastal plain has revealed the diagenetic properties of the sediment. Several diagenetic trends can be identified with increasing distance (and a proposed increasing age) from the modern shoreline landwards.

XRD analysis of sediment samples has revealed a general increase in low-Mg calcite content with proposed age. Sediment samples closer to the modern shoreline, and presumably younger, retain high values of aragonite and high-Mg calcite and may be classed as diagenetically immature. Farther inland, in older deposits, aragonite and high-Mg calcite are replaced by low-Mg calcite. Some of the most inland sites, such as Dartmoor Cemetery and Mingbool village within the Dismal Range, are up to 88% low-Mg calcite, and aragonite content is < 2%. Such deposits may be classed as diagenetically mature with regard to carbonate mineralogy.

Thin section analysis has allowed for assessment of grain composition within sediment samples. Grain composition is generally similar in the majority of deposits and includes constituents such as molluscan fragments, foraminifera, bryozoan and echinoid fragments. These constituents primarily reflect a marine source, though varying proportions of quartz indicate partial terrestrial sources, primarily in aeolianite deposits, where changing wind direction may have introduced different source materials. However, analysis of quartz under the microscope reveals that grains are commonly clear and angular, reflecting coastal transport. These grains may therefore be derived from the River Murray, which transports terrigenous sediment to the coast, followed by deposition on the Bonney Shelf through longshore transport. Descriptions of cements between framework grains have allowed establishment of the diagenetic environments to which sediments may have been exposed. Most sediments are found to have been subjected to meteoric-vadose environments, with some of the more inland sites indicative of shallow marine environments. These conclusions generally support stratigraphic interpretations of units as proposed in Chapter 3. While a weak correlation can be highlighted between the extent of cementation within a sample and the relative age of the deposit, the degree of cementation is more likely a result of the diagenetic and depositional environments, rather than the relative age of the deposit.

Karst features have been described at each of the study sites. A positive correlation between the volume of karstic features and proposed age of a deposit may be drawn to a

certain extent. Samples near to the modern shoreline show limited karst features, with no karst present on modern and Holocene beaches. Robe Range equivalent deposits are indicative of some subaerial exposure as indicated by calcrete profiles, but no solution pipes are evident. Solution pipes are best developed within Compton Range at Baxter's Quarry and Heritage Industries. These sites are likely to be significantly older than those at more seaward locations and perhaps suggest that solution pipe size and density increase with length of subaerial exposure. However, within the most inland study sites of the Mingbool and Dismal Ranges, few or no solution pipes or calcrete horizons are identified. This may be due to the fact that these deposits have all been identified as subaqueous and perhaps they have not been exposed at the surface for the entire length of time that they were deposited and were previously capped by aeolian deposits that have since been eroded away. As suggested by Budd *et al.* (2002) local climatic factors may also have affected the distribution of solution pipes across the coastal plain.

Examination of foraminiferal test surfaces reveals tests within barriers farther inland from the present shorelines to commonly be more cemented than those of a proposed younger age. Thick calcitic crusts on test surfaces were more common on tests from more inland regions. However, this may be a result of the diagenetic environment that a test is exposed to, with samples in near-surface marine environments perhaps subjected to more phreatic conditions, where cementation is greater. Other identifiable textural surfaces such as abrasion and dissolution processes are indicative of the environment of deposition and transportation of the test. In general, textural surface conclusions complemented the stratigraphic interpretations proposed in Chapter 3.

If diagenetic models of calcarenite alteration, as proposed by Land *et al.* (1967), are applied to samples across the Mount Gambier coastal plain, exposures of calcarenite would range from stage 1, where sediment is unconsolidated, as found at the modern and Holocene beaches, to stage 4 where calcarenite is in the process of aragonite loss by dissolution, as found at inland sites such as Dartmoor Cemetery and Fort O'Hare Quarry. If diagenetic grades proposed by Reeckman and Gill (1981) are applied to samples of the Bridgewater Formation, samples may range from stage 1 to stage 2. However, rather than the primary loss of high-Mg calcite over aragonite, as reported by Reeckman and Gill (1981) on calcarenite deposits from Warrnambool, Victoria, samples from the Mount Gambier coastal plain appeared to exhibit total loss of aragonite before loss of high-Mg calcite. In contrast to Hearty and O'Leary's (2008) adaptation of diagenetic grades, hardness of calcarenite was not necessarily associated

with older samples. This may result from sample sites being from differing depositional environments. Capping soils were not identified at all study sites and therefore could not be used to determine diagenetic grade in this regard, as used by Hearty and O'Leary (2008).

Table 4.5 summarises the diagenetic properties identified at representative study sites across the coastal plain. Gardner and McLaren (1994) warn against applying diagenetic models outside of the region where the original model was developed. Therefore, rather than directly apply the diagenetic grades suggested by Land *et al.* (1967), Reeckman and Gill (1981) and Hearty and O'Leary (2008) to samples from the Mount Gambier coastal plain, the samples are rated on their diagenetic maturity from the features examined in this study (Table 4.5).

In this thesis, ratings of diagenetic maturity range from highly immature to highly mature. Highly immature samples exhibit limited to no cements on grain contacts, high proportions of aragonite and high-Mg calcite within samples, no karst features are identified, and foraminifera are well-preserved. Immature samples may exhibit slight micritic meniscus cements, slightly lower proportions of aragonite and high-Mg calcite, limited karst features, and foraminifera may show only slight textural differences from live specimens. Weakly mature samples exhibit the following features: moderate proportions of aragonite and high-Mg calcite, development of some karst features such as calcrete horizons, micritic and spar cements are found to connect grains but pore spaces are not completely filled, and foraminifera may show significant textural differences from modern samples. Sediments that are diagenetically mature may exhibit significantly reduced proportions of aragonite and high-Mg calcite, display well-developed karst features and well-developed spar cements that partially fill pore spaces, and foraminifera may be significantly altered. Highly mature sediments include samples that have little or no aragonite and Mg-calcite. The majority of the mature samples are composed of low-Mg calcite, and are dominated by well-developed spar cements that fill the majority of pore spaces. Well-developed karst features such as wide solution pipes and foraminifera that are significantly altered or are unrecognisable at the species level are also common within older deposits.

As shown in Table 4.5, the diagenetic maturity of the sample does not directly correlate to the proposed age of the deposit. Samples found farthest inland (and presumably older) have only a rating of 'mature', as exposures at these sites do not exhibit any karst features. As previously mentioned, the development of karst features may relate to local climatic conditions (Budd *et al.*, 2002) and the length of subaerial exposure, which at these study sites may not correlate with the age of the deposit. Therefore, it is apparent that this

diagenetic classification system may also be flawed, as other factors such as depositional environment and climate, influence the extent of diagenesis, as well as age. The classification system is therefore used here solely as a coarse tool to identify the range of diagenetic features at sample locations. Such features do not necessarily show a direct relation to the age of a deposit due to differences in local climatic regimes, diagenetic and depositional environments and more varying erosional processes which can cause subaerial exposure to be more recent than the time of original structure deposition.

**Table 4.5:** Summary of the diagenetic features observed through petrographic analysis of sediments on the Mount Gambier coastal plain, southern Australia

Dune Range	Sample site	Diagenetic features observed	Diagenetic environment	Diagenetic maturity
Holocene	Port MacDonnell Beach, modern	None observed – no cement, or karst recognised. High-Mg calcite proportions are high. Foraminifera are well-preserved.		Highly immature
	Shelly Beach, modern	None observed – no cement, or karst recognised. High aragonite and high-Mg calcite proportions		Highly immature
	Holocene Beach, Port MacDonnell	Fine micritic, meniscus cement on outer grains edges in intra-grain pores. No karst recognised. High aragonite proportions.		Immature
Robe	Upper aeolianite, Port MacDonnell	Meniscus micritic cement and patches of blocky spar identified. Moderate aragonite proportions. 75 cm thick rubbly calcrete overlying unit. Foraminifera primarily show signs of abrasion.	Meteoric-vadose	Weakly mature
	Upper aeolianite, Shelly Beach	Moderate aragonite and high-Mg calcite proportions. 1 m thick massive to rubbly calcrete overlying unit. Foraminifera primarily show signs of abrasion and minor dissolution.	Meteoric-vadose	Weakly mature
	Lower aeolianite, Port MacDonnell	Moderate aragonite and high-Mg calcite proportions. 75 cm thick massive calcrete and overlying 10-30 cm thick red palaeosol. Foraminifera primarily show signs of abrasion and few solution pits on surface.	Meteoric-vadose	Weakly mature
	Lower aeolianite, Shelly Beach	Moderate aragonite proportions. Undercut region 15 cm potentially representing an eroded palaeosol. Foraminifera show signs of abrasion and are coated in a calcitic crust.	Meteoric-vadose	Weakly mature
	Weathered aeolianite, Port MacDonnell	Meniscus micritic cement identified upon which dog-tooth spar has developed. Inter-grain pores commonly filled with micritic cements. Moderate to lower aragonite and high-Mg calcite proportions.	Meteoric-vadose	Mature
	MacDonnell Swarts Road	Fine micritic meniscus cement is observed on grain edges. Moderate aragonite and high-Mg calcite proportions. 30 cm thick rubbly calcrete horizon and 1 m thick layer of rhizoliths. Foraminifera primarily show signs of abrasion.	Meteoric-vadose	Mature
Burleigh	Narrawong	Foraminifera generally well-preserved and only show minor abrasion features and dissolution appears the primary destructive process.		Weakly mature
	Rabbitors Road	Meniscus cements observed. Moderate aragonite and moderate-lower high-Mg calcite proportions. Patches of rhizoliths up to 1 m high, solution pipes 50 cm to 3 m tall. Foraminifera are severely abraded and coated in thick calcitic crusts.	Meteoric-vadose	Mature
Caveton	Laslett Road	No karst identified. Foraminifera are generally well-preserved with only minor abrasion features observed.		Weakly mature
	Rabbitors Road	Micritic meniscus cements observed on grain edges and dog-tooth spar identified in intra-grain pores. Moderate aragonite proportions. 15 cm thick rubbly calcrete. Foraminifera primarily show signs of dissolution.	Meteoric-vadose	Weakly mature
	Bucks Hill	Fine meniscus cements are observed. Low aragonite and high-Mg calcite proportions. No karst identified. Foraminifera are difficult to identify as ornamentation is severely reduced.	Meteoric-vadose	Mature
Gambier	Gooch Road	Highly cemented sample. Fine, micritic cement observed on grain edges upon which a dog-tooth spar and drusy spar have developed. Very low aragonite and low high-Mg calcite proportions. No karst identified. Foraminifera generally well-preserved and dissolution is the primarily destructive process.	Near surface marine	Mature
Compton	Baxter's Quarry	Two stages of cement development identified. Micritic cement on grains edges upon which a blocky spar has developed and filled pore spaces. Very low aragonite and high-Mg calcite proportions. Rhizoliths identified and wide solution pipes (up to 1 m) partially filled with <i>terra rossa</i> soils. Foraminifera are generally coated in thick calcitic crusts.	Meteoric-vadose to near surface marine	Highly mature
	Heritage Industries	No aragonite and low high-Mg calcite proportions. Wide (up to 1 m) and densely packed solution pipes. Foraminifera are severely abraded.	Meteoric-vadose to near surface marine	Highly Mature
Mingbool	Don's Quarry	Very low aragonite and high-Mg calcite proportions. No karst identified. Foraminifera are partially abraded and dissolution features are more common. Calcitic crystals are identified over much of the test.	Meteoric-vadose to near surface marine	Mature
Dismal	Dartmoor Cemetery	Highly cemented sample. Micritic rim found on grains. Dog-tooth spar and blocky spar fill pore spaces. No aragonite and low high-Mg calcite proportions. Small solution pipes identified near top of exposure. Foraminiferal tests are severely exfoliated and highly cemented.	Near surface marine	Mature
	Fort O'Hare Quarry	Cement dominated sample. Micritic rim on grains upon which a dog-tooth and drusy spar have developed. Very low aragonite and high-Mg calcite proportions – sample is almost completely calcite. 1 m thick laminar calcrete capping unit, and a potential solution pipe. Dissolution features are common of foraminiferal surfaces. Thick calcite crusts commonly identified.	Near surface marine	Mature
	Mingbool village	Sediment is significantly iron-stained. Meniscus micritic cements identified upon which isopachous dog-tooth spar has developed. Syntaxial overgrowth cements are identified on echinoid fragments. Very low aragonite and high Mg-calcite proportions – sample is almost completely calcite. No karst identified. Foraminiferal test surface are severely exfoliated and thick calcitic crusts are common.	Near surface marine	Mature
Naracoorte	Henschke Quarry	Highly cemented sample. Micritic cement is more common than in previously examined sample, but cements also show a similar pattern with micrite found on grain edges upon which dog-tooth and blocky spars have developed.	Near surface marine	Mature

In conclusion, this chapter has highlighted that sediments from sample sites across the coastal plain are affected by diagenesis differently, and this alteration may not necessarily relate to sample age but to variations in climate, depositional and diagenetic environments. In general, the petrographic analysis of sediments supports the lithostratigraphic interpretations of study sites proposed in Chapter 3. Identification of the mineralogical and compositional data from sediment samples will be potentially useful in accounting for varying results from the AAR analysis of bioclastic sediment using the whole-rock technique conducted in Chapter 5. Identification of textural differences in foraminifera will aid in interpretation of results of single-grain AAR analysis conducted on foraminifera in Chapter 5, and may assist in accounting for any anomalous data points.



# Chapter 5

## **Amino acid racemisation, radiocarbon and optically stimulated luminescence dating of the Bridgewater Formation, Mount Gambier coastal plain, southern Australia**

### **5.1 Introduction**

Sprigg (1952) suggested that the shoreline barriers of the Bridgewater Formation across the Mount Gambier coastal plain formed during successive sea-level highstands. Building upon the work of previous investigations (Murray-Wallace *et al.*, 1996; 1999; 2001) this chapter presents a geochronological framework for these successions to provide a critical evaluation of the original hypothesis formulated by Sprigg (1952). The geochronological methods applied within this thesis are introduced and reasons for their selection are discussed. Amino acid racemisation (AAR) analysis is the primary geochronological tool used in this study and a review of its principles and its application as a dating tool to coastal carbonate deposits is presented. Following this, the sampling strategy and methods for applying AAR in this study are outlined. Radiocarbon and optically stimulated luminescence (OSL) dating were also used to aid in constraining the time of deposition of the coastal deposits and in calibrating rates of racemisation. A brief outline of these methods is also presented as well as the approaches to calibrating AAR. The geochronological results derived from the use of AAR, radiocarbon and OSL are then presented for each of the coastal successions analysed. A summary of these results will then be outlined and initial patterns within these results discussed.

### **5.2 Geochronological methods adopted in this study**

To constrain the timing of deposition of the coastal barriers on the Mount Gambier coastal plain and associated sea-level highstands, a suite of geochronological techniques was used. AAR was performed on both fossil molluscs and carbonate sediments from within the dune ranges. Radiocarbon dating was conducted on shell presumed to be younger than 50,000 years and optically stimulated luminescence (OSL) was used on dune sediment samples which can be assumed to have been bleached prior to burial.

AAR was chosen as the primary geochronological tool as the dune limestones and fossils within them are particularly suited to this method. AAR dating is applicable in this region on a timeframe between 100 years and 1.2 million years, as shown by Murray-Wallace *et al.* (2001) through their use of whole-rock dating on the Robe coastal plain.

Radiocarbon and OSL dating were used to calibrate the rate of racemisation and aid in determining numerical ages from AAR analysis. Radiocarbon dating can be used to determine the time of cessation of  $^{14}\text{C}$  uptake of living organisms (commonly found to correspond with death for short-lived organisms) assuming that a closed system has existed since the death of the organism, there has been a constant production of  $^{14}\text{C}$  over time, the ratio of  $^{14}\text{C}:^{12}\text{C}$  in the biosphere and hydrosphere is in equilibrium with the ratio in the atmosphere, and that the decay rate of  $^{14}\text{C}$  is constant. The isotope  $^{14}\text{C}$  has a half-life of  $5730 \pm 40$  years and thus can only date samples reliably that are younger than 50 ka. Radiocarbon dating was used in this study to aid in calibrating Holocene and latest late Pleistocene fossil shell. The chosen specimen was cut in two; half of the sample was radiocarbon dated and the other half analysed using AAR. While radiocarbon is applicable to only a small proportion of fossil shell analysed within this study, it is useful as a calibration tool for the early portion of the kinetic pathway. An advantage of using radiocarbon dating for calibrating the rate of racemisation is that AAR analysis can be conducted on the same sample and both techniques are dating the same event, namely, the death of the organism.

While most of the coastal barriers on the Mount Gambier coastal plain are composed primarily of calcium carbonate (in the form of low-Mg calcite, aragonite and high-Mg calcite) quartz also comprises a significant component (up to 10% in some samples), and thus aeolian sediment samples were suitable for OSL analysis. OSL analyses yield ages that correspond to when sediments were last exposed to light. Areas of potential reworking or units suspected to have experienced pedogenic alteration should therefore be avoided when sampling for OSL. The age range of OSL varies depending upon the dose rate, but can range to approximately 500 ka under particularly favourable conditions, though is commonly only 100-200 ka. Therefore, the use of OSL aids in constraining the age of late Pleistocene deposits on the Mount Gambier coastal plain. A potential limitation of using OSL analysis to aid in calibrating the rate of racemisation is that it records a different event than AAR. OSL determines when the sediment was last exposed to light, and thus records the time of burial or deposition, while AAR defines the cessation of protein formation in carbonate-secreting organisms. The two events may not necessarily coincide and accordingly, caution must be exercised when using

OSL as a calibration tool. Furthermore, while OSL can be used reliably on most quartz-bearing aeolian sediments, where grains are quickly 'bleached' by light, OSL dating of marine sediments is more experimental, as there may be incomplete bleaching. Additional stratigraphical analyses are commonly required to assess these age-event relationships.

### 5.3 Amino acid racemisation dating - a review

As AAR is the principal geochronological technique within this study, the following discussion reviews the literature on previous AAR studies and in particular those focused on coastal successions. The review details the principles of the technique, how the application of AAR has varied its history of application, parameters influencing racemisation, the application of AAR as a geochronological tool, the kinetics of the racemisation reaction, potentially datable material, limitations of AAR, and examples of AAR application to other marginal marine sequences.

#### 5.3.1 Principles of amino acid racemisation dating

Amino acid racemisation has been widely used as a dating technique since the 1970s. The principle of the technique is based upon the preservation and time-dependent degradation of protein within fossils. Amino acids that are found within fossilised skeletal remains represent the diagenetic alteration products of the original mineralised proteins (Wehmiller, 1993). Amino acids are low in molecular weight, non-volatile, crystalline compounds (Rutter *et al.*, 1979). They are present in all living organisms and are used in protein synthesis. Structurally, all amino acids except glycine contain a central tetrahedral carbon atom (or centre of symmetry) which is connected to four different atoms or groups of atoms: a carboxylic acid group (-COOH), an amino group (-NH<sub>2</sub>), a hydrogen atom (-H) and a hydrocarbon group (-R).

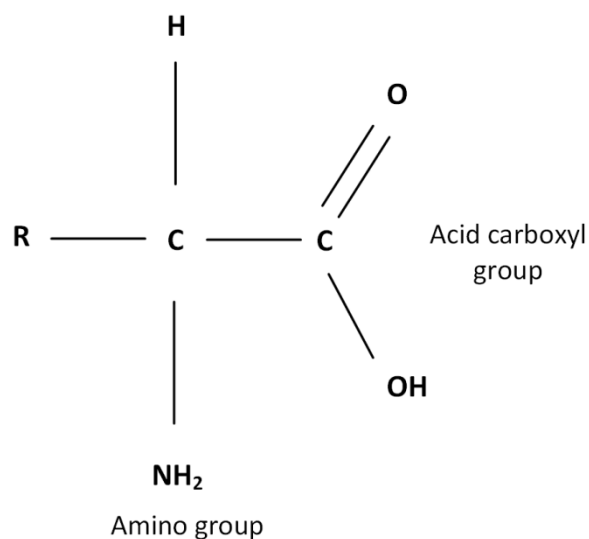


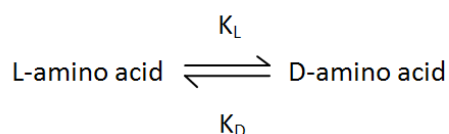
Figure 5.1: Diagrammatic representation of amino acid structure.

Amino acids are chiral molecules, in that their mirror images cannot be superimposed (Miller and Clarke, 2007). Chiral forms of the same amino acid can be identified by how they rotate plane polarised light; with L-amino acids (levorotatory) rotating light to the left, and D-amino acids (dextrorotatory) rotating light to the right.

Abelson (1954) noted that living organisms almost exclusively use L-amino acids in protein synthesis. After cessation of protein synthesis, usually associated with death of an organism, biological constraints are removed and diagenetic reactions begin to degrade proteinaceous residues into their constituent amino acids, which spontaneously interconvert into their D-configurations (Bada and Schroeder, 1975) until equilibrium is reached.

The process by which L-amino acids readily convert to a D-configuration is known as racemisation and it is a reversible reaction. The mechanism of racemisation involves the abstraction of the  $\alpha$  proton by the hydroxide ion, leading to the formation of a planar carbanion (Bada and Schroeder, 1975). In principle, the D value for each amino acid preserved within the fossil will increase with time from 0 in living organisms, to an equilibrium value of 1.

Racemisation can be illustrated through the following equation;



Where  $K_L$  and  $K_D$  are the rate constant for the forward and reverse reactions.

The diastereoisomer isoleucine, unlike most other amino acids, contains two centres of asymmetry. L-isoleucine undergoes a reaction around only one of these centres, the  $\alpha$ -carbon atom, and produces different molecules: D-alloisoleucine, through the process of epimerisation. The equilibrium value of D-alloisoleucine is ca. 1.25-1.30, but a range of values have been reported as noted by Williams and Smith (1977).

### 5.3.2 Historical review

The first report of the presence of amino acids in fossil shells, bones and teeth was by Phillip Abelson (1954). Abelson examined a fish bone of Devonian age and concluded that it contained a range of amino acids. He recognised that amino acids could survive up to millions of years at ambient Earth temperatures and suggested that the rate of protein degradation in fossils could provide the basis for a dating method. In 1968, Hare and Abelson observed that there was a distinct correlation between the extent of isoleucine epimerisation and fossil age,

while Hare and Mitterer (1969) were the first to estimate an age for a fossil based on the stereochemistry of amino acids.

Amino acid separation methods have progressed with initial methods using stereospecific enzymes to destroy one chiral form preferentially (Hare and Abelson, 1968). More robust separation methods are based on either gas or liquid chromatography with ion-exchange liquid chromatography (IEC) also a commonly used technique (Penkman, 2009). Gas chromatography (GC) can separate multiple DL isomers from single samples, allowing for the cross-checking of unreliable results across a suite of amino acids. Sample preparation for GC, however, is highly time consuming, resulting in few samples analysed under time and budget constraints. IEC, on the other hand, requires minimal sample preparation yet can only resolve a single pair of amino acids; L-isoleucine and D-alloisoleucine. Kaufman and Manley (1998) suggested that reverse-phase, high-performance liquid chromatography (RP-HPLC) combines the advantages of both IEC and GC in that sample preparation is simple and the instrumentation is fully automated. RP-HPLC allows amino acids to be derivatised before their separation on a reverse phase column allowing for higher sensitivity with regard to separation of D/L amino acids (Kaufman and Manley, 1998). IEC, however, employs post-column derivitisation of amino acids.

### **5.3.3 Parameters that influence racemisation within natural systems**

The rate of racemisation and/or epimerisation of amino acids within fossils are sensitive to a range of factors including temperature, the matrix in which the amino acid is imbedded, the position of the amino acid within the peptide chain, the amino acid being analysed, the species of the analysed organism, and external diagenetic factors such as moisture content and pH.

#### **Temperature**

The rate of racemisation/epimerisation of amino acids is temperature-dependent, and can be described by the Arrhenius equation:

$$\ln(k_1) = \ln(A) - E_a/RT$$

Whereby  $k_1$  is the forward rate constant;  $A$  is a constant, commonly referred to as the Arrhenius factor;  $E_a$  is the activation energy;  $R$  is the universal gas constant; and  $T$  is the integrated thermal history  $T_{eff}$  in Kelvin.

As racemisation/epimerisation reactions are highly sensitive to temperature, knowledge of the temperature history of a deposit is required before a reliable assessment of age can be derived. Through a range of laboratory studies, aimed at determining the

temperature sensitivity of the epimerisation of isoleucine in a variety of samples (e.g. Mitterer, 1975; McCoy, 1987), it has been concluded that a 1°C increase in temperature will yield an 18% increase in the rate of racemisation/epimerisation; thus a 5°C rise in temperature will more than double the reaction rate. A 5°C reduction in temperature will decrease the rate of racemisation by about 60% (Clarke and Murray-Wallace, 2006). Due to the exponential dependence of racemisation on temperature, specimens that are exposed to high-amplitude seasonal temperature fluctuations will have a resultant reaction rate equivalent to a higher temperature than those of deeply buried samples of the same age (Miller *et al.*, 1997). Thus, in environments characterised by large temperature fluctuations it is necessary to ensure that fossils have been sufficiently buried by overlying sediment in order to calculate an age accurately. If palaeoclimatic information is available the Effective Quaternary Temperature (EQT) can be calculated and uncertainties minimised (Wehmiller, 1982). EQT is the integrated kinetic effect of temperature and provides a weighted average rate constant for a sample of a certain age. However, to calculate EQT closely, you first need to know the age of the material you are dating. Sampling from depth is recommended to be more than 1 m (Murray-Wallace, 1995) and can aid in avoiding the effects of (seasonal and diurnal) temperature fluctuations on fossils, so that the long-term influence on diagenetic racemisation is the effect of temperature variations associated with climate change.

The effects of temperature differences on racemisation rates have been reported from a range of AAR studies. Hearty and Aharon (1988) documented the rapid epimerisation in the giant clam *Tridacna* during the Holocene and last interglacial maximum on the Huon Peninsula, Papua New Guinea. They found that when calibrated with radiocarbon and Th/U ages the majority of epimerisation occurred during warm interglacial intervals between 130 and 80 ka and within the last 10 ka of the Holocene. On the island of Bermuda, samples deposited at the beginning of MIS 5e (130 ka) were found to have experienced more interglacial warmth than those deposited later in the last interglacial maximum (120 ka), and this was attributed to epimerisation Alloseucine/Isoleucine (Ala/Ile) differences found in deposits between the beginning and end of MIS 5e (Hearty, 2002). Hearty (1986; 1987) also recognised this 'interglacial effect' within *Helix* (land snails) and *Glycymeris* (marine pelyceps) from the Mediterranean basin. However, Muhs *et al.* (2002) and Rowe *et al.* (2014) dated the same deposits on Bermuda analysed by Hearty (2002) to MIS 7 (~200 ka), and not MIS 5e, which therefore brings the effect of interglacial temperature on D/L values into contention.

In a study of AAR within molluscs from last interglacial (*sensu lato*) sites, Miller and Mangerud (1985) also identified a temperature effect on epimerisation rates. They detected that D/L ratios were substantially lower in molluscs found along the Arctic coast of Russia, due to low thermal histories, when compared with European counterparts.

Understanding the influence of temperature on racemisation/epimerisation rates is thus crucial to the validity of amino acid racemisation as a geochronological method. The diagenetic temperature history of fossils since their death and incorporation into sediments is an important factor influencing the racemisation reaction (Murray-Wallace and Kimber, 1988) and should be accounted for when comparing D/L values between sites.

### **Taxonomic effects**

Another factor influencing racemisation rates of amino acids is the taxonomic form in which the amino acid is contained. Variations of racemisation rates have been found to be inter-species specific (e.g. King and Hare, 1972; King and Neville, 1977) and intra-species specific (e.g. Brigham, 1983; Sejrup and Haugen, 1994).

Isoleucine epimerisation rates in fossil planktonic foraminifera were studied from the equatorial Pacific core V28-238 by King and Neville (1977), who found a strong species-dependent relationship. King and Hare (1972) also studied the amino acid analyses of planktonic foraminifera and concluded that each species has a unique pattern of racemisation that differs from that of other species. Therefore, chronological studies should focus on monospecific samples in order to eliminate error and obtain a higher degree of precision in results (King and Neville, 1977).

Racemisation rates have also been found to vary significantly within individual molluscs. From studying five anatomically different portions in the mollusc species *Hiatella arctica*, Brigham (1983) noted that the concentration of certain amino acids (including; aspartic acid, serine, glutamic acid, glycine, alanine, valine, alloisoleucine, isoleucine and leucine) were significantly higher in the hinge and central part of the shell, and lower towards the shell's outer edge. Brigham (1983) suggested that possible reasons for this difference in amino acid concentration could be due to leaching of the thinner, more vulnerable shell growth edge, or due to a protein rich layer lining the valve near the central and hinge region of the shell. Sejrup and Haugen (1994) studied the molluscan species *Arctica islandica* at sites in Norway, Scotland and the North Sea and found that there was an increase in the degree of isoleucine epimerisation and decreasing amino acid concentrations from the inner part of the valve to the outer. By comparing amino acid concentrations of fossil shells with their recent



counterparts, Sejrup and Haugen (1994) found a more uniform amino acid concentration throughout the modern shells, and suggested that the exposure to amino-acid-consuming bacteria in fossil shells may be an explanation for the observed gradient.

Previous research has shown variations in amino acid racemisation rates can be inter- and intra-species specific (e.g. King and Hare, 1972; Brigham, 1983; Sejrup and Haugen, 1994). Therefore, when sampling, it is advised where possible to sample the same species and within the same physical location (e.g. the hinge) in order to maintain consistency and to eliminate factors other than age and temperature influencing the D/L value.

### **Molecular environment of the amino acid**

The location of an amino acid within a peptide chain, the neighbouring amino acids and the characteristic R-group are also known to affect the rate of racemisation (e.g. Wehmiller and Hare, 1971; Kriaušakul and Mitterer, 1978; Bada and Man, 1980; Mitterer and Kriaušakul, 1984; Bada, 1985). Through an investigation into rates of epimerisation of isoleucine, Kriaušakul and Mitterer (1978) proposed that isoleucine would preferentially epimerise at a terminal position within the polypeptide chain and that rates of epimerisation are substantially lower in the interior and free positions. Kriaušakul and Mitterer (1978) suggested that reasons for this slower epimerisation rate at interior positions may be due to the reduced stability of the intermediate carbanion in the interior position, or due to the restriction in the rearrangement of the carbanion structure as a consequence of intra-molecular hydrogen bonding. Laboratory experiments have indicated that epimerisation of isoleucine occurs more rapidly at the NH<sub>2</sub> terminal position than at the COOH terminal (Kriaušakul and Mitterer, 1978; Bada, 1985). Other researchers have noted that the free amino acid fraction is consistently more extensively racemised than the total hydrolysate (Wehmiller and Hare, 1971; Schroeder and Bada, 1976; Murray-Wallace and Kimber, 1987). Initially, most amino acids will be in the interior portion of a peptide chain. Through hydrolysis the interior amino acids will be hydrolysed to terminal positions (Figure 5.2) where they will preferentially racemise. Over time, a greater number of slowly racemising amino acids, in the form of free amino acids, will be present, causing a reduction in racemisation rates (Kriaušakul and Mitterer, 1978).

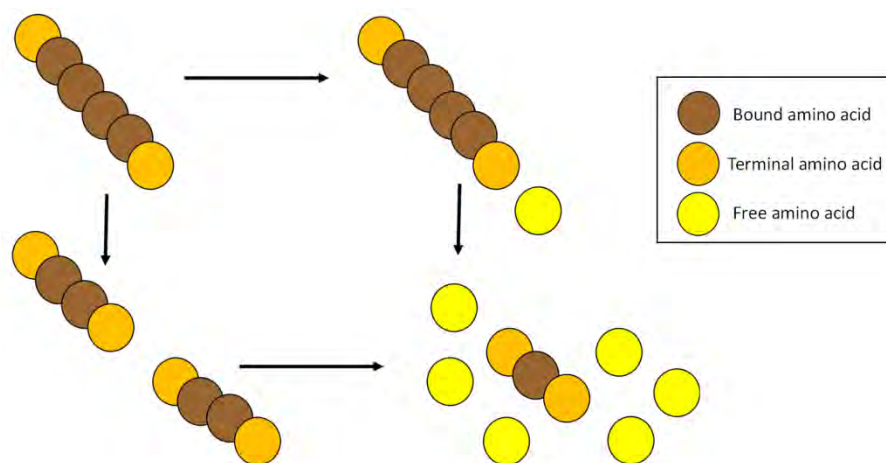


**Figure 5.2:** Hydrolysis of peptide bonds in a protein chain, creating terminal and free amino acids. Modified from Penkman (2009).

Bada and Man (1980) have suggested that the rate of hydrolytic decomposition of amino acids may depend upon the sedimentary environment in which the amino acid is contained, and proposed that hydrolysis is faster in calcareous sediments. The strength of the peptide bonds also has an influence over the rate of racemisation (Kriaušakul and Mitterer, 1978) causing different amino acids to reach D/L equilibrium faster than others.

Rates of racemisation vary depending on which amino acid is being considered (Kvenvolden *et al.*, 1971) in accordance with the ability of the R groups to stabilise a carbanion intermediate (Miller and Clarke, 2007). As amino acids racemise at different rates, different amino acids are thus useful for analysing certain time frames (Goodfriend, 1991). Isoleucine and leucine are commonly the primary choice for dating carbonate fossils as both racemise/epimerise relatively slowly (Miller and Brigham-Grette, 1989) whereas faster racemising amino acids (such as aspartic acid and serine) are commonly a more appropriate option for dating the last ca. 1000 years (Goodfriend, 1991) or the Holocene.

## pH

The pH value of the dated material also influences the racemisation rate. It has been shown that between pH values of 3 and 9, the racemisation rates in bone are largely independent of pH (Bada and Shou, 1980). A more recent study, quantifying the effects of varying alkaline pH values on the racemisation rates of amino acids in the fresh water species *Margaritifera falcata*, found pH values of pore water greater than 9 to have a significant influence (Orem and Kaufman, 2011). However, the effect of changes in pH to racemisation rates in molluscs may be limited due to the buffering effects of the shell carbonate (McCoy, 1987; Smith *et al.*, 1978).

### **Presence of water**

The presence of water has been demonstrated to accelerate the racemisation reaction (Bada, 1985), yet it may also provide a mechanism for leaching, resulting in the progressive loss of amino acids from a fossil (Hare, 1974; Murray-Wallace and Kimber, 1988), particularly the more labile, lower-molecular-weight fractions. The matrix surrounding the fossil will also affect the availability of water depending upon its permeability (Rutter and Blackwell, 1995). Murray-Wallace and Kimber (1987) suggested that a plot of aspartic acid and glutamic acid D/L values in molluscs can be used to identify discrete groups. Distinct outliers from these groups may indicate leaching. High serine concentration may be used to indicate secondary contamination (Miller and Brigham-Grette, 1989).

### **Inter- and intra-crystalline fractions of amino acids**

The intra-crystalline fraction of amino acids comprises the amino acids that are found within the carbonate crystals of fossils, whereas the inter-crystalline amino acids are found between the plates of crystalline carbonate. The inter-crystalline fraction of amino acids may therefore undergo a wider range of diagenetic pathways which may lead to variation in the acid concentration and abundance with age, even for shells that have been deposited within the same depositional environment (Penkman *et al.*, 2008) and is again a function of the integrity of the diagenetic environment. Penkman *et al.* (2008) suggested that the intra-crystalline fraction approximates a closed system of amino acids, as they are effectively isolated from external rate-affecting factors such as contamination by allochthonous material (Sykes *et al.*, 1995), leaching, and microbial decomposition.

It is therefore proposed that the intra-crystalline amino acid population provides a superior subset of amino acids that will most likely produce reliable samples for geochronological applications (Sykes *et al.*, 1995; Penkman *et al.*, 2008). Penkman *et al.* (2008) suggested that in order to isolate the intra-crystalline fraction and remove the organic matrix between mineral crystals, powdered mollusc shells be exposed to concentrated NaOCl for 48 hours. Through the treatment of land snails with NaOCl, Sykes *et al.* (1995) found that the D/L ratio of isoleucine was increased compared to previous analysis without NaOCl.

The above discussion has shown that the racemisation/epimerisation of amino acids is not just temperature-dependent, but also influenced by intra- and inter-species specific effects, the particular amino acid being used, the position of the amino acid within the peptide chain, adjacent amino acids, the strength of the peptide bonds, and whether the inter- or intra-crystalline fraction of an amino acid is analysed. The pH value and presence of water

within a sample have relatively low to minimal impact. The utility of racemisation as a geochronological tool depends on a thorough understanding of these diagenetic reactions of amino acids (Wehmiller and Hare, 1971).

#### **5.3.4 Amino acid racemisation as a dating technique**

Rutter and Blackwell (1995) describe two methods in using amino acid racemisation data in determination of numerical ages: the uncalibrated and calibrated methods. The uncalibrated approach does not use age data derived from other geochronological methods to calibrate amino acid racemisation rates. This method requires a precise knowledge of the temperature history of the fossil, the racemisation rate constant of the pertinent amino acid and the D/L value of the amino acid within the fossil being dated. The fossil age can then be determined by placing these values in an appropriate integrated rate equation based upon amino acid racemisation kinetics. Problems associated with this technique include the accurate assessment of diagenetic temperature over time, which can never be known with any certainty. The calibrated method requires the D/L value of an amino acid to be obtained for the fossil being dated by alternative, independent means, such as by radiocarbon dating. The main assumption associated with this method is that the temperature history of the calibrated fossil is the same as that of the fossil which is to be dated (Rutter *et al.*, 1979).

One of the strengths of amino acid racemisation as a dating tool is the timeframe to which the method can be applied. Currently, radiocarbon dating can confidently be used to date samples back to approximately 50 ka BP, though this is preparation and measurement dependent and is also influenced by the nature of 'background'. Amino acid geochronology is thought to provide independent geochronological control beyond the limited range of radiocarbon techniques (Schroeder and Bada, 1976; Miller and Brigham-Grette, 1989). Miller and Hare (1980) also noted that amino acid dating can be performed faster and at a lower cost than radiocarbon measurements.

However, as the racemisation of amino acids is dependent on temperature, the age range of the method relies on the climate in which the sample has been deposited, as well as the differential rates of racemisation between amino acids, (e.g. aspartic acid and valine). The temperature experienced at a site has the greatest control on the resolving power of AAR application. In tropical regions, where mean annual temperatures (MAT) are greater than 25°C, D/L equilibrium may be attained in 150-300 ka. In mid-latitudinal regions, (where MAT is >10°C) equilibrium may require 2 Ma, with resolution no greater than 10-20 ka, while in Arctic sites (where MAT <-10°C), it may take more than 10 Ma for equilibrium to occur (Miller and

Brigham-Grette, 1989). Thus the temperature experienced at a site has the greatest control on the resolving power of AAR application.

Aminostratigraphy involves the classification of facies or strata into chronostratigraphic units that correspond to intervals of time called geochronologic units (Bowen, 1978; Murray-Wallace and Kimber, 1987; Murray-Wallace, 2000). Aminostratigraphy is most widely used in the aminostratigraphical subdivision of sedimentary successions, particularly in coastal areas (Murray-Wallace, 2000). D/L values from closely spaced, but discontinuous deposits are grouped into 'aminozones', which refer to single stratigraphical units that represent specific intervals of time. An aminozone may be defined by the clustering of amino acid D/L values on replicable molluscan or sedimentary fossils from a lithostratigraphical unit (Murray-Wallace, 2000). Litho-, bio- and morphostratigraphical evidence, in addition to calibration by other geochronological methods, is commonly used to support the chronostratigraphically derived units (Murray-Wallace, 2000). The main assumption in the use of aminostratigraphy is that the closely spaced localities have had similar temperature histories, in which case differences in D/L values can be attributed to age differences (Wehmiller, 1982). Miller and Hare (1980) proposed that the use of the aminostratigraphy technique was the least ambiguous application of amino acid geochronology as the method remains independent of kinetics of racemisation and eliminates the thermal history term. The success of aminostratigraphy is dependent upon the nature of the preserved geologic record, the detail of conducted stratigraphic analysis and the resolving power of the technique(s) employed (Wehmiller, 1993).

The use of aminozones to define substages within the last interglacial (MIS 5) has been largely unsuccessful. Rutter and Blackwell (1995) suggested that this is because the time interval of ~50 ka during MIS 5 does not statistically resolve differences in significant ratios due to the slow reaction rate. However, the use of aminostratigraphy has proven useful in separating MIS 5 from other isotopic stages, such as MIS 1 and MIS 7. Wehmiller (2013a) proposed that across United States coastal deposits, between latitudes 48°N and 30°N, relative age resolution of aminostratigraphy appears successful at the scale of interglacial intervals.

Aminochronology, however, uses independent age control for one or more aminozones and kinetic modelling to aid in estimation of samples within a particular aminostratigraphic region (Wehmiller, 1993). A numerical-based chronology requires an understanding of the sequential change in the thermal history of the deposit and the kinetics of racemisation. When the age of a sample in a region is derived from an independent

calibration (e.g. radiocarbon dating) it can be applied to a kinetic model and allows the determination of other sample ages in the region. Amino chronology is dependent upon the availability of another suitable geochronological technique. Radiocarbon is commonly used as a calibration tool for marine molluscs up to ~50 ka, but beyond this, calibrating reaction rates becomes more challenging due to the limited reliability of U-series analysis on shell deposits. Molluscs do not incorporate uranium from sea water while living (unlike corals) and have been found to behave as open-systems in relation to U-series isotopes *post-mortem* (Kaufman *et al.*, 1971; Kaufman *et al.*, 1996) deeming them unsuitable to this technique. OSL and thermoluminescence (TL) are commonly used in calibration, but technically date the burial of a unit rather than the cessation of protein synthesis (which usually coincides with death).

### 5.3.5 Kinetics

The kinetics of the amino acid racemisation reaction is central to the application of the method for deriving numerical ages. Amino acid racemisation can be used as a semi-quantitative tool of age estimation and temperature or age differences if appropriate models of racemisation kinetics are used (Wehmiller, 1982). The kinetic pathways of racemising amino acids have been contended.

Two conflicting models of racemisation kinetics were proposed in the earlier development and application of AAR in Quaternary stratigraphy and include: the 'extended linear' model (Kvenvolden *et al.*, 1979; 1981) and the 'nonlinear' model (Wehmiller and Belknap, 1978; Wehmiller, 1981). These two kinetic plots are compared in Figure 5.3.

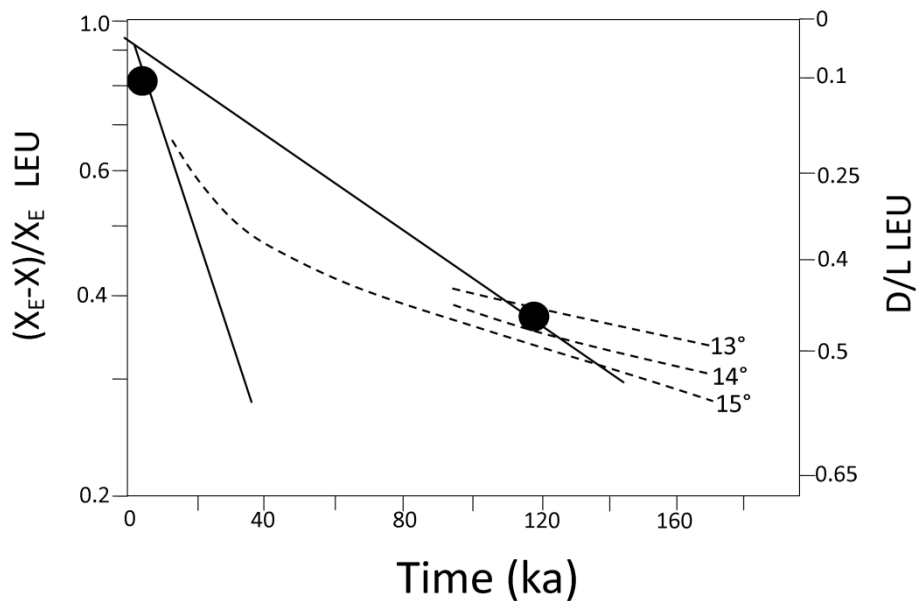


**Figure 5.3:** Comparison of the 'extended linear' and 'non-linear' kinetic model options for leucine racemisation in *Protothaca*, with solid lines representing the extended linear model and dashed lines the non-linear model.  $X = D / (D+L)$  at time  $T$ ,  $X_E = X$  at equilibrium, for leucine  $X_E = 0.50$ . From Wehmiller (1984).

It was initially suggested that the kinetic pathways of amino acids could be described using the extended linear model which assumes that the racemisation of amino acids follow linear, first-order kinetics from the cessation of protein synthesis to the attainment of racemisation equilibrium. This was argued to be simpler in concept, was thought to be more universal in its application and is used where  $D/L$  values are less than  $\sim 0.5$  (Kvenvolden *et al.*, 1981). However, it has since been suggested that racemisation kinetics in molluscs are non-linear. Accordingly, the kinetic pathway is characterised by two linear components with an intermediate transition zone (Wehmiller and Belknap, 1978). In the non-linear kinetic plot, the curve is linear to a  $D/L$  value of approximately 0.2, and then follows a steady decrease in slope gradient until a  $D/L$  value of approximately 0.35, where the racemisation rate is only about 10% of the initial rate (Wehmiller, 1984). The transition zone seen in the non-linear model represents a significant slowing of the racemisation reaction and is likely to signify the effect of a number of diagenetic reactions of high-molecular weight fossil polypeptides (Wehmiller and Hare, 1971; Wehmiller, 1982). Wehmiller's results are temperature-, genus- and amino-acid-specific. These kinetic phases are illustrated in Figure 5.4.



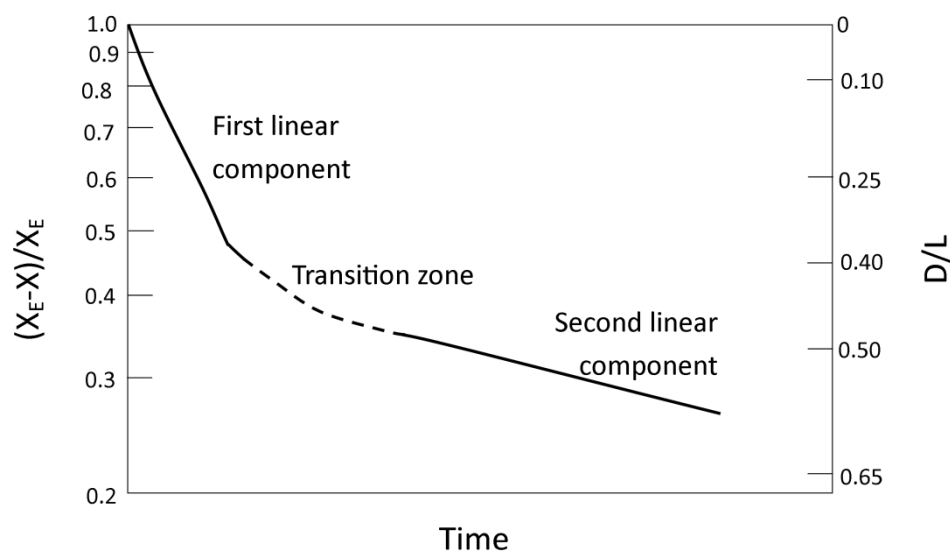


**Figure 5.4:** A kinetic plot demonstrating the general nature of probable racemisation kinetic pathways in molluscs,  $X = D / (D+L)$  at time  $T$ ,  $X_E = X$  at equilibrium (Wehmiller, 1982).

Support for the non-linear model comes from studies of the giant clam *Tridacna gigas* on the Huon Peninsula, Papua New Guinea and the Great Barrier Reef, Australia. Hearty and Aharon (1988) measured the D/L ratios of *Tridacna gigas* and calibrated their results against radiometrically dated coral reefs. Their results indicated three distinct phases of epimerisation: a fast rate for the first 8 ka; a transitional interval for the next 60 ka; and a final phase between 60 and 180 ka whereby D/L values obtained a quasi-equilibrium (Hearty and Aharon, 1988).

Bada and Schroeder (1975) proposed that epimerisation rates of isoleucine in calcareous marine sediments followed first order kinetics up to a *alle/Ile* value of 0.35, but that for values greater than this, the observed ratio was less than expected on the basis of linear kinetics. These results support the conclusions of Wehmiller and Hare (1971) who considered the epimerisation rates of isoleucine in foraminifera from several deep sea cores which had already been dated by a range of methods. Wehmiller and Hare (1971) found that at lower *in situ* temperatures D/L values of isoleucine greater than 0.3-0.4 do not obey reversible first order kinetics.

As mentioned previously, the rate of racemisation of amino acids is affected by its molecular environment. Initially, almost all of the amino acids are in interior positions in the peptide chain. Hydrolysis results in breakage of peptide bonds and thus transfers some of the interior amino acid to terminal positions where they are preferentially epimerised. This accounts for the first linear portion of the reaction (Mitterer and Kriausakul, 1989) as the rate of hydrolysis of proteins and peptides is nearly constant during this time period (Wehmiller

and Hare, 1971). Further hydrolysis results in some terminal amino acids converting to free amino acids which are racemised at a slower rate, and thus the overall reaction rate decreases. This is thought to represent the transitional zone (Mitterer and Kriausakul, 1989). Once the amino acid is almost entirely in the free state, the racemisation reaction rate again follows reversible first-order kinetics, although at a slower rate due to the slower racemising potential of free amino acids, and thus signifies the second linear component of the non-linear kinetic plot (Mitterer and Kriausakul, 1989). While non-linear kinetic plots of amino acid racemisation have been widely accepted, Mitterer and Kriausakul (1989) stated that the model proposed by Wehmiller and Belknap (1978) is complex and based upon a number of uncertainties and assumptions, most importantly the uncertainty of the limiting D/L value for the portion of the reaction within the transition zone, which will also be a function of the particular amino acid and temperature history.

Mitterer and Kriausakul (1989) instead proposed the use of parabolic kinetics which yields a linear relationship between the square root of age of samples and values of  $D/L < 1.0$ . Mitterer and Kriausakul (1989) stated that the change in the D/L value of isoleucine with time resembles a parabolic curve and therefore the reaction can be modelled by parabolic kinetics. A plot of the product yield against the square root of time will produce a straight line if parabolic kinetics are followed, and deviation from this line only occurs when parabolic kinetics are no longer followed. Figure 5.5 illustrates the parabolic kinetics for modern *Mercenaria campechiensis*, whereby the data are linear to  $alle/Ile \sim 1$ , suggesting the epimerisation of isoleucine follows apparent parabolic kinetics for this section of the reaction range (Mitterer and Kriausakul, 1989).

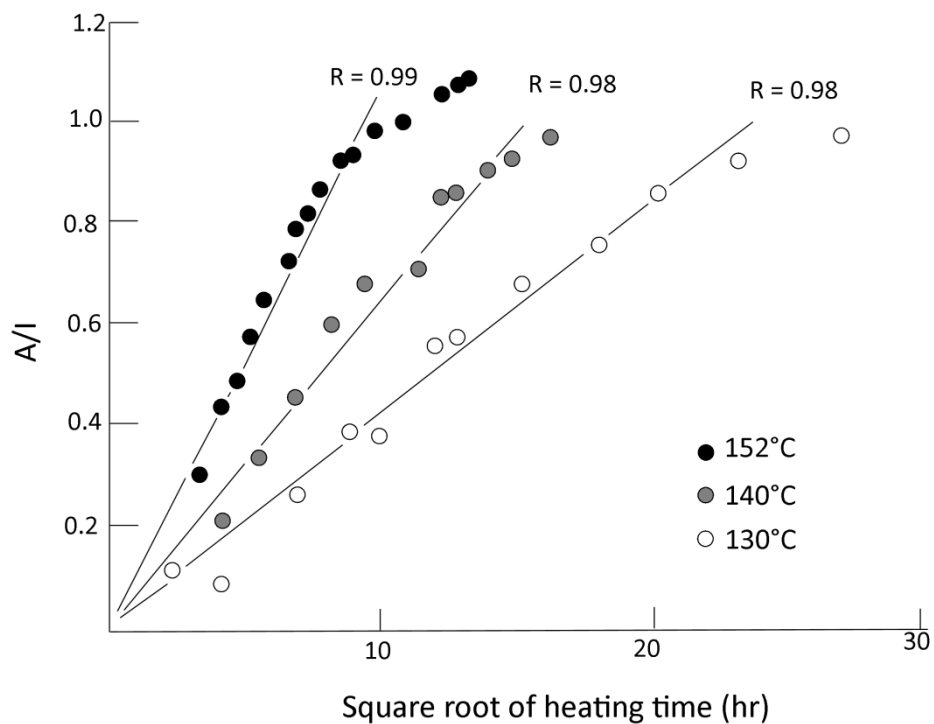


**Figure 5.5:** Laboratory-induced isoleucine epimerisation at a range of temperatures in modern *Mercenaria campechiensis* plotted as *alle/Ile* against the square root of time. From Mitterer and Kriausakul (1989).

Support for the use of parabolic kinetics comes from research in southern Australia by Murray-Wallace and Kimber (1993) who concluded that the racemisation in carbonate fossils may be described using parabolic kinetics of fossils up to 225,000 years old (MIS 7). Goodfriend (1991) studied the patterns of racemisation and epimerisation of amino acids in land snails from the Negev Desert, Southern Israel, and found further support for parabolic kinetics.

Application of a parabolic kinetic model has several advantages if a suitable calibration sample is available. Firstly, the parabolic relationship can be used to determine fossil age over a large portion of the reaction range (Mitterer and Kriausakul, 1989). Secondly, the parabolic model overcomes the uncertainties experienced within the non-linear model, such as the limiting value to which the reaction follows first order kinetics (Mitterer and Kriausakul, 1989) and the difficulty of deriving ages from samples that have undergone limited diagenesis (Murray-Wallace and Kimber, 1993). The parabolic model can also be applied without the knowledge of the thermal history of the fossil if a sufficient number and range of calibration points exist, and that calibration samples of fossils have experienced similar diagenetic temperatures (Clarke and Murray-Wallace, 2006).

However, limitations have also been documented with the use of parabolic kinetic racemisation plots. It has been suggested that the method does not discriminate ages reliably where D/L values exceed 0.8 and approach equilibrium due to the curvature of the parabola and the poor age-resolving power of slowly racemising amino acids (Murray-Wallace and Kimber, 1993; Clarke and Murray-Wallace, 2006). The extrapolation of kinetic models from results calibrated from the Holocene or late Pleistocene to older samples will underestimate the ages of the older samples (Wehmiller and Hare, 1971; Wehmiller and Belknap, 1978). Several kinetic models and mathematical expressions have been used to describe amino acid racemisation rates over time, with different approaches suited to different time frames. These are further outlined in an extensive review by Clarke and Murray-Wallace (2006).

### **5.3.6 Datable material**

Amino acid dating can be used on a range of material, including carbonate fossils, wood, bone, eye lenses and teeth. In principle, amino acid racemisation dating is useful for any skeletal amino acid material, though the largest number of studies have generally concentrated on calcareous shell structures (Wehmiller, 1986). The following discussion focuses on the application of AAR to carbonate fossils and bioclastic carbonate sediments as these are the materials analysed within this thesis.

#### **Carbonate fossils**

Carbonate fossils are particularly well suited to the amino acid dating technique due to their relatively sturdy shells and the natural buffering effect of the carbonate matrix which minimises significant losses of protein residues with time (Miller and Hare, 1980; Murray-Wallace and Kimber, 1988). Other than temperature, buffering also effectively excludes the effects of other environmental parameters.

In carbonate fossils, proteins and peptides aid in the calcification process, with protein membranes acting as templates upon which the calcium carbonate is crystallised (Crenshaw, 1980). During the biomineralisation phase, each successive organic layer is enveloped by the mineral phase and the surrounding carbonate effectively isolates the organic compounds from biological degradation and they may be preserved for long periods of time (Miller and Brigham-Grette, 1989).

Articulated (paired) bivalves are favoured for AAR analysis of molluscs as they are commonly indicative of the growth position of the fossil and suggest limited transport and reworking since deposition (Murray-Wallace and Kimber, 1988). Gastropods are also used as their thicker shell components, such as the opercula or columella, commonly retain amino

acids well. The ease of identification of molluscs also prevents errors that may result from generic effects (Murray-Wallace and Kimber, 1988).

Foraminifera have also been dated using the amino acid racemisation technique. King and Neville (1977) noted that the enclosing calcite skeleton found in planktonic foraminifera aids in protection of the internal organic matrix from the attack of bacteria and physiochemicals as well as sheltering the matrix from possible contamination. The major contribution from foraminiferal studies is the recognition of non-linear kinetic pathways (Wehmiller and Hare, 1971) and generic effects of racemisation (King and Neville, 1977). Technological improvements have allowed for AAR application on single grains (for example using RP-HPLC), and promoted the analysis of AAR on individual foraminifers.

More recently, foraminifera have been analysed by AAR from the Arctic Ocean (Kaufman *et al.*, 2008) and from Quaternary sediment cores within the Pacific, Atlantic and Arctic Oceans (Kaufman *et al.*, 2013). From the application of modelled power functions to the planktonic foraminifer *Pulleniatina oliquiloculata* within sediment cores from the Northern Queensland margin, Australia, Hearty *et al.* (2004) suggested depositional age estimates can be derived for up to 500 ka in this region.

### **Whole-rock**

AAR analysis has also been conducted on bioclastic carbonate sediments using the whole-rock technique. This method analyses aggregates of comminuted skeletal and carbonate grains that have formed offshore over time (Hearty *et al.*, 2000). Mitterer (1968) first demonstrated concentrations of amino acids, similar to those found in molluscs, are present in coated grains and aragonite muds. The whole-rock method was then pioneered by Hearty *et al.* (1992) and has since been successfully applied to shorelines globally. The method of using whole-rock samples is applicable to AAR as skeletal calcarenites contain abundant amino acids within bioclastic carbonate sands (Hearty and Vacher, 1994). The method is reliant upon the averaging effect of the variety of racemisation/epimerisation extent among the different bioclast components that comprise the sample (Hearty *et al.*, 1992). In a 150 mg sand sample of the 250-500 µm size fraction there are approximately 2500 grains. The extent of racemisation within whole-rock sediment therefore reflects an integrated effect of amino acid concentration and D/L values within multiple carbonate grains of varying age and mass (Murray-Wallace *et al.*, 2010). Murray-Wallace *et al.* (2001) stated that the whole-rock technique conforms to the acceptability criteria of AAR listed by Wehmiller (1984) in the context of marine molluscs, whereby samples must have: good mineralogical and chemical

preservation; stratigraphical and thermal consistency and; the ability to illustrate increasing racemisation with increasing age.

A distinct advantage of the whole-rock AAR technique is that it allows for the dating of Quaternary carbonates that contain limited, or no, microfossils (Hearty and O'Leary, 2008). The whole-rock method can therefore be used in supplementing lithostratigraphic correlations and provides a means of estimating the ages of depositional units that are lacking material datable by other geochronological methods (Hearty *et al.*, 1992). On the island of Bermuda, amino acid ratios have been found to be concordant with the established stratigraphy in approximately 97% of cases (Hearty *et al.*, 1992).

Hearty *et al.* (1992) stated that the development of the whole-rock method has made the Quaternary depositional record accessible to geochronology between 300 ka and >1 Ma. The rate of racemisation of the suite of amino acids within the carbonate sediment is temperature-dependent and thus the age limit to the whole-rock technique varies globally. Hearty and Kaufman (2000) suggested that the practical age limit of the whole-rock method on the Bahamas is approximately 450 - 500 ka (~MIS 13), where current mean annual temperature (CMAT) is ~23-25°C. On the Robe coastal plain, South Australia where CMAT is 14.5-14.7°C, Murray-Wallace *et al.* (2001) suggested that the age limit of the method may extend to approximately 1.2 Ma. Leucine concentrations within aeolianite whole-rock samples on the Coorong coastal plain have been found to display kinetic behaviour similar to that of aspartic acid in the coral *Porites australiensis* from the Great Barrier Reef (Goodfriend *et al.*, 1992). Murray-Wallace *et al.* (2001) suggested that while aspartic acid and leucine are known to racemise at very different rates the similar kinetic behaviour indicates the integrity of whole-rock samples in retaining indigenous amino acids for lengthy periods of time.

AAR whole-rock dating has proven to be a reliable method and is often found to be consistent with ages provided by a range of other techniques. For example, whole-rock ages are consistent with: TL and U-Th ages from aeolianite on Lord Howe Island (Brooke *et al.*, 2003); U-Th ages from aeolianite in Western Australia (Hearty and O'Leary, 2008) and; TL ages from the Coorong coastal plain, South Australia (Murray-Wallace *et al.*, 2001). The whole-rock approach can also be used in other forms of geochronological analysis. Roy (1990) reported the use of radiocarbon analysis on shell hash (sand samples comprised of hundreds of biogenic-carbonate fragments). Despite the mixing problem, Roy (1990) found that the ages derived from radiocarbon analyses corresponded well to depositional models of Holocene coastal sand barriers and estuaries.

The whole-rock method analyses grains that have formed offshore over time and therefore entirely 'modern' material cannot be expected (Hearty *et al.*, 2000) as a certain amount of time will have passed between sediment production and deposition on the beach. The residence time of the sediment on the beach and inner continental shelf needs to be considered in numerical age calculations. Therefore, each whole-rock sample will have some 'inherited' age. The main assumption is that the inherited age will be similar for all samples of the same age (Hearty *et al.*, 2000). For example, in whole-rock samples taken from a modern active beach on the Robe coastal plain, Murray-Wallace *et al.* (2001) found that D/L values of leucine were  $0.225 \pm 0.002$ ; while on Rottnest Island whole-rock samples from a modern beach at Fairbridge Bluff were found to yield an isoleucine value of 0.049 and a radiocarbon age of  $1581 \pm 112$  cal yr BP (Hearty and O'Leary, 2008). Thus, when calculating the age of a deposit, it is necessary to subtract this value (or the value of a range of modern beach samples from the region) in order to account for the residence time of the sediment on the shoreface.

As whole-rock samples are comprised of a variety of bioclasts, there is the possibility that a proportion or component of the sediment is reworked, and thus yielding an apparent age based on the extent of racemisation is potentially challenging. This element of reworking is not experienced in other datable material such as molluscs, whereby any sediment that enters the sample can be washed or etched away, though whole molluscs can be reworked and are sometimes difficult to discern. Hearty and Vacher (1994) suggested that older sediment that is reworked into younger sediment may not significantly influence the D/L value, but this is a question of scale and depends on the volumes and ages of both the original and introduced material. As sediment increases in age, the concentration of amino acids within it reduces (Corrado *et al.*, 1986), and thus the presence of older sediment within a sample would have little influence on the decisive whole-rock D/L ratio (Hearty and Vacher, 1994; Hearty and Kaufman, 2000). It is still possible for younger material to be reworked into a sample, and thus the argument in reverse is that this sediment would have higher amino acid concentrations and a significantly higher influence on the D/L value. The averaging of the racemisation extent of a range of bioclasts is vital to balance out these possibly younger/older reworked grains.

The effects of reworking and inherited age on the extent of racemisation can be illustrated when comparing whole-rock samples from the modern active beach with modern shell samples. On the South Australian coastline, modern shells may typically yield a D/L value for valine of approximately 0.02 - 0.03 (Murray-Wallace and Kimber, 1988). Much higher valine D/L values of  $0.189 \pm 0.006$  are yielded from the bioclastic sediment collected from



Parsons Beach, southern Fleurieu Peninsula, South Australia. Therefore sediment sub-samples are likely to yield higher D/L values, and a higher extent of racemisation, than molluscs sampled from the same deposit.

Other parameters that may influence the observed extent of racemisation within whole-rock sediment, besides reworking of grains, include variable thermal histories of sedimentary constituents and the potential genus-specific contrasts of individual grains (Murray-Wallace *et al.*, 2010). Within each whole-rock sample there is a variety of skeletal fragments of different genera of carbonate organisms. Brooke *et al.* (2003) noted that the significant variations in the proportions of different genera within deposits may result in significant differences in their D/L values. They stressed the importance of assessing the petrology and granular composition of each whole-rock sample collected.

Whole-rock aminostratigraphy has proven to be a useful and reliable method of amino acid analysis. It allows for the dating of material lacking in microfossils and yields an average racemisation extent of the bioclast constituents. The whole-rock method allows for dating of sediments back to more than one million years in some parts of the world depending on the diagenetic temperature of the region. However, limitations include the possibility of reworking of both younger and older sedimentary constituents into the deposit and the range of different racemisation rates and extents of bioclasts, thus also requiring an accurate petrological description of each whole-rock sample. While whole-rock AAR analysis is a useful geochronological tool it is recommended that other means of dating, such as AAR analysis of molluscan samples if present, are also conducted.

### **5.3.7 Limitations of the AAR technique**

While the amino acid racemisation technique has experienced success in dating samples, and exceeds the dating limit of radiocarbon, there are several limitations and uncertainties inherent with the technique. The primary uncertainties are the Arrhenius parameters and the estimated diagenetic temperature history that the sample has experienced since deposition (McCoy, 1987). The racemisation of an amino acid is highly dependent on temperature and if the temperature that a fossil has been exposed to is calculated incorrectly, the results will prove to be inaccurate. For example, with the epimerisation of isoleucine, a small temperature uncertainty of  $\pm 2^{\circ}\text{C}$  may produce an estimated age with a uncertainty of ca.  $\pm 36\%$  (Rutter *et al.*, 1979).

A major consideration, when using amino acid dating techniques, is the possibility of sample contamination (Rutter *et al.*, 1979). Contamination of the fossil with amino acids other than present at the time of death may lead to an overestimation or underestimation of the numerical age of the dated material. As the overall quantity of amino acids decrease, the potential influence of contamination increases (Wehmiller and Hare, 1971). Murray-Wallace and Kimber (1988) list four main areas of contamination: 1) groundwater leaching; 2) diagenetic formation of amino acids; 3) bacterial and algal contamination and; 4) contamination during sample collection and preparation. Leaching of amino acids has also been found to be a factor altering 'true' racemisation extents. The molecules that are most susceptible to leaching are those low in molecular weight such as free amino acids and small peptides (Miller and Clarke, 2007).

Errors may result from species misinterpretation (Murray-Wallace and Kimber, 1987). When correlating the chronostratigraphy of different geological deposits the effects of reworking, variations in diagenetic conditions, differential weathering, erosion and subaerial exposure should be addressed, as the ultimate precision of the technique is partly dependent on the degree of control placed on these factors (Murray-Wallace and Kimber, 1987).

The racemisation reaction is dependent upon the matrix in which the amino acids are imbedded and therefore an individual amino acid would be expected to racemise at a different rate in shell than in bone or wood (Rutter *et al.*, 1979). Therefore, caution must be undertaken when comparing racemisation rates from different matrices and when comparing D/L values from differing climatic regions.

#### **5.3.8 Examples from coastal deposits/marginal marine sequences**

Bowen *et al.* (1985) used amino acid dating techniques to identify D/L values in marine molluscs along the coast of southwest Britain. They studied species that epimerised at similar rates and used U-series dating as a form of geochronological calibration and exerted lithostratigraphical correlation. Bowen *et al.* (1985) were able to identify three highstands of sea-level, during MIS 7 to MIS 5, and were able to place constraints on the timing and extent of Late Devensian glaciation in southwest Britain.

Using whole-rock aminostratigraphy to aid in dating carbonate deposits along the coastline of Eleuthera, the Bahamas, Hearty *et al.* (2000) were able to identify eight soil-bounded limestone sequences, representing at least six full interglacials, from the Holocene to MIS 13. Hearty *et al.* (2000) associated the *terra rossa* bound units with glacials and the

limestone deposits with interglacial sea-level highstands. Parabolic kinetics were used to derive age estimates for aminozones, which supplemented lithostratigraphic correlation within the sequences examined. Due to the largely non-coraliferous sedimentary deposits found along the Bahamas, radiometric dating of corals is commonly inapplicable, and thus aminostratigraphy proves to be a valuable dating and correlation tool along this coastline (Hearty, 1998).

Hearty *et al.* (1999) used whole-rock aminostratigraphy to suggest that marine deposits at  $+20 \pm 3$  m APSL on the supposedly tectonically stable coastlines of Bermuda and the Bahamas support the hypothesis of a partial collapse of the Antarctica icesheet during MIS 11. As well as on Bermuda (Hearty *et al.*, 1992), and the Bahamas (Kindler and Hearty, 1997) whole-rock aminostratigraphy has also been successfully used on aeolianite deposits in Hawaii (Hearty *et al.*, 2000), South Australia (Murray-Wallace *et al.*, 2001), Western Australia and Rottnest Island (Hearty and O'Leary, 2008), and Lord Howe Island (Brooke *et al.*, 2003).

#### 5.3.9 Discussion

While amino acid dating can extend beyond the age range of radiocarbon dating and commonly requires small sample sizes, it is a less precise technique than other conventional isotopic techniques due to the range of environmental factors that influence racemisation rates (Schroeder and Bada, 1976). Limitations in precision result in uncertainties associated with numerical ages derived from the dating method. The primary uncertainties are the Arrhenius parameters and estimates of the effective diagenetic temperature a sample has experienced (McCoy, 1987). Kosnik *et al.* (2008) stated that determining analytical precision is relatively easy, yet incorporating the uncertainty related to the variability within a specimen, collection of shells, or among amino acids is more complicated. Miller and Brigham-Grette (1989) suggested that with reliable independent calibration samples, interpolation up until  $\sim D/L < 0.3$  is reliable to about  $\pm 15 - 20\%$ , whereas after the transition phase, interpolation is less reliable and carries an uncertainty of  $\pm 30 - 40\%$ . McCoy (1987) proposed that numerical ages can be calculated with a precision no better than  $\pm 40 - 50\%$  if the age equation is not calibrated locally.

The temporal resolution of amino acid dating is also of concern. There is the possibility that the natural variability of the D/L values in shells is large enough to create an overlap between aminozones, thus complicating the identification of reworked material (McCarroll, 2002). Defining the existence and division between aminogroups and aminozones can also be subjective (Penkman, 2009). It is therefore imperative that detailed site

descriptions and consistent facies architecture descriptions are maintained throughout sample collection.

Data screening and the recognition of outlying data can aid in increasing the precision of the technique. Kosnik and Kaufman (2008) listed and examined a variety of screening criteria including high serine concentrations, covariance of aspartic acid and glutamic acid concentrations, replication of measurements, and the relations between aspartic acid and glutamic acid concentrations. High serine concentrations can be indicative of modern contamination, as serine is known to decompose rapidly, and therefore its abundance can be compared with other amino acids to account for the expected reduction with time. Unusually high concentrations of D-glutamic acid, D-aspartic acid or D-alanine can be indicative of modern contamination as each are significant components of some bacterial cell walls (Murray-Wallace and Kimber, 1988). Specimens that yield values greater than  $2\sigma$  outside the group range are commonly excluded from calculations as samples with unusually high D/L values have been potentially reworked into the younger population (Kosnik and Kaufman, 2008). It is therefore recommended that a hybrid approach and range of data screening criteria are utilised, as samples from different studies may rank differently using various criteria (Kosnik and Kaufman, 2008). It is also suggested to analyse multiple amino acids, as the presence of outlying data may be undetected when using data from a single amino acid (Kosnik *et al.*, 2008).

Amino acid racemisation is an influential and cost-effective geochronological tool. It has the versatility to be applied to both marine and non-marine samples, and a range of datable material including shell, whole-rock sediment samples, wood and bone, over a wide range timeframe. It is therefore one of the most useful techniques available in Quaternary geochronology (McCarroll, 2002). However, caution should be exercised when undertaking amino acid dating as assumptions of the temperature history of a sample is required. Thus, the degree of resolution is dependent on the natural variability and temperature history of the sample. It is also crucial to evaluate the stratigraphical context effectively and consider other environmental indicators surrounding the deposit to help clarify the significance of the data (Penkman, 2009). Amino acid ratios alone may be considered as a guide to a relative age, while an independent calibration and suitable kinetic models are required before numerical ages can be attained.

### 5.3.10 Conclusions

1. Amino acid racemisation can be used to date a range of material including: wood; bone; eye lenses; and teeth, yet the majority of studies have concentrated on dating calcareous shell structures due to their robustness and the buffering effects provided by the carbonate matrix which minimises the loss of protein residues. Whole-rock aminostratigraphy is also a popular technique as it can be used on sediments lacking in microfossils and provides an average of racemisation rates from a range of bioclastic constituents.
2. It was initially suggested that the kinetic pathways of racemising amino acids followed linear first-order kinetics, yet this has been shown to be incorrect. In fact, racemisation kinetics are non-linear with the kinetic pathway characterised by two linear components with an intermediate transition zone. This non-linear pathway has been shown to occur as amino acids exist as different fractions within a sample and reaction rates differ between free and bound fractions.
3. Amino acid racemisation is not solely time and temperature dependent. The molecular environment of the amino acid, the presence of water, the pH content of the dated material as well as taxonomic effects can also influence the rate at which amino acids racemise. However, effective sampling techniques can aid in limiting the significance of each of these factors.
4. Amino acid racemisation is a significant geochronological tool providing geochronological control beyond the limited range of radiocarbon dating, and can be performed faster and at a lower cost. While aminostratigraphy is dependent upon stratigraphic analysis it is proposed to be the least ambiguous application of amino acid geochronology, while aminochronology requires an understanding of the sequential change of the thermal history of the deposit. There are several limitations and uncertainties associated with the technique. These include uncertainties with the Arrhenius parameters and the estimated diagenetic temperature history of the sample, as well as the possibility of sample contamination.

## 5.4 Amino acid racemisation methods used in this study

This section describes the methods used for AAR analysis throughout this study. Firstly the terms used are described. The sampling procedure is then outlined before the laboratory techniques are discussed. A range of data screening techniques were employed after results were obtained from the RP-HPLC and these are also outlined.

#### **5.4.1 Definition of terms**

A 'sample' refers to an individual mollusc, whereas a sub-sample may identify several portions taken and analysed from that individual. It has been noted that the rates of racemisation of certain amino acids vary within individual shells (Sejrup and Haugen, 1994). Thus, by analysing sub-samples from one individual, this variation can hopefully be minimised. In this study, where possible, molluscan sub-samples were obtained from the hinge/umbo area in bivalves (where shells tend to be thickest) and the aperture in gastropods in order to minimise intra-species variation. In fragmented shells where the umbo region was not present, the outer growth edge was sampled.

Where sediment was analysed using the whole-rock method, a 'sample' refers to sediment that was collected from within a certain unit (note that several samples may be collected from a unit). Sub-samples refer to sediment that has been taken from this initial sample and processed individually. Within this study it was general practice to analyse ten sub-samples from an individual whole-rock sample to assess the degree of variation within the sample. By determining a mean and standard deviation from a sample, the D/L value is likely to be more representative of the sample as a whole rather than if only one sub-sample was analysed, and permits the integrity of the data to be visualised.

#### **5.4.2 Sample selection**

The material collected at sample site locations within the Bridgewater Formation was dependent upon exposed facies at the site and the material suitable for AAR analysis. Molluscan shells were collected preferentially, but where they were unavailable, whole-rock samples were collected. Whole-rock samples were also collected at sites where shells were abundant in order to establish a comparison between the two materials. Foraminifera were hand-picked from sediment samples and used as a comparison between the whole-rock and mollusc shell techniques. The foraminifer *Elphidium crispum* was identified at the majority of sample sites and proved an important comparison in racemisation extent between sites.

#### **Molluscs**

Well-preserved molluscan samples were preferentially chosen for analysis over whole-rock samples. While individual molluscs may have been reworked into a deposit of a different age or amino acids may leach from the shell, material cannot be reworked into the shell matrix. Samples that were fragmented, discoloured or chalky in appearance were discarded, as these are characteristics that may indicate recrystallisation, oxidation, or severe weathering. Similarly, articulated valves were preferentially sampled where available as they may indicate

life position and limited transportation from the site of death. Where possible, up to six individuals from the same genus were sampled from a given unit and site. As many different genera as possible were collected to aid in a detailed description of taphonomy and to help constrain an accurate AAR numerical age at the site. Sampling of multiple genera also aided in site comparison of D/L values, as the same genera were not present at all study sites.

#### **Whole-rock**

Whole-rock samples were taken from road side cuttings, recent quarries and drainage exposures. Where possible all whole-rock samples (except for modern beach samples) were taken from >1 m below the ground surface to minimise the effects of diurnal temperature changes. Sediment samples were selected from facies displaying the least diagenetic alteration and/or weathering within the cutting and away from areas of potential reworking such as truncation surfaces or solution pipes.

#### **Foraminifera**

Three common species of foraminifera identified within Bridgewater Formation deposits on the Mount Gambier coastal plain were preferentially hand-picked from sediment samples. Tests that were large, whole and clearest in colour were assumed to be the least affected by diagenesis and deemed to yield the most representative D/L values. Multiple foraminifera were analysed from each sediment sample where present. The number of reported D/L values of foraminifera differs between study sites due to species availability and the number of samples rejected. For example, at several older sites, such as Dartmoor Cemetery and Fort O'Hare Quarry, up to 30 vials of foraminifera were analysed but many rejected due to low serine (SER) values. Single grain analysis was conducted preferentially on larger foraminifera, yet where tests were small, multiple (up to ten) tests were analysed within one vial in order to yield more significant amino acid concentrations.

#### **5.4.3 Laboratory procedure**

Before processing, all samples were washed with double distilled water to remove any foreign constituents on their surfaces. Mollusc samples were also treated with a dental drill to remove the outer layer of shell under which foreign matter may have lodged. Whole-rock and mollusc samples were etched with 2 M hydrochloric acid (HCl) to remove a third of their mass and to remove any non-indigenous amino acids or leached material. Samples were then rinsed and bathed in 3% hydrogen peroxide and rinsed once more. Samples were hydrolysed in 8 M HCl for 22 hours at 110°C, and sub-samples were then dried under a vacuum. Due to the small sample masses of foraminifera (commonly less than 0.1 mg), the etch of tests was omitted and



individuals were placed in high-purity 6 M HCl for hydrolysis. Free amino acids (FAA) were taken as sub-samples prior to the hydrolysis stage in order to compare with total hydrolysable amino acids (THAA) and to assess the integrity of the results. L-Homoarginine was added to the dried sample at the same volume of sub-sample taken, and samples were run using the reverse-phase, high-performance liquid chromatography (RP-HPLC) method. A full description of methods for each analysed material is outlined in Appendix B.

#### **5.4.4 Reverse-phase, high-performance liquid chromatography (RP-HPLC)**

Kaufman and Manley (1998) developed the reverse-phase high performance liquid chromatography (RP-HPLC) method for analysing amino acid concentrations from fossil samples. RP-HPLC separates at least 9 pairs of DL amino acids with baseline resolution within 75 minutes using commercially available reagents and equipment, and is able to analyse milligram-sized samples allowing for single grain analysis (Kaufman and Manley, 1998). The advantages of using RP-HPLC over IEC is that it allows for the analysis of a suite of amino acids providing the opportunity to choose which amino acid is best suited to represent the sample (as different amino acids racemise at different rates). It also allows for cross-checking of amino acids to establish the reliability of results. RP-HPLC may be favourable over GC as preparation time is greatly reduced with RP-HPLC and thus more samples can be analysed within a given amount of time. This study used the RP-HPLC method and followed the procedure outlined by Kaufman and Manley (1998).

#### **5.4.5 Data screening**

A range of rejection criteria were established to aid in screening the data sets produced by the RP-HPLC and aid in establishing the 'most reliable' D/L value of a sample. These are as follows:

##### **Cross-correlation of amino acids**

D/L values for different amino acids were cross-correlated with each other in a bivariate plot to assess whether values clustered significantly or not. In this study, the amino acids aspartic acid (ASP) and glutamic acid (GLU) were commonly cross-correlated to aid in cluster analysis. Kosnik and Kaufman (2008) noted that under ideal conditions the extent of racemisation of different amino acids should covary according to a predictable function. As each amino acid racemises at a different rate, comparison of two or more amino acids will aid in assessing their internal consistency (Kosnik and Kaufman, 2008).

##### **Identification of high serine concentrations**

An over-abundance of serine is a commonly used screening criterion in AAR studies (Kosnik and Kaufman, 2008). As serine decomposes rapidly compared with other amino acids,

excessive volumes are indicative of contamination by modern amino acids. Caution was advocated where recorded concentrations of serine were high in comparison to other amino acids. Low serine D/L values are also indicative of the introduction of modern material into the sample (if samples are suspected to be greater than Holocene age). To screen for this, samples yielding D/L values for serine of  $< 0.1$  were rejected (as used by Lachlan, 2011) when a sample was expected to be greater than 11 ka in age.

#### **Comparison of total and free amino acids fractions**

Previous AAR studies have used the covariance between different fractions of amino acids within the same specimen to assess the internal consistency of the results, and the integrity of the diagenetic system (e.g. Kosnik and Kaufman, 2008). Studies such as those conducted by Miller and Brigham-Grette (1989) and Murray-Wallace and Kimber (1989) found the free amino acid fractions to be higher compared with the total hydrolysable fraction. In this study, where the free fraction D/L values were lower than total fraction, values were immediately rejected. Comparing the variance in D/L values in the free fraction with total amino acids allowed for identifying signs of leaching and assessing the integrity of the results.

#### **Identification of values more than 2 standard deviation outside the mean**

Samples yielding D/L values more than 2 standard deviations outside of the standard mean of the group were excluded from calculations, as suggested by Kosnik and Kaufman (2008). Samples yielding unusually high D/L values represent potentially reworked older material into a younger population. Unusually low D/L values may indicate contamination from post-depositional sources, the effects of diagenesis, or laboratory procedures. The loss of free and lower molecular weight peptides may also result in D/L values for the THAA fraction weighted towards the lower degree of racemisation in the larger peptides.

### **5.5 Radiocarbon and OSL methods used in this study**

Radiocarbon and optically stimulated luminescence (OSL) analysis were conducted on selected samples to aid in calibrating rates of amino acid racemisation. Radiocarbon dating was conducted on fossil shells thought to be less than 50 ka in age and samples were analysed at the University of Waikato, New Zealand. OSL analysis was conducted in the OSL laboratory, Centre of Archaeological Science, University of Wollongong, and at Macquarie University.

#### **5.5.1 Radiocarbon dating methods**

Radiocarbon dating was conducted on *Turbo undulatus* opercula from the Holocene gravel beach facies at Port MacDonnell and on *Turbo undulatus* opercula found within a well-cemented flint conglomerate. From stratigraphical analysis, the flint conglomerate is

suggested to be a palaeo-beach of Late Pleistocene, interstadial age (section 3.8.2). Radiocarbon analyses were conducted by accelerator mass spectrometry. The surfaces of the opercula were cleaned in an ultrasonic bath, given a light etch with 0.1 N HCl and were subsequently rinsed in distilled water and dried. The calcium carbonate was then analysed by XRD and confirmed to be primary aragonite. Stable isotope analyses revealed that the aragonite was consistent with  $\delta^{13}\text{C}$  values for marine carbonate ( $2.3 \pm 0.2$  ‰ for the Holocene and  $2.1 \pm 0.2$  ‰ for the Pleistocene shells respectively).

### 5.5.2 OSL dating methods

OSL analysis was conducted on four aeolianite samples from exposures of Bridgewater Formation aeolianite: one sample from the upper aeolianite unit of the cliffs at Port MacDonnell Beach, suspected to be a correlative to the Robe Range; one sample from a small sand quarry within MacDonnell Range; one sample taken from a siliceous cover sand on a strongly weathered portion of the Bridgewater Formation north of Mount Gambier township; and another from the aeolian facies exposed within Compton Range at Baxter's Quarry. The location of sample sites is shown in Figure 3.11. Each sample was collected using a light-proof tube and sealed with black plastic caps and tape to prevent light exposure. The samples from Robe Range, MacDonnell Range and siliceous sand overlying Bridgewater Formation sediments north of Mount Gambier were analysed at UOW OSL laboratory. The sample collected from Compton Range at Baxter's Quarry was analysed at Macquarie University OSL laboratory.

Samples analysed at UOW used the following method. Coarse quartz grains of 180-212  $\mu\text{m}$  diameter were prepared for OSL analysis following the standard procedures outlined by Aitken (1998). Prepared grains were mounted as a monolayer onto stainless-steel discs, and placed into a Risø OSL/TL-DA-15 (Risø 2) dating instrument for analysis. Optical stimulations were performed using blue LEDs ( $470 \pm 30$  nm) for 40 s at 125°C. Photocounting of the resulting ultraviolet emissions was conducted by Electron Tubes 9235B photomultiplier tube coupled with two 3 mm Hoy U-340 filters. Laboratory irradiations (regenerative doses), which allowed for the construction of dose response curves for each sample aliquot, were performed using a calibrated  $^{90}\text{Sr}/^{90}\text{Y}$  beta source attached to the OSL/TL-DA-15.

For each sample, of 24 multi-grains with 1 mm mask aliquots (each containing approximately 40 grains), the OSL equivalent dose ( $D_e$ ) was measured using a modified single-aliquot regenerative dose (SAR) protocol (Wintle and Murray, 2006). Small aliquot masks were used to assess the adequacy of light exposure to the sediment prior to deposition (Olley *et al.*, 1999), though this was not suspected to be a significant problem as all samples were collected

from aeolian facies. Standard protocol checks were conducted, including checks for thermal transfer from heat treatment applied to each aliquot before optical stimulation, and the adequacy of the test-dose correction procedure used to compensate for any changes in OSL sensitivity between successive regenerative-dose cycles (Wintle and Murray, 2006). Dose recovery tests (whereby grains are bleached at a given dose) were undertaken at a range of preheats and cutheats to determine the most appropriate experimental conditions for each sample. A preheat cutheat of 240°C for 10 s was deemed most appropriate, and all aliquots were exposed to this before measuring the natural and regenerative-dose signals. Before each test dose the aliquots were also heated to 160°C for 5 s prior to optical stimulation.

Beta-dose rate estimation was conducted following the methods of Bøtter-Jensen and Mejdahl (1998) and Ankjærgaard and Murray (2007). Estimations of uranium and thorium concentrations were undertaken following the thick source alpha counting methods outlined in Aitken (1985) and Jacobs (2004). Geiger Muller beta counting was utilised to calculate percentages of potassium. Concentrations were then converted to gamma dose rates using conversion factors of Guérin *et al.* (2011).

OSL dose-response curves were generated for each aliquot. The regeneration dose points in all aliquots were fitted with an exponential plus linear term (Jacobs *et al.*, 2003);

$$I = I_0 + I_{max} \left( 1 - e^{-\frac{D}{D_0}} \right) + k \cdot D$$

Whereby  $I$  is the sensitivity corrected luminescence intensity;  $D$  is the given laboratory dose; and  $D_0$  and  $k$  are constants. This function was used to fit all data. By using the function above the corresponding  $D_e$  values were determined from the integration for the first 0.64 s of OSL signal, using the count rate over the final 8 s of simulation as background. Methods of data analysis and error estimation follow Yoshida *et al.* (2003). Sediment moisture content was estimated by dividing the difference of the weight of wet and dry sediment by the weight of the dry sediment and multiplying by 100.

The sample from Baxter's Quarry, analysed at Macquarie University, was subjected to a similar method. Again, quartz grains of 180-212 µm were analysed and separated from the matrix using standard purification procedures which included an etch in 40% hydrofluoric acid for 45 minutes to remove external alpha-dosed rinds (Aitken, 1998). OSL techniques used UV emissions from single quartz grains and incorporated a modified SAR protocol (Murray and Wintle, 2000) whereby between 500-1000 single grains were loaded onto aluminium single-

grain discs and measured in a TL-DA-20 Risø unit which contained a single-grain attachment (Bøtter-Jensen *et al.*, 2000, 2003). Each quartz grain was stimulated for 2 s using a 10 mW 532 nm Nd:YVO<sub>4</sub> solid-state diode pumped green laser. Resultant UV emissions were detected by an Electron Tubes Ltd photomultiplier tube fitted with 7.5 mm of Hoya U-340 filter. High-resolution gamma spectrometry was conducted on dried and powdered sediment samples to determine concentrations of <sup>238</sup>U, <sup>235</sup>U, <sup>232</sup>Th (and their decay products) and <sup>40</sup>K. These measurements were converted to dose rates (following Mejdal, 1979; Stokes *et al.*, 2003) allowing for estimated long-term water contents, estimates of cosmic-ray dose rate (Prescott and Hutton, 1994) and internal dose rate of 0.03 Gy/kyr<sup>-1</sup> (Feathers and Migliorini 2001).

## 5.6 Pyrolysis experiments

The rate of racemisation varies for each amino acid. Several pyrolysis experiments were conducted to provide a context to understand the field-based observations for racemisation kinetics in different genera or different fossil matrices. These experiments allowed for comparison of racemisation rates between amino acids and comparison of racemisation rates in shell, foraminifera and whole-rock samples.

*Ostrea* and *Katelysia* were the most commonly collected genera at exposures of Bridgewater Formation across the Mount Gambier coastal plain. Pyrolysis experiments were therefore conducted on these genera to compare racemisation rates between the molluscs which may account for any identified differences in D/L values of samples at the same site. Shells were live-collected and thoroughly cleaned with a dental drill and washed in distilled water. Once dried, samples were crushed into a coarse powder, measured into sub-samples and placed in glass vials. A known volume of sterile quartz sand was added to the shell powder to act as a substrate, with a small volume of Millipore water to moisten the material. Tubes were sealed and placed in an oven at 110°C and were subsequently removed at set time intervals for up to 180 days. Once removed from the oven, samples were dried, the shell was sieved from the quartz sand substrate, and weighed shell samples were processed following the method for shell described in Appendix B.1.

Pyrolysis experiments were also conducted on *Elphidium crispum* and *Discorbis dimidiatus*, which were commonly identified foraminifera within Bridgewater Formation exposures. Tests were hand-picked from modern substrate collected at Port MacDonnell Beach. Between 5 and 10 tests of each species were placed into heating tubes with a small volume of Millipore water, sealed, and placed in an oven at 110°C for set time intervals. On removal from the oven tests were dried and processed as outlined in Appendix B.3.

Sub-samples of whole-rock collected at Shelly Beach, Cape Northumberland were also analysed through pyrolysis experiments. Sub-samples of 150 mg were weighed and put in tubes with Millipore water and placed in the 110°C oven for designated time intervals. Once removed from the oven samples were processed as following the methods for whole-rock outlined in Appendix B.2.

Pyrolysis experiments demonstrate that different species and different amino acids racemise at variable rates (Table 5.1). As shown in Figure 5.6 for each medium analysed, differing amino acids followed the same pattern; serine D/L values increased rapidly within a short period of time and obtained the largest D/L values, though these were not always consistent at later times and indicates the poor stability of this amino acid. Aspartic acid was the second fastest racemising amino acid, quickly reaching high D/L values and subsequently plateauing out. Through pyrolysis experiments on Holocene and Pleistocene fossil shells, Kimber and Griffin (1987) identified a reversal in aspartic acid D/L values within 64 days of heating and suggested caution against using this amino acid for dating purposes. Glutamic acid and leucine were similarly matched with a shallower curve, with glutamic acid generally racemising slightly faster. Valine was usually the slowest amino acid to racemise.

A constrained power law model (Kaufman, 2000; Manley *et al.*, 2000; Clarke and Murray-Wallace, 2006) was used to determine the forward rates of reaction for aspartic acid and glutamic acid within the materials analysed. Through iterative calculation processes it was found that the power function 1.9 produced the best linear correlation for all amino acids across all analysed materials. Manley *et al.* (2000) found the modification of the power law function (from the simpler power function used by Goodfriend *et al.* (1996)) to provide a better linear fit for ASP D/L ratios, and thus this technique is adopted here. Calculation of forward rates was conducted by applying the following equation (after Kaufman, 2000; Manley *et al.*, 2000) to the D/L data derived from pyrolysis experiments;

$$\left( \frac{1 + D/L}{1 - K'D/L} \right)^n = (1 + K')kt + C$$

Where  $K'$  is the reciprocal of the equilibrium constant,  $k$  is the forward rate constant ( $\text{yr}^{-1}$ ) for a given temperature (110°C in this case),  $t$  is the length of time the sample has been heated (yr),  $n$  is the power function that resulted in the most linear relationship (found here to be 1.9), and  $C$  is an analytical constant equivalent to the left hand side of the above equation at  $t=0$ . Forward rate constants are calculated by multiplying the gradient of the slope by 0.5. Results are shown in Table 5.2 and Figure 5.7.

Forward rate constants for aspartic acid are constantly greater than for glutamic acid across all materials. The extent of racemisation of glutamic acid is greater in *Katelsysia* compared with *Ostrea*. This may account for higher D/L values reported for *Katelsysia* compared with *Ostrea* fossils of equivalent age. The racemisation extent of glutamic acid is found to be greater in fossil shell than whole-rock samples and this may reflect the lengthy residence time of whole-rock on the modern beach. Racemisation rates of glutamic acid within foraminifera are found to be greater for *Discorbis* than *Elphidium*, but the reverse is found for aspartic acid, with faster racemisation rates recorded in *Elphidium*. Rates of glutamic acid racemisation for foraminifera are found to be greater than in whole-rock sediment, similar to *Ostrea*, but not as fast as racemisation rates in *Katelsysia*.

Previous investigations (e.g. Kimber and Griffin, 1987) have shown that concentrations of valine and glutamic acid are well maintained in older specimens, and are the most appropriate for use in geochronological analysis of late Pleistocene samples. Pyrolysis experiments conducted in this study show that glutamic acid and valine racemise relatively slowly. Valine is eluted later in the chromatographic analysis and was commonly found to yield smaller, unreliable, non-Gaussian peaks, an issue of column performance based on the chemical composition of the stationary phase. Therefore, glutamic acid, which elutes earlier within the run, was the preferentially reported amino acid throughout this study.



**Table 5.1:** AAR D/L values derived from pyrolysis experiments on modern molluscs *Kataysia*, *Ostrea*, whole-rock samples and the foraminifers *Discorbis* and *Elphidium*

Heating time (hrs)	<i>Kataysia</i> D/L values			<i>Ostrea</i> D/L values		Whole-rock D/L values			<i>Discorbis</i> D/L values		<i>Elphidium</i> D/L values	
	ASP	GLU	SER	ASP	GLU	ASP	GLU	SER	ASP	GLU	ASP	GLU
0	0.073	0.035	0.057	0.079	0.039	0.340	0.192	0.361	0.062	0.039	0.076	0.054
24	0.274 ± 0.003	0.112 ± 0.015	0.636 ± 0.003	0.248	0.066	0.374 ± 0.016	0.211 ± 0.008	0.413 ± 0.110	0.270 ± 0.007	0.072 ± 0.001	0.150	0.061
48	0.336 ± 0.029	0.173 ± 0.015	0.675 ± 0.049	0.377 ± 0.015	0.141 ± 0.004	0.389 ± 0.008	0.212 ± 0.007	0.457 ± 0.010	0.336 ± 0.002	0.092 ± 0.013	0.248 ± 0.019	0.081 ± 0.001
72				0.376 ± 0.010	0.114 ± 0.003	0.388 ± 0.002	0.218 ± 0.007	0.528 ± 0.024	0.360 ± 0.008	0.115 ± 0.003	0.135 ± 0.125	0.086 ± 0.006
96	0.481 ± 0.020	0.239 ± 0.014	0.781 ± 0.007	0.379	0.115	0.392 ± 0.012	0.212 ± 0.010	0.569 ± 0.029			0.312	0.123
168						0.429 ± 0.001	0.231 ± 0.006	0.724 ± 0.182				
192	0.572 ± 0.001	0.294 ± 0.050	0.863 ± 0.002	0.461 ± 0.0	0.175 ± 0.004	0.449 ± 0.001	0.246 ± 0.001	0.592 ± 0.027	0.410	0.220 ± 0.023	0.313 ± 0.021	0.184 ± 0.025
288				0.497 ± 0.011	0.219 ± 0.008	0.462 ± 0.001	0.255 ± 0.005	0.549 ± 0.003				
384	0.643 ± 0.023	0.342 ± 0.024	0.817 ± 0.085			0.489 ± 0.004	0.268 ± 0.002	0.521 ± 0.007	0.504	0.257	0.377 ± 0.019	0.178 ± 0.037
576	0.707 ± 0.017	0.422 ± 0.029	0.889 ± 0.010			0.528 ± 0.004	0.315 ± 0.006	0.621 ± 0.008				
672						0.562 ± 0.013	0.377 ± 0.005	0.577 ± 0.003				
768	0.732 ± 0.023	0.451 ± 0.034	0.737 ± 0.238	0.591 ± 0.008	0.324 ± 0.002	0.553	0.349	0.252	0.569 ± 0.052	0.403 ± 0.109	0.487 ± 0.130	0.302 ± 0.087
960	0.758 ± 0.013	0.499 ± 0.010	0.888 ± 0.003	0.616 ± 0.015	0.344 ± 0.00	0.567 ± 0.016	0.355 ± 0.001	0.613 ± 0.052				
1056				0.601 ± 0.010	0.327 ± 0.003							
1152	0.782 ± 0.013	0.545 ± 0.037	0.860 ± 0.013	0.625 ± 0.006	0.346 ± 0.013	0.589 ± 0.002	0.361 ± 0.002	0.560 ± 0.115				
1296				0.647	0.375	0.598 ± 0.001	0.386 ± 0.004	0.629 ± 0.009				
1344	0.783 ± 0.002	0.536 ± 0.004	0.871 ± 0.016								0.619	0.349
1440						0.615 ± 0.004	0.408 ± 0.005	0.534 ± 0.095				
1536	0.799	0.568	0.847						0.597 ± 0.001	0.396 ± 0.040	0.79	0.353
2160				0.700 ± 0.006	0.449 ± 0.005							
2880	0.852	0.651	0.756	0.710 ± 0.006	0.478 ± 0.006	0.679 ± 0.017	0.497 ± 0.024	0.486 ± 0.148	0.685 ± 0.042	0.558 ± 0.07	0.730 ± 0.002	0.489 ± 0.014
4320				0.772 ± 0.004	0.591 ± 0.005							

**Table 5.2:** Forward rate constants derived from pyrolysis experiments for aspartic acid (ASP) and glutamic acid (GLU)

Amino Acid	Forward rate constant (k) (yr <sup>-1</sup> )				
	<i>Kataysia</i>	<i>Ostrea</i>	Whole-rock sediment	<i>Elphidium crispum</i>	<i>Discorbis dimidiatus</i>
ASP	180.69	44.158	29.883	49.189	31.917
GLU	27.355	10.941	8.824	9.283	13.939

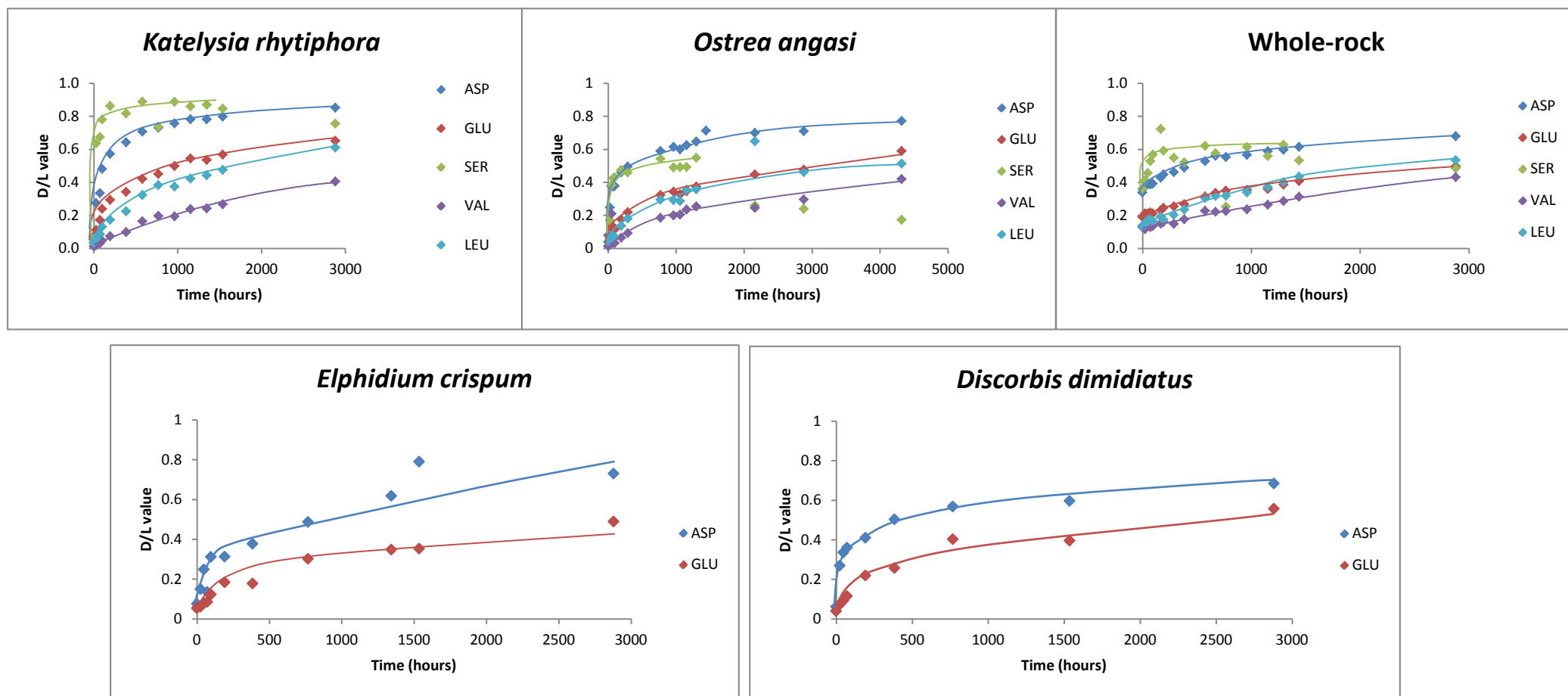


**Figure 5.6:** Scatter plots of pyrolysis experiments for *Katelysia rhytiphora*, *Ostrea angasi*, whole-rock, *Elphidium crispum* and *Discorbis dimidiatus* for a range of amino acids.

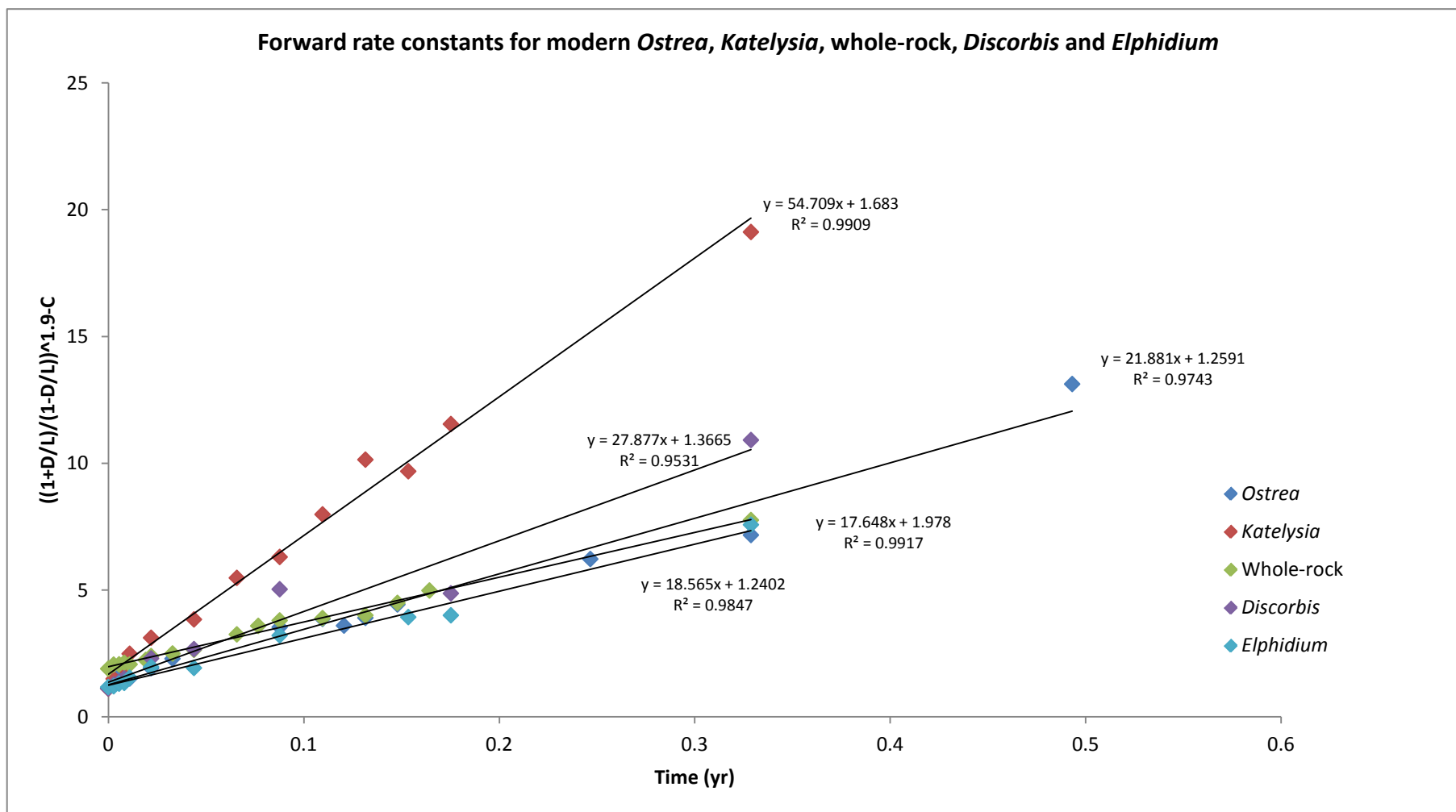


**Figure 5.7:** Constrained power law functions for D/L data derived from pyrolysis experiments from a range of carbonate material across the Mount Gambier coastal plain to yield forward rate constants for glutamic acid.

## 5.7 Deriving numerical ages - calibration and kinetic modelling

Numerical AAR ages were derived by calibrating samples dated using OSL and radiocarbon analyses. Glutamic acid (GLU) D/L values are modelled using apparent parabolic kinetics (Mitterer and Kriausakul, 1989). The following section presents the results of radiocarbon and OSL analysis before discussing the details of AAR calibration for each analysed material.

### 5.7.1 Results of radiocarbon and OSL analysis

Results of radiocarbon and OSL analyses aid in constraining the depositional timing of deposition of the Bridgewater Formation at specific sites across the Mount Gambier coastal plain (Tables 5.3 and 5.4). XRD analyses associated with radiocarbon analyses revealed the shell carbonate to be primary aragonite. Measured  $\delta^{13}\text{C}$  values (Table 5.3) are consistent with marine carbonate. Radiocarbon analysis of *Turbo undulatus* operculum from the raised Holocene cobble beach unit at Port MacDonnell yielded an age of  $2473 \pm 25$  yr BP (Wk-34195) and precludes a late Pleistocene age for the gravel beach facies. Radiocarbon dating of the operculum of *Turbo undulatus* from within the flint conglomerate beach unit at Port MacDonnell yielded a 'finite' minimum age of  $47,910 \pm 2100$  yr BP (Wk-34733). This result precludes a Holocene age for the fossil shells from the flint, partially-lithified, conglomerate. As this sample yields an age close to the practical limit of radiocarbon dating, and the 'true' age likely exceeds the derived value, it was not used as a calibration point for determining AAR numerical ages. Reported radiocarbon ages are not calibrated. Radiocarbon ages of the middle Holocene may underestimate the 'true age' of a fossil, and thus uncalibrated radiocarbon ages may differ from AAR ages of the same fossil. However, the *Turbo* from the flint conglomerate is regarded as a minimum age due to its proximity to the age limit for radiocarbon dating and is not used in calibration of racemisation rates. As the radiocarbon age from the raised Holocene beach is of late Holocene age there is likely a close approximation between this and the 'true age' of the fossil, and thus can be used confidently in calibrating racemisation rates for amino acids.

The Central Age Model (CAM; Galbraith *et al.*, 1999) was used to determine a weighted mean  $D_e$  for OSL samples collected from Robe Range, MacDonnell Range and inland siliceous sands covering an exposure of Bridgewater Formation. Overdispersion within these samples was relatively low (i.e.  $< 20\%$ ) which supports the assumption of a single-dose population (Table 5.4; Figure 5.8) Three upper values were excluded from the CAM for the Robe Range sample due to the possibility that a significant percentage of poorly bleached grains were present within these aliquots. Two aliquots were rejected from the siliceous sand and none were rejected from the MacDonnell Range sample. The sample from Compton

Range (BaQu) is aeolian and it can be assumed that the grains would have been well-bleached during deposition. The Finite Mixture Model (FMM) is therefore appropriate to use to assess the distribution of the grains which indicated three dose populations, with the largest proportion of grains (58%) being in the highest dose population. If the majority of grains have been bleached, which in this aeolian sample it is assumed they have, a conservative approach is to use the largest dose population to represent the depositional dose. The younger populations highlighted by the FMM may indicate some sediment mixing. The sample was taken near a small truncation surface (Figure 3.39) and while the sample was taken at depth from solution pipes, these features are common throughout the exposure and indicate that some mixing and transport of younger sediment to depths in the profile may have occurred.

OSL analysis suggests that the upper aeolianite unit within Port MacDonnell coastal cliffs, suspected to be Robe II from stratigraphical analysis, was deposited  $53 \pm 4$  ka, during the early portion of MIS 3 (25-60 ka). Accordingly, this aeolianite unit post-dates Robe II, *sensu* Schwebel (1978), which is suggested to have formed during MIS 5a. The findings from this study are more comparable with those of Banerjee *et al.* (2003) who used SAR OSL to date the sediments of Robe II aeolianite near to the township of Robe and reported an age of  $63 \pm 3.6$  ka. The findings from Port MacDonnell, 80 km southeast of Robe, confirm that Robe II cannot be a local deposit, as suggested by Banerjee *et al.* (2003), and has much wider stratigraphical expression. Bathymetric data suggest that if sea level during MIS 3 was 40 to 65 m lower than present (Lambeck and Chappell, 2001) the shoreline would have been approximately 13 km seaward from that of present at Port MacDonnell (Geoscience Australia, 2009). It is plausible that with strong winds reactivated sands may have blown this far inland. Similar aeolian reworking of skeletal carbonate sands during the late Pleistocene has been noted on the Swan Coastal Plain, Western Australia (Price *et al.*, 2001).

Interestingly, an OSL age very similar to that within Robe II was derived from a siliceous cover sand 25 km landward of Port MacDonnell. OSL analysis of this deposit yielded an age of  $54 \pm 4$  ka. Therefore, three aeolian deposits, at Robe (Banerjee *et al.*, 2003), Port MacDonnell and north of Mount Gambier, all seem to have been deposited at a similar time and potentially indicate aeolian reactivation of sands during the interstadial of MIS 3, when conditions were significantly more arid and windier (e.g. Bowler, 1976; Nanson *et al.*, 1992; Fujioka and Chappell, 2010). While much further sampling would be necessary to confirm such a hypothesis this suggestion is further discussed, in light of other research on dune reactivation in continental Australia, within the thesis synthesis (section 6.2.10).

The OSL sample from MacDonnell Range, 7 km inland of Port MacDonnell, yielded an age of  $124 \pm 10$  ka and suggests that this is an extension of the last interglacial *sensu stricto* (MIS 5e) Woakwine Range, a prominent barrier feature to the northwest of the present study area. This value was used in calibrating whole-rock and foraminifera AAR numerical ages.

The OSL sample from Baxter's Quarry, collected from the eastern side of the exposure, was obtained from steeply dipping aeolian cross-beds which are overlain by a truncation surface likely representing the bottom-set of a dune. As outlined in Chapter 3 (section 3.8.8) the aeolian facies within Baxter's Quarry is separated from the underlying subaqueous calcarenite by a laterally extensive undercut layer representing an unconformity surface and indicative of a short diastem. Morphological evidence suggests that Compton Range, in which Baxter's Quarry lies, is the fifth barrier shoreline landward from the modern shoreline and is accordingly a correlative of MIS 13. The OSL sample from the aeolian facies within Baxter's Quarry yielded an age of  $390 \pm 35$  ka and at face value indicates deposition during MIS 11.

Two potential scenarios may account for the observed OSL age. Firstly, the MIS 11 age may represent a minimum age of the deposit due to the proximity of quartz grains to saturation at high palaeodoses and the potential for mixing of grains from younger sources. In this interpretation, the OSL result simply suggests that the barrier is at least MIS 11 in age, and combined with geomorphological evidence it may be indicative of deposition during MIS 13.

A second potential interpretation is to assume that the OSL age is accurate and that the aeolian facies exposed within Baxter's Quarry was deposited during MIS 11 and potentially overlies a core of MIS 13 subaqueous calcarenite. Compton Range may therefore be a composite structure, similar to that observed within Woakwine Range, which is found to have a core sediment body of MIS 7 age and overlying MIS 5e calcarenite (Murray-Wallace *et al.*, 1999), and Robe Range which formed during successive sea-level highstands of MIS 5c, MIS 5a and MIS 1 (Schwebel, 1978; 1984). As suggested from geochronological analysis of Robe II at Port MacDonnell, it is possible that aeolian sands can travel up to 13 km onshore and it is therefore plausible that during the MIS 11 sea-level highstand aeolian sediment could have been transported to the inland MIS 13 shoreline barrier. It is also possible that the MIS 11 sea-level highstand may have been significantly higher (as suggested from several other studies, e.g. Bowen, 2010; Raymo and Mitrovica, 2012) and thus the coastline during MIS 11 would have been significantly closer to the previously deposited Compton Range.

The defining question is therefore the duration of the depositional hiatus that is indicated by the disconformity found between the aeolian and subaqueous facies at Baxter's Quarry. Is this surface indicative of ~100 ka of subaerial exposure? The undercut layer above the unconformity surface may represent a soil layer that has since been eroded yet left red/orange staining of the unit. This layer is approximately 15 cm thick and extends laterally throughout the exposure. Narrow bands of caliche within the undercut layer are evident, but no extensive calcrete or rhizolith development is recognised. When this deposit is compared with the 75 cm thick, massive calcrete and overlying red palaeosol at Port MacDonnell Beach, which separates aeolian units of Robe Range, it is evident the disconformity at Baxter's Quarry is significantly thinner. The calcrete and palaeosol unit within Port MacDonnell aeolianite cliffs is suggested to represent a depositional hiatus between interstadial events, potentially lasting between ~20 ka (if the deposits are MIS 5a and MIS 5c in age) and ~50 ka (if the upper aeolianite is MIS 3 in age). While comparison of the thickness of the disconformities between Compton and Robe Range is limited by the assumption of similar climatic conditions at the time of formation for both units, it is evident that the calcrete palaeosol within Robe Range is more developed and potentially reflects a longer period of subaerial exposure.

While the undercut layer within Baxter's Quarry is laterally extensive, due to the lack of a well-developed calcrete and rhizoliths, the reduced thickness of this unit (compared to that within the Robe Range) suggests that this deposit does not represent a depositional hiatus of 100 ka between interglacial sea-level highstands. The presence of soil remnants and caliche, and the development of small solution pipes within this unit do suggest some period of subaerial exposure of the underlying subaqueous deposit before deposition of aeolian sediment. The 15-cm-thick undercut layer within Baxter's Quarry may therefore represent a former protosol. On the island of Bermuda, Vacher *et al.* (1995) proposed that where protosols are located between an underlying marine unit and an overlying aeolianite unit they mark a transition from an erosional coastline to a depositional one. At Baxter's Quarry it may be that the lower subaqueous facies were deposited during MIS 13, but as sea level rose during MIS 11 some of this sediment (potentially remnants of a subaerial exposure surface or overlying dunes) was eroded. As sea-level fell towards the end of the MIS 11 highstand, the subaqueous sediment may have been exposed for a short time interval allowing the formation of a protosol prior to deposition of aeolian dunes at the end of MIS 11. However, another possibility is that the period of subaerial exposure at Baxter's Quarry was long, but much of the palaeosol representing that period has simply been eroded away. Further analysis is required to examine these hypotheses further.



**Table 5.3:** Numerical ages derived from radiocarbon analysis of *Turbo undulatus* opercula from Port MacDonnell, South Australia

Sample site	Lab code	Species	$\delta^{13}\text{C}$	Radiocarbon age (years BP)
Raised Holocene beach, Port MacDonnell	Wk-34195	<i>Turbo undulatus</i>	$2.3 \pm 0.2 \text{ ‰}$	$2470 \pm 25$
Flint conglomerate, Port MacDonnell	Wk-34733	<i>Turbo undulatus</i>	$2.1 \pm 0.2 \text{ ‰}$	$47910 \pm 2106$

The isotopic fraction  $\delta^{13}\text{C}$  is expressed as ‰ with regards to PDB.

**Table 5.4:** Results of OSL analysis from aeolian sand samples across the Mount Gambier coastal plain, southern Australia

Sample site	Lab code	Field moisture content (as a % dry mass) <sup>f</sup>	Total dose rate (Gy/ka) <sup>a,b</sup>	N/ $\sigma_d$ (%) <sup>c</sup>	D <sub>e</sub> (Gy) <sup>d</sup>	Age (ka) <sup>b,e</sup>
Robe Range	UOW-848	3.1	$0.515 \pm 0.037$	17 / $9.9 \pm 2.1$	$27 \pm 1$	$53 \pm 4$
MacDonnell Range	UOW-849	3.2	$0.418 \pm 0.031$	24 / $11.4 \pm 2.1$	$52 \pm 1$	$124 \pm 10$
Inland siliceous sand	UOW-850	0.3	$0.629 \pm 0.048$	22 / $15.5 \pm 2.6$	$34 \pm 1$	$54 \pm 5$
Compton Range	BaQu	$1/5 \pm 2$	$0.87 \pm 0.08$		$340 \pm 7$	$390 \pm 35$

<sup>a</sup> Includes an assumed internal alpha dose rate of  $0.03 \pm 0.01$  Gy/ka; cosmic ray dose-rates estimated as a function of geomagnetic latitude, elevation, and depth, after Prescott and Hutton (1994); dose-rates are adjusted for water content and beta attenuation (Aitken, 1985, 1998; Brennan, 2003; Nathan and Mauz, 2008). <sup>b</sup> Mean  $\pm$  total uncertainty (68 % confidence interval), calculated as the quadratic sum of the random and systematic uncertainties. <sup>c</sup> Number of aliquots used in the final D<sub>e</sub> estimation (N) / relative standard deviation of D<sub>e</sub> distribution after accounting for measurement uncertainties (overdispersion,  $\sigma_d$ ). <sup>d</sup> Central age model (CAM) D<sub>e</sub> (Galbraith et al. 1999).

<sup>e</sup> Uncertainty includes a systematic component of  $\pm 2 \%$  associated with laboratory beta-source calibration. <sup>f</sup> An assumed moisture content of  $10 \pm 5 \%$  was used in the age calculation to account for loss during sampling and storage, and uncertainty in this parameter over time.

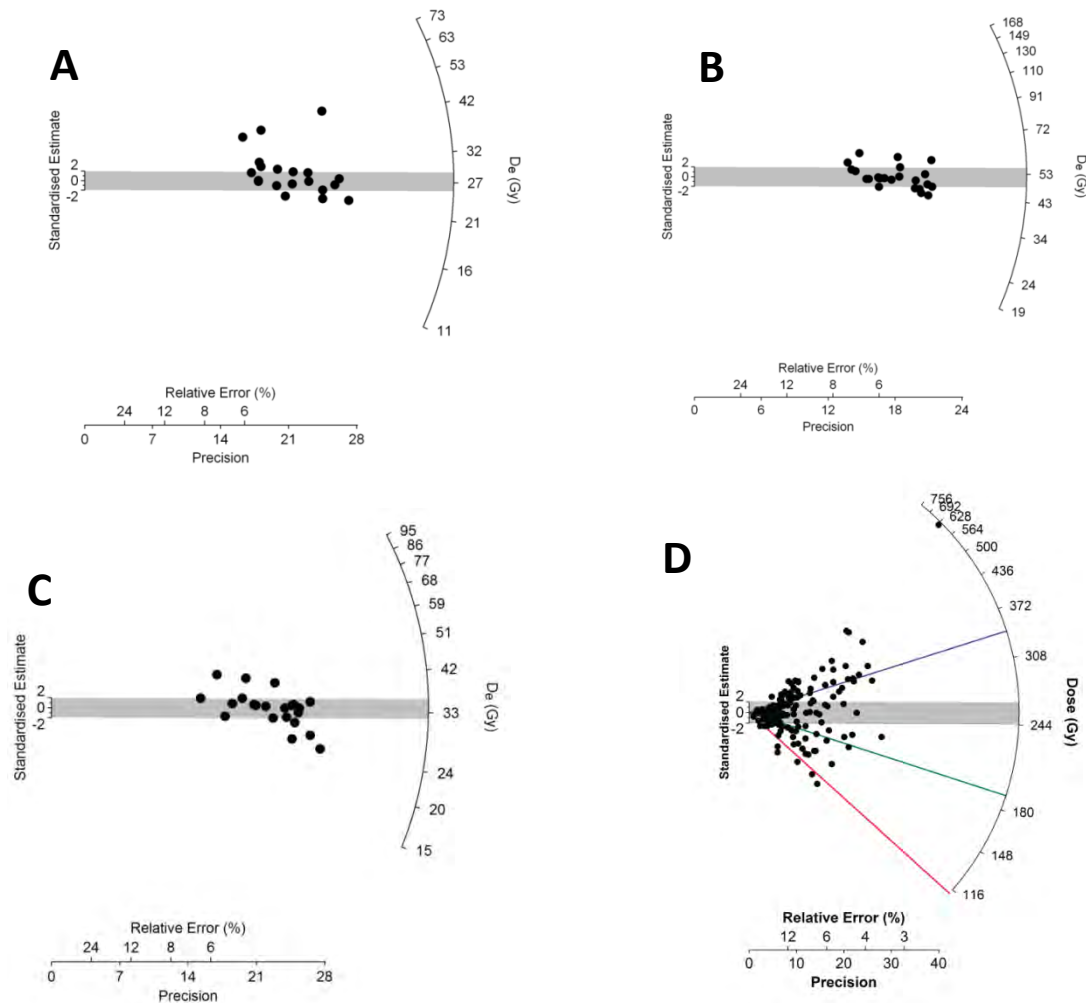


**Figure 5.8:** Single-aliquot OSL equivalent dose (D<sub>e</sub>) distributions (as radial plots) for **A:** Robe II, Port MacDonnell aeolianite centred on CAM  $27.014 \pm 0.72$  Gy, **B:** MacDonnell Range centred on CAM  $51.98 \pm 1.36$  Gy, **C:** Siliceous sand overlying Bridgewater Formation centred on CAM  $34.01 \pm 1.18$  Gy, and **D:** Baxter's Quarry centred on 255 Gy as this is the central age using the CAM for palaeodoses of the grains analysed. The palaeodose for this sample is the upper dose population defined by FMM and highlighted by the blue line.

### 5.7.2 AAR calibration curve construction

AAR numerical ages are determined using calibration curves. In this study calibration points are fitted using the apparent parabolic kinetic model after Mitterer and Kriausakul (1989). This section discusses the construction of calibration curves for each type of material analysed using AAR in turn.

#### Molluscs

Rates of amino acid racemisation have been found to vary for different mollusc genera (Lajoie *et al.*, 1980). Therefore, where possible within this study, calibration curves were created for separate species. Where there was no calibration points for separate species, calibration curves were used from a similar class, for example the calibration curve for one gastropod might be adapted for a second gastropod known to experience similar rates of racemisation. The associated uncertainties of this are discussed in the following section (5.7.3).

For the species *Turbo undulatus* three calibration points were used: (1) opercula collected from the modern beach face were used to represent time zero; (2) operculum from the raised Holocene beach dated by radiocarbon analysis; and (3) opercula previously dated by Murray-Wallace *et al.* (2010) from the Last Interglacial Glanville Formation at Traeger's Quarry, Goolwa, near the River Murray mouth. Limited options were available for intermediate calibration points. Due to the nature of highstand deposits, no suitable fossil shell was identified for the MIS 3 (~60 ka) highstand, as the coast was likely approximately ~13 km seaward of its present position at this time.

*Katelysia rhytiphora* calibration curves were constructed using two calibration points: live-collected *Katelysia* were used to represent time zero, and *Katelysia* analysed from the site of Murray-Wallace and Belperio (1991) near Lake Hawdon South (CCP 1) back-barrier lagoon facies of the last interglacial Woakwine Range, which have previously been identified as MIS 5e in age by AAR analyses. Here, the molluscs were analysed by RP-HPLC and derived D/L values used for calibration adopted the U-series age previously derived by Schwebel (1978; 1984). Schwebel (1978; 1984) conducted U-series on both shell and sediment from Woakwine Range at Drain L near Robe. Commonly, a significant amount of time may pass between the death of a mollusc and the burial of that individual by landward transgressing dunes. However, Murray-Wallace *et al.* (1999) suggested that *Katelysia rhytiphora* within a back-barrier lagoon of the Woakwine Range were moving upwards through the overlying sediment as the dune rapidly transgressed over the lagoonal facies, resulting in asphyxiation of the organisms. In this case, therefore, burial time and time of death were very similar, and thus the age derived by

Schwebel for molluscs from the Woakwine Range is suggested to be representative of the time of death of the organisms and associated time of barrier construction. As radiocarbon dating of fossil shell is limited to  $\sim 50$  ka, the U-series age derived by Schwebel (1978; 1984) of  $125 \pm 20$  ka for shell within the Woakwine Range is used within this study as an independent calibration point for fossil shell from Lake Hawdon South. This calibration point has also been adopted by previous AAR studies along the South Australian coastline (e.g. Murray-Wallace 1999; Lachlan, 2011).

Calibration curves for *Ostrea angasi* also used two calibration points; live-collected *Ostrea* yielded time zero values and specimens from Lake Hawdon South calibrated with Schwebel's (1978; 1984) U-series value of  $125 \pm 20$  ka. Other molluscan species analysed adopted one of these three calibration curves and the difference in racemisation rates between genera was accounted for by using an additional uncertainty (calculated by the mean difference of all genera at the same site).

#### **Whole-rock and foraminifera**

The high-energy environment of beaches across the Mount Gambier coastal plain results in common mixing of sediments. Depending on the surrounding deposits of the beach shoreface, reworking of older grains can affect the overall D/L value of a whole-rock sample. Four separate modern beach samples were collected across the coastal plain: Longbeach, Guichen Bay, near Robe; Shelly Beach, Cape Northumberland; Port MacDonnell Beach; and Bridgewater Bay, Cape Bridgewater. The average of these four modern beach whole-rock samples was defined as time zero to provide a more statistically accurate value as residence time in a region may vary temporally and spatially. Time zero ( $T_0$ ) represents the average time sediments may reside on a beach before being transported into the dune system. The individual D/L values of these whole-rock samples and potential reasons for their variation are discussed later in the chapter (section 5.8.1). The second whole-rock calibration point used the OSL age derived from MacDonnell Range of  $124 \pm 10$  ka. While OSL and AAR date different events, the burial of sediments and the cessation of protein synthesis in organisms respectively, this is statistically accounted for by subtracting the time zero (or residence time) of sediment (calculated as the average of 10 sub-samples from 4 sample sites of modern beaches across the coastal plain) from derived D/L values prior to calibration of AAR numerical ages. The OSL age confirms a MIS 5e age for MacDonnell Range and was deemed more suitable for AAR calibration curve construction than the U-series age derived by Schwebel (1978; 1984) due to its lower analytical uncertainty.

Foraminifera were also calibrated using two calibration points. A separate calibration curve was constructed for each foraminiferal species analysed. *Elphidium crispum*, *Ammonia beccarii* and *Discorbis dimidiatus* were sampled from the Port MacDonnell Beach modern sediment (which yielded the lowest D/L values of all modern whole-rock samples) and was used to represent time zero. Foraminifera sampled from sediment within MacDonnell Range were used as the second calibration point and adopted the OSL derived age of  $124 \pm 10$  ka at this site.

#### **Apparent parabolic kinetic model**

The basis of this kinetic model is that as the rate of racemisation decreases over time, this pattern can be fitted with a parabola (Mitterer and Kriausakul, 1989). This model was deemed suitable for calibration of AAR samples across the Mount Gambier coastal plain as it can be applied without the knowledge of the thermal history of the fossils as long as a suitable number of calibration points are used and that the fossils have been subjected to a similar thermal history (Clarke and Murray-Wallace, 2006). Other curve fitting methods such as the integrated rate equation were regarded as unsuitable. The racemisation kinetic model based on the application of the integrated rate equation does not accurately describe D/L values over the entire range to equilibrium if a sample observes reversible first order reaction kinetics. This model is therefore unsuitable to middle Pleistocene samples, especially where there are gaps in the sedimentary record (Clarke and Murray-Wallace, 2006) such as on the Mount Gambier coastal plain. Several other studies across the South Australian coastline have also successfully applied the apparent parabolic kinetic model (e.g. Murray-Wallace *et al.*, 2001, 2010).

The equation for the apparent parabolic kinetic model is;

$$t = \left( \frac{[(D/L)_s - (D/L)_{t_0}]}{M_c} \right)^2$$

Where  $t$  represents the derived AAR numerical age,  $(D/L)_s$  is the extent of racemisation at one sample site derived from the averaging of multiple sub-samples of whole-rock or multiple individuals of foraminifer or molluscs of the same species,  $(D/L)_{t_0}$  represents the time zero of material analysed, while  $M_c$  is the slope of linear regression between calibrated samples and is given as:

$$M_c = \frac{(D/L)}{\sqrt{t}}$$

While it is recognised that the calibration curve for *Turbo undulatus* only has three calibration points, the degree of fit is very good ( $r^2=0.999$ ) as shown in Figure 5.9. The calibration points used are the modern beach samples ( $t=0$ ), the raised Holocene beach sample ( $t=2.473$  ka), and the sample from the Glanville Formation, Goolwa ( $t=125$  ka).  $M_c$  for this calibration is 0.0374.



Figure 5.9: Calibration curve used to derive AAR numerical ages for *Turbo undulatus* at Port MacDonnell.

### 5.7.3 Uncertainties

Uncertainties were calculated by the square root of the sum of the squares of a range of sources of potential uncertainty. These included: (1) the analytical precision for the RP-HPLC; (2) the variation within sampled material at each sampling site; (3) the variation in diagenetic temperature; (4) the variation in modern temperatures between sample sites; (5) the uncertainty in calibration values; and, in the case of genera not analysed at calibration sites, (6) the variation in D/L values between different genera.

The laboratory uncertainty term and RP-HPLC reproducibility was derived by running multiple inter-laboratory comparison (ILC) standards after Wehmiller (1984). In this study, ILCs were generally analysed with most runs. The standard deviation of the derived D/L values for each ILC was then derived and converted into a percentage. The average of these three values yielded 1.4% and was used in final uncertainty estimates of AAR numerical ages.

Variation within sample sites was accounted for by averaging multiple sub-samples. Where shell was used, at least two and commonly three sub-samples were analysed from the umbo region of the same individual to account for any intra-shell variation. Where possible, three shells or more of the same species were analysed to account for any variation to D/L

values that may have been caused to a particular shell by localised weathering effects. Multiple foraminifers were hand-picked and analysed from whole-rock samples. Multiple vials containing single foraminifers were analysed, as were vials containing up to 10 foraminifera which yielded higher amino acid concentrations but may not necessarily have yielded values as precise as that from a single test. Up to ten sub-samples were analysed for whole-rock samples to account for D/L variation within sites. Within each analysed unit the multiple samples and sub-samples were averaged and the co-efficient of variance of each sample calculated. This value was used in the final AAR numerical age calculation for each sample.

The AAR reaction is temperature sensitive and it is necessary to account for the potential changes in temperature that a fossil has been exposed to before the extent of racemisation can be interpreted. The diagenetic temperature of a sample site refers to the integrated temperatures that fossils have experienced during the burial history from the onset of racemisation to analysis of the sample. It is not possible to derive the complete change in temperature at sample sites across the Mount Gambier coastal plain for the entire time molluscs or sediment have been deposited, but where possible samples were collected from 1 m or more below the land surface where temperature differences are suggested to be minimal (Miller and Clarke, 2007). When using AAR to determine the age of shoreline deposits of presumed last interglacial shoreline age along the south-eastern Australian coastline, Belperio *et al.* (1995) suggested that a 1°C temperature uncertainty in diagenetic temperature be accounted for in age assessments and correlation. When applied to the CMAT of the Mount Gambier coastal plain this results in an approximate temperature variation of 10%.

CMAT varies across the Mount Gambier coastal plain. As AAR numerical ages are calibrated by samples from a wide spread of localities the temperature difference is accounted for in each calibration curve. For *Turbo undulatus*, calibration points are compared from Goolwa (CMAT = 15.5°C) and Port MacDonnell (CMAT = 14.0°C). This temperature difference is 9.4% and is incorporated into uncertainty calculations. All other molluscan species and foraminifera are collected from between Robe and Dartmoor, which yields a temperature difference of 3.27%. Whole-rock samples are collected between Robe and Cape Bridgewater (13.4°C) and a temperature difference of 7.5% is incorporated into uncertainty calculations.

Determination of AAR numerical ages is dependent on the calibration of D/L values with independently dated samples. The uncertainties associated with these derived ages are incorporated in the AAR numerical age determination as a percentage of the age (e.g. 125 ± 20, gives an error value of 16%).

For some mollusc genera that were not identified at a calibration site (Lake Hawdon South) or where live-collected samples of this genus were not analysed, numerical ages were derived using the calibration curve of another mollusc. While this would add additional uncertainty to deriving a numerical age it is suggested the magnitude of this uncertainty would be low, though this may be dependent on the species. Statistical results of GLU D/L values of molluscs collected from the *in situ* shell bed at Lake Hawdon South reveal there is no statistical difference between the extent of racemisation in *Katelysia*, *Tellina*, *Fulvia*, and *Anadara* (Appendix C). Statistical difference was found between these genera and *Brachidontes*, and therefore numerical ages were not calculated for the latter genus. Where possible, bivalves were calibrated with the *Katelysia* calibration curve, while gastropods were calibrated using the curve derived for *Turbo*. At Lake Hawdon South the largest range of molluscan species were identified. The average of *Katelysia*, *Anadara*, *Tellina*, *Chlamys*, and *Fulvia* were averaged and their co-efficient of variance was derived to be 7.198. This value was incorporated into the uncertainty of AAR numerical age calculations of shells not belonging to the genera *Katelysia*, *Ostrea*, or *Turbo*.

## 5.8 Presentation of AAR results

This section presents the AAR results derived from analysis of molluscs, foraminifera and whole-rock samples from the Bridgewater Formation across the Mount Gambier coastal plain. Sample site locations are shown in Figure 3.11. Results are presented by sample site from the modern coastline landward. As discussed earlier, it is hypothesised that barrier shorelines should increase in age with increased distance landward. D/L values are presented for both total hydrolysable amino acids and free amino acids where analysed. Standard deviation values presented are to  $1\sigma$ . Statistical analysis was conducted on D/L values to determine whether there was any significant difference between the sample sites. Statistical tests conducted included analysis of variance (ANOVA) of mean values and post-hoc Tukey tests using the SPSS statistical package (IBM Corp., 2010). Statistical results are presented in Appendix C.

Where D/L values were significantly low in relation to the distance landward of the modern shoreline and did not correlate with stratigraphical interpretations of significantly older deposits, AAR numerical ages were not calculated. The low D/L values, especially found within whole-rock samples, potentially reflect leaching of lower-molecular-weight amino acids or diagenetically altered samples, and thus AAR numerical ages would not represent the true age of the deposit.



### 5.8.1 Modern beach and shell samples

AAR analysis of sediment using the whole-rock technique is reliant on the averaging of D/L values in thousands of carbonate grains (up to 2500 in a 150 mg sample). These grains may reside on the modern beach for lengthy periods of time before they are transported landward into dune systems. A range of whole-rock samples was collected from beaches along the Mount Gambier coastal plain coastline to compare residence times. Sample sites include: Longbeach, Guichen Bay, near Robe (collected by Murray-Wallace *et al.*, 2001); Shelly Beach, Cape Northumberland; Port MacDonnell Beach; and Cape Bridgewater, Victoria. D/L values from these four modern beach sites were averaged and used as  $T_0$  in whole-rock numerical age calibration. Operculum of the marine gastropod *Turbo undulatus* were collected from the modern beach at Port MacDonnell to compare with the residence time of whole-rock samples. Live-collected *Katelysia rhytiphora* and *Ostrea angasi* were also analysed for AAR to compare D/L values. Aspartic acid, glutamic acid and valine D/L values are presented in Table 5.5.

Statistical analysis of whole-rock samples at modern beach sites indicates that there is a significant difference between derived D/L values. The modern sand at Port MacDonnell Beach yielded significantly lower D/L values than those at Shelly Beach, Cape Bridgewater and Longbeach (Figure 5.10), while no significant difference was found between the other three sample sites. This result highlights the difference in residence times of bioclastic grains within the beach environment, and may potentially result from the age and erosional potential of surrounding deposits. At Guichen Bay, where Longbeach is the modern beach, up to 80 Holocene beach ridges (relict foredunes) have been identified (Sprigg, 1952; Murray-Wallace *et al.*, 2002). It is highly likely that during high tides and storm conditions this older sediment may be reworked into modern beach sediment. At Shelly Beach, aeolianite cliffs and offshore stacks, suspected to be last interglacial *sensu lato* (MIS 5a and MIS 5c) in age from stratigraphical correlation with Robe Range, surround the modern beach and sediment from these deposits may have been reworked within the modern beach grains. At Cape Bridgewater, there are stacked aeolianites of the Bridgewater Formation that formed during multiple sea-level highstands (Boutakoff, 1963) and these deposits back the modern beach. Reworked older sediment from this cliff may also have contributed to the modern beach material. At Port MacDonnell Beach, while aeolianite cliffs are found at the western end of the beach, only a small Holocene beach deposit is found to the rear of the modern beach, and may have not increased D/L values as significantly compared with the other modern beach sample sites.

**Table 5.5:** Results of AAR analysis from samples at modern beaches across the Mount Gambier coastal plain, southern Australia

Sample site	Facies	Material analysed	UWGA (UOW AAR lab. code)	n replicates	Amino acid D/L value $\pm 1 \sigma$		
					ASP	GLU	VAL
Port MacDonnell	Beach	Whole-rock	9883a-i	9	T: 0.117 $\pm$ 0.010 F: 0.553 $\pm$ 0.013	T: 0.083 $\pm$ 0.005 F: 0.425 $\pm$ 0.008	T: 0.038 $\pm$ 0.002 F: 0.490 $\pm$ 0.087
Shelly Beach, Cape Northumberland	Beach	Whole-rock	9630a-i	9	T: 0.332 $\pm$ 0.012 F: 0.687 $\pm$ 0.020	T: 0.192 $\pm$ 0.007 F: 0.378 $\pm$ 0.010	T: 0.148 $\pm$ 0.013 F: 0.365 $\pm$ 0.021
Longbeach, Guichen Bay (AAB2)	Beach	Whole-rock	9838a-i	9	T: 0.327 $\pm$ 0.014 F: 0.737 $\pm$ 0.007	T: 0.212 $\pm$ 0.008 F: 0.488 $\pm$ 0.009	T: 0.152 $\pm$ 0.014 F: 0.525 $\pm$ 0.086
Cape Bridgewater, VIC	Beach	Whole-rock	9620a-i	9	T: 0.355 $\pm$ 0.007 F: 0.722 $\pm$ 0.013	T: 0.214 $\pm$ 0.012 F: 0.485 $\pm$ 0.038	T: 0.169 $\pm$ 0.019 F: 0.592 $\pm$ 0.046
<b>AVERAGE OF ALL MODERN BEACH WHOLE-ROCK SAMPLES</b>					<b>T: 0.283 <math>\pm</math> 0.098</b> <b>F: 0.669 <math>\pm</math> 0.098</b>	<b>T: 0.175 <math>\pm</math> 0.107</b> <b>F: 0.712 <math>\pm</math> 0.068</b>	<b>T: 0.127 <math>\pm</math> 0.054</b> <b>F: 0.497 <math>\pm</math> 0.115</b>
Live-collected		<i>Katelysia rhytiphora</i>	10028a-d	4	T: 0.073 $\pm$ 0.004	T: 0.035 $\pm$ 0.003	T: 0.013 $\pm$ 0.001
Live-collected		<i>Ostrea</i>	10212	5	T: 0.079 $\pm$ 0.007	T: 0.039 $\pm$ 0.003	T: 0.014 $\pm$ 0.001
Port MacDonnell	Beach	<i>Turbo undulatus</i> operculum	9856 a,b,c,e 9811 c,d	6	T: 0.153 $\pm$ 0.053	T: 0.063 $\pm$ 0.017	T: 0.019 $\pm$ 0.008
Port MacDonnell (older tests)	Beach	<i>Elphidium crispum</i>	10206 ai, aii, aiv, avi, avii, aviii	10 vials (6x10pv and 4x1pv)	T: 0.076 $\pm$ 0.022	T: 0.054 $\pm$ 0.01	T: 0.033 $\pm$ 0.013
			10206 aiii, av	2 vials (1x10, 1x1 pv)	T: 0.166 $\pm$ 0.056	T: 0.157 $\pm$ 0.056	T: 0.131 $\pm$ 0.091
		<i>Discorbis dimidiatus</i>	10206 bi- biii	3 vials (2x1, 1x5pv)	T: 0.062 $\pm$ 0.021	T: 0.039 $\pm$ 0.005	T: 0.020 $\pm$ 0.003

n replicates refers to the number of individual shells (note; usually at least 3 sub-samples taken from each individual shell), whole-rock sub-samples, or vials of foraminifera averaged. In relation to analysed foraminifera, pv indicates the number of foraminifera per vial. For example, 10 vials (6x10 pv, 4x1 pv) means that D/L values from 10 vials were averaged, and of those 10, 6 vials contained 10 tests and 4 vials contained 1 test per vial. T = total hydrolysable amino acids while F = free amino acids.

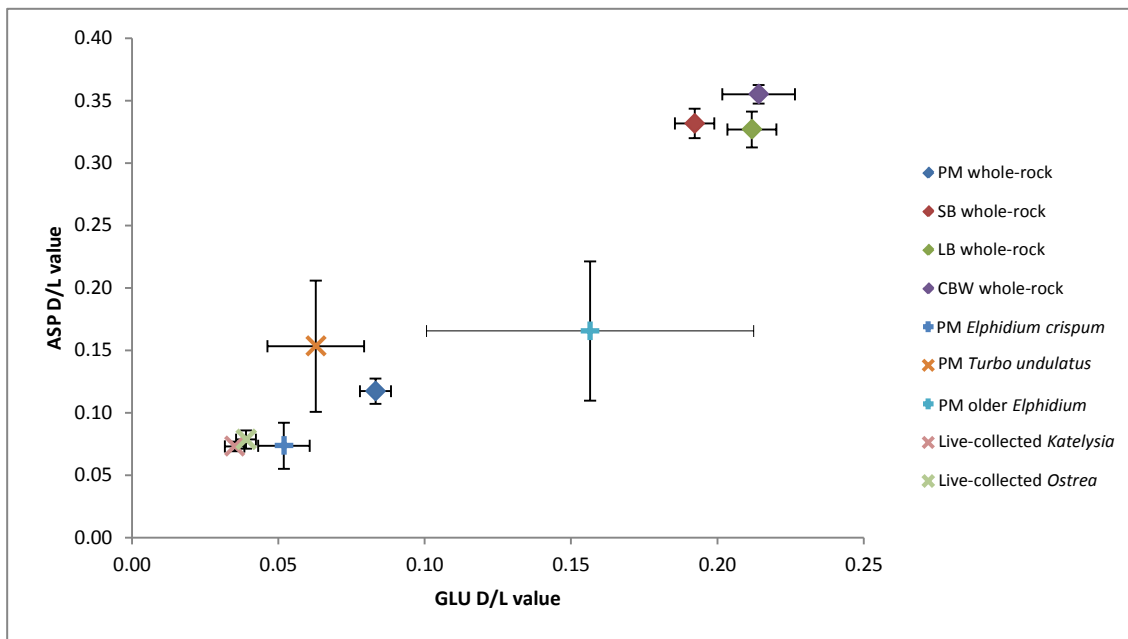


**Figure 5.10:** Scatter plot of aspartic acid (ASP) and glutamic acid (GLU) D/L values derived from AAR analysis of whole-rock, shell and foraminifera at modern beach sample sites. Whole-rock samples from Shelly Beach, Longbeach and Cape Bridgewater yielded significantly higher D/L values and reflect reworking of older grains into modern beach sediment. Foraminifera D/L values at Port MacDonnell Beach show a wide spread of D/L values potentially indicating the reworking of grains. [PM = Port MacDonnell, SB = Shelly Beach, LB = Longbeach, CBW = Cape Bridgewater]. D/L values were derived from single injections and averaged from up to ten sub-samples for whole-rock, analyses of single and multiple (up to ten) tests for foraminifera and at least four individual molluscs which were sub-sampled at least twice. For exact numbers of sub-samples see Table 5.5.

D/L values for modern whole-rock samples are consistently higher than those derived from live-collected molluscs or *Turbo undulatus* collected from Port MacDonnell Beach (Figure 5.10). This likely reflects the lengthy residence times of bioclastic grains on the beach face and reworking of older grains from the actively eroding exposures of late Pleistocene aeolianite. There is no significant difference between GLU D/L values for live-collected *Ostrea* or *Katelaysia*. D/L values of foraminifera from the whole-rock sample collected at Port MacDonnell Beach were found to vary significantly. Some *Elphidium crispum* yielded D/L values similar to the live-collected molluscan values, while others yielded higher D/L values and potentially reflect lengthier residence times on the continental shelf.

By comparing the hydrolysable amino acid (THAA) and free amino acid (FAA) fractions derived from multiple sub-samples of sediment analysed using the whole-rock method from the same deposits at the modern beaches of the Mount Gambier coastal plain the structure of the data can be observed (Figure 5.11). This structure is sometimes masked when D/L values are averaged. It is evident that FAA are consistently higher than THAA. D/L values are most consistent within the Port MacDonnell Beach sample and most varied within the Cape Bridgewater modern beach sample. This variation may reflect the reworking of older grains from the nearby stacked aeolianites of the Bridgewater Formation and the inherent inhomogeneity of these contrasting samples with regard to the age of individual carbonate grains.

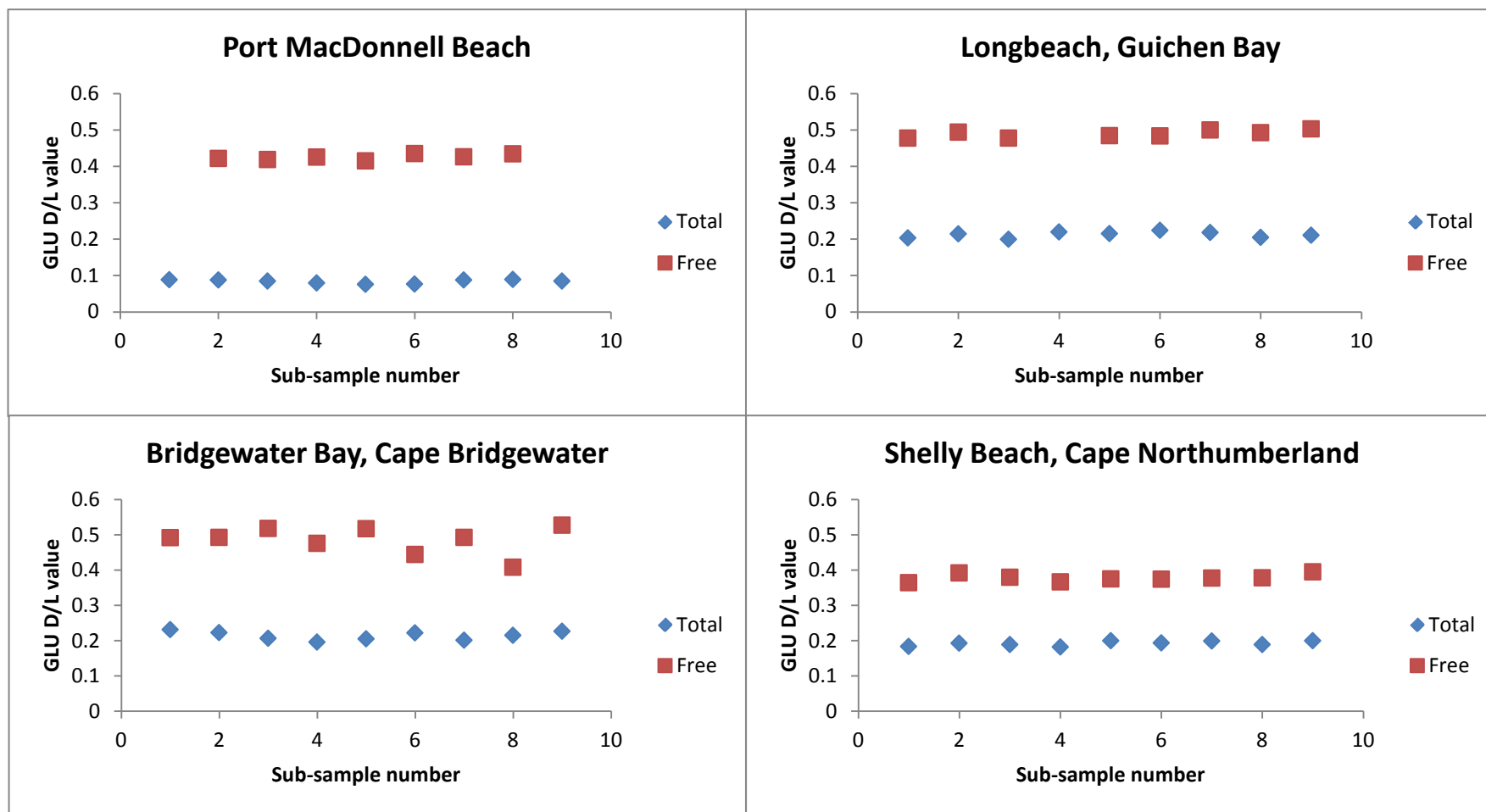


**Figure 5.11:** Plots of glutamic acid total hydrolysable (THAA) and free amino acid (FAA) fraction D/L values derived from multiple sediment sub-samples at modern beaches across the Mount Gambier coastal plain, analysed through the whole-rock technique. Results show the structure of the data within a sample and allow for identification of possible reworked skeletal carbonate grains. Results indicate FAA are continually higher than THAA and variance of D/L values is low between sub-samples.

### 5.8.2 Port MacDonnell (0-3 m APSL)

Samples were collected and analysed from a range of units at Port MacDonnell Beach. *Turbo undulatus* opercula were collected from the raised Holocene beach landward of Port MacDonnell Beach (the stratigraphy of this site is described in section 3.8.2). The opercula from this deposit were analysed for both AAR and radiocarbon dating. Sediment for whole-rock analysis was also collected from this unit as well as *Elphidium crispum* and *Discorbis dimidiatus* which were hand-picked from the sediment. *Turbo undulatus* opercula were collected and analysed for AAR from the midden found on the raised Holocene beach. Whole-rock samples were collected from the upper and lower aeolianite units of the proposed equivalent of Robe Range at the western end of Port MacDonnell Beach and Shelly Beach (section 3.8.3 describes the stratigraphy of these deposits). *Elphidium crispum* and *Discorbis dimidiatus* were hand-picked from these sediment samples. A whole-rock sample was also collected from Robe III at Robe Harbour by Murray-Wallace *et al.* (2001) and was re-analysed in this study using RP-HPLC. Finally, *Turbo undulatus* opercula were sampled from the flint conglomerate which overlies Gambier Limestone on Port MacDonnell Beach and was analysed using both radiocarbon and AAR analysis. AAR D/L values and derived numerical ages are given for all units at Port MacDonnell in Table 5.6.

**Table 5.6:** Results from AAR analysis of samples from a range of coastal facies at Port MacDonnell, Mount Gambier coastal plain, southern Australia

Sample site	Facies	Material analysed	UWGA	n replicates	Amino acid D/L value $\pm 1 \sigma$			Age estimate (ka) using GLU
					ASP	GLU	VAL	
Port MacDonnell back beach area	Holocene beach	Whole-rock	10044a-j	10	T: 0.456 $\pm$ 0.012 F: 0.759 $\pm$ 0.007	T: 0.291 $\pm$ 0.009 F: 0.577 $\pm$ 0.019	T: 0.232 $\pm$ 0.010 F: 0.525 $\pm$ 0.012	44 $\pm$ 6
		<i>Turbo undulatus</i> operculum	9840, 9841, 9847a-d, 9850a-f	12	T: 0.308 $\pm$ 0.037 F: 0.586 $\pm$ 0.061	T: 0.133 $\pm$ 0.017 F: 0.255 $\pm$ 0.03	T: 0.069 $\pm$ 0.015 F: 0.206 $\pm$ 0.035	3.5 $\pm$ 1
		<i>Elphidium crispum</i>	10205ai, aii, av, avi, avii	5 (3x10, 2x1pv)	T: 0.399 $\pm$ 0.026	T: 0.202 $\pm$ 0.018	T: 0.193 $\pm$ 0.004	46 $\pm$ 7
Port MacDonnell, Robe Range equivalent	Midden Upper aeolianite in cliff	<i>Discorbis dimidiatus</i>	10205 bi-bvii	7 (4x10, 3x1pv)	T: 0.377 $\pm$ 0.068	T: 0.182 $\pm$ 0.048	T: 0.213 $\pm$ 0.102	29 $\pm$ 4
		<i>Turbo undulatus</i> operculum	9806a-d	4	T: 0.342 $\pm$ 0.061	T: 0.134 $\pm$ 0.025	T: 0.047 $\pm$ 0.018	4 $\pm$ 1
		Whole-rock	9837a-j	10	T: 0.462 $\pm$ 0.012 F: 0.692 $\pm$ 0.023	T: 0.300 $\pm$ 0.021 F: 0.518 $\pm$ 0.014	T: 0.238 $\pm$ 0.009 F: 0.457 $\pm$ 0.033	52 $\pm$ 8
Shelly Beach, Robe Range equivalent	Upper aeolianite in cliff	<i>Elphidium crispum</i>	9864ai, aii, bi, bii, 10033ai, aiii, aiv, avi, avii 10095ai-aiv	13 (8x10, 2x5, 3x1pv)	T: 0.491 $\pm$ 0.027	T: 0.258 $\pm$ 0.043	T: 0.242 $\pm$ 0.058	87 $\pm$ 19
		<i>Discorbis dimidiatus</i>	10095bi, bii, 10033bi, biii	4 (2x10, 2x1 pv)	T: 0.486 $\pm$ 0.033	T: 0.234 $\pm$ 0.030	T: 0.203 $\pm$ 0.013	54 $\pm$ 10
		Whole-rock	10047a-j	10	T: 0.519 $\pm$ 0.005 F: 0.774 $\pm$ 0.003	T: 0.333 $\pm$ 0.006 F: 0.581 $\pm$ 0.012	T: 0.297 $\pm$ 0.01 F: 0.588 $\pm$ 0.011	79 $\pm$ 12
Port MacDonnell, Robe Range equivalent	Lower aeolianite in cliff	<i>Elphidium crispum</i>	10214aii-aviii	7 (3x10, 4x1 pv)	T: 0.480 $\pm$ 0.046	T: 0.244 $\pm$ 0.028	T: 0.246 $\pm$ 0.018	75 $\pm$ 10
		<i>Discorbis dimidiatus</i>	10214bi-biii	3 (2x10, 1x1 pv)	T: 0.523 $\pm$ 0.019	T: 0.259 $\pm$ 0.035	T: 0.342 $\pm$ 0.039	69 $\pm$ 13
		Whole-rock	10048a-j	10	T: 0.534 $\pm$ 0.025 F: 0.747 $\pm$ 0.001	T: 0.354 $\pm$ 0.030 F: 0.588 $\pm$ 0.018	T: 0.328 $\pm$ 0.026 F: 0.662 $\pm$ 0.004	106 $\pm$ 18
Shelly Beach, Robe Range equivalent	Lower aeolianite in cliff	<i>Elphidium crispum</i>	10065aii-avii	5 (5x10 pv)	T: 0.477 $\pm$ 0.006	T: 0.229 $\pm$ 0.018	T: 0.187 $\pm$ 0.015	64 $\pm$ 10
		<i>Discorbis dimidiatus</i>	10065biii	1 (1x10 pv)	T: 0.548	T: 0.277	T: 0.277	81 $\pm$ 11
		Whole-rock	10046a-e, 9520a-g	12	T: 0.467 $\pm$ 0.027 F: 0.736 $\pm$ 0.009	T: 0.320 $\pm$ 0.035 F: 0.599 $\pm$ 0.097	T: 0.188 $\pm$ 0.041 F: 0.593 $\pm$ 0.028	69 $\pm$ 13
Robe Harbour, Robe Range Port MacDonnell conglomerate	Beach	<i>Elphidium crispum</i>	10215ai-avii	7 (3x10, 4x1 pv)	T: 0.496 $\pm$ 0.02	T: 0.264 $\pm$ 0.029	T: 0.290 $\pm$ 0.036	92 $\pm$ 12
		<i>Discorbis dimidiatus</i>	10215bi-biv	4 (2x10, 2x1 pv)	T: 0.477 $\pm$ 0.027	T: 0.249 $\pm$ 0.023	T: 0.326 $\pm$ 0.047	63 $\pm$ 10
		Whole-rock	9839a-i	9	T: 0.576 $\pm$ 0.008 F: 0.791 $\pm$ 0.008	T: 0.400 $\pm$ 0.008 F: 0.567 $\pm$ 0.018	T: 0.340 $\pm$ 0.006 F: 0.573 $\pm$ 0.009	167 $\pm$ 25
Traeger's Quarry, Goolwa	Beach	<i>Turbo undulatus</i> operculum	9851, 10058, 10061, 10062	4	T: 0.345 $\pm$ 0.023 F: 0.597 $\pm$ 0.019	T: 0.137 $\pm$ 0.01 F: 0.258 $\pm$ 0.021	T: 0.062 $\pm$ 0.012 F: 0.145 $\pm$ 0.013	4 $\pm$ 1
			9852, 10057, 10059, 10060	4	T: 0.650 $\pm$ 0.040 F: 0.822 $\pm$ 0.076	T: 0.443 $\pm$ 0.037 F: 0.618 $\pm$ 0.016	T: 0.353 $\pm$ 0.052 F: 0.534 $\pm$ 0.022	103 $\pm$ 23
		<i>Turbo undulatus</i> operculum	5387a-e	5	T: 0.730 $\pm$ 0.012	T: 0.480 $\pm$ 0.010	T: 0.415 $\pm$ 0.010	~125*

UWGA = lab code for University of Wollongong, Australia; n replicates refers to the number of individual shells (at least 2 sub-samples from each) whole-rock sub-samples, or vials of foraminifera averaged; pv = number of tests per vial; \*D/L values yielded by Murray-Wallace *et al.* (2010) for Traeger's Quarry and deemed to be MIS 5e in age; T= total amino acid fraction, F= free amino acid fraction.

AAR analysis of sediment by the whole-rock technique and foraminifera within the raised Holocene beach deposit landward of Port MacDonnell Beach yielded surprisingly high D/L values, while *Turbo undulatus* within the deposit yielded much lower D/L values. Radiocarbon analysis of the same fossil shell gave an age of  $2470 \pm 25$  yr BP (Wk-34195) and precludes a late Pleistocene age for the deposit. Whole-rock D/L values from the Holocene beach were found to be statistically significantly different from all modern beach samples, but were not significantly different from the upper aeolianite units at Port MacDonnell and Shelly Beach, indicating that sediment may have been reworked from these deposits into the Holocene unit. The lack of aeolianite on Port MacDonnell Beach indicates that had any been present previously, it has been eroded by the Holocene sea-level highstand and during this phase of erosion, bioclastic sediment originally deposited as aeolianite may have been reworked into the Holocene beach deposit. This potentially explains why D/L values were higher for sediment than *Turbo undulatus* within this unit. *Turbo undulatus* from the midden deposit yielded similar D/L values to the Holocene beach deposit and a numerical age estimate of  $3.6 \pm 1$  ka was derived.

The well-defined 75 cm calcrete palaeosol separating aeolianite units in the cliffs at Port MacDonnell and Shelly Beach (Figures 3.19c,d and 3.21) indicates a significant hiatus in sediment deposition. If the upper aeolianite units correlate with Robe II as described by Banerjee *et al.* (2003) and suggested by OSL analysis from this study (Table 5.4) then the lower aeolianite unit may represent a correlative of Robe III of MIS 5c age estimate ( $\sim 105$  ka). This would be in accord with the previously derived TL age of  $116 \pm 6$  ka for Robe III near the type locality at Robe (Huntley *et al.*, 1994).

Whole-rock GLU D/L values from the upper and lower aeolianite units at Port MacDonnell are not significantly different from each other or from the lower aeolianite at Shelly Beach. This indicates that they were likely deposited at a similar time. Whole-rock and foraminifera D/L values from the upper aeolianite units at Port MacDonnell correlate well with the OSL result of this deposit and indicate a late MIS 3 age, while the samples from the upper aeolianite at Shelly Beach yield slightly higher values and indicate a MIS 5a age ( $79 \pm 12$  ka). Whole-rock samples from the lower Port MacDonnell aeolianite unit yielded an AAR numerical age estimate of  $106 \pm 18$  ka indicating deposition during MIS 5. Foraminifera from this deposit yielded slightly lower D/L values and indicate that AAR does not have the age resolution to distinguish between interstadial events. This is also highlighted in derived numerical ages of foraminifera from Shelly Beach aeolianites which range from  $63 \pm 10$  ka to  $92 \pm 2$  ka.

Murray-Wallace *et al.* (2001) used gas chromatography (GC) to analyse Bridgewater Formation whole-rock samples across the Robe coastal plain. A sample collected from an aeolianite unit of Robe III near Robe Harbour yielded an AAR age estimate of  $127 \pm 24$  ka. This sample was re-analysed in this study using RP-HPLC and yielded an AAR numerical age of  $167 \pm 22$  ka. The lower age derived by Murray-Wallace *et al.* (2001) for this sample may reflect differences between GC and RP-HPLC analysis. Murray-Wallace *et al.* (2010) suggested that lower degrees of racemisation in whole-rock samples derived by GC compared with RP-HPLC may reflect the grain size fraction analysed, with finer particles potentially yielding higher extents of racemisation. The difference in derived numerical ages and the age derived by RP-HPLC (which suggests deposition during the sea level lowstand, which unless sediment has been reworked, is unlikely) could also reflect diagenetic temperature differences that were not accounted for accurately enough, between Robe Harbour and MacDonnell Range, where the calibration sediment was sampled.

The flint and shell-rich conglomerate found on Port MacDonnell Beach underlies weathered Bridgewater Formation aeolianite stratigraphically similar (in terms of bedding, sediment characteristics and elevation) to the lower aeolianite unit identified in cliffs at the western end of the beach (Figure 3.20). This weathered aeolianite is thought to be MIS 5c in age, as is the lower aeolianite within what is proposed to be an equivalent of Robe Range. Schwebel (1978; 1984) considered Robe Range to include units of interstadial age capped by Holocene dunes. As the flint conglomerate is stratigraphically beneath this lower aeolianite it must therefore be the same age (MIS 5c) or older. Because the last interglacial (MIS 5e) shoreline of MacDonnell Range is found 7 km inland, the flint conglomerate cannot be MIS 5e in age, and is therefore suggested to have been deposited during a last interglacial interstadial. Radiocarbon analysis of a *Turbo undulatus* operculum within the conglomerate yielded a 'finite' minimum age of  $47,910 \pm 2100$  yr BP (Wk-34733) and precludes a Holocene age for the fossil shells within the deposit. AAR analysis of *Turbo undulatus* opercula fragments within the conglomerate suggest two phases of shell deposition within the conglomerate. Of the eight fragments analysed by AAR, four yielded significantly lower D/L values and a numerical age of  $4 \pm 1$  ka, which is almost identical to the values and age determined for *Turbo sp.* within the raised Holocene beach to the rear of this deposit. The other four *Turbo sp.* fragments within the conglomerate yielded higher D/L values which were more comparable to D/L values of *Turbo sp.* within the last interglacial (MIS 5e) Glanville Formation at Traeger's Quarry, Goolwa (Table 5.6). The AAR numerical age derived from the analysed shell fragments within the flint conglomerate at Port MacDonnell is  $103 \pm 23$  ka, and suggests a last interglacial *sensu lato* age,



while its geographic location, 7 km seaward of the MIS 5e barrier shoreline, indicates that it is a relict shoreline feature younger than the last interglacial maximum. This finding is significant as it is the first reported subaqueously deposited, late Pleistocene interstadial beach strata found above present sea level on the Australian continent (Blakemore *et al.*, 2014). The significance of this finding is discussed further in the context of palaeo-sea level in Chapter 6.

### **5.8.3 Last interglacial (MIS 5e) deposits (~9-16 m APSL)**

The location of MacDonnell Range, 7 km landward from and sub-parallel to the modern coastline, reveals it as a potential correlative of the last interglacial (MIS 5e) Woakwine Range and this is supported by OSL analysis (Table 5.4). Woakwine Range has been mapped as extending for over 300 km from the mouth of the River Murray to Kongorong (Murray-Wallace *et al.*, 1999; Murray-Wallace *et al.*, 2010), approximately 20 km southwest of Mount Gambier. Whole-rock samples were collected from an aeolian unit along Swarts Road, near Allendale East. *Elphidium crispum*, *Discorbis dimidiatus* and *Ammonia beccarii* were hand-picked and analysed for AAR. Sherwood *et al.* (1994) reported a MIS 5e age shell bed at Narrawong, Victoria. This site was not identified through fieldwork in this study but sediment and a loose shell were sampled from a nearby road cutting. No last interglacial, *sensu stricto*, shell beds in an *in situ* position were located in the Mount Gambier region. This may be attributed to the large aeolian dunes covering any lagoonal facies as they transgressed landward and a lack of road cuttings through the barrier exposing such facies. Hypothesised last interglacial shells were therefore sampled from Lake Hawdon South, landward of the Woakwine Range at Biscuit Drain (Figure 3.23). A nearby site at Lake Hawdon South (CCP1) has been identified as MIS 5e in age (Murray-Wallace and Belperio, 1991), and therefore, the samples collected from Biscuit Drain are used to calibrate other shell D/L values. *Katelsia rhytiphora* from Lake Hawdon South (CCP1) were also analysed by RP-HPLC in this study and used in calibration curve construction for this species. AAR results for all proposed last interglacial (MIS 5e) shell, sediment and foraminifera are presented in Table 5.7.

**Table 5.7:** Results from AAR analysis of samples from proposed last interglacial sites within MacDonnell Range; Woakwine Range, Lake Hawdon South; and Narrawong, Victoria

Sample site	Facies	Material analysed	UWGA	n replicates	Amino acid D/L value $\pm 1 \sigma$			Age estimate (ka) using GLU
					ASP	GLU	VAL	
Swarts Road, MacDonnell Range	Aeolianite	Whole-rock	9836a-g, 9540a-j	17	T: 0.552 $\pm$ 0.009 F: 0.785 $\pm$ 0.006	T: 0.369 $\pm$ 0.009 F: 0.537 $\pm$ 0.011	T: 0.188 $\pm$ 0.078 F: 0.524 $\pm$ 0.012	Used as calibration value 124 $\pm$ 10 ka
		<i>Elphidium crispum</i>	9844a-h, j, l, 9866aai	9 (2x10, 7x1 pv)	T: 0.530 $\pm$ 0.052	T: 0.298 $\pm$ 0.045	T: 0.306 $\pm$ 0.081	
		<i>Discorbis dimidiatus</i>	9865ai, aii, bi	3 (2x10, 1x1 pv)	T: 0.562 $\pm$ 0.005	T: 0.334 $\pm$ 0.006	T: 0.396 $\pm$ 0.024	
Narrawong road cutting	Unknown	Whole-rock	10045a-j	10	T: 0.523 $\pm$ 0.030 F: 0.759 $\pm$ 0.007	T: 0.349 $\pm$ 0.035 F: 0.577 $\pm$ 0.019	T: 0.310 $\pm$ 0.036 F: 0.525 $\pm$ 0.012	100 $\pm$ 17.9  100 $\pm$ 13.3 78 $\pm$ 10.7 155 $\pm$ 33*
		<i>Elphidium crispum</i>	10081ai-aiii	3 (3x10 pv)	T: 0.504 $\pm$ 0.002	T: 0.273 $\pm$ 0.003	T: 0.218 $\pm$ 0.003	
		<i>Discorbis dimidiatus</i>	10081bi, bii, biv	3 (3x10 pv)	T: 0.565 $\pm$ 0.011	T: 0.325 $\pm$ 0.011	T: 0.364 $\pm$ 0.015	
		<i>Spisula</i>	10214	1	T: 0.576 $\pm$ 0.011 F: 0.751 $\pm$ 0.006	T: 0.395 $\pm$ 0.021 F: 0.586 $\pm$ 0.006	T: 0.375 $\pm$ 0.014 F: 0.540 $\pm$ 0.007	
		Whole-rock	9855a-j	10	T: 0.532 $\pm$ 0.020 F: 0.749 $\pm$ 0.007	T: 0.362 $\pm$ 0.045 F: 0.574 $\pm$ 0.015	T: 0.357 $\pm$ 0.036 F: 0.658 $\pm$ 0.043	
		Whole-rock	9855a-j	10	T: 0.532 $\pm$ 0.020 F: 0.749 $\pm$ 0.007	T: 0.362 $\pm$ 0.045 F: 0.574 $\pm$ 0.015	T: 0.357 $\pm$ 0.036 F: 0.658 $\pm$ 0.043	
Woakwine Range (AAB6) Lake Hawdon South	Lagoonal	<i>Katelsysia rhytiphora</i>	10066, 10067, 10087-93	9	T: 0.534 $\pm$ 0.067 F: 0.806 $\pm$ 0.011	T: 0.386 $\pm$ 0.058 F: 0.588 $\pm$ 0.026	T: 0.287 $\pm$ 0.091 F: 0.509 $\pm$ 0.039	148 $\pm$ 36  127 $\pm$ 27*  115 $\pm$ 29*  124 $\pm$ 38* 125 $\pm$ 20^
		<i>Anadara trapezia</i> *	10065, 10094	2	T: 0.638 $\pm$ 0.013 F: 0.827 $\pm$ 0.019	T: 0.361 $\pm$ 0.018 F: 0.527 $\pm$ 0.061	T: 0.286 $\pm$ 0.022 F: 0.443 $\pm$ 0.055	
		<i>Tellina deltoidalis</i>	10068	1	T: 0.609 $\pm$ 0.011 F: 0.824 $\pm$ 0.011	T: 0.412 $\pm$ 0.025 F: 0.654 $\pm$ 0.032	T: 0.380 $\pm$ 0.029 F: 0.439 $\pm$ 0.043	
		<i>Chlamys bifrons</i> *	10069	1	T: 0.399 $\pm$ 0.012 F: 0.661 $\pm$ 0.005	T: 0.345 $\pm$ 0.052 F: 0.648 $\pm$ 0.021	T: 0.326 $\pm$ 0.017 F: 0.814 $\pm$ 0.018	
		<i>Brachidontes rostratus</i>	10070, 10071, 10202	3	T: 0.667 $\pm$ 0.036 F: 0.900 $\pm$ 0.008	T: 0.475 $\pm$ 0.038 F: 0.654 $\pm$ 0.025	T: 0.365 $\pm$ 0.061 F: 0.877 $\pm$ 0.148	
		<i>Fulvia tenuicostata</i> *	10083, 10073, 10201	3	T: 0.441 $\pm$ 0.061 F: 0.740 $\pm$ 0.029	T: 0.357 $\pm$ 0.081 F: 0.661 $\pm$ 0.028	T: 0.253 $\pm$ 0.086 F: 0.512 $\pm$ 0.043	
		<i>Ostrea angasi</i>	10076-79, 10034a,b, d, e, h	8	T: 0.519 $\pm$ 0.037	T: 0.371 $\pm$ 0.049	T: 0.355 $\pm$ 0.083	
		<i>Katelsysia rhytiphora</i>	10024	7	T: 0.591 $\pm$ 0.020 F: 0.809 $\pm$ 0.044	T: 0.358 $\pm$ 0.032 F: 0.559 $\pm$ 0.074	T: 0.296 $\pm$ 0.035 F: 0.517 $\pm$ 0.018	
		<i>Katelsysia rhytiphora</i>	9878a,c,e, 10016a-e	10	T: 0.639 $\pm$ 0.032 F: 0.839 $\pm$ 0.099	T: 0.470 $\pm$ 0.032 F: 0.680 $\pm$ 0.020	T: 0.396 $\pm$ 0.037 F: 0.634 $\pm$ 0.024	
		<i>Katelsysia rhytiphora</i>	9878a,c,e, 10016a-e	10	T: 0.639 $\pm$ 0.032 F: 0.839 $\pm$ 0.099	T: 0.470 $\pm$ 0.032 F: 0.680 $\pm$ 0.020	T: 0.396 $\pm$ 0.037 F: 0.634 $\pm$ 0.024	

UWGA = lab code for University of Wollongong, Australia; n replicates refers to the number of individual shells, whole-rock sub-samples, or vials of foraminifera averaged; pv = per vial. \*Uses *Katelsysia* as a calibration curve; ^Uses U-series age of Schwabel (1978; 1984) of 125  $\pm$  20 ka, and is a calibration point in curve construction after Murray-Wallace and Belperio (1991).

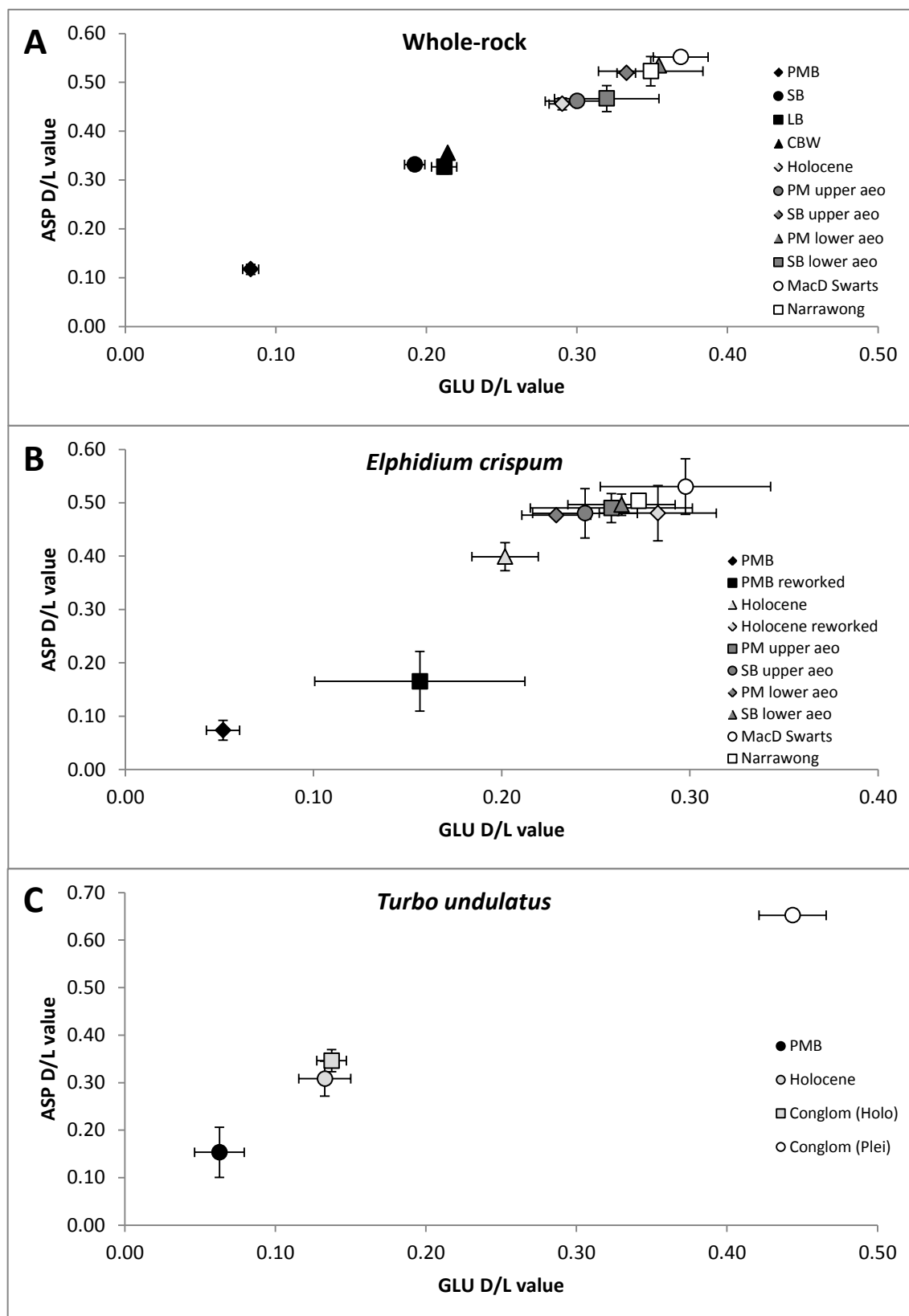


**Figure 5.12:** Scatter plot of ASP and GLU D/L values from modern beach, Holocene and last interglacial sites across the coastal plain for **A: Whole-rock**, **B: *Elphidium crispum***, and **C: *Turbo undulatus***. Scatter plots highlight how modern and MIS 5 samples can be clearly separated, but how AAR cannot distinguish clearly between interstadial sub-stages (dark grey points). [PM = Port MacDonnell, SB = Shelly Beach, LB = Longbeach, CBW = Cape Bridgewater, MacD = MacDonnell, Conglom = Flint conglomerate at Port MacDonnell, WR = whole-rock, aeo = aeolianite]. D/L values are derived from single injections and the averaging of up to ten sub-samples for whole-rock, multiple analyses of single and multiple tests for foraminifers and the average of at least 4 individual molluscs at a sample site, which were sub-sampled at least twice. Table 5.7 identifies the exact number of sub-samples for each individual.

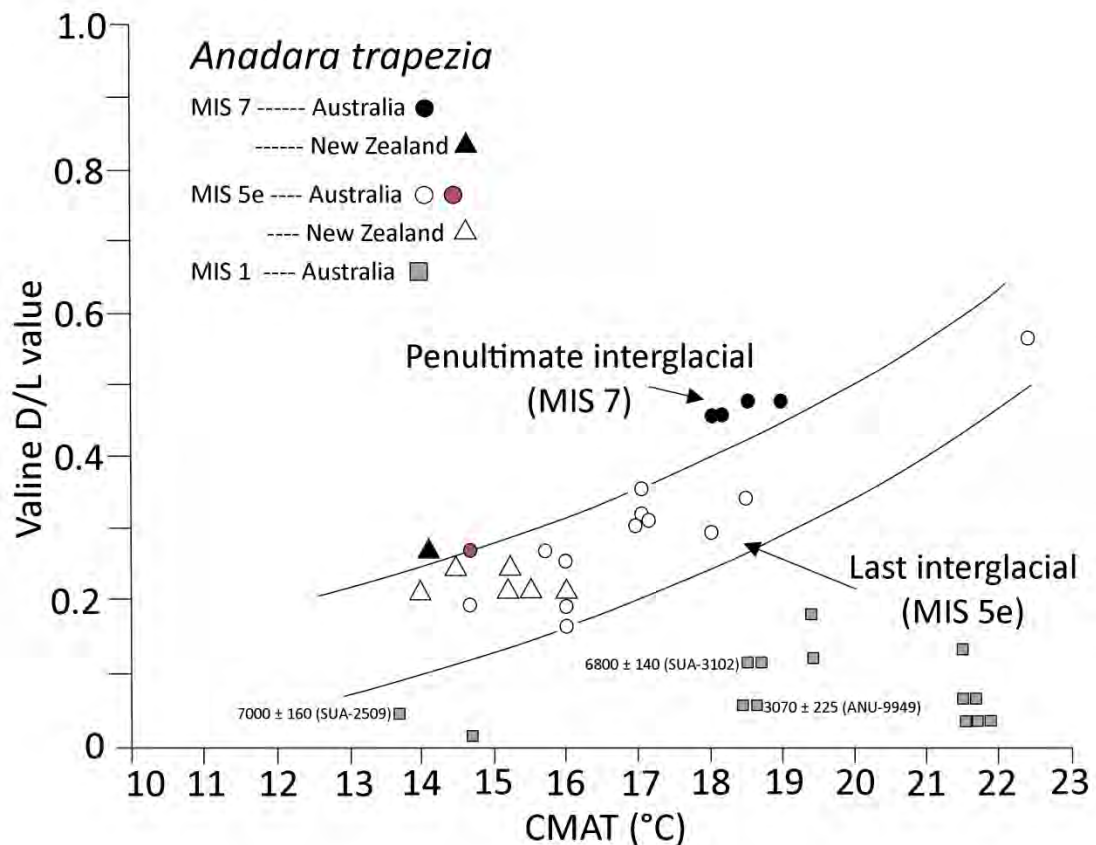


**Figure 5.13:** Extent of valine racemisation within *Anadara trapezia* specimens from Australia and New Zealand plotted against current mean annual temperature (CMAT) at each locality, modified from Murray-Wallace *et al.* (2000). Red circle denotes *Anadara trapezia* analysed in this study from Lake Hawdon South and AAR analyses was done for this using the RP-HPLC method. All other AAR analyses in the image were derived by Gas Chromatography.

From Figure 5.12 it is evident that specimens analysed from Robe Range and MacDonnell Range are distinctly different in age from the raised Holocene beach deposit or the modern beach at Port MacDonnell. It is not possible to separate between foraminifera or whole-rock D/L values derived from the Robe and MacDonnell Ranges, and this indicates the inability of AAR to resolve between interstadial events.

Whole-rock GLU D/L values from MacDonnell Range were found to show statistically significant differences from the upper aeolianite at Shelly Beach, the lower aeolianite at Port MacDonnell, and the Narrawong road cutting. *Elphidium crispum* analysed from within the MacDonnell Range sand quarry were not found to be significantly different from those analysed within the aeolianite cliffs at Shelly Beach and Port MacDonnell, or those analysed at Narrawong. This indicates that bioclastic grains may have been deposited at similar times.

Sediment and foraminifera from the road cutting at Narrawong yielded last interglacial *sensu lato* ages, and support the age of the deposit suggested by Sherwood *et al.* (1994). A single *Spisula* shell from this site was analysed by AAR and also yielded a last interglacial age.

Foraminifera within the sediment sampled at Narrawong yielded GLU D/L values that were not significantly different from those within MacDonnell Range sand quarry, the aeolianite units at Port MacDonnell and Shelly Beach, or the raised Holocene beach which further indicates the Holocene beach contains reworked last interglacial sediment. The calcarenite identified at Narrawong is therefore an extension of the last interglacial Woakwine Range and MacDonnell Range in western Victoria.

Murray-Wallace *et al.* (2001) analysed (using GC) a whole-rock sample from the Woakwine Range (AAB6) within the same unit that Schwebel (1978; 1984) determined to be  $125 \pm 20$  ka using U-series dating. In this thesis the same sediment sample was re-analysed by RP-HPLC and an age of  $119 \pm 21$  ka was obtained. Derived D/L values are not significantly different from those within the lower aeolianite at Port MacDonnell, Robe III at Robe, MacDonnell Range sand quarry or Narrawong, which are all suggested to be last interglacial *sensu lato* in age. This further illustrates that AAR does not have the age-resolving power to discriminate the substages of MIS 5.

At Lake Hawdon South, landward of the Woakwine Range, a wide range of fossil mollusc species were identified within a lagoonal facies. No significant difference was identified between GLU D/L values yielded from analyses of *Fulvia tenuicostata*, *Anadara trapezia*, *Chlamys bifrons* and *Ostrea angasi*. *Katelysia rhytiphora* and *Tellina deltoidalis* were not found to be significantly different from any other species. Samples of *Brachidontes rostratus* yielded higher D/L values than other species and significantly higher values than *Fulvia*, *Anadara*, *Tellina*, *Chlamys* and *Ostrea*, indicating a major disparity between certain genera of the same age, supporting the findings of King and Neville (1977) and Lajoie *et al.* (1980) that racemisation rates are inter-species specific. Comparing the derived valine D/L value for *Anadara trapezia* from Lake Hawdon South with other AAR analyses of this species from around Australia and New Zealand (Figure 5.13) it is apparent that the D/L value fits within their curve band derived for MIS 5e by Murray-Wallace *et al.* (2000) depending on current mean annual temperature. The D/L value from Lake Hawdon South fits on the upper limit of this curve, however, and this may be a result of using RP-HPLC for AAR analysis rather than GC which was used to analyse all other *Anadara trapezia* specimens.

At German Creek, landward of the Woakwine Range in the area of Kongorong, analysed *Katelysia rhytiphora* yielded higher D/L values and an AAR numerical age of  $227 \pm 46$  ka, suggesting that these molluscs were potentially reworked from a MIS 7 deposit. The

elevation and morphostratigraphic position of this deposit precludes this sediment being deposited during MIS 7.

#### **5.8.4 Burleigh Range (~32-34 m APSL)**

Whole-rock samples were collected from three locations on the western face of the Rabbitors Road cutting through the Burleigh Range and from one location at Laslett Road cutting (Figures 3.27 and 3.29). Foraminifera were hand-picked from these sediment samples. Shell fragments of *Katelsia rhytiphora* were sampled throughout Rabbitors Road cutting and analysed for AAR analysis. Additional well-preserved *Chlamys bifrons* were also collected for analysis. Whole, disarticulated, *Anapella cycladea* and *Brachidontes rostratus* were sampled from Laslett Road cutting. Results of AAR analysis for Burleigh Range are shown in Table 5.8.

**Table 5.8:** Results from AAR analysis within Burleigh Range and Reedy Creek Range, Mount Gambier and Robe coastal plains, southern Australia

Sample site	Facies	Material analysed	UWGA	n replicates	Amino acid D/L value $\pm 1 \sigma$			Age estimate (ka) using GLU
					ASP	GLU	VAL	
Rabbitors Road, Burleigh Range	Beach	Whole-rock	9680a-i	9	T: 0.648 $\pm$ 0.005 F: 0.821 $\pm$ 0.006	T: 0.517 $\pm$ 0.009 F: 0.655 $\pm$ 0.014	T: 0.495 $\pm$ 0.014 F: 0.660 $\pm$ 0.008	297 $\pm$ 45
	Beach	Whole-rock	9650a-e	5	T: 0.592 $\pm$ 0.008 F: 0.820 $\pm$ 0.004	T: 0.475 $\pm$ 0.015 F: 0.698 $\pm$ 0.007	T: 0.400 $\pm$ 0.034 F: 0.765 $\pm$ 0.006	
	Beach	Whole-rock	9854a-j	10	T: 0.464 $\pm$ 0.012 F: 0.679 $\pm$ 0.010	T: 0.347 $\pm$ 0.029 F: 0.561 $\pm$ 0.024	T: 0.281 $\pm$ 0.046 F: 0.692 $\pm$ 0.080	
	Beach	<i>Elphidium crispum</i>	9871a,c,d,e, 10219ai, aiv-avii pv)	8 (4x1, 2x5, 2x10 pv)	T: 0.675 $\pm$ 0.037	T: 0.454 $\pm$ 0.044	T: 0.427 $\pm$ 0.069	
	Beach	<i>Ammonia beccarii</i>	9872a,b, 100219ci, cii	4 (4x1 pv)	T: 0.715 $\pm$ 0.010	T: 0.526 $\pm$ 0.021	T: 0.533 $\pm$ 0.027	229 $\pm$ 31
	Beach	<i>Discorbis dimidiatus</i>	10219bi, biv, bv	3 (1x1, 2x10 pv)	T: 0.662 $\pm$ 0.005	T: 0.440 $\pm$ 0.007	T: 0.571 $\pm$ 0.002	
	Beach	<i>Katelsysia rhytiphora</i>	9809a-c, 10095- 97, 10200	7	T: 0.732 $\pm$ 0.029 F: 0.844 $\pm$ 0.069	T: 0.630 $\pm$ 0.040 F: 0.747 $\pm$ 0.068	T: 0.595 $\pm$ 0.027 F: 0.698 $\pm$ 0.030	
		<i>Chlamys bifrons</i> *	10006, 9849	2	T: 0.484 $\pm$ 0.018 F: 0.701 $\pm$ 0.019	T: 0.402 $\pm$ 0.012 F: 0.616 $\pm$ 0.045	T: 0.646 $\pm$ 0.025 F: 0.855 $\pm$ 0.017	161 $\pm$ 33*
Laslett Road, Burleigh Range	Lagoonal	<i>Elphidium crispum</i>	10064ai-aiii, 10064avi-avxii	10 (8x10, 2x1 pv)	T: 0.569 $\pm$ 0.055	T: 0.382 $\pm$ 0.031	T: 0.273 $\pm$ 0.048	224 $\pm$ 35
		<i>Anapella cycladea</i>	9879, 10017, 10018	3	T: 0.648 $\pm$ 0.026 F: 0.807 $\pm$ 0.014	T: 0.521 $\pm$ 0.017 F: 0.806 $\pm$ 0.054	T: 0.494 $\pm$ 0.033 F: 0.809 $\pm$ 0.028	283 $\pm$ 59*
		<i>Brachidontes rostratus</i>	10020	1	T: 0.859 $\pm$ 0.004 F: 0.920	T: 0.827 $\pm$ 0.010 F: 0.874	T: 0.789 $\pm$ 0.032 F: 0.866	
Reedy Creek (AAB10)	Aeolian?	Whole-rock	9845k-t	10	T: 0.532 $\pm$ 0.006 F: 0.712 $\pm$ 0.004	T: 0.414 $\pm$ 0.012 F: 0.582 $\pm$ 0.040	T: 0.373 $\pm$ 0.049 F: 0.753 $\pm$ 0.088	189 $\pm$ 29

UWGA = lab code for University of Wollongong, Australia; n replicates refers to the number of individual shells, whole-rock sub-samples, or vials of foraminifera averaged; pv = number of tests analysed per vial;

\*= uses calibration curve of *Katelsysia*; T = total amino acid fraction, F = free amino acid fraction.

Whole-rock samples from three locations along the Rabbitors Road cutting, Burleigh Range yield a range of GLU D/L values. The morphostratigraphical location of Burleigh Range, the next landward barrier from the last interglacial (MIS 5e) MacDonnell Range, suggests that it could date to the MIS 7 highstand. D/L values from whole-rock sample UWGA 9854 are significantly lower than expected based on the morphostratigraphic position of the barrier and a numerical age was not calculated in view of poor data integrity. The low values may reflect leaching of lower-molecular-weight amino acids from the sediment. In contrast, D/L values derived from two other whole-rock samples are significantly higher than expected and suggest that sediment has been reworked from older deposits. Tests of *Elphidium crispum* and *Ammonia beccarii* also yielded significantly higher D/L values than what would be expected from a MIS 7 deposit, as did fragments of *Katelsia rhytiphora*, which further suggests reworking of older sediment and shells. The fragmented nature of *Katelsia* indicates high-energy transport, which may have occurred through reworking. Tests of *Discorbis dimidiatus* and the better preserved *Chlamys bifrons* yielded numerical ages more comparable with MIS 7 and indicate the possibility that some deposition at this locality occurred during the penultimate interglacial.

The Laslett Road cutting exposes lagoonal facies within the Burleigh Range. D/L values derived from analysis of *Elphidium crispum* and *Anapella cycladea* yield numerical ages that indicate deposition of these species during MIS 7. *Brachidontes rostratus* yielded significantly higher D/L values and have potentially been reworked. Alternatively, this species may simply racemise at a faster rate than others as seen at Lake Hawdon South and may therefore require a greater number of robust calibration points to obtain a numerical age accurately.

Murray-Wallace *et al.* (2001) analysed whole-rock sediment from Reedy Creek Range, the northern extension of Burleigh Range. Using GC Murray-Wallace *et al.* (2001) yielded an AAR numerical age of  $258 \pm 25$  ka. AAR analysis of the same sample using RP-HPLC in this study yielded an age of  $189 \pm 29$  ka, placing deposition in the later stages of MIS 7.

#### **5.8.5 Caveton Range (~32-45 m APSL)**

Samples from Caveton Range were collected at two locations; the Rabbitors Road lagoonal facies and Bucks Hill aeolianite. Whole-rock samples were collected from units 2 and 8 at Rabbitors Road and Bucks Hill. *In situ* fossil shells were sampled from unit 2 at Rabbitors Road (Figure 3.31). Foraminifera were hand-picked from sediment samples within the Rabbitors Road lagoon facies, but were not identifiable within the aeolian facies at Bucks Hill. Results of AAR analysis from Caveton Range are presented in Table 5.9.



**Table 5.9:** Results of AAR analysis from the Caveton Range, Mount Gambier coastal plain, southern Australia

Sample site	Facies	Material analysed	UWGA	n replicates	Amino acid D/L value $\pm 1 \sigma$			Age estimate (ka) using GLU
					ASP	GLU	VAL	
Rabbitors Road, Caveton Range, Unit 2	Lagoonal	Whole-rock	9650a-h	8	T: 0.585 $\pm$ 0.028 F: 0.737 $\pm$ 0.012	T: 0.421 $\pm$ 0.033 F: 0.515 $\pm$ 0.010	T: 0.408 $\pm$ 0.036 F: 0.565 $\pm$ 0.017	200 $\pm$ 34
		<i>Tellina deltoidalis</i>	9827a,b, 9828a-d, 9883, 9888, 9889	10	T: 0.697 $\pm$ 0.075 F: 0.816 $\pm$ 0.127	T: 0.547 $\pm$ 0.059 F: 0.623 $\pm$ 0.153	T: 0.517 $\pm$ 0.058 F: 0.655 $\pm$ 0.202	314 $\pm$ 73*
		<i>Anapella cycladea</i>	9807a-d, 9808, 9826a-e	9	T: 0.657 $\pm$ 0.037 F: 0.824 $\pm$ 0.010	T: 0.440 $\pm$ 0.029 F: 0.652 $\pm$ 0.037	T: 0.407 $\pm$ 0.023 F: 0.676 $\pm$ 0.028	196 $\pm$ 42*
		<i>Katelsysia rhytiphora</i>	9829a, b, c, 9884, 9885, 9887, 9836, 9837, 9838, 9840	10	T: 0.601 $\pm$ 0.086 F: 0.849 $\pm$ 0.026	T: 0.504 $\pm$ 0.064 F: 0.753 $\pm$ 0.018	T: 0.492 $\pm$ 0.070 F: 0.747 $\pm$ 0.032	263 $\pm$ 61
		<i>Niothus pyrrhus</i>	9825a, b, c, d, e, f, g	2	T: 0.648 $\pm$ 0.011 F: 0.741 $\pm$ 0.096	T: 0.453 $\pm$ 0.006 F: 0.545 $\pm$ 0.077	T: 0.436 $\pm$ 0.033 F: 0.768 $\pm$ 0.136	
		<i>Fulvia tenuicostata</i> *	10204	1	T: 0.531 $\pm$ 0.071 F: 0.765 $\pm$ 0.018	T: 0.463 $\pm$ 0.091 F: 0.722 $\pm$ 0.025	T: 0.301 $\pm$ 0.121 F: 0.697 $\pm$ 0.016	219 $\pm$ 62*
		Whole-rock	9640a-j	10	T: 0.647 $\pm$ 0.008 F: 0.816 $\pm$ 0.012	T: 0.524 $\pm$ 0.011 F: 0.657 $\pm$ 0.023	T: 0.507 $\pm$ 0.018 F: 0.755 $\pm$ 0.021	402 $\pm$ 60
Rabbitors Road, Caveton Range, Unit 8	Lagoonal	<i>Elphidium crispum</i>	9869ai, aii, bi, bii, 10031av, ai, 10220ai, aii, avii, aviii, ax	11 (5x10, 2x5, 3x1pv)	T: 0.659 $\pm$ 0.069	T: 0.447 $\pm$ 0.094	T: 0.433 $\pm$ 0.103	322 $\pm$ 80
		<i>Ammonia beccarii</i>	9863ai, aii, bi, bii, 9867ai-aiii, bi, biii- bv, 10220bi	12 (6x10, 2x5, 4x1 pv)	T: 0.664 $\pm$ 0.059	T: 0.453 $\pm$ 0.056	T: 0.447 $\pm$ 0.074	366 $\pm$ 66
		<i>Discorbis dimidiatus</i>	10020ci	1 (1pv)	T: 0.665	T: 0.475	T: 0.538	271 $\pm$ 36
Bucks Hill, Caveton Range	Aeolian	Whole-rock^	9886k-t	10	T: 0.578 $\pm$ 0.009 F: 0.734 $\pm$ 0.033	T: 0.461 $\pm$ 0.015 F: 0.810 $\pm$ 0.041	T: 0.470 $\pm$ 0.025 F: 0.679 $\pm$ 0.129	270 $\pm$ 41

UWGA = University of Wollongong, Australia lab code; n replicates = number of whole-rock sub-samples and individual molluscs analysed; pv = number of foraminiferal tests per vial.

\*Calibrated using *Katelsysia*; ^treated with a 24 hour bleach; T = total amino acid fraction, F = free amino acid fraction.

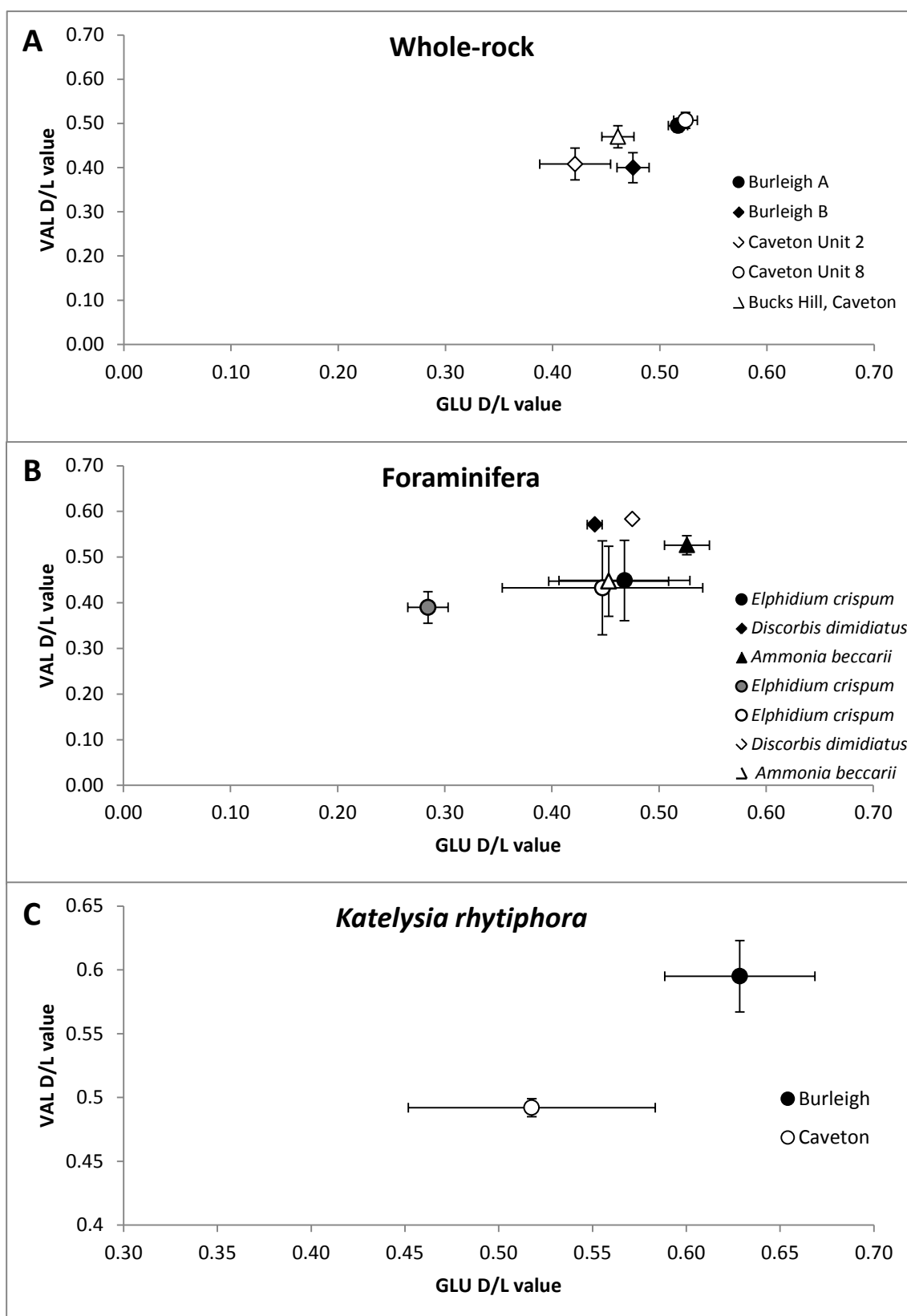


**Figure 5.14:** Scatter plots comparing glutamic acid (GLU) and valine (VAL) D/L values between samples of **A:** whole-rock, **B:** foraminifera, and **C:** *Katelaysia rhytiphora* from Burleigh Range (filled data points; note black points represent Rabbitors Road exposure while the grey point is Laslett Road lagoonal facies) and Caveton Range (empty data points). There is no significant difference between derived D/L values and it suggests that sediment from Burleigh Range (proposed to be MIS 7 based on geographical position) has been reworked from older sources, potentially Caveton Range. D/L values for all scatter plots were determined using a single injection. Whole-rock values are averaged from up to ten sub-samples. Foraminifera are averaged from multiple analyses of single and multiple (up to 10) tests, while *Katelaysia* D/L values are derived from the average of up to ten analyses of separate individuals, which were each sub-sampled at least twice. Exact numbers of sub-samples are shown in Table 5.9.

The geographical location of the Caveton Range as the third prominent barrier shoreline inland from the modern coastline suggests it could date to MIS 9. Results from AAR analysis of *Tellina deltoidalis* and foraminifera collected from a lagoonal facies of the Caveton Range support this hypothesis, as does whole-rock AAR analysis of aeolianite sampled at Bucks Hill. GLU D/L values of various mollusc species are found to be significantly different at this site, indicating the variability in the extent of racemisation in differing genera. For example, the gastropod *Niothus pyrrhus* yielded GLU D/L values significantly different from all other genera at this site. No significant difference was identified between *Katelsysia rhytiphora* and *Tellina deltoidalis*. GLU D/L values of fossil molluscs are statistically different from those collected from the lagoonal facies (at Laslett Road) at Burleigh Range, seaward of Caveton Range. Whole-rock GLU D/L values from Caveton Range are significantly higher than those from the last interglacial MacDonnell Range, yet derived whole-rock numerical ages overlap with those from the seaward Burleigh Range and landward Gambier and Compton Ranges, reflecting the limited resolution of this technique within older sediments.

The sediments and molluscs within Burleigh Range, seaward of Caveton Range, should (based on their geographical position) yield a younger age and lower D/L values than those from the Caveton Range. However, this is not evident from the results. As shown in Figure 5.14, Caveton and Burleigh Range whole-rock D/L values are very similar and cannot be confidently separated. *Katelsysia* from Burleigh Range yield significantly higher D/L values than those from Caveton Range, while the foraminifera from Burleigh Range at Rabbitors Road cutting and the Caveton Range lagoonal facies cannot be clearly distinguished based on D/L values either. These results suggest there is no significant difference in sediment age between the Burleigh Range at Rabbitors Road and the Caveton lagoonal facies. This supports the hypothesis that sediment within Burleigh Range at this location could have been reworked from an older deposit, potentially Caveton Range. The higher D/L values derived from *Katelsysia* within Burleigh Range suggest these may have been reworked from a deposit even older than Caveton Range. As *Elphidium* from Burleigh Range lagoonal facies (Laslett Road) are significantly lower than those from Rabbitors Road and Caveton Range (Figure 5.14), it is suggested that the back-barrier lagoon sediments of Burleigh Range were deposited during the penultimate interglacial.

#### 5.8.6 Gambier Range (~55 m APSL) and Compton Range (~45-60 m APSL)

A suitable sample site within the Gambier Range was only located at one point along Gooch Road (Figure 3.11, 3.35) as it was difficult to obtain a representative sample for this barrier. Two whole-rock samples were collected at Gooch Road from which foraminifera were hand-picked. No fossil shell was identified at the site. Compton Range was sampled at Baxter's Quarry, Heritage Industries and a road cutting through Grey Street, Mount Gambier. No shell was found at Baxter's Quarry but a whole-rock sample was taken from the subaqueously deposited calcarenite (Figure 3.39) and foraminifera were hand-picked from this, both of which were analysed for AAR. At Heritage Industries, three distinct shell horizons were identified. *Ostrea angasi*, the principal species in the lower shell beds, were sampled and analysed for AAR. The upper shell bed consisted primarily of fossil shell fragments but a largely well-preserved *Placamen* was sampled and analysed by AAR. A whole-rock sample was collected from near the lower shell layer. Foraminifera were also hand-picked from this sediment. Where initial D/L values on shell and whole-rock sediment yielded SER D/L values lower than 0.1, samples were reanalysed with a 24 bleach soak replacing the 2 hour hydrogen peroxide soak in an attempt to analyse the intra-crystalline fraction (after Penkman *et al.*, 2008). At Grey Street, fragmented samples of shell were analysed for AAR. AAR values and derived numerical ages are shown in Table 5.10.

**Table 5.10:** Results of AAR analysis from Gambier Range and Compton Range, Mount Gambier coastal plain, southern Australia

Sample site	Facies	Material analysed	UWGA	n replicates	Amino acid D/L value $\pm 1 \sigma$			Age estimate (ka) using GLU
					ASP	GLU	VAL	
Gooch Road, Gambier Range	Subaqueous	Whole-rock	10041b-j, 10042a-e	14	T: $0.529 \pm 0.026$ F: $0.664 \pm 0.017$	T: $0.392 \pm 0.060$ F: $0.659 \pm 0.049$	T: $0.307 \pm 0.085$ F: $0.684 \pm 0.067$	581 $\pm$ 90
		<i>Elphidium crispum</i>	10063di – div, ei-eviii	12 (9x10, 3x1 pv)	T: $0.729 \pm 0.033$	T: $0.582 \pm 0.047$	T: $0.473 \pm 0.072$	
East Avenue Range	Aeolian	Whole-rock	10040a-i	9	T: $0.516 \pm 0.036$ F: $0.742 \pm 0.009$	T: $0.363 \pm 0.040$ F: $0.609 \pm 0.044$	T: $0.249 \pm 0.051$ F: $0.749 \pm 0.117$	
Grey Street, Compton Range	Aeolian	<i>Anapella?</i>	10013a-b	1	T: $0.730 \pm 0.024$ F: $0.870 \pm 0.008$	T: $0.687 \pm 0.031$ F: $0.797 \pm 0.078$	T: $0.893 \pm 0.077$ F: $0.953 \pm 0.004$	509 $\pm$ 107
Baxter's Quarry, Compton Range	Subaqueous	Whole-rock^	9820a-j	10	T: $0.569 \pm 0.007$ F: $0.694 \pm 0.024$	T: $0.471 \pm 0.041$ F: $0.520 \pm 0.060$	T: $0.484 \pm 0.016$ F: $0.596 \pm 0.051$	289 $\pm$ 50
		<i>Elphidium crispum</i>	9862a,b, di 10029bi, biv, bv,	6 (5x10, 1x1 pv)	T: $0.669 \pm 0.056$	T: $0.488 \pm 0.063$	T: $0.458 \pm 0.053$	393 $\pm$ 81
		<i>Ammonia beccarii</i>	9863a, b, 9862ei, 10029ai, aiv	5 (3x10, 1x5, 1x1 pv)	T: $0.712 \pm 0.038$	T: $0.560 \pm 0.058$	T: $0.557 \pm 0.068$	576 $\pm$ 97
Heritage Industries, Compton Range	Beach	Whole-rock	9821a-i	9	T: $0.554 \pm 0.006$ F: $0.708 \pm 0.005$	T: $0.443 \pm 0.009$ F: $0.548 \pm 0.009$	T: $0.347 \pm 0.053$ F: $0.612 \pm 0.095$	
		<i>Elphidium crispum</i>	8960a-c	3 (2x10, 1x1pv)	T: $0.637 \pm 0.089$	T: $0.471 \pm 0.057$	T: $0.499 \pm 0.126$	363 $\pm$ 65
		<i>Ammonia beccarii</i>	9859a-c, i	4 (4x10 pv)	T: $0.750 \pm 0.056$	T: $0.611 \pm 0.061$	T: $0.645 \pm 0.102$	693 $\pm$ 115
	Upper shell layer	<i>Placamen flindersi</i>	10010	1 (5 sub-samples)	T: $0.717 \pm 0.013$ F: $0.832 \pm 0.015$	T: $0.623 \pm 0.011$ F: $0.763 \pm 0.020$	T: $0.653 \pm 0.019$ F: $0.912 \pm 0.067$	411 $\pm$ 85*
	Lower shell layer	<i>Ostrea angasi</i> ^	9830, 9831, 9834, 9834	4	T: $0.675 \pm 0.038$ F: $0.834 \pm 0.015$	T: $0.616 \pm 0.075$ F: $0.757 \pm 0.01$	T: $0.655 \pm 0.026$ F: $0.857 \pm 0.032$	377 $\pm$ 86
		<i>Ostrea angasi</i>	9802, 9877	2	T: $0.664 \pm 0.048$ F: $0.826 \pm 0.011$	T: $0.51 \pm 0.057$ F: $0.771 \pm 0.064$	T: $0.526 \pm 0.103$ F: $0.894 \pm 0.027$	

UWGA = University of Wollongong, Australia lab code; n replicates = number of whole-rock sub-samples; individual molluscs analysed; pv = number of foraminiferal tests per vial; ^samples treated with 24 hour bleach soak instead of 2 hour hydrogen peroxide soak; \*Uses calibration curve of *Kataysia*; T = total amino acid fraction, F = free amino acid fraction.

Whole-rock samples from the exposure of the Gambier Range at Gooch Road yielded significantly lower D/L values and numerical age estimates than expected. The position of the dune range as the fourth significant barrier shoreline landward from the coastline suggests that Gambier Range could date to the MIS 11 highstand. The whole-rock sample yielded unexpectedly low GLU D/L values, indicating either poor sample integrity and/or leaching of amino acids from the sediment; therefore it was deemed inappropriate to derive a numerical age for this sample. Foraminifera from this sample site yielded a numerical age ( $581 \pm 90$  ka) which is older than the hypothesised MIS 11, and is more comparable with MIS 13 or 15. The variability in D/L values from Gambier Range may reflect differential diagenetic impacts to bioclastic grains within the deposit, whereby foraminifera are potentially preferentially preserved compared with other grains. It may be that within this highly cemented sample, cements were not completely removed from the whole-rock samples prior to processing and this material reduced the overall D/L value of the sample. Another possible explanation is the leaching of lower molecular weight, highly racemised amino acids from the sediment.

Murray-Wallace *et al.* (2001) analysed a whole-rock sample from the northern correlative of Gambier Range; East Avenue Range on the Robe coastal plain. Using GC, Murray-Wallace *et al.* (2001) found that the sediment within this barrier shoreline also yielded D/L values that were significantly lower than expected and suggested that this was possibly a result of *in situ* leaching. This may also be the reason for the lower than expected whole-rock D/L values from Gambier Range.

The geographical location of Compton Range, north of Mount Gambier and the fifth barrier inland from the present coastline, should correlate the barrier shoreline to MIS 13 if the hypothesis that each barrier formed in successive interglacial highstands is correct. Whole-rock samples from both Baxter's Quarry and Heritage Industries yielded D/L values significantly lower than expected and may indicate leaching of the sediment or diagenetic influences on the skeletal carbonate grains. Foraminifera analysed from Heritage Industries and Baxter's Quarry yield significantly higher D/L values. *Ammonia beccarii* from the lower subaqueous facies at Baxter's Quarry yield an age of  $576 \pm 97$ , placing deposition within MIS 13 to 15. AAR numerical ages derived from *Elphidium crispum* from the subaqueous facies at Baxter's Quarry correspond well with the OSL age derived from the overlying aeolian facies at this site. D/L values and numerical ages derived from *Ammonia beccarii* were higher than analysed *Elphidium crispum* at both sample sites and possibly reflect inter-generic differences or preferential preservation of *Ammonia beccarii*. Molluscs were identified only in the

successions at Heritage Industries. *Ostrea angasi* is the main species found and certain samples were treated with a 24 hour bleach while others were subjected to a 2 hour hydrogen peroxide soak. Samples analysed with bleach yielded higher D/L values and possibly reflect the potential contamination of the non-intra-crystalline portion of shell matrix. However, these values were still lower than expected and may reflect leaching of amino acids from the shell matrix. Analysed *Placamen* yielded higher D/L values than *Ostrea* and a numerical age within MIS 11, or possibly (when uncertainties are included) the latter part of MIS 13. The higher values recorded from this specimen may indicate a better retention of amino acids in this species.

#### **5.8.7 Mingbool Range (~45 m APSL) and Dismal Range (~40-70 m APSL)**

Mingbool Range was sampled at Don's Quarry, western Victoria, where a whole-rock sample was collected, as were fragments of *Ostrea angasi* found along the surface of the small quarry (Figure 3.44). Foraminifera were hand-picked and analysed for AAR from the sediment samples. The Dismal Range was sampled near Dartmoor Cemetery, and at Fort O'Hare Quarry, western Victoria, and in a small quarry near Mingbool village, South Australia. Fossil shell was found sporadically, approximately 6 m beneath the surface, throughout the exposure of Bridgewater Formation at Dartmoor Cemetery and suggests the shell has been transported *post mortem* (Figures 3.46, 3.47). A whole-rock sample was also collected from Dartmoor Cemetery and from which foraminifera were also identified. At Fort O'Hare Quarry shell samples were collected along the distinct shell bed. *Ostrea angasi* were collected *in situ* within the shell bed at the eastern extent of the exposure (Figures 3.48, 3.49b). Shells were also collected for analysis approximately half way along the exposure where material had fallen during excavation and included specimens of *Chlamys* and *Pecten*. Foraminifera were hand-picked from whole-rock samples collected at two locations beneath the shell layer across the exposure. At Mingbool village fragments of *Ostrea angasi* found at the quarry surface were collected for AAR analysis. Whole-rock samples were collected from units displaying distinctive low-angle cross-bedding. Foraminifera were hand-picked from these whole-rock samples. Some samples were re-treated with a 24 hour hydrogen peroxide soak, replacing the 2 hour peroxide soak, where initial serine (SER) D/L values were less than 0.1. Shell samples were preferentially analysed for AAR at the umbo region. Where only fragments were collected, shells were sometimes analysed on their outer growth edge (OGE). Results of AAR analysis and the age yielded from calibration are displayed in Table 5.11.

**Table 5.11:** Results of AAR analysis from samples within Mingbool Range and Dismal Range, Mount Gambier coastal plain, southern Australia

Sample site	Facies	Material analysed	UWGA	<i>n</i> replicates	Amino acid D/L value $\pm 1 \sigma$			Age estimate (ka) using GLU
					ASP	GLU	VAL	
Don's Quarry, Mingbool Range	Subaqueous	Whole-rock^	9888k-m, o-t	9	T: 0.560 $\pm$ 0.010 F: 0.699 $\pm$ 0.013	T: 0.439 $\pm$ 0.035 F: 0.586 $\pm$ 0.032	T: 0.676 $\pm$ 0.208 F: 0.811 $\pm$ 0.145	778 $\pm$ 118
		<i>Elphidium crispum</i>	10027av, 10027axi, axii, 10027di, diii	5 (5x10 pv)	T: 0.761 $\pm$ 0.036	T: 0.665 $\pm$ 0.049	T: 0.626 $\pm$ 0.087	
		<i>Ostrea angasi</i>	9893, 10009, 10019, 10021-22	5	T: 0.637 $\pm$ 0.042 F: 0.749 $\pm$ 0.046	T: 0.641 $\pm$ 0.086 F: 0.799 $\pm$ 0.040	T: 0.697 $\pm$ 0.125 F: 0.982 $\pm$ 0.184	411 $\pm$ 96
Dartmoor Cemetery, Dismal Range	Subaqueous	Whole-rock^	9889k, l, m, o, p, q, s, t	8	T: 0.539 $\pm$ 0.011 F: 0.753 $\pm$ 0.019	T: 0.442 $\pm$ 0.028 F: 0.642 $\pm$ 0.033	T: 0.410 $\pm$ 0.078 F: 0.910 $\pm$ 0.131	577 $\pm$ 79
		<i>Elphidium crispum</i>	10025bii, bv, 10213ai, avii	4 (2x10, 2x1 pv)	T: 0.668 $\pm$ 0.012	T: 0.580 $\pm$ 0.020	T: 0.575 $\pm$ 0.028	
		<i>Pecten benedictus</i>	10051-53	3	T: 0.611 $\pm$ 0.018 F: 0.734 $\pm$ 0.029	T: 0.485 $\pm$ 0.024 F: 0.650 $\pm$ 0.052	T: 0.472 $\pm$ 0.042 F: 0.735 $\pm$ 0.107	
		<i>Ostrea angasi</i>	10054, 10056, 9873, 10007	4	T: 0.623 $\pm$ 0.069 F: 0.811 $\pm$ 0.047	T: 0.565 $\pm$ 0.084 F: 0.792 $\pm$ 0.092	T: 0.522 $\pm$ 0.124 F: 0.898 $\pm$ 0.166	
Fort O'Hare Quarry, Dismal Range	Subaqueous	Whole-rock	9890a-j	10	T: 0.586 $\pm$ 0.033 F: 0.768 $\pm$ 0.032	T: 0.443 $\pm$ 0.037 F: 0.586 $\pm$ 0.026	T: 0.456 $\pm$ 0.044 F: 0.736 $\pm$ 0.055	743 $\pm$ 100
		<i>Elphidium crispum</i>	10212avii, aix	2 (2x10 pv)	T: 0.747 $\pm$ 0.004	T: 0.651 $\pm$ 0.018	T: 0.718 $\pm$ 0.016	
		<i>Ostrea angasi</i>	9874, 9875, 10003-5, -in shell layer	9	T: 0.702 $\pm$ 0.050 F: 0.799 $\pm$ 0.064	T: 0.582 $\pm$ 0.063 F: 0.710 $\pm$ 0.090	T: 0.641 $\pm$ 0.114 F: 0.858 $\pm$ 0.172	
		-from fallen material	10083-6 9896-7	2	T: 0.687 $\pm$ 0.022 F: 0.817 $\pm$ 0.031	T: 0.556 $\pm$ 0.046 F: 0.714 $\pm$ 0.068	T: 0.558 $\pm$ 0.082 F: 0.912 $\pm$ 0.114	
		<i>Pecten benedictus</i> - (OGE)* fallen material	9876a-d	4	T: 0.590 $\pm$ 0.027 F: 0.730 $\pm$ 0.007	T: 0.467 $\pm$ 0.031 F: 0.654 $\pm$ 0.042	T: 0.621 $\pm$ 0.106 F: 1.010 $\pm$ 0.074	
		<i>Chlamys bifrons</i> (OGE)* fallen material	9898	1 (3 sub-samples)	T: 0.514 $\pm$ 0.022 F: 0.711 $\pm$ 0.001	T: 0.424 $\pm$ 0.037 F: 0.837 $\pm$ 0.120	T: 0.395 $\pm$ 0.093 F: 0.983 $\pm$ 0.005	
		Whole-rock^	9892k-s	9	T: 0.604 $\pm$ 0.005 F: 0.728 $\pm$ 0.008	T: 0.528 $\pm$ 0.024 F: 0.611 $\pm$ 0.014	T: 0.555 $\pm$ 0.108 F: 0.827 $\pm$ 0.092	
		<i>Elphidium crispum</i>	10015aiii, av, 10030civ, cv, dii, diiii, div, dvi	8 (8x10 pv)	T: 0.803 $\pm$ 0.029	T: 0.712 $\pm$ 0.041	T: 0.675 $\pm$ 0.052	
		<i>Ammonia beccarii</i>	10030ai, aii, aiv, cii, 10015eii	6 (2x10, 1x5, 3x1pv)	T: 0.790 $\pm$ 0.024	T: 0.705 $\pm$ 0.031	T: 0.717 $\pm$ 0.040	
Mingbool village, Dismal Range	Subaqueous	<i>Ostrea angasi</i>	9894-5, 10023	3	T: 0.659 $\pm$ 0.040 F: 0.822 $\pm$ 0.026	T: 0.638 $\pm$ 0.049 F: 0.804 $\pm$ 0.083	T: 0.737 $\pm$ 0.052 F: 0.910 $\pm$ 0.098	407 $\pm$ 84

UWGA = University of Wollongong, Australia lab code; *n* replicates = number of whole-rock sub-samples, individual molluscs analysed; pv = number of tests per vial; ^ Samples treated with a 24 hour bleach; \*Calibrated using *Katetylsia*; T = total amino acid fraction, F = free amino acid fraction.



The geographical position of Mingbool Range and Dismal Range as the sixth and seventh barriers respectively, landward from the present coastline suggests that they could correlate with MIS 15 and 17 respectively if each barrier is formed in a successive interglacial highstand. Whole-rock AAR analysis of sediment from sample sites across the barrier shorelines, however, reveals significantly lower D/L values than expected for these hypothesised ages. Sediment from the exposure of Dismal Range at Mingbool village yields the oldest numerical ages derived from whole-rock analysis across the coastal plain but is still significantly lower than expected. D/L values were expected to be consistently greater in sediment analysed by the whole-rock technique than in fossil shells due to the lengthy residence times of bioclastic grains on the continental shelf and beach face. This trend was not identified within the derived data. This may result from the diagenetic processes affecting sediments, and indicates limitations of the whole-rock technique in this instance.

*Ostrea angasi* was identified at each of the study sites across Mingbool Range and Dismal Range. Numerical ages derived for *Ostrea* were significantly higher than those derived using whole-rock technique on sediment samples, but still much lower than expected for Ranges of Bridgewater Formation at such a distance inland. It may be possible that the platy structure of *Ostrea* increases the likelihood of leaching of amino acids from the shell, and thus lower D/L values than expected are recorded. Wide variation within D/L values of *Ostrea* have been reported from previous studies (e.g. Kvenvolden *et al.*, 1979; Kimber and Griffin, 1987) and it is therefore suggested that *Ostrea* is not a reliable matrix for the retention of indigenous amino acids.

The highest GLU D/L values and corresponding numerical ages were derived from foraminifera within sediment samples from the Mingbool and Dismal Ranges. The derived numerical ages for *Elphidium crispum* and *Ammonia beccarii* yielded ages that better correspond with the proposed timing of deposition of these barriers during MIS 15 and 17 and reflect the potential precision of single-grain AAR analysis. The hand-picking of single grains allows selection of better preserved samples, and tests yielding SER values lower than 0.1 can be rejected. For example, *Discorbis dimidiatus* was identified at each of the above samples sites, but when tests were analysed SER D/L values were too low and therefore results were omitted. However, while analysed foraminifera from Fort O'Hare Quarry yielded a numerical age of  $743 \pm 100$  ka, which correlates with the inferred MIS 17 age of this deposit based on its geographical position, only 2 vials, each with 10 foraminifers within them, yielded results with acceptable SER D/L values. From these results it is therefore not possible to distinguish the

Bridgewater Formation from the lower Werrikoo Limestone (section 3.8.10) confidently at this locality and further analysis is required.

#### **5.8.8 Discussion of AAR results**

Overall, there is a strong correlation between increasing D/L values of shells, foraminifera and whole-rock sediment samples analysed in this study with increasing distance of sample sites from the modern shoreline. These results support the notion that barriers increase in age landward. Stratigraphical analysis confirms that barriers are coastal deposits, and the slow epeirogenic uplift of the coastline suggests they are likely to have been deposited during successive interglacials. However, barriers may have not formed during a single sea-level highstand and may be composite deposits formed during multiple interglacials and interstadials.

Bioclastic sediment, foraminifera and fossil shell from the MacDonnell Range and correlative Woakwine Range are clearly identifiable as last interglacial in age and can be easily distinguished from modern and mid-Holocene deposits. Deposits from the Burleigh Range likely correlate with MIS 7, but may include reworked material. For successions older than MIS 7, it is more difficult to correlate AAR values with the marine isotope stage inferred from the geographical position of the barrier in relation to the modern coastline. This may be related to differing diagenetic processes preferentially affecting different sample sites and different fossils, varying kinetic pathways of amino acids and poor data (particularly regarding whole-rock) resulting in differing D/L values.

At sites where multiple mollusc genera are identified, such as Lake Hawdon South (MIS 5e) and Caveton Range lagoonal facies (MIS 9), it is evident that there is a significant range in D/L values between different genera presumed to be of the same age (Figure 5.15). As both sample sites are lagoonal and many shells remain articulated, it is proposed that both sites represent thanatocoenoses fossil assemblages. The observed difference in D/L values within these assemblages is likely a result of differing racemisation rates between genera rather than differences in age, as has been previously observed by King and Neville (1977).

A range of molluscan species were analysed using AAR across the Mount Gambier coastal plain and in general glutamic acid D/L values were found to increase with distance inland, as shown in Figure 5.16 for a range of species. Samples are assigned a marine isotope stage based on the geographical location of the barrier from the present shoreline. Unfortunately, a single species common to all sample sites was not found and a genus effect

on D/L values has been identified. Therefore, each common (more than 10 fossils) species is illustrated in a separate graph. *Turbo undulatus* was only identified at sites within the Port MacDonnell region of the Mount Gambier coastal plain and thus was not found in successions hypothesised to be older than the last interglacial (MIS 5e).

A distinct difference between glutamic acid D/L values is found between Holocene and last interglacial age *Turbo* shells as shown in Figure 5.16a. The Port MacDonnell conglomerate sample is much more comparable to the *Turbo* from last interglacial Glanville Formation identified at Traeger's Quarry (Murray-Wallace *et al.*, 2010). The *Turbo* opercula cemented onto the upper surface of the conglomerate is very similar in age to those from the raised Holocene beach.

While, *Katelsia rhytiphora* GLU D/L values generally increase with distance inland, fragments from Burleigh Range (hypothesised to be MIS 7 in age) are significantly greater than from all other sites, including the more landward Caveton Range (Figure 5.16b). Last interglacial *Katelsia rhytiphora* shells yield considerably higher D/L values compared with modern specimens as expected. Shells from Burleigh Range at Rabbitors Road are significantly higher than those from Lake Hawdon South (MIS 5e) and Caveton Range (MIS 9). As all samples were collected from at least 1.5 m depth of burial it is suggested that temperature histories of fossils would have been similar and thus this cannot account for varying extents of racemisation. As a result, it is inferred that fragments of *Katelsia* from Burleigh Range at Rabbitors Road have been reworked from an older deposit.

GLU D/L values of *Ostrea angasi* from Compton, Mingbool and Dismal Range are significantly higher than those of last interglacial (MIS 5e) age (Figure 5.16c). However, D/L values cannot be confidently separated between these three barriers which, based on their geographical position, are proposed to correlate to MIS 13, 15 and 17 respectively. This again indicates that *Ostrea* is a poor matrix for the retention of indigenous amino acids and identifies the limited resolution of AAR on middle Pleistocene *Ostrea* within this region.

A considerable range of D/L values is noted from the modern beach sites, as discussed previously this is potentially due to highly active erosion and sediment supply of reworked bioclasts from surrounding late Pleistocene deposits. Figure 5.17 illustrates the spread of GLU D/L values in whole-rock samples within barriers across the coastal plain. Whole-rock GLU D/L values from the raised Holocene beach are not significantly different from last interglacial *sensu lato* samples, again indicative of reworking of older grains from the

nearby Robe Range into the sample. This finding highlights the potential mixing of bioclastic grains that can occur within high-energy sampling sites and the potential limitations of using whole-rock AAR analysis alone to determine the numerical age of a deposit. GLU D/L values from interstadial deposits of the last interglacial complex cannot be confidently distinguished from one another, highlighting the limited resolution of AAR. Whole-rock GLU D/L values from Burleigh Range at Rabbitors Road are significantly higher than those from last interglacial samples, but not from those within Caveton Range (proposed MIS 9 based on geographical position). This further suggests that sediment has been reworked from an older deposit, potentially Caveton Range, as Burleigh Range was formed. While a weak trend of increasing GLU D/L values with increased distance from the present shoreline can be observed (Mingbool village sample, the farthest distance from the shoreline, yields the highest GLU D/L value), discrepancies are evident. Samples from both Burleigh and Caveton Range yielded higher D/L values than for the Gambier, Compton and Mingbool Ranges, farther inland. This may reflect reworking of older sediment within the younger barriers (as proposed for Burleigh Range) and/or leaching of amino acids in the older successions.

The spread of GLU D/L values from foraminifera yields the clearest pattern of increasing D/L value with distance inland (Figures 5.18; 5.19; 5.20). It was decided to present results of GLU D/L values in comparison with proposed MIS age based on geographical position of the barrier inland over the use of bivariate plots comparing GLU with ASP D/L values. With increased age, ASP loses the power to discriminate, as seen within pyrolysis experiments (Figure 5.6), and eventually ASP D/L values will start to decrease, as noted by Kimber and Griffin (1987). Due to issues with column performance and the late elution time of VAL, D and L, peaks for this slow racemising amino acid were commonly small with unreliable derived D/L values not suited to using within bivariate plots. While clear trends are apparent between the increased distance of barriers from the present shoreline and increased GLU D/L value of foraminifera, it is noted that presenting results this way may mask the fact that some barriers are composite deposits formed during multiple sea-level highstands. Stratigraphical interpretations of site descriptions are also necessary in determining a chronostratigraphy and this is established for the Mount Gambier coastal plain in the following chapter.

Foraminifera consistently yielded AAR numerical ages closer to those hypothesised, based on the geographical positioning of sample sites, especially in the more inland barriers, compared with whole-rock and mollusc AAR analysis. Figure 5.21 compares D/L values from a range of analysed material for the oldest sample sites within Mingbool Range and Dismal

Range. As illustrated, foraminifera consistently yield the highest D/L values with the lowest spread indicating a potentially greater precision of dating. Whole-rock consistently yielded the lowest D/L values and whilst GLU D/L values in *Ostrea* were also higher, the spread of values is wide and represents a lack of precision.

The fact that foraminifera yielded numerical ages more similar to those expected based on geographical location than analysis of whole-rock samples or fossil shell may relate to the use of a single grain over a shell matrix or multiple grains whereby sources of contamination are harder to identify. Due to the high availability of foraminifera within carbonate-rich sediment, many single grains could be analysed, and samples were easily rejected where SER D/L values were less than 0.1. The averaging of D/L values from multiple grains within whole-rock samples may have resulted in the presence of diagenetically altered grains, thus reducing the overall D/L value. It may also be possible that foraminifera represent a better closed system or retain indigenous amino acids better than some fossil shell.

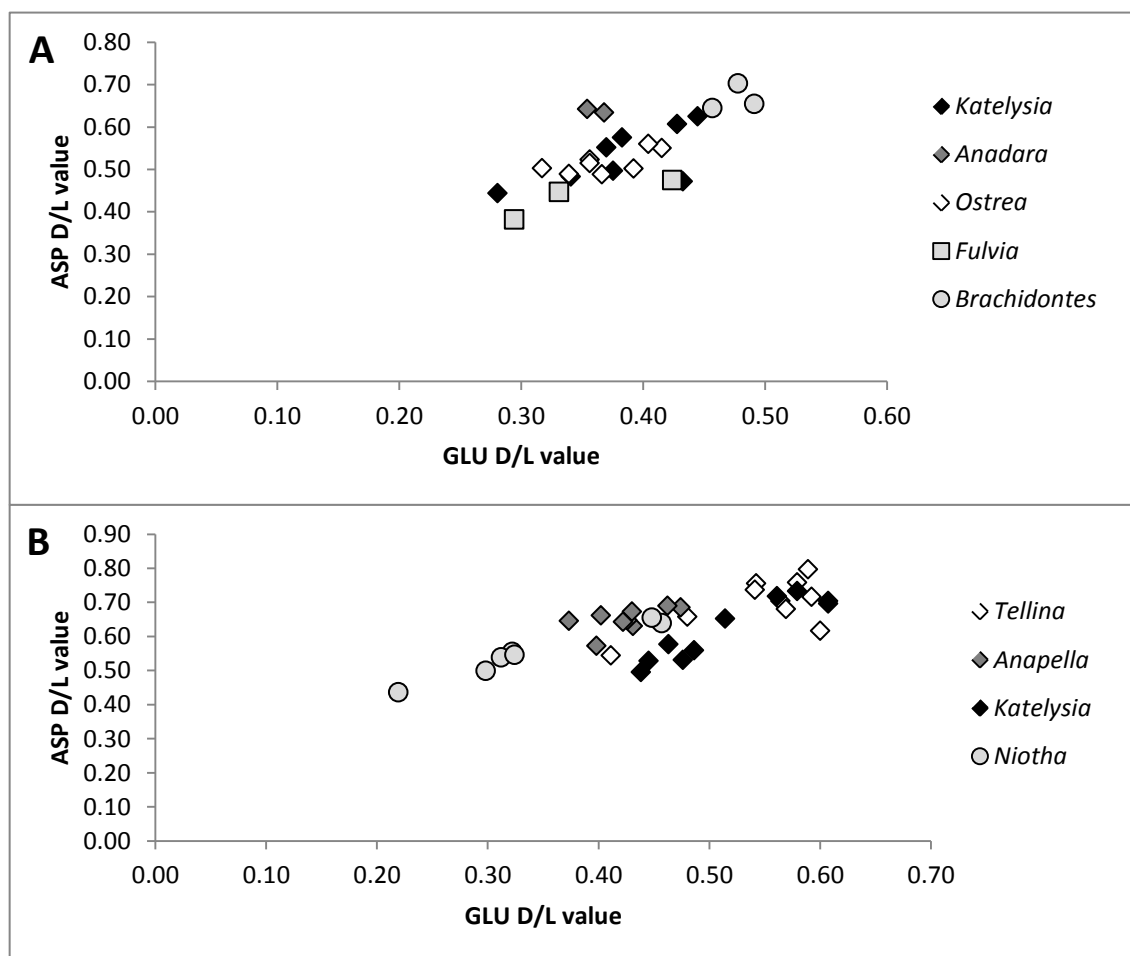


**Figure 5.15:** Scatter plots of aspartic acid (ASP) and glutamic acid (GLU) D/L values derived from AAR analysis of a variety of molluscan genera from **A:** landward of the Woakwine Range (MIS 5e) at Lake Hawdon South, and **B:** the Caveton Range lagoonal facies, Rabbitors Road (MIS 9). Scatter plots shows a wide spread of D/L values within genera at the same sample site. D/L values were derived from single injections and are displayed for individual molluscs but comprised of the average of D/L values derived from at least three sub-samples from each shell to avoid intra-shell variation.

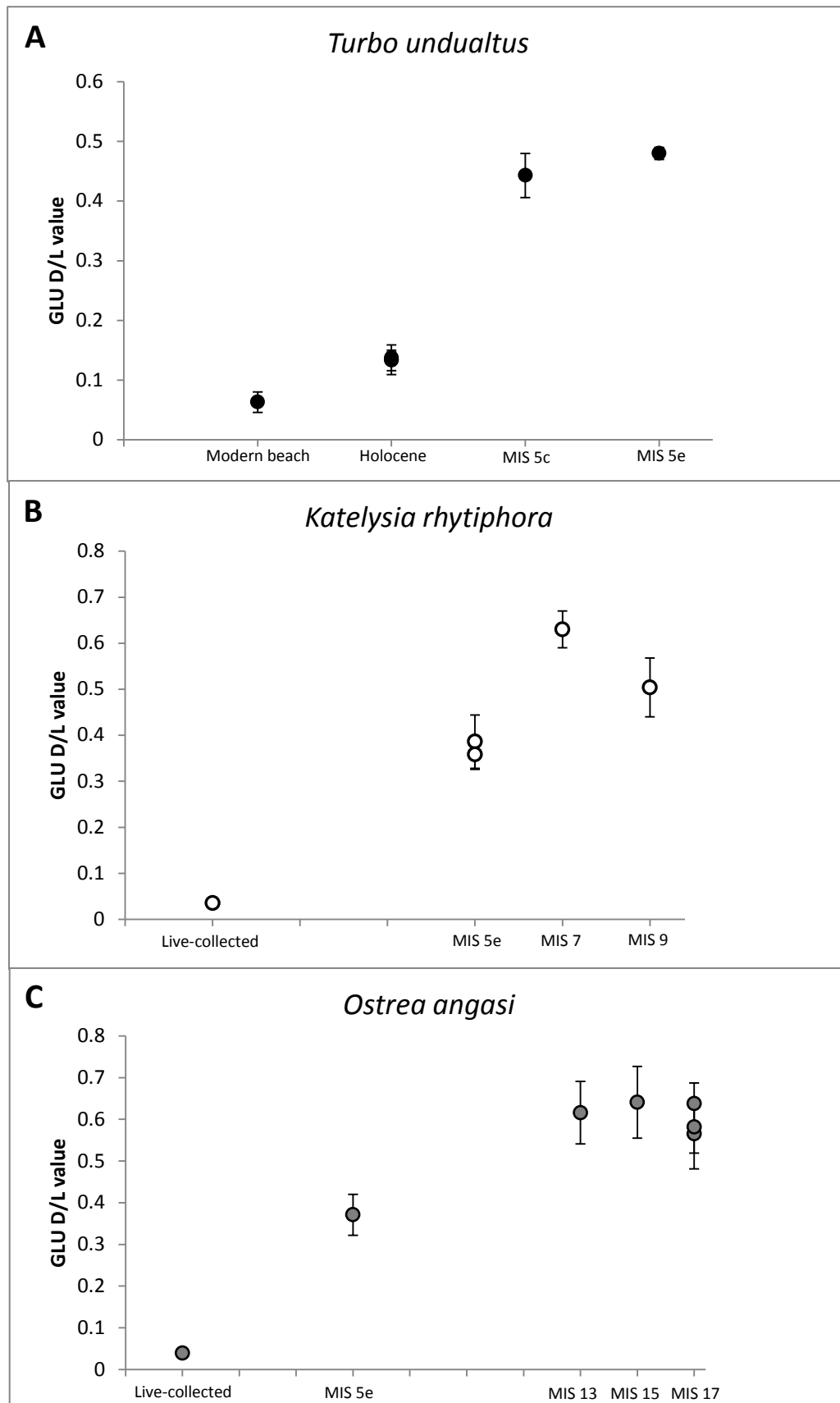


**Figure 5.16:** Plots of GLU D/L values against proposed MIS based on geographical location of barriers from molluscs across the Mount Gambier coastal plain. D/L values are derived from single injections and averaging of at least three individuals at each site. Each individual mollusc was sub-sampled at least twice to account for intra-shell variation and these derived D/L values were averaged also. Note MIS 5e *Turbo* is that reported by Murray-Wallace *et al.* (2010) from Traeger's Quarry, Goolwa. Error bars represent  $1\sigma$ .

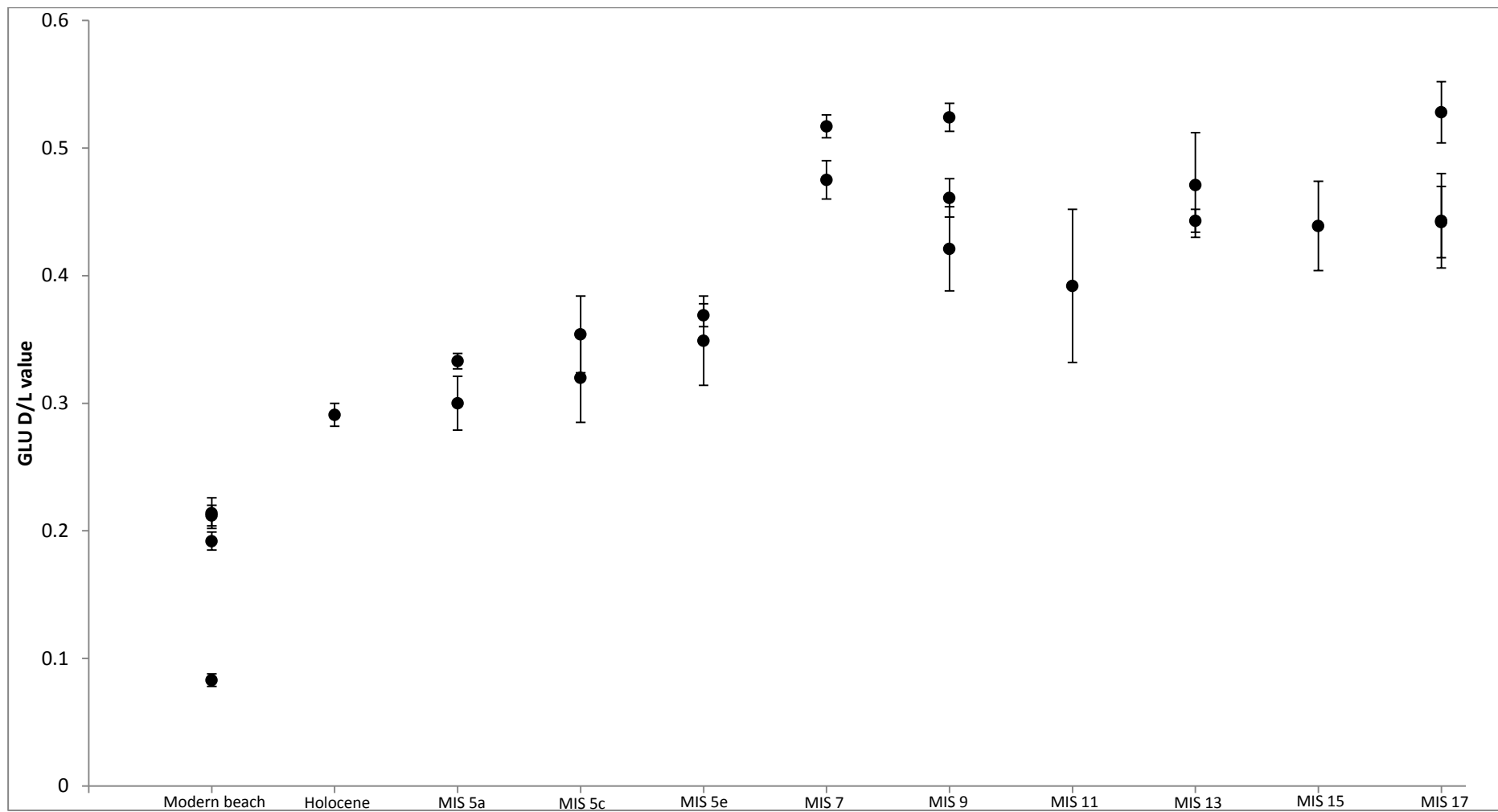


**Figure 5.17:** Plot of GLU D/L values derived from whole-rock samples across the Mount Gambier coastal plain plotted against proposed MIS based on the geographical position of corresponding barrier in relation to the modern shoreline. A weak trend of increasing GLU D/L values with increased distance inland from the present coastline is evident, but values appear to plateau past MIS 9 (Caveton Range). Leaching of amino acids may have resulted in lower than expected D/L values in older barriers. D/L values are derived from single injections and the averaging of up to ten separately analysed sub-samples at each site. Exact sub-sample numbers are shown in tables throughout the chapter. Error bars represent  $1\sigma$ .

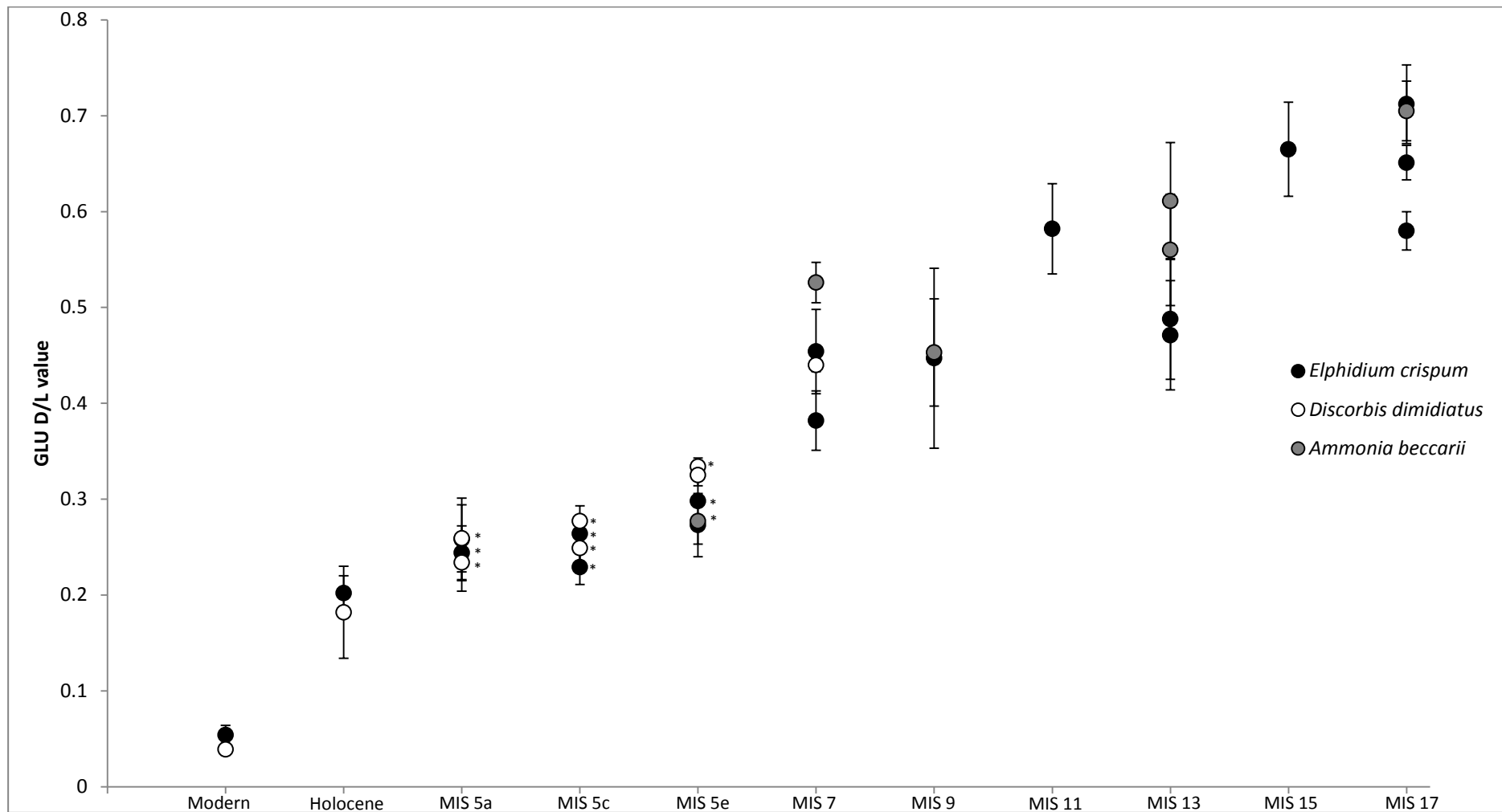


**Figure 5.18:** Plot of GLU D/L values derived from multiple individuals of foraminifers at sample sites across the Mount Gambier coastal plain plotted against proposed MIS based on geographical position of barrier from the present shoreline. A clear trend of increasing D/L value with increased distance from the present shoreline is evident. The greater clarity of this trend in foraminifera when compared with whole-rock may relate to the increased precision of single-grain analysis. \*represents samples from aeolianite facies. D/L values are derived from single injections and averaging of single and multiple (up to 10) tests analysed at a sample site. Exact numbers of sub-samples are identified in tables within the Chapter.



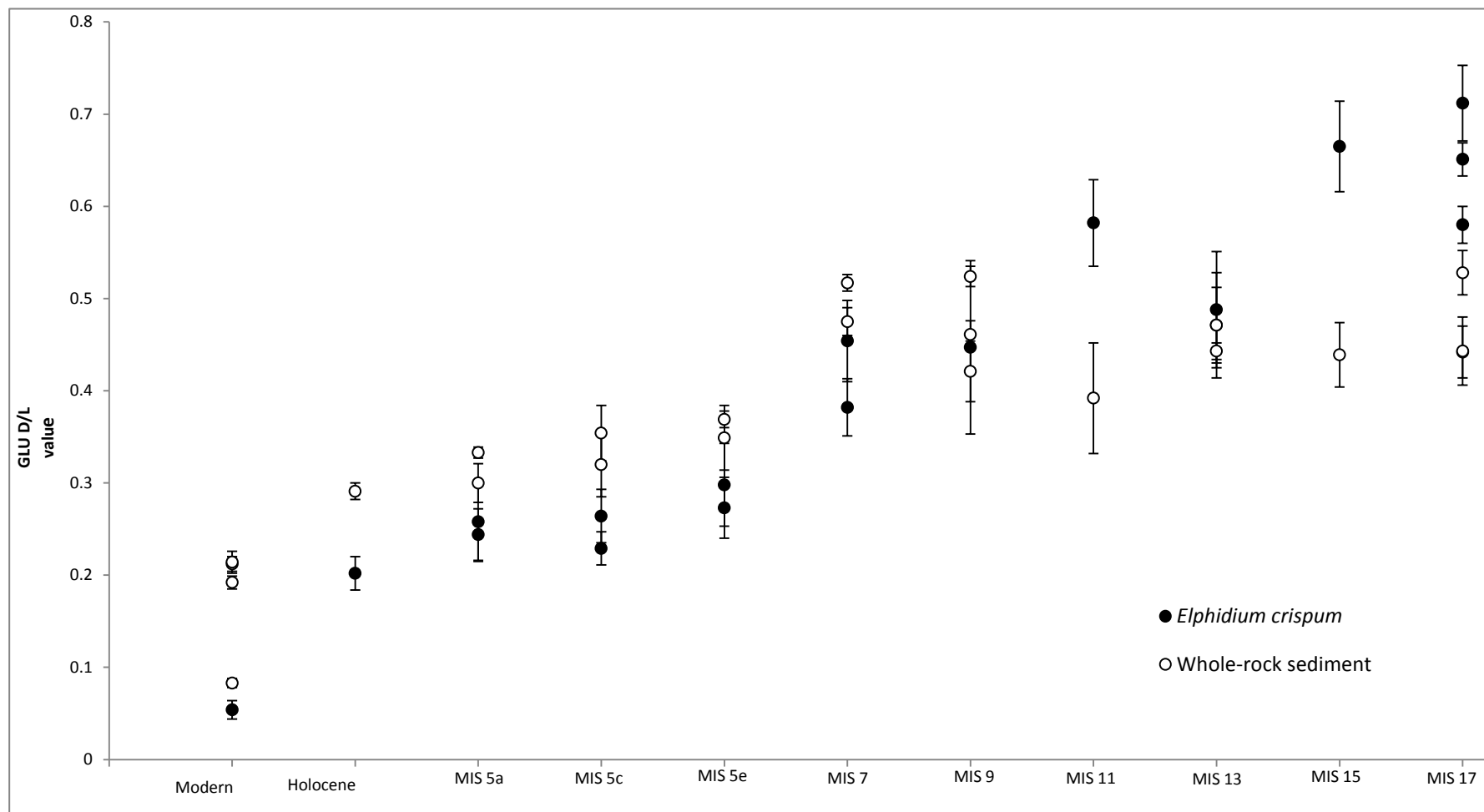


**Figure 5.19:** Plot compares D/L values of whole-rock samples and *Elphidium crispum* with the proposed MIS of the barrier sediment was sampled from based on its geographical position. It is evident from the plot that after MIS 9 whole-rock D/L values plateau off and lose their ability to resolve, while foraminifera GLU D/L values continue to increase with proposed age. Whole-rock values are represented by the averaging of 10 separately analysed sub-samples from one unit at a site, while foraminifera D/L values are represented by an average of multiple single tests and several analyses of up to 10 tests averaged in one vial. Exact numbers of sub-samples for each site are indicated in tables throughout the chapter. Analyses were subjected to single injections by the RP-HPLC. Error bars represent 1 $\sigma$ .

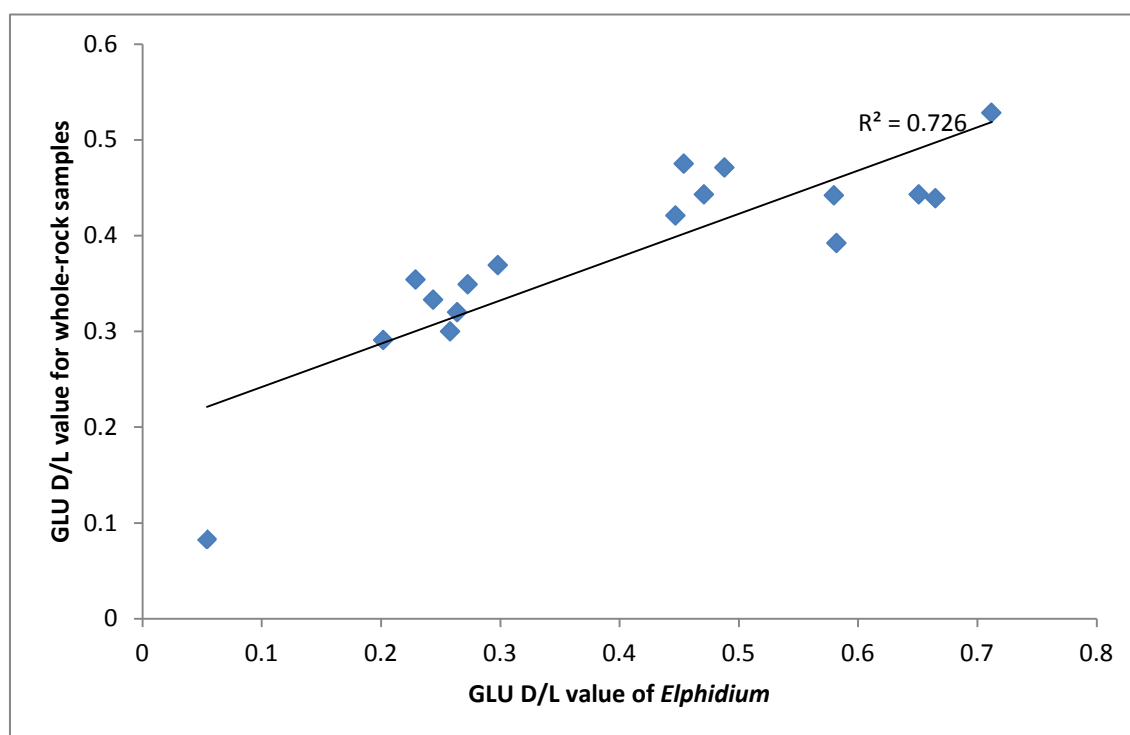


**Figure 5.20:** Scatter plot of GLU D/L values between whole-rock and *Elphidium crispum* samples; illustrates the wider range of D/L values expressed through foraminifera compared with bioclastic sediment samples. Whole-rock values are represented by the averaging of 10 separately analysed sub-samples from one unit at a site, while foraminifera D/L values are represented by an average of multiple single tests and several analyses of up to 10 tests averaged in one vial. Exact numbers of sub-samples for each site are indicated in tables throughout the chapter. Analyses were subjected to single injections by the RP-HPLC.

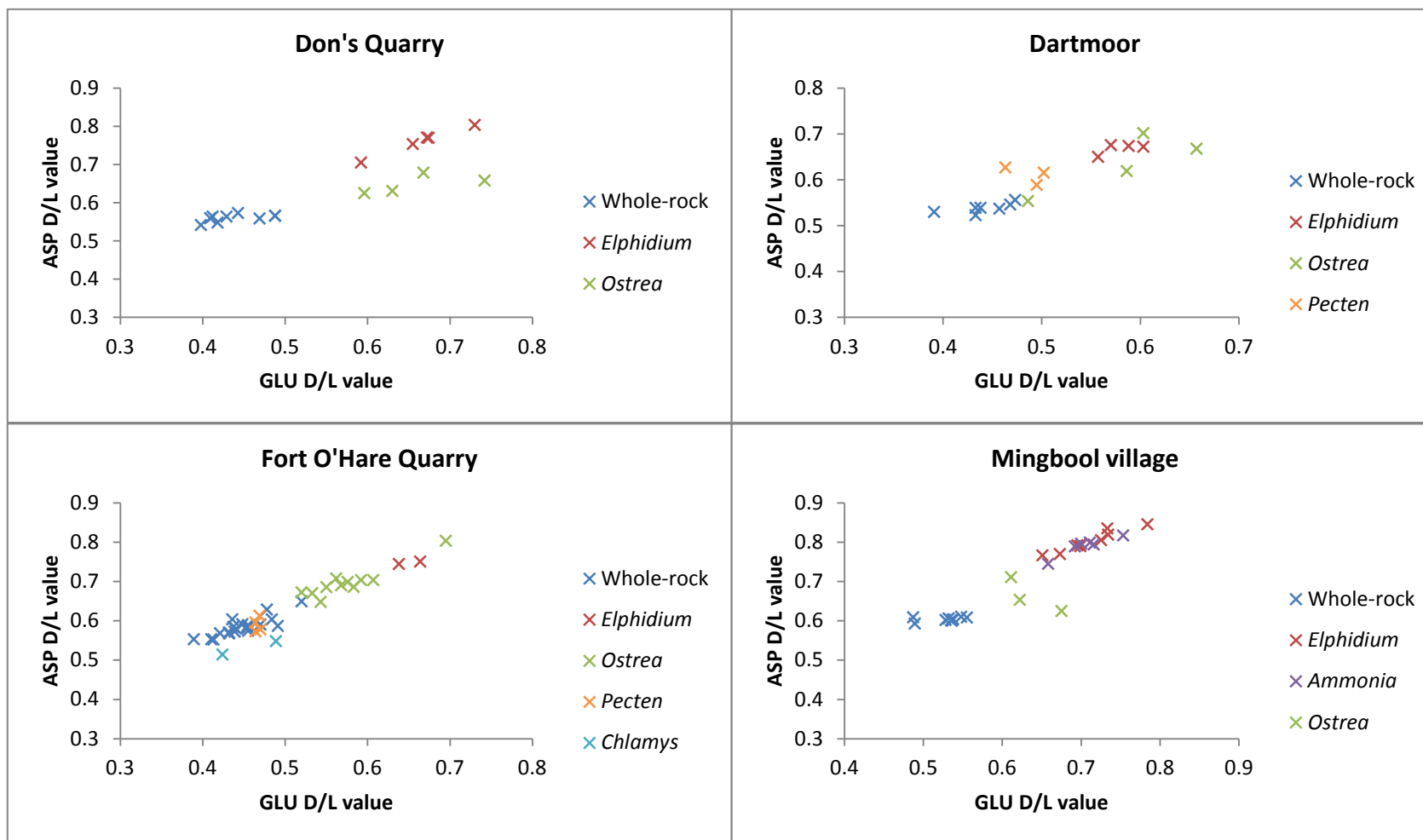


**Figure 5.21:** Scatter plots of D/L values from whole-rock, foraminifera and fossil shells analysed at four of the most inland sites of Early Pleistocene Bridgewater Formation on the Mount Gambier coastal plain. Whole-rock samples continually yield the lowest D/L values at a site, while foraminifera generally yield the highest with the least variance. All samples represent single injection analyses of the RP-HPLC. Whole-rock values are derived from averaging of up to ten sub-samples. Foraminifera values are derived from averaging of single and multiple (up to 10) tests, while shell D/L values are derived from up averaging up to 4 samples at a site and at least 3 sub-samples from individual molluscs. Exact numbers of sub-samples are shown in Table 5.11.

## 5.9 Conclusions

Geochronological analysis has aided in constraining the timing of deposition of barrier shorelines on the Mount Gambier coastal plain and supports the hypothesis proposed by Sprigg (1952) that ranges were deposited during successive sea-level highstands.

Whole-rock analysis of modern beach sediments highlights the range in residence times that sediment may rest upon a beach and the inner continental shelf before being finally incorporated within dune deposits. OSL analysis confirmed that the aeolianites at the western end of Port MacDonnell Beach are at least MIS 3 in age, and is consistent with the age reported by Banerjee *et al.* (2003) for Robe II near the town of Robe, 80 km northwest of Port MacDonnell. These findings highlight that Robe II is not a local deposit, as suggested by Banerjee *et al.* (2003), as proposed equivalents are also recognised at Port MacDonnell and thus the deposit has a much wider stratigraphic expression. As Robe Range is not observed continuously along the entire extent of coastline between Cape Northumberland and Robe, it is in a sense an amalgam of regional and local processes. Deposits are only preserved in certain locations, such as at Robe and Cape Northumberland, but were formed by sea-level highstands which affected the region as a whole. The localisation of these deposits may be a result of varying energy regimes along the coastline, resulting in differing preservation potential between regions. For example, on Port MacDonnell Beach, remnants of the Robe Range are found in the form of highly weathered 20 cm thick aeolianite units, yet 100 m farther west deposits of the same unit are over 3 m thick.

OSL suggests confirms MacDonnell Range, 7 km inland from the present coastline, is an extension of the MIS 5e Woakwine Range. Due to the gentle uplift of the coastal plain the aeolianites at Port MacDonnell must therefore be younger and are suggested to have formed during warm interstadials of the last interglacial. Radiocarbon dating of *Turbo undulatus* within a palaeo-beach deposit at Port MacDonnell reveals that it is older than Holocene and yielded a minimum age of 47 ka, while AAR analysis suggests the shell is of last interglacial age.

AAR analysis of shell, whole-rock sediment and foraminifera from Burleigh Range at Rabbitors Road cutting yielded a large range of D/L values significantly higher than the proposed MIS 7 interglacial based on its geographical position. Foraminifera from Laslett Road cutting, a lagoonal facies directly landward of Burleigh Range, yielded values more consistent with MIS 7 and therefore it is suggested that some sediment within the high wave energy gravel beach facies at Rabbitors Road has been reworked from an older deposit. It is possible

that as sea level regressed at the end of an earlier interglacial, sediment was entrained seaward and was reworked into Burleigh Range as sea level transgressed during MIS 7.

Numerical ages derived from AAR analysis of bioclastic sediments, foraminifera and *Tellina deltoidalis* from Caveton Range confirm that it is MIS 9 in age, which corresponds with the proposed age of this deposit based on its geographical location in relation to the present coastline. Shell from this site yielded lower-than-expected numerical ages and may reflect leaching of amino acids from the shell matrix. Lower than expected values were also reported from analysis of fossil shell at this site by Murray-Wallace *et al.* (1996).

At Gooch Road, within the Gambier Range, whole-rock analysis yielded significantly lower numerical ages than the hypothesised MIS 11. This may be due to the highly cemented nature of the sediment, which may have lowered the overall D/L value. However, *Elphidium crispum* from this site yielded higher numerical ages than anticipated. SEM analysis (section 4.7.3) confirms tests have not been significantly abraded; therefore it is not likely tests have been reworked from an older deposit. It is possible tests resided on the inner continental shelf for a significantly longer timeframe than tests analysed at other deposits. *Discorbis dimidiatus* analysed from this deposit all yielded low SER values (0.013 to 0.057), indicative of diagenetic alteration, and potential preferential preservation of *Elphidium*. Through geochronological analysis it is not possible to conclusively confirm that this is a MIS 11 barrier shoreline, though AAR numerical ages from foraminifera indicate sediment is older than MIS 9.

OSL analysis of quartz grains from an aeolian facies exposed at Baxter's Quarry within Compton Range yielded a MIS 11 age. *Elphidium crispum* from the lower subaqueous facies at this site also yielded a MIS 11 age, while *Ammonia beccarii* are suggestive of deposition during MIS 13, though uncertainty is high and this may be related to differential kinetics between species. The combined geochronological and stratigraphical interpretations of this site suggest that it may be a composite deposit formed during multiple sea-level highstands; with a core sediment body of MIS 13 age separated by a laterally extensive disconformity from an overlying aeolian facies of MIS 11 age. Foraminifera from Heritage Industries, also in the Compton Range, yield MIS 11 to MIS 13 ages. Geochronological analysis suggests, therefore, the Compton Range formed during MIS 11 or MIS 13.

Fossil shell and whole-rock sediment from Mingbool and Dismal Range yielded significantly lower AAR numerical ages than expected, possibly due to diagenetic alteration of

this material. Foraminifera, however, yielded numerical ages similar to those hypothesised based on the geographical positions of the relict shorelines across the coastal plain. Associated uncertainty values are high for the derived numerical ages from Don's Quarry, proposed to lie within Mingbool Range, and cannot be distinguished from the more inland Dismal Range samples. It is possible that these two dunes were formed during the same sea-level highstand, but there is insufficient precision to assess this hypothesis. AAR numerical ages derived from these sample sites are significantly greater than those within Compton Range and geochronological analysis indicates deposition during MIS 15 and 17.

This study has contributed to the body of AAR analyses previously conducted on the southern Australian coastline. Whole-rock analysis did not yield the lengthy time span of deposition recorded by Murray-Wallace *et al.* (2002) farther north on the Coorong coastal plain, and this may be due to greater diagenetic impacts and poorer preservation of samples from the Mount Gambier region. Karst weathering prevails across the Mount Gambier regional landscape, as is evidenced by doline structures in the outcropping Gambier Limestone, and may attribute to different preservation potential in this region. The limited extent of the whole-rock technique in the Mount Gambier area may also relate to the chosen amino acid. The slowly racemising leucine was used by Murray-Wallace *et al.* (2001) and derived from GC analysis. Within this study RP-HPLC was used and the late elution of both leucine and valine within runs and problems with column performance resulted in unreliable D/L values for these amino acids. Foraminifera have not previously been analysed to such an extent within the shoreline barriers across the South Australian coastal plains. The use of single foraminifer analyses allows immediate rejection of contaminated samples which do not lower the overall average D/L value for a deposit. This research has shown the high potential of this single-grain technique to extend further into the middle Pleistocene in this region.

The geochronological results from this research will be compared with previous results derived farther north on the Coorong coastal plain (Murray-Wallace *et al.*, 1996; 1999; 2001; 2010) in the following chapter. This final chapter will also provide a synthesis of the geomorphological evolution of the Mount Gambier coastal plain, drawing together stratigraphical, petrographical and geochronological interpretations derived in this research to construct a palaeo-sea level record for the region and critically evaluate these findings with regard to the global sea-level history as it is presently understood.



# Chapter 6

## Quaternary coastal evolution of the Mount Gambier coastal plain, southern Australia and the successive development of the Bridgewater Formation

### 6.1 Introduction

This chapter provides a synthesis of the development of the Bridgewater Formation on the Mount Gambier coastal plain, southern Australia, by combining the results of stratigraphical, petrological and geochronological interpretations established in this thesis. The barrier shoreline complexes on the Mount Gambier coastal plain were formed in successive sea-level highstands, as proposed by Sprigg (1952) and correlate with the barriers of the Robe coastal plain as described by Murray-Wallace *et al.* (2001). By identifying the elevation of palaeo-sea level indicators associated with each of the barriers on the Mount Gambier coastal plain and applying previously determined uplift rates to the proposed age of deposits a palaeo-sea level record for the last 680 ka is presented. Few locations in the world preserve such a lengthy archive of local sea-level change. The principal findings of this thesis are compared with a framework of interglacial sea-level records that were presented in Chapter 2 to determine their global significance. Barrier morphology of the shoreline successions on the Mount Gambier coastal plain are described using SRTM data and compared with other global coastal interglacial calcarenite deposits. The relative thickness of calcarenite deposits between interglacials on the Mount Gambier coastal plain is found to compare well with those on Eleuthera Island, the Bahamas, while the successive and composite barrier morphology compares with calcarenite deposits in South Africa. Trends between interglacial intensity, independently identified based on ice-core records, and overall shoreline barrier volume are also identified, with more intense interglacials found to deposit larger volumes of calcareous sediment. Finally, the conclusions of this thesis are discussed and topics for further research are proposed.

### 6.2 Chronostratigraphy of the Bridgewater Formation on the Mount Gambier coastal plain

Stratigraphical and petrological analyses conducted in this thesis have determined the depositional and diagenetic environment of certain exposures of facies within barrier



successions across the Mount Gambier coastal plain. Geochronological analyses, through the use of AAR, OSL, and radiocarbon dating, have constrained the age of barrier formation. Table 6.1 summarises each of these findings for key deposits across the coastal plain. The following discussion ties each of these aspects together to create a chronostratigraphy for barrier shoreline deposition and highlights coastal evolution of the plain and the potential pitfalls of geochronological techniques in a dynamic coastal system. Determination of such a chronostratigraphy will ascertain whether the hypothesis of Sprigg (1952), that each shoreline barrier was deposited in a successive interglacial, is correct. Combined with the identification of palaeo-sea level markers a chronostratigraphy will enable the construction of a palaeo-sea level record for the Mount Gambier coastal plain.

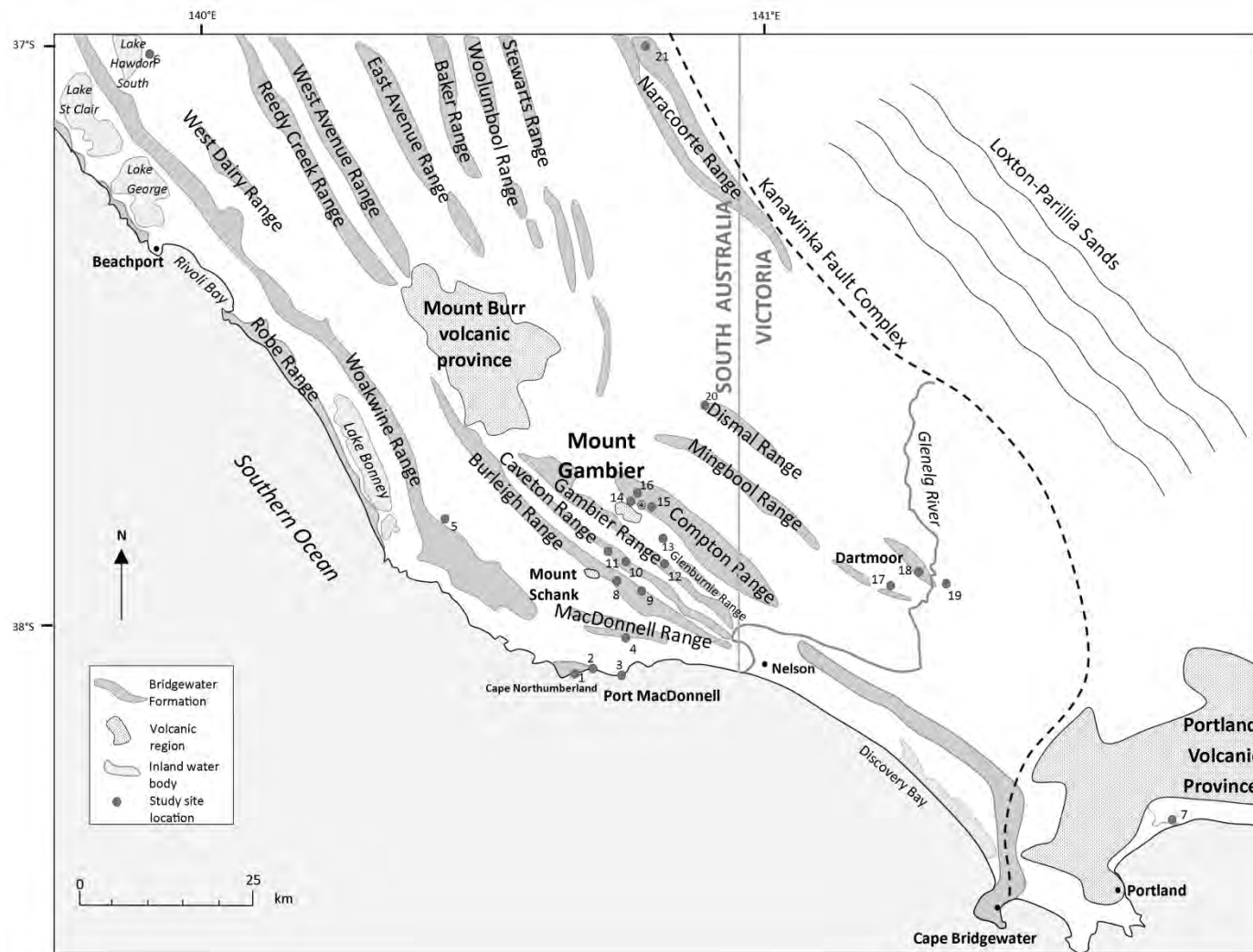


**Figure 6.1:** Map of the Mount Gambier coastal plain highlighting the successive barrier deposits and sample study sites. 1 = Shelly Beach; 2 = Port MacDonnell Beach; 3 = Racecourse Bay; 4 = Swarts Road sand quarry; 5 = German Creek shell bed; 6 = Shell beds in Biscuit Drain, Lake Hawdon South; 7 = Narawong Road cutting, as Surry River crosses Princes Highway; 8 = Rabbitors Road cutting; 9 = Laslett Road cutting; 10 = Caveton Range on Rabbitors Road; 11 = Bucks Hill; 12 = Gooch Road; 13 = Caroline Main Road; 14 = Road cutting through Grey St; 15 = Heritage Industries; 16 = Baxter's Quarry; 17 = Don's Quarry, Mumbannar; 18 = Dartmoor Cemetery; 19 = Fort O'Hare Quarry; 20 = Small quarry near Mingbool village; 21 = Henschke Quarry, Naracoorte. \* = siliceous sand deposit.

### 6.2.1 Modern coastline

Stratigraphical descriptions (section 3.8.2) of the coastline at Port MacDonnell, Shelly Beach and Racecourse Bay have identified that the coast in this region differs from that northwest of Robe and at Discovery Bay in Victoria, in that they lack significant Holocene dunes. The presence of older aeolianites stacked on the beaches at Port MacDonnell and Shelly Beach indicate aeolian deposition occurred in this region previously.

AAR analysis reveals that the age of sediments on the beachface can vary dramatically depending on the age and proximity of surrounding deposits. For example, fossil shell within the raised Holocene beach at Port MacDonnell is significantly younger than the sediment within which it is deposited, indicating that this sediment has been potentially reworked from the surrounding stacked, late Pleistocene aeolianites during a Holocene sea-level highstand. Therefore, while the steadily uplifting coastal plain may separate successive barrier shorelines, sediment can still be eroded, deposited and reworked from previously deposited units during successive interstadial and interglacial sea-level highstands.

### 6.2.2 Robe Range

Stratigraphical interpretation of aeolianite cliffs at Port MacDonnell and Shelly Beach has suggested the deposits at these locations are correlative with those of Robe Range, as described by Schwebel (1978; 1984) in the vicinity of Robe. This is based on their proximity to the modern coastline, thick calcrete profiles (indicating they are older than Holocene) and the composition of the cliffs, revealing at least two separate phases of aeolian deposition separated by a significant hiatus. OSL analysis of the upper aeolianite at Port MacDonnell yielded a late MIS 3 age for sediment deposition, during which time the coastline would have been 13 km shoreward of its present position. Strong winds may have blown sediment this far inland, or sediment may have been reworked by aeolian processes following initial deposition (this suggestion is further discussed in section 6.2.10).

AAR does not have the resolution to distinguish between the two proposed interstadial units at Port MacDonnell and Shelly Beach confidently. However, these aeolianites must be younger than MIS 5e, as OSL has confirmed the MacDonnell Range, 7 km inland from the modern coastline to be  $124 \pm 10$  ka in age. If the lower aeolianite at Port MacDonnell is of MIS 5c age (as suggested for the lower aeolianite unit at Robe dated by Huntley *et al.*, 1993a), then it constrains the depositional timing of a palaeo-beach facies identified stratigraphically below remnants of this lower aeolianite unit 100 m farther east (Figure 6.2).

AAR analysis on *Turbo undulatus* within the flint conglomerate palaeo-beach facies indicates deposition at  $103 \pm 23$  ka and a younger, Holocene episode of deposition on its upper surface. It is therefore suggested that interstadial aeolianite units would have once covered the beach at Port MacDonnell but much of this was eroded during the successive Holocene sea-level highstand, forming the Holocene shore platform. The presence of two temporally different episodes of shell deposition within the conglomerate indicate how younger shell and sediment can be intermixed into older deposits (and vice versa), complicating interpretations of the 'true' age of shelly successions.

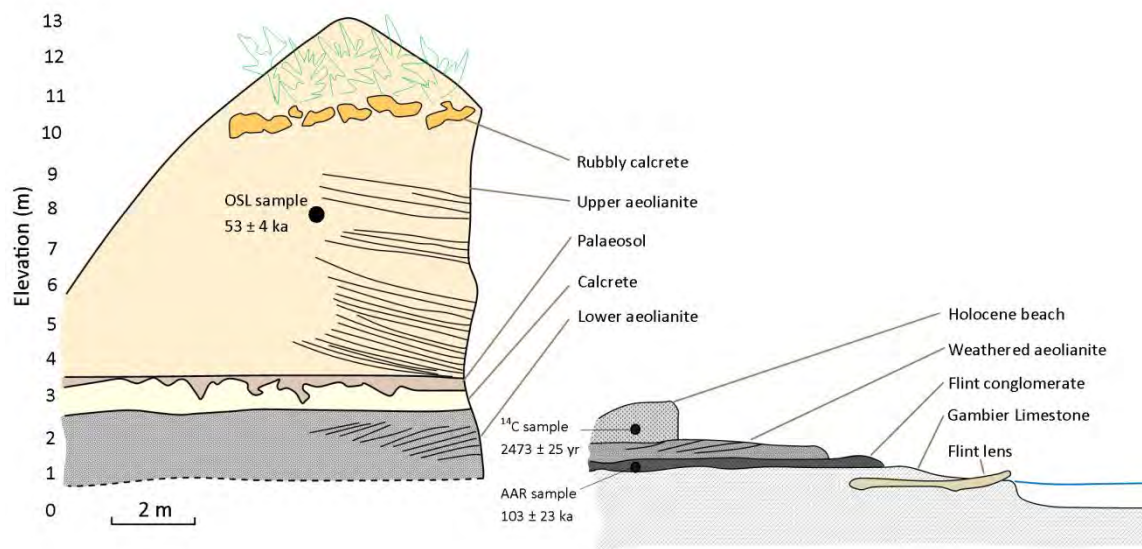


**Figure 6.2:** Stratigraphical cross-sections of coastal deposits on Port MacDonnell Beach illustrating chronostratigraphical interpretations. Sites are located 100 m from each other along the shoreline.

### 6.2.3 MacDonnell Range

Geographically, the MacDonnell Range appears as an extension of the last interglacial (MIS 5e) Woakwine Range. OSL analysis of quartz grains within aeolian facies of MacDonnell Range confirms this correlation, yielding an age of  $124 \pm 10$  ka. Shell collected from Lake Hawdon South was presumed to be last interglacial in age due to the presence of fauna such as *Anadara trapezia*, and this was confirmed through AAR results. AAR analysis of whole-rock sediment and foraminifera within a road cutting at Narrawong confirm the findings of Sherwood *et al.* (1994) that this is also a last interglacial (MIS 5) deposit.

### 6.2.4 Burleigh Range

Burleigh Range is the second significant barrier succession on the Mount Gambier coastal plain. A cutting along Rabbitors Road exposes three flint lenses capped by aeolian sands, indicative of a prograding coastline. The present day coastline at Racecourse Bay is currently

dominated by flint clasts and may be an analogue for this facies. AAR results for fragmented fossil shell, skeletal carbonate sands and foraminifera within this exposure yielded significantly higher-than-expected D/L values when compared to the geographical position of the barrier 13 km inland from the modern shoreline. AAR results from a lagoonal facies landward of the barrier indicate deposition during MIS 7. It is therefore suggested that Burleigh Range formed during the penultimate interglacial but that the sediment and fossil shell within the barrier were reworked from an older source during sea-level regression and subsequent transgression.

#### **6.2.5 Caveton Range**

Caveton Range is the third barrier on the coastal plain and is located approximately 15 km inland from the modern coastline. Results of AAR analysis of *Tellina deltoidalis* and foraminifers within a lagoonal facies and of skeletal carbonate sands from an aeolian facies analysed by the whole-rock method indicate a probable MIS 9 time of deposition. These values, along with the results from MacDonnell Range and some of the data from Burleigh Range, support the suggestion that each successive barrier has been deposited during sequential interglacial highstands. Other fossil shell species within the lagoonal facies yielded significantly lower D/L values than *Tellina sp.*, potentially resulting from the leaching of amino acids from shell matrices.

#### **6.2.6 Gambier Range**

Gambier Range is a particularly tall barrier on the coastal plain as indicated by SRTM data (Figure 3.12) and is the fourth barrier inland from the modern coastline. AAR whole-rock analysis within a subaqueous facies of Gambier Range, yielded D/L values that are significantly lower than expected based on the geographical position of the barrier in relation to the modern shoreline and lower than those derived from the seaward Burleigh and Caveton Ranges, which likely reflects post-depositional leaching. AAR results of foraminifers within the same facies were, however, significantly higher. Geochronological analysis from this deposit cannot be relied upon to infer depositional age, and may relate to the mature diagenesis of this deposit. Consequently, age determination of this barrier as MIS 11 is based on its morphostratigraphical position relative to the modern shoreline.

#### **6.2.7 Compton Range**

Compton Range is the fifth barrier inland from the present coastline, found 23 km landward of Port MacDonnell. From Grey Street, Mount Gambier, a fragmented bivalve was analysed through AAR and yielded an age of  $509 \pm 107$  ka, placing deposition of the unit within MIS 13.

At Baxter's Quarry, Mount Gambier, the lower subaqueous facies is separated from the overlying aeolian unit by a laterally extensive truncation surface which reflects an eroded protocol. OSL analysis of the aeolian facies at Baxter's Quarry yielded a MIS 11 age. Results of AAR analysis of *Elphidium crispum* within the lower subaqueous facies yielded an age of  $392 \pm 80$  ka. If the OSL result is accurate (which it may not be due to the proximity to the age limit of the method and the high palaeo-dose of the sample), it suggests that Compton Range may be a composite deposit, with sediment deposited at this locality during two successive interglacials. While several studies in the global literature have proposed a MIS 11 sea-level highstand significantly higher than present (e.g. Bowen, 2010; Raymo and Mitrovica, 2012; Muhs *et al.*, 2014), a sea-level of similar elevation to present during MIS 11 may have also extended to this location previously.

At Heritage Industries, 3 km southeast of Baxter's Quarry, AAR numerical ages derived from *Ostrea* and *Elphidium* indicate a MIS 11 age. However, in older sites within this study and from pyrolysis experiments conducted by Kimber and Griffin (1987), *Ostrea* has been identified as a poor matrix for retaining indigenous amino acids. Results of AAR analysis of *Elphidium crispum* yielded a numerical age of  $363 \pm 65$  ka.

The geographical position of Compton Range in relation to the present shoreline suggests it should correlate with MIS 13 if barriers are deposited in successive interglacial highstands. Geochronological analysis has suggested that sediments were potentially deposited during both MIS 11 and MIS 13 and stratigraphical interpretations at Baxter's Quarry have indicated the presence of two distinctive units, separated by a lateral unconformity (Figure 6.3). Therefore, Compton Range potentially reflects a composite barrier, similar to that described on the Robe coastal plain within Robe Range (Schwebel, 1978; 1984) and Woakwine Range (e.g. Murray-Wallace *et al.*, 1999).

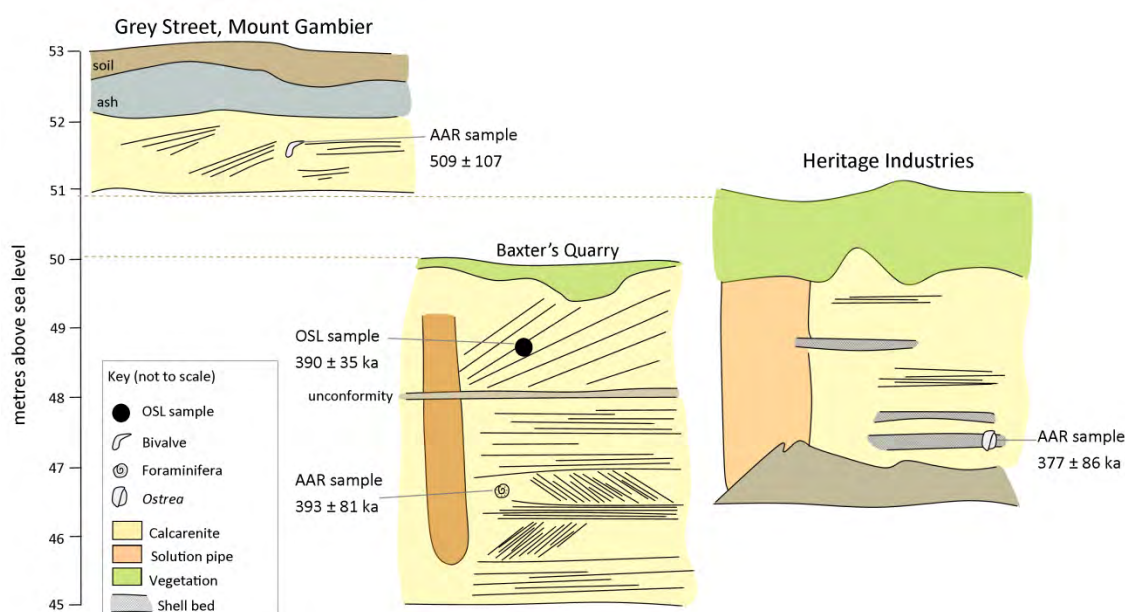


**Figure 6.3:** Interpretive sketches and the chronostratigraphical interpretation of exposures within Compton Range, South Australia.

### 6.2.8 Mingbool Range

Mingbool Range is located approximately 33 km inland from Port MacDonnell and is the sixth barrier landward of the present coastline. If the hypothesis of Sprigg (1952) is correct, this barrier should correlate with MIS 15. An exposure within Mingbool Range is described in this thesis at Don's Quarry, near Dartmoor, western Victoria (Figure 6.1). AAR analysis from *Ostrea angasi* fragments yielded a MIS 11 age, while foraminifers yielded significantly higher AAR numeric ages at  $778 \pm 118$  ka, placing deposition during MIS 19-21. The greater age of these tests may be a product of a lengthy residence time on the continental shelf. The barriers in this region are also vertically subdued and visible as isolated patches of raised elevation. It may be that this site forms a second arm to the landward Dismal Range. While geographical positioning of Mingbool Range in relation to the present shoreline indicates it should correlate with MIS 15, AAR analysis cannot confidently confirm this.

### 6.2.9 Dismal Range

Dismal Range is the seventh barrier inland from the modern coast and is approximately 40 km landward of Port MacDonnell. Each sample site reveals a subaqueous facies and lacks a distinctive overlying calcrete horizon, indicative of limited subaerial exposure, or more likely erosion of a calcrete that once existed. AAR analysis of skeletal carbonate sands by the whole-rock method and of fossil shell yielded lower than expected D/L values and may reflect the leaching of lower molecular weight peptide residues resulting in lower D/L values for the total hydrolysable amino acids. AAR analysis of foraminifera at each site yielded significantly higher

values and results are indicative of deposition during MIS 15 age and between MIS 17 and MIS 19 for Dartmoor Cemetery and Fort O'Hare sites respectively. At Mingbool village *Elphidium crispum* yielded an even greater age of  $903 \pm 167$  ka.

The geographical position of Dismal Range as the seventh barrier landward from the present coast indicates it was deposited during MIS 17 if the hypothesis that each barrier shoreline was deposited in a successive sea-level highstand is correct. AAR is not precise enough to resolve whether the barrier was constructed during MIS 17 but indicates foraminifera within the examined exposures of Dismal Range are significantly older than barriers seaward of it.

#### **6.2.10 Factors that may have altered the morphology of barrier successions**

Barrier formation on the Mount Gambier coastal plain is intrinsically linked to sea-level highstands. However, a range of other factors may have also influenced the morphology of the barriers subsequent to their deposition. Pleistocene volcanism associated with the Mount Burr volcanic province has resulted in gradual uplift of the coastal plain and has effectively spaced barrier shoreline formations. The Holocene eruptions of Mount Gambier and Mount Schank may have recently affected rates of uplift within the region and the possible effects of this on barrier morphology are discussed later in this Chapter (section 6.4).

#### **Aeolian reworking during the last glacial cycle**

OSL analysis has yielded three similar ages for aeolian deposition in areas over 80 km apart on the Mount Gambier coastal plain. Banerjee *et al.* (2003) reported an age of  $63 \pm 3.6$  ka for the aeolianite unit of Robe II near the town of Robe. In this thesis an equivalent unit in aeolian cliffs at Port MacDonnell, 80 km southeast of Robe, was also analysed using OSL and yielded an age of  $53 \pm 4$  ka. These ages do not correspond with the suggestion of Schwebel (1978; 1984) that Robe II was formed during MIS 5a, and potentially indicate an additional phase of aeolian deposition during early MIS 3. At this time sea level was 50 m below present (Lambeck and Chappell, 2001), and the shoreline at Port MacDonnell would have been 13 km south of its present position. OSL analysis of a siliceous cover sand, overlying Bridgewater Formation deposits, 25 km north of Port MacDonnell (Figure 6.1) yielded an age of  $54 \pm 5$  ka. The contrasting mineralogy of this siliceous deposit indicates it has a different source to the carbonate aeolianites of Robe II. The similarity of the timing of deposition of three units spread over a wide spatial scale potentially reflects a phase of aeolian reworking associated with more arid and windier conditions between the last interglacial and the Holocene.



Several studies across continental Australia have identified numerous intervals of aeolian reworking of linear dunes associated with increased aridity between the last interglacial (MIS 5e) and the Holocene. In central Australia, desert dune construction predominantly occurred when sediment was available for aeolian transport during cool, drier climates in MIS 4, late MIS 3 and MIS 2 (Fitzsimmons *et al.*, 2007a, b). This differs from the timing of coastal dune construction which is associated with sea-level highstands, offshore carbonate production and predominant onshore winds. Through OSL analysis of 26 sites across the Strzelecki and Tirari Deserts, south-eastern central Australia, Fitzsimmons *et al.* (2007a) identified phases of dune activity between 73-66 ka, 35-32 ka, 22-18 ka and 14-10 ka which they found to correlate with cold, arid conditions during MIS 4, late MIS 3 and MIS 2. Surrounding Lake Frome within the Strzelecki Desert, Fitzsimmons *et al.* (2007b) used OSL analysis to suggest that linear dune activity was initiated no later than 66 ka, and they identified specific reworking intervals between 67-57 ka, 43-28 ka and 22-11 ka. Also within the Strzelecki Desert, South Australia, Lomax *et al.* (2003) used OSL analysis to suggest that peak aridity occurred between 65 and 45 ka. A more extensive study by Lomax *et al.* (2011) within the western Murray Basin, South Australia, identified phases of aeolian deposition between 111-80 ka, 67-63 ka and 38-18 ka.

The burial age of the coastal aeolianite and siliceous sands on the Mount Gambier coastal plain are within 63 to 53 ka, and generally fall outside the proposed cooler periods of MIS 4 and late MIS 3, when continental aeolian activity is suggested to have been regionally more active (Fitzsimmons *et al.*, 2007a, 2007b; Lomax *et al.*, 2011). However, these ages do correlate with the bracket of peak aridity within the Strzelecki Desert suggested by Lomax *et al.* (2003) to have occurred between 65 and 45 ka. The identified delay between the aeolian reworking of more coastal sites on the Mount Gambier coastal plain compared with reworking of dunes in central Australia may relate to the coastward spread of aridity. Nanson *et al.* (1992) identified such a trend both within the cessation of operating river channels and the reworking of dune systems. They noted that palaeochannels within central Australia stopped flowing around 80 ka, while in coastal regions they were still active until ~70 ka. Nanson *et al.* (1992) also noted that dunes formed around the Lake Eyre Basin ~90 ka but did not form on the more coastal Riverine Plain until 70 to 50 ka. They suggested that the delayed spread of aridity to coastal regions occurred as the glacial period intensified.

A working hypothesis of aeolian reworking of both coastal and siliceous sands on the Mount Gambier coastal plain during MIS 3 associated with drier and windier conditions is

inferred. Robe Range may have thus been formed during MIS 5a as initially suggested by Schwebel (1978), but likely further southward on the continental shelf and sand was blown landward during a phase of aeolian reworking associated with a more arid climate. This may account for discrepancies between AAR and OSL numeric ages, as AAR would indicate the cessation of protein synthesis of skeletal carbonate while OSL determines the most recent burial of sediment. However, due to its limited resolution, AAR cannot confidently distinguish that the aeolianites at Port MacDonnell were initially formed during MIS 5a and MIS 5c. There is a paucity of evidence in this dataset but it would appear from the preliminary results that aeolian reworking of the aeolianite successions occurred during the last glacial cycle. These findings are significant as they help to inform the dichotomy of whether aeolianites were deposited during sea-level highstands or lowstands.

The more recent reworking of some of the coastal aeolianite successions remains an interesting working hypothesis and requires sampling and analysis of a larger number of deposits from across a wider portion of the coastal plain. A study of palaeo-wind directions, based on these successions, would usefully supplement such an investigation and is a potential topic for future research.

#### **Variation in the course of local rivers**

Morphology of barrier successions may have also been influenced by a potential change in the course of local rivers. The only modern river local to the Mount Gambier coastal plain is the Glenelg River in western Victoria, which currently flows from the Grampian Mountains southward down the South Australian border before reaching the Southern Ocean at Nelson (Figure 6.1). A change in the course of the river may have disrupted the aeolian system and modified dune morphology. If the river valley was to transverse across the width of the barrier system it would have resulted in an obvious distribution of barrier sediment towards the ocean. If the course of the river was to have flowed between barrier successions it may have caused potential erosion of sediment at the base of barriers and deposition of terrestrial sediment transported by the river.

Through an assessment of bathymetric data in the southeast of South Australia and western Victoria, Boutakoff (1963) identified three offshore canyons and associated delta systems between Beachport and Cape Northumberland, and suggested that these may have been former mouths of the Glenelg River. Offshore river gorges, formed due to the scouring of the continental shelf by former river channels during glacial maxima, may locally disrupt carbonate production and onshore transportation of skeletal carbonate sands. For example,

sediment may be trapped within a former river gorge as it is transported landwards, effectively depriving the area directly onshore of the same volumes of sediment deposition found at different localities along the coast.

Due to the karst landscape of the Mount Gambier region, few rivers are present on the land surface. Palaeo-river channels may therefore have also flowed below the surface and evidence of their former pathways is not present in the surficial geology. Underground waterways may have resulted in lowering of the landscape in certain regions and the formation of dolines or collapsed structures. While the analysis of underground palaeo-river courses is beyond the course of this study, further investigation could further determine how the landscape and specifically the shoreline barriers have evolved over the Quaternary in response to variation in the local fluvial system.

**Table 6.1:** Summary table of stratigraphic descriptions, diagenetic maturity derived from petrologic analysis and derived numeric ages for representative sample sites across the Mount Gambier coastal plain, southern Australia

Dune Range	Sample site	Inferred age from geographical position of barrier	Depositional environment derived from stratigraphical analysis	Diagenetic environment and maturity derived from petrological analysis	Numeric age derived from geochronological analysis (results are for AAR analysis unless otherwise listed)
	Raised Holocene beach Port MacDonnell	1-8 ka	Beach facies		Shell: $2.5 \pm 0.25$ yr BP ( $^{14}\text{C}$ ), to $3.5 \pm 1$ ka <b>MIS 1</b> Whole-rock: $45 \pm 7$ ka Forams: $29 \pm 4$ ka to $46 \pm 7$ ka
Robe Range	Aeolianites at Port MacDonnell and Shelly Beach	MIS 5a / MIS 5c	Aeolian facies	Meteoric-vadose. Weakly mature.	Whole-rock: $52 \pm 9$ ka to $106 \pm 18$ ka Forams: $54 \pm 10$ ka to $92 \pm 12$ ka <b>MIS 5</b>
	Flint conglomerate palaeo-beach		Beach facies		$103 \pm 23$ ka <b>MIS 5</b>
MacDonnell Range	Swarts Road, Allendale East	MIS 5e	Aeolian facies	Meteoric-vadose. Mature.	$124 \pm 10$ ka (OSL) <b>MIS 5</b>
	Narrawong road cutting		Unknown	Weakly mature	Whole-rock: $108 \pm 18$ ka, Forams: $78 \pm 11$ ka to $100 \pm 11$ ka Shell: $155 \pm 33$ ka <b>MIS 5</b> $125 \pm 20$ ka (uses U-series calibration of Schwebel; 1978. 1984)
Woakwine Range	Biscuit drain, Lake Hawdon South		Lagoonal facies		
Burleigh Range	Rabbitors Road	MIS 7	Beach facies with overlying aeolian sands	Meteoric-vadose. Mature.	Shell: $161 \pm 33$ ka to $424 \pm 86$ ka <b>MIS 5-11</b> Whole-rock: $297 \pm 45$ to $386 \pm 58$ ka <b>MIS 7-11</b> Forams: $229 \pm 31$ ka to $504 \pm 67$ ka <b>MIS 7 – 11</b>
	Laslett Road		Lagoonal facies	Weakly mature	Forams: $224 \pm 35$ ka to $283 \pm 59$ ka <b>MIS 7</b> Shell: $283 \pm 59$ ka
Caveton Range	Rabbitors Road	MIS 9	Lagoonal facies	Meteoric-vadose. Weakly mature.	Whole-rock: $200 \pm 34$ ka to $402 \pm 60$ ka <b>MIS 7-11</b> Shell: $196 \pm 42$ ka to $314 \pm 73$ ka <b>MIS 7-9</b> Forams: $271 \pm 36$ ka to $366 \pm 66$ ka <b>MIS 9</b>
Gambier Range	Bucks Hill		Aeolian facies	Meteoric-vadose. Mature.	Whole-rock: $270 \pm 41$ ka <b>MIS 9</b>
	Gooch Road	MIS 11	Subaqueous facies	Near surface marine. Mature.	Forams: $581 \pm 90$ ka <b>MIS 15-17</b>
Compton Range	Baxter's Quarry	MIS 13	Aeolian facies Subaqueous facies	Meteoric-vadose to near surface marine. Highly mature.	Aeolian: $390 \pm 35$ ka (OSL) <b>MIS 11</b> Forams: $393 \pm 81$ to $576 \pm 97$ ka <b>MIS 11-13</b>
	Heritage Industries	MIS 13	Subaqueous facies with potential swash zone	Meteoric-vadose to near surface marine. Highly mature.	Forams: $363 \pm 65$ to $693 \pm 115$ ka <b>MIS 11-17</b>
Mingbool Range	Don's Quarry	MIS 15	Subaqueous facies	Meteoric-vadose to near surface marine. Mature.	Shell: $377 \pm 86$ to $411 \pm 85$ ka <b>MIS 11</b> Forams: $778 \pm 118$ ka <b>MIS 19-21</b>
Dismal Range	Dartmoor Cemetery	MIS 17	Subaqueous facies with potential swash zone	Near surface marine. Mature.	Forams: $577 \pm 79$ ka <b>MIS 15</b>
	Fort O'Hare Quarry Mingbool village		Subaqueous facies Subaqueous facies	Near surface marine. Mature. Near surface marine. Mature.	Forams: $743 \pm 100$ ka <b>MIS 19</b> Forams: $903 \pm 167$ ka to $936 \pm 130$ ka <b>MIS 21-23</b>

### 6.2.11 Discussion of chronostratigraphy

Geochronological analysis of each barrier across the coastal plain indicates an increase in barrier age with increased distance from the present shoreline. It is evident from AAR results that each of the four most seaward barriers (Robe, MacDonnell, Burleigh and Caveton Ranges) correlates with a successively older interglacial highstand. Landward of Caveton Range uncertainties associated with AAR numeric ages are high and it is difficult to assign each barrier to an interglacial based on AAR results alone.

Interglacials may not be defined by a single sea-level highstand, as highlighted in Chapter 2, but multiple. For example, MIS 5 is comprised of three highstands; MIS 5e (~125 ka), MIS 5c (~105 ka) and MIS 5a (~82 ka), with all three highstands occurring within 50 ka of each other. It is therefore possible that each coastal barrier does not necessarily relate to individual interglacial maximum sea-level highstands but that some of the barriers may be interstadial in age. While sea level during these interstadials may have been lower and thus barriers formed in a more seaward position relative to interglacial maximum barriers, tectonic uplift of the coastal plain could have exposed these barriers above present sea level.

Interstadial sea levels are commonly several metres lower than sea level elevation attained in interglacial maximum highstands and are commonly of a shorter duration. It is therefore suggested that these barriers would be substantially smaller. The barriers described within this thesis are significant features and clearly identifiable within the landscape. The coastal barriers of MacDonnell, Burleigh and Caveton Ranges have been confidently dated to MIS 5e, MIS 7 and MIS 9 respectively through OSL (on MacDonnell Range) and AAR dating (both within this thesis) and TL analyses (Murray-Wallace *et al.*, 1996). MIS 5, MIS 7, and MIS 9 are suggested to have consisted of multiple highstands; up to three during MIS 5 and MIS 7 and at least two during MIS 9 (see Chapter 2). While deposits of MIS 5c and MIS 5a age are identified at Port MacDonnell, no other interstadial barriers have yet been identified and dated between MacDonnell, Burleigh and Caveton Ranges, and it may be that they have not been preserved in the sedimentary record. MIS 11 is suggested to have been a longer interglacial (Loutre and Berger, 2003) consisting of a single sea-level highstand (Imbrie *et al.*, 1984) and is assigned to Gambier Range, the next barrier inland from the MIS 9 Caveton Range. While the more inland barriers are more difficult to define, and Compton Range especially is composed of what appears to be a wide field of dune ridges, the large uncertainties associated with dating these older deposits mean it is not possible to resolve whether certain ridges were formed during interstadials rather than interglacial maximum.

Therefore, with no stratigraphic evidence to the contrary, and in light of the geochronological evidence presented within this thesis, it is proposed that each barrier on the Mount Gambier coastal plain relates to a separate interglacial, as previously proposed by Sprigg (1952).

However, composite barriers, such as Robe Range and Compton Range which potentially formed during more than one sea-level highstand, are also identified through a combination of geochronological analysis and stratigraphic interpretations. As only two to three exposures are analysed along each barrier within this thesis it is possible that other barriers are also composite features but have not been identified because of incomplete exposures of single barriers. It is also possible that the older barriers of Mingbool and Dismal Ranges may have once been overlain by younger sediment (as occurs at Compton Range) but this has been removed through erosional processes.

Reworking of sediments has also been identified through geochronological analysis. D/L values from Burleigh Range were significantly high and potentially reflect sediment reworked from an older source. Sediment within the Holocene beach at Port MacDonnell is significantly older than fossil shell within the same unit and indicates reworking and erosion of older aeolianite units during the Holocene sea-level highstand. Aeolian sands within Robe Range are also suggested to have been reworked during the more arid MIS 3.

Huntley *et al.* (1993a) used TL dating to correlate each successive barrier on Robe coastal plain to a successive interglacial marine oxygen isotope stage. Figure 6.4 attempts to do the same for the Mount Gambier coastal plain barrier successions, and compares these with the correlation of Huntley *et al.* (1993a). Confirmation of each barrier succession with a marine isotope stage will allow for comparison of palaeo-sea level data from the Mount Gambier coastal plain with other global interglacial sea-level highstand records.

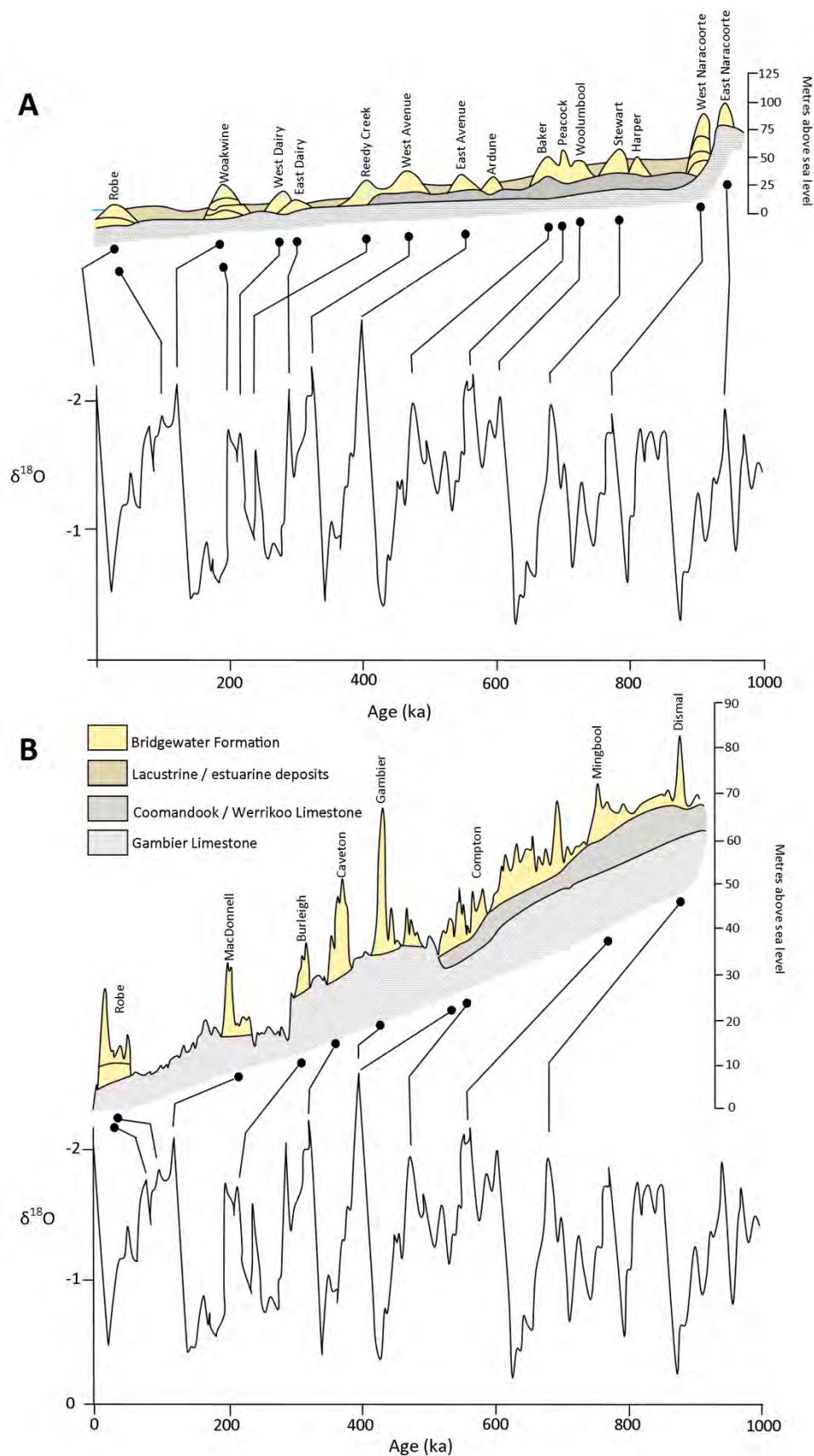


**Figure 6.4:** Correlation of barrier successions on the Robe and Mount Gambier coastal plains with sea-level highstands as identified through the marine oxygen isotope record (Imbrie *et al.* 1984, modified after Huntley *et al.*, 1993). **A:** Transect of barrier successions between Robe and Naracoorte modified after Murray-Wallace *et al.* (1998) and Huntley *et al.* (1993a) and **B:** Transect from Port MacDonnell to Dismal Range, near Mingbool. The location of these transects is highlighted in Figure 6.9.

#### **6.2.12 Comparison of the Bridgewater Formation on the Mount Gambier coastal plain with the stratotype at Bridgewater Lakes, Victoria**

The stratotype of the Bridgewater Formation has been described at Bridgewater Lakes, western Victoria by Boutakoff (1963). At Bridgewater Lakes, calcareous aeolianites are stacked in cliffs and separated by what Boutakoff (1963) describes as an abrasion platform which he related to the Mindel-Riss interglacial sea level in the middle Pleistocene. The aeolianites above and below this abrasion surface were therefore designated to the Lower and Upper Pleistocene respectively. Boutakoff further described reddish-pink to brown soils truncating the dune aeolianites, and identified five separate horizons within the Upper Pleistocene successions exposed within coastal cliffs at Portland. Boutakoff (1963) suggested that the dunes were formed during interglacials and specifically during the gradual regression of the ocean towards the end of a highstand, while the soils developed in advance of more continental environments during glacials. At Bridgewater Lakes, Boutakoff (1963) noted the well-developed karst topography on the aeolianites, including rhizoliths and solution pipes. Aeolian cross-bedding was suggested to be a common feature, with lee slopes identified within high-angle dipping beds.

At the time of Boutakoff's geological descriptions of the Bridgewater Formation in Victoria the marine isotope stages of the Quaternary had yet to be defined in detail (as they were later by Shackleton and Opdyke, (1973) who developed the original work of Emiliani, (1955)). While Boutakoff was able to correlate dune formation to three episodes during the Pleistocene he did not identify specific sea-level highstands that resulted in formation of successive aeolian deposits. However, Boutakoff (1963) correlated the stacked aeolianites in the Portland region with the distinctive barriers on the Mount Gambier coastal plain and suggested that epeirogenic warping had resulted in spatial separation of the units. He suggested that the stacking of the aeolianites within the Portland area indicated the stability of this region and how it acted as a pivot for warping farther to the northwest. Neotectonics in the Mount Gambier region has spatially separated the barriers and allowed for clearer identification of facies architecture and palaeo-sea level indicators.

Previous authors have suggested that the barrier shorelines on the Mount Gambier coastal plain only represented the Middle and Upper Pleistocene (e.g. Crocker and Cotton, 1946; Fairbridge, 1953). However, Boutakoff (1963) supported the hypothesis of Sprigg (1952) that the barriers extended to the Lower Pleistocene, and suggested that deposits under the forested area north of Gambier Dune and south of Mingbool Dune represented such a time period.



The work of Boutakoff (1963) was limited by a lack of geochronological data and the assignment of episodes of dune building relied strictly on litho-stratigraphical interpretations. Since the work of Boutakoff, several geochronological investigations have been conducted on the Robe coastal plain and indicate that barriers do extend to the Lower Pleistocene (e.g. Huntley *et al.*, 1994; Murray-Wallace *et al.*, 2001). This thesis provides further support for Boutakoff's suggestions, and is the first to have conducted geochronological analysis of the older, more landward barriers on the Mount Gambier coastal plain. The present study has identified that the Compton Range, in the region suggested by Boutakoff (1963) to represent the Lower Pleistocene, between Gambier Range and Mingbool Range correlates with MIS 13, while the more landward barriers of Mingbool Range and Dismal Range correlate with MIS 15 and MIS 17 respectively.

A distinct difference can be identified in the spacing of aeolianites of the Bridgewater Formation on the Mount Gambier coastal plain compared with the Portland District, some 75 km southeast (Figure 6.5). It is evident that the closer proximity of the Mount Gambier region to the centres of Quaternary uplift (associated with the Mount Burr – Mount Gambier volcanic province) has resulted in significantly different morphostratigraphical characteristics of the Bridgewater Formation at this locality compared with the stratotype at Bridgewater Lakes.

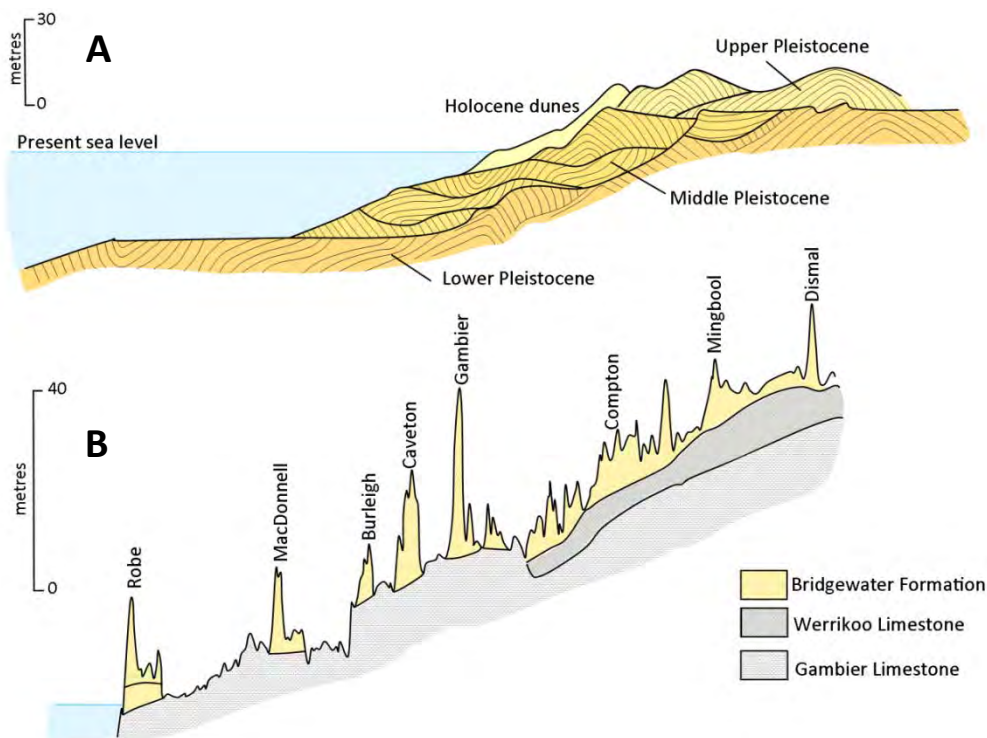


**Figure 6.5:** Comparison of cross-sections of the Bridgewater Formation at its type section locality at Cape Bridgewater (A; after Boutakoff, 1963) with the Mount Gambier coastal plain examined in this thesis (B).

### 6.3 Sea-level history of the Mount Gambier coastal plain

The global Quaternary palaeo-sea level record provides an important archive and potential analogue for inclusion in models of future sea-level change. Few records of palaeo-sea level, derived from palaeo-shorelines, span more than the past four interglacial sea-level highstands. The determination of a chronostratigraphy for the Mount Gambier coastal plain has identified that the succession of barrier shorelines in this region spans at least seven interglacial sea-level highstands back to and including MIS 17 (~680 ka). The palaeo-sea level record preserved on the Mount Gambier coastal plain is significant due to the location of the southern Australian margin within a far field with respect to glacio-isostasy adjustment effects from Quaternary ice sheets, which results in a sea-level record not significantly affected by glacio-isostasy. While the Mount Gambier coastal plain preserves only a local sea-level record for the middle Pleistocene to Holocene, it can be compared with other global records to aid in further understanding the controls and dynamics of past climatic and oceanic systems.

The calculation of past sea level relies on knowledge of the tectonic history of a region, the identification of reliable sea-level indicators, and a modern analogue with which to compare sea-level indicators to current mean sea level. On the Mount Gambier coastal plain rates of uplift have previously been calculated to  $0.13 \text{ mm yr}^{-1}$  by Murray-Wallace *et al.* (1996). They proposed that 16 m of uplift had occurred during the past 125 ka by identifying a lagoonal facies 18 m APSL at the south-eastern extent of Woakwine Range, which they determined was of last interglacial age through AAR analysis of fossil shell. Murray-Wallace *et al.* (1996) then applied the last interglacial sea-level datum of +2 m (derived by Murray-Wallace and Belperio (1991) from Eyre Peninsula, South Australia) to determine the rate of uplift. Quaternary volcanism associated with the Mount Burr volcanic province is suggested to have resulted in steady, continual uplift of the coastal plain over the middle Pleistocene (Murray-Wallace *et al.*, 1998), and has been further confirmed by Murray-Wallace *et al.* (2001), who identified a linear correlation with interglacial back-barrier lagoon facies and distance from the present shoreline. Mount Gambier and Mount Schank erupted during the Holocene, after the formation of the barrier shorelines, with Mount Schank erupting through the side of Burleigh Range. The influence of these Holocene volcanoes on the rates of uplift within the region is unknown. In view of the limited data available to evaluate the effects of these more recent volcanic eruptions on uplift rates, this thesis adopts the uplift rates previously determined by Murray-Wallace *et al.* (1996) but acknowledges the complexities of this issue and discusses this further with respect to the limitation and reliability of results in the following section (6.4).

Within this thesis, palaeo-shoreline indicators are identified as far west as Lake Hawdon South near Robe and as far east as Narrawong, Victoria (Figure 6.1). Uplift rates have yet to be determined for the eastern portion of the Mount Gambier coastal plain. Narrawong, unlike all other sites analysed within this thesis, is found to the east of the Kanawinka Fault, and therefore the uplift history of this region is complicated by the presence of this and the Swan Lake fault (White, 2000). Results of AAR analysis on foraminifera and skeletal carbonate sands by the whole-rock method from this thesis confirm the findings of Sherwood *et al.* (1994) that this site is last interglacial in age.

The last interglacial shoreline in Australia has been shown to vary significantly around its margin (Murray-Wallace and Belperio, 1991). U-series dating of coral reefs in Western Australia have suggested that MIS 5e sea level was 3-4 m APSL (e.g. Stirling *et al.*, 1998) with recent findings suggesting a large jump in sea level at the end of the interglacial to +9 m (O'Leary *et al.*, 2013). However, this has yet to be validated by the identification of other last interglacial deposits at this height within its vicinity. In Victoria, analyses of last interglacial sedimentary successions have suggested that sea level was up to 7.5 m APSL between Cape Nelson and Warrnambool (Gill, 1967, 1988; Kenley, 1988). Therefore, it is not valid to apply the last interglacial sea-level datum of +2 m of Eyre Peninsula to the Narrawong region due to the variability of MIS 5e sea level around the Australian coastline and the distance (700 km) between the two sites. Further understanding of the tectonic uplift of the region is also required. A palaeo-sea level estimate for the Narrawong region is therefore not calculated within this thesis. Several study sites within this thesis, especially within the more landward barrier successions, are located in western Victoria, near the town of Dartmoor, 50 km east of Mount Gambier (Figure 6.1). As the elevation of a last interglacial shoreline within the Nelson region, directly shoreward of Dartmoor, has not been identified, there are no valid data to construct an uplift rate for this region. Palaeo-sea-level estimations for western Victoria are therefore not calculated either.

Chappell (1987) described sea-level indicators as being either fixed or relational. Fixed sea-level indicators are always located within a restricted elevation with respect to sea level, such as intertidal mangrove forests or coral microatolls. Relational sea-level indicators are less reliable as they only infer a sea-level elevation relative to that marker and may occupy a wide elevation range with respect to mean sea level. Examples of relational sea-level indicators include marine molluscs which can occupy a wide range of depths, such as *Ostrea angasi*, which may be found within the tidal zone or up to 30 m below the sea surface (Ludbrook,

1984). Aeolian deposits are also relational sea-level indicators as they are always deposited above mean sea level. A range of palaeo-sea level markers are identified across the Mount Gambier coastal plain, including lagoonal, subaqueous, beach and aeolian facies. The stratigraphy of each of these deposits is described in Chapter 3. Palaeo-beach facies, such as the flint conglomerate at Port MacDonnell and flint lenses within Burleigh Range, can be used as fixed sea-level indicators if modern analogues of these facies are present at the modern coastline and the position of these facies can be inferred in relation to present sea-level. The modern beach at Port MacDonnell and the flint-cobble-dominated beach ridges at Racecourse Bay provide direct analogues to both the flint conglomerate and the exposure within Burleigh Range respectively. Lagoonal facies are suggested to provide a more reliable indicator of mean sea level at their time of deposition (Murray-Wallace, 2002). However, accurate determination of post-depositional influences such as compaction and denudation are required before assessment of palaeo-sea level can be confidently undertaken. Lagoonal facies are identified on the Mount Gambier coastal plain in the lee of Burleigh and Caveton Ranges. Other subaqueous facies (deposited on the sea floor in the shoreface or offshore zones) have predominantly been identified in older barriers across the coastal plain and this pattern may be a result of denudation through lengthier exposure to erosion, causing removal of any overlying aeolian facies. Subaqueous facies (i.e. non-lagoonal) are thus a relational sea-level indicators as sea-level must have been at least as high as this in the past. Results of palaeo-sea level elevation across the Mount Gambier coastal plain are presented in Table 6.2.

**Table 6.2:** Interglacial palaeo-sea levels derived from sample sites within Bridgewater Formation successions across the Mount Gambier coastal plain, southern Australia

Dune Range / sample site	Geochronological age*	Palaeo-sea level indicator and current height APSL	Relational or fixed indicator?	Rate of uplift	Palaeo-sea level height
Raised Holocene beach, Port MacDonnell	3 ka (MIS 1)	Flint cobble and shell beach deposit – 1 m APSL	Fixed	0.13 mm yr <sup>-1</sup>	0.5 m ± 2 m
Robe Range, Port MacDonnell, flint conglomerate	105 ka (MIS 5c)	Well-cemented palaeo-beach – present sea level	Fixed	0.13 mm yr <sup>-1</sup>	-14 ± 2 m
Woakwine Range, Lake Hawdon South	125 ka (MIS 5e)	Lagoonal facies landward of Woakwine Range – 9 m APSL	Fixed	0.07 mm yr <sup>-1</sup>	0.25 m ± 1 m
Burleigh Range, Rabbitors Road	250 ka (MIS 7e)	Flint cobble beach facies – 34 m APSL	Fixed	0.13 mm yr <sup>-1</sup>	1.5 m ± 2 m
Burleigh Range, Laslett Road	250 ka (MIS 7)	Lagoonal facies – 36 m APSL	Fixed	0.13 mm yr <sup>-1</sup>	3.5 m ± 1 m
Caveton Range, Rabbitors Road	322 ka (MIS 9)	Lagoonal facies – 38 m APSL	Fixed	0.13 mm yr <sup>-1</sup>	-3.5 m ± 1 m
Gambier Range, Gooch Road	420 ka (MIS 11)	Subaqueous facies – 50 m APSL	Relational	0.13 mm yr <sup>-1</sup>	Higher than -2 m
Compton Range, Baxter's Quarry	488 ka (MIS 13)	Subaqueous facies – 45.85 m APSL	Relational	0.13 mm yr <sup>-1</sup>	Higher than -18 m
Compton Range, Heritage Industries	490 ka (MIS 13)	Subaqueous facies – 47 m APSL	Relational	0.13 mm yr <sup>-1</sup>	Higher than -16.5 m
Mingbool Range, Don's Quarry	570 ka (MIS 15)	Subaqueous facies – 46 m APSL	Relational		
Dismal Range, Dartmoor Cemetery	680 ka (MIS 17)	Subaqueous facies – 50 m APSL	Relational		
Dismal Range, Fort O'Hare Quarry	680 ka (MIS 17)	Subaqueous facies – 45 m APSL	Relational		
Dismal Range, Mingbool village	680 ka (MIS 17)	Subaqueous facies - 70 m APSL	Relational	0.13 mm yr <sup>-1</sup>	Higher than -14.5 m

\*Geochronological age is based on AAR, radiocarbon and OSL analysis and correlation with the marine oxygen isotope record (e.g. Lisiecki and Raymo, 2005) for more inland deposits where precision is reduced.

## 6.4 Reliability and significance of results

Uncertainties in palaeo-sea level estimations are derived from limitations of the geochronological techniques applied and the precision of palaeo-sea level indicators. The following discussion outlines the limitations of both these variables and the methods sought to overcome these in order to evaluate the significance to the sea-level record derived from the Mount Gambier coastal plain.

Three geochronological techniques were applied to barrier successions within this study, each with specific limitations. Radiocarbon analysis was conducted on fossil marine shell of proposed late Pleistocene and Holocene age. The timing of deposition of several aeolian successions on the Mount Gambier coastal plain was constrained by OSL analysis. Murray-Wallace and Woodroffe (2014) suggested that OSL is potentially the most accurate method for determining the age of coastal landforms, as it determines the timing of deposition, yet is less precise than radiocarbon or U-series dating. The limitations of both radiocarbon and OSL analysis have previously been outlined in section 5.2.

AAR is the primary geochronological method used in this thesis, and while it can potentially date samples back to over one million years in this region, several limitations of the technique are recognised (section 5.3.7). AAR can generate numerical ages when rates of racemisation are calibrated against independently dated deposits, as has been done in this thesis using radiocarbon and OSL. AAR and radiocarbon compare well as dating techniques as both generally, within short-lived organisms, date the time of death of an organism. OSL, however, dates the timing of deposition of sediment, which may not directly correlate with the death of organisms within that sediment. The OSL sample used for calibration curve construction was deemed suitable as it yielded a more reliable age than that previously derived for the correlative of the deposit through U-series dating by Schwebel (1978; 1984). Due to the non-linear kinetic pathway of AAR (Wehmiller, 1981), multiple calibration points are required at varying time intervals to create a robust calibration curve. Within this thesis, calibration points of Holocene and last interglacial (MIS 5e) age were used, though to increase the accuracy of numerical ages derived, more calibration points, particularly between the two existing points, would be required. However, due to the slow uplift of the Mount Gambier coastal plain and as sea level was significantly lower during MIS 3 (~50 m BPSL, Lambeck and Chappell, 2001), suitable calibration deposits of ~60 ka are not preserved above present sea level. U-series dating is commonly used in dating palaeo-coastal successions and to calibrate

AAR, but the temperate waters of the Bonney Shelf do not promote coral growth and U-series analysis of fossil shell is inappropriate (Kaufman *et al.*, 1971).

The use of AAR in constraining the age of deposits is limited in its resolution. While AAR can be used to determine the interglacial that sediment was deposited in, it does not have the resolution to differentiate interstadial events or ascertain when during an interglacial a sea-level highstand maximum was attained. This information would be useful in constraining sea-level highstand maxima in the far-field with respect to Quaternary icesheets compared with near-field zones. Higher-resolution U-series dating has been conducted primarily on coral reef terraces in the near field to Quaternary ice sheets (e.g. the Bahamas) and highlights a limitation of the palaeo-sea level data derived from the Mount Gambier coastal plain.

Throughout this research, multiple methods have been adopted to overcome the potential limitations in geochronological applications. These include: the collection of multiple sub-samples to account for reworked sediment or shell and intra-shell variation, the use of multiple geochronological techniques where possible at samples sites to increase dating accuracy, SEM analysis of foraminifera to identify extensive diagenesis, the rejection of samples that appear cemented or recrystallised before analysis, and the rejection of samples yielding D/L values of less than 0.1 for the unstable amino acid serine, which may indicate contamination of the sample with younger carbonates.

The primary limitation in the estimation of palaeo-sea level on the Mount Gambier coastal plain is the assumption associated with tectonic uplift history and how this has varied spatially and temporally. Uplift calculations are based on the assumption that MIS 5e sea-level reached +2 m APSL 125 ka, which is suggested by Murray-Wallace and Belperio (1991) to be the most consistent sea-level datum within southern Australia. As the distance between Eyre Peninsula and Mount Gambier is only 500 km, this datum is assumed to be applicable. It is also assumed that tectonic uplift of the coastal plain has been constant since the middle Pleistocene, as suggested by Murray-Wallace *et al.* (2001) from the linear relationship between the elevation of successive back-barrier lagoonal facies and distance from the present coastline. However, the effects of Holocene volcanism associated with Mount Gambier and Mount Schank on rates of uplift have not previously been identified. From the subcrop map of Gambier Limestone (Figure 6.6), it is evident that some crustal doming is associated with Mount Gambier and to a lesser extent with Mount Schank. The lack of previous data concerning exploration of this concept prevents an accurate evaluation of the volcanoes' influence on uplift rates; this is acknowledged as a limitation of the derived dataset with

further work suggested to concentrate on constraining uplift rates with greater precision. Coastal successions of last interglacial age have not been described landward of the town of Dartmoor, hampering the determination of uplift rates specific to western Victoria.

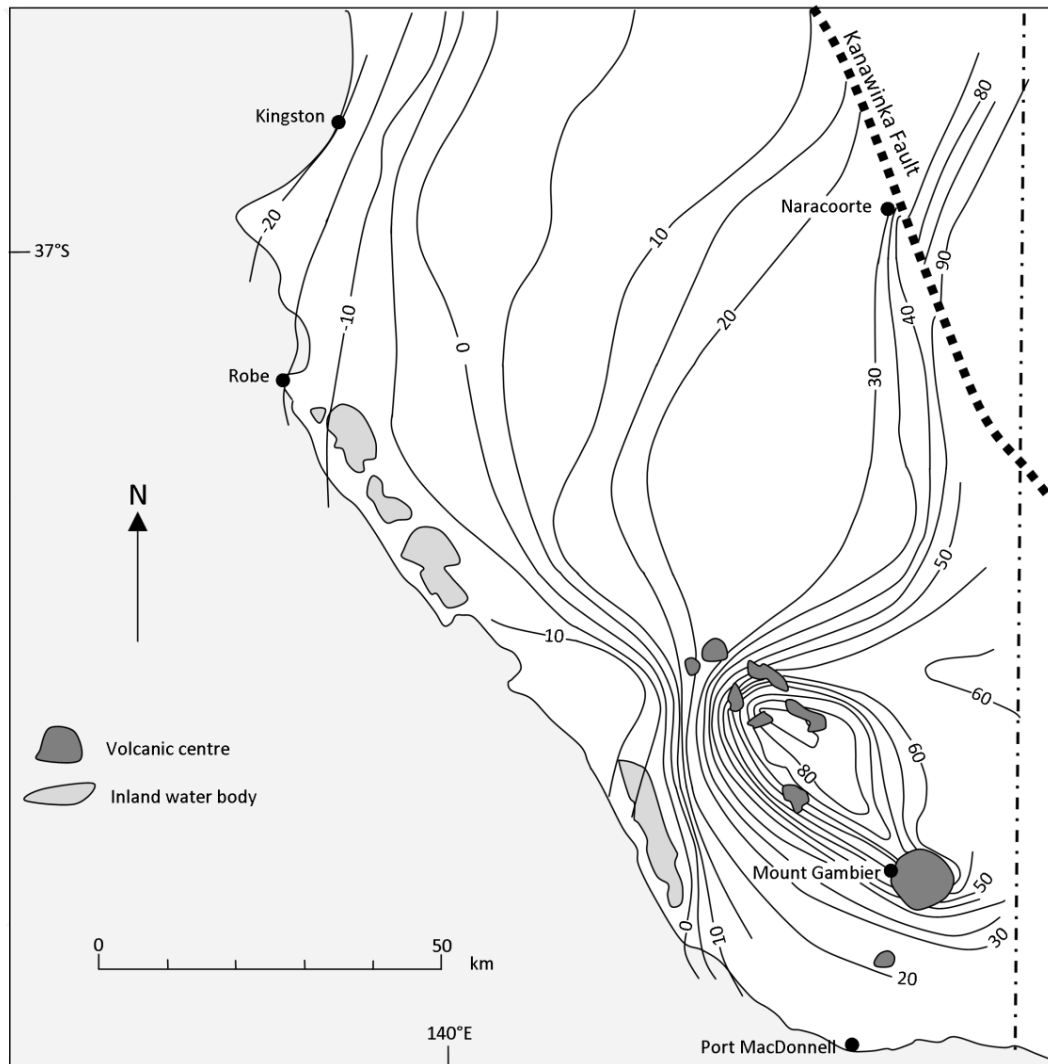


**Figure 6.6:** Subcrop map of the elevation of the upper surface of the Oligo-Miocene Gambier Limestone indicating crustal doming associated with centres of Quaternary volcanism (modified from Murray-Wallace *et al.*, 1998).

Palaeo-sea level estimations across the Mount Gambier coastal plain are also limited by the types of sea-level indicators recognised. Fixed sea-level indicators are identified as palaeo-beach facies within Burleigh Range and the flint conglomerate on Port MacDonnell Beach as well as lagoonal facies leeward of Burleigh and Caveton Ranges. However, the majority of identified sea-level indicators are relational subaqueous or aeolian facies. The correlation of lagoonal and aeolian facies to sea-level elevation is restricted by the lack of modern analogues within the Port MacDonnell region and relies on comparisons with the



Younghusband Peninsula and Coorong lagoon, approximately 100 km northwest of Port MacDonnell. Estimates of past sea level are also limited by the extensive vertical depth range of several commonly identified molluscan species (*Pecten benedictus*, *Ostrea angasi*, and *Chlamys asperrima asperrima* can be located up to 30 m below sea level; Ludbrook; 1984), and the high energy conditions of the coastline, which results in a fair-weather wave-base depth of 100 m (James *et al.*, 1992).

### Summary

Certain limitations are recognised within this research. Where possible, the limitations of geochronological techniques have been minimised by analysing multiple sub-samples and various material within each barrier succession. All possible uncertainties associated with these methods have been accounted for in calculation of numeric ages; resulting in a reduction in precision, but accurate results. Palaeo-sea level estimations are limited by assumptions associated with uplift, the unknown uplift rate of the Dartmoor region and the influence of Holocene volcanism on uplift rates. However, in light of a lack of evidence to evaluate otherwise, the previously determined uplift rate of Murray-Wallace *et al.* (1996) is used and further work on constraining uplift rates is proposed later in the chapter (section 6.8). Estimations of past sea level are also limited by the number of identified relational sea-level indicators and the lack of direct analogues at the Port MacDonnell coastline, relying on the relationship of these facies to present sea level north of Robe (Younghusband Peninsula) and east of Nelson (Discovery Bay).

It is recognised that the sea-level indicators identified on the Mount Gambier coastal plain commonly only define sea-level at one time during the interglacial highstand, and may not represent the maximum sea level attained. While derived geochronological results are not as precise as those from U-series dating of coral reefs (for example, within the Caribbean and tropical Pacific), the sea-level record on the Mount Gambier coastal plain is significant as an extensive archive of palaeo-sea level within a far field site from Quaternary ice sheets.

## 6.5 Comparison with barrier successions of the Robe coastal plain

The coastal plain from Robe to Naracoorte also preserves a lengthy record of interglacial sea-level highstands. Previous research has concentrated on constraining the depositional timing of these successions (Huntley *et al.*, 1993a, 1994; Murray-Wallace *et al.*, 1999, 2001). The following discussion compares the geochronology and inferred palaeo-sea level elevations between the Mount Gambier and Robe coastal plains to assess if they are correlative features and to resolve any discrepancies between depositional timing and sea-level elevation. The

overall morphology of the barriers is also compared using SRTM data. This section concludes by summarising the principal contributions of this thesis to the understanding of the palaeo-sea level history of southern Australia throughout the Quaternary.

#### **6.5.1 AAR geochronology**

AAR was used to constrain the timing of sea-level highstands on the coastal plain between Robe and Naracoorte (Murray-Wallace *et al.*, 2001) and in the River Murray mouth region (Murray-Wallace *et al.*, 2010). Farther northwest along the coastline, with increased distance from the Mount Burr - Mount Gambier volcanic province, shoreline barriers are more closely spaced and commonly coalesce in the River Murray mouth region.

D/L values from whole-rock analysis of interglacial deposits from the Mount Gambier coastal plain derived in this study were compared with D/L values of whole-rock analysis on Bridgewater Formation sediments from the River Murray mouth and Robe regions (Figure 6.7). Results from the River Murray mouth and this study are reported for glutamic acid and were derived using RP-HPLC. On the Robe coastal plain results are reported for leucine and were derived by GC. Leucine D/L values were not reported for this study as D- and L-peaks were derived towards the end of the run and commonly found to be small and unreliable; a problem previously noted with the RP-HPLC technique (Wehmiller, 2013b). To overcome this problem, comparisons were made to results in this study for glutamic acid because leucine is shown to have a similar rate of racemisation to glutamic acid (Figure 5.6). Murray-Wallace *et al.* (2010) compared whole-rock D/L values derived from GC analysis with those derived by RP-HPLC from the River Murray mouth and revealed that consistently lower D/L values were derived by GC.

D/L values are generally lower for whole-rock samples from the Mount Gambier coastal plain across the middle Pleistocene compared with the Robe coastal plain and the River Murray mouth region (Figure 6.7). Whole-rock D/L values are also generally lower at Robe than in the River Murray mouth region. This likely reflects the temperature difference between the regions. Current mean annual temperatures (CMAT) for the River Murray mouth, Robe and Mount Gambier coastal plains are 15.5°C, 14.7°C and 14.04°C respectively. It is likely that effective Quaternary temperature (EQT) has always been higher farther northwest along the coastline, and thus racemisation rates will have been higher at the River Murray mouth with respect to Robe and Mount Gambier. This finding highlights how racemisation rates can vary within only 400 km between sample sites and the problems associated with comparing D/L values or amino zones from different global sites.

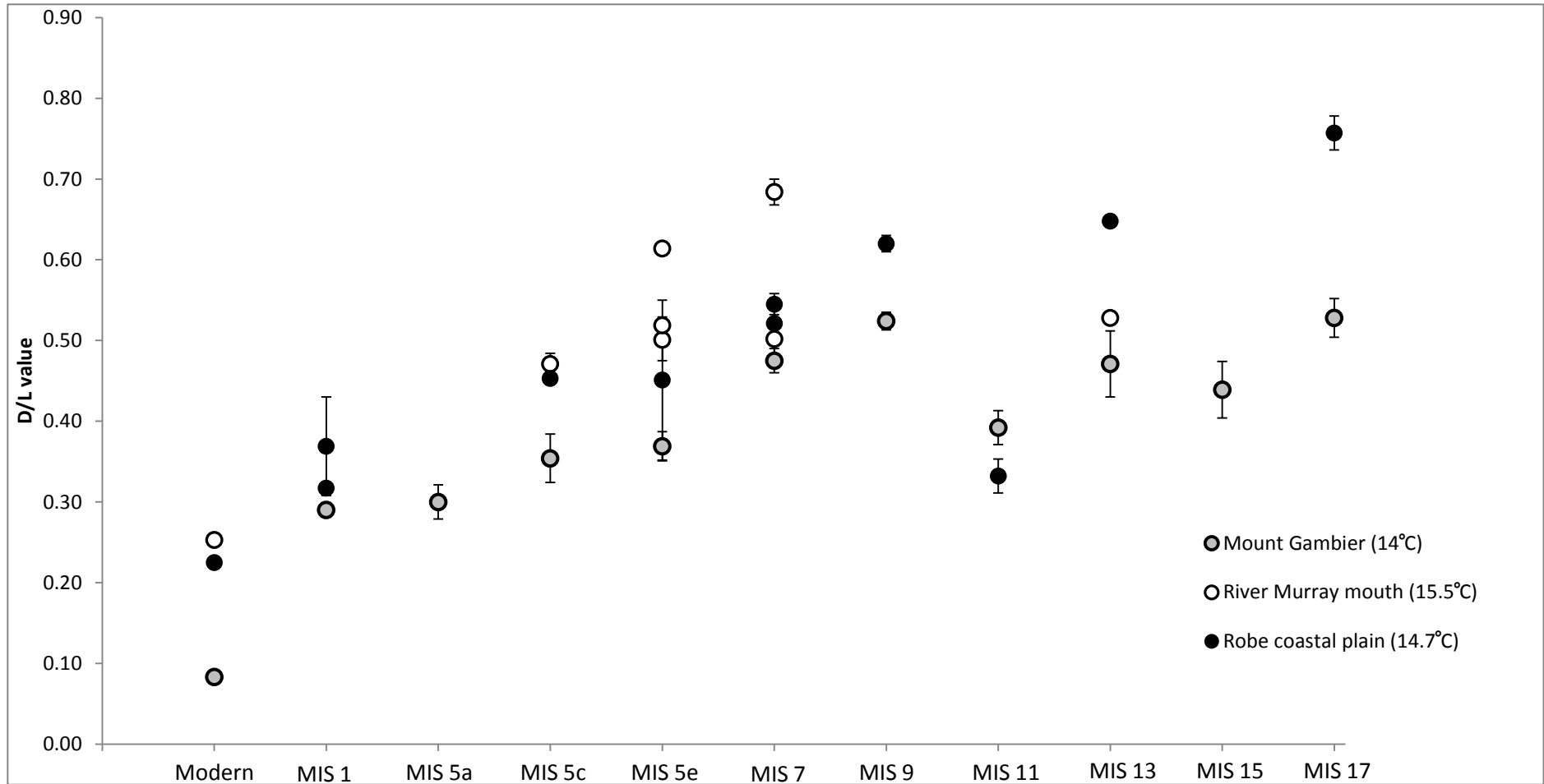


**Figure 6.7:** Extent of racemisation (total hydrolysable amino acids) within skeletal carbonate sands analysed by whole-rock analysis from Bridgewater Formation successions on the Mount Gambier coastal plain (this study), Robe coastal plain (Murray-Wallace *et al.*, 2001) and the River Murray mouth region (Murray-Wallace *et al.*, 2010). D/L values are plotted against the proposed MIS that the barrier was deposited during, based on the geographical location and dating of the deposit by other geochronological techniques. Uncertainties are to 1  $\sigma$ . D/L values from Mount Gambier and the River Murray mouth are presented for GLU while those from Robe are for LEU. Up to 10 sub-samples are averaged for samples from Mount Gambier and 3-6 sub-samples from the River Murray mouth.

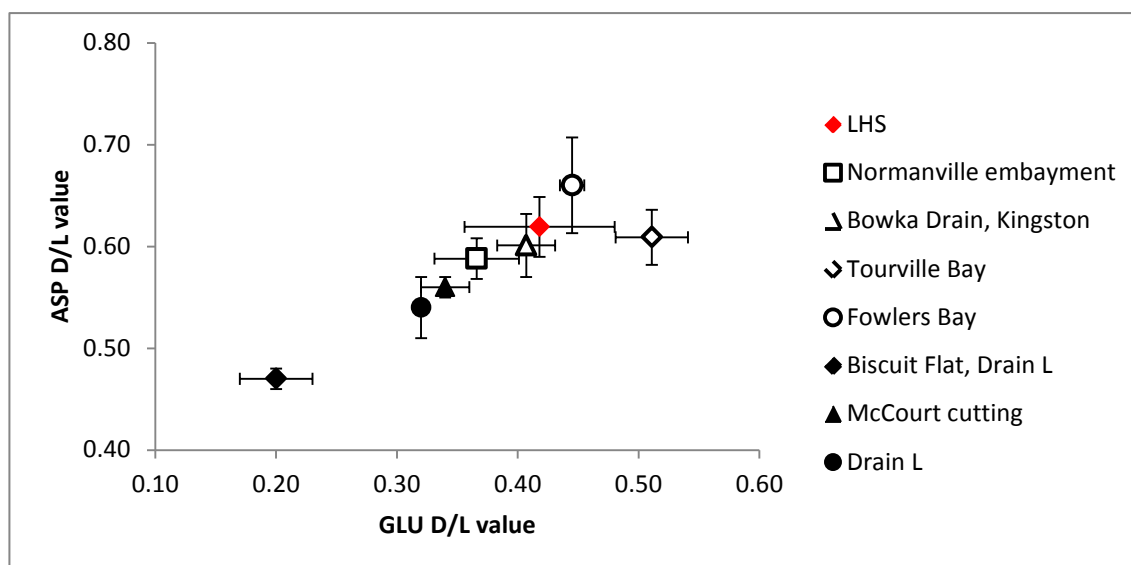


**Figure 6.8:** Scatter plot of aspartic acid (ASP) and glutamic acid (GLU) D/L values derived from *Katelaysia rhytiphora* from last interglacial deposits between Robe and the River Murray mouth. Solid-filled data points were derived by GC and are reported by Murray-Wallace *et al.* (1999) from the Woakwine Range near Beachport. Open data points were derived by RP-HPLC and were derived and reported by Murray-Wallace *et al.* (2010) from the River Murray mouth region. LHS = Lake Hawdon South, and was derived in this study using RP-HPLC.

D/L values derived for whole-rock increase with older interglacials back to and including MIS 9 (Figure 6.7). The MIS 11 barriers on the Robe and Mount Gambier coastal plain (East Avenue and Gambier Ranges respectively) both yielded lower D/L values than anticipated. In East Avenue Range Murray-Wallace *et al.* (2001) attributed this to the loss of lower molecular weight, highly racemised amino acids from the sediment. While D/L values on the Robe coastal plain continue to increase with later interglacials, D/L values from the Mount Gambier and the River Murray mouth regions do not obtain values as high as those recorded for MIS 9 in older sediments. This may indicate a potential age ceiling to the whole-rock method within these regions. This also reflects leaching of amino acids from sediments within older barriers within the Mount Gambier region. The lack of a distinct calcrete surface overlying these deposits indicates that they may have been poorly preserved. Results might also suggest leucine is a more suitable amino acid to use compared with glutamic acid for whole-rock analysis of middle Pleistocene deposits.

The extent of racemisation in *Katelaysia rhytiphora* from several last interglacial sites across southern Australia can also be compared (Figure 6.8). No significant difference is identified between samples from the River Murray mouth region and those from Lake Hawdon South, near Robe (derived in this thesis), despite differences in EQT.

The geochronology from the Mount Gambier coastal plain generally compares well with that of the Robe coastal plain derived by Murray-Wallace *et al.* (2001). OSL analysis suggests that MacDonnell Range is a correlative of the last interglacial (MIS 5e) Woakwine Range. Results of AAR analysis of foraminifera from a back-barrier lagoonal facies of Burleigh Range confirm it is a correlative of MIS 7 Reedy Creek Range. Caveton Range is confirmed to have been deposited during MIS 9 and correlated with West Avenue Range, while Gambier Range correlates with East Avenue Range. Older barriers are not as laterally extensive along their strike and thus determining correlative units based on their geomorphological positioning alone is difficult. OSL analysis of aeolian facies in Compton Range confirm it is at least MIS 11 in age, while its geographical position as the fifth barrier landward of the present coastline indicates core deposition occurred during MIS 13, and thus corresponds with Baker Range. AAR uncertainty terms increase significantly within the most landward barriers, though age ranges overlap between Harper and Dismal Ranges which are suggested to have formed during MIS 17. The aminostratigraphic correlation between the two regions supports the early work of Sprigg (1952) who suggested that the barriers within each region were correlatives.

#### **6.5.2 Palaeo-sea level reconstruction**

The elevation of palaeo-sea level reconstruction from the Mount Gambier and Robe coastal plains compare well in general (Table 6.3), despite varying uplift rates between the two regions. Palaeo-sea level estimates from the Robe coastal plain (Murray-Wallace *et al.*, 2001) have been defined from lagoonal facies, which have a greater precision as sea-level markers than the range of beach facies identified on the Mount Gambier coastal plain.

MIS 5c sea level is estimated at -9 m for Robe III at Robe Harbour, while a lower sea level of  $-14 \pm 2$  m is suggested for Port MacDonnell. Sea-level estimates vary for MIS 7, with sea level similar to present as indicated from lagoonal facies of the Reedy Creek Range, while interpretations from Burleigh Range suggest a MIS 7 sea level between +1.5 and +3.5 m APSL. MIS 9 sea level is indicated to be lower than present in both regions; -1m at West Avenue Range and -3.5 m at Caveton Range. A sea level of -3 m is reported for MIS 11 from lagoonal facies at East Avenue Range (Murray-Wallace *et al.*, 2001), while a minimum sea level of -2 m is suggested from subaqueous deposits within Gambier Range. Sea level for MIS 13 is estimated at -1 m from Baker Range, while estimates from Compton Range are limited by the dominance of exposures of subaqueous facies and suggest sea level must have been higher than -16.5 m. Lagoonal facies of the Harper Range suggest a MIS 17 sea level of -1 m, while

subaqueous facies analysed within this study suggest that MIS 17 sea level was at least -14.5 m at Dismal Range.

The elevation of palaeo-sea level markers varies between the Mount Gambier and Robe coastal plains due to differences in regional uplift rates (Figures 6.10 and 6.11). Figure 6.14 compares the sea-level elevations derived by Murray-Wallace *et al.* (2001) for the Robe coastal plain with the morphology of the barriers of the Mount Gambier coastal plain as determined by SRTM data, accounting for the differential uplift rates within this region. From Figure 6.14 it is observed that certain sea-level highstands can flood behind previously formed barrier successions, resulting in the formation of composite deposits. For example, the MIS 11 highstand (even when a value of -1 m is used) may have at some point during the interglacial (possibly before Gambier Range was so vertically extensive) flooded the previously deposited Compton Range, assuming the height of Compton Range has not varied significantly since that time. This provides an explanation for the MIS 11 aeolian facies, recognised through OSL analysis, at Baxter's Quarry within Compton Range.

From Figure 6.14 it may also be suggested that denudation has occurred within the landward regions of the Mount Gambier coastal plain. Derived MIS 15 and MIS 17 palaeo-sea levels (from the Robe coastal plain record) flood over Mingbool and Dismal Ranges, with no sediment found above sea-level for either barrier. This supports the stratigraphical evidence; a lack of capping calcrete horizons and aeolian facies, that more sediment previously overlaid these deposits but has since been eroded resulting in a more subdued barrier profile.

Differences between palaeo-sea level elevations within the two regions may relate to the precision of preserved palaeo-sea level markers. Lagoonal facies are recognised behind each successive barrier on the Robe coastal plain, but not within the Mount Gambier region, where a greater range of sea-level indicators with increased tidal ranges are identified. A paucity of reliable palaeo-sea level indicators within older barrier successions, especially in the Mount Gambier region means that distinguishing palaeo-sea level elevation is challenging.

Variation in sea-level estimations may also be related to differences in uplift history calculations, where these have not been accurately described spatially and temporally for each region or inaccuracies in geochronological analysis, whereby an incorrect interglacial age is assigned to a deposit significantly altering the calculation of palaeo-sea level. Ultimately, estimations rely on the preservation of sedimentary structures representing reliable sea-level indicators.

**Table 6.3:** Comparison of derived numeric ages and palaeo-shorelines between the Robe and Mount Gambier coastal plains, southern Australia

Direct comparison of derived radiocarbon ages and palaeo shorelines between the Robe and Mount Gambier coastal plains, southern Australia								
Robe coastal plain					Mount Gambier coastal plain			
Dune Range	Geochronological age (ka)	Derived palaeo-sea level (m)	Reference	CaCO <sub>3</sub> (%)	Equivalent dune range	Geochronological age (ka)	Derived palaeo-sea level (m)	CaCO <sub>3</sub> (%)
Younghusband Holocene (Fresh Dip Lake)	(estimated 7 ka) 3.68 ± 0.11 ( <sup>14</sup> C)	0	Murray-Wallace (2002) Murray-Wallace <i>et al.</i> (1996)		Holocene raised beach, Port MacDonnell	2.8 ± 0.25 ( <sup>14</sup> C) 3.5 ± 0.9 (AAR)	+0.5 ± 2	99
					Robe II, Port MacDonnell & Shelly Beach	53 ± 4 (OSL) 52 ± 8 to 87 ± 19 (AAR)		99
Robe III (MIS 5c)	116 ± 6 (TL) 127 ± 24 (AAR)	-9	Huntley <i>et al.</i> (1993a, 1994) Murray-Wallace <i>et al.</i> (2001)	81	Robe III, Port MacDonnell and Shelly Beach	63 ± 10 to 106 ± 18 (AAR)		99
					Flint conglomerate, Port MacDonnell	103 ± 23 (AAR)	-14 ± 2	
Woakwine I (MIS 5e)	132 ± 9 (TL)	+2	Huntley <i>et al.</i> (1993a, 1994)	81	MacDonnell Range	124 ± 10 (OSL)		97
Woakwine at Narrawong (MIS 5e)			Sherwood <i>et al.</i> (1994)		MacDonnell Range at Narrawong	100 ± 13 to 155 ± 33 (AAR)		94
					Biscuit Drain, Lake Hawdon South	115 ± 29 to 170 ± 36 (AAR)	+ 0.3 ± 1	
Woakwine II (MIS 7a)	230 ± 11 (TL) 214 ± 41 (AAR)	-6	Huntley <i>et al.</i> (1993a, 1994) Murray-Wallace <i>et al.</i> (2001)	82				
Reedy Creek (MIS 7e)	258 ± 25 (TL) 251 ± 48 (AAR)	0	Huntley <i>et al.</i> (1993a, 1994) Murray-Wallace <i>et al.</i> (2001)	55	Burleigh Range, Laslett Road	224 ± 35 to 289 ± 59 (AAR)	+ 3.5 ± 1	
Burleigh Range (Beach facies)	237 ± 16 (TL)				Burleigh Range, Rabbitors Road	98 ± 17 to 427 ± 57 (AAR)	+1.5 ± 2	93
West Avenue (MIS 9)	342 ± 32 (TL) 382 ± 73 (AAR)	-1	Huntley <i>et al.</i> (1993a, 1994) Murray-Wallace <i>et al.</i> (2001)	83	Caveton Range, Bucks Hill	270 ± 41		97
Caveton Range (Lagoonal facies)	320 ± 22 (TL)		Huntley <i>et al.</i> (1993a, 1994)		Caveton Range, Rabbitors Road	184 ± 40 to 402 ± 60 (AAR)	-3.5 ± 1	87
East Avenue (MIS 11)	414 ± 29 (TL)	-3	Huntley <i>et al.</i> (1993a, 1994)	55	Gambier Range, Gooch Road	581 ± 90 ka (AAR)	Higher than -2	88
Baker (MIS 13)	456 ± 37 (TL) 438 ± 83 (AAR)	-1	Huntley <i>et al.</i> (1993a, 1994) Murray-Wallace <i>et al.</i> (2001)	73	Compton Range, Baxter's Quarry	390 ± 35 (OSL) 393 ± 81 to 488 ± 82 (AAR)	Higher than -18	66
					Compton Range, Heritage Industries	363 ± 65 to 587 ± 97 (AAR)	Higher than -16.5	90
Peacock/Woolumbool (MIS 15)		0	Murray-Wallace (2002)		Mingbool Range, Don's Quarry (MIS 15)	411 ± 97 to 778 to 118 (AAR)		96
Harper/Stewart (MIS 17)	585 ± 44 (TL) 693 ± 132 (AAR)	-1	Huntley <i>et al.</i> (1993a, 1994) Murray-Wallace <i>et al.</i> (2001)	58	Dismal Range, Dartmoor Cemetery	577 ± 79 (AAR)		96
					Dismal Range, Fort O'Hare Quarry	743 ± 100 (AAR)		75
					Dismal Range, Mingbool village	793 ± 110 to 903 ± 167 (AAR)	Higher than -14.5	99
West Naracoorte (MIS 19)	800 ± 100 (TL) 543 ± 102 (AAR)	0	Huntley <i>et al.</i> (1993a, 1994)	90				

### 6.5.3 Morphology of the barrier shorelines

SRTM imagery allows for direct comparison of the overall morphology of barrier shorelines between the Mount Gambier and Robe coastal plains. Figure 6.12 displays transects across both coastal plains derived from SRTM data and ArcGIS software. The significant difference in uplift rates between the two regions is visible resulting from the proximity of each site to centres of Quaternary volcanism. The base of Dismal Range is 65 m APSL and 45 km landward of the coast, while the base of the correlative Harper Range is only 45 m APSL and 80 km from the present coastline, illustrating the closer spacing of barriers as a result of slower uplift rates on Robe coastal plain. In western Victoria, SRTM data yields a spatially different transect (Figure 6.13). The increased distance from Quaternary volcanic centres of the Mount Burr - Mount Gambier volcanic province results in an apparent coalescing of barriers in the Nelson region, whereby barrier shorelines of successive interglacials have potentially formed on top of one another. Further geochronological analysis, and potential drilling of the deposit would be necessary to confirm this hypothesis. Mingbool Range and Dismal Range are identifiable landward of the Glenelg River; potentially suggesting the Glenelg River has redistributed sediment associated with shoreline barriers shoreward of Mingbool Range.

The only significant difference in barrier morphology between the Mount Gambier and Robe coastal plains is identified within the hypothesised MIS 11 barrier. Gambier Range is significantly taller than all other barriers on Mount Gambier coastal plain and reaches 30 m above the surrounding landscape. East Avenue Range, however, only extends to 20 m in height, and is not significantly different from other barriers on the Robe coastal plain. This difference could relate to variations in sediment supply or predominant wind and wave directions between the two locations. This is presently observed on the modern coastline where Holocene dunes of Younghusband Peninsula are found shoreward of the Coorong lagoon but no Holocene dunes are identified at Port MacDonnell.

Shoreline barriers generally contain higher proportions of carbonate in the Mount Gambier region compared with Robe (Table 6.2). This likely reflects the greater distance of Mount Gambier from the River Murray mouth compared with Robe. The River Murray transports silicate-rich terrestrial sediment to the Southern Ocean, and through longshore sediment transport this may be moved southward along the coastline. Greater volumes of silicate-rich terrigenous sediment are likely deposited on the continental shelf directly south of Robe compared with Mount Gambier, and thus more terrigenous clasts, such as quartz, are available for onshore transport and barrier construction in the Robe region. The variance in



calcium carbonate percentages between the two regions may also reflect variation in bioproductivity across the shelf, with a more productive region directly south of Mount Gambier.

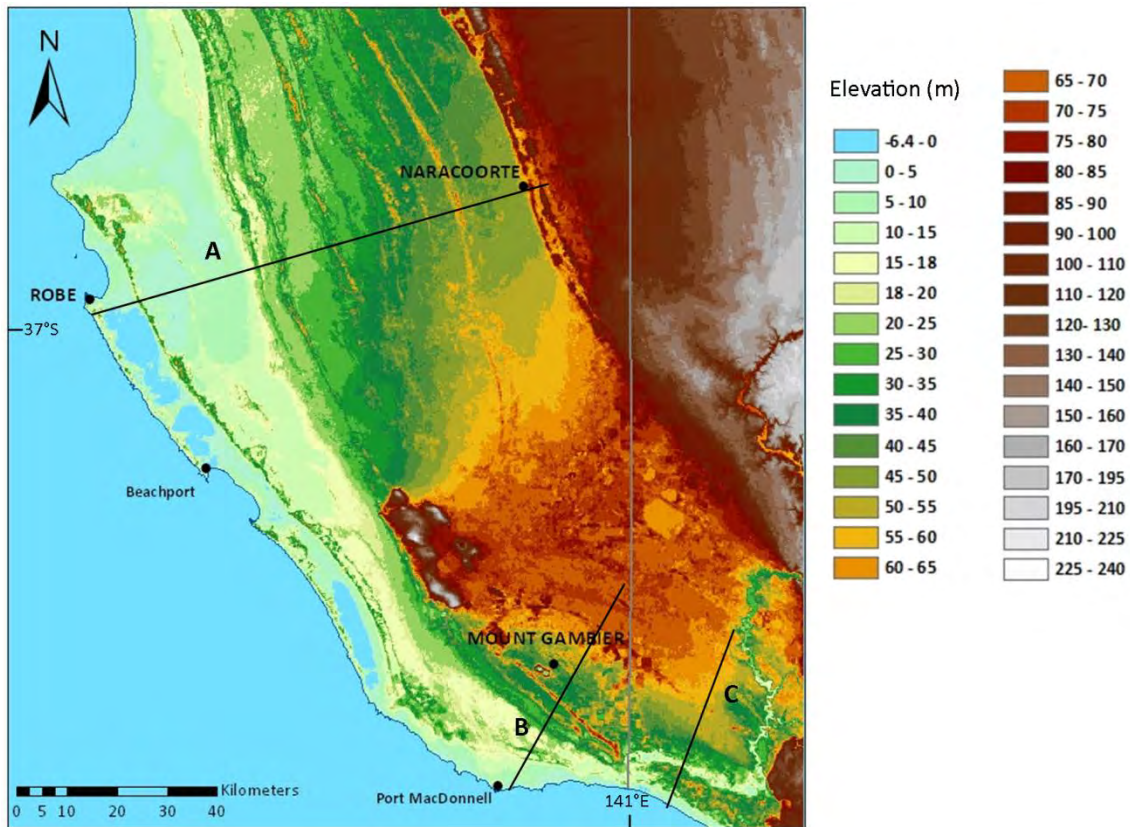


**Figure 6.9:** Map locating transects across the coastal plain from which SRTM data in Figures 6.10 to 6.14 are derived. Transects are located between Robe and Naracoorte (A), Port MacDonnell and Mingbool village (B) and Nelson and Dartmoor (C).

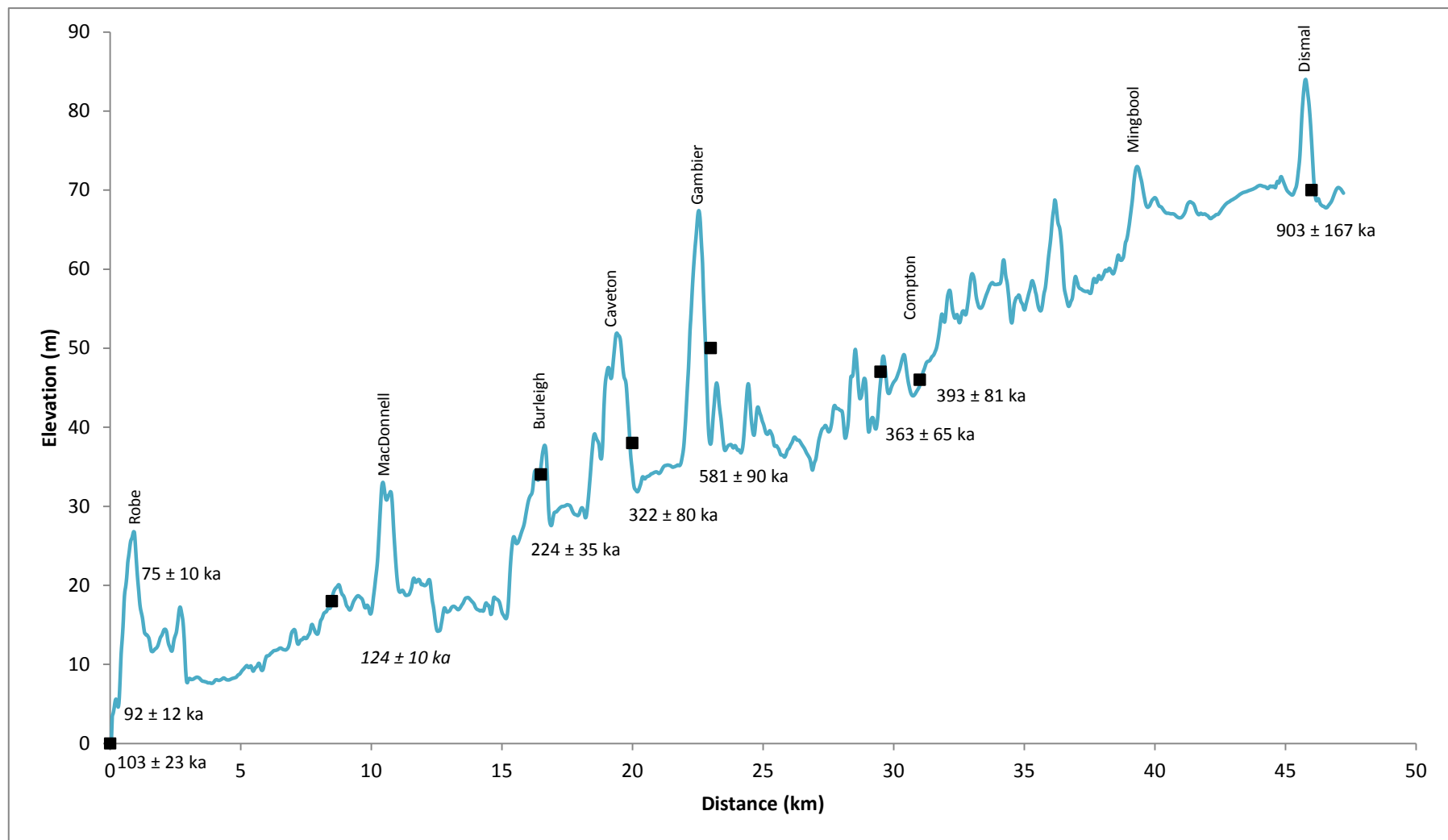


**Figure 6.10:** Transect across the Mount Gambier coastal plain from Port MacDonnell to Dismal Range derived by SRTM data, highlighting the difference in barrier morphology and the elevation of palaeo-sea level markers and the derived numerical age of these deposits from AAR analysis. Ages in italics indicate results were derived from OSL analysis.

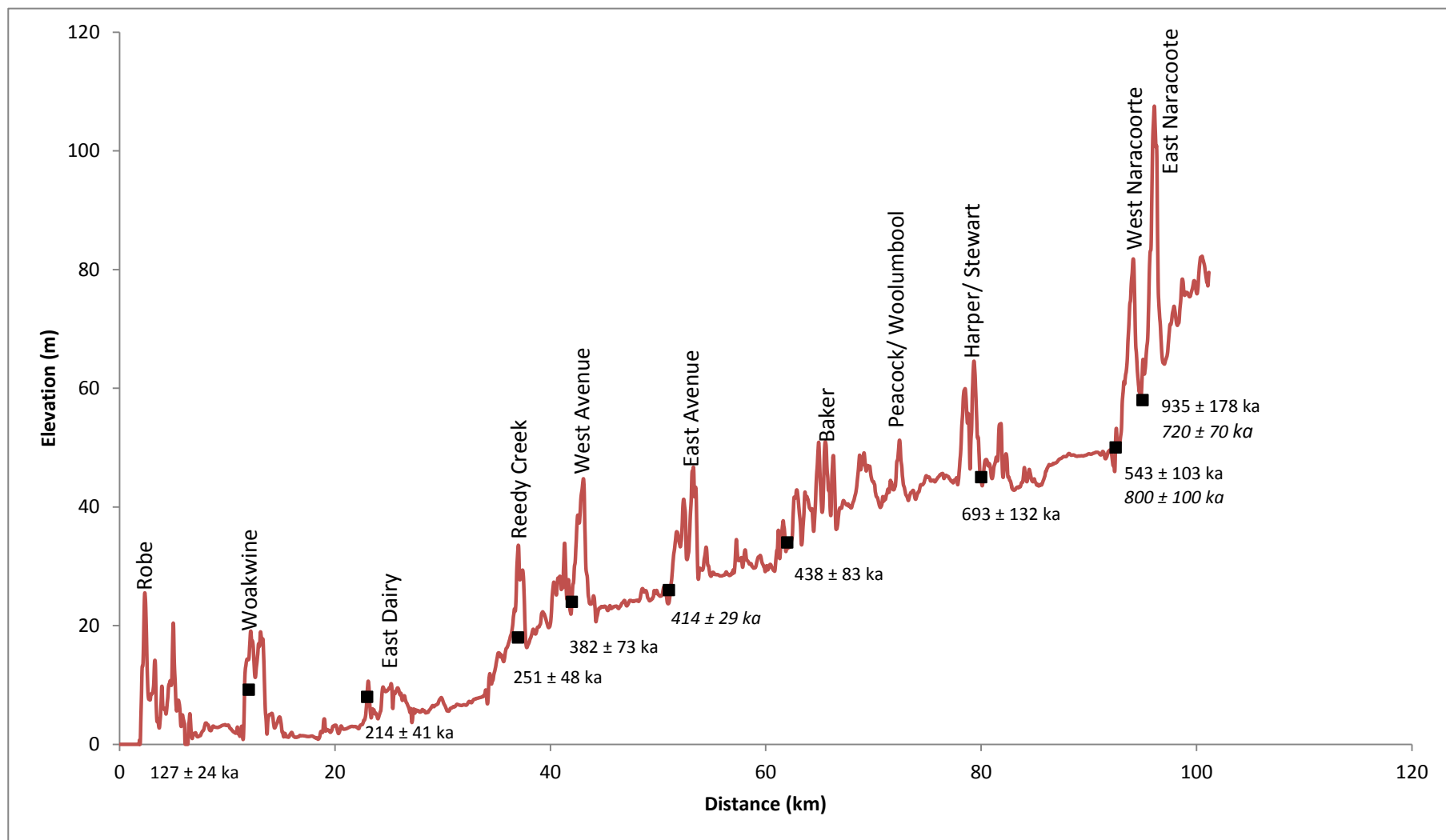


**Figure 6.11:** Transect across the Robe coastal plain derived by SRTM data, highlighting the morphology of the barrier shorelines and the elevation and numeric ages (derived by AAR, or TL if in *italics*) of palaeo-shoreline deposits as described by Murray-Wallace *et al.* (2001).

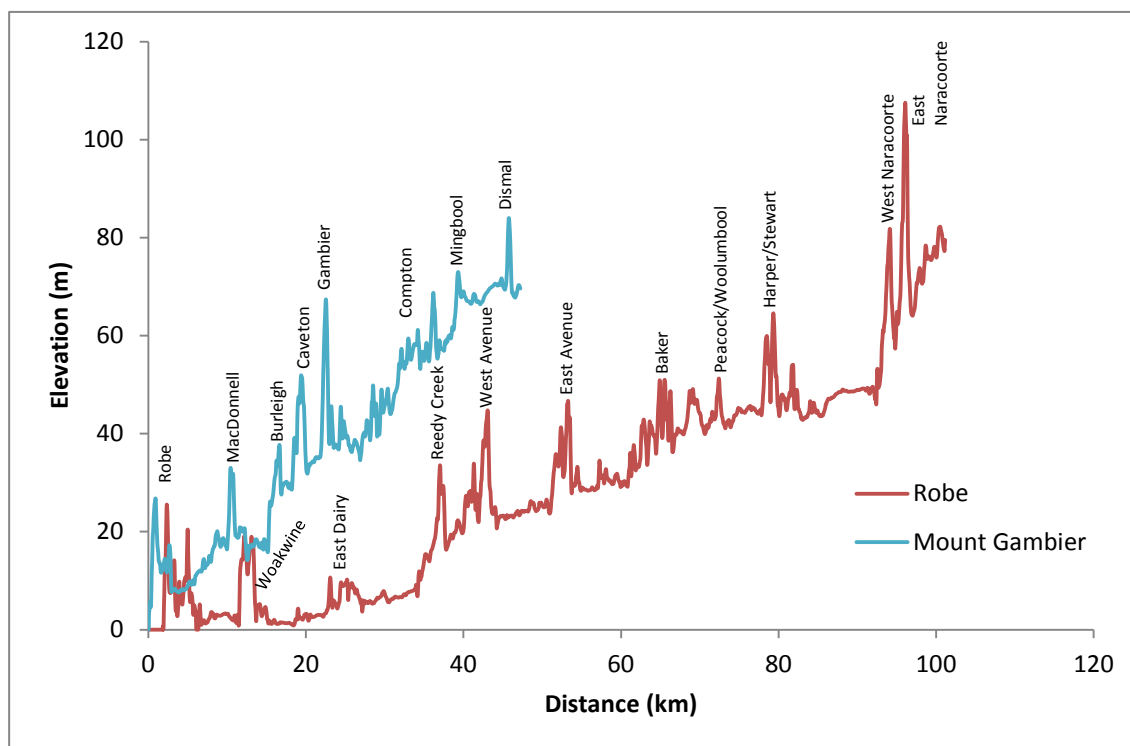


**Figure 6.12:** Comparison of transects (from SRTM data) from the Mount Gambier and Robe coastal plains highlighting the difference in the rate of uplift between the two regions.

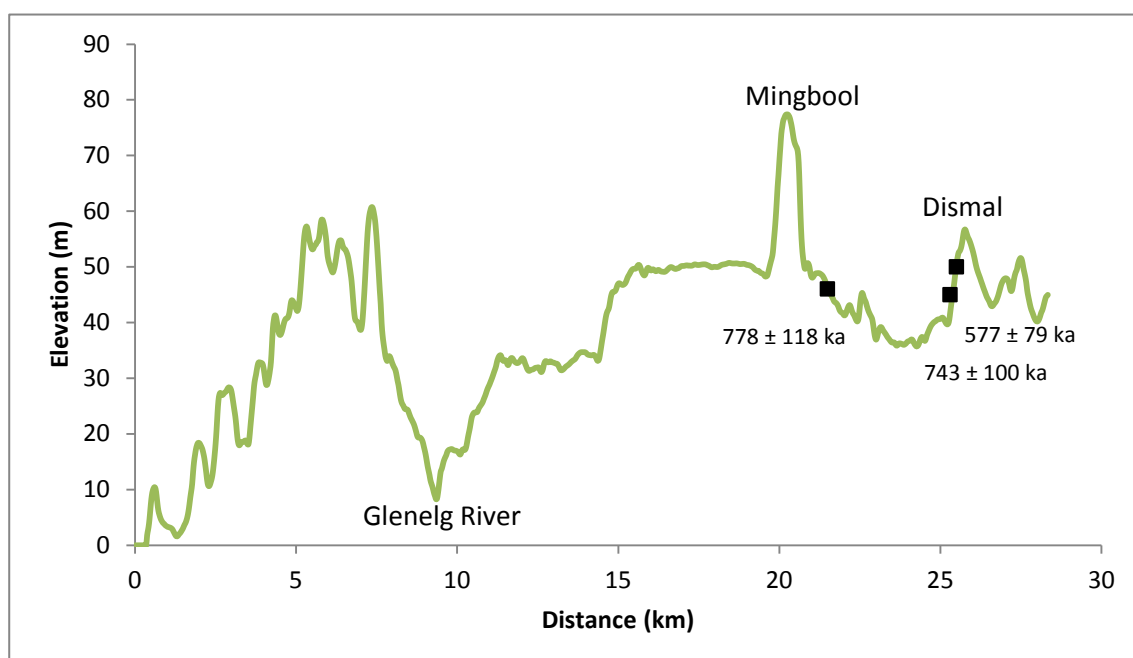


**Figure 6.13:** Transect across the Mount Gambier coastal plain between Nelson and Dartmoor using SRTM data and highlighting subaqueous facies identified at Don's Quarry, Fort O'Hare Quarry and Dartmoor Cemetery. Numeric ages are derived from AAR analysis of foraminifera at these sites. Shoreline barriers seaward of the Glenelg River are not as widely geographically separated as they are in the Mount Gambier or Robe region and potentially form a composite deposit.

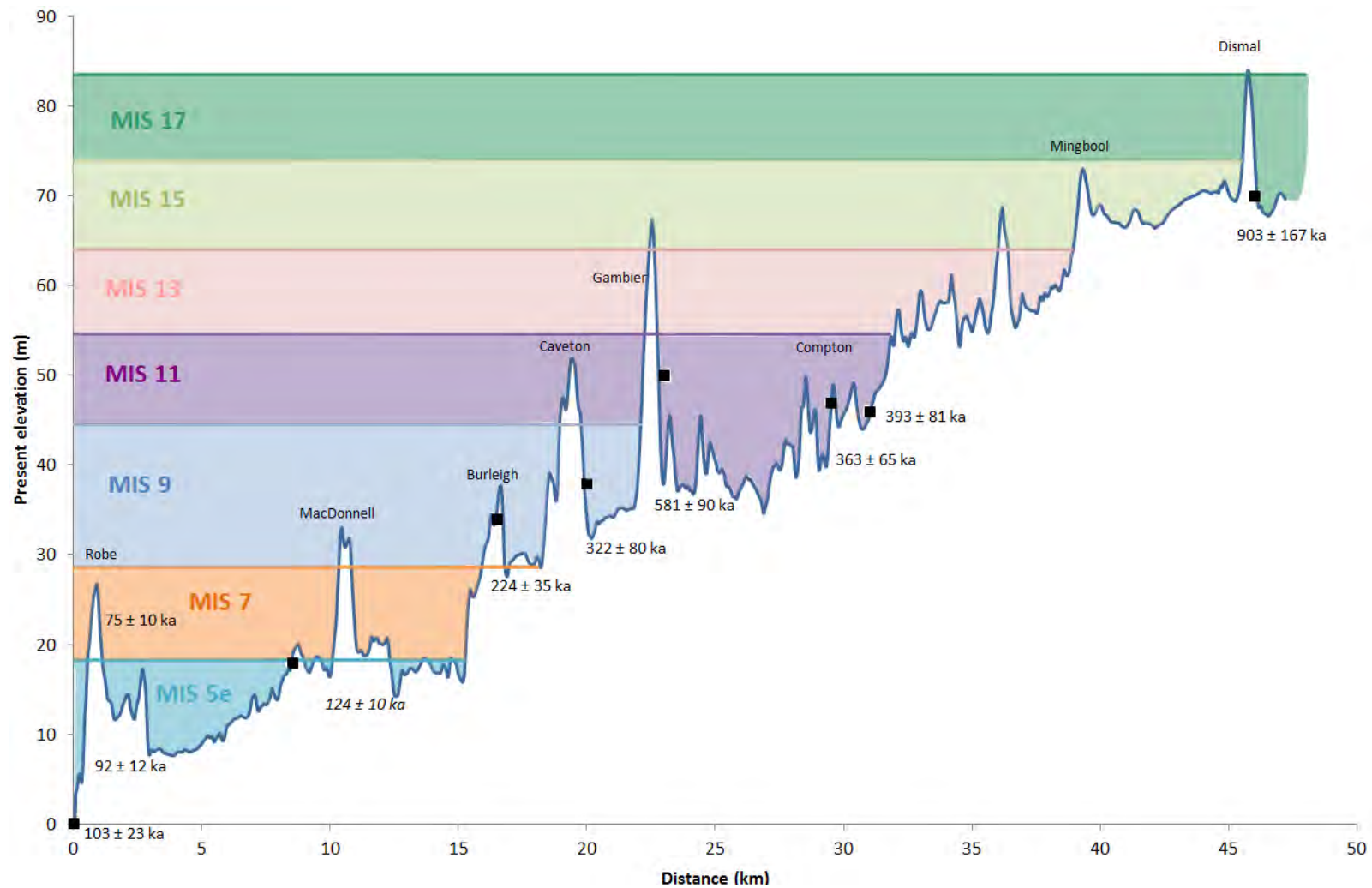


**Figure 6.14:** Transect of barrier shorelines of the Mount Gambier coastal plain with interglacial sea-level elevations as proposed by Murray-Wallace *et al.* (2001) adjusted for tectonic uplift in the Mount Gambier region. Even with a lower than global average sea-level of -3 m it is evident that MIS 11 may have flooded parts of the Compton Range assuming that the Compton Range was at the same volume during MIS 11 as it is now. Sea levels for MIS 15 and 17 also extend above the Mingbool and Dismal Ranges which were deposited within these interglacials indicating that sediment has been eroded from these barriers.

#### 6.5.4 New contributions to the southern Australia palaeo-sea level record

The findings reported within this thesis compare well with those farther northwest on the Coorong coastal plain and confirm that interglacial palaeo-sea levels did not extend more than 5 m APSL throughout the 680 ka in southern Australia. This research increases the confidence and accuracy of palaeo-sea level reconstruction from this region in a far-field site from Quaternary ice sheets.

The flint conglomerate palaeo-beach facies described at Port MacDonnell provides a more accurate minimum sea-level elevation for MIS 5c of  $-14 \pm 2$  m, than previously reported from the toe of the Robe III dune (Huntley *et al.*, 1993a, 1994) from which a palaeo-sea level of -9 m has been inferred (Murray-Wallace, 2002). The palaeo-beach facies at Port MacDonnell is the first reported subaqueously deposited late Pleistocene interstadial (MIS 5c) coastal strata found above present sea level within Australia (Blakemore *et al.*, 2014).

Geochronological analysis within this study confirms the shoreline barriers of the Mount Gambier coastal plain are correlative with those analysed on the Robe coastal plain as inferred by Sprigg (1952). Similar uplift-corrected palaeo-sea level estimations from two regions of varying tectonic uplift increase the confidence in these interpretations. Single-grain AAR analysis of foraminifera from barriers on the Mount Gambier coastal plain confirms the deposition of interglacial shoreline barriers back to MIS 17 in the region. Single grain AAR analysis has not previously been conducted on the Robe coastal plain and its use within this thesis yields a potentially more precise chronology than whole-rock analysis which was found not to be reliable past MIS 9 on the Mount Gambier coastal plain, due to greater diagenesis and leaching of amino acids. The use of single grain AAR analysis enables the more accurate identification of reworked or diagenetically altered grains, which can potentially lower the overall D/L value of a sample.

SRTM data have also not previously been used to determine the morphology of barrier shorelines in the Robe to Mount Gambier region. In this thesis, SRTM data were used to compare sediment volumes between correlative barriers. SRTM data can also be used to compare the morphology of the barriers with proposed interglacial duration and intensity, which is discussed further in the following section (6.6.3), whereby results derived from the Mount Gambier coastal plain are compared with global data sets of last interglacial deposits.

## 6.6 Comparison with global interglacial studies

Orbital forcing has been widely-accepted as a driver of glacial and interglacial climates, with variation in interglacial intensity proposed to correlate with differences in these cycles (e.g. Jouzel *et al.*, 2007). The following discussion compares the Mount Gambier sea-level record with other global archives and identifies differences in glacio-hydro-isostasy, calculation of long-term uplift rates and uncertainties associated with palaeo-sea level markers as potential reasons for variation between records. Results from the Mount Gambier coastal plain are compared with insolation forcing maximum in the Northern Hemisphere to try and infer whether the timing of barrier deposition supports the Milankovitch (1941) hypothesis. The volumetric size of barrier shorelines on the Mount Gambier coastal plain is compared with variation in interglacial intensity to establish whether there is any correlation between the two. Global records of interglacial aeolianite deposition are then compared to establish whether this trend is evident in other regions. Comparisons of this nature highlight the significance of the palaeo-sea level record derived from the Mount Gambier coastal plain.

### 6.6.1 Global interglacial sea-level

Global sea-level records are derived from a range of successions, though few extend back past MIS 5e due to erosional processes and the lack of preservation potential of certain coastal deposits. As outlined in Chapter 2, the estimation of palaeo-sea level from these relict deposits is found to vary significantly due to differences in local neotectonics, glacio-hydro-isostasy and the extrapolation of rates of uplift. The following discussion compares the global sea-level literature with the record derived from the Mount Gambier coastal plain by exploring potential reasons for variance in sea-level elevation and the timing of highstands from contrasting datasets within the far and near-field of former ice sheets. This section concludes by evaluating how the sea-level record derived from the Mount Gambier coastal plain contributes to the global literature.

Sea-level elevations are found to vary with location, in relation to their proximity to former ice sheets, for each of the last four interglacials and beyond. Figure 6.15 illustrates this variation in derived palaeo-sea level records (including the Mount Gambier record), with zone 1 being closest to former ice sheets and zone 5 being farthest away. Figure 6.16 compares results from the Mount Gambier coastal plain with global sea-level estimates and the marine oxygen isotope records of Lisiecki and Raymo (2005) and Siddall *et al.*, (2003).



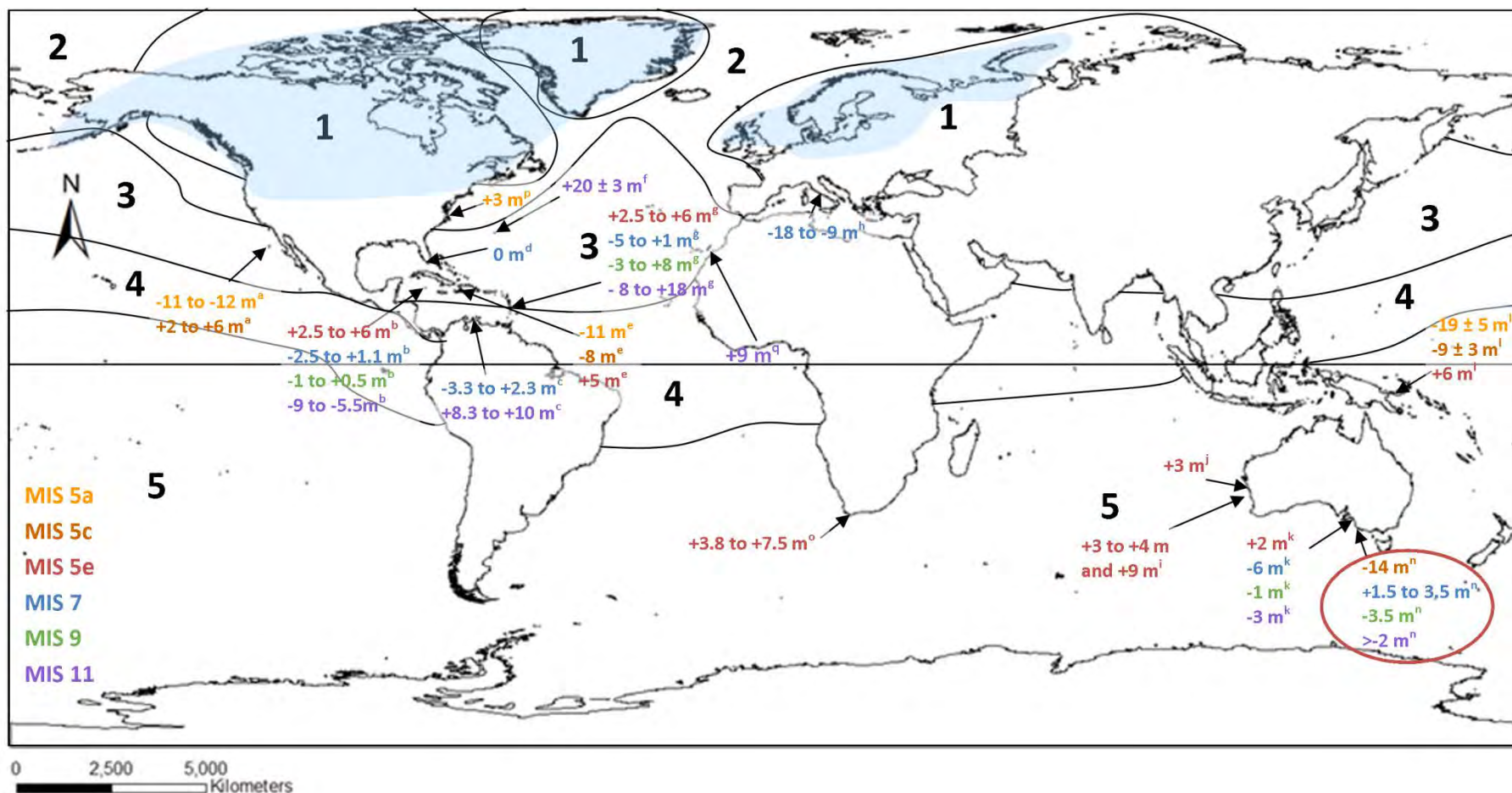


**Figure 6.15:** Various interglacial sea-level deposits plotted in regards to zonation from former Quaternary ice sheets after Clark *et al.* (1978) and compared with the new data derived from this research from the Mount Gambier coastal plain (circled). <sup>a</sup>San Nicolas Island, California, Muhs *et al.* (2012a); <sup>b</sup>Ironshore Formation, Grand Cayman Island, Vezina *et al.* (1999); <sup>c</sup>Curaçao, Leeward Antilles Islands, Muhs *et al.* (2012a); <sup>d</sup>Florida Keys, Muhs *et al.* (2011); <sup>e</sup>North-western Peninsula, Haiti, Dumas *et al.* (2006); <sup>f</sup>Government Quarry, Bermuda, Hearty *et al.* (1999); <sup>g</sup>Barbados, Schellmann and Radtke (2004) – note that MIS 5e sea level in Barbados is assumed; <sup>h</sup>Argentarola Cave, Italy, Bard *et al.* (2002); <sup>i</sup>Quobba Ridge, Western Australia, O’Leary *et al.* (2013); <sup>j</sup>Cape Range, Western Australia, Stirling *et al.* (1998); <sup>k</sup>Coorong coastal plain, South Australia, Murray-Wallace (2002); <sup>l</sup>Huon Peninsula, Papua New Guinea, Chappell and Shackleton (1986); <sup>m</sup>Mount Gambier coastal plain (this study, note >-2 m reflects that this is a minimum sea level of 2 m BPSL); <sup>n</sup>Cape Agulhas, South Africa, Carr *et al.* (2010); <sup>o</sup>Virginia, USA, Wehmiller *et al.* (2004); <sup>p</sup>Canary Islands, Spain, Muhs *et al.* (2014). Note, world map produced using data from ESRI (2002).



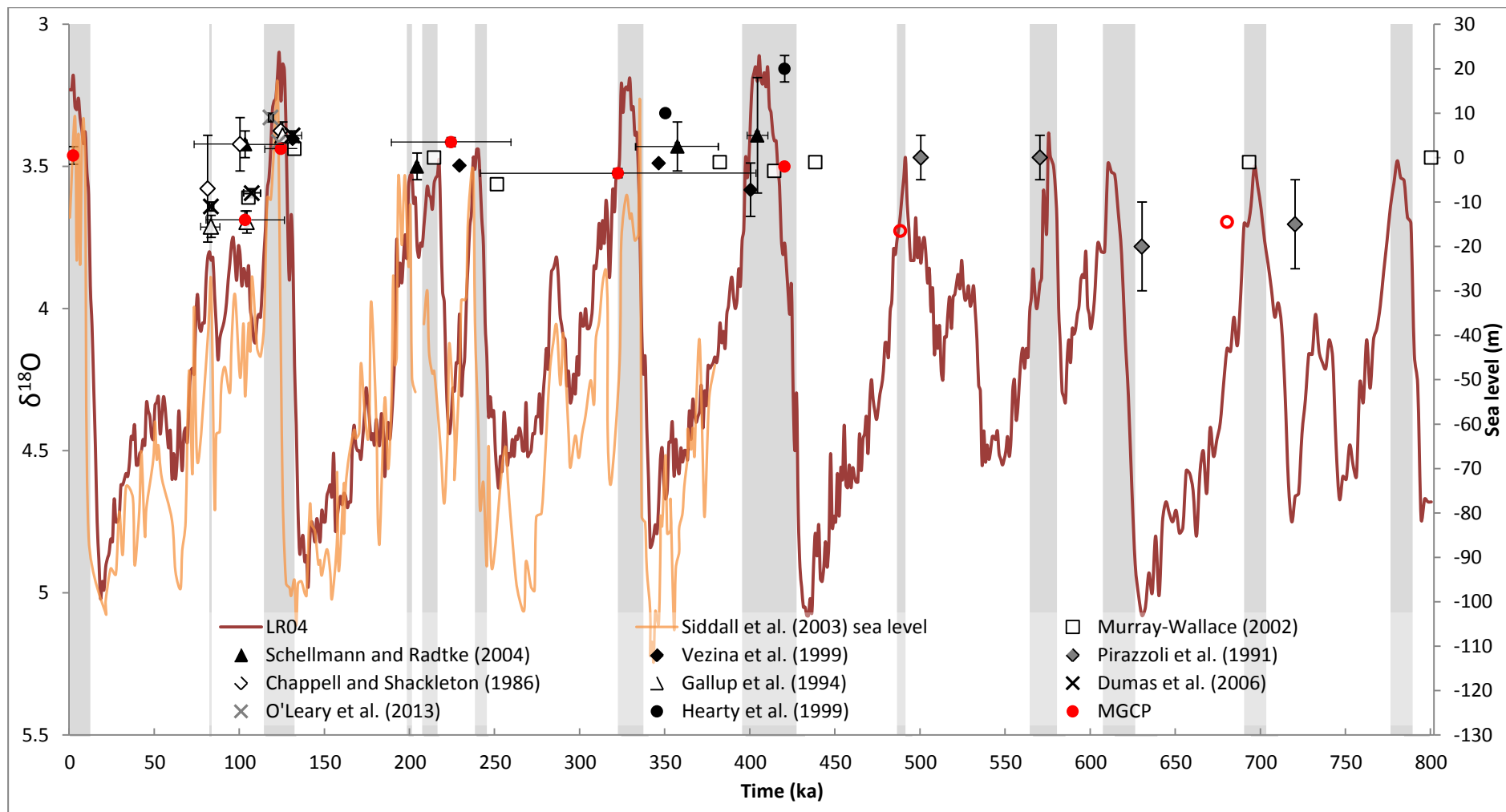


**Figure 6.16:** Comparison of palaeo-sea levels derived from the Mount Gambier coastal plain (MGCP) with marine oxygen isotope records (from the Red Sea: Siddall *et al.*, 2003 and LR04 stack of Lisiecki and Raymo, 2005) and other morphological indicators from palaeo-shorelines. Grey shaded regions depict interglacials, defined by Schilt *et al.* (2010) where  $\delta D$  is greater than  $-408\text{‰}$  from the ice core record published by Jouzel *et al.* (2007). Open circles from the Mount Gambier coastal plain represent minimum sea-level estimates derived from subaqueous facies.

Few geomorphic sea-level records preserve successions of older interglacials due to the erosion and denudation of former coastal deposits. One such record is preserved on the uplifted coral reefs of Sumba Island, Indonesia. From U-series and ESR analysis of these successions, Pirazzoli *et al.* (1991) suggested that sea-level during MIS 13 and MIS 15 was similar to present, while sea level was only -20 and -25 m during MIS 17 and MIS 19 respectively. These values compare well with the orbitally tuned oxygen isotope record (Figure 6.16), which indicates that prior to the Mid-Brunhes Event (Jansen *et al.*, 1986), interglacials were less intense (Masson-Delmotte *et al.*, 2010). However, diagenetic changes to coral and reoccupation of reef terraces during successive sea-level highstands may prevent accurate interpretations at this site. Sea-level estimates of MIS 13, 15 and 17 from the Mount Gambier coastal plain are limited by the paucity of accurate sea-level indicators due to poorer preservation of more landward barriers. Sea-level estimations are therefore based on subaqueous facies from which only minimum sea level can be derived.

As mentioned in Chapter 2, sea level during MIS 11 has been highly contended. MIS 11 has been described as a lengthy and warmer interglacial (Loutre and Berger, 2003; Howard, 1997; Droxler and Farrell, 2000). On the islands of Bermuda and the Bahamas, coastal deposits of MIS 11 age are identified as illustrating a sea-level highstand up to 20 m above present (Hearty, 1998; Olson and Hearty, 2009), while global records indicate that MIS 11 sea level was more similar to present (Murray-Wallace, 2002). This variation maybe due to incorrect appraisal of the effects of glacio-isostatic adjustment in the Caribbean as suggested by Raymo and Mitrovica (2012). The elevated coastal deposits are not indicative of a sustained sea-level highstand, as a distinct coral terrace would be, and therefore these deposits may simply represent an abnormal event such as a tsunami (McMurtry *et al.*, 2007) where sediment is deposited significantly above mean sea-level. On the Mount Gambier coastal plain minimum MIS 11 sea level is suggested to be -2 m as identified from subaqueous calcarenite deposits within Gambier Range. This estimation is limited by the resolution of AAR dating, the leaching of lower molecular amino acids from the sediment, and the lack of a fixed sea-level indicator. However, a range (between +8 m and +24 m) of palaeo-sea level estimates during MIS 11 have been derived from the Leeward Antilles Islands (Muhs *et al.*, 2012a), and from the Canary Islands (Muhs *et al.*, 2014). It is therefore imperative to more accurately understand the glacio-isostatic effects on sea-level during this interglacial. Further constraining the MIS 11 sea-level from other global coastal successions is limited by the lack of preserved deposits and from the large uncertainties associated with geochronological dating techniques applied to samples of this age.

Global sea-level variations are also identified within MIS 9 and MIS 7. From the Bahamas and Bermuda, Hearty and Kindler (1995) suggested sea-level during MIS 9 may have reached +4 m, while on Grand Cayman Island, Vezina *et al.* (1999) proposed MIS 9 sea-level ranged from -3 to +0.5 m and that MIS 7 sea-level was between -2.5 and +1.1 m. Several studies have recorded substantially lower sea-levels during MIS 7; such as -6 m in the Bahamas (Li *et al.*, 1989); -18 to -19 m at Argentarola Cave, Italy (Bard *et al.*, 2002), and -11 to -17 m in French Polynesia (Camoin *et al.*, 2001). Other studies have recorded MIS 7 sea-level as closer to present; such as the Florida Keys (Muhs *et al.*, 2011). The higher sea level for this site may relate to its position within a near zone to former Quaternary ice sheets as has been identified for varying elevations of interstadial deposits on the Atlantic coastal plain (Potter and Lambeck, 2003). However, estimates from Curaçao, significantly farther south, suggest that sea level during MIS 7 was similar to present (Muhs *et al.*, 2012a). MIS 9 sea-level for the Mount Gambier region is identified at -3.5 m from a lagoonal facies landward of Caveton Range. This lower than present sea-level estimate may be a result of denudation processes following deposition, such as potential dissolution of the underlying Gambier Limestone at this locality which may have resulted in lowering of the ground surface. This is simply a hypothesis, however, and further work would be required to determine its accuracy. MIS 7 sea-level from the Mount Gambier coastal plain is derived from two facies within Burleigh Range: the palaeo-gravel-beach facies indicates a palaeo-sea level of +1.5 m with an uncertainty of + 2 m (derived from the current tidal range at Racecourse Bay, which is used as an analogue); and the lagoonal facies along Laslett Road, which suggests that sea-level may have been up to +3.5 m at some point during the MIS 7 sea-level highstand.

There are several factors that contribute to spatially varied interglacial sea-level estimates which may account for differences between the Mount Gambier sea-level record and other global archives. One of the best examples of the variability in sea-level on a spatial scale is derived from palaeo-sea level estimation of the interstadials of the last interglacial. From the marine oxygen isotope record (e.g. Lisiecki and Raymo, 2005) it is derived that global ice volume during MIS 5a and MIS 5c were significantly greater than during MIS 5e and thus corresponding sea-level should be lower during these interstadials. Several reported interstadial sea-levels support the marine oxygen isotope records. For example, MIS 5c sea level has been identified as low as -10 to -17 m and MIS 5a sea level between -13 to -18 m in Barbados (Gallup *et al.*, 1994; Schellmann and Radtke, 2004). On Haiti, Dumas *et al.* (2006) suggested MIS 5c sea level reached -8 m while MIS 5a sea level was -11 m. From oxygen isotope analysis of the Red Sea, Rohling *et al.* (2004) suggested MIS 5c sea level was as low as

-17 m. These datasets compare relatively well with the minimum sea-level for MIS 5c of  $-14 \pm 2$  m derived from the Mount Gambier coastal plain from a palaeo-beach facies at Port MacDonnell. However, a range of other studies, specifically along the Atlantic coastal plain of the United States, have recorded MIS 5a sea-level near to and above present (e.g. Muhs *et al.*, 2002; Wehmiller *et al.*, 2004). Potter and Lambeck (2003) noted a northward gradient in MIS 5a sea-level across the western Atlantic and attributed the higher proposed sea-level estimates to differences in glacio-isostatic rebound between regions in relation to the proximity of sites to former Quaternary ice sheets. Differences in isostasy may be a factor that results in variability between sea-level records from Mount Gambier with other global sites.

Isostasy is the result of crustal adjustment to varying overlying loads. Isostasy can occur both on land, with the growth and decay of ice sheets, and in the ocean with the loading and unloading of increased water volumes as a result of glaciation and deglaciation. Potter and Lambeck (2003) associated the higher elevation of MIS 5a deposits along the United States Atlantic coastal plain with the collapse of the peripheral forebulge associated with the North American ice sheets following the Last Glacial Maximum. Variance in elevation of sea-level markers in relation to glacio-hydro-isostasy is not constrained to interstadial events, but applies to all previous interglacials. Variances in sea level between sites reported in the studies above may result from inappropriate modelling of isostatic influences within these regions. The adjustment of the mantle to varying overlying loads is not immediate. Certain shorelines, such as those in Scotland, are still uplifting in response to the removal of the Last Glacial Maximum ice sheets from this region, over 14 ka ago (Lambeck, 1995). Lambeck *et al.* (2012) stated that the global variability observed in respect to the elevation of the last interglacial shoreline is a function of glacio-hydro-isostatic effects occurring before, during and following an interglacial. Therefore, to accurately compare palaeo-sea levels from global locations a more accurate model of isostatic processes at each site is required.

Variability in global sea-level estimates may also arise from differences in neotectonics of a region and errors in how rates of uplift, for example, are calculated. Rates of uplift on tectonically rising coastlines are commonly calculated by identifying the elevation of a last interglacial (MIS 5e) shoreline deposit and applying the generally well-accepted global sea-level datum of + 6 m (after Veeh, 1966) to determine rates of uplift over the past  $125 \pm 8$  ka. Nevertheless, while MIS 5e sea-level has been identified to vary spatially, as previously discussed, this uncertainty is suggested to be relatively small in comparison with the magnitude of uplift (Murray-Wallace and Woodroffe, 2014). Potential errors are encountered

when long-term rates of uplift are presumed to be constant and extrapolated beyond the last interglacial. For example, on segments of Huon Peninsula, Papua New Guinea, Chappell *et al.* (1996) recognised episodic uplift had occurred.

Another source of disparity between geomorphological sea-level records may be accounted for in the uncertainty associated with the relation of the described indicator to sea level. While corals known to grow at a certain depth may record the maximum sea-level elevation during a highstand (as indicated by their final growth position), other sea-level markers may not. For example, palaeo-beach deposits may be formed at any point during a sea-level transgression, maximum or regression, and it cannot always be presumed that deposits formed in sea-level maxima will always be preserved. Variance in the preservation potential of sea-level indicators can also influence derived ages of deposits. For example, ages derived from U-series dating of corals can be significantly skewed if the coral specimen has been diagenetically altered. The elevation at which a palaeo-sea level indicator is found can be altered by denudation and landscape lowering associated with erosion as well as tectonic uplift, thus adding uncertainty to palaeo-sea level estimates in some regions.

Potter and Lambeck (2003) stated that one of the inherent problems of palaeo-sea level reconstruction is that past sea levels are compared with those of the present, but that sea-level is not presently in an equilibrium isostatic state. Can it be asked, therefore, whether interglacial sea-level is ever in an equilibrium isostatic state? For example, Scottish shorelines are still rebounding 14 ka after the removal of former ice sheets (Lambeck, 1995), which is the proposed duration of several past interglacials.

While the Mount Gambier sea-level record generally compares well with other global archives, discrepancies may occur as a result of variations in glacio-hydro-isostasy, local neotectonics and the preservation and precision of specific sea-level indicators. Ultimately, however, the Mount Gambier interglacial sea-level record is a significant archive as it reveals a more eustatically-driven palaeo-sea level record due to the position of southern Australia in a far field zone from Quaternary ice sheets.

### **6.6.2 Insolation forcing**

The orbital hypothesis, suggested by Milankovitch (1941) has been widely accepted as a driver of glacial and interglacial cycles. The hypothesis suggests that interglacials will follow shortly after intervals of summer insolation maximum at 65°N. Evidence of the timing of these events derived by orbital cycles has been identified in a range of marine and terrestrial sources (e.g.

Hays *et al.*, 1976; Hooghiemstra *et al.*, 1993; Kukla, 1987; EPICA community members, 2004). Figure 6.17 compares the derived ages of barrier shoreline formation from the Mount Gambier coastal plain with the timing of Northern Hemisphere insolation maximum as defined by Berger and Loutre (1991).

MacDonnell Range has been suggested by OSL analysis to be last interglacial (MIS 5e) in age. An OSL age of  $124 \pm 10$  ka is derived from an aeolian deposit within the barrier succession, and the mean of this age slightly postdates Northern Hemisphere insolation maximum at 126 ka. However, when  $1 \sigma$  uncertainty is accounted for this age suggests deposition may have occurred between 114 and 134 ka, straddling the timing of insolation maximum. Foraminifera from the back-barrier lagoon facies of Burleigh Range indicate deposition at  $224 \pm 35$  ka which postdates insolation maximum at 241 ka, though when uncertainties are accounted for the upper limit for deposition also coincides with and slightly predates insolation maxima. An AAR numeric age of  $322 \pm 80$  ka was derived from *Elphidium crispum* within a lagoonal facies of Caveton Range, and although the majority of this age estimate postdates the insolation maximum at 333 ka, the large uncertainty values associated with the derived age prevent a confident correlation between time of deposition and Northern Hemisphere insolation maximum.

Landward of Caveton Range derived AAR numeric ages have large uncertainty values. Successive barrier complexes are assigned a time of deposition in correlation with the marine oxygen isotope record (e.g. Lisiecki and Raymo, 2005) based on both geochronological analysis (AAR and OSL) and geographical positioning of the barrier in relation to the present coastline. Comparing the timing of barrier deposition to Northern Hemisphere maximum for barriers inland of Caveton Range is therefore a circular argument as the marine oxygen isotope record is orbitally tuned. Figure 6.17, therefore, only indicates barrier deposition for successions shoreward and including Caveton Range.

Comparison of barrier shoreline deposition across the Mount Gambier coastal plain with Northern Hemisphere insolation forcing to determine whether the successions provide further support for Milankovitch forcing is ultimately limited by the resolution of geochronological techniques applied, in particular AAR. Peaks in insolation are identified approximately every 20 ka, and thus uncertainty values associated with deposition need to be lower than this to confidently determine a relationship. As uncertainty values are commonly higher than 20 ka it cannot be confidently determined that the timing of barrier deposition on the Mount Gambier coastal plain is determined by the Milankovitch (1941) orbital hypothesis.

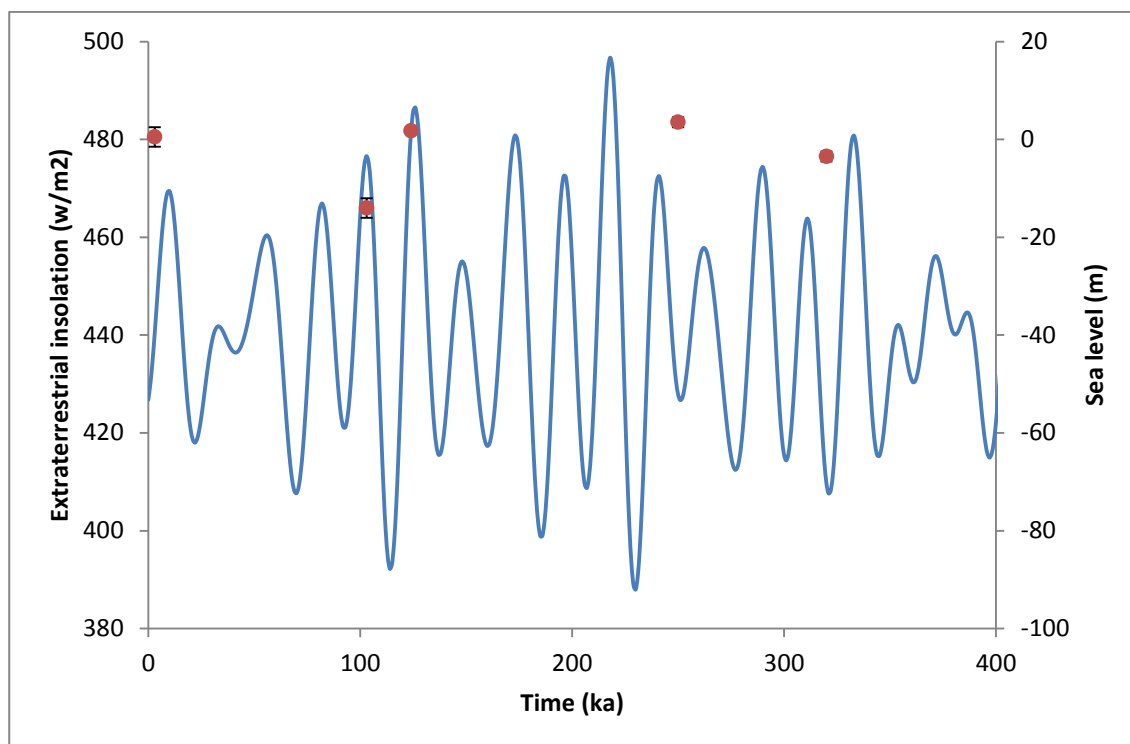


**Figure 6.17:** Comparison of depositional timing of barrier successions on the Mount Gambier coastal plain with Northern Hemisphere insolation maximum as derived by Berger and Loutre (1991).

### 6.6.3 Interglacial intensity

The intensity of interglacials has been shown to vary over the Quaternary. After the Mid-Brunhes Event (MBE) ~430 ka (Jansen *et al.*, 1986), interglacials and glacials are found to be greater in amplitude, as is reflected in ice- (EPICA community members, 2004) and marine-core records (Lisiecki and Raymo, 2005). Before the MBE, interglacial climates are interpreted to have recorded cooler Antarctic temperatures, lower atmospheric CO<sub>2</sub> concentrations, larger ice sheets and lower global sea levels (Yin and Berger, 2010 and references therein). Following the MBE, interglacials, including MIS 11, are inferred to have been warmer. Yin and Berger (2010) proposed that this is due to increased temperatures during Northern Hemisphere winters as a result of increased insolation.

Masson-Delmotte *et al.* (2010) compared the relative intensities of the last nine interglacials based on a range of proxies identified from EPICA Dome C ice-core. These proxies included temperature derived from the  $\delta D$  record (Jouzel *et al.*, 2007), dust, carbon dioxide, methane, sodium and calcium concentrations. Masson-Delmotte *et al.* (2010) ranked each interglacial according to temperature, ice-core proxies and relative sea-level (derived from past ice volumes of Bintanja *et al.*, 2005). Based on these proxies they concluded that MIS 5e and MIS 11 were the most intense interglacials. The warmest temperatures were recorded during MIS 5e whereas sea-level and rankings from other ice-core proxies were highest during

MIS 11. The weakest interglacials were MIS 13 and MIS 17, both of which occurred before the MBE.

It is interesting to evaluate whether evidence of these more intense interglacials is present within the barrier shoreline successions of the Mount Gambier coastal plain. Table 6.4 compares the relative intensity of interglacials as derived by Masson-Delmotte *et al.* (2010) with interglacial duration and the width and height of palaeo-shoreline barriers on the Mount Gambier coastal plain. An average volume of the barriers may be approximated by taking the average height of the barrier (from trough to crest) and multiplying it by its average width. Volumetrically, MacDonnell and Gambier Range are the largest barriers. MacDonnell Range does not extend as high above the surrounding coastal plain as Gambier Range, but it is wider in cross-sectional extent. Gambier Range is very prominent in the landscape and is clearly visible in transects across the coastal plain (Figures 6.10, 6.12 and 6.14) and in SRTM imagery (Figure 3.12). The larger volume of these barriers compares well with the intensity of their corresponding interglacials; MacDonnell Range is confirmed to have formed during MIS 5e and Gambier Range is proposed to have formed during MIS 11. The smallest barriers observed on the coastal plain are the most landward Mingbool and Dismal Ranges, proposed to have formed during MIS 15 and MIS 17 respectively. MIS 15 and MIS 17 occurred before the MBE, and thus the subdued topography of Mingbool and Dismal Range may reflect the weaker intensity of these interglacials. However, the lack of distinct calcrete horizons, the paucity of fixed sea-level indicators, and the absence of aeolian facies within exposures of these barriers potentially indicates denudation of the barriers has occurred through erosional processes.

### **Summary**

Sediment volume of barrier successions is found to be greatest in MacDonnell and Gambier Range formed during MIS 5e and MIS 11 respectively, and correlate with the most intense interglacials as recognised by Masson-Delmotte *et al.* (2010). Figure 6.18 compares barrier height with Antarctic temperature derived from the  $\delta D$  record of Jouzel *et al.* (2007), and a weak positive trend is identified. During warmer interglacials, warmer waters may have covered the Bonney Shelf. Cann and Clarke (1993) suggested that the Leeuwin Current extended farther eastward across the Great Australia Bight during MIS 5e, bringing warmer water to the region as is reflected in the faunal associations. Relatively warmer temperatures may have increased carbonate production on the Bonney Shelf, resulting in greater volumes of carbonate sediment available for landward transportation and barrier shoreline construction. Volumetrically, the smallest barriers on the coastal plain are Mingbool and Dismal Range, which were formed in interglacials of proposed weaker intensity. The subdued topography of



these barriers is likely a result of a combination of factors. The lower amplitude of interglacials before the MBE may have resulted in cooler temperatures and reduced carbonate production on the Bonney Shelf, thus reducing the volume of sediment available for barrier construction. However, the older barriers have also been subjected to lengthier extents of erosion and weathering which have potentially resulted in landscape lowering. A further limitation of this correlation is the assumption that barriers (e.g. MacDonnell and Gambier) have formed during a single interglacial highstand. For example, on the Robe coastal plain, Woakwine Range and Robe Range are morphologically significant barriers in comparison with the others, but it has been shown that they are composite features having formed in multiple sea-level highstands. Woakwine Range is predominantly MIS 5e in age but has a core body of MIS 7 sediment (Murray-Wallace *et al.*, 1999), while Robe Range formed during MIS 5c, MIS 5a and is capped with Holocene sands (e.g. Schwebel, 1978; 1984). Therefore, while the basis of a correlation between interglacial intensity and barrier volume has been provided, further sampling and geochronological analysis of barrier sediments is required to determine whether they are composite features or whether all sediment within the complex was deposited during a single interglacial.

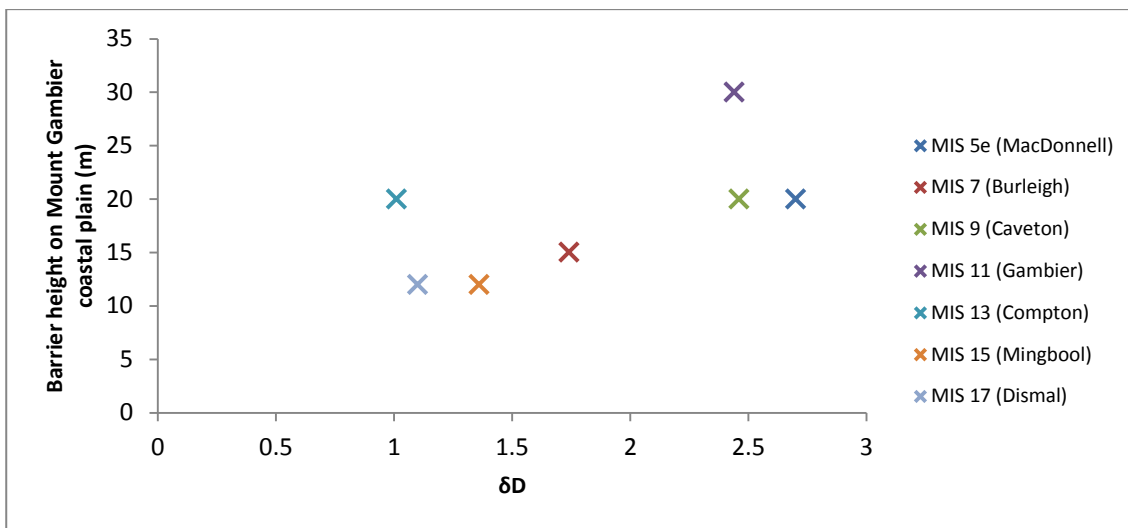


**Figure 6.18** Scatter plot of barrier height on the Mount Gambier coastal plain against  $\delta D$  from the EPICA Dome C ice-core (Jouzel *et al.*, 2007) for the corresponding marine isotope stage the barriers were deposited within. A weak trend between Antarctic temperature and barrier height is observed and potentially reflects increased carbonate production on the Bonney Shelf during warmer interglacials which has possibly resulted in increased barrier height.

**Table 6.4:** Comparison of interglacial intensity as defined by Masson-Delmotte *et al.* (2010) with the height and width of barrier shorelines on the Mount Gambier coastal plain, southern Australia

Marine isotope stage (MIS)	Rank based on EDC temperature*''	Rank based on a range of ice-core proxies*^	Rank based on sea-level*#	Rank based on duration of interglacial~	Corresponding barrier on MGCP	Height of barrier (m)	Width of barrier (km)	Rank based on barrier size
1	4	4	4	9				
5e	1	2	2	3	MacDonnell	20	3	1
7e	5	8	7	2	Burleigh	15	2	5
9	3	3	3	6	Caveton	20	2	4
11	2	1	1	1	Gambier	30	2	1
13	10	9	10	10	Compton	20	2.5	3
15a	8	6	5	5	Mingbool	12	2	6
15e	6	5	9	4				
17	9	10	8	8	Dismal	12	0.7	7
19	7	7	6	7				

\*Ranking for interglacial intensity as derived by Masson-Delmotte *et al.* (2010) based on: "EPICA Dome C  $\delta D$  records from Jouzel *et al.* (2007); ^other proxies include dust, sodium, calcium, methane and CO<sub>2</sub>; #Sea level based on ice volume record from Bintanja *et al.* (2005). ~Duration based on length of interglacial as defined by Schilt *et al.* (2010) as being greater than -408‰  $\delta D$  from the EPICA ice core record derived by Jouzel *et al.* (2007). MGCP = Mount Gambier coastal plain. The width and height of each barrier was calculated by taking multiple (>10) transects across the SRTM digital elevation model of the coastal plain. Barrier width was defined as the distance from trough to trough in each barrier and height was calculated by taking the average maximum elevation of each barrier and subtracting the elevation of the surrounding land surface. Estimations are given to the nearest metre.

#### **6.6.4 Comparison of the thickness of calcarenite deposits on the Mount Gambier coastal plain with other global interglacial calcarenite successions**

Aeolianite deposition has been associated with interglacial sea-level highstands at a range of global locations, including South Africa, Brazil, the Bahamas, Bermuda and the Mediterranean, as outlined in Chapter 3 (section 3.4). The larger barriers of MacDonnell and Gambier Range on the Mount Gambier coastal plain are tentatively linked with more intense interglacials. The following discussion compares the vertical thickness of global interglacial aeolianite deposits to determine whether this trend is observed in other sequences.

Few interglacial shorelines are confidently identified as greater than MIS 5e in age. Barrier shorelines across the Mount Gambier coastal plain are relatively well-preserved in respect to other global successions due to the gentle tectonic uplift and the formation of protective calcrete horizons. Where climate does not promote calcrete formation and where coastlines are stable, aeolianite deposits are more susceptible to erosion by successive sea-level highstands. Table 6.5 describes numerous calcarenite deposits, primarily from stable coastlines where aeolianite units are commonly stacked. Therefore, comparisons between volumes of aeolianite deposition during successive interglacials are challenging as it is difficult to identify the volumes of sediment removed from underlying layers as successive units are deposited above.

Volumes of aeolianite deposition may be correlated with carbonate production in the continental offshore shelf. Vertical thickness of global interglacial aeolianite deposits may therefore vary with differences in carbonate production associated with temperature and volumes of terrigenous sediment transported offshore disrupting carbonate production, though this is minimal in the Mount Gambier region. Thus, while vertical thicknesses of aeolianite successions may compare well in certain regions for specific interglacials (such as the thickness of units described in Table 6.5 for last interglacial interstadials), it is necessary to identify the relative thickness of aeolianite units for successive interglacials to determine whether the correlation between larger barrier successions on the Mount Gambier coastal plain and interglacial intensity is recognised in other global aeolianite sequences.

**Table 6.5:** Comparison of global coastal calcarenite deposits during differing interstadial and interglacial sea-level highstands

Location	Carbonate production environment	Facies	Time of deposition (dating technique)	Vertical thickness of facies	Reference
Wilderness embayment, South Africa	Temperate	Landward Barrier – aeolian	MIS 7, and likely a MIS 9 core to barrier (OSL)	~250 m	Bateman <i>et al.</i> (2011)
		Middle Barrier – aeolian	Mainly MIS 5 with some MIS 7 sedimentation	>200 m	
Lord Howe Island, South-west Pacific	Subtropical	Seaward Barrier – aeolian	MIS 5 and MIS 1 (6 ka and younger)	150 m	Brooke <i>et al.</i> (2003)
		Searles Point Formation – beach and aeolian	MIS 7 and likely older	Max. 8 m at Neds Beach	
		Neds Beach Formation – aeolian Cobbys Corner Member		Max. 20 m at North Bay	
		Middle Beach – aeolian and beach – top aeolian unit	MIS 5e-5c	11 m	
			MIS 5e-5c	35 m at Middle Beach	
			MIS 5a	23 m at Middle Beach	
Rio Grande do Sol coastal plain, Brazil	Temperate-warm	Pleistocene Barrier (III) Last interglacial barrier	MIS 5e	~20 m	Tomazelli and Dillenberg (2007)
North Eleuthera Island, Bahamas	Sub-tropical	Aeolian	MIS 5a	5 m	Hearty (1998)
		Aeolian/beach	MIS 5e	8 m	
		Aeolian	MIS 7	Max. 12 m	
		Beach/washover/aeolian	MIS 9/11	20 m	
		Aeolian	>MIS 13	Up to 10 m	
Kaiehu Point, NW Molokai, Hawaii	Sub-tropical	Lower aeolianite	MIS 5c?	1-2 m	Fletcher <i>et al.</i> (2005)
		Middle aeolianite	MIS 5a	3 m	
Kaua'i, Hawaii	Sub-tropical	Pā'ā member	MIS 1	20 m	Blay and Longman (2001)
		Makawehi member	MIS 5e	12 m	
		Pā'ō'ō member	MIS 5e/MIS 7	14 m	
		Punahoa member	MIS 7/MIS 9	25 m	
Levant Coast, East Mediterranean, Ga'ash, Israel	Temperate	Marine sands	MIS 5e	25 m	Mauz <i>et al.</i> (2013)
		Aeolian sands	80-51 ka (MIS 3?)	32 m	
		Aeolian sands	51-40 ka	15m	
Bermuda	Sub-tropical	Southampton Formation – aeolian	MIS 5a	1.5 m	Hearty (2002)
		Hungry Bay Formation – aeolian	MIS 5c	4 m	
		Devonshire Formation – marine	MIS 5e	3 m	
		Grape Bay Member of Rock Bay Formation	MIS 5e	3.5 m	
Rottneest Island, Western Australia	Temperate	Fish Hook Bay – aeolian	MIS 3	4 m	Hearty (2003)
			MIS 5a?	4m	
			MIS 5c?	5 m	
		Fairbridge Bluff (Unit IV) – subtidal	MIS 5e	4 m	
		Mary Cove (Unit IV) – subtidal	MIS 5e	5 m	

As previously mentioned, few interglacial aeolianite successions are preserved that are greater than MIS 5e in age. One such succession is that of the Wilderness Embayment, South Africa, where the slowly uplifting coastline preserves three barrier shorelines, which extend over 250 m APSL (Bateman *et al.*, 2011). The barriers are suggested to have been composite deposits, with core sediment within the barrier complex deposited in previous interglacial highstands (Bateman *et al.*, 2011). Without further stratigraphical interpretation of facies architecture and more extensive sampling to determine the elevation of truncation surfaces separating successive interglacial deposits it is difficult to determine the volume of sediment that is attributed to a single sea-level highstand. It is evident, however, that these barriers are substantially larger than those on the Mount Gambier coastal plain and potentially signify a more productive offshore carbonate shelf off the South African coast. On Eleuthera Island, Bahamas, Hearty (1998) has described at least four aeolianite units associated with MIS 5a, MIS 5e, MIS 7 and MIS 9/11. Vertically, the thickest of these is the MIS 9/11 deposit, which would correlate well with the tallest barrier shoreline on the Mount Gambier coastal plain, Gambier Range. This may provide support for a more intense MIS 11 interglacial, in which warmer temperatures may have resulted in greater volumes of carbonate production and thus sediment available for onshore deposition. However, further geochronological and stratigraphical analysis is required of both regions to constrain the age of successions and to determine whether any underlying units within the Gambier Range are older than MIS 11 in age. Without more extensive sampling in other global interglacial aeolianite deposits it is not possible to determine whether the trend in increased interglacial intensity with increased shoreline barrier volume is evident.

## 6.7 Conclusions

This thesis has examined the successive development of the Bridgewater Formation on the Mount Gambier coastal plain, southern Australia through extensive stratigraphical, petrographical and geochronological analysis. The facies architecture of multiple exposures within barrier shorelines has been described to reconstruct the depositional history and coastal evolution of the region. Stratigraphical descriptions have also identified both fixed and relational palaeo-sea level indicators within each successive barrier. The extent of diagenesis within exposures of Bridgewater Formation has been assessed from the large scale in terms of karst development to the small scale through SEM analyses of single foraminifer tests. This has allowed for modes of sediment transport, diagenetic environments and overall preservation of barrier successions to be determined, further enhancing knowledge of coastal evolution within the region. Geochronological analysis in the form of radiocarbon, OSL and AAR dating has

constrained the formation of barrier shorelines to successive interglacials (with the identification of several composite barriers) and confirms the hypothesis of Sprigg (1952) that barriers correlate with those on the Robe coastal plain. Assemblage of a chronology for barrier deposition and application of predetermined rates of uplift to the coastal plain has allowed for the construction of an interglacial palaeo-sea level record extending back over 680 ka. From these findings several significant conclusions can be drawn:

1. Barrier shorelines across the Mount Gambier coastal plain were formed during successive interglacial sea-level highstands extending back to MIS 17 and are correlative to those on the Robe coastal plain, confirming the hypotheses of Sprigg (1952). Due to the resolution of AAR, it was not possible to determine with certainty whether barriers were deposited following periods of Northern Hemisphere insolation maximum and thus it was not possible to determine whether deposition timing was determined by the Milankovitch (1941) orbital cycles. However, age estimates from AAR geochronology do not rule out such a possibility.
2. A sea-level record for sequential interglacial highstands over the past 680 ka is presented from a far-field site from Quaternary ice-sheets. Significant aspects of this record include; the identification of a palaeo-beach facies at Port MacDonnell Beach that has been constrained to be of MIS 5c age and thus represents the first subaqueously deposited coastal strata of this age above present sea level to be described on the Australian continent. The derived MIS 5c palaeo-sea level of  $-14 \pm 2$  m compares well with other interstadial deposits within far-field zones of Quaternary ice sheets such as Haiti (Dodge *et al.*, 1983; Dumas *et al.*, 2006) and Papua New Guinea (Chappell and Shackleton, 1986). OSL analysis has confirmed MacDonnell Range is a southern extension of the last interglacial (MIS 5e) Woakwine barrier shoreline. Derived palaeo-sea level for MIS 7 and 9 are not significantly lower than present and suggest sea-level was within 3.5 m of its current elevation. Lowest sea-level was derived for MIS 11, 13 and 17. While derived minimum sea level from these deposits is lower than present sea level it is suggested that this reflects erosion of older successions. Few palaeo-sea level records from coastal deposits extend this far into the middle Pleistocene, and the Mount Gambier coastal plain record compares well with others that do, including the record from Sumba Island, Indonesia (Pirazzoli *et al.*, 1991) and the record derived from the Robe coastal plain (Murray-Wallace *et al.*, 2001).
3. The use of SRTM data has allowed the overall morphology of barrier successions across the coastal plain to be determined. This is the first time this technique has been used within the region to determine barrier morphology and provides a platform for further work. The use of

SRTM data in this thesis has allowed for estimations of sediment volumes within barriers to be calculated and the comparison of volumetric size of these features with correlative features on the Robe coastal plain and other calcarenite successions globally. A trend was identified between proposed interglacial intensity and barrier sediment volume, potentially reflecting an increase in carbonate production on the Bonney Shelf during more intense interglacials.

4. While barriers were found to be formed during successive interglacials, detailed petrological and geochronological assessments allowed for further detailed descriptions of coastal evolution within the region. For example, it was identified that sediment within Burleigh Range had been reworked from older deposits potentially through the regression and subsequent transgression of sea-level cycles. Within the raised Holocene beach at Port MacDonnell it is suggested that the older age of sediment in comparison to shell within the same succession may relate to the reworking of older sediment during the Holocene sea-level highstand. The combination of geochronological and stratigraphical analysis allowed for the identification of composite deposits, where sediments within barriers were deposited during more than one sea-level highstand, such as Robe and Compton Ranges. Analysis of karst structures at sample sites suggested that denudation had occurred within the most landward barriers, and provided reasoning for their subdued topography.

5. AAR analyses of single tests of foraminifers within calcarenite was found to be more accurate than whole-rock analysis of multiple skeletal carbonate grains, which were commonly found to have leached lower molecular amino acids, and from fossil shell which may have recrystallised. The use of single test analysis of foraminifera allowed for the identification of diagenetically altered tests which could easily be omitted from calculations of mean age. Single test analyses have not previously been applied to foraminifera on the coastal plain and it is suggested that potential further AAR work in the region, especially within older study sites, use or incorporate this method.

In light of the previous discussion throughout this chapter the significance of the Mount Gambier sea-level record becomes evident. Despite the limitations described, the results of this thesis are important for several reasons. Firstly, the location of the southern Australian continental margin within a far-field zone from Quaternary ice sheets indicates that the derived sea-level record within this region is primarily a eustatic archive. Secondly, palaeo-sea level records of such length (up to 680 ka) are rarely identified in the morphological record. On the Mount Gambier coastal plain the preservation of barrier shorelines is a result of the gentle tectonic uplift of the region and the development of pervasive calcrete horizons

overlying the successions which have been promoted in the semi-arid climate. While further research will continue to constrain the geochronology and relative sea-level associated with the formation of each barrier, this thesis has set the premise for the development of a globally significant sea-level record.

## **6.8 Further research**

As with increased study of any topic, several new research questions are proposed that were beyond the scope of this thesis. To further constrain palaeo-sea level records of the Mount Gambier coastal plain a more detailed investigation into Quaternary uplift rates is required. These are especially necessary in western Victoria, where Bridgewater Formation is exposed within Mingbool and Dismal Ranges, and should encompass the influence of other volcanic provinces within western Victoria. Identification of a last interglacial shoreline within the Nelson area would aid in constraining the rates of uplift for the last 125 ka at least, though extrapolation of uplift rates beyond this time may be less reliable. Drilling into the barrier succession shoreward of the Glenelg River within the Nelson region may lead to the identification of a range of coastal facies associated with past interglacial sea-level highstands and application of geochronological techniques may constrain the depositional timing of these deposits.

The identification of more accurate or fixed sea-level markers across the Mount Gambier coastal plain is required to further constrain palaeo-sea level estimates. For example, within barrier shoreline successions landwards of and including Gambier Range only subaqueous facies are identified, from which only minimum palaeo-sea level elevations can be derived. Extensive drilling across the coastal plain could aid in the identification of more palaeo-beach deposits, especially within regions where they may presently be covered by once landward transgressing aeolian dunes, for example MacDonnell Range. Palaeo-beach deposits could further constrain past sea-levels if they can be accurately correlated with present tidal ranges.

Additional research could investigate the potential aeolian reworking of barrier successions during glacials over a wider study area. This would aid in evaluating the long-standing debate of whether coastal aeolianites were deposited during sea-level highstands or lowstands. Such a study could also investigate palaeo-wind directions in coastal regions compared with continental Australia and further enhance knowledge of palaeo-climate during the last glacial.



Several fault systems are identified across the Mount Gambier coastal plain, such as the Kanawinka Fault and Tartwaup Fault. Further research could investigate the relationship between the fault networks and the formation of barrier shorelines to determine whether faults have constrained barrier morphology. Investigation into the presence and elevation of the water table within these barrier successions may also reveal how dissolutional and erosional processes have influenced barrier morphology or resulted in denudation of the barrier shoreline complexes.

One specific site of interest for further research is Cape Northumberland. Within the coastal cliffs at this locality, described in this study as an extension of the Robe Range, multiple aeolianite deposits are separated by undercut units approximately 30 cm thick, potentially reflecting former protosols or palaeosols. Five cross-bedded aeolianite units are identified and potentially represent shorter (than interglacial or perhaps even interstadial) sea-level highstands. Further research is proposed to scale the aeolianite cliffs, describing the stratigraphy and sub-sampling sediment from each unit. Geochronological analysis would aid in constraining the depositional timing of these units. AAR would not be a suitable technique as its resolution is too poor, and thus OSL is suggested to be more appropriate. Detailed chronostratigraphy of these deposits could reveal if they formed during shorter sea-level highstands such as Heinrich events or Dansgaard-Oeschger events that have been described in the North Atlantic but have not commonly been detailed within the Southern Ocean.

# Bibliography

- Abegg, R.E., Loope, D.B. and Harris, P.M. (2001) Carbonate eolianites – Depositional models and diagenesis, *In* Abegg, F.E., Harris, P.M., Loope, D.B. (Eds.) *Modern and ancient carbonate eolianites: sedimentology, sequence stratigraphy, and diagenesis*, p17-30, SEPM Special Publication, **71**.
- Abelson, P.H. (1954) Amino acids in fossils, *Science*, **119**, 576.
- Aharon, P. (1983) 140,000 yr isotope climatic record from raised coral reefs in New Guinea, *Nature*, **304**, 720-723.
- Aharon, P. (1984) Implications of the coral-reef record from New Guinea concerning the astronomical theory of ice ages, *In* Berger, A., Imbrie, J., Hays, J., Kukla, G. and Saltzman, B. (Eds.) *Milankovitch and Climate: Understanding the Response to Astronomical Forcing* p379-389, Reidel, Dordrecht, The Netherlands.
- Aitken, M.J. (1985) *Thermoluminescence Dating*, Academic Press, London, pp 359.
- Aitken, M.J. (1988) *An introduction to optical dating*, Oxford University Press, Oxford, pp 267.
- Alley, N.F. (1995) Late Palaeozoic, *In* Drexel, D.F. and Preiss, W.V. (Eds.) *The geology of South Australia, Volume 2, The Phanerozoic*, p63-91, South Australia Geological Survey, Bulletin **54**.
- Alley, N.F. and Lindsay, J.M. (1995) Tertiary, *In* Drexel, D.F. and Preiss, W.V. (Eds.) *The geology of South Australia, Volume 2, The Phanerozoic*, p151-217, South Australia, Geological Survey, Bulletin **54**.
- Anderson, M.B., Stirling, C.H., Potter, E-K., Halliday, A.N., Blake, S.G., McCulloch, M.T., Ayling, B.F., O'Leary, M.J. (2010) The timing of sea-level high-stands during Marine Isotope Stages 7.5 and 9: Constraints from the uranium-series dating of fossil corals from Henderson Island, *Geochimica et Cosmochimica Acta*, **74**, 3598-3620.
- Ankjærsgaard, C. and Murray, A.S. (2007) Total beta and gamma dose rates in trapped charge dating based on beta counting, *Radiation Measurements*, **42**, 352-359.
- Bada, J.L. (1985) Racemization of amino acids, *In* Barrett, G.C. (Ed.) *Chemistry and Biochemistry of the amino acids*, p399-414, Chapman & Hall.
- Bada, J.L. and Man, E.H. (1980) Amino acid diagenesis in deep sea drilling project cores: Kinetics and mechanisms of some reactions and their application in geochronology and in paleotemperature and heat flow determinations, *Earth Science Reviews*, **16**, 21- 55.
- Bada, J.L. and Schroeder, R.A. (1975) Amino acid racemization reactions and the geological implications, *Naturwissenschaften*, **62**, 71-79.

- Bada, J.L. and Shou, M.-Y. (1980) Kinetics and mechanism of amino acid racemization in aqueous solution and in bones, *In* Hare, P.E., Hoering, T.C. and King, K. Jr. (Eds.) *Biogeochemistry of Amino Acids*, p235-255, Wiley, New York.
- Banerjee, D., Hildebrand, A.N., Murray-Wallace, C.V., Bourman, R.P., Brooke, B.P. and Blair, M. (2003) New quartz SAR-OSL ages from the stranded beach dune sequence in south-east South Australia, *Quaternary Science Reviews*, **22**, 1019-1025.
- Barbetti, M. and Sheard, M.J. (1981) Palaeomagnetic results from Mounts Gambier and Schank, South Australia, *Journal of the Geological Society of Australia*, **28**, 385-394.
- Bard, E., Fairbanks, R.G., Hamelin, B., Zindler, A. and Hoang, C.T. (1991) Uranium-234 anomalies in corals older than 150,000 years, *Geochimica et Cosmochimica Acta*, **55**, 2385-2390.
- Bard, E., Antonioli, F. and Silenzi, S. (2002) Sea-level during the penultimate interglacial period based on a submerged stalagmite from Argentarola Cave (Italy), *Earth and Planetary Science Letters*, **196**, 135-146.
- Barwis, J.H. and Tankard, A.J. (1983) Pleistocene shoreline deposition and sea-level history at Swartklip, South Africa, *Journal of Sedimentary Petrology*, **53**, 1281-1294.
- Bateman, M.D., Holmes, P.J., Carr, A.S., Horton, B.P. and Jaiswal, M.K. (2004) Aeolianite and barrier dune construction spanning the last two glacial-interglacial cycles from the southern Cape coast, South Africa, *Quaternary Science Reviews*, **23**, 1681-1698.
- Bateman, M.D., Carr, A.S., Dunajko, A.C., Holmes, P.J., Roberts, D.L., McLaren, S.J., Bryant, R.G., Marker, M.E. and Murray-Wallace, C.V. (2011) The evolution of coastal barrier systems: a case study of the Middle-Late Pleistocene Wilderness barriers, South Africa, *Quaternary Science Reviews*, **30**, 63-81.
- Bathurst, R.G. (1972) *Carbonate sediments and their diagenesis*, Developments in sedimentology **12**, Elsevier Publication Company, Amsterdam, pp 620.
- Belknap, D.F. and Kraft, J.C. (1981) Preservation potential of transgressive coastal lithosomes on the U.S. Atlantic shelf, *Developments in Sedimentology*, **32**, 429-442.
- Belperio, A.P. (1988) Fowlers Bay rotary drilling report and revision of the Quaternary geology around Fowlers Bay, *South Australia Department of Mines and Energy, Report Book 88*.
- Belperio, A.P. (1995) Quaternary, *In* Drexel, J.F. and Preiss, W.V. (Eds.) *The geology of South Australia, Volume 2, The Phanerozoic*, p219-281, South Australia, Geological Survey, Bulletin **54**.
- Belperio, A.P. and Bluck, R.G. (1990) Coastal palaeogeography and heavy mineral sand exploration targets in the western Murray Basin, South Australia, p5-10, *Australian Institute of Mining and Metallurgy, Proceedings*, **295**.

- Belperio, A.P. and Cann, J.H. (1990) Quaternary evolution of the Robe-Naracoorte coastal plain: an excursion guide, *South Australia, Department of Mines and Energy, Report Book*, 90/27.
- Belperio, A.P. and Fotheringham, D.G. (1990) Geological setting of two Quaternary footprint sites, western South Australia, *Australian Journal of Earth Sciences*, **37**, 37-42.
- Belperio, A.P., Murray-Wallace, C.V. and Cann, J.H. (1995) The last interglacial shoreline in southern Australia: Morphostratigraphic variations in a temperate carbonate setting, *Quaternary International*, **26**, 7-19.
- Belperio, A.P., Harvey, N., Bourman, R.P. (2002) Spatial and temporal variability in the Holocene palaeosea-level record around the South Australian coastline, *Sedimentary Geology*, **150**, 153-169.
- Bender, M.L., Fairbanks, R.G., Taylor, F.W., Matthews, R.K., Goddard, J.G. and Broecker, W.S. (1979) Uranium-series dating of the Pleistocene reef tracts of Barbados, West Indies, *Geological Society of America Bulletin*, **90**, 557-594.
- Bender, M., Sowers, T., Dickson, M-L., Orchardo, J., Grootes, P., Mayewski, P.A. and Meese, D.A. (1994) Climate correlations between Greenland and Antarctica during the past 100,000 years, *Nature*, **372**, 663-666.
- Berger, A. and Loutre, M.F. (1991) Insolation values for the climate of the last 10 million years, *Quaternary Science Reviews*, **10**, 297-317.
- Berstad, I.M., Lundberg, J., Lauritxen, S.-E., and Linge, H.C. (2002) Comparison of the climate during marine isotope stage 9 and 11 inferred from a speleothem isotope record from Northern Norway, *Quaternary Research*, **58**, 361-371.
- Billeaud, I., Tessier, B., Lesueur, P., Caline, B. (2007) Preservation potential of highstand coastal sedimentary bodies in a macrotidal basin: Example for the Bay of Mont-Saint-Michel, NW France, *Sedimentary Geology*, **202**, 745-775.
- Bintanja, R., van der Wal, R.S.W. and Oerleman, J. (2005) Modelled atmospheric temperatures and global sea levels over the past million years, *Nature*, **437**, 125-128.
- Birch, G.F. (1977) Surficial sediments on the continental margin off the west coast of South Africa, *Marine Geology*, **23**, 305-377.
- Blackburn, G. (1962) Stranded coastal dunes in northwestern Victoria, *Australian Journal of Science*, **24**, 95-96.
- Blackburn, G., Bond, R.D. and Clarke, A.R.P. (1965) Soil development associated with stranded beach ridges in south-east South Australia, *Soil Publication No 22*, Commonwealth Scientific and Industrial Research Organisation, Melbourne, Australia.
- Blackburn, G., Allison, G.B. and Leaney, F.W.J. (1982) Further evidence of the age of tuff at Mt. Gambier, South Australia, *Royal Society of South Australia, Transactions*, **106**, 163-167.

- Blakemore, A.G., Murray-Wallace, C.V. and Lachlan, T.J. (2014) First recorded evidence of subaqueously-deposited late Pleistocene interstadial (MIS 5c) coastal strata above present sea level in Australia, *Marine Geology*, **355**, 377-383.
- Blatt, H., Middleton, G. and Murray, R. (1980) *Origin of Sedimentary Rocks*, Prentice-Hall, New Jersey, pp 782.
- Blay, C.T. and Longman, M.W. (2001) Stratigraphy and sedimentology of Pleistocene and Holocene carbonate eolianites, Kaua'i, Hawai'i, USA, *SEPM Special Publication*, **71**, 93-115.
- Boggs, S. (2001) *Principles of Sedimentology and Stratigraphy*, Prentice Hall, New Jersey, pp 726.
- Boreen, T., James, N., Wilson, C. and Heggie, D. (1993) Surficial cool-water carbonate sediments on the Otway continental margin, southeastern Australia, *Marine Geology*, **112**, 35-56.
- Bøtter-Jensen, L., Mejdahl, V. (1988) Assessment of beta dose-rate using a GM multicounter system. *Nuclear Tracks and Radiation Measurements*, **14**, 187-191.
- Bøtter-Jensen, L., Bulur, E., Duller, G.A.T., Murray, A.S. (2000) Advances in luminescence instrument systems, *Radiation Measurements*, **32**, 523-528.
- Bøtter-Jensen, L., Andersen, C.E., Duller, D.A.T., Murray, A.S. (2003) Developments in radiation, stimulation and observation facilities in luminescence measurements, *Radiation Measurements*, **37**, 535-541.
- Boutakoff, N. (1952) The structural pattern of south-west Victoria, *Mining and Geological Journal of Victoria*, **4**, 21-29.
- Boutakoff, N. (1963) The geology and geomorphology of the Portland area, *Victoria Geological Survey, Memoir* **22**.
- Boutakoff, N., and Sprigg, R.C. (1953) Summary report on the petroleum possibilities of the Mt. Gambier sunklans, *Mining and Geological Journal, Department of Mines, Victoria*, **5**, 28-42.
- Bowen, D.Q. (1978) *Quaternary Geology: A Stratigraphic Framework for Multidisciplinary Work*, Pergamon Press, London, pp 221.
- Bowen, D.Q. (2010) Sea Level ~400,000 years ago (MIS 11): analogue for present and future sea level? *Climate of the Past*, **6**, 9-19.
- Bowen, D.Q. and Sykes, G.A. (1985) Amino acid geochronology of raised beaches in south west Britain, *Quaternary Science Reviews*, **4**, 279-318.
- Bowler, J.M. (1975) Deglacial events in southern Australia: their age, nature and palaeoclimatic significance, In: Suggate, R.P. and Cresswell, M.M. (Eds.) *Quaternary Studies*, The Royal Society of New Zealand, 75-82.

- Bowler, J.M. (1976) Aridity in Australia: age, origins and expression in aeolian landforms and sediments, *Earth-Science Reviews*, **12**, 279-310.
- Bowler, J.M. (1982) Aridity in the late Tertiary and Quaternary in Australia, *In* Barker, W.R. and Greenslade, P.J.M. (Eds.) *Evolution of the flora and fauna of arid Australia*, p35-45, Peacock Publications, Adelaide.
- Bradley, R.S. (1985) *Quaternary Paleoclimatology: methods of paleoclimatic reconstruction*. Allen and Unwin, Boston, pp 472.
- Brennan, B.J. (2003) Beta doses to spherical grains, *Radiation Measurements*, **37**, 299-303.
- Brett, C.E. and Baird, G.C. (1986) Comparative taphonomy: a key to palaeoenvironmental interpretation based on fossil preservation, *Palaaios*, **1**, 207-227.
- Bretz, J.H. (1960) Bermuda: A partially drowned, late mature Pleistocene karst: *Geological Society of America Bulletin*, **71**, 1729-1754.
- Bricker, O.P. and Mackenzie, F.T. (1970) Limestones and red soils of Bermuda, Discussion, *Geological Society of America Bulletin*, **81**, 2523-2524.
- Brigham, J.K. (1983) Intrashell variations in amino acid concentrations and isoleucine epimerization ratios in fossil *Hiatella arctica*, *Geology*, **11**, 509-513.
- Broecker, W.S. (1963) A preliminary evaluation of uranium series inequilibrium as a tool for absolute age measurement on marine carbonates, *Journal of Geophysical Research*, **68**, 2817-2834.
- Broecker, W.S. and van Donk, J. (1970) Insolation changes, ice volumes and the O<sup>18</sup> record in deep-sea cores, *Reviews of Geophysics and Space Physics*, **8**, 169-198.
- Broecker, W.S., Thurber, D.L., Goddard, J., Ku, T., Matthews, R.K. and Mesolella, K.J. (1968) Milankovitch hypothesis supported by precise dating of coral reefs and deep sea sediments, *Science*, **159**, 297-300.
- Brooke, B. (1999) *Quaternary stratigraphy and evolution of aeolianite on Lord Howe Island*, unpublished Ph.D thesis, School of Geosciences, University of Wollongong, Australia.
- Brooke, B. (2001) The distribution of carbonate eolianite, *Earth Science Reviews*, **55**, 135-164.
- Brooke, B., Murray-Wallace, C.V., Woodroffe, C.D. and Heijnis, H. (2003) Quaternary aminostratigraphy of eolianite on Lord Howe Island, Southwest Pacific Ocean, *Quaternary Science Reviews*, **22**, 387-406.
- Brookfield, M.E. (1977) The origin of bounding surfaces in ancient aeolian sandstones, *Sedimentology*, **24**, 303-332.
- Brookfield, M.E. (1992) Eolian Systems, *In* Walker, R.G. and James, N.P. (Eds.) *Facies Models Response to Sea Level Change*, p143-156, Geological Association of Canada.

Budd, D.A. (1988) Aragonite-to-calcite transformation during freshwater diagenesis of carbonate: insights from pore water chemistry: *Geological Society of America Bulletin*, **100**, 1260-1270.

Budd, D.A., Gaswirth, S.B. and Oliver, W.L. (2002) Quantification of macroscopic subaerial exposure features in carbonate rocks, *Journal of Sedimentary Research*, **72**, 917-928.

Bureau of Meteorology (2013) Climate data online  
<http://www.bom.gov.au/climate/data/index>

Butzer, K.W. and Cuerda, J. (1962) Coastal stratigraphy of Southern Mallorca and its implication for the Pleistocene chronology of the Mediterranean Sea, *The Journal of Geology*, **70**, 398-416.

Buzas-Stephens, P. and Buzas, M.A. (2005) Population dynamics and dissolution of foraminifera in Nueces Bay, Texas, *Journal of Foraminiferal Research*, **35**, 248-258.

Camoin, G.F., Ebren, Ph., Eisenhauer, A., Bard, E., Faure, G. (2001) A 300,000 year coral reef record of sea level changes, Mururoa atoll (Tuamotu archipelago, French Polynesia), *Palaeogeography, Palaeoclimatology, Palaeoecology*, **175**, 325-341.

Cann, J.H. and Clarke, J.D.A. (1993) The significance of *Marginopora vertebralis* (Foraminifera) in surficial sediments at Esperance, Western Australia, and in last interglacial sediments in northern Spencer Gulf, South Australia, *Marine Geology*, **111**, 171-187.

Cann, J.J. and Gostin, V.A. (1985) Coastal sedimentary facies and foraminiferal biofacies of the St Kilda Formation at Port Gawler, South Australia, *Royal Society of South Australia, Transactions*, **109**, 121-142.

Cann, J.H., Murray-Wallace, C.V., Belperio, A.P. and Brenchley, A.J. (1999) Evolution of Holocene coastal environments near Robe, southeastern South Australia, *Quaternary International*, **56**, 81-97.

Carew, J.L. and Mylroie, J.E. (1991) Some pitfalls in paleosol interpretation in carbonate sequences, *Carbonates and Evaporites*, **6**, 69-74.

Carew, J.L. and Mylroie, J.E. (1995) Quaternary tectonic stability of the Bahamian archipelago: evidence from fossil coral reefs and flank margin caves, *Quaternary Science Reviews*, **14**, 145-153.

Carew, J.L. and Mylroie, J.E. (2001) Quaternary carbonate eolianites of the Bahamas: Useful analogues for the interpretation of ancient rocks, In Abegg, F.E., Harris, P.M., Loope, D.B. (Eds.) *Modern and ancient carbonate eolianites: sedimentology, sequence stratigraphy, and diagenesis*, p33-45, SEPM Special Publication, 71.

Carr, A.S., Bateman, M.D. and Holmes, P.J. (2007) Developing a 150 ka luminescence chronology for the barrier dunes of the Southern Cape, South Africa, *Quaternary Geochronology*, **2**, 110-116.

- Carr, A.S., Bateman, M.D., Roberts, D.L., Murray-Wallace, C.V., Jacobs, Z. and Holmes, P.J. (2010) The last interglacial sea-level highstand on the southern Cape coastline of South Africa, *Quaternary Research*, **73**, 351-363.
- Carter, R.W.G. (1986) The morphology of beach-ridge formation: Magilligan, Northern Ireland, *Marine Geology*, **73**, 191-214.
- Carter, R.W.G. and Orford, J.D. (1984) Coarse clastic barrier beaches: A discussion of the distinctive dynamic and morphosedimentary characteristics, *Marine Geology*, **60**, 377-389.
- Cavenave, A., Dominh, K., Rabinowicz, M. and Ceuleneer, G. (1988) Geoid and depth anomalies over ocean swells and troughs: evidence of an increasing trend of the geoid to depth ration with age of plate, *Journal of Geophysical Research*, **93**, 8064-8077.
- Chappell, J. (1974a) Geology of coral terraces, Huon Peninsula, New Guinea: A study of Quaternary tectonic movements and sea-level changes, *Geological Society of America Bulletin*, **85**, 553-570.
- Chappell, J. (1974b) Relationships between sea levels,  $^{18}\text{O}$  variations and orbital perturbations, during the past 250,000 years, *Nature*, **252**, 199-202.
- Chappell, J. (1987) Late Quaternary sea-level changes in the Australia region, *In* Tooley, M.J. and Shennan, I. (Eds.) *Sea-level Changes*, p296-331, Institute of British Geographers Special Publication Series, Blackwell.
- Chappell (2002) Sea level changes forced ice breakouts in the Last Glacial cycle: new results from coral terraces, *Quaternary Science Reviews*, **21**, 1229-1240.
- Chappell, J. and Polach, H. (1991) Post-glacial sea-level rise from a coral record at Huon Peninsula, Papua New Guinea, *Nature*, **349**, 147-149.
- Chappell, J. and Shackleton, N.J. (1986) Oxygen isotopes and sea level, *Nature*, **324**, 137-140.
- Chappell, J. and Veeh, H.H. (1978) Late Quaternary tectonic movements and sea-level changes at Timor and Atauro Island, *Geological Society of America Bulletin*, **89**, 356-368.
- Chappell, J., Ota, Y. and Berryman, K. (1996) Late Quaternary coseismic uplift history of Huon Peninsula, Papua New Guinea, *Quaternary Science Reviews*, **15**, 7-22.
- Chave, K.E. (1967) Recent carbonate sediments – an unconventional view, *Journal of Geological Education*, **15**, 200-204.
- Chen, J.H., Curran, H.A., White, B. and Wasserburg, G.J. (1991) Precise chronology of the last interglacial period:  $^{234}\text{U}$ - $^{230}\text{Th}$  data from fossil coral reefs in the Bahamas, *Geological Society of America Bulletin*, **103**, 82-97.
- Clark, J.A. (1978) Global changes in postglacial sea level: A numerical calculation, *Quaternary Research*, **9**, 265-287.



Clarke, S.J. and Murray-Wallace, C.V. (2006) Mathematical expression used in amino acid racemisation geochronology – A review, *Quaternary Geochronology*, **1**, 261-278.

Clemmensen, L.B., Fornos, J.J. and Rodriguez-Perea, A. (1997) Morphology and architecture of a late Pleistocene cliff-front dune, Mallorca, Western Mediterranean, *Terra Nova*, **9**, 251-254.

Clifton, H.E. (1969) Beach lamination: nature and origin, *Marine Geology*, **7**, 553-559.

Clifton, H.E., Hunter, R.E. and Phillips, R.L. (1971) Depositional structures and processes in the non-barred high-energy nearshore, *Journal of Sedimentary Petrology*, **3**, 651-670.

Colhoun, E.A., Kiernan, K., Barrows, T.T. and Geode, A. (2010) Advances in Quaternary studies in Tasmania, In Bishop, P. and Pillans, B. (Eds.) *Australian Landscapes*, p165-183, Geological Society Special Publication **346**.

Collinson, J.D. and Thompson, D.B. (1989) *Sedimentary Structures*, Unwin Hyman, London, pp 207.

Cook, P.J., Colwell, J.B., Firman, J.B., Lindsay, J.M., Schwebel, D.A. and von der Borch, C.C. (1977) The late Cainozoic sequence of southeast South Australia and Pleistocene sea-level changes, *BMR Journal of Australian Geology and Geophysics*, **2**, 81-88.

Cooper, J.A.G. (2007) Sea-level studies – High energy coasts sedimentary indicators, In Elias, S. *Encyclopedia of Quaternary Science*, 2983-2993, Elsevier.

Copyright ©Commonwealth of Australia (Geoscience Australia) 2011

Corliss, B.H. and Honjo, S. (1981) Dissolution of deep-sea benthonic foraminifera, *Micropaleontology*, **27**, 356-378.

Corrado, J.C., Weems, R.E., Hare, P.E. and Bamback, R.K. (1986) Capabilities and limitations of applied aminostratigraphy, as illustrated by analyses of *Mulinia lateralis* from the late Cenozoic marine beds near Charleston, South Carolina, *South Carolina Geology*, **30**, 19-46.

Cotter, T.L. and Hallock, P. (1988) Test surface degradation in *Archaias angulatus*, *Journal of Foraminiferal Research*, **18**, 187-202.

Crenshaw, M.A. (1980) Mechanisms of shell formation and dissolution. In Rhoads, D.C. and Lutz, R.A. (Eds.), *Skeletal Growth of Aquatic Organisms*, p115-132, Plenum, New York.

Crocker, R.L. (1946) Post-Miocene climate and geological history and its significance in relationship to the genesis of the major soil types of South Australia, *CSIRO Australia Bulletin* **193**.

Crocker, R.L. and Cotton, B.C. (1946) Some raised beaches of the lower south-east of South Australia and their significance, *Royal Society of South Australia, Transactions*, **70**, 64-82.

Croll, J. (1887) On the change in the obliquity of the ecliptic, its influence on the climate of the polar regions and on the level of the sea, *Philosophical Magazine*, **28**, 121-137.

Copper, M.L., White, S. and Neilson, J.L. (2003) Quaternary, *In* Birch, W.D. (Ed.) *Geology of Victoria*, p337-359, Geological Society of Australia, Special Publication **23**.

Dansgaard, W., Johnsen, S.J., Clausen, H.B., Dahl-Jensen, D., Gundestrup, N.S., Hammer, C.U., Hvidberg, C.S., Steffensen, J.P., Sveinbjornsdottir, A.E., Jouzel, J. and Bond, G. (1993) Evidence for general instability of past climate from a 250-kyr ice-core record, *Nature*, **364**, 218-220.

Davaud, E. and Septfontaine, M. (1995) Post-mortem onshore transportation of epiphytic foraminifera: Recent example from the Tunisian coastline, *Journal of Sedimentary Research*, **65**, 136-142.

Davidson-Arnott, R.G.D. and Greenwood, B. (1976) Facies relationships on a barred coast, Kouchibouguac Bay, New Brunswick, Canada *In* Dravis Jr., R.A. and Ethington, R.L. (Eds.) *Beach and Nearshore Sedimentation*, p149-168, SEPM special publication, **24**.

Davies, J.L. (1957) The importance of cut and fill in the development of sand beach ridges, *Australian Journal of Science*, **20**, 105-111.

Davis Jr, R.A. and Fitzgerald, D.M. (2004) *Beaches and Coasts*, Blackwell Science Ltd, Oxford, pp 419.

Dawson, A.G. (1992) *Ice Age Earth*, Routledge, London, pp 293.

Desperat, S., Sánchez Goñi, Naughton, F., Turon, J.-L., Duprat, J., Malaize, B., Cortijo, E. and Peypouquet, J.-P. (2007) Climate variability of the last five isotopic interglacials: Direct land-sea-ice correlation from the multiproxy analysis of north-western Iberian margin deep-sea cores, *In* Sirocko, F., Litt, T., Claussen, M. and Sanches-Goni, M.F. (Eds.). *The climate of past interglacials*, p375-386, Elsevier, Amsterdam.

Diz, P. and Francès, G. (2009) Postmortem processes affecting benthic foraminiferal assemblages in the Ria de Vigo, Spain: Implications for paleoenvironmental studies, *Journal of Foraminiferal Research*, **39**, 166-179.

Dodson, J.R. (1974) Vegetation history and water fluctuations at Lake Leake, south-eastern Australia I. 10,000 BP to present, *Australian Journal of Botany*, **22**, 719-741.

Dott, R.H. and Bourgeois, J. (1982) Hummocky stratification: Significant of its variable bedding sequences, *Geological Society of America Bulletin*, **8**, 663-680.

Dravis, J.J. (1996) Rapidity of freshwater calcite cementation-implications for carbonate diagenesis and sequence stratigraphy, *Sedimentary Geology*, **107**, 1-10.

Droxler, A. and Farrell, J. (2000) Marine isotope stage 11 (MIS 11): new insights for a warm future, *Global and Planetary Change*, **24**, 1-5.

Duddy, I.R. (2003) Mesozoic: a time of change in tectonic regime, *In* Birch, W.D. (Ed.) *Geology of Victoria*, p239-286, Geological Society of Australia, Special Publication **23**.

Dumas, B., Hoang, C. T., Raffy, J. (2006) Record of MIS 5 sea-level highstands based on U/Th dated coral terraces of Haiti, *Quaternary International*, **145-146**, 106-118.

- Dunham, R.J. (1962) Classification of carbonate rocks according to depositional texture, *In* Ham, W.E. (Ed.) *Classification of Carbonate Rocks*, p108-121, AAPG Memoir **1**.
- Dutton, A. and Lambeck, K. (2012) Ice volume and sea level during the last interglacial, *Science*, **337**, 216-129.
- Dutton, A., Bard, E., Antonioli, F., Esat, T.M., Lambeck, K. and McCulloch, M.T. (2009) Phasing and amplitude of sea-level and climate change during the penultimate interglacial, *Nature Geoscience*, **2**, 355-359.
- Edwards, R.L., Chen, J.H., Ku, T.-L. and Wasserburg, G.J. (1987) Precise timing of the Last Interglacial period from mass spectromic determination of Thorium-230 in corals, *Science*, **236**, 1547-1553.
- Eisenhauer, A., Zhu, Z.R., Collins, L.B., Wyrwoll, K.H. and Eichst tter, (1996) The Last interglacial sea level change: New evidence from the Abrolhos Islands, Western Australia, *Geologische Rundschau*, **85**, 606-614.
- Elliot, T. (1986) Siliclastic Shorelines, *In* Reading, H.G. (Ed.) *Sedimentary Environments and Facies*, p155-188, Blackwell, Oxford.
- Emiliani, C. (1955) Pleistocene temperatures, *Journal of Geology*, **63**, 538-578.
- EPICA community members (2004) Eight glacial cycles from an Antarctic ice core, *Nature*, **429**, 623-628.
- Esat, T.M. (1999) Rapid fluctuations in sea level recorded at Huon Peninsula during the Penultimate Deglaciation, *Science*, **283**, 197-201.
- ESRI (2002) World Continents: ESRO Data & Maps 2002, Environmental Systems Research Institute, Inc. (ESRI), Redlands, California, USA.
- Esteban, M. And Klappa, C.F. (1983) Subaerial exposure environments *In* Scholle, P.A., Bebout, D.G. and Moore, C.H. (Eds.) *Carbonate Depositional Environments*, p1-54, AAPG Memoir **33**, American Association of Petroleum Geologists, Tulsa.
- Fairbanks, R.G. (1989) A 17,000 glacio-eustatic sea level record: influence of the glacial melting rates on the Younger Dryas event and deep-ocean circulation *Nature*, **342**, 637-642.
- Fairbridge, R.W. (1953) *Australian stratigraphy*, University of Western Australia Text Books Board.
- Fairbridge, R.W. and Johnson, D.L. (1978) Eolianite, *In* Fairbridge, R.W. and Bourgeois, J. (Eds.) *The Encyclopedia of Sedimentology*, p279-282, Dowden, Hutchinson and Ross, Stroudsburg.
- Fairbridge, R.W. and Teichert, C. (1953) Soil horizons and marine bands in the coastal limestones of Western Australia, *Proceedings of the Royal Society of New South Wales*, **86**, 68-87.

- Feathers, J.K. and Migliorini, E. (2001) Luminescence dating at Katanda – a reassessment, *Quaternary Science Reviews*, **20**, 961-966.
- Fenner, C. (1930) The major structural and physiographic features of South Australia, *Transactions of the Royal Society of South Australia*, **54**, 1-36.
- Ferranti, L., Antonioli, F., Mauz, B., Amorosi, A., Dai Pra, G., Mastronuzzi, G., Monaco, C., Orrù, Pappalardo, M., Radtke, U., Renda, P., Romano, P., Sanso, P. and Verrubbi, V. (2006) Markers of the last interglacial sea-level high stand along the coast of Italy: Tectonic implications, *Quaternary International*, **145-146**, 30-54.
- Fitzsimmons, K.E., Rhodes, E.J., Magee, J.W. and Barrows, T.T. (2007a) The timing of linear dune activity in the Strzelecki and Tirari Deserts, Australia, *Quaternary Science Reviews*, **26**, 2598-2616.
- Fitzsimmons, K.E., Bowler, J.M., Rhodes, E.J. and Magee, J.M. (2007b) Relationships between desert dunes during the late Quaternary in the Lake Frome region, Strzelecki Desert, Australia, *Journal of Quaternary Science*, **22**, 549-558.
- Fletcher, C.H., Murray-Wallace, C.V., Glenn, C.R., Sherman, C.E., Popp, B. and Hessler, A. (2005) Age and origin of Late Quaternary eolianite, Kaiehu Point (Moomomi), Molokai, Hawaii, *Journal of Coastal Research Special Issue*, **42**, 97-112.
- Flügel, E. (2004) *Microfacies of carbonate rocks: analysis, interpretation and application*, Springer, Berlin, pp 976.
- Folk, R.L. (1959) Practical, petrographic classification of limestones, *Bulletin of the American Association of Petroleum Geologists*, **43**, 1-38.
- Folk, R.L. (1962) Spectral subdivision of limestone types, *In* Ham, W.E. (Ed.) *Classification of carbonate rocks*, p62-84, AAPG Memoir, **1**.
- Fornos, J.J. and Ahr, W.M. (1997) Temperate Carbonates on a modern, low-energy, isolated ramp: The Balearic platform, Spain, *Journal of Sedimentary Research*, **2**, 364-373.
- Fornos, J.J., Bromley, R.G., Clemmensen, L.B. and Rodriguez-Perea, A. (2002) Tracks and trackways of *Myotragus balearicus* Bate (Artiodactyla, Caprinae) in Pleistocene aeolianites from Mallorca (Balearic Islands, Western Mediterranean), *Palaeogeography, Palaeoclimatology, Palaeoecology*, **180**, 277-313.
- Fornos, J.J., Clemmenson, L.B., Gomez-Pujol, L. and Murray, A.S. (2009) Late Pleistocene carbonate aeolianites on Mallorca, Western Mediterranean: a luminescence chronology, *Quaternary Science Reviews*, **28**, 2697-2709.
- Forsström, L. (2001) Duration of interglacials: a controversial question, *Quaternary Science Reviews*, **20**, 1577-1586.
- Franceschini, G. and Compton, J.S. (2007) Abrasion of foraminifera tests along an active dune cordon, Western Cape, South Africa, *Palaios*, **22**, 686-690.

- Frebourg, G., Hasler, C-A., Le Geurn, P. and Davaud, E. (2008) Facies characteristics and diversity in carbonate eolianites, *Facies*, **54**, 175-191.
- Fryberger, S.G. and Schenk, C. (1981) Wind sedimentation tunnel experiments on the origins of aeolian strata, *Sedimentology*, **28**, 805-821.
- Fujioka, T. and Chappell, J. (2010) History of Australian aridity: chronology in the evolution of arid landscapes, In Bishop, P. and Pillans, B. (Eds.) *Australian Landscapes*, p121-139, Geological Society, London.
- Galbraith, R.F., Roberts, R.G., Laslett, G.M., Yoshida, H., Olley, J.M. (1999) Optical dating of single and multiple grains of quartz from Jinmium rock shelter, northern Australia: Part I, experimental design and statistical models, *Archaeometry*, **41**, 339-364.
- Gallup, C.D., Edwards, R.L. and Johnson, R.G. (1994) The timing of high sea levels over the past 200,000 years, *Science*, **263**, 796-800.
- Gallup, C.D., Cheng, H., Taylor, F.W. and Edwards, R.L. (2002) Direct determination of the timing of sea level change during Termination II, *Science*, **295**, 310-313.
- Gardner, R.A.M. and McLaren, S.J. (1994) Variability in early vadose carbonate diagenesis in sandstones, *Earth Science Reviews*, **36**, 27-45.
- Garrett, P. and Gould, S.J. (1984) Geology of New Providence Island, Bahamas, *Geological Society of America Bulletin*, **95**, 209-220.
- Gehrels, W.R. (2007) Sea-level studies - Microfossil reconstructions, In Elias, S., *Encyclopedia of Quaternary Science*, p3015-3024, Elsevier.
- Gill, E.D. (1967) Evolution of the Warrnambool-Port Fairy coast and the Tower Hill Eruption, western Victoria, In Jennings, J.N. and Marbutt, J.A. (Eds.) *Landform studies from Australia and New Guinea*, p340-364, Australian National University.
- Gill, E.D. (1988) Warrnambool – Port Fairy District, In Douglas, J.G. and Ferguson, J.A. (Eds.) *Geology of Victoria*, p374-379, Geological Society of Australia, Sydney.
- Goodfriend, G.A. (1991) Patterns of racemization and epimerization of amino acids in land snails shells over the course of the Holocene, *Geochimica et Cosmochimica Acta*, **55**, 293-302.
- Goodfriend, G.A., Hare, P.E. and Druffel, E.R.M. (1992) Aspartic acid racemisation and protein diagenesis in corals over the last 350 years, *Geochimica et Cosmochimica Acta*, **56**, 3847-3850.
- Goodfriend, G.A., Brigham-Grette, J. and Miller, G.H. (1996) Enhanced age resolution of the marine Quaternary record in the Arctic using aspartic acid racemization dating of bivalve shells, *Quaternary Research*, **45**, 176-187.
- Gostin, V.A., Belperio, A.P. and Cann, J.H. (1988) The Holocene non-tropical coastal and shelf carbonate province of southern Australia, *Sedimentary Geology*, **60**, 51-70.

- Goudie, A.S. and Sperling, C.H.B. (1977) Long distance transport of foraminiferal tests by wind in the Thar Desert, Northwest India, *Journal of Sedimentary Petrology*, **47**, 630-633.
- Greenwood, B. and Sherman, D.J. (1986) Hummocky cross-stratification in the surf zone: flow parameters and bedding genesis, *Sedimentology*, **33**, 33-45.
- Grimes, K.G. (1994) The South-East karst province of South Australia, *Environmental Geology*, **23**, 134-148.
- Guérin, G., Mercier, N., Adamiec, G. (2011) Dose-rate conversion factors: update. *Ancient TL*, **29**, 5-8.
- Hails, J.R., Belperio, A.P. and Gostin, V.A. (1984) Quaternary sea levels, Northern Spencer Gulf, Australia, *Marine Geology*, **61**, 373-389.
- Hamelin, B., Bard, E., Zindler, A. and Fairbanks, R.G. (1991)  $^{234}\text{U}/^{238}\text{U}$  mass spectrometry of corals: How accurate is the U-Th age of the last interglacial period? *Earth and Planetary Science Letters*, **106**, 169-180.
- Haq, B.U., Hardenbol, J., Vail, P.R. (1987) Chronology of fluctuating sea levels since the Triassic, *Science*, **235**, 1156-1167.
- Hare, P.E. (1974) Amino acid dating of bone - the influence of water, *Carnegie Institution of Washington Year Book*, **73**, 576-581.
- Hare, P.E. and Abelson, P.H. (1968) Racemization of amino acids in fossil shells, *Carnegie Institution of Washington Year Book*, **66**, 526-528.
- Hare, P.E. and Mitterer, R.M. (1969) Laboratory simulation of amino acid diagenesis in fossils, *Carnegie Institution of Washington Year Book*, **67**, 205-208.
- Harmon, R.S., Mitterer, R.M., Kriaušakul, N., Land, L.S., Schwarcz, H.P., Garrett, P., Larson, G.J., Vacher, H.L. and Rowe, M. (1983) U-series and amino-acid racemization geochronology of Bermuda: Implications for eustatic sea-level fluctuation over the past 250,000 years, *Palaeogeography, Palaeoclimatology, Palaeoecology*, **44**, 41-70.
- Harms, J.C., Southard, J.B., Spearing, D.R. and Walker, R.G. (1975) Depositional environments as interpreted from primary sedimentary structures and stratification sequences, *Society of Economic Paleontologists and Mineralogists Short Course Notes*, **2**, 161.
- Harrison, R.S. (1977) Caliche profiles: indicators of near-surface subaerial diagenesis, Barbados, West Indies, *Bulletin of Canadian Petroleum Geology*, **25**, 123-173.
- Harrison, R.S. and Steinen, R.P. (1978) Subaerial crusts, caliche profiles, and breccia horizons: Comparison of some Holocene and Mississippian exposure surfaces, Barbados and Kentucky, *Geological Society of America Bulletin*, **89**, 385-396.
- Hays, J.D., Imbrie, J. and Shackleton, N.J., (1976) Variations in the Earth's Orbit: Pacemaker of the Ice Ages, *Science*, **194**, 1121-1132.

- Hearty, P.J. (1986) An inventory of last interglacial (*sensu lato*) age deposits from the Mediterranean basin: A study of isoleucine epimerization and U-series dating, *Zeitschrift für Geomorphologie*, **62**, 61-69.
- Hearty, P.J. (1987) New data on the Pleistocene of Mallorca, *Quaternary Science Reviews*, **6**, 245-257.
- Hearty, P.J. (1998) The geology of Eleuthera Island, Bahamas: A Rosetta Stone of Quaternary stratigraphy and sea-level history, *Quaternary Science Reviews*, **17**, 333-355.
- Hearty, P.J. (2002) Revision of the late Pleistocene stratigraphy of Bermuda, *Sedimentary Geology*, **153**, 1-21.
- Hearty, P.J. (2003) Stratigraphy and timing of eolianite deposition on Rottneest Island, Western Australia, *Quaternary Research*, **60**, 211-222.
- Hearty, P.J. and Aharon, P. (1988) Amino acid chronostratigraphy of late Quaternary coral reefs: Huon Peninsula, New Guinea, and the Great Barrier Reef, Australia, *Geology*, **16**, 579-583.
- Hearty, P.J. and Kaufman, D.S. (2000) Whole-rock aminostratigraphy and Quaternary sea-level history of the Bahamas, *Quaternary Research*, **54**, 163-173.
- Hearty, P.J. and Kindler, P. (1993) New perspectives on Bahamian Geology: San Salvador Island, Bahamas, *Journal of Coastal Research*, **9**, 577-594.
- Hearty, P.J. and Kindler, P. (1995) Sea-level highstand chronology from stable carbonate platforms (Bermuda and the Bahamas), *Journal of Coastal Research*, **11**, 675-689.
- Hearty, P.J. and Kindler, P. (1997) The stratigraphy and surficial geology of New Providence Island, Bahamas, *Journal of Coastal Research*, **13**, 798-812.
- Hearty, P.J. and Neumann, A.C. (2001) Rapid sea level and climate change at the close of the Last Interglaciation (MIS 5e): evidence from the Bahama Islands, *Quaternary Science Reviews*, **20**, 1881-1895.
- Hearty, P.J. and O'Leary, M.J. (2008) Carbonate eolianites, quartz sands, and Quaternary sea-level cycles, Western Australia: A chronostratigraphic approach, *Quaternary Geochronology*, **3**, 26-55.
- Hearty, P.J. and Vacher, H.L. (1994) Quaternary stratigraphy of Bermuda: A high resolution pre-Sangamonian rock record, *Quaternary Science Reviews*, **13**, 685-697.
- Hearty, P.J., Vacher, H.L. and Mitterer, R.M. (1992) Aminostratigraphy and ages of Pleistocene limestones of Bermuda, *Geological Society of America Bulletin*, **104**, 471-480.
- Hearty, P.J., Kindler, P., Cheng, H. and Edwards, R.L. (1999) A +20m middle Pleistocene sea-level highstand (Bermuda and the Bahamas) due to partial collapse of Antarctic ice, *Geology*, **27**, 375-378.

Hearty, P.J., Kaufman, D.S., Olson, S.L. and James, H.F. (2000) Stratigraphy and whole-rock amino acid geochronology of key and last interglacial carbonate deposits in the Hawaiian Islands, *Pacific Science*, **54**, 423-442.

Hearty, P.J., O'Leary, M.J., Kaufman, D.S., Page, M.C. and Bright, J. (2004) Amino acid geochronology of individual foraminifer (*Pulleniatina obliquiloculata*) tests, north Queensland margin, Australia: A new approach to correlating and dating Quaternary tropical marine sediment cores, *Paleoceanography*, **19**, doi:10.1029/2004PA001059.

Hearty, P.J., Hollin, J.T., Neumann, A.C., O'Leary, M.J. and McCulloch, M. (2007) Global sea-level fluctuations during the Last Interglaciation (MIS 5e), *Quaternary Science Reviews*, **26**, 2090-2112.

Henderson, G.M. and Slowey, N.C. (2000) Evidence from U-Th dating against Northern Hemisphere forcing of the penultimate deglaciation, *Nature*, **404**, 61-66.

Henderson, G.M., Cohen, and O'Nions, R.K. (1993)  $^{234}\text{U}/^{238}\text{U}$  ratios and  $^{230}\text{Th}$  ages for Hateruma Atoll corals: implications for coral diagenesis and seawater  $^{234}\text{U}/^{238}\text{U}$  ratios, *Earth and Planetary Science Letters*, **115**, 65-75.

Henderson, G.M., Robinson, L.F., Cox, K. and Thomas, A.L. (2006) Recognition of non-Milankovitch sea-level highstands at 185 and 343 thousand years ago from U-Th dating of Bahamas sediment, *Quaternary Science Reviews*, **25**, 3346-3358.

Herrero, C. and Canales, M.L. (2002) Taphonomic processes in selected Lower and Middle Jurassic foraminifera from the Iberian Range and Basque-Cantabrian Basin (Spain), *Journal of Foraminiferal Research*, **32**, 22-42.

Herwitz, S.R. (1993) Stemflow influences on the formation of solution pipes in Bermuda eolianite, *Geomorphology*, **6**, 253-271.

Hesp, P.A. (1984) Foredune Formation, In Thom, B.G. (Ed.) *Coastal geomorphology in Australia*, p69-98, Academic Press, Sydney.

Hodell, D.A., Charles, C.D. and Ninnemann, U.S. (2000) Comparison of the southern ocean for the past 450kyr: implications for Marine Isotope Stage (MIS) 11, *Global and Planetary Change*, **27**, 7-26.

Holdgate, G.R. and Gallagher, S.J. (2003) Tertiary: a period of transition to marine basin environments, In Birch, W.D. (Ed.) *Geology of Victoria*, p289-335, Geological Society of Australia, Special Publication **23**.

Hooghiemstra, H., Melice, J.L., Berger, A. and Shackleton, N.J. (1993) Frequency spectra and paleoclimatic variability of the high-resolution 30-1450 ka Funza I pollen record (Eastern Cordillera, Columbia), *Quaternary Science Reviews*, **12**, 141-156.

Hossfeld, P.A. (1950) The Late Cainozoic history of the south-east of South Australia, *Royal Society of South Australia, Transactions*, **73**, 232-279.



- Howard, W.R. (1997) A warm future in the past, *Nature*, **388**, 418-419.
- Howard, J.D. and Reineck, H-E. (1981) Depositional facies of high-energy beach-to-offshore sequence: Comparison with low-energy sequence, *AAPG Bulletin*, **65**, 807-830.
- Howchin, W. (1935) Notes on the geological sections obtained by several borings situated on the plain between Adelaide and Gulf St. Vincent, *Royal Society of South Australia, Transactions*, **59**, 68-102.
- Hunter, R.E. (1977) Basic types of stratification in small eolian dunes, *Sedimentology*, **24**, 361-387.
- Hunter, R.E. (1981) Stratification styles in eolian sandstones: some Pennsylvanian to Jurassic examples from the Western Interior USA, In Ethridge, F.G. and Flores, R.M. (Eds.) *Recent and Ancient Nonmarine Depositional Environments: Models for Exploration*, p315-329, Society of Economic Paleontologists Mineralogists, Special Publication **31**.
- Hunter, R.E., Clifton, H.E. and Phillips, R.L. (1979) Depositional processes, sedimentary structures, and predicted vertical sequences in barred nearshore systems, southern Oregon coast, *Journal of Sedimentary Petrology*, **49**, 711-726.
- Huntley, D.J., Hutton, J.T. and Prescott, J.R. (1993a) The stranded beach-dune sequence of south-east South Australia: a test of thermoluminescence dating, 0-800 ka, *Quaternary Science Reviews*, **12**, 1-20.
- Huntley, D.J., Hutton, J.T. and Prescott, J.R. (1993b) Optical dating using inclusions within quartz grains, *Geology*, **21**, 1087-1090.
- Huntley, D.J., Hutton, J.T. and Prescott, J.R. (1994) Further thermoluminescence dates from the dune sequence in the southeast of South Australia, *Quaternary Science Reviews*, **13**, 201-207.
- IBM Corp. (2010) *IBM SPSS Statistics for Windows*, version 19, Armonk, New York, IBM Corp.
- Idnurm, M. and Cook, P.J. (1980) Palaeomagnetism of beach ridges in South Australia and the Milankovitch theory of ice ages, *Nature*, **286**, 699-702.
- Imbrie, J., Hays, J.D., Martinson, D.G., McIntyre, A., Mix, A.C., Morley, J.J., Pisias, N.G., Prell, W.L. and Shackleton, N.J. (1984) The orbital theory of Pleistocene climate: Support from a revised chronology of the marine  $\delta^{18}\text{O}$  record, In Berger, A., Imbrie, J., Hays, J., Kukla, G. and Saltzman, B. (Eds.) *Milankovitch and Climate: Understanding the Response to Astronomical Forcing*, p269-305, Reidel, Dordrecht, The Netherlands.
- Imbrie, J., Mix, A.C. and Martinson, D.G. (1993) Milankovitch theory viewed from Devil's Hole, *Nature*, **363**, 531-533.
- IPCC (2007) Climate Change 2007: The physical science basis. Contribution of working group I to the Fourth Assessment Report of the Intergovernmental Panel on Climate Change {S. Solomon, D. Qin, M. Manning, Z. Chen, M. Marquis, K.B. Averyt, M. Tignor and H.L. Miller (Eds.)}, *Cambridge University Press*, Cambridge.

Irving, A.J. and Green, D.H. (1976) Geochemistry and petrogenesis of the newer basalts of Victoria and South Australia, *Journal of the Geological Society of Australia*, **23**, 45-66.

Jacobs, Z. (2004) Development of luminescence techniques for dating Middle Stone Age sites in South Africa. Unpublished Ph.D thesis, University of Wales, Aberystwyth.

Jacobs, Z., Wintle, A. G. and Duller, G. A. T. (2003) Optical dating of dune sand from Blombos Cave, South Africa: I—multiple grain data. *Journal of Human Evolution*, **44**, 599-612.

James, N.P. (1997) The cool-water carbonate depositional realm. In James, N.P., Clarke, J.A.D. (Eds.) *Cool-water Carbonates*, p1-21, SEPM Special Publication No. **56**, Society for Sedimentary Geology, Tulsa.

James, N.P. and Bone, Y. (1989) Petrogenesis of Cenozoic, temperate water calcarenites, South Australia: A model for meteoric/shallow burial diagenesis of shallow water calcite sediments, *Journal of Sedimentary Petrology*, **59**, 191-203.

James, N.P. and Bone, Y. (2010) *Neritic Carbonate Sediments in a Temperate Realm: Southern Australia*, Springer, London, pp 263.

James, N.P. and Choquette, P.M. (1989) Diagenesis 9: In Scholle, P.A., James, N.P. and Read, J.F. (Eds.) *Short Course in Geology: Volume 4, Carbonate Sedimentology and Petrology*, p41-79, American Geophysical Union, Washington, D.C.

James, N.P. and von der Borch, C.C. (1991) Carbonate shelf edge off southern Australia: A prograding open-platform margin, *Geology*, **19**, 1005-1008.

James, N.P., Bone, Y., von der Borch, C.C. and Gostin, V.A. (1992) Modern carbonate and terrigenous clastic sediments on a cool water, high energy, mid-latitude shelf: Lacepede, southern Australia, *Sedimentology*, **39**, 877-903.

James, N.P., Bone, Y., Hageman, S., Gostin, V.A. and Feary, D.A. (1997) Cool-water carbonate sedimentation during the Terminal Quaternary, high-amplitude, sea-level cycle: Lincoln shelf, southern Australia, In James, N.P. and Clarke, J.A.D. (Eds.) *Cool-water Carbonates*, p53-76, SEPM, Special Publication, **56**.

James, N.P., Bone, Y. and Kyser, T.K. (2005) Where has all the aragonite gone? Mineralogy of Holocene neritic cool-water carbonates, southern Australia, *Journal of Sedimentary Research*, **75**, 454-463.

Jansen, E. (1989) The use of stable oxygen and carbon isotope stratigraphy as a dating tool, *Quaternary International*, **1**, 151-166.

Jansen, J.H.F., Kuijpers, A., Troelstra, S.R. (1986) A Mid-Brunhes Climatic Event: Long-term changes in global atmosphere and ocean circulation, *Science*, **232**, 619-622.

Jenkin, J.J. (1968) *The geomorphology and Upper Cainozoic geology of S.E. Gippsland, Victoria*, Geological Survey of Victoria, Memoir, **27**.

Jorry, S.J., Hasler, C-A. and Davaud, E. (2006) Hydrodynamic behaviour of *Nummulites*: implication for depositional models, *Facies*, **52**, 391-404.

Jouzel, J., Barkov, N.I., Barnola, J.M., Bender, M.B., Chappellaz, J., Genthon, C., Kotlaykor, V.M., Lipenkov, V., Louris, C., Petit, J.R., Raynaud, D., Raisbeck, G., Ritz, C., Sowers, T., Stievenard, M., Yiou, F. and Yiou, P. (1993) Extending the Vostok ice core record of palaeoclimate to the penultimate glacial period, *Nature*, **364**, 407-412.

Jouzel, J., Hoffman, G., Parrenin, F. and Waelbroeck, C. (2002) Atmospheric oxygen 18 and sea-level changes, *Quaternary Science Reviews*, **21**, 307-314.

Jouzel, J., Masson-Delmotte, V., Cattani, O., Dreyfus, G., Falourd, S., Hoffman, G., Minster, B., Nouet, J., Barnola, J.M., Chappellaz, J., Fischer, H., Gallet, J.C., Johnsen, S., Leuenberger, M., Loulergue, L., Luethi, D., Oerter, H., Parrenin, F., Raisbeck, G., Raynaud, D., Schilt, A., Schwander, J., Selmo, E., Souchez, R., Spahni, R., Stauffer, B., Steffensen, J.P., Stenni, B., Stocker, T.F., Tison, J.L., Werner, M. and Wolff, E.W. (2007) Orbital and millennial Antarctic climate variability over the past 800,000 years, *Science*, **317**, 793-796.

Joyce, E.B. (1975) Quaternary volcanism and tectonics in southeastern Australia, *Bulletin of the Royal Society of New Zealand*, **13**, 169-176.

Kaufman, D.S. (2000) Amino acid racemization in ostracods, In Goodfriend, G.A., Collins, M.J., Fogel, M.L., Macko, S.A., Wehmiller, J.F. (Eds.) *Perspectives in Amino Acid and Protein Geochemistry*, p145-161, Oxford University Press, New York.

Kaufman, D.S. and Manley, W.F. (1998) A new procedure for determining DL amino acid ratios in fossils using reverse phase liquid chromatography, *Quaternary Geochronology*, **17**, 987-1000.

Kaufman, A., Broecker, W.S., Ku, T-L. and Thurber, D.L. (1971) The status of U-series methods of mollusc dating, *Geochimica et Cosmochimica Acta*, **35**, 1115-1183.

Kaufman, A., Ghaleb, B., Wehmiller, J.F. and Hillaire-Marcel, C. (1996) Uranium concentration and isotope ratio profiles within *Mercenaria* shells: Geochronological implications, *Geochimica et Cosmochimica Acta*, **60**, 3735-3746.

Kaufman, D.S., Polyak, L., Adler, R., Channell, J.E.T. and Xuan, C. (2008) Dating late Quaternary planktonic foraminifer *Neogloboquadrina pachyderma* from the Arctic Ocean using amino acid racemization, *Palaeoceanography*, **23**, doi:10.1029/2008PA001618.

Kaufman, D.S., Cooper, K., Behl, R., Billups, K., Bright, J., Gardner, K., Hearty, P., Jakobsson, M., Mendes, I., O'Leary, M., Polyak, L., Rasmussen, T., Rosa, F. and Schmidt, M. (2013) Amino acid racemization in mono-specific foraminifera from Quaternary deep-sea sediments, *Quaternary Geochronology*, **16**, 50-61.

Kendrick, G.W., Wyrwoll, K.-H. and Szabo, B.J. (1991) Pliocene-Pleistocene coastal events and history along the western margin of Australia, *Quaternary Science Reviews*, **10**, 419-399.

- Kenley, P.R. (1971) Cainozoic geology of the eastern part of the Gambier Embayment, southwestern Victoria, *In* Wopfner, H. and Douglas, J.G. (Eds.), *The Otway Basin of Southeastern Australia*, p89-153, Special Bulletin, Geological Surveys of South Australia and Victoria.
- Kenley, P.R. (1988) Southwestern Victoria, *In* Douglas, J.G. and Ferguson, J.A. (Eds.) *Geology of Victoria*, p365-374, Geological Society of Australia, Sydney.
- Kimber, R.W.L. and Griffin, C.V. (1987) Further evidence of the complexity of the racemization process in fossil shells with implications for amino acid racemization dating, *Geochimica et Cosmochimica Acta*, **51**, 839-846.
- Kindler, P. and Davaud, E. (2001) Sedimentological, petrological and diagenetic evidence for greenhouse eolianites in the Lower Cretaceous Chambotte Formation, Saleve Chain, France, *SEPM Special Publication*, **71**, 141-150.
- Kindler, P. and Hearty, P.J. (1997) Geology of the Bahamas: architecture of Bahamian Islands, *In* Vacher, H.L. and Quinn, T.M. (Eds.) *Geology and Hydrogeology of Carbonate Islands*, p141-160, Developments in Sedimentology, **54**, Elsevier, Amsterdam.
- Kindler, P. and Hearty, P.J. (2000) Elevated marine terraces from Eleuthera (Bahamas) and Bermuda: sedimentological, petrographic and geochronological evidence for important deglaciation events during the middle Pleistocene, *Global and Planetary Change*, **24**, 41-58.
- Kindler, P., Reyss, J., Cazala, C. and Plagnes, V. (2007) Discovery of a composite reefal terrace of middle and late Pleistocene age in Great Inagua Island, Bahamas. Implications for regional tectonics and sea-level history, *Sedimentary Geology*, **194**, 141-147.
- King, K. and Hare, P.E. (1972) Amino acid composition of planktonic foraminifera: A paleobiochemical approach to evolution, *Science*, **175**, 1461-1463.
- King, K. and Neville, C. (1977) Isoleucine epimerization for dating marine sediments: Importance of analysing monospecific foraminiferal samples, *Science*, **195**, 1333-1335.
- Kocurek, G.A. (1996) Desert aeolian systems, *In* Reading, H.G. (Ed.) *Sedimentary Environments: Processes, Facies and Stratigraphy*, p125-153, Third Edition, Blackwell Science, Oxford.
- Kopp, R.E., Simons, F.J., Mitrovica, J.X., Maloof, A.C. and Oppenheimer, M. (2009) Probabilistic assessment of sea level during the last interglacial stage, *Nature*, **462**, 863-868.
- Kosnik, M.A. and Kaufman, D.S. (2008) Identifying outliers and assessing the accuracy of amino acid racemization measurements for geochronology: II. Data screening, *Quaternary Geochronology*, **3**, 328-341.
- Kosnik, M.A., Kaufman, D.S. and Hua, Q. (2008) Identifying outliers and assessing the accuracy of amino acid racemization measurements for geochronology: I. Age calibration curves, *Quaternary Geochronology*, **3**, 308-327.

- Kotler, E., Martin, R.E. and Liddell, W.D. (1992) Experimental analysis of abrasion and dissolution resistance of modern reef-dwelling foraminifera: Implications for the preservation of biogenic carbonate, *Palaeo*, **7**, 244-276.
- Kraft, J.C. and Chrzastowski, M.J. (1985) Coastal Stratigraphic Sequences, *In* Davis, R.A. (Ed.) *Coastal Sedimentary Environments*, p625-664, Springer-Verlag, New York.
- Kriausakul, N. and Mitterer, R.M. (1978) Isoleucine epimerization in peptides and proteins: Kinetic factors and application to fossil proteins, *Science*, **201**, 1011-1014.
- Kroopnick, P. and Craig, H. (1972) Atmospheric oxygen: Isotopic composition and solubility fractionation, *Science*, **175**, 54-55.
- Kuenen, H. and Perdok, W.G. (1962) Experimental Abrasion 5: Frosting and defrosting of quartz grains, *The Journal of Geology*, **70**, 648-658.
- Kukla, G. (1987) Loess Stratigraphy in Central China, *Quaternary Science Reviews*, **6**, 191-219.
- Kukla, G., McManus, J.F., Rousseau, D. and Chuine, I. (1997) How long and how stable was the last Interglacial? *Quaternary Science Reviews*, **16**, 605-612.
- Kutzbach, J.E. and Street-Perrott, F.A. (1985) Milankovitch forcing of fluctuations in the level of tropical lakes from 18 to 9 kyr BP, *Nature*, **317**, 130-134.
- Kvenvolden, K.A., Lawless, J.G. and Ponnamperuma, C. (1971) *Proceedings of the National Academy of Sciences US*, **68**, 486-90.
- Kvenvolden, K.A., Blunt, D.J. and Clifton, H.E. (1979) Amino-acid racemization in Quaternary shell deposits at Willapa Bay, Washington, *Geochimica et Cosmochimica Acta*, **43**, 1505-1520.
- Kvenvolden, K.A., Blunt, D.J. and Clifton, H.E. (1981) Age estimates based on amino acid racemization: reply to comments of J.F. Wehmiller, *Geochimica et Cosmochimica Acta*, **45**, 265-267.
- Lachlan, T.J. (2011) *Aminostratigraphy and luminescence dating of the Pleistocene Bridgewater Formation, Kangaroo Island, South Australia: An archive of long term climate and sea-level change*, Unpublished Ph.D thesis, University of Wollongong, Australia.
- Lajoie, K.R., Peterson, E. and Gerow, B. (1980) Amino acid bone dating: A feasibility study, South San Francisco Bay region, California. *In* Hare, P.E., Hoering, T.C. and King, K. Jr. (Eds.) *Biogeochemistry of Amino Acids*, p477-490, Wiley, New York.
- Lambeck, K. (1995) Late Devensian and Holocene shorelines of the British Isles and North Sea from models of glacio-hydro-isostatic rebound, *Journal of the Geological Society, London*, **152**, 437-448.
- Lambeck, K. and Chappell, J. (2001) Sea level change through the last glacial cycle, *Science*, **292**, 679-686.

- Lambeck, K., Nakada, M. (1990) Late Pleistocene and Holocene sea-level change along the Australian coast, *Palaeogeography, Palaeoclimatology, Palaeoecology* **89**, 143-176.
- Lambeck, K. and Nakada, M. (1992) Constraints on the age and duration of the last interglacial period and sea level variations, *Nature*, **357**, 125-128.
- Lambeck, K., Purcell, A. and Dutton, A. (2012) The anatomy of interglacial sea levels: The relationship between sea levels and ice volumes during the Last Interglacial, *Earth and Planetary Science Letters*, **315-316**, 4-11.
- Land, L.S., MacKenzie, F.T. and Gould, S.J. (1967) Pleistocene history of Bermuda, *Geological Society of America Bulletin*, **78**, 993-1006.
- Larsen, G. and Chilingar, C.V. (1979) *Diagenesis in sediments and sedimentary rocks*, Elsevier, Amsterdam, pp579.
- Leckie, D.A. and Walker, R.G. (1982) Storm- and tide-dominated shorelines in Cretaceous Moosebar-Lower Gates Interval – outcrop equivalents of deep basin gas trap in Western Canada, *American Association of Petroleum Geologists Bulletin*, **66**, 138-157.
- Lees, A. and Buller, A.T. (1972) Modern temperate-water and warm-water shelf carbonate sediments contrasted, *Marine Geology*, **13**, 67-73.
- Leighton, C.L., Bailey, R.M. and Thomas, D.S.G. (2013) The utility of desert sand dunes as Quaternary chronostratigraphic archives: evidence from the northeast Rub' al Khali, *Quaternary Science Reviews*, **78**, 303-318.
- Lewis, S.E., Sloss, C.R., Murray-Wallace, C.V., Woodroffe, C.D. and Smithers, S.G. (2013) Post-glacial sea-level changes around the Australian margin: a review, *Quaternary Science Reviews*, **74**, 115-138.
- Li, W.-X., Lundberg, J., Dickin, A.P., Ford, D.C., Schwarcz, H.P., McNutt, R. and Williams, D. (1989) High-precision mass-spectrometric uranium-series dating of cave deposits and implications for palaeoclimate studies, *Nature*, **339**, 534-536.
- Li, Q., McGowran, B., James, N.P., Bone, Y., Cann, J.H. (1996) Mixed foraminiferal biofacies on the mesotrophic, mid-latitude Lacedpede Shelf, South Australia, *Palaios*, **11**, 176-191.
- Li, Q., James, N.P., McGowran, B., Bone, Y. and Cann, J. (1998) Synergetic influence of water masses and Kangaroo Island barrier on foraminiferal distribution, Lincoln and Lacedpede shelves, South Australia: A synthesis, *Alcheringa: An Australasian Journal of Palaeontology*, **22**, 153-176.
- Lisiecki, L.E., and Raymo, M.E. (2005) A Pliocene-Pleistocene stack of 57 globally distributed benthic  $\delta^{18}\text{O}$  records, *Palaeoceanography*, **20**, doi:L101.1029/2004PA001071.
- Lomax, J., Hilgers, A., Wopfner, H., Grün, R., Twidale, C.R. and Radtke, U. (2003) The onset of dune formation in the Strzelecki Desert, South Australia, *Quaternary Science Reviews*, **22**, 1067-1076.

Lomax, J., Hilgers, A. and Radtke, U. (2011) Palaeoenvironmental change recorded in the palaeodune fields of the western Murray Basin, South Australia – New data from single grain OSL-dating, *Quaternary Science Reviews*, **30**, 723-736.

Longman, M.W. (1980) Carbonate diagenetic textures from nearsurface diagenetic environments, *American Association of Petroleum Geologists Bulletin*, **64**, 461-487.

Loope, D.B. (1985) Episodic deposition and preservation of eolian sands: A late Paleozoic example from southeastern Utah, *Geology*, **13**, 73-76.

Loope, D.B. (1988) Rhizoliths in ancient eolianites, *Sedimentary Geology*, **56**, 301-314.

Loope, D.B. and Abegg, F.E. (2001) Recognition and geologic preservation of ancient carbonate eolianites, In Abegg, F.E., Harris, P.M., Loope, D.B. (Eds.) *Modern and ancient carbonate eolianites: sedimentology, sequence stratigraphy and diagenesis*, p3-16, SEPM Special Publication, **71**.

Loucks, R.G. and Ward, W.C. (2001) Eolian stratification and beach-to-dune transition in a Holocene carbonate eolianite complex, Isla Cancun, Quintana Roo, Mexico, In Abegg, F.E., Harris, P.M., Loope, D.B. (Eds.) *Modern and ancient carbonate eolianites: sedimentology, sequence stratigraphy and diagenesis*, p57-76, SEPM Special Publication, **71**.

Loutre, M.F. and Berger, A. (2003) Marine Isotope Stage 11 as an analogue for the present interglacial, *Global and Planetary Change*, **36**, 209-217.

Love, A.J., Herczeg, A.L., Armstrong, D., Stadter, F. and Mazor, E. (1993) Groundwater flow regime within the Gambier Embayment of the Otway Basin, Australia: evidence from hydraulics and hydrochemistry, *Journal of Hydrology*, **143**, 297-338.

Lower, C.S., Cann, J.H. and Haynes, D. (2013) Microfossil evidence for salinity events in the Holocene Coorong Lagoon, South Australia, *Australian Journal of Earth Sciences*, **60**, 573-587.

Ludbrook, N.H. (1961) Stratigraphy of the Murray Basin in South Australia, *Geological Survey of South Australia, Bulletin*, **36**.

Ludbrook, N.H. (1976) The Glanville Formation at Port Adelaide, South Australia, *Geological Survey, Quarterly Geological Notes*, **57**, 4-7.

Ludbrook, N.H. (1978) Quaternary molluscs of the western part of the Eucla Basin, Western Australia, *Geological Survey, Bulletin*, **125**.

Ludbrook, N.H. (1984) Quaternary molluscs of South Australia, *South Australia, Department of Mines and Energy, Handbook*, **9**.

Ludwig, K.R., Muhs, D.R., Simmons, K.R., Halley, R.B. and Shinn, E.A. (1996) Sea-level records at ~80 ka from tectonically stable platforms: Florida and Bermuda, *Geology*, **24**, 211-214.

Lundberg, J. and Ford, D.C. (1994) Late Pleistocene sea level change in the Bahamas from mass spectrometric U-series dating of submerged speleothem, *Quaternary Science Reviews*, **13**, 1-14.

- Mallett, C.W. (1977) Studies in Victorian Tertiary foraminifera: Neogene planktonic faunas, unpublished Ph.D thesis, University of Melbourne.
- Manley, W.F., Miller, G.H., Czywczynski, J. (2000) Kinetics of aspartic acid racemization in *Mya* and *Hiatella*: modelling age and palaeotemperature of high-latitude Quaternary mollusks, *In* Goodfriend, G.A., Collins, M.J., Fogel, M.L., Macko, S.A. and Wehmiller, J.F. (Eds.) *Perspectives in Amino Acid and Protein Geochemistry*, p202-219, Oxford University Press, New York.
- Marshall, J.F. and Thom, B.G. (1976) The sea level in the last interglacial, *Nature*, **263**, 120-121.
- Martin, R.E. and Liddell, W.D. (1991) The taphonomy of foraminifera in modern carbonate environments: Implications for the formation of foraminifera assemblages, *In* Donovan, S.K. (Ed.) *The processes of Fossilisation*, p170-193, Belhaven Press, London.
- Martin, R.E., Harris, M.S. and Liddell, W.D. (1995) Taphonomy and time-averaging of foraminiferal assemblages in Holocene tidal sediments, Bahia la Choya, Sonora, Mexico (northern Gulf of California), *Marine Micropaleontology*, **26**, 187-206.
- Martinson, D.G., Pisias, N.G., Hays, J.D., Imbrie, J., Moore, T.C. and Shackleton, N.J. (1987) Age dating and the orbital theory of the ice ages: Development of a high-resolution 0 to 300,000-year chronostratigraphy, *Quaternary Research*, **27**, 1-29.
- Maslin, M.A. and Ridgwell, A.J. (2005) Mid-Pleistocene revolution and the 'eccentricity myth', *Geological Society London, Special Publications*, **247**, 19-34.
- Masson-Delmotte, V., Stenni, B., Pol, K., Braconnot, P., Cattani, O., Falourd, S., Kageyama, M., Jouzel, J., Landaise, A., Minster, B., Barnola, J.M., Chappellaz, J., Krinner, G., Johnsen, S., Rothlisberger, R., Hansen, J., Mikolajewicz, U. and Otto-Bliesner, B. (2010) EPICA Dome C record of glacial and interglacial intensities, *Quaternary Science Reviews*, **29**, 113-128.
- Mauz, B., Hijma, M.P., Amorosi, A., Porat, N., Galili, E. and Bloemendal, J. (2013) Aeolian beach ridges and their significance for climate and sea level: Concept and insight from the Levant coast (East Mediterranean), *Earth-Science Reviews*, **121**, 31-54.
- McCarroll, D. (2002) Amino-acid geochronology and the British Pleistocene: secure stratigraphical framework or a case of circular reasoning? *Journal of Quaternary Science*, **17**, 647-651.
- McCoy, W.D. (1987) The precision of amino acid geochronology and paleothermometry, *Quaternary Science Reviews*, **6**, 43-54.
- McCulloch, M.T. and Esat, T. (2000) The coral record of last interglacial sea levels and sea surface temperatures, *Chemical Geology*, **169**, 107-129.
- McDougall, I., Embleton, B.J., Stone, D.B. (1981) Origin and evolution of Lord Howe Island, southwest Pacific Ocean, *Journal of the Geological Society of Australia*, **28**, 155-176.



- McGowran, B., Li, Q., Cann, J., Padley, D., McKirdy, D.M. and Shafik, S. (1997) Biogeographic impact of the Leeuwin Current in southern Australia since the late middle Eocene, *Palaeogeography, Palaeoclimatology, Palaeoecology*, **136**, 19-40.
- McDougall, I., Allsopp, H.L. and Chamalaun, F.H. (1966) Isotopic dating of the new volcanics of Victoria, Australia, and geomagnetic polarity epochs, *Journal of Geophysical Research*, **71**, 6107-6118.
- McKee, E.D. and Ward, W.C. (1983) Eolian environment, In Scholle, P.A., Bedout, D.G. and Moore, C.H. (Eds.), *Carbonate Depositional Environments*, p132-169, AAPG Memoir, **33**, American Association of Petroleum Geologists, Tulsa.
- McKee, E.D. and Weir, G.W. (1953) Terminology for stratification and cross-stratification in sedimentary rocks, *Bulletin of the Geological Society of America*, **64**, 381-390.
- McLaren, S., Wallace, M.W., Gallagher, S.J., Miranda, J.A., Holdgate, G.R., Gow, L.J., Snowball, I. and Sandgren, P. (2011) Palaeogeographic, climate and tectonic change in southeastern Australia: the Late Neogene evolution of the Murray Basin, *Quaternary Science Reviews*, **30**, 1086-1111.
- McManus, J.F., Bond, G.C., Broecker, W.S., Johnsen, S., Labeyrie, L. and Higgins, S. (1994) High-resolution climate records from the North Atlantic during the last interglacial, *Nature*, **371**, 326-329.
- McMurtry, G.M., Tappin, D.R., Sedwick, P.N., Wilkinson, I., Fietzke, J. and Sellwood, B. (2007) Elevated marine deposits in Bermuda record a late Quaternary megatsunami, *Sedimentary Geology*, **200**, 155-165.
- Mejdahl, V. (1979) Thermoluminescence dating: beta-dose attenuation in quartz grains, *Archaeometry*, **21**, 61-72.
- Mesolella, K.J. (1967) Zonation of uplifted Pleistocene coral reefs on Barbados, West Indies, *Science*, **156**, 638-640.
- Milankovitch, M. (1941) *Canon of Insolation and the Ice-Age Problem*. Royal Serbian Academy Special Publication. No. 132. (Translated from the German by the Israel Program for Scientific Translations, Jerusalem, 1969).
- Miller, G.H. and Brigham-Grette, J. (1989) Amino acid geochronology: Resolution and precision in carbonate fossils, *Quaternary International*, **1**, 111-128.
- Miller, G.H. and Clarke, S.J. (2007) Amino-acid dating, In Elias, S. (Ed.) *Encyclopedia of Quaternary Science*, p41-52, Elsevier, Amsterdam.
- Miller, G.H. and Hare, P.E. (1980) Amino acid geochronology: Integrity of the carbonate matrix and potential of molluscan fossils, In Hare, P.E., Hoering, T.C. and King, K. Jr. (Eds.) *Biogeochemistry of Amino Acids*, p415-443, Wiley, New York.

- Miller, G.H. and Mangeurd, J. (1985) Aminostratigraphy of European marine interglacial deposits, *Quaternary Science Reviews*, **4**, 215-278.
- Miller, G.H., Magee, J.W. and Jull, A.J.T. (1997) Low-latitude glacial cooling in the Southern hemisphere from amino-acid racemization in emu eggshells, *Nature*, **385**, p241-244.
- Milnes, A.R. and Ludbrook, N.H. (1986) Provenance of microfossils in aeolian calcarenites and calcretes in southern South Australia, *Australian Journal of Earth Sciences*, **33**, 145-159.
- Miranda, J.A., Wallace, M.W. and McLaren, S. (2008) The Norwest Bend Formation: Implication for the evolution of Neogene drainage in southeastern Australia, *Sedimentary Geology*, **205**, 53-66.
- Miranda, J.A., Wallace, M.W. and McLaren, S. (2009) Tectonism and eustasy across a Late Miocene strandplain: The Loxton-Parilla Sands, Murray Basin, southeastern Australia, *Sedimentary Geology*, **219**, 24-43.
- Mitterer, R.M. (1968) Amino acid composition of organic matrix in calcareous oolites, *Science*, **162**, 1498-1499.
- Mitterer, R.M. (1975) Ages and diagenetic temperatures of Pleistocene deposits of Florida based on isoleucine epimerization in *Mercenaria*, *Earth and Planetary Science Letters*, **28**, 275-282.
- Mitterer, R.M. and Kriaušakul, N. (1984) Comparison of rates and degrees of isoleucine epimerization in dipeptides and tripeptides, *Organic Geochemistry*, **7**, 91-98.
- Mitterer, R.M. and Kriaušakul, N. (1989) Calculation of amino acid racemization ages based on apparent parabolic kinetics, *Quaternary Science Reviews*, **8**, 353-357.
- Mix, A.C. and Ruddiman, W.F. (1984) Oxygen-isotope analyses and Pleistocene ice volumes, *Quaternary Research*, **20**, 1-20.
- Morton, J.G.G. (1995) Otway Basin, In Drexel, D.F. and Preiss, W.V. (Eds.) *The geology of South Australia, Volume 2, The Phanerozoic*, p142-149, South Australia, Geological Survey, Bulletin **54**.
- Morton, J.G.G. and Drexel, J.F. (Eds.) (1995) *The petroleum geology of South Australia, Volume 1: Otway Basin*. South Australia, Department of Mines and Energy, Report Book 95/12.
- Mountney, N. and Howell, J. (2000) Aeolian architecture, bedform climbing and preservation space in the Cretaceous Etjo Formation, NW Namibia, *Sedimentology*, **47**, 825-849.
- Muhs, D.R. (2002) Evidence for the timing and duration of the last interglacial period from high-precision Uranium-series ages of corals on tectonically stable coastlines, *Quaternary Research*, **58**, 36-40.
- Muhs, D.R., Budahn, J., Avila, A., Skipp, G., Freeman, J. and Patterson, D. (2010) The role of African dust in the formation of Quaternary soils on Mallorca, Spain and implications for the genesis of Red Mediterranean soils, *Quaternary Science Reviews*, **29**, 2518-2543.

- Muhs, D.R., Simmons, K.R., Schumann, R.R. and Halley, R.B. (2011) Sea-level history of the past two interglacial periods: new evidence from U-series dating of reef corals from south Florida, *Quaternary Science Reviews*, **30**, 570-590.
- Muhs, D.R., Pandolfi, J.M., Simmons, K.R. and Schumann, R.R. (2012a) Sea-level history of past interglacial periods from uranium-series dating of corals, Curaçao, Leeward Antilles islands, *Quaternary Research*, **78**, 157-169.
- Muhs, D.R., Budahn, J.R., Prospero, J.M., Skipp, G. and Herwitz, S.R. (2012b) Soil genesis on the island of Bermuda in the Quaternary: The importance of African dust transport and deposition, *Journal of Geophysical Research*, **117**, F03025, doi: 10.1029/2012JF002366.
- Muhs, D.R., Meco, J. and Simmons, K.R. (2014) Uranium-series ages of corals, sea level history, and palaeozoogeography, Canary Islands, Spain: An exploratory study for two Quaternary interglacial periods, *Palaeogeography, Palaeoclimatology, Palaeoecology*, **394**, 99-118.
- Mullins, H.T., Dolan, J., Breen, N., Anderson, B., Gaylord, M., Petruccione, J.L., Wellner, R.W., Melillo, A.J. and Jurgens, A.D. (1991) Retreat of carbonate platforms: Response to tectonic processes, *Geology*, **19**, 1089-1092.
- Murray, J.W. (1989) Syndepositional dissolution of calcareous foraminifera in modern shallow-water sediments, *Marine Micropaleontology*, **15**, 117-121.
- Murray, J.W. (1991) *Ecology and palaeoecology of benthic foraminifera*, Longman, Harlow, Essex, pp 397.
- Murray, J.W. (2006) *Ecology and applications of benthic foraminifera*, Cambridge University Press, Cambridge, pp 426.
- Murray, J.W. and Alve, E. (1999) Natural dissolution of modern shallow water benthic foraminifera: taphonomic effects on the palaeoecological record, *Palaeogeography, Palaeoclimatology, Palaeoecology*, **146**, 195-209.
- Murray, A.S. and Wintle, A.G. (2000) Luminescence dating of quartz using an improved single-aliquot regenerative dose protocol, *Radiation Measurements*, **32**, 57-73.
- Murray, J.W. and Wright, C.A. (1970) Surface textures of calcareous foraminiferids, *Palaeontology*, **13**, 184-187.
- Murray-Wallace, C.V. (1987) *Evaluation and application of the amino acid racemisation reaction in studies of Quaternary coastal and marine sediments in Australia*, Unpublished Ph.D thesis, The University of Adelaide, Adelaide.
- Murray-Wallace, C.V. (1993) A review of the application of the amino acid racemisation reaction to archaeological dating, *Artefact*, **16**, 19-26.
- Murray-Wallace, C.V. (1995) Aminostratigraphy of Quaternary coastal sequences in Southern Australia – an overview, *Quaternary International*, **26**, 69-86.

Murray-Wallace, C.V. (2000) Quaternary coastal aminostratigraphy: Australian data in a global context, *In* Goodfriend, G.A., Collins, M.J., Fogel, M.L., Macko, S.A. and Wehmler, J.F. (Eds.) *Perspectives in Amino Acid and Protein Geochemistry*, p279-300, Oxford University Press, Oxford.

Murray-Wallace, C.V. (2002) Pleistocene coastal stratigraphy, sea-level highstands and neotectonism of the southern Australian passive continental margin – a review, *Journal of Quaternary Science*, **171**, 469-489

Murray-Wallace, C.V. (2007) Eustatic sea-level changes, Glacial-Interglacial cycles, *In* Elias, S. *Encyclopedia of Quaternary Science*, p3024-3034, Elsevier.

Murray-Wallace, C.V. and Belperio, A.P. (1991) The last interglacial shoreline in Australia – A review, *Quaternary Science Reviews*, **10**, 441-461.

Murray-Wallace, C.V. and Cann, J.H. (2007) Quaternary history of the Coorong Coastal Plain, South Australia, Excursion Guide (A6), XVII INQUA Congress, Cairns, Australia, School of Earth and Environmental Sciences, University of Wollongong.

Murray-Wallace, C.V. and Geode, A. (1991) Aminostratigraphy and electron spin resonance studies of late Quaternary sea level change and coastal neotectonics in Tasmania, Australia, *Zeitschrift für Geomorphologie*, **35**, 129-149.

Murray-Wallace, C.V. and Geode, A. (1995) Aminostratigraphy and electron spin resonance dating of Quaternary coastal neotectonism in Tasmania and the Bass Strait Islands, *Australian Journal of Earth Sciences*, **42**, 51-67.

Murray-Wallace, C.V. and Kimber, R.W.L. (1987) Evaluation of amino acid racemization reaction in studies of Quaternary marine sediments in South Australia, *Australian Journal of Earth Sciences*, **34**, 279-292.

Murray-Wallace, C.V. and Kimber, R.W.L. (1988) A review of amino acid racemisation dating and its application to Australian Quaternary marine molluscs – Current trends and future prospects *In* J.R. Prescott (Ed.) *Archaeometry: Australian Studies 1988*, p6-21. Department of Physics and Mathematical Physics, The University of Adelaide.

Murray-Wallace, C.V. and Kimber, R.W.L. (1989) Quaternary marine aminostratigraphy: Perth Basin, Western Australia, *Australian Journal of Earth Sciences*, **36**, 553-568.

Murray-Wallace, C.V. and Kimber, R.W.L. (1993) Further evidence for apparent ‘parabolic’ racemisation kinetics in Quaternary molluscs, *Australian Journal of Earth Sciences*, **40**, 313-317.

Murray-Wallace, C.V., Woodroffe, C.D. (2014) *Quaternary Sea-Level Changes: A global perspective*, Cambridge University Press, Cambridge, pp 484.

Murray-Wallace, C.V., Belperio, A.P., Cann, J.H., Huntley, D.J. and Prescott, J.R. (1996) Late Quaternary uplift history, Mount Gambier region, South Australia, *Zeitschrift für Geomorphologie*, **106**, 41-56.

Murray-Wallace, C.V., Belperio, A.P. and Cann, J.H. (1998) Quaternary neotectonism and intra-plate volcanism: the Coorong to Mount Gambier Coastal Plain, Southeastern Australia: a review. In Stewart, I.S. and Vita-Finzi, C. (Eds.) *Coastal Tectonics*, p255-267, Geological Society, London, Special Publications, **146**.

Murray-Wallace, C.V., Belperio, A.P., Bourman, R.P., Cann, J.H. and Price, D.M. (1999) Facies architecture of a last interglacial barrier: a model for Quaternary barrier development from the Coorong to Mount Gambier Coastal Plain, southeastern Australia, *Marine Geology*, **158**, 177-195.

Murray-Wallace, C.V., Beu, A.G., Kendrick, G.W., Brown, L.J., Belperio, A.P. and Sherwood, J.E. (2000) Palaeoclimatic implications of the occurrence of the arcoid bivalve *Anadara trapezia* (Deshayes) in the Quaternary of Australasia, *Quaternary Science Reviews*, **19**, 559-590.

Murray-Wallace, C.V., Brooke, B.P., Cann, J.H., Belperio, A.P. and Bourman, R.P. (2001) Whole-rock aminostratigraphy of the Coorong Coastal Plain, South Australia: towards a 1 million year record of sea-level highstands, *Journal of the Geological Society*, **158**, 111-124.

Murray-Wallace, C.V., Banerjee, D., Bourman, R.P., Olley, J.M. and Brooke, B.P. (2002) Optically stimulated luminescence dating of Holocene relict foredunes, Guichen Bay, South Australia, *Quaternary Science Reviews* **21**, 1007-1086.

Murray-Wallace, C.V., Bourman, R.P., Prescott, J.R., Williams, F., Price, D.M. and Belperio, A.P. (2010) Aminostratigraphy and thermoluminescence dating of coastal aeolianites and the later Quaternary history of a failed delta: The River Murray mouth region, South Australia, *Quaternary Geochronology*, **5**, 28-49.

Mylroie, J.E. (2008) Late Quaternary sea-level position: Evidence from Bahamian carbonate deposition and dissolution cycles, *Quaternary International*, **183**, 61-75.

Nakamori, T., Iryu, Y. and Yamada, T. (1995) Development of coral reefs of the Ryukyu Islands (southwest Japan, East China Sea) during Pleistocene sea-level change, *Sedimentary Geology*, **99**, 215-231.

Nanson, G.C., Price, D.M. and Short, S.A. (1992) Wetting and drying of Australia over the past 300 ka, *Geology*, **20**, 791-794.

Nathan, R.P., Mauz, B. (2008) On the dose-rate estimate of carbonate-rich sediments for trapped charge dating, *Radiation Measurements*, **43**, 14-25.

NASCN (1983) North American Stratigraphic Code, *The American Association of Petroleum Geologists Bulletin*, **67**, 841-875.

Nelson, C.S. (1988) An introductory perspective on non-tropical shelf carbonates, *Sedimentary Geology*, **60**, 3-12.

Neumann, A.C. and Hearty, P.J. (1996) Rapid sea-level changes at the close of the last interglacial (substage 5e) recorded in Bahamian island geology, *Geology*, **24**, 775-778.

- Neumann, A.C. and Moore, W.S. (1975) Sea level events and Pleistocene coral ages in the northern Bahamas, *Quaternary Research*, **5**, 215-224.
- O'Leary, M.J., Hearty, P.J., Thompson, W.G., Raymo, M.E., Mitrovica, J.X. and Webster, J.M. (2013) Ice sheet collapse following a prolonged period of stable sea level during the last interglacial, *Nature Geoscience*, **6**, 796-800.
- Olley, J. M., Caitcheon, G. G. and Roberts, R.G. (1999) The origin of dose distributions in fluvial sediments, and the prospect of dating single grains of quartz from fluvial deposits using optically stimulated luminescence, *Radiation Measurements*, **30**, 207-217.
- Olson, S.L. and Hearty, P.J. (2009) A sustained +21 m sea-level highstand during MIS 11 (400 ka): direct fossil and sedimentary evidence from Bermuda, *Quaternary Science Reviews*, **28**, 271-285.
- Orem, C.A. and Kaufman, D.S. (2011) Effects of basic pH on amino acid racemisation and leaching in freshwater mollusk shell, *Quaternary Geochronology*, **6**, 233-245.
- Orford, J.D., Murdy, J.M. and Wintle, A.G. (2003) Prograded Holocene beach ridges with superimposed dunes in north-east Ireland: mechanisms and timescales of fine and coarse beach sediment decoupling and deposition, *Marine Geology*, **194**, 47-64.
- Ota, Y. and Chappell, J. (1996) Late Quaternary coseismic uplift events on the Huon Peninsula, Papua New Guinea, deduced from coral terrace data, *Journal of Geophysical Research*, **101**, 6071-6082.
- Ota, Y. and Omura, A. (1992) Contrasting styles and rates of tectonic uplift of coral reef terraces in the Ryukyu and Daito Islands, southwestern Japan, *Quaternary International*, **15/16**, 17-29.
- Otvos, E.G. (2000) Beach ridges – definitions and significance, *Geomorphology*, **32**, 38-108.
- Paillard, D. (1998) The timing of Pleistocene glaciations from a simple multiple-state climate model, *Nature*, **391**, 378-381.
- Patience, A.J. and Kroon, D. (1991) Oxygen isotope chronostratigraphy, In Smart, P.L. and Frances, P.D. (Eds.) *Quaternary Dating Methods: A User's Guide*, Quaternary Research Association Technical Guide no. 4, Cambridge, pp 233.
- Peebles, M.W. and Lewis, R.D. (1991) Surface textures of benthic foraminifera from San Salvador, Bahamas, *Journal of Foraminiferal Research*, **21**, 285-292.
- Peebles, M.W. and Lewis, R.D. (1988) Differential infestation of shallow-water benthic foraminifera by microboring organisms: Possible biases in preservation potential, *Palaios*, **3**, 345-351.
- Pell, S.D., Chivas, A.R. and Williams, I.S. (2001) The Mallee dunefield: development and sand provenance, *Journal of Arid Environments*, **48**, 149-170.

- Peltier, W.R. (2002) On eustatic sea level history: last glacial maximum to Holocene, *Quaternary Science Reviews*, **21**, 377-396.
- Penkman, K. (2009) Amino acid geochronology: its impact on our understanding of the Quaternary stratigraphy of the British Isles, *Journal of Quaternary Science*, **25**, 501-514.
- Penkman, K.E.H., Kaufman, D.S., Maddy, D. and Collins, M.J. (2008) Closed-system behaviour of the intra-crystalline fraction of amino acids in mollusc shells, *Quaternary Geochronology*, **3**, 2-25.
- Penny, C.L. (1983) Climate, In Tyler, M.J., Twidale, C.R., Ling, J.K. and Holmes, J.W. (Eds.), *Natural History of the South East*, p85-94, Royal Society of South Australia, Adelaide.
- Petit, J.R., Jouzel, J., Raynaud, D., Barkov, N.I., Barnola, J.-M., Basile, I., Bender, M., Chappellaz, J., Davis, M., Delaygue, G., Delmotte, M., Kotlyakov, V.M., Legrand, M., Lipenkov, V.Y., Louris, C., Pepin, Ritz, C., Saltzman, E., Stievenard, M. (1999) Climate and atmospheric history of the past 420,000 years from the Vostok ice core, Antarctica, *Nature*, **399**, 429-436.
- Pickett, J.W., Thompson, C.H., Kelley, R.A. and Roman, D. (1985) Evidence of high sea level during isotope stage 5c in Queensland, Australia, *Quaternary Research*, **24**, 103-114.
- Pickett, J.W., Ku, T.L., Thompson, C.H., Roman, D., Kelley, R.A. and Huang, Y.P. (1989) A review of age determinations on Pleistocene corals in Eastern Australia, *Quaternary Research*, **31**, 392-395.
- Pillans, B. (1982) Amino Acid Racemization Dating: A review, In Ambrose and Duerdon (Eds.) *Archaeometry: An Australian Perspective*, p228-234, The Australian National University, Canberra.
- Pirazzoli, P.A. (1993) Global sea-level changes and their measurement, *Global and Planetary Change*, **8**, 135-148.
- Pirazzoli, P.A. (1996) *Sea-level changes – the last 20,000 years*, Wiley, New York, pp 211.
- Pirazzoli, P.A. (2007) Sea-level studies - Geomorphological indicators, In Elias, S. *Encyclopedia of Quaternary Science*, p2974-2983, Elsevier.
- Pirazzoli, P.A., Radtke, U., Hantoro, W.S., Jouannic, C., Hoang, C.T., Causse, C., Borel Best, M. (1991) Quaternary raised coral-reef terraces on Sumba Island, Indonesia, *Science*, **252**, 1834-1836.
- Pisias, N.G., Martinson, D.G., Moore, T.C., Shackleton, N.J., Prell, W., Hays, J. and Boden, G. (1984) High resolution stratigraphic correlation of benthic oxygen isotopic records spanning the last 300,000 years, *Marine Geology*, **56**, 119-136.
- Playford, P.E. (1997) Geology and hydrogeology of Rottnest Island, Western Australia, In Vacher, H.L. and Quinn, T.M. (Eds.) *Geology and Hydrogeology of Carbonate Islands*, p783-810, *Developments in Sedimentology*, **54**.

- Playford, P.E. and Leech, R.E.J. (1977) Geology and hydrology of Rottnest Island, *Geological Survey of Western Australia, Report 6*.
- Playford, P.E., Cockbain, A.E. and Low, G.H. (1976) Geology of the Perth Basin, Western Australia, *Geological Survey of Western Australia Bulletin*, **124**.
- Poore, R.Z. and Dowsett, H.J. (2001) Pleistocene reduction of polar ice caps: Evidence from Cariaco Basin marine sediments, *Geology*, **29**, 71-74.
- Potter, E-K. and Lambeck, K. (2003) Reconciliation of sea-level observation in the Western North Atlantic during the last glacial cycle, *Earth and Planetary Science Letters*, **217**, 171-181.
- Prell, W.L., Imbrie, J., Martinson, D.G., Morley, J.J., Pisias, N.G., Shackleton, N.J. and Streeter, H.F. (1986) Graphic correlation of oxygen isotope stratigraphy application to the late Quaternary, *Paleoceanography*, **1**, 137-162.
- Prescott, J.R. and Hutton, J.T. (1994) Cosmic-ray contributions to dose-rates for luminescence and ESR dating – large depths and long-term variations, *Radiation Measurements*, **23**, 497-500.
- Price, D.M., Brooke, B.P. and Woodroffe, C.D. (2001) Thermoluminescence dating of aeolianites from Lord Howe Island and South-West Western Australia, *Quaternary Science Reviews*, **20**, 841-846.
- Price, R.C., Nicholls, I.A. and Gray, C.M. (2003) Cainozoic igneous activity, *In* Birch, W.D. (Ed.) *Geology of Victoria*, p361-375, Geological Society of Australia, Special Publication **23**.
- Pye, K. and Tsoar, H. (1990) *Aeolian Sand and Sand Dunes*, Unwin Hymen Ltd, London, pp 396.
- Rao, C.P. (1996) *Modern carbonates, tropical, temperate, polar: introduction to sedimentology and geochemistry*, University of Tasmania, Hobart, pp 206.
- Raymo, M.E. and Mitrovica, J.X. (2012) Collapse of polar ice sheets during the stage 11 interglacial, *Nature*, **483**, 453-456.
- Raynaud, D., Barnola, J., Souchez, R., Lorrain, R., Petit, J., Duval, P. and Lipenkov, V.Y. (2005) The record for marine isotopic stage 11, *Nature*, **436**, 39-40.
- Reading, H.G. (1996) *Sedimentary Environments: Processes, Facies and Stratigraphy*, Blackwell, Oxford, pp 688.
- Reading, H.G. and Collinson, J.D. (1996) Clastic coasts, *In* Reading, H.G. (Ed.) *Sedimentary Environments: Processes, Facies and Stratigraphy*, p154-231, Blackwell, Oxford.
- Reeckman, S.A. and Gill, E.D. (1981) Rates of vadose diagenesis in Quaternary dune and shallow marine calcarenites, Warrnambool, Victoria, Australia, *Sedimentary Geology*, **30**, 157-172.
- Richards, D.A. and Dorale, J.A. (2003) Uranium-series chronology and environmental applications of speleothems, *In* Bourdon, B., Henderson, G.M., Lundstrom, C.C. and Turner,



S.P. (Eds.) *Uranium Series Geochemistry, Reviews in Mineralogy and Geochemistry*, p407-460, Mineralogical Society of America, **52**.

Richards, D.A., Smart, P.L. and Edwards, R.L. (1994) Maximum sea levels for the last glacial period from U-series ages of submerged speleothems, *Nature*, **367**, 357-360.

Riordan, N.K., James, N.P. and Bone, Y. (2011) Oligo-Miocene seagrass-influenced carbonate sedimentation along a temperate marine palaeoarchipelago, Padthaway Ridge, South Australia, *Sedimentology*, **59**, 393-418.

Roberts, D.L. and Berger, L. (1997) Last Interglacial (c.117 kyr) human footprints South Africa, *South African Journal of Science*, **93**, 349-350.

Roberts, D.L., Bateman, M.D., Murray-Wallace, C.V., Carr, A.S. and Holmes, P.J. (2008) Last Interglacial fossil elephant trackways dated by OSL/AAR in coastal aeolianites, Still Bay, South Africa, *Palaeogeography, Palaeoclimatology, Palaeoecology*, **257**, 261-279.

Robertson, G.B., Prescott, J.R. and Hutton, J.T. (1996) Thermoluminescence dating of volcanic activity at Mount Gambier, South Australia, *Royal Society of South Australia, Transactions*, **120**, 7-12.

Robinson, L., F., Henderson, G.M. and Slowey, N.C. (2002) U-Th dating of marine isotope stage 7 in Bahamas slope sediments, *Earth and Planetary Science Letters*, **196**, 175-187.

Rodgers, J. (1957) The distribution of marine carbonate sediments: A review. In Leblanc, R.J. and Breeding, J.G. (Eds.) *Regional Aspects of Carbonate Deposition – SEPM Special Publication* **5**, 2-14.

Rohling, E.J., Fenton, M., Jorissen, F.J., Bertrand, P., Ganssen, G. and Caulet, J.P. (1998) Magnitudes of sea-level lowstands of the past 500,000 years, *Nature*, **394**, 162-165.

Rohling, E.J., Grant, K., Hemleben, C.H., Siddall, M., Hoogakker, B.A.A., Bolshaw, M. and Keucera, M. (2008) High rates of sea-level rise during the last interglacial period, *Nature Geoscience*, **1**, 38-42.

Rohling, E.J., Grant, K., Bolshaw, M., Roberts, A.P., Siddall, M., Hemleben, Ch. And Kucera, M. (2009) Antarctic temperature and global sea level closely coupled over the past five glacial cycles, *Nature Geoscience*, **2**, 500-504.

Rowe, M.P., Wainer, K.A.I., Bristow, C.S. and Thomas, A.L. (2014) Anomalous MIS 7 sea level recorded on Bermuda, *Quaternary Science Review*, **90**, 47-59.

Roy, P.S. (1990) Shell hash dating and mixing models for marine sediments, In Gillespie, R. (Ed.) *Quaternary Dating Workshop, 1990*, p19-23, Department of Biogeography and Geomorphology, RSPacS, ANU.

Roy, P.S., Cowell, P.J., Ferland, M.A. and Thom, B.G. (1994) Wave-dominated coasts, In: Carter, R.W.G. and Woodroffe, C.D. (Eds.) *Coastal Evolution: late Quaternary shoreline morphodynamics*, Cambridge University Press, Cambridge, p121-186.

- Rubin, D.M. and Hunter, R.E. (1982) Bedform climbing in theory and nature, *Sedimentology*, **29**, 121-138.
- Ruddiman, W.F., Raymo, M. and McIntyre, A. (1986) Matuyama 41,000-year cycles: North Atlantic Ocean and northern hemisphere ice sheets, *Earth and Planetary Science Letters*, **80**, 117-129.
- Rutter, N.W. and Blackwell, B. (1995) Amino acid racemization dating, In Rutter, N.W. and Catto, N.R. (Eds.) *Dating methods for Quaternary deposits*, p125-164, Geological Association of Canada, Newfoundland.
- Rutter, N.W. and Crawford, R.J. (1984) Utilizing wood in amino acid dating, Reprinted from Mahaney, W.C. (Ed.) *Quaternary Dating Methods*, p195-209, Elsevier Science Publishers, Amsterdam.
- Sasaki, K., Omura, A., Murakami, K., Sagawa, N., Nakamori, T. (2004) Interstadial coral reef terraces and relative sea-level changes during marine oxygen isotope stages 3-4, Kikai Island, central Ryukyus, Japan, *Quaternary International*, **120**, 51-64.
- Sayles, R.W. (1931) Bermuda during the ice age, *Proceeding of the America Academy of Arts and Science*, **66**, 381-467.
- Schahinger, R.B. (1987) Structure of coastal upwelling events observed off the south-east coast of South Australia during February 1983 – April 1984, *Australian Journal of Marine and Freshwater Research*, **38**, 439-59.
- Schellmann, G. and Radtke, U. (2004) A revised morpho- and chronostratigraphy of the Late and Middle Pleistocene coral reef terraces on Southern Barbados (West Indies), *Earth Science Reviews*, **64**, 157-187.
- Schilt, A., Baumgartner, M., Blunier, T., Schwander, J., Spahni, R., Fischer, H. and Stocker, T.F. (2010) Glacial-interglacial and millennial-scale variations in the atmospheric nitrous oxide concentration during the last 800,000 years, *Quaternary Science Reviews*, **29**, 182-192.
- Scholle, P.A. and Ulmer-Scholle, D.S. (2003) A color guide to the petrography of carbonate rocks: grains, textures, porosity, diagenesis, *AAPG Memoir 77*, 474pp.
- Scholz, D., Mangini, A. and Felis, T. (2004) U-series dating of diagenetically altered fossil reef corals, *Earth and Planetary Science Letters*, **218**, 163-178.
- Schroeder, R.A. and Bada, J.L. (1976) A review of the geochemical applications of the amino acid racemization reaction, *Earth Science Reviews*, **12**, 347-391.
- Schwebel, D.A. (1978) *Quaternary stratigraphy of the southeast of South Australia*, Unpublished Ph.D thesis, Flinders University of South Australia.
- Schwebel, D.A. (1984) Quaternary stratigraphy and sea-level variation in the southeast of South Australia, In Thom, B.G. (Ed.) *Coastal Geomorphology in Australia*, p291-311, Academic Press, Sydney.

- Sedgwick, P.E. and Davis Jr., R.A. (2003) Stratigraphy of washover deposits in Florida: implications for recognition in the stratigraphic record, *Marine Geology*, **200**, 31-48.
- Sejrup, H.P. and Haugen, J-E. (1994) Amino acid diagenesis in the marine bivalve *Arctica islandica* Linné from northwest European sites: only time and temperature? *Journal of Quaternary Science*, **9**, 301-309.
- Shackleton, N.J. (1967) Oxygen isotope analyses and Pleistocene temperatures reassessed, *Nature*, **215**, 15-17.
- Shackleton, N.J. (1969) The last interglacial in the marine and terrestrial record, *Proceedings of the Royal Society of London*, **147**, 135-154.
- Shackleton, N.J. (1987) Oxygen isotopes, ice volume and sea level, *Quaternary Science Reviews*, **6**, 183-190.
- Shackleton, N.J. (2000) The 100,000-year ice-age cycle identified and found to lag temperature, carbon dioxide and orbital eccentricity, *Science*, **289**, 1897-1902.
- Shackleton, N.J. (2006) Formal Quaternary stratigraphy – What do we expect and need? *Quaternary Science Reviews*, **25**, 3458-3462.
- Shackleton, N.J. and Opdyke, N.D. (1973) Oxygen isotope and palaeomagnetic stratigraphy of equatorial Pacific core V28-238: Oxygen isotope temperatures and ice volumes on a  $10^5$  and  $10^6$  year scale, *Quaternary Research*, **3**, 39-55.
- Shackleton, N.J., Imbrie, J. and Hall, M.A. (1983) Oxygen and carbon isotope record of East Pacific core V19-30: implications for the formation of deep water in the late Pleistocene North Atlantic, *Earth and Planetary Science Letters*, **65**, 233-244.
- Sheard, M.J. (1978) Geological history of the Mount Gambier volcanic complex, southeast South Australia, *Transactions of the Royal Society of South Australia*, **102**, 125-139.
- Sheard, M.J. (1983) Volcanoes, In Tyler, M.J., Twidale, C.R., Ling, J.K. and Holmes, J.W. (Eds.), *Natural History of the South East*, p7-14, Royal Society of South Australia, Adelaide.
- Sheard, M.J. (1990) A guide to Quaternary volcanoes in the lower south-east of South Australia, *Mines and Energy Review*, **157**, 40-50.
- Sheard, M.J. (1995) Quaternary volcanic activity and volcanic hazards, In Drexel, J.F. and Preiss, W.V. (Eds.) *The Geology of South Australia, Volume 2: The Phanerozoic*, p264-268, South Australia, Geological Survey, Bulletin **54**.
- Sheard, M.J. and Smith, P.C. (1995) Karst and mound spring deposits, In Drexel, J.F. and Preiss, W.V. (Eds.) *The Geology of South Australia, Volume 2: The Phanerozoic*, p257-260, South Australia, Geological Survey, Bulletin **54**.
- Sherwood, J., Barbetti, M., Ditchburn, R., Kimber, R.W.L., McCabe, W., Murray-Wallace, C.V., Prescott, J.R. and Whitehead, N. (1994) A comparative study of Quaternary dating techniques

applied to sedimentary deposits in southwest Victoria, Australia, *Quaternary Geochronology*, **13**, 95-110.

Short, A.D. (2006) *Beaches of the South Australian coast and Kangaroo Island*, Australian Beach Safety and Management Program, Sydney University Press, Sydney, pp 346.

Short, A.D. and Hesp, P.A. (1982) Wave, beach and dune interactions in southeastern Australia, *Marine Geology*, **48**, 259-284.

Short, A.D. and Hesp, P.A. (1999) Beach and Dune Stratification, *In* Short, A.D. (Ed.) *Handbook of Beach and Shoreface Morphodynamics*, p279-292, John Wiley and Sons Ltd, Chichester.

Shroba, C. (1993) Taphonomic features of benthic foraminifera in a temperate setting: Experimental and field observations on the role of abrasion, solution and microboring in the destruction of foraminiferal tests, *Palaios*, **8**, 250-266.

Shulmeister, J., Goodwin, I., Renwick, J., Harle, K., Armand, L., McGlone, M.S., Cook, E., Dodson, J., Hesse, P.P., Mayewski, P. and Curran, M. (2004) The Southern Hemisphere westerlies in the Australasia sector over the last glacial cycle: a synthesis, *Quaternary Science Reviews*, **118-119**, 23-53.

Siddall, M., Rohling, E.J., Almogi-Labin, A., Hemleben, Ch., Meischner, D., Schmelzer, I. and Smeed, D.A. (2003) Sea-level fluctuations during the last glacial cycle, *Nature*, **423**, 853-858.

Siddall, M., Chappell, J. and Potter, E.-K. (2007) Eustatic sea level during past interglacials, *In* Sirocko, F., Litt, T., Claussen, M. and Sanches-Goni, M.F. (Eds). *The climate of past interglacials*, p75-92, Elsevier, Amsterdam.

Singleton, O.P., McDougall, I. and Mallett, C.W. (1976) The Pliocene-Pleistocene boundary in southeastern Australia, *Journal of the Geological Society of Australia*, **23**, 299-311.

Sloss, C.R., Murray-Wallace, C.V. and Jones, B.J. (2007) Holocene sea-level change on the southeast coast of Australia: a review, *The Holocene*, **17**, 999-1014.

Smith, B.W. and Prescott, J.R. (1987) Thermoluminescence dating of the eruption at Mt Schank, South Australia, *Australian Journal of Earth Sciences*, **34**, 335-342.

Smith, G.G., Williams, K.M. and Wonnacott, D.M. (1978) Factors affecting the rate of racemization of amino acids and their significance to geochronology, *Organic Chemistry*, **43**, 1-5.

Sprigg, R.C. (1952) The geology of the South-East Province, South Australia, with special reference to Quaternary coast-line migrations and modern beach developments, *South Australia, Geological Survey, Bulletin*, **29**.

Sprigg, R.C. (1979) Stranded and submerged sea-beach systems of Southeast South Australia and the aeolian desert cycles, *Sedimentary Geology*, **22**, 53-96.

Squires, D.F. (1963) Carbon-14 dating of the fossil dune sequence, Lord Howe Island, *The Australian Journal of Science*, **25**, 412-413.

- Staines, H.R.E. (1985) Field geologist's guide to lithostratigraphic nomenclature in Australia, *Australian Journal of Earth Science*, **32**, 83-106.
- Stapor, F.W. (1975) Holocene beach ridge plain development, northwest Florida, *Zeitschrift für Geomorphologie*, **22**, 116-144.
- Stirling, C.H., Esat, T.M., McCulloch, M.T. and Lambeck, K. (1995) High-precision U-series dating of corals from Western Australia and implications for the timing and duration of the last interglacial, *Earth and Planetary Science Letters*, **135**, 115-130.
- Stirling, C.H., Esat, T.M., Lambeck, K. and McCulloch, M.T. (1998) Timing and duration of the last interglacial: evidence for a restricted interval of widespread coral reef growth, *Earth and Planetary Science Letters*, **160**, 745-762.
- Stirling, C.H., Esat, T.M., Lambeck, K., McCulloch, M.T., Blake, S.G., Lee, D.-C. and Halliday, A.N. (2001) Orbital forcing of the marine isotope stage 9 interglacial, *Science*, **291**, 290-293.
- Stokes, S., Ingram, S., Aitken, M.J., Sirocko, F., Anderson, R. and Leuschner, D. (2003) Alternative chronologies for Late Quaternary (last interglacial-Holocene) deep sea sediments via optical dating of silt-sized quartz, *Quaternary Science Reviews*, **22**, 925-941.
- Sugihara, K., Nakamori, T., Irvu, Y., Sasaki, K. and Blanchon, P. (2003) Holocene sea-level change and tectonic uplift deduced from raised reef terraces, Kikai-jima, Ryukyu Islands, Japan, *Sedimentary Geology*, **159**, 5-25.
- Sykes, G.A., Collins, M.J. and Walton, D.I. (1995) The significance of a geochemically isolated intracrystalline fraction within biominerals, *Organic Geochemistry*, **23**, 1059-1065.
- Szabo, B.J. (1985) Uranium-series dating of fossil corals from marine sediments of southeastern United States Atlantic Coastal Plain, *Geological Society of America Bulletin*, **96**, 398-406.
- Szabo, B.J., Ludwig, K.R., Muhs, D.R. and Simmons, K.R. (1994) Thorium-230 ages of corals and duration of the Last Interglacial sea-level high stand on Oahu, Hawaii, *Science*, **266**, 93-96.
- Taylor, M.J. and Stone, G.W. (1996) Beach ridges: a review, *Journal of Coastal Research*, **12**, 612-621.
- Thom, B.G. (1964) Origin of sand beach-ridges, *Australian Journal of Science*, **26**, 351-352.
- Thom, B.G. (1965) Late Quaternary coastal morphology of the Port Stephens-Myall Lakes area, NSW, *Journal of Royal Society of NSW*, **98**, 345-364.
- Thom, B.G. (1984) Transgressive and regressive stratigraphies of coastal sand barriers in eastern Australia, *Marine Geology*, **7**, 161-168.
- Thom, B.G. and Murray-Wallace, C.V. (1988) Geological note: last interglacial (stage 5e) estuarine sediments at Largs, New South Wales, *Australian Journal of Earth Sciences*, **35**, 571-574.

- Thompson, W.G. and Goldstein, S.L. (2005) Open-system coral ages reveal persistent suborbital sea-level cycles, *Science*, **308**, 401-404.
- Thompson, W.G. and Goldstein, S.L. (2006) A radiometric calibration of the SPECMAP timescale, *Quaternary Science Reviews*, **25**, 3207-3215.
- Tomazelli, L.J. and Dillenberg, S.R. (2007) Sedimentary facies and stratigraphy of a last interglacial coastal barrier in south Brazil, *Marine Geology*, **244**, 33-45.
- Tucker, M.E. (1990) Diagenetic processes, products and environments, *In* Tucker, M.E. and Wright, V.P. (Eds.) *Carbonate Sedimentology*, p314-364, Blackwell Scientific Publishing, Oxford.
- Tucker, M.E. and Wright, V.P. (1990) *Carbonate Sedimentology*, Blackwell Scientific Publishing, Oxford, pp 482.
- Twidale, C.R., Campbell, E.M. and Bourne, J.A. (1983) Granite forms, karsts and lunettes, *In* Tyler, M.J., Twidale, C.R., King, J.K. and Holmes, J.W. (Eds.), *Natural History of the South East*, p25-38, Royal Society of South Australia, Adelaide.
- Tzedakis, C. (2003) Timing and duration of last interglacial conditions in Europe: a chronicle of a changing chronology, *Quaternary Science Reviews*, **22**, 763-768.
- Vacher, H.L. and Hearty, P.J. (1989) History of stage 5 sea level in Bermuda: Review with new evidence of a brief rise to present sea level during substage 5a, *Quaternary Science Reviews*, **8**, 159-168.
- Vacher, H.L. and Rowe, M.P. (1997) Geology and hydrogeology of Bermuda, *In* Vacher, H.L. and Quinn, T.M. (Eds.) *Geology and Hydrogeology of Carbonate Islands*, p35-90, Elsevier, Amsterdam.
- Vacher, H.L., Hearty, P.J. and Rowe, M.P. (1995) Stratigraphy of Bermuda: nomenclature, concepts, and status of multiple systems of classification, *In* Curran, H.A. and White, B. (Eds.) *Terrestrial and Shallow Marine Geology of the Bahamas and Bermuda*, p271-294, Geological Society of America Special Paper, **300**, Geological Society of America, Boulder.
- van Hengstum, P.J., Scott, D.B. and Javaux, E. (2009) Foraminifera in elevated Bermudian caves provide further evidence for +21 m eustatic sea level during Marine Isotope Stage 11, *Quaternary Science Reviews*, **28**, 1850-1860.
- Veeh, H.H. (1966)  $\text{Th}^{230}/\text{U}^{238}$  and  $\text{U}^{234}/\text{U}^{238}$  ages of Pleistocene high sea level stand, *Journal of Geophysical Research*, **71**, 3379-3386.
- Veeh, H.H. and Chappell, J. (1970) Astronomical theory of climate change: support from New Guinea, *Science*, **167**, 862-865.
- Veevers, J.J. (1986) Breakup of Australia and Antarctica estimated as mid-Cretaceous ( $95 \pm 5$  Ma) from magnetic and seismic data at the continental margin, *Earth and Planetary Science Letters*, **77**, 91-99.

- Vezina, J., Jones, B. and Ford, D. (1999) Sea-level highstands over the last 500,000 years: evidence from the Ironshore Formation on Grand Cayman, British West Indies, *Journal of Sedimentary Research*, **69**, 317-327.
- von der Borch, C.C., Bada, J.L. and Schwebel, D.L. (1980) Amino acid racemisation dating of late Quaternary strandline events of the coastal plain sequence near Robe, southeastern South Australia, *Transactions of the Royal Society of South Australia*, **104**, 167-170.
- Waelbroeck, C., Frank, N., Jouzel, J., Parrenin, F., Masson-Delmotte, V., Genty, D. (2008) Transferring radiometric dating of the last interglacial sea level high stand to marine and ice core records, *Earth and Planetary Science Letters*, **265**, 183-194.
- Walker, R.G. (1992) Facies, facies models and modern stratigraphic concepts, *In* Walker, R.G. and James, N.P. (Eds.) *Facies Models Response to Sea Level Change*, p1-14, Geological Association of Canada.
- Walker, S.E. and Goldstein, S.T. (1999) Taphonomic tiering: experimental field taphonomy of molluscs and foraminifera above and below the sediment-water interface, *Palaeogeography, Palaeoclimatology, Palaeoecology*, **149**, p227-244.
- Walker, R.G., Duke, W.L. and Leckie, D.A. (1983) Hummocky stratification: Significance of its variable bedding sequences: Discussion and reply: Discussion, *Geological Society of America Bulletin*, **94**, 1245-1249.
- Wallace, M.W., Dickinson, J.A., Moore, D.H. and Sandiford, M. (2005) Late Neogene strandlines of Southern Victoria: a unique record of eustasy and tectonics in southeast Australia, *Australian Journal of Earth Sciences*, **52**, 279-297.
- Ward, W.C. (1973) Influence of climate on the early diagenesis of carbonate eolianites, *Geology*, **1**, 171-174.
- Warren, J.K. (1983) Pedogenic calcrete as it occurs in Quaternary calcareous dunes in coastal South Australia, *Journal of Sedimentary Petrology*, **53**, 787-796.
- Wehmiller, J.F. (1981) Kinetic model options for interpretation of amino acid enantiomeric ratios in Quaternary molluscs: comments on a paper by Kvenvolden *et al.*, (1979) *Geochimica et Cosmochimica Acta*, **45**, 261-264.
- Wehmiller, J.F. (1982) A review of amino acid racemization studies in Quaternary mollusks: Stratigraphic and chronologic applications in coastal and interglacial sites, Pacific and Atlantic coasts, United States, United Kingdom, Baffin Island, and tropical islands, *Quaternary Science Reviews*, **1**, 83-120.
- Wehmiller, J.F. (1984) Relative and absolute dating of Quaternary molluscs with amino acid racemization: Evaluation, applications and questions, Reprinted from Mahaney, W.C. (Ed.) *Quaternary Dating Methods*, p171-193, Elsevier Science Publishers, Amsterdam.

Wehmiller, J.F. (1986) Amino acid racemization geochronology, *In* Hurford, A.J., Jäger, E. and Ten Cate, J.A.M. (Eds.) *Dating Young Sediments*, p139-158, Committee of co-ordination of joint prospecting for mineral resources in Asian offshore areas (CCDO) Technical Publication, 16.

Wehmiller, J.F. (1993) Applications of organic geochemistry for Quaternary research: Aminostratigraphy and Amino chronology, *In* Engel, M.H. and Macko, S.A. (Eds.) *Organic Geochemistry: principles and applications* p755-783, Plenum Press, New York.

Wehmiller, J.F. (2013a) United States Quaternary coastal sequences and molluscan racemisation geochronology – What have they meant for each other over the past 45 years? *Quaternary Geochronology*, **16**, 3-20.

Wehmiller, J.F. (2013b) Interlaboratory comparison of amino acid enantiomeric ratios in Pleistocene fossils, *Quaternary Geochronology*, **16**, 173-182.

Wehmiller, J.F. and Belknap, D.F. (1978) Alternative kinetic models for the interpretation of amino acid enantiomeric ratios in Pleistocene molluscs: Examples from California, Washington and Florida, *Quaternary Research*, **9**, 330-348.

Wehmiller, J.F. and Hare, P.E. (1971) Racemization of amino acids in marine sediments, *Science*, **173**, 907-911.

Wehmiller, J.F., Simmons, K.R., Cheng, H., Edwards, R.L., Martin-McNaughton, J., York, L.L., Krantz, D.E. and Shen, C-C. (2004) Uranium-series coral ages from the US Atlantic Coastal plain – the '80 ka problem' revisited, *Quaternary International*, **120**, 3-14.

White, M.R. (1995) Subdivision of the Gambier Limestone: formal description of three new members, *South Australia, Department of Mines and Energy*, Report Book 95/7.

White, S. (2000) Thermoluminescence dating of dune ridges in western Victoria, *Helictite*, **36**, 38-40.

Williams, M. (1977) *The changing rural landscape of South Australia*, Heinemann Educational Australia Pty Ltd, Richmond, pp 90.

Williams, K.M. and Smith, G.G. (1977) A critical evaluation of the application of amino acid racemization to geochronology and geothermometry, *Origins of Life*, **8**, 91-144.

Williams, D.F., Thunell, R.C., Tappa, E., Rio, D. and Raffi, I. (1988) Chronology of the Pleistocene oxygen isotope record: 0-1.88 m.y. B.P. *Palaeogeography, Palaeoclimatology, Palaeoecology*, **64**, 221-240.

Williams, M., Dunkerley, D., De Deckker, P., Kershaw, P. and Chappell, J. (1998) *Quaternary Environments, Second Edition*, Arnold, London, pp 329.

Winograd, I.J., Coplen, T.B., Landwehr, J.M., Riggs, A.C., Ludwig K.R., Szabo, B.J., Kolesar, P.T. and Revesz, K.M. (1992) Continuous 500,000-year climate record from vein calcite in Devils Hole, Nevada, *Science*, **258**, 255-260.



- Winograd, I., Landwehr, J.M., Ludwig, K.R., Coplen, T.B. and Riggs, A.C. (1997) Duration and structure of the past four interglacials, *Quaternary Research*, **48**, 141-154.
- Wintle, A.G., Murray, A.S. (2006) A review of quartz optically stimulated luminescence characteristics and their relevance in single-aliquot regeneration dating protocols. *Radiation Measurements*, **41**, 369-391.
- Woillard, G.M. (1978) Grande Pile peat bog: a continuous pollen record for the last 140,000 years, *Quaternary Research*, **9**, 1-21.
- Woodroffe, C.D. (2003) *Coasts: form, process and evolution*, Cambridge University Press, Cambridge, pp 623.
- Woodroffe, C.D., Stoddard, D.R., Harmon, R.S. and Spencer, T. (1983) Coastal morphology and Late Quaternary history, Cayman Islands, West Indies, *Quaternary Research*, **19**, 64-84.
- Woodroffe, C.D., Kennedy, D.M., Brooke, B.P. and Dickson, M.E. (2006) Geomorphological evolution of Lord Howe Island and carbonate production at the latitudinal limit to reef growth, *Journal of Coastal Research*, **22**, 188-201.
- Woodroffe, C.D., McGregor, H.V., Lambeck, K., Smithers, S.G. and Fink., D. (2012) Mid-Pacific microatolls record sea-level stability over the past 5000 yr, *Geology*, **40**, 951-954.
- Wopfner, J., and Douglas, J.G. (1971) *The Otway Basin of southeastern Australia*, Special Bulletin, Geological Surveys of South Australia and Victoria, 464 pp.
- Wright, V.P. and Smart, P.L. (1994) Paleokarst (dissolution diagenesis): Its occurrence and hydrocarbon exploration significance, In Wolf, K.H. and Chilingarian, G.V. (Eds.) *Diagenesis, IV*, p477-517, Developments in Sedimentology **51**, Elsevier, Amsterdam.
- Wu, G. and Hillaire-Marcel, C. (1994) Oxygen isotope compositions of sinistral *Neogloboquadrina pachyderma* tests in surface sediments: North Atlantic Ocean, *Geochimica et Cosmochimica Acta*, **58**, 1303-1312.
- Yin, Q.Z. and Berger, A. (2010) Insolation and CO<sub>2</sub> contribution to the interglacial climate before and after the Mid-Brunhes Event, *Nature Geoscience*, **3**, 243-246.
- Yokoyama, Y., Esat, T.M. and Lambeck, K. (2001) Coupled climate and sea-level changes deduced from Huon Peninsula coral terraces of the last ice age, *Earth and Planetary Science Letters*, **193**, 579-587.
- Yoshida, H., Roberts, R. G. and Olley, J. M. (2003) Progress towards single grain optical dating of fossil mud-wasp nests and associated rock art in northern Australia. *Quaternary Science Reviews*, **22**, 1273-1278.
- Zazo, C. (1999) Interglacial sea levels, *Quaternary International*, **55**, 101-113.

Zhou, L., Williams, M.A.J. and Peterson, J.A. (1994) Late Quaternary aeolianites, palaeosols and depositional environments on the Nepean Peninsula, Victoria, Australia, *Quaternary Science Reviews*, **13**, 225-239.

Zhu, Z.R., Wyroll, K.-H., Collins, L.B., Chen, J.H., Wasserburg, G.J. and Eisenhauer, A. (1993) High-precision U-series dating of last interglacial events by mass spectrometry: Houtman Abrolhos Islands, Western Australia, *Earth and Planetary Science Letters*, **11**, 281-293.



## **Appendices**

### **Appendix A: Microstructural features of skeletal carbonate grains identified within samples across the Mount Gambier coastal plain, southern Australia**

This appendix serves to list the attributes by which carbonate (and other) grains were identified through thin section analysis of sediment samples discussed in Chapter 4.

#### **A.1 Echinoid**

Echinoderms form in both shallow- and deep-marine environments. Echinoids are covered with elongated, moveable spines that commonly detach from the organism after death, and the spines themselves can be a large contributor to sediment volumes (Scholle and Ulmer-Scholle, 2003). Plates and spines of echinoderms are punctuated with a regular meshwork of pores that are approximately 15 – 25  $\mu\text{m}$  in diameter and produce a dusty appearance. Echinoid spines are recognisable in cross section as pores have a radial symmetry and thus produce a flower-like appearance (Scholle and Ulmer-Scholle, 2003). Fractions of echinoderms are easily recognisable under cross-polarised light in thin section as they appear as a single calcite crystal with complete unit extinction.

#### **A.2 Foraminifer**

Foraminifers are present within most sediment analysed across the Mount Gambier coastal plain and have been used to aid in palaeo-environmental reconstruction and to aid in constraining the chronostratigraphy of deposits. Tests of most benthic foraminifera are composed of calcite, though some species construct walls of aragonite or silica (Scholle and Ulmer-Scholle, 2003). Foraminifers are easily identifiable in thin section due to their small size (typically less than 1 mm; much smaller than most gastropods) and their hollowed- and multi-chambered, thin-walled tests.

#### **A.3 Mollusc**

As discussed within the thesis, molluscs are a common component on both beaches across the Mount Gambier coastal plain and the Bonney shelf. High-energy conditions along the southern Australian coastline therefore results in molluscan fragments comprising high proportions of beach and dune sediment. Both gastropods and bivalves are recognisable under thin section. Gastropods commonly display multiple chambers when cut in cross-section and are generally larger in size than most foraminifera. Bivalve fragments are typically more elongate in shape and may increase in thickness towards a hinge area. Bivalves will generally

also display layers of elongated crystals several microns in length. A cross-lamellar structure may be discernable in cross-polarised light whereby elongate aragonite crystals, of up to three orders of lamination, may be arranged parallel to sub-parallel to the surface of the shell. In cross-polarised light a homogenous structure may also be visible within some fragments whereby large areas will display uniform extinction and exhibit a patchwork of polarisation colours.

#### **A.4 Algal fragment**

Red or coralline algae are common within limestones. Under thin section they are recognisable due to their laminae and lattice-like patterns. Under high resolution the layers of medulla filaments are visible cased within a cortex filament, creating a mesh-like structure. In some instance the individual growth rings of the algae may also be visible. Algal fragments will commonly appear as a distinctive dark brown colour in thin section due to the micrite found between algal cell walls.

#### **A.5 Bryozoan fragment**

Bryozoan carbonates are marine, active suspension feeders, dominant in shelf areas and abundant between the intertidal zone and depths of up to 80 m (Flügel, 2004). Bryozoan biocalsts are abundant on temperate water shelves and are a dominant component within the Oligo-Miocene Gambier Limestone. In thin section bryozoan are commonly identifiable by their characteristic fan-like or dendritic pattern as a result of their zooecia (which are round, elongated tubes) composition. Individual zooecia are generally less than 1 mm in diameter, and their walls consist of foliated calcium carbonate crystals (Scholle and Ulmer-Scholle, 2003).

#### **A.6 Lithoclast**

Lithoclasts describe reworked grain aggregates. Commonly these grains are composed of fragments of molluscs, calcareous algae and foraminifera and found within strong cement. Under polarised light lithoclasts may be recognised as arrangements of multiple unorientated grains of a variety of shades; commonly yellows and browns.

#### **A.7 Quartz**

Quartz grains are easily identifiable in thin section under cross-polarised light as they are bright white and exhibit complete extinction.

#### **A.8 Opaque grains**

Within some thin section samples grains appeared dark and no structure within the grain was visible. In these instances grains were simply classed as opaque grains.

### **A.9 Cement**

Cement may form between grains during diagenesis. Several types of cement may be observed within sediment from the Mount Gambier coastal plain. Micritic cement is commonly brown to grey when examined under a microscope and commonly lack any internal structure. Micrite is also smaller in size than other cements and in the original definition of Folk (1959) the grain size limit is  $<4\ \mu\text{m}$ .

Spar cement is generally larger in size. Cement can be distinguished from bioclastic grains within a thin section by a range of factors: it commonly has a clear and clean appearance; spars generally have well-defined crystal boundaries; sharp contacts between spar and other grains; spars will not overlap grains; the long axis of spar crystals are commonly perpendicular to grains surfaces; and spar crystal sizes will generally increase away from the grain surface (Flügel, 2004).

Cement types are commonly indicative of depositional environments and several of these cement types are identified in thin sections of samples from the Mount Gambier coastal plain. Meniscus cement is where calcite cement precipitates at grain to grain contacts within pores and may exhibit a curved surface below grains. Meniscus cements are commonly indicative of diagenesis in the meteoric-vadose zone. Dog-tooth spar described sharply pointed acute calcite crystals that are generally found normal to the grain surface and are commonly of elongated or rhombodedral form, with sometimes blunted terminations (Flügel, 2004). Drusy cements describe those that fill pore spaces and is characterised by equant to elongated calcite crystals that increase in size towards the centre of a void. Drusy cements are indicative of near-surface meteoric and burial diagenetic environments (Flügel, 2004). Granular cements are similar to drusy cements. However, crystals are slightly smaller and do not increase in size towards the centre of a void. Granular cements are commonly formed within meteoric-vadose, meteoric-phreatic and burial environments, though may also form from the recrystallization of pre-existing cements (Flügel, 2004). Blocky spar cement also forms within pores but is coarser in size and crystals are of various sizes with no preferred orientation. Syntaxial overgrowth cements form where substrate-controlled overgrowth occurs around a host grain, commonly echinoderm fragments. Differences in colour between the skeletal grain and the overgrowth cement may be noticeable and indicate diagenesis within a near-surface marine, vadose-marine or meteoric-phreatic environment (Flügel, 2004).

## **Appendix B: AAR Laboratory procedure**

The laboratory procedure for preparation and analysis of samples for AAR is outlined within this appendix which presents the procedures for molluscs, whole-rock, foraminifera and pyrolysis experiments.

### **B.1 Molluscs**

#### **Cleaning**

Prior to processing molluscs, samples were cleaned to eliminate any foreign constituents that may be embedded within the sample. This was done using a dentist's drill to remove the outer layer of shell, which is where cements and conglomerates of sediment are most likely to reside. When using the dentist's drill, the sample and the drill were kept constantly wet in order to keep temperatures low and to prevent inducing racemisation of the shell sample. Once the outer shell layer was removed the shell was cut into several sub-samples of an appropriate size for analysis. This was again conducted using the dentist's drill.

Each sub-sample was placed in a sterile test tube, and covered in purified (Millipore) water before placing in an ultrasonic bath for ten minutes. Samples were then washed three times with Millipore water before returning to the ultrasonic bath for a further ten minutes. This flushing aims to remove any further sediment or cement which may not have been washed off after the use of the drill. Where molluscan samples were too small to cut using the dentist's drill, whole shells were sampled. When whole gastropods were analysed they were broken into several fragments (beneath two pieces of sterile tissue using a pair of tweezers) and then placed into the ultrasonic bath. This was done as the whorls present within gastropods are a favourable locality for the accumulation of sediment and foreign matter.

#### **Acid etch**

Once samples were sufficiently cleaned they were subjected to an acid etch which aimed to remove any non-indigenous amino acids or leached material. It is desirable to remove approximately 33% of the sample mass. This is therefore done by accurately measuring the sample after it has dried, and adding 0.0033 mL of 2 M hydrochloric acid (HCl) per 1 mg of sample mass.

For example, if the dried sample weighs 50 mg:

Volume of 2 M HCl to add =  $0.0033 \text{ mL} \times 50 \text{ mg} = 0.165 \text{ mL}$  (or 165  $\mu\text{L}$ ).

Prior to adding the HCl, samples were placed in sterile test tubes and covered with a small amount of Millipore water (to prevent all of the shell from dissolving). After acid was

added the sample was left until it was visibly seen to stop reacting. Once this had occurred, each sample was washed 3 to 5 times with Millipore water to remove any acid. Once as much of the water and acid residue as possible had been removed, the sample was subjected to its final cleaning step; a peroxide soak. Samples remained in the test tube and were covered (using a pasteur pipette) with 3% hydrogen peroxide ( $\text{H}_2\text{O}_2$ ) and left for a minimum of two hours, in the aim of removing absorbed contaminating organic material. Samples were then rinsed again with Millipore water, before being placed in sterile plastic trays and left to air-dry once more.

Note, where samples were thought to be particularly old (mid to early Pleistocene) and previous analysis has yielded D/L values lower than expected, the peroxide soak may be exchanged for a 24 hour bleach soak which is aimed to analyse the intra-crystalline fraction, suggested by Penkman *et al.* (2008) to be a better closed system.

### **Hydrolysis**

Once samples had dried they were accurately weighed again and placed into sterile 4 mL vials, and then subjected to hydrolysis prior to analysis. Hydrolysis releases the amino acids from their peptide chains by subjecting the sample to acidic conditions under elevated temperatures. In this study samples were dissolved in 8 M HCl and placed in an 110°C oven for 22 hours. Excess 8 M HCl was added to the sample, so that when the shell is completely dissolved the solution will still remain highly acidic, in this case at 7M.

In order to calculate the volume of 8 M HCl to add to the sample the following formula may be used;

For example, if the specimen weighs 50 mg after the 2 M HCl acid etch;

$$0.02 \text{ mL} \times 50 \text{ mg} = 1 \text{ mL}$$

Therefore 1000  $\mu\text{L}$  8 M HCl is added to the specimen.

Samples were dissolved in the same vial they were to be hydrolysed in to minimise loss and contamination. 8 M HCl was added slowly to the sample (to avoid sample reacting quickly and 'boiling over'), with a pipette. Samples should then be totally dissolved.

Free amino acid samples were taken from each sub-sample once samples had been dissolved but prior to hydrolysis. 50  $\mu\text{L}$  was taken from each sub-sample and then placed in a vacuum to dry out. Once dry, free sub-samples followed the procedure outlined for the total fraction as outlined below after hydrolysis.



As each vial was capped, the sample was flushed with nitrogen gas for approximately 15 seconds to remove any oxygen left in the atmosphere that would result in oxidation of any protein residue within the acidic solution. Caps were securely fitted before samples were placed in an oven set at 110°C for 22 hours. After 30 minutes the caps were re-tightened.

After 22 hours samples were removed from the oven and allowed to cool. 50 µL was then drawn from each sample and dried in a vacuum desiccator. Once completely dry samples were re-hydrated with 50 µL of a rehydration solution (0.01 mM L-Homoarginine + 0.01 M HCl and 0.77 mM sodium azide), in which the L-Homoarginine acted as an internal standard that allows concentrations of amino acids to be calculated.

Samples were then thoroughly mixed with the vortex mixer and were ready for insertion into the RP-HPLC Autosampler.

## **B.2 Whole-rock**

Whole rock samples required a series of additional sample preparation steps prior to amino acid analysis. If the whole rock sample was highly consolidated, a section needed to be broken off and ground down using a mortar and pestle to separate all the grains. This was done, not by placing great force on the sediment, but by gently grinding and rolling the grains. The samples were then sieved using a nest of sieves and the 250 – 500 µm fraction was used in this study for analysis. Samples were studied under the microscope to check if all grains have been separated from one another, if they have not, samples are again gently grinded using the mortar and pestle and sieved once more.

Samples were then placed in a beaker with distilled water and sonicated for 5 to 10 minutes. Samples were then washed and sonicated once more before being left to dry overnight. This step aimed to remove any silt, clay or organic material that may be within the sample.

It is necessary to determine the percentage of calcium carbonate with the whole-rock sample in order to accurately calculate the volumes of 2M and 8M HCl that are to be added to the sample throughout sample preparation procedures. This was done through placing a measured volume of the sample within a beaker and adding 8M HCl to the sample until it stopped reacting. The acid was then washed off and the sample left to dry overnight in a 110°C oven before the remainder of the sample was re-weighed. The net loss is the carbonate content within the sample. Once the sample had been sonicated and left to dry ten sub-

samples of 150-200 mg were taken and placed in ten individual test tubes for the acid etch stage.

For whole-rock, the calculations to determine the volumes of 2 M and 8 M HCl are slightly different to those used for molluscs, and incorporate the carbonate content of the sample. The calculations for whole rock are as follows;

Volume of 2 M HCl to add for acid etch:

$$= [(initial\ mass\ of\ sample \times \% \text{ carbonate of initial mass}) \times 0.0033] \times 1000$$

For example, suppose the sample is 150 mg and has a carbonate content of 80 %;

$$[(150\ \text{mg} \times 0.8) \times 0.0033] \times 1000 = 396\ \mu\text{L of 2 M HCl to etch whole-rock sample with}$$

Volume of 8 M HCl to add to sample for hydrolysis:

$$= [(Total\ mass\ of\ carbonate\ within\ initial\ sample \times 0.67) \times 0.02] \times 1000$$

$$= [[(150 \times 0.8) \times 0.67] \times 0.02] \times 1000$$

$$= 1608\ \mu\text{L of 8 M to add to the sample for hydrolysis.}$$

Samples are then processed in much the same way as with molluscs, and are treated with nitrogen gas before being capped and placed in the 110°C oven for 22 hours (free amino acid samples are also taken prior to placing sub-samples in the oven).

On removal from the oven sub-samples were allowed to cool. Each whole-rock sub-sample was then filtered prior to drying in the vacuum, to remove any of the constituents that have not dissolved (the non-carbonate portion of the sample). After filtration, 50 µL was taken from each sub-sample and placed in sterile vials in the vacuum to dry. From this stage onwards samples were processed in the same way as mollusc samples.

### **B.3 Foraminifera**

Where foraminifera were analysed, they also generally followed the procedure outlined for molluscs, however several of the steps were modified or omitted to account for the fact that only single grain analysis was performed.

Firstly foraminifera were hand-picked from samples, with well persevered (translucent and unabraded) specimens being favoured. Specimens were then placed in a test tube with distilled water and sonicated twice for five minutes at a time. Samples were flushed with distilled water between sonications. Samples were then flushed three times with Millipore

water, placed in a test tube and left to soak in 3% hydrogen peroxide for 2 hours (the 2 M HCl etch step was omitted due to the small size of each of the specimens). Samples were once again flushed with Millipore water and left to dry overnight.

Once dry, individual tests were placed in separate sterile vials. Samples were then subjected to 5  $\mu$ L of high purity 6 M HCl. It proved difficult to establish a mass for individual foraminifera so 5  $\mu$ L was used as a control measure to add to each specimen. When multiple foraminifera (usually 10) were analysed in one vial 10  $\mu$ L of 6 M HCl was added. Samples were then flushed with nitrogen gas before being capped and placed in the 110 °C oven for 22 hours. Samples were then left to dry in the vacuum. Once dry samples were rehydrolysed with 5  $\mu$ L of L-homoarginine (the same volume as the 6 M high purity HCl used for hydrolysis) and were ready for analysis in the HPLC.

Due to their low mass and a low volume of 6 M HCl was added, it was impossible to take a sub-sample to analysis the free amino acid fraction of the foraminifera, and thus this step was also omitted from procedure.

#### **B.4 Pyrolysis experiments**

In an attempt to model the kinetics of racemisation of glutamic acid, valine, aspartic acid, leucine and serine, heating (pyrolysis) experiments were conducted on whole-rock samples collected from the sediment of the modern Shelly Beach, Cape Northumberland, on live-collected *Ostrea* and *Katelysia* and on foraminifera (*Elphidium crispum* and *Discorbis dimidiatus*) hand-picked from Port MacDonnell Beach sediment. Whole-rock samples were derived from the 250-500  $\mu$ m fraction, sonicated and flushed with Millipore water. 400 mg samples were then weighed and placed in sterile glass vials with approximately 15 mL of Millipore water and sealed. Samples were placed in an oven heated to 110°C and removed at varying times over a period of 120 days for processing. On removal from the oven samples were left to dry. Two-sub-samples were taken from the vial and processed as outlined in B.2.

Live-collected *Ostrea* were first cleaned by hand and dental drill to remove any algae and non-indigenous material from the shell. Four *Ostrea* shells were used, and from these the umbo region was cut from the shell using a dental drill. These samples were then cleaned in an ultrasonic bath for five minutes before being rinsed and left to dry. Once dry samples were crushed using a mortar and pestle into a coarse powder. Sub-samples of ~300 mg were weighed, and placed in sterile vials. ~800 mg of quartz sand was added to these vials. Millipore water was finally added to the vials before they were sealed and placed in the 110°C

oven. Samples were again taken out at varying times (see Table 5.1) over the course of 120 days. On removal from the oven samples were left to dry. The quartz sand was then removed from the shell through sieving. Two ~50 mg sub-samples of shell were taken from each vial and processed following the procedure outlined in B.1. The same process was adopted for *Katelsysia*, though the umbo of five shells was sampled and crushed into a coarse powder.

Foraminifera were subtracted from whole-rock samples, placed in sterile test tubes. and sonicated for 5 minutes in distilled water. Previous attempts at pyrolysis experiments had resulted in tests dissolving within the test tubes after lengthy time intervals in the oven. Therefore, multiple tests, and specifically the largest and most robust tests present were placed within each test tube. Millipore water was added to the test tubes and they were then sealed and placed in the 110°C oven for set intervals of time. On removal, water was drained and tests were dried and then processed following the procedure outlined in B.3.

## **Appendix C: Statistical analysis of results**

To determine whether derived GLU D/L values were statistically different from those derived at other sample sites one way analysis of variance (ANOVA) tests were conducted on raw data sets using the IBM SPSS Statistics program (IBM Corp., 2010). If the results of ANOVA revealed there was a statistical difference between derived D/L values then post-hoc Tukey tests were conducted on data sets to determine which samples yielded significantly different GLU D/L values. Tests were conducted to compare whole-rock samples, analysed *Elphidium crispum* and also the variance in GLU D/L values between certain molluscan genera (*Ostrea*, *Katelsysia* and *Turbo*) across sample sites.

The results of these tests are presented in the following tables; C.1, C.2, C.3, C.4, C.5, C.6 and C.7. Where derived values are greater than 0.05 it suggests that there is no significant difference between derived GLU D/L values at a confidence interval of 95%.

**Table C.1:** Results of Post-Hoc Tukey statistical tests on GLU D/L values from the foraminifer *Elphidium crispum* in sample sites across the Mount Gambier coastal plain

Elphid	PMB	PMB(o)	HB	HB(o)	PM Ua	SB Ua	PM La	SB La	Ma Sw	Ma Na	Bu Ra	Bu La	Ca La	Gam	Baxt	Heri	Don's	Dart	FOH	Ming v
PMB	x	0.271	0	0	0	0	0	0	0	0	0	0	0	0	0	0	0	0	0	0
PMB(o)	0.271	x	1	0.401	0.296	0.672	0.936	0.3	0.019	0.39	0	0	0	0	0	0	0	0	0	0
HB	0	1	x	0.843	0.705	0.989	1	0.729	0.036	0.843	0	0	0	0	0	0	0	0	0	0
HB(o)	0	0.401	0.843	x	1	1	0.997	1	1	1	0.001	0.384	0.001	0	0	0.003	0	0	0	0
PM Ua	0	0.296	0.705	1	x	1	1	1	0.905	1	0	0	0	0	0	0	0	0	0	0
SB Ua	0	0.672	0.989	1	1	x	1	1	0.726	1	0	0	0	0	0	0	0	0	0	0
PM La	0	0.936	1	0.997	1	1	x	0.999	0.453	0.999	0	0	0	0	0	0	0	0	0	0
SB La	0	0.3	0.729	1	1	1	0.999	x	0.995	1	0	0	0	0	0	0	0	0	0	0
Ma Sw	0	0.019	0.036	1	0.905	0.726	0.453	0.995	x	1	0	0.016	0	0	0	0	0	0	0	0
Ma Na	0	0.39	0.843	1	1	1	0.999	1	1	x	0	0.053	0	0	0	0	0	0	0	0
Bu Ra	0	0	0	0.001	0	0	0	0	0	0	x	0.116	1	0	0.998	1	0	0.003	0	0
Bu La	0	0	0	0.384	0	0	0	0	0.016	0.53	0.116	x	0.14	0	0.003	0.286	0	0	0	0
Ca La	0	0	0	0.001	0	0	0	0	0	0	1	0.14	x	0	0.969	1	0	0	0	0
Gam	0	0	0	0	0	0	0	0	0	0	0	0	0	x	0.012	0.036	0.096	1	0.903	0
Baxt	0	0	0	0	0	0	0	0	0	0	0.998	0.003	0.969	0.012	x	1	0	0.205	0.05	0
Heri	0	0	0	0.003	0	0	0	0	0	0	1	0.286	1	0.036	1	x	0	0.2	0.05	0
Don's	0	0	0	0	0	0	0	0	0	0	0	0	0	0.096	0	0	x	0.396	1	0.958
Dartm	0	0	0	0	0	0	0	0	0	0	0.003	0	0	1	0.205	0.2	0.396	x	0.958	0.001
FOH	0	0	0	0	0	0	0	0	0	0	0	0	0	0.903	0.005	0.005	1	0.958	x	0.98
Ming vi	0	0	0	0	0	0	0	0	0	0	0	0	0	0	0	0	0.958	0.01	0.98	x

No statistical difference between D/L values is recognised to a confidence interval of 95% when p values are greater than 0.05.

PMB = Port MacDonnell Beach, (o) = presumed older or reworked grains, HB = Holocene Beach, Port MacDonnell, PM Ua = Port MacDonnell upper aeolianite, SB Ua = Shelly Beach upper aeolianite, PM La = Port MacDonnell lower aeolianite, SB La = Shelly Beach lower aeolianite, Ma Sw = MacDonnell Range, Swarts Road, Ma Na = MacDonnell Range at Narrawong, Bu Ra = Burleigh Range at Road, Bu La = Burleigh Range at Laslett Road, Ca La = Caveton Range lagoonal facies, Gam = Gambier Range, Baxt = Baxter's Quarry, Heri = Heritage Industries, Don's = Don's Quarry, Mingbool Range, Dart = Dartmoor Cemetery, FOH = Fort O'Hare Quarry, Ming v = Mingbool village, Dismal Range.

**Table C.2:** Results of Post-Hoc Tukey statistical tests on GLU D/L values from whole-rock analysis of bioclastic sediment at sample sites across the Mount Gambier coastal plain

WR	PMB	SB	CBW	LB	Holo	PMUa	SBUa	PMLa	SBLa	WeA	MaSw	MaNa	BuA	BuB	BuC	CaU2	CaU8	Buck	Gam	Baxt	Heri	Don's	Dart	FOH	Min
PMB	x	0	0	0	0	0	0	0	0	0	0	0	0	0	0	0	0	0	0	0	0	0	0	0	0
SB	0	x	0.994	0.999	0	0	0	0	0	0.946	0	0	0	0	0	0	0	0	0	0	0	0	0	0	0
CBW	0	0.994	x	1	0	0	0	0	0	1	0	0	0	0	0	0	0	0	0	0	0	0	0	0	0
LB	0	0.99	1	x	0	0	0	0	0	1	0	0	0	0	0	0	0	0	0	0	0	0	0	0	0
Holo	0	0	0	0	x	1	0.01	0	0.066	0	0	0	0	0	0	0	0	0	0	0	0	0	0	0	0
PMUa	0	0	0	0	1	x	0.204	0	0.63	0	0	0.001	0	0	0.002	0	0	0	0	0	0	0	0	0	0
SBUa	0	0	0	0	0.01	0.204	x	0.914	1	0	0.017	0.998	0	0	1	0	0	0	0	0	0	0	0	0	0
PMLa	0	0	0	0	0	0	0.914	x	0.276	0	0.996	1	0	0	1	0	0	0	0.018	0	0	0	0	0	0
SBLa	0	0	0	0	0.066	0.63	1	0.276	x	0	0	0.711	0	0	0.839	0	0	0	0	0	0	0	0	0	0
WeA	0	0.946	1	1	0	0	0	0	0	x	0	0	0	0	0	0	0	0	0	0	0	0	0	0	0
MaSw	0	0	0	0	0	0	0.017	0.996	0	0	x	0.845	0	0	0.71	0	0	0	0.419	0	0	0	0	0	0
MaNa	0	0	0	0	0	0.001	0.998	1	0.711	0	0.845	x	0	0	1	0	0	0	0.002	0	0	0	0	0	0
BuA	0	0	0	0	0	0	0	0	0	0	0	0	x	0.238	0	0	1	0	0	0.009	0	0	0	0	1
BuB	0	0	0	0	0	0	0	0	0	0	0	0	0.238	x	0	0.026	0.049	1	0	1	0.807	0.6	0.815	0.996	0.023
BuC	0	0	0	0	0	0.002	1	1	0.839	0	0.71	1	0	0	x	0	0	0	0.023	0	0	0	0	0	0
CaU2	0	0	0	0	0	0	0	0	0	0	0	0	0	0.026	0	x	0	0.118	0	0.006	0.972	0.998	0.994	0.529	0
CaU8	0	0	0	0	0	0	0	0	0	0	0	0	1	0.049	0	0	x	0	0	0	0	0	0	0	1
Buck	0	0	0	0	0	0	0	0	0	0	0	0	0	1	0	0.118	0	x	0	1	0.998	0.971	0.997	1	0
Gam	0	0	0	0	0	0	0	0.018	0	0	0.419	0.002	0	0	0.023	0	0	0	x	0	0	0.002	0.004	0	0
Baxt	0	0	0	0	0	0	0	0	0	0	0	0	0.009	1	0	0.006	0	1	0	0	0.74	0.472	0.774	0.998	0
Heri	0	0	0	0	0	0	0	0	0	0	0	0	0	0.807	0	0.972	0	0.998	0	0.74	x	1	1	1	0
Don's	0	0	0	0	0	0	0	0	0	0	0	0	0	0.6	0	0.998	0	0.971	0.002	0.472	1	x	1	1	0
Dart	0	0	0	0	0	0	0	0	0	0	0	0	0	0.815	0	0.994	0	0.997	0.004	0.774	1	1	x	1	0
FOH	0	0	0	0	0	0	0	0	0	0	0	0	0	0.996	0	0.529	0	1	0	0.998	1	1	1	x	0
Min v	0	0	0	0	0	0	0	0	0	0	0	0	1	0.023	0	0	0	0	0	0	0	0	0	0	x

No statistical difference between D/L values is recognised to a confidence interval of 95% when p values are greater than 0.05.

PMB = Port MacDonnell Beach, (o) = presumed older or reworked grains, SB = Shelly Beach, Cape Northumberland, HB = Holocene Beach, Port MacDonnell, PMUa = Port MacDonnell upper aeolianite, SBUa = Shelly Beach upper aeolianite, PMLa = Port MacDonnell lower aeolianite, SBLa = Shelly Beach lower aeolianite, WeA = weathered aeolianite, Port MacDonnell, MaSw = MacDonnell Range, Swarts Road, MaNa = MacDonnell Range at Narrawong, BuA = Burleigh Range at Rabbitors Road A, BuB = Burleigh Range at Rabbitors B, BuC = Burleigh Range at Rabbitors Road C, CaU2 = Caveton Range lagoonal facies unit 2, CaU8 = Caveton Range lagoonal facies unit 8, Gam = Gambier Range, Baxt = Baxter's Quarry, Heri = Heritage Industries, Don's = Don's Quarry, Mingbool Range, Dart = Dartmoor Cemetery, FOH = Fort O'Hare Quarry, Min v = Mingbool village, Dismal Range.

**Table C.3:** Results of post-hoc Tukey statistical tests for GLU D/L values from *Katelsysia rhytiphora* samples across the Mount Gambier coastal plain

<i>Katelsysia rhytiphora</i>	Live-collected	Lake Hawdon South	CCP 1	German Creek	Burleigh (Rabbitors)	Caveton
Live-collected	x	0	0	0	0	0
Lake Hawdon South	0	X	0.798	0.251	0	0.001
CCP 1	0	0.798	X	0.002	0	0
German Creek	0	0.251	0.002	X	0	0.05
Burleigh (Rabbitors)	0	0	0	0	X	0
Caveton	0	0.001	0	0.05	0	X

No statistical difference between D/L values is recognised to a confidence interval of 95% when p values are greater than 0.05.

**Table C.4:** Results of post-hoc Tukey statistical tests for GLU D/L values from *Ostrea angasi* samples across the Mount Gambier coastal plain

<i>Ostrea</i>	Live-collected	Lake Hawdon S.	Heritage	Heri w. bleach	Don's	Dartmoor	FOH shell bed	FOH fallen	Mingb. Village
Live-collected	x	0	0	0	0	0	0	0	0
Lake Hawdon S.	0	x	0.158	0	0	0.001	0	0.001	0
Heritage	0	0.158	x	0.783	0.921	0.997	0.382	0.701	0.655
Heri w. bleach	0	0	0.783	x	1	0.976	0.999	1	1
Don's	0	0	0.921	1	x	0.999	0.943	0.996	0.996
Dartmoor	0	0.001	0.997	0.976	0.999	x	0.638	0.93	0.912
FOH shell bed	0	0	0.382	0.999	0.943	0.638	x	1	1
FOH fallen	0	0.001	0.701	1	0.996	0.93	1	x	1
Mingb. village	0	0	0.655	1	0.996	0.912	1	1	x

No statistical difference between D/L values is recognised to a confidence interval of 95% when p values are greater than 0.05.

**Table C.5:** Results of post-hoc Tukey statistical tests for GLU D/L values from *Turbo undulatus* samples across the Mount Gambier coastal plain

<i>Turbo</i>	Port MacDonnell	Midden	Holocene beach	Conglomerate (Holo)	Conglomerate (Plei)
Port MacDonnell	x	0	0	0	0
Midden	0	x	0.697	0.956	0
Holocene beach	0	0.697	x	0.992	0
Conglomerate (Holo)	0	0.992	0.992	x	0
Conglomerate (Plei)	0	0	0	0	x

No statistical difference between D/L values is recognised to a confidence interval of 95% when p values are greater than 0.05.

**Table C.6:** Results of post-hoc Tukey statistical test for GLU D/L values for a range of genera collected from an *in situ* assemblage at Lake Hawdon, lagoonal facies, proposed to be MIS 5e in age.

Genera	<i>Fulvia</i>	<i>Anadara</i>	<i>Katelsysia</i>	<i>Tellina</i>	<i>Brachidontes</i>
<i>Fulvia</i>	X	1	0.842	0.819	0.001
<i>Anadara</i>	1	X	0.936	0.887	0.005
<i>Katelsysia</i>	0.842	0.936	X	0.999	0.067
<i>Tellina</i>	0.819	0.887	0.999	X	0.731
<i>Brachidontes</i>	0.001	0.005	0.067	0.731	X

**Table C.7:** Results of post-hoc Tukey statistical tests for GLU D/L values for a range of genera collected from a lagoonal facies within Caveton Range, proposed to be MIS 9 in age.

Genera	<i>Katelsysia</i>	<i>Tellina</i>	<i>Niotha</i>	<i>Fulvia</i>
<i>Katelsysia</i>	X	0.12	0	0.814
<i>Tellina</i>	0.12	X		0.166
<i>Niotha</i>	0	0	X	0.021
<i>Fulvia</i>	0.814	0.166	0.021	X